UNIVERSITAT DE BARCELONA

The role of the G-protein coupled receptor 120 (GPR120) on the FGF21 system in white and brown adipose tissues

Tania Paloma Quesada López

The role of the G-protein coupled receptor 120 (GPR120) on the FGF21 system in white and brown adipose tissues

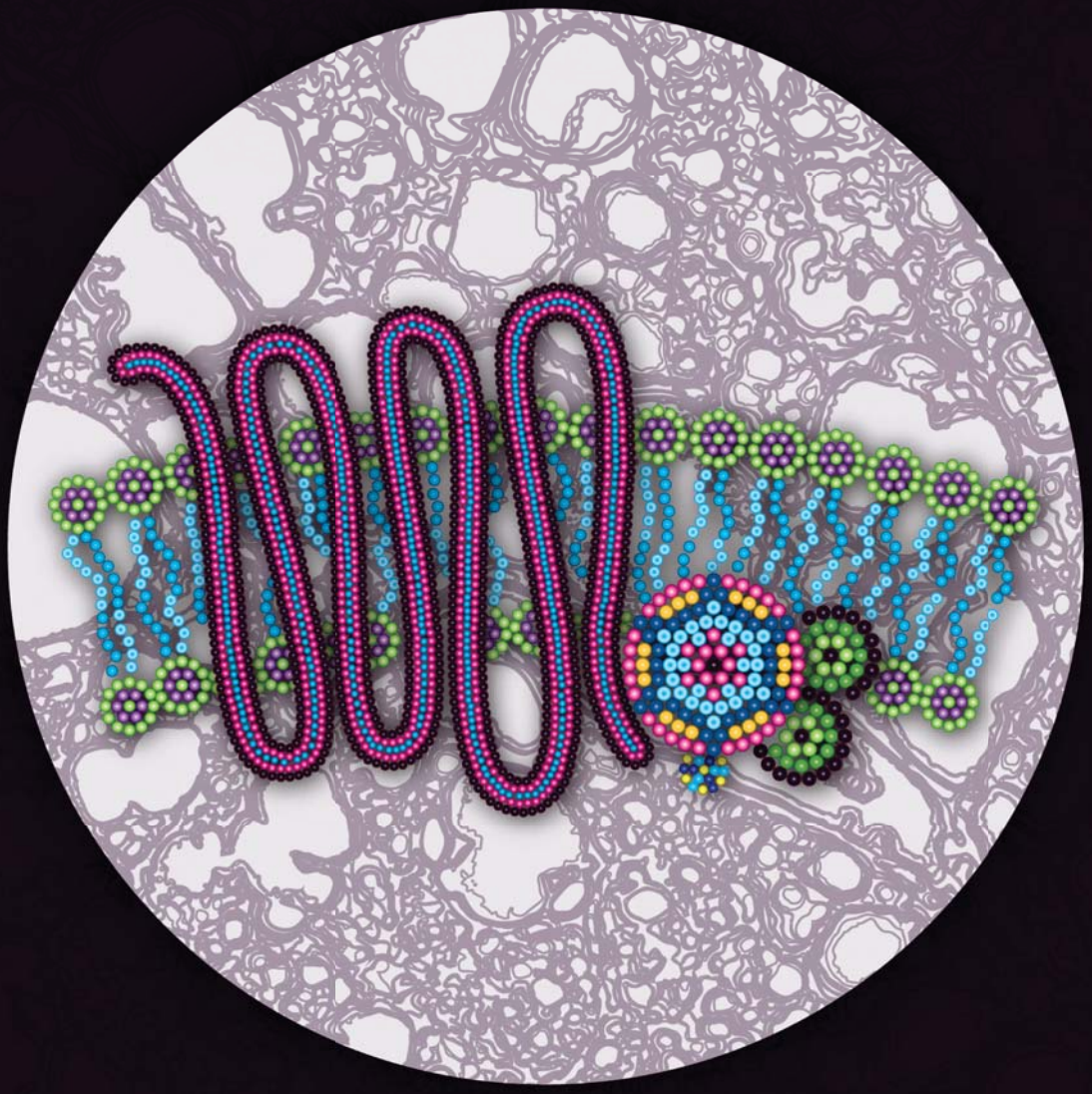

Tania Paloma Quesada López

Doctoral Thesis

2018

Tania Paloma Quesada López

The role of the G-protein coupled receptor 120 (GPR120) on the FGF21 system in white and brown adipose tissues

Doctoral Thesis 2018

Facultad de Biología

Programa de Doctorado en Biomedicina

Departamento de Bioquímica y Biomedicina Molecular

Grupo de Genética y Biología Molecular de Proteínas Mitocondriales y Patologías Asociadas

The role of the G-protein coupled receptor 120 (GPR120) on the FGF21 system in white and brown adipose tissues

Memoria presentada por

Tania Paloma Quesada López

para optar al grado de doctor por la Universidad de Barcelona

Firma de los directores

Dr. Francesc Villarroya Gombau

Dra. Marta Giralt Oms

Barcelona, 2018

UNIVERSITAT DE BARCELONA

Biomedicine Doctorate Program

Biochemistry and Molecular Biomedicine Department

Genetics and Molecular Biology of Mitochondrial Proteins

and Associated Pathologies Laboratory

The role of the G-protein coupled receptor 120 (GPR120) on the FGF21 system in white and brown adipose tissues

Doctoral Thesis

Tania Paloma Quesada López

Barcelona

2018

“Science knows no country, because knowledge belongs to humanity, and is the torch which illuminates the world.”

Louis Pasteur

A mi familia

Agradecimientos [Acknowledgements]

Siempre se me había hecho curioso leer aquella frase al inicio de los agradecimientos de las tesis. Esa frase que menciona una copa de vino o unas cuantas cervezas. No voy a mentir, me he sentado frente a una colección de botellas con la intención de tomar un poco de inspiración para soltar las palabras. Lo curioso es que he volteado a ver el tequila y el vino (*algunos me quitarían el pasaporte por esta última frase*) y me hace darme cuenta que, sin duda, 'la tesis' me ha marcado de muchas maneras dejándome una huella bastante mestiza. Y es que, es real. Es bastante resonante el momento de sentarse y mirar hacia atrás. No por el hecho de arrepentirse de las decisiones tomadas -*o de las muestras no guardadas en el -80°C*- sino por todo aquello que se ha vivido. El montón de personas que van marcando el camino que hemos elegido. Además, en mi caso, también se piensa en aquellas personas que se quedan en la lejanía pero que al final siempre encuentran la manera de hacerse sentir a un lado nuestro. Hoy, a punto de entregar este gran cúmulo de páginas, me doy cuenta que ha sido un gran camino. No lo digo por los 8'000 kms que me he desplazado desde casa para lograrlo (*¡Cielos! Suenan menos de los que se sienten...*). Lo digo porque sé que he crecido bastante gracias a todas las personas que han estado a mi lado estos años. Los primeros en estar siempre ahí, esté donde esté, son mis padres. Gracias, mamá y papá, por apoyarme siempre en mis aventuradas decisiones. No importa que tan descabellado o difícil parezca aquello que elijo, siempre he podido contar con su apoyo aunque ello represente estar alejados. Sé que no es fácil vivir con la duda de cuando nos volveremos a abrazar pero siempre han encontrado la forma de hacerme sentir amada y apoyada. Otro par de estrellas en mi camino que siempre se hacen notar, de lejos y de cerca, son Abril y Joel. Mis pequeños (*ya grandes*) hermanos que siempre encuentran la manera de comunicarse conmigo y alegrarme el día. A los cuatro, los llevo siempre conmigo. No puedo dejar de mencionar al resto de la familia, gracias por estar siempre pendientes de mí y recibirme con los brazos abiertos en cuanto piso *tierras aztecas*. Abuelos, tíos, primos… gracias!

Si bien no es fácil estar lejos de la tierra que te ha visto crecer, la verdad es que me han 'acogido' dos personas maravillosas. Ambos han hecho que mi estancia se convirtiera en una experiencia fantástica al grado de convertir el laboratorio en mi segundo hogar estos últimos 5 años (bueno, casi 5). Dr. Francesc, Dra. Marta: estoy muy agradecida con ustedes por darme la oportunidad de entrar al TAM, por permitirme aprender de ustedes y con ustedes, por TODA la paciencia y guía durante este tiempo y por compartir una nueva cultura conmigo siempre haciéndome sentir incluida y bienvenida. Sin duda, pocos doctorandos tienen la suerte de encontrar a dos magníficos directores y excelentes personas por el camino. Moltíssimes gràcies!

Igualmente, tengo que agradecer a la gran familia TAM. ¡Una familia padrísima! ☺ Con diferentes integrantes a lo largo de este tiempo pero siempre con un gran sentimiento de compañerismo, un buen ambiente y buenas experiencias. Gracias a todos ustedes porque de todos he aprendido un poco, tanto de ciencia como de cultura y costumbres.

La verdad es que han sido un excelente grupo de trabajo y de vida. No pude haber encontrado un grupo más *chingón* que éste. He sido muy afortunada de tener siempre alguien con quien hablar, chismear, hacer la **'***hora de la balada mexicana*', consultar protocolos, cantar, no morir en el intento por subir (*y bajar*) el Pedraforca, comer calçots o nachos, tacos y margaritas. Gracias por su apertura cultural, por hacerme sentir integrada siempre, por sus oídos, por sus historias, por las risas y el sushi (*PUFAs!!!!*). Gracias por haber dejado en mí una huella de cada uno de ustedes. Sin duda han hecho que para mí el TAM sea un lugar especial (*multicultural, miltimusical, obesogénico, etc*). Muchísisisisimas gracias!!!

Y qué decir de mi más grande cómplice de esta *pato*-aventura. Nada sería lo mismo sin tu compañía y apoyo. Gracias por tomarme de la mano y compartir esa mirada de –*al chile, allá vamos*- y alcanzar nuestras metas más *guajiras* del otro lado del planeta juntos. Por todas las carcajadas, el apoyo, la paciencia, las preguntas, la sazón, las risas, los bailes, el canto y tu amor. ¡Gracias, babe, por compartir cada milisegundo de esta gran decisión! #TnT <3

No puedo olvidarme de aquellos que han hecho de esta vida en Barcelona toda una travesía. Gente que da sabor a los días y color a los malos momentos. Gracias a mis *fantastics*: César, Josué y Linette; tres personas maravillosas con las que he podido contar y compartir *físico-algoritmo-pasteleramente*. A mi sector Latinoamérica (Liska) del departamento por compartir experiencias, la terapia del *homesick* y cupcakes. A Rod y Quim, gracias por ser una pequeña familia de este lado del mundo. Por compartir cenas, comidas, *calçotadas*, diadas, arte, historia y un poco de vino. A los amigos que están por aquí, a los que han venido y se han vuelto a casa y a aquellos amigos que están en México o en algún otro lugar del mundo y se han tomado el tiempo para ver 'cómo va la tesis' y ponernos al día. Dentro de ellos, especialmente a Andrea V. Gracias, amiga, porque siempre estás ahí para escuchar, compartir las frustraciones de este camino paralelo, por las canciones de *Nirvana* y las carcajadas simultáneas por teléfono. A todos ustedes, gracias, por las comidas los findes, las risas hasta llorar, los picnics, los *mezcales*, los *panellets*, las *Skypeadas*, los *mails*, los *whatsapps*, las caminatas o lo que fuera. Gracias por estar ahí y preguntar por mis ratones, por mis células y por cantar conmigo en el karaoke.

En verdad, me alegra mucho haberlos tenido a todos ustedes en este camino. Porque no es fácil y porque se precisa contar con grandes personas para tener grandes días. Así que hoy me siento feliz porque en este tiempo he logrado comprender la letra de aquella canción: <*tantos siglos, tantos mundos, tanto espacio y coincidir*>.

¡MIL GRACIAS A TODOS!

CONTENTS

Contents

This doctoral thesis is organized according to current regulations regarding the format of “Thesis as a compendium of publications” established by the Faculty of Biology of the University of Barcelona. For this reason, it presents the following structure:

Index

Figures' index

Tables' index

Abbreviations

7TM	Seven transmembrane
β2AR	β-2 adrenergic receptor
ACC	Acetyl coenzyme a carboxylase
ACTH	Adrenocorticotropic hormone
DNA	Deoxyribonucleic acid
AdipoQ	Adiponectin
ADP	Adenosine diphosphate
AGPATs	Acyl-glycerol phosphate acyltransferases
Akt	Protein kinase B
ALA	Alpha-linolenic acid
AP-2	Adaptor protein-2
AT	Adipose Tissue
ATF(x)	Activating transcription factor (x=2,4)
ATGL	Adipose Triglyceride Lipase
ATP	Adenosine triphosphate
BAT	Brown Adipose Tissue
BMI	Body Mass Index
BMP (x)	Bone morphogenetic protein (x=1-7,8b)
BMMSCs	Bone marrow mesenchymal stem cells
bZIP	Basic Leucine Zipper Domain
BRET	Bioluminescence resonance energy transfer
cDNA	Complementary DNA
cAMP	3'-5'-cyclic adenosine monophosphate
CCK	Cholecystokinin
CD36	Cluster of differentiation 36
CDK	Cyclin dependent kinase
C/EBP (x)	CCAAT(cytosine-cytosine-adenosine-adenosine-thymidine)-enhancer-binding proteins (x=α,β, ɣ)
ChRE	Carbohydrate response element
ChREBP	Carbohydrate response element-binding protein
CNS	Central Nervous System
CPT1	Carnitine palmitoyltransferase I
COX (x)	Cyclooxygenase (x=2,4)
CRE	cAMP Response Element
CREB	cAMP Response Element Binding
CRF	Corticotrophin-releasing factor
CRH	Corticotrophin-releasing hormone
DAG	Diacylglycerol
DHA	Docosahexaenoic acid
DHAP	Dihydroxyacetone phosphate
cGMP	Cyclic guanosine monophosphate
DIO	Diet induced obesity
DIO (x)	Iodothyronine deiodinase (x=2)
DMEM	Dulbecco's Modified Eagle's Medium
DNA	Deoxyribonucleic acid

dNTPs	Deoxynucleotide Triphosphates
DRY motif	Asp-Arg-Tyr (DRY) motif
ECL (x)	Extracellular loop (1-3)
ECN-1	Ectodermal-neural cortex 1
EGF	Epidermal growth factor
Elk-1	Ets-like protein-1
ELOV	Fatty Acid Elongases family
EPA	Eicosapentaenoic Acid
ER	Endoplasmic reticulum
ERK1/2	Extracellular signal-regulated protein kinases 1 and 2 (Also known as MAPK3/MAPK1)
FA	Fatty Acids
FABP(4)	Fatty Acid Binding Protein (4)
FAS	Fatty Acid Synthase
FBS	Fetal Bovine Serum
FDG-PET	Positron Emission Tomography for measuring [$_{18}$F]- fluoro-deoxi-glucose uptake
FFA (s)	Free fatty acid (s)
FFAR(x)	Free fatty acid receptor (x=1-4)
FGF (x)	Fibroblast growth factor (x=1-23)
FGFR (x)	FGF receptors (x=1-4, and isoforms a ,b, c)
FOXA	Forkhead Box A1
FOXC2	Transcription factor Forkhead box protein C2
FOXO	Forkhead Box O1
FRET	Fluorescence resonance energy transfer
GH	Growth Hormone
GIP	Gastric inhibitory polypeptide
Glut(x)	Glucose transporter type (x=1,2,4)
GlyK	Glycerol kinase
GLP-1	Glucagon-like peptide-1
GPCRs or GPRs	G-protein coupled receptors
GPTAs	Glycerol-3-phosphate O-acyltransferase
GR	Glucocorticoid response elements
GRAFS families	Glutamate, Rhodopsin, Adhesion, Frizzled and Secretin families
GRKs	G-protein coupled receptor kinase
GSK3β	Glycogen synthase kinase 3 beta
H8	Intracellular amphipathic helix (GPCRs)
HFD	High fat diet
HDL	High density lipoprotein
HIV	Human immunodeficiency virus
HOXC8	Homeobox C8
HPA	Hypothalamic-pituitary-adrenal axis
HPG	Hypothalamic pituitary-gonadal axis
HSGAG	Heparan sulfate glycosaminoglycan
HSL	Hormone Sensitive Lipase
IBMX	3-isobutyl-1-methylxanthine
ICL (x)	Intracellular loop (x=1-3)

IDF	International Diabetes Federation
Ig (x)	Immunoglobulin-type domains (x= I-III)
IGF-1	Insulin-like growth factor 1
IL (x)	Interleukin (x=1,2,6,8,12)
IP3	inositol 1,4,5-trisphosphate
IR	Insulin Resistance
IRS	Insulin receptor substrate
JNK1	c-Jun N-terminal kinase 1
KDa	Kilodaltons
KLB	β-Klotho
KLFs	Kruppel-like factors
LPL	Lipoprotein lipase
MAPK	Mitogen-activated protein kinase
MCE	Mitotic Clonal Expansion
MCP-1	Monocyte chemoattractant protein 1
MGL	Monoacylglycerol lipase
mRNA	Messenger RNA
miRNA	Micro RNA
mtDNA	Mitochondrial DNA
mTOR	Mammalian target of rapamycin
MS	Metabolic Syndrome
MSCs	Mesenchymal Stem or Stromal Cells
MUFAs	Monounsaturated fatty acids
Myf5+	Myogenic factor 5
NADH	Nicotinamide adenine dinucleotide (reduced)
NAFLD	Non-alcoholic fatty liver disease
NCD-RisC	Non-Communicable Diseases Risk Factor Collaboration
NE or NA	Norepinephrine or Noradrenaline
NEFAs	Non-esterified fatty acids
NFκB	Nuclear factor kappa-light-chain-enhancer of activated B cells
NPY	Neuropeptide Y
NST	Non-shivering thermogenesis
p38 MAPK	p38 mitogen-activated protein kinase
paO_2	Partial pressure of oxygen in blood
Pax-7	Paired-box 7
PBS	Phosphate-Buffered Saline
PEPCK	Phosphoenolpyruvate carboxykinase
PGC-1α or PPARGC1A	Peroxisome proliferator-activated receptor gamma coactivator 1-alpha
PTH	Parathyroid hormone
PI3K	Phosphoinositide 3-kinase
PIP2	Phosphatidylinositol 4,5-bisphosphate
PK(x)	Protein kinase (x=A,B,C)
PLC	Phospholipase C
POA	Preoptic Area
POS	Polycystic Ovary Syndrome
PP2A	Protein phosphatase 2A

PPAR(x=α, β, ɣ)	Peroxisome proliferator-activated receptor (x=alpha, delta, gamma)
PPRE	PPARs response element
PRDM16	PRD1-BF-RIZ1 homologous domain containing protein-16
Pref-1	Pre-adipocyte factor 1
P/S	Penicillin Streptomycin
PTH	Parathyroid hormone
PUFAs	Polyunsaturated fatty acids
PYY	Peptide YY hormone
Rcf	Relative centrifuge force
qPCR	Quantitative polymerase chain reaction (real time)
RBP4	Retinol binding protein 4
RGS	Regulators of G-protein signaling
RNA	Ribonucleic Acid
RXR	Retinoid receptor X
SIRT(x)	Sirtuin (x=1,3)
SFA	Saturated fatty acids
SI	Sequence Identities
SMAD3	Mothers against decapentaplegic homolog 3
Src	Proto-oncogene tyrosine-protein kinase
SRF	Transcription factor: serum response factor
SREBP	Sterol regulatory element-binding protein
STAT5A	Signal transducer and activator of transcription 5A
SVF	Stromal Vascular Fraction
SWI/SNF	SWItch/Sucrose Non-Fermentable nucleosome remodeling complex
T2DM	Type 2 Diabetes Mellitus
T3	Triiodothyronine
T4	Tetraiodothyronine
TAB1	TAK1 binding protein
TAK1	Transforming growth factor beta-activated kinase 1
TBX15	T-box transcription factor 15
TG	Triglycerides
TGFβ	Transforming growth factor beta
TGR5	G protein-coupled bile acid receptor 1
TH	Tyrosine hydroxylase
TM (x)	Transmembrane-spanning α-helices (x=1-7)
TNFα	Tumor necrosis factor alpha
UCP1	Uncoupling protein 1
VLDL	Very low density lipoproteins
WAT	White Adipose Tissue
WHO	World health organization
WNT	Wingless-related integration site transduction pathways
ZFP423	Zinc finger protein 423

INTRODUCTION

Introduction

1. Obesity and metabolic syndrome

More than a hundred years have passed since the first ideas of homeostatic regulation under the control of fat mass were exposed (Neumann 1902; Gulick 1922). Descriptions on the balance between food intake and energy expenditure and their relationship with the increase in obesity prevalence led to new questions regarding the mechanisms by which this so called homeostasis was achieved. It still took nearly 40 years for the first definitions of metabolic syndrome (MS) to emerge (Himsworth, 1939; Vague, 1956; Albrink and Meigs, 1965). Himsworth (1939) first reported insulin resistance (IR) to be the antecedent of Type 2 *Diabetes Mellitus* (T2DM). Several long observational studies and prospective randomized trials were needed before the association between the excess of fat mass, MS, IR and T2DM was finally established (Haffner *et al.*, 1990; Ferrannini *et al*., 1990; Pyörälä *et al.*, 1998).

Nowadays, the concepts of obesity and MS are the center of attention regarding public health issues and policies since it is related to most of the main causes of dead worldwide (i.e. heart failure, T2DM and cancer) (Popkin *et al.*, 2012). Obesity is a complex metabolic state influenced by genetics, environmental features and lifestyle. It is defined as an abnormal or excessive fat accumulation that may impair health. The main index for determining or classifying a patient with obesity is the body mass index (BMI). BMI is an index of weight-for-height and is obtained from dividing the person's weight in kilograms by the square of his/her height in meters (kg/m^2). Based on this value, a person can be classified as obese when the BMI range is above 30 (BMI≥30) for average height populations or above 25 (BMI≥25) for short-heightened populations (García and Méndez, 2011; Zapata *et al*., 2016; Ortiz-Dominguez, 2008). The central characteristic of MS is obesity. As a consequence of this excessive fat, individuals may develop IR and several cardiopathies such as atherosclerosis or hypertension (Morales-Villegas *et al.*, 2006; Garcia-Garcia, 2008; Anagnostis *et al.*, 2013; Recio *et al*., 2018).

Unfortunately, in the past 30 years the prevalence of this disease has increased alarmingly. It is estimated by the World Health Organization (WHO, 2018) that almost 2 billion adults and nearly 340 million children present an excess of fat mass accumulation in the body. Obesity trends for children and adults are shown in figure 1. This second group of the population is the most preoccupying since a compromised growth and several other complications are related to excessive fat mass (i.e. polycystic ovary syndrome (POS) and infertility) (Sam, 2007; de Onis *et al.,* 2010). Obesity and MS endanger life and compromise life quality by affecting growth, professional development and even family environmental health (Olaiz-Fernández *et al.*, 2006). It is estimated that 75% of adult mortality is related to obesity in those countries with higher index of prevalence (i.e. USA). This situation is disturbing since the prevalence of the disease has been increasing without intermission in the majority of the industrialized populations worldwide. This trend affects in great measure the health status of the population, especially of those people in an economically active age (situation that affects in a great extent global macroeconomy) (García-García *et al.*, 2008). For this reason, the international scientific community has oriented efforts to seek for new strategies for its treatment and the prevention of its comorbidities (WHO, 2018).

Altogether, this information gives us a hint for focusing research and resources on the study of potential therapeutic targets for the treatment of obesity. For this reason, the main responsible tissue for energy storage, the adipose tissue (AT), has been at the spotlight. To this day the concept of AT has evolved from a simple storage organ to a multitasked regulatory organ and it is important to study and understand the processes by which AT modulates hormonal and metabolic status in physiological and pathological conditions. (Fantuzzi and Mazzone, 2007).

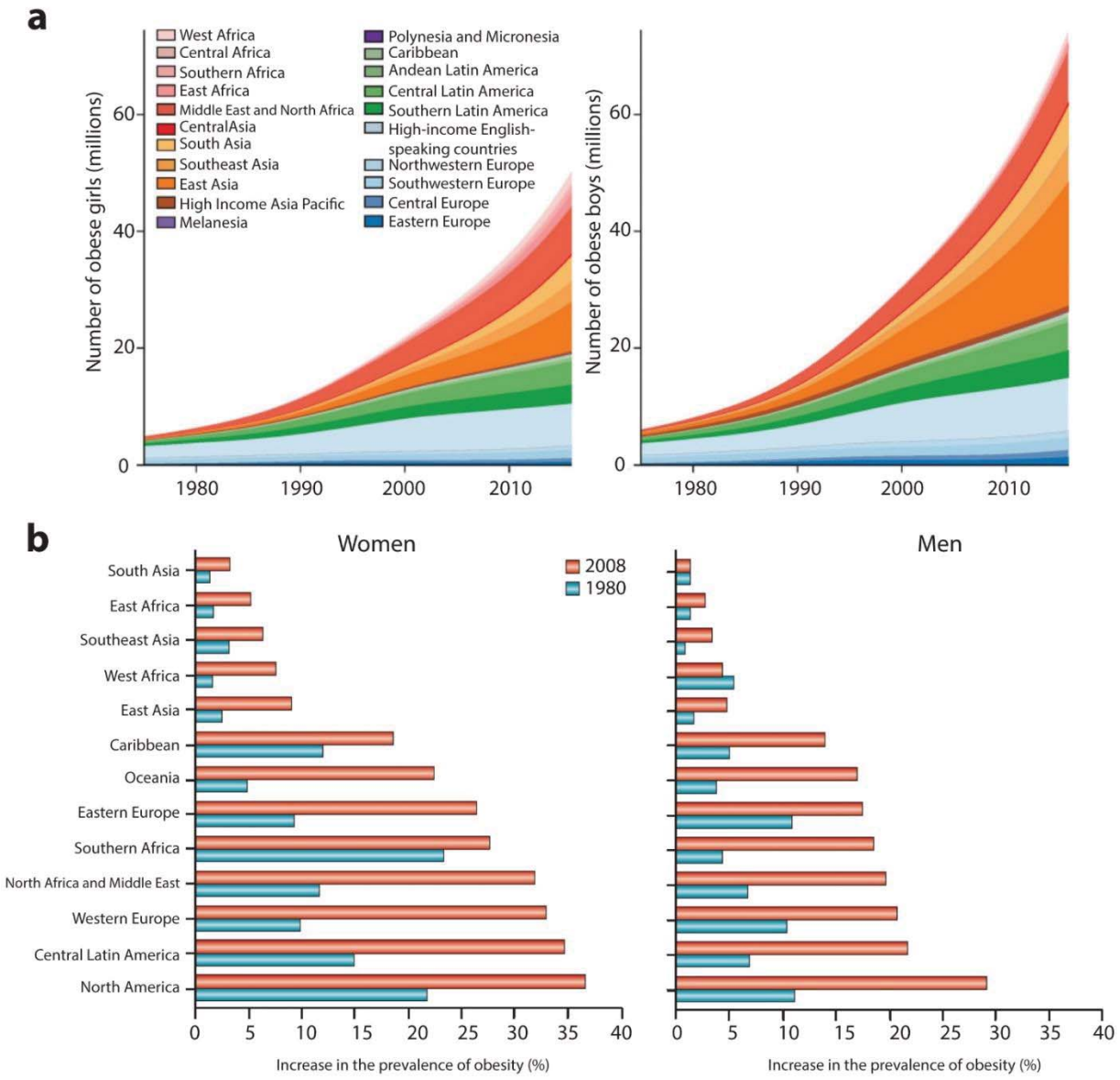

Figure 1. Global trends of obesity in worldwide population. The upper panel shows the obesity trends in children, girls and boys, from 1975 to 2016 (Graph obtained and modified from NCD Risk Factor Collaboration (NCD-RisC). 2017) **(a)**. The lower panel shows adulthood trends in obesity for women and men (Graph obtained and modified from Malik *et al.*, 2013.) **(b)**.

2. The Adipose Tissue

We know from not so long ago that the AT plays a major role in energy homeostasis. Recently, it was revealed that the adipose depots are more than just an inert reservoir of energy. The correlations of the increased size adipose depots with the appearance of different metabolic pathologies gave rise to a concept of the AT as an active and regulatory organ (Ailhaud, 2001; Rosen and Spiegelman, 2014).

Consecutive to this idea, AT is considered as a highly specialized tissue. It stores the excessive energy consumed to cover periods of energy scarcity but it is also important for the regulation and response to physiological processes (i.e. nutritional status, development, appetite control, insulin sensitivity, temperature maintenance and even reproduction). Abnormalities in AT regulation can lead either to an excess accumulation of fat, to a redistribution of the adipose depots (lipodystrophy), or to an induced catabolism like in cachexia. (Ailhaud, 2001; Cinti, 2005; Fantuzzi and Mazzone, 2007). Fat can be placed at different anatomical sites in the body of an organism and each depot may develop different specialized functions. The fat mass percentage of an individual can fluctuate from 20% to 70% and this difference in the amount of fat stored in the body can be the root in the development of different metabolic pathologies (Cinti, 2005; Fantuzzi and Mazzone, 2007; Rosen and Spiegelman, 2014).

AT is a very heterogeneous tissue not only composed of adipocytes, the anatomical subunits of the adipose tissue. It also comprises the stromal vascular fraction (SVF) which is important for AT biology. SVF includes nerve ends, mesenchymal stem cells (MSCs), T regulatory cells, endothelial precursor cells, macrophages and pre-adipocytes in distinct differentiation status (figure 2). All of these cell types may play critical roles in the development of pathologies linked to AT abnormalities (i.e. obesity) (Cinti, 2005). The last members mentioned, the pre-adipocytes, are the ones that bring plasticity to the tissue due to their proliferation and differentiation capacity (Dani and Billon, 2012). AT is a highly dynamic and finely regulated cell population. It is estimated that nearly 50% of the human adipocytes are replaced every 8 years. On the other hand, tissue size

showed to be related to adipocyte size and differentiated cell number as will be described later on this section (Spalding *et al.*, 2008).

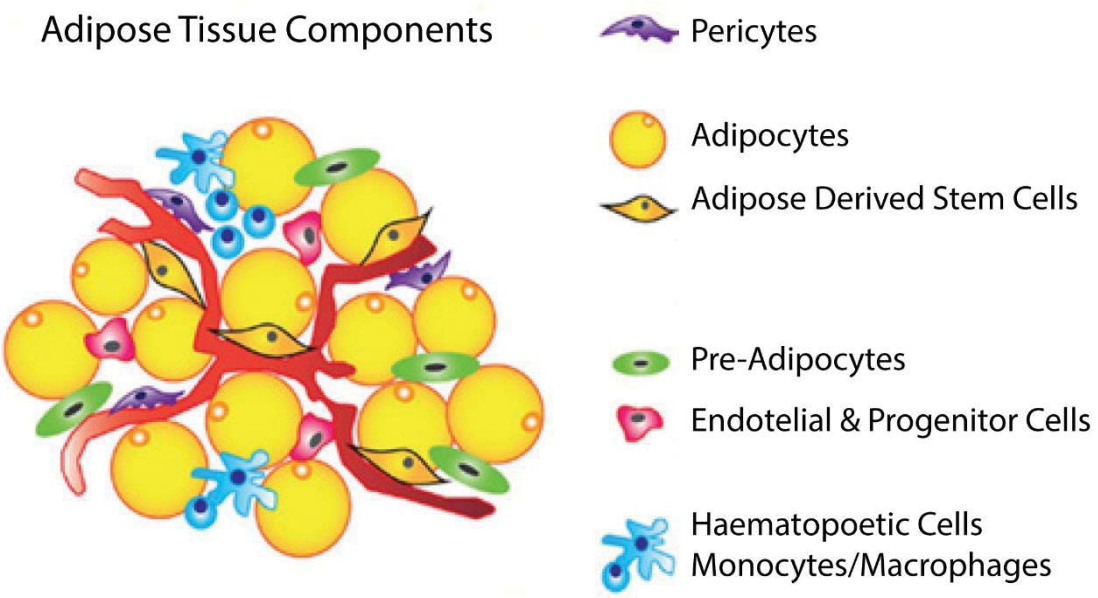

Figure 2. Adipose tissue constitution. This image shows a small representation of the AT cell populations (Image obtained and modified from Shukla *et al.*, 2015).

2.1. Adipose Tissue Distribution and Classification

Considering its visual characteristics, AT is divided in two major types: the white adipose tissue (WAT) and the brown adipose tissue (BAT). These two groups not only differ in their chromatic appearance, they appear to have opposite functions. (Nicholls and Locke, 1984; Dani and Billion, 2012; Rosen and Spiegelman, 2014; Moreno-Navarrete and Fernández-Real, 2012: Saely *et al*., 2012). Both types share the ability to store triglycerides in the form of lipid droplets, however for different purposes. WAT is the main energy storage tissue. Besides its repository role, it has proven to be related to a great amount of endocrine functions for the control of intermediate metabolism. BAT has also shown to accumulate lipid droplets nonetheless to generate heat by dissipating energy in a process now denominated non-shivering thermogenesis (NST). BAT function and thermogenesis have also been linked to the maintenance of homeostasis in the organism (Dani and Billion, 2012; Saely *et al*., 2012; Rosen and Spiegelman, 2014).

Some researchers rather prefer to classify WAT in a different manner. Anatomically, the WAT is localized in several depots along the body of the individual, either mice or human. These different depots can vary in function and in content during life but most of the time localization and appearance are consistent. Therefore, another classification of WAT can be made by localization. This classification divides WAT in two groups: subcutaneous and visceral. The first one refers to those depots found underneath the skin while the second one refers to the depots found in between the inner tissues. Both types of tissues share the main adipogenic characteristics, especially regarding the expression profiles. However, they differ a lot in their activity and for this reason sometimes they are considered as different tissues (Gesta *et al*., 2006; Tchkonia *et al.*, 2006).

2.2. Mice and human adipose depots distribution

Mice

It is important to mention that the most common model to study the adipose tissue is the rodent model (*Mus musculus* and *Ratus norvericus*, being the first one our lab's animal model). They are used to investigate distribution (with special considerations) and also function. Mice (*Mus musculus*) and humans' (*Homo sapiens*) ATs share a great spectrum of characteristics but still some differences can be found. Mice subcutaneous AT is very well defined by the localization. Three segments have been described; the anterior, dorsal and posterior subcutaneous WAT (a summarized distribution is presented in table 1 and depicted in figure 3). (Virtanen *et al*., 2009; Chusyd *et al*., 2016). The three segments described and the fact that epididymal WAT is not present in humans are the main differences between mice and humans.

Table 1. Brown and White adipose tissue distribution in mice	
BAT	**WAT**
Interscapular Cervical Subscapular (axillar) Mediastinal Perirenal	*Subcutaneous* Posterior: dorsolumbar, inguinal, gluteus. Dorsal: above interscapular BAT Anterior: In between the skin and the muscle from the frontal extremities.
	Visceral Cardiac: surrounding heart Mesenteric: around intestines Omental: above stomach Retroperitoneal: dorsal area Perigonadal: epididymal and periovaric

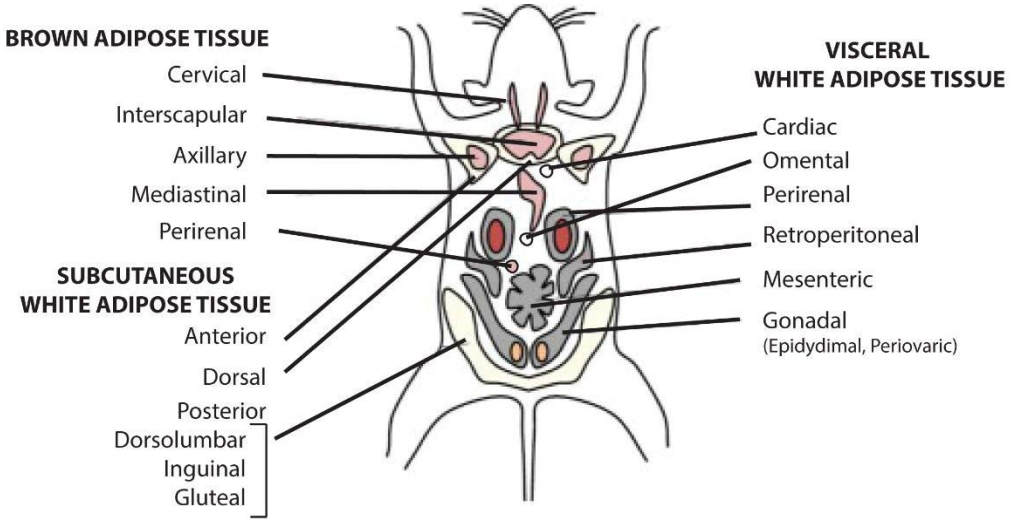

Figure 3. Distribution of the adipose depots in mice (image taken and updated from Choe *et al.*, 2016).

Humans

In the case of humans the division is somewhat different. A distribution of subcutaneous WAT is difficult to determine since almost all the area under the skin can present a minimal quantity of AT. This is due to the fact that it also serves as an insulating barrier to keep body temperature. In the case of visceral AT, the distribution and anatomical classification shares some similarity with rodents. However, epididymal AT in male rodents, the main visceral adipose tissue analyzed in this model, is not found in human males. In contrast, omental AT is the main visceral depot in humans but barely found in rodents.

Nonetheless, in the case of BAT, it was well recognized in human newborns due to its activity regulating temperature at the beginning of life. Unfortunately, this depot was believed to be inexistent in adults. This knowledge was changed last century when physicians started to use Positron Emission Tomography for measuring [$_{18}$F]- fluoro-deoxi-glucose uptake (FDG-PET) in the detection and study of tumors. This technique identified, due to marked glucose, those regions that could be more metabolically active. At the beginning, clinicians found a marked area close to the chest that appeared to have an increased metabolic rate and they believed it to be WAT. It was until 2009 that profound results in the study of this tissue confirmed the expression of markers related to thermogenesis. In addition to this, it was detected that there were different types of adipocytes coexisting in BAT discovered in adult humans (brown and beige adipocytes, which will be described later). Finally, the idea of functionally active BAT in human adults and that this BAT activity inversely correlated with body mass index (BMI) and age, suggested that there was a downregulation of BAT associated to both circumstances. (Nedergaard *et al*., 2007; Cypess *et al*., 2009; Saito *et al.*, 2009; Zingarretti *et al.*, 2009). Table 2 briefly describes the distribution of human AT and this distribution is depicted in figure 4.

Table 2. Brown and white adipose tissue distribution in humans

BAT	**WAT**
Classical • Newborn: Interscapular • Adult: cervical	Subcutaneous • Abdominal • Craniofacial • Gluteus-femoral
Inducible • Supraclavicular • Paravertebral • Peritirodeal • Mediastinal • Perirenal • Intermediate-cervical	Visceral • Mesenteric • Pericardial • Omental • Retroperitoneal • Pararenal • Perigonadal

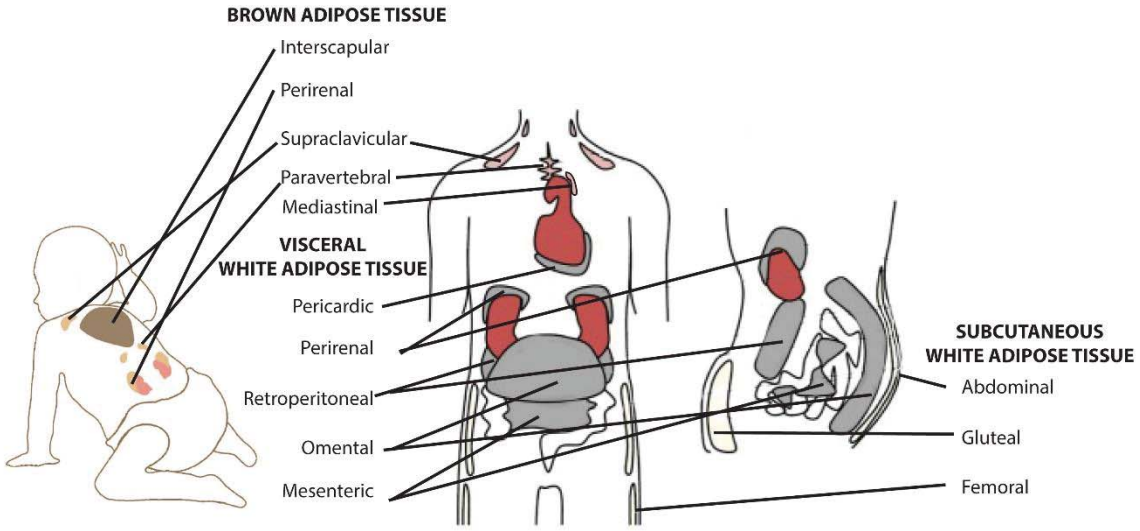

Figure 4. Distribution of the adipose depots in humans (image taken and updated from Chusyd *et al*., 2016 and Choe *et al.*, 2016).

Many of the characteristics, functions and metabolic roles of the depots depend on whether they fall into BAT, WAT or an intermediate type of AT (*Beige Adipose Tissue*, which will be described latter in this section). Still, the primary role of AT is to regulate the nutritional status of the organism and to coordinate responses to achieve homeostasis. Besides this main job, the different depots of AT complement each other in other roles. For example, WAT serves as an organ to isolate the inner tissues of the body in order to help maintain temperature. At the same time, BAT is in charge of the production of heat to contribute to the temperature maintenance (Zwick *et al.*, 2018). As for the roles that are typical of each type of tissue, meaning their main characteristics and potential differences, they are going to be described in the next few pages.

2.3. White Adipose Tissue

Due to evolutionary purposes, organisms have developed the capacity to sustain life and homeostasis in every life-limiting situation. These situations may include food scarcity. WAT is the tissue mainly described to store energy (Dani and Billion, 2012). It is characteristic of this tissue, in comparison with BAT, to house the white adipocytes

(described in a subsequent section). These adipocytes are the store units of WAT able to synthesize triglycerides (TG) from free fatty acids (FFA). The synthesized TG are accumulated as lipid droplets. In periods of fasting or cold exposure, these lipid droplets are broken down by lipolytic enzymes and produce FFAs and glycerol, metabolites that will contribute to maintain the organism functions (Rosen and Spiegelman, 2014). The final decision of an organism to store or to use the available energy will be determined by the energy balance. This energy balance is resolved by the difference between the ingested energy (from the diet) and the energy consumed by the organism. It is estimated that a healthy individual can store an approximate of 0.4 to 0.6 µg of TG in each adipocyte but a hypertrophic adipocyte can house nearly 1.2 µg. Under any of these circumstances the lipid droplet occupies around 90% of the cytosolic volume in these cells. When the maximum amount of lipids has been stored in each cell, the cell itself helps the proximate fibroblasts to induce proliferation and differentiation in order to store the extra energy reaching the tissue. As a consequence adipocytes will increase in number in a process denominated hyperplasia. (Dani and Billion, 2012; Tamucci *et al*., 2018). The maximal expression of adipose tissue expansion would be obesity, pathological condition in which hypertrophy shows the most dangerous secondary effects (Taube *et al.*, 2012). When it is demanded by the nutritional status, WAT needs to liberate the stored substrates in order to sustain the main functions of the organism. Then, WAT derived substrates can reach high metabolically active tissues such as kidney, liver, heart and muscle under stress conditions, cold exposure or fasting (Saely *et al.*, 2012; Tamucci *et al.*, 2018). In addition to both, the harvest and the breakdown of energy, WAT has important hormonal activity and for so, when the activity or the status of this tissue is altered, metabolic abnormalities can occur (Bays, 2011).

The current lifestyles have led the population to break the equilibrium between energy ingested and energy consumed. This imbalance is a consequence of a high availability of rich-energy foods and a decreased need to move. Also, modern cities' urban planning prevent their citizens to be exposed to harsh weather and temperature circumstances. This leads to a poor activation of thermogenesis and, as consequence, a decreased energy expenditure contributing to the development of obesity since early stages of life (Berthoud, 2012; Mustajoki, 2015).

Due to the previously described role of WAT, this tissue is equipped with a specialized machinery to control assembly (triglyceride synthesis) and the degradation (lipolysis) of TG.

2.4. Triglyceride synthesis

Triglyceride synthesis results from the set of processes that leads to the synthesis of fatty acids (FA) and their esterification into triglycerides (TG). Many cell types are able to process and form TG; however hepatocytes and adipocytes will play the major role in the control of this procedure (Kersten, 2001). For a great period of time, it was considered that the TG incorporated in AT were only coming from lipoproteins sent from other organs (i.e. intestine). It is now well assumed that the adipocyte is also equipped with the pertinent enzymes for TG synthesis (Gesta and Kahn, 2012).

Upon feeding, lipids from the diet will enter circulation packed as chylomicrons to be transported all along the body. Feeding also causes an increase in blood glucose, when this metabolite reaches the liver, it will start *de novo lipogenesis* to be converted into TG. These newly synthesized TG will be packaged into very low density lipoproteins (VLDL) to be transported to other tissues. Both packages of TG (chylomicrons and VLDL) can reach adipocytes where they can be harvested with other lipids synthesized by this cell type or they can be transported to other tissues (Strable and Ntambi, 2010). Before entering the target cells, endothelial cells will trigger a reaction by the enzyme lipoprotein lipase (LPL) which will convert this TG in non-esterified fatty acids (NEFAs). When entering the cell as NEFAs they will be broken down to acetyl-CoA units and used as a metabolic substrate or re-esterified to form TG.

As for *de novo lipogenesis* in the adipocyte, this process starts with the entrance of glucose through the specialized glucose transporter 4 (Glut4). Cytosolic glucose will be metabolized to pyruvate to later be converted to acetyl-CoA (by the *pyruvate*

descarboxylase) in mitochondria. This synthesized acetyl-CoA will enter the Krebs cycle (also known as the Citric Acid Cycle) where one of the intermediates, citrate, will leave the mitochondria. Once outside the mitochondria, this cytosolic citrate will be metabolized into acetyl-CoA by the activity of *citrate lyase* to subsequently become malonyl-CoA (due to *acetyl-coA carboxylase* activity). With this substrate, the enzyme fatty acid synthase (FAS) will drive the elongation of the FA by reducing NADPH and adding two carbon atoms in the form of acetyl-CoA every cycle until palmitic acid is synthesized. Once formed, palmitic acid will be the precursor FA for other FAs as a product of elongation or unsaturation by the family of enzymes ELOV (fatty acid elongases) (Jump, 2009).The resulting fatty acids can be targeted and incorporated to the membrane or gathered in the lipid droplet for energy harvest. In order to be packed in the adipocyte's lipid droplet, FAs must be assembled in a greater molecule, TG. Krebs cycle intermediates are substrates for the enzyme *phosphoenolpyruvate carboxykinase* (PEPCK). PEPCK activity will produce a glycerol-3-phosphate molecule. This glycerol-3-phosphate will undergo acylation of two free hydroxyl groups with two molecules of fatty acyl-CoA; these molecules will produce a fosfatidic acid by the GPTAs (*Glycerolphosphate acyltransferases*) and AGPATs (*acyl-glycerolphosphate acyltransferases*). Together (as a diacylglycerol), they will become a TG by the inclusion of a third fatty acyl-CoA (Gesta and Kahn, 2012; Strable and Ntambi, 2010). The whole process is to be carried at the lumen of the endoplasmic reticulum (ER). The fact that the formed TGs tend to agglomerate helps the lipid droplet to start its formation at the ER. The formation of these droplets will include the assembly of other lipid species such as cholesterol and other proteins which will be important for the control of lipid mobilization (i.e.caveolin-1, perilipins) (Brasaemle, 2009). The resulting structure is what is commonly known as lipid droplet. Figure 5a shows a summarized diagram of this process.

The action of these enzymes will be regulated by circulating hormones (i.e. Insulin and growth hormone), different intermediate molecules and changes in the energetic ratios (ATP/ADP) (Kersten, 2001; Strable and Ntambi, 2010). After feeding, an increase in the circulating levels of glucose will induce an increase in circulating insulin. Insulin will cause the translocation of Glut4 to the membrane, this will lead to an

increase in glucose uptake. The cytosolic glucose will trigger the start of FA synthesis in the adipocyte. On the other hand, glucagon has the inverse effect provoking not the synthesis of TGs but their degradation as we will describe in the next section (Kersten, 2001).

2.5. Lipolysis

Contrary to the metabolic situations that lead to lipogenesis, during circumstances where there is a need of substrates for oxidation the adipocyte receives signals either from the peripheral tissues or through sympathetic innervation in order to start a process for the breakdown of lipids. The classic signal that triggers this TGs breakdown is norepinephrine or noradrenaline (NE), a hormone that will act through the adrenergic receptors (α and β) and will lead to TGs breakdown (Frühbeck *et al*., 2014). Another example is a drop in the ratio insulin/glucagon. Glucagon is a hormone that modulates the metabolic profile in fasting conditions and targets a GPCR. Upon activation, the $G_{\alpha s}$-protein coupled to this receptor will induce PKA phosphorylation (Sztalryd *et al*., 2003). Once phosphorylated, PKA will trigger the breakdown of lipids since it will lead to a phosphorylation of the enzyme HSL. HSL binds perilipin, a protein that normally would play a role inhibiting the enzyme's entrance to the lipid droplet. However, upon phosphorylation perilipin helps enzyme to enter to the lipid droplet. As a result, ATGL (Adipose triglyceride lipase), HSL (hormone sensitive lipase) and MGL (monoacylglycerol lipase) enter the lipid droplet and starts TGs breakdown (Gesta and Kahn, 2012; Sztalryd *et al.*, 2003). Nevertheless, the direct activation by glucagon is not critical. Insulin is a powerful inhibitor of lipolysis so a decrease in insulin signaling will also lead to lipid breakdown (Chakrabarti *et al*., 2013).

ATGL activity provokes the separation of a FA from the TG and in turn produces diacylglycerol. This byproduct will be substrate of the second enzyme, HSL, and will produce monoacylglycerol while liberating another FA. For its part, MGL will target this lipid and separate the missing FA and glycerol. The resulting FAs are oxidized inside the cell on, with the help of the fatty acid binding protein 4 (FABP4), the resulting FFAs will be mobilized outside the cell and reach other tissues. In the case of glycerol it can either

be recycled or moved outside the cell, through Aquaporin 7 (Aqp7), to subsequently reach the liver where it will undergo gluconeogenesis (Jaworski *et al.*, 2007, Gesta and Kahn, 2012; Sztalryd *et al.*, 2003). Figure 5b shows a summarized diagram of this process. In the case of brown and beige adipocytes, under a high energy demanding situation, lipids coming from circulating lipoproteins can also be used as energy substrates. LPL will help, in these cases, the uptake of FA from these structures in order to make them available for β-oxidation. (Goldberg *et al.*, 2009)

Once the NEFAs reach the cells to be metabolized, the protein transporter CD36 (cluster of differentiation 36) will facilitate their entrance to the cell and with the help of CPT1 (Carnitine palmitoyltransferase I), the FA will be incorporated to the mitochondria to follow β-oxidation/oxidative phosphorylation (Frühbeck *et al.*, 2014).

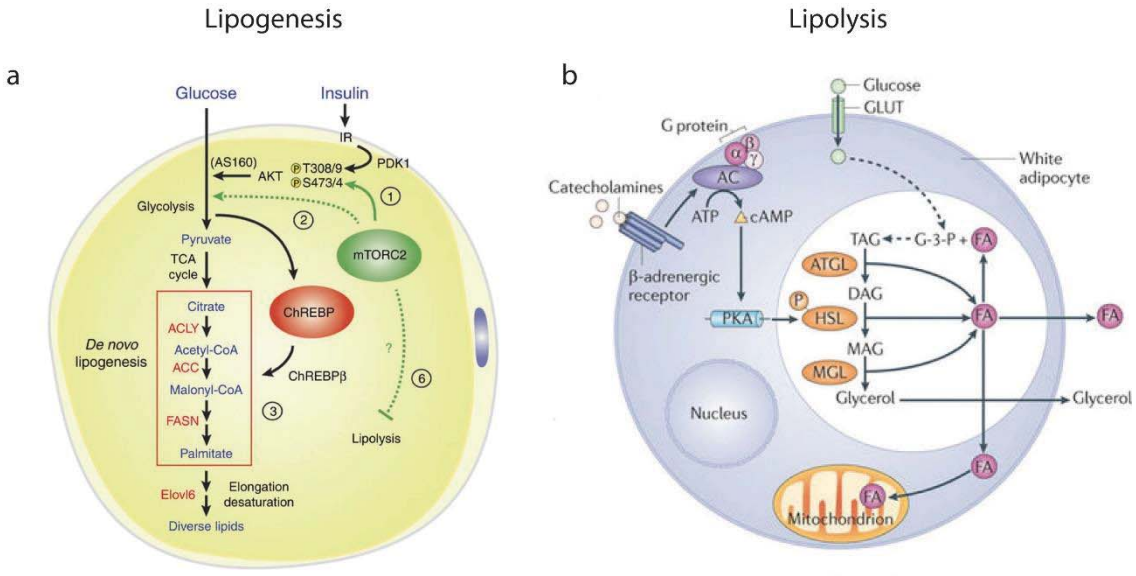

Figure 5. Lipid metabolism in adipocytes. **(a)** Summarized diagram of *de novo lipogenesis* (Image taken and modified from Tang *et al.*, 2016). **(b)** Metabolic pathway of lipolysis (Image taken and modified from Altarejos and Montminy, 2011).

2.6. Adipokines, WAT as a secretory organ

As mentioned earlier, AT functions are not limited to energy storage. AT is also an endocrine organ which is important for a great number of physiological processes. It secretes and modulates the response to several hormones and cytokines. The molecules that are released from adipocytes with a potential impact on physiology are denominated adipokines. The following table numbers some of the most relevant adipokines and their functions.

Table 3. Examples of WAT adipokines

Adipokine	Described effects
Leptin	Informs the CNS about the nutritional status of the AT Satiety signal Reduces circulating glucose (improves insulin sensitivity) Inhibits lipogenesis Stimulates lipolysis
Adiponectin	Increases insulin sensitivity in peripheral tissues FA oxidation in muscle (AMPK dependent) Inhibits gluconeogenesis in liver Inhibits lipolysis in adipocytes Inhibits monocyte adhesion Anti-inflammatory effects over endothelial cells
Resistin	Effects have been suggested over glucose metabolism and insulin sensitivity In the presence of obesity, has been linked to insulin resistance in muscle and liver
PAI-1	Inhibits the activity of the protein tissue type plasminogen activator Anticlotting factor
IL-6	Impairs appetite Mediates inflammation Inhibits gluconeogenesis Inhibits *de novo lipogenesis* Contributes to thermogenic activation
TNFα	FFA release from adipocytes Mediates inflammation Reduces adiponectin release and expression Impairs insulin sensitivity Linked to the development of fibrosis in AT
**Other molecules secreted by adipocytes can modulate processes like thermogenesis and will be described in another section. Friedman and Halaas, 1998; Ronti *et al*., 2006; Antuna-Puente *et al*., 2008; Yiannikouris *et al*., 2010.	

These are just some examples of the main adipokines expressed and secreted from adipocytes (and AT). Also, as a result of lipolysis, NEFAs can act as signaling molecules that mediate communication between several tissues and the AT through GPCRs (G-protein coupled receptors) (Yore *et al*., 2014). Some authors have linked distinct species of circulating NEFAs in obese patients to the development of the metabolic comorbidities (Harwood, 2012).

Regarding the pathophysiology of obesity, AT function seems impaired in hypertrophic and hyperplasic situations. Some researchers consider hypertrophy as a situation most often identified in obese and overweighed people. Hyperplasia has been more related to the severity and progression of the metabolic complications product of obesity (Hirsch and Batchelor, 1976). However, the presence of hypertrophic adipocytes is always considered a limiting condition for insulin resistance and the risk of developing T2DM (Moreno-Navarrete and Fernández-Real, 2012). Even so, both conditions lead to intracellular and extracellular abnormalities. These abnormalities conduct to a dysregulation in metabolic performance of the adipocyte itself and to a dysregulation in the expression, modulation and circulating levels of adipokines (Torres, 2009).

2.7. Brown adipose tissue (BAT)

Also known as brown fat, due to its color, BAT function opposes that of WAT in the sense that it stores energy for its own use. This tissue has a major role on temperature maintenance. Such duty will represent a higher input and consumption of energy compared to WAT but not as unfeasible as muscle contraction. BAT was first described as a 'hibernating gland' due to its capacity to produce heat and contributing to the survival during cold winter of marmots (species where it was initially described), small well-known hibernating animals (Rasmussen, 1923; Ballinger and Andrews, 2018). BAT subunits are the brown adipocytes (described profoundly later in this dissertation), these cells show increased and smaller lipid droplets inside each cell. The process by which these adipocytes help maintain body temperature is known as non-shivering thermogenesis (NST) or adaptive thermogenesis (Cannon and Nedergaard, 2004).

Brown adipocytes show high number of mitochondria inside the cell. This characteristic gives rise to the increased energy expenditure and the color of the tissue. These mitochondria are rich in uncoupling protein 1 (UCP1) which is a protein with the special ability to uncouple the respiratory chain and provoke a proton leak in the membranes from these organelles. As a consequence they produce heat. This is the reason why UCP1 is the main BAT marker known. (Cannon and Nedergaard, 2004; Morrison *et al*., 2014a). Also important to this tissue and its physiology is the great abundance of sympathetic nervous system innervation which helps activate the tissue in a fast and appropriate manner during thermal stress. Upon BAT activation, the blood that has been warmed up in the vessels that surround BAT is put in motion. An extensive irrigative network special in this tissue contributes to this process. Furthermore, this high irrigation favors a continuous flux and abundance not only of energy substrates (i.e. glucose and triglycerides) but also of oxygen (Cannon and Nedergaard, 2004; Giralt and Villarroya; 2013).

2.8. Beige –or brite– adipose tissue

Approximately a decade ago, a third type of fat tissue was described. Apparently, and promising to the actual obesity pandemic, WAT is able to recruit brown-like adipocytes upon a strong thermal stress. This process is denominated as *browning*. These cells are then referred as beige (*or brite*) adipocytes due to the color they acquire product of the increased number of mitochondria (not completely white, however not brown) (Meigal, 2002; Rosenwald and Wolfrum, 2014). Although these cells have differences compared to brown adipocytes, the process by which these adipocytes trigger thermogenesis are very alike and will be described ahead (Cannon and Nedergaard, 2004; Morrison *et al*., 2012; Morrison *et al*., 2014; Cereijo *et al*., 2015; Ishibashi and Seale, 2010; Wu *et al*., 2012).

2.9. Thermogenesis

2.9.1. Acute and chronic response to cold

Cold winter has been a common stressor for animals. This cold stress represented an increase in the energy transference from the living organism to the environment. In order to be able to compensate the temperature drop, animals developed a mechanism to be able to maintain body temperature. Most of them increase their WAT depots and their BAT capacity in autumn season so that during winter. WAT harvest could serve as fuel for BAT and achieve survival (Ballinger and Andrews, 2018). When the temperature drops, animals increase their heat production in a process denominated as adaptive thermogenesis. On the contrary when the environmental temperature increases, evaporation helps the release of all that extra heat. When none of these processes are being held, it is believed that the animal is under a thermoneutral temperature. This means that the organism does not need any extra mechanism in order to maintain body temperature (also known as basal metabolism) (Golozoubova *et al*., 2004; Cannon and Nedeergard, 2004; Ballinger and Andrews, 2018).

Thermogenesis is the process by which most of the animals can achieve temperature maintenance during long periods of cold exposure. Nevertheless, it should be mentioned that this is not the only process by which an organism can cope with a cold environment. Any sensed temperature below the 26°C by the skin drives the activation of TRPM8 (transient receptor potential action channel subfamily M member 8) in the skin's sensory neurons. These neurons will mediate the sensation of cold to the central nervous system (CNS). The signal will target the primary somatosensory cortex and the preoptic area (POA) of the hypothalamus. Is precisely in the hypothalamus where the thermosensory signals will be integrated and a response will be propitiated. Hypothalamus will facilitate the secretion of norepinephrine (NE), catecholamine that will mediate through several pathways the global responses to maintain body temperature. These responses include: vasoconstriction, aimed to limit the amount of heat lost in dissipation through skin; shivering thermogenesis, increasing the input of

energy in muscles for the production of heat; non-shivering thermogenesis (NST), activating a less unsustainable mechanism in BAT for temperature maintenance; and an appropriate increase in blood-flow to BAT in order to assure oxygen and substrates availability for NST (Haman, 2006; Betz and Enerbäck, 2017).

The first strategy, and commonly described to be the one driven under short periods of cold exposure, is based on vasoconstriction and muscle shivering. The former one implies an excessive input of energy to maintain body temperature during longer periods of time. It is considered to be unfeasible due to the high demand of ATP required to produce enough heat for temperature maintenance. For this reason, a more sustainable process for keeping body temperature should take place. So, regulated by CNS and its catecholamine production, NST takes the lead in temperature maintenance (Cannon and Nedeergard, 2004; Whittle *et al*., 2011).

2.9.2. CNS pulls the trigger: Noradrenergic activation of thermogenesis

It is the 'high energy (as heat)' demand what activates BAT through different neurotransmitters. BAT activation includes a remodeling of the tissue and total re-adjustment of BAT cell machinery. Both will be achieved by the interface of both types of neurons with the tissue. To start, a recruitment of nerve terminals from the NPY+ neurons and blood vessels will reach and embrace the tissue. This high innervation and vascularization will increase the infiltration of substrates and oxygen at the same time that it will favor the modification of the cell profile in the tissue (i.e. an increase in brown adipocyte differentiation from mesenchymal stem cells and pre-adipocytes (*hyperplasia*) and an increase in macrophage infiltration) (Haman, 2006; Morrison *et al*., 2014; Tamucci *et al*. 2018). At the same time that all these modifications occur, other nerve terminals (from NPY+ and NPY- neurons) reach the differentiated adipocytes. As described above, upon cold stimulus, the hypothalamus response induces an increase in catecholamine's secretion. On these BAT targeting neurons the production of the preferred catecholamine to induce thermogenesis upon cold will be synthesized, norepinephrine. NE will then be secreted and activate three potential receptors in brown adipocytes: adrenergic receptor β1, β2, and β3. β3-adrenergic receptor will play

the major role in the signal transduction for the activation of thermogenesis in these adipocytes. This receptor is a GPCR (described later in this dissertation) coupled to Gs. Gs is a G-protein that has the ability to activate *adenylyl cyclase* which induces the formation of cAMP from ATP. The obtained cAMP will cause an activation of protein-kinase A (PKA) (Cannon and Nedergaard, 2004). PKA has a key-role in thermogenesis (both in BAT and WAT) since it modulates lipolysis producing NEFAs for oxidation while inducing the expression of the thermogenic machinery genes (i.e. *UCP1, PGC-1α, BMP8b*). This induction is achieved due to its potential action over cAMP response element-binding (CREB) and activating transcription factor 2 (ATF2). Then both are able to bind the pertinent response elements (i.e. CRE) in the promoter regions of some of these genes. Other effects of PKA activation include, the activation of ERK1/2 and p38 MAPK, both important for the activation and maintenance of the thermogenic activity. In the case of ERK1/2, it will inhibit apoptosis, contributing to the maintenance of the cell number in this highly demanded tissue. On the other hand, p38 MAPK seems to mediate thermogenic activation through the phosphorylation of PGC-1α which is a master regulator of mitochondrial biogenesis and the activity of UCP1 (Thonberg *et al*., 2002; Cao *et al*., 2004; Cannon and Nedergaard, 2004). While this transcription is enhanced, the translation of the mRNAs produced will be prompted, and the process by which mitochondria (and other relevant proteins) are to be degraded will be stopped (autophagy). An increased flow of substrates will take place and, if the cold exposure is sustained, a massive degradation of the intracellular reserves could occur (lipophagy) (Haman, 2006; Morrison *et al*., 2014; Cairo *et al*., 2016; Tamucci *et al*., 2018). Activation of lipolysis will also produces an increase in FA in the cell. These endogenous FAs are able to bind PPARs (Peroxisome proliferator-activated receptors). PPARs are key regulators of lipid metabolism that are activated by lipids to promote gene transcription. One of this receptors is PPARα which, upon activated by FFAs, is able to target the binding sites in the promoter regions of thermogenic marker genes (i.e. *PGC-1α* and *UCP1*) (Mottillo *et al*., 2012). A diagram of catecholamine-mediated activation of thermogenesis can be observed in figure 6.

It is important to mention that the response to be achieved by the tissue is to be determined by previous experiences of cold exposure. This means that an organism that

has never been or has been lightly exposed to cold will present a decreased number in mitochondria and a decreased expression of the protein UCP1. This situation in BAT is known as *whitening* and, as it implies, is the completely opposite effect of *browning*. Whitening is achieved in brown adipocytes that decrease the number of lipid droplets and mitochondria (and UCP1 expression) while increasing their size. These will lead to a reduced thermogenic capacity of the tissue (Feldmann *et al*., 2009).

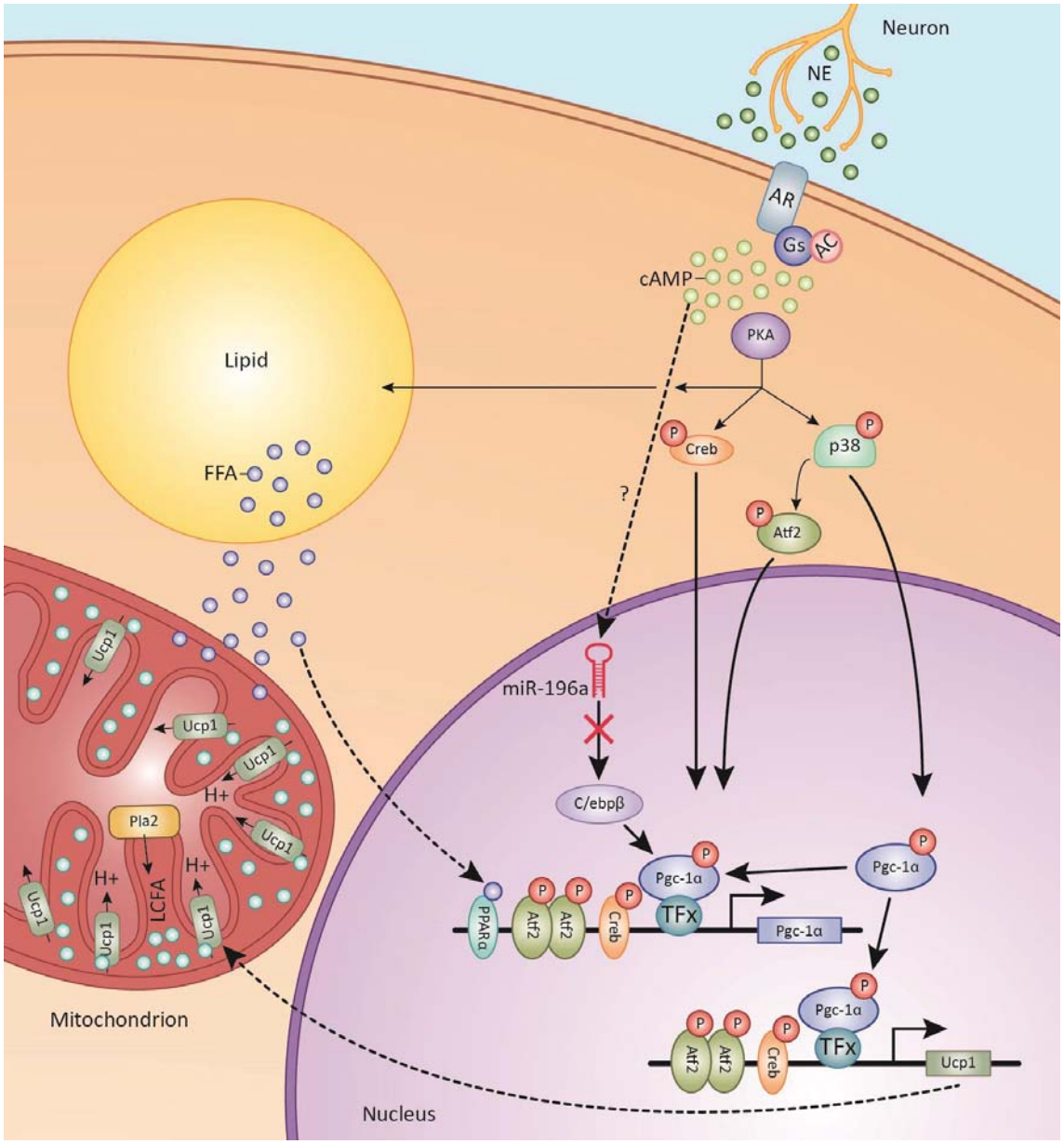

Figure 6. Diagram on the signaling cascade of noradrenergic activation of the adipocyte. (Image obtained from Harms and Seale, 2013)

2.9.3. Perinatal thermogenesis

Due to its primary described role, BAT activation and recruitment has been associated to early stages of life. BAT appearance starts around the mid-gestational period in the fetus (process that is yet to be elucidated). Newborn BAT activity is enhanced upon delivery and gradually lost (or decreased in function) during childhood until adulthood. This developmental characteristic of BAT is relevant since it plays a major role at birth allowing the newborn to adapt to the new (extra uterine) atmosphere (Cannon *et al*., 1998; Clarke *et al*., 1997). Actually, the localization, protein status (especially regarding mitochondria), and vascularization (enhancing blood supply) at the moment of birth assures a maximal activation of BAT. This maximal activation is very unlikely to be reached again in life (Cannon and Nedergaard, 2004). A key component in this transition (uterine to extra uterine environment) is an adequate maturation of the hypothalamic-pituitary-adrenal (HPA) axis at the moment of birth. HPA axis is crucial for the control in the cocktail of hormones and neurotransmitters (i.e. NE, cortisol) that are to target and activate the tissue at the early stages of life (Symonds *et al*., 2013; Gnanalingham *et al.*, 2005).

Based on thermoregulatory properties, there exist three groups of species when talking about newborn BAT: altricial (i.e. mice and rats), immature (i.e. Syrian Hamsters) and precocial (i.e. humans, guinea pigs and calves) newborns. Precocial species are believed to be born with a mature and recruited BAT while altricial and immature are to recruit it after birth (the former one, in a delayed timing (not described in this text)) (Cannon and Nedergaard, 2004). Altricial newborns (i.e. mice) depend on nesting, with the rest of the litter and the mother, to maintain body temperature while precocial (humans) newborns are able to cope with cold stress more independently. This nesting adaptation seems to be important to the development and functioning of the depot in later stages of life (Malik and Fewell, 2003). The difference between these two groups of newborns is believed to be due to previous observations that stated that precocial newborns were born with a mature HPA axis and a recruited BAT while altricial newborns induced maturation and recruitment immediately after birth. However, it has recently been reported that at day 18.5 of embryonic age (E18.5), mice BAT is competent

for uncoupling respiration. This competence seems to be mediated by IL-33 and its receptor ST2 since the absence of either of them (*Il33-/-* and *Il1rl1−/−*, respectively) resulted in a decreased expression of UCP1 protein (in E18.5). In addition, 12h pups (P0.5) showed an increase in UCP1 protein expression compared to E18.5 (Odegaard *et al*., 2016). This suggests the existence of an active thermogenic machinery at the moment of birth in mice. Figure 7 described the induction of UCP1 upon birth and the dynamics of oxygen and oxidative substrate in precocial species.

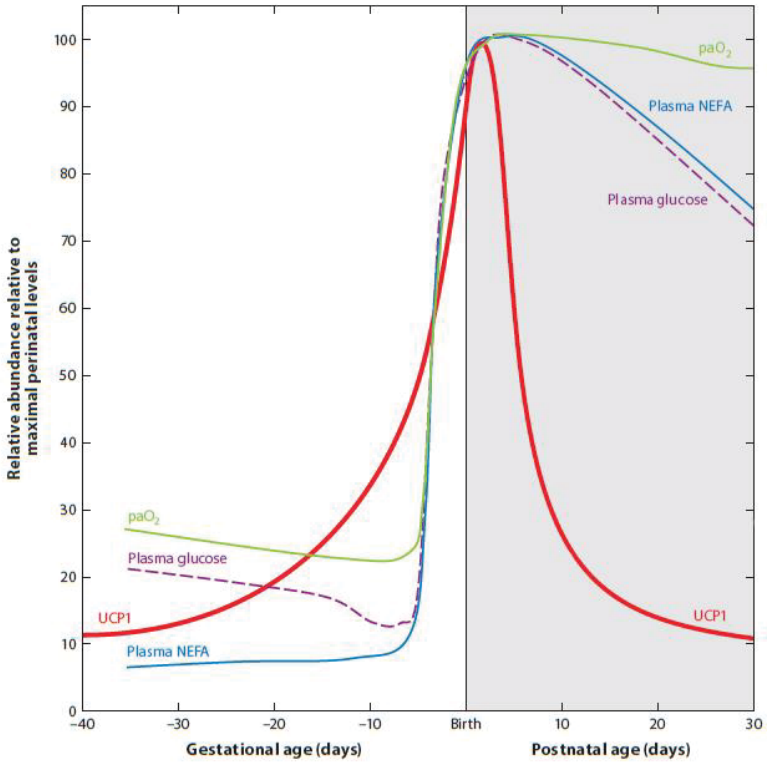

Figure 7. Perinatal metabolic and UCP1 profiles. Perinatal primary changes in the metabolic profile as described for precocial species; abundance of substrates and UCP1 expression are shown. (Image obtained and modified from Symonds *et al*., 2015)

2.9.4. The mechanics of heat production

Activated adipocytes, brown and beige, are able to produce heat due to a protein very well-known, UCP1. Although UCP1 is not the only uncoupling protein described (there are also UCP2, UCP3, UCP4 and UCP5), it is the only one related and confirmed important for noradrenergic stimulation of thermogenesis (Nedergaard *et al*., 2001).

Electron transport chain takes place at the inner membrane of the mitochondrial membrane. This transport (from complex I to IV) helps create the gradient between mitochondrial matrix and mitochondrial intermembrane necessary for ATP formation (in complex V). UCP1 is located at the inner membrane of the mitochondrion. There it promotes a proton leak from the intermembrane space to the matrix. This leak modifies the proton gradient and provokes the dissipation of energy as heat (Terada, 1990; Nedergaard *et al*., 2001; Cannon and Nedergaard, 2004). During the production of ATP, proton ratio mediates the activity of the gradient created by the complexes thus modulating the oxidation of substrates. In uncoupled respiration, UCP1 creates a continuous leak which leads to a continuous transport by the complexes. Altogether, it promotes a continuous mitochondrial catabolism of substrates making brown adipocyte a highly oxidative cell (Golozoubova, 2001; Krauss, Zhang and Lowell, 2005). Figure 8 illustrated the components of coupled and uncoupled respiration.

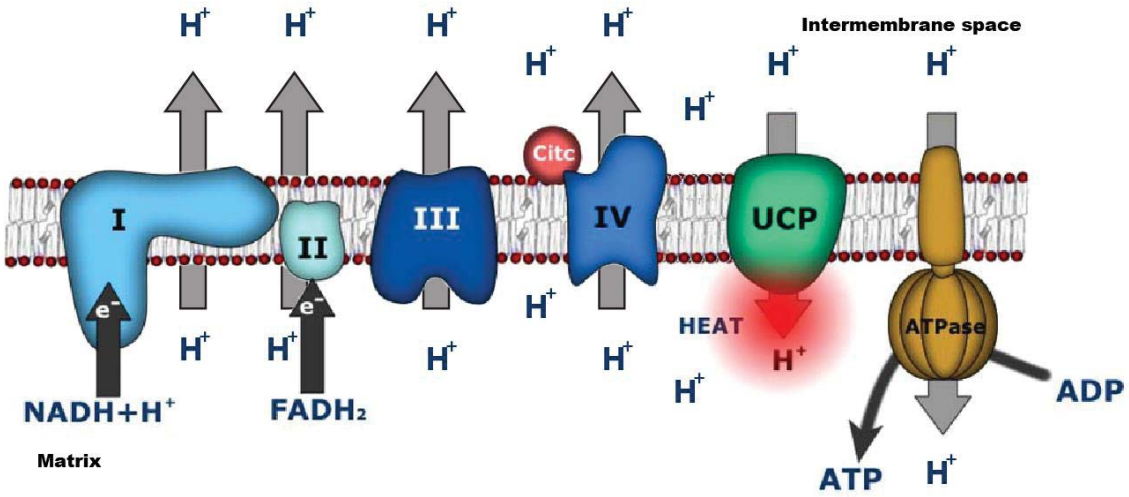

Figure 8. The components of coupled and uncoupled respiration. (Image obtained and modified from Valle *et al.*, 2010)

2.9.5. Activation not mediated by adrenergic stimuli

It was of great interest that the animal model ADRB3-deficient (gene coding for β3-receptor) was able to activate thermogenesis and even induce browning (always in a decreased level) (Konkar *et al*., 2000). At the beginning, it was believed to be due to a compensatory effect inducing β1 adrenergic receptor. However, now there have been

identified alternative factors also contributing to the activation of BAT and the *browning* of WAT independently from noradrenergic activation. Here some examples:

Table 4. Alternative factors contributing to BAT activation	
Factor	**Function**
Retinoids	Retinoids, vitamin A derivatives, are potent activators of BAT recruitment and UCP1 expression. They have been related to an increase in the expression of RBP4 (Retinol binding protein 4) which, when released from brown adipocytes, causes a paracrine activation (Alvarez *et al.*, 1995; Rosell *et al*., 2012).
Thyroid hormones	Thyroid hormones are important BAT activators. DIO2 (iodothyronine deiodinase 2) in BAT suggests that it is able to synthesize T3 (triiodothyronine) from tetraiodothyronine (T4). This is of relevance for the thermogenic activation since T3 has been reported to activate the expression of thermogenic markers such as UCP1 (López *et al*., 2010).
Prostaglandins	COX2 (cyclooxygenase-2), a limiting enzyme in the synthesis of prostaglandins appears to have a role in the induction of UCP1 when browning of WAT is taking place. This has not been observed in the case of BAT. The action appears to be related to PPARs since a similar effect is observed in MSC, where the cell is differentiated into a brown adipocyte but has not yet been confirmed (Madsen *et al*., 2010; Vegiopoulos *et al.*, 2010).
PPAR agonists	PPARɣ has been described to mediate brown adipocyte differentiation whereas PPARα is involved in the induction of the thermogenic machinery (as it will be explained in the next section). Then, it is of no surprise that the use of synthetic agonists for this receptors result in the activation of BAT and the *browning* of WAT (i.e. rosiglitazone induces browning and through PGC-1α dependent mechanism) (Hondares *et al*., 2006).
Bile Acids	Liver produces bile acids that activate TGR5 in BAT which induces DIO2 unleashing the thermogenic activation (Watanabe *et al*., 2006)
FGF21	The fibroblast growth factor 21 (FGF21) is an endocrine factor that is produced by and activates brown fat cell. This factor will be described latter in this dissertation but it is relevant for this chart due to its capacity to induce PGC-1α and ultimately UCP1, both leading to the induction of thermogenesis (Hondares *et al*., 2010; Hondares *et al.*, 2011).
Bmp8b	BMP8b is a member of the family of the Bone morphogenetic proteins (BMPs). It is able to sensitize the brown adipocyte to the noradrenergic stimuli and at the same time it signals hypothalamic hormones. This causes an induction in the signaling mechanism for BAT activation from the CNS (Whittle *et al*., 2012).

Dietary factors	Some dietary factors described to mediate thermogenic activation are: aminoacid (especially methionine restriction), resveratrol, capsaicin, some non-esterified fatty acids, etc. All of them have proven either to induce brown adipocyte differentiation or the browning of WAT (Bonet *et al*., 2013). In this group, a great variety of mediators of thermogenic activation take part (i.e. receptors and kinases). Families of receptors that are target of these dietary modulators have resulted interesting and important in the development of therapeutic approaches. One of these families is the GPCR family (described later in this text). β3-adrenergic receptor, the main receptor mediating thermogenic activation, is part of this great family. Likewise, a recently explored subgroup of GPCRs activated by dietary metabolites has been subject of study due to their potential role in BAT physiology. Also, regarding GPCRs activity and thermogenesis, ketone bodies, fatty acids and even bile acids have shown to modulate BAT activity.

2.9.6. BAT as metabolic regulator

Important to our knowledge of the tissue, and to the attempts to use BAT activation to treat obesity, it has been observed that upon feeding there can also be an induction in BAT thermogenesis. Also known as, *diet induced thermogenesis*, this phenomenon is present after feeding. This thermogenesis is probably mediated by the increase in circulating metabolites (i.e. glucose and FFAs) and some hormones like insulin, cholecystokinin, enterostatin and leptin (the most importantly proposed to regulate this response). Nevertheless, β3-adrenergic activation may also be involved. The real purpose of the activation after meals is yet to be elucidated but it has been suggested as a strategy by the BAT to modulate the replenishment of AT depots in order to avoid hypertrophy and obesity. This proposes BAT and its thermogenic activity as a homeostasis regulator to control the nutritional status not just in BAT but all AT depots (Rothwell and Stock, 1981; Commins *et al*., 2001; von Essen *et al*., 2017; Kawada, 2018). Also, upon several stimuli received (i.e. exercise, HFD in fuel) BAT is able to secrete cytokines able to regulate global metabolism and the activation of other AT depots. Some of these cytokines include IGF1, IL6, FGF21 and Bmp8b (Cereijo *et al*., 2013).

Table 5 summarizes basic characteristics of the three types of AT described. Now that the tissues and the different processes that they exert have been described, it is time to define how those adipocytes achieve specialization and their important and unique characteristics.

Table 5. Brown and white fat characteristics			
	White Adipose Tissue	**Brown Adipose Tissue**	**Beige Adipose Tissue**
Function	**Energy storage**	**Heat production**	**Heat production and energy source**
Adipocyte Morphology	One large lipid droplet Few mitochondria	Small and multiple lipid droplets Abundant mitochondria	Smaller size of lipid droplets compared to WAT Increased mitochondria (Approx. 10% of UCP1 compared to BAT
Characteristic markers	Leptin	UCP1	UCP1, FOXC2, TBX15
Development	Mainly coming from Myf5-negative precursors	Mainly Myf5-positive cells (we could also find Myf5-negative cells, derived from other lineages)	My5+/Myf5-
Impact of aging	In relation to age, its size increases	Tends to decrease with age	Tends to decrease to be recruited with age
Obesity effect	Increases the tissue size	Decreases tissue size and activity (	Decreased availability with increased BMI
Extracted and modified from Saely *et al*., 2012.			

2.10. The adipocytes

Although most eukaryote organisms are able to store energy in the form of lipid droplets, only vertebrates have a specialized cell-type able to store these droplets. These cells are the adipocytes and represent the functional subunits of both WAT and BAT (also beige adipose tissue) as shown in figure 9. Other cell types such as cardiomyocites and

hepatocytes can contain lipid droplets inside. However, in the case of these cells the consistent appearance of lipid droplets is considered to be pathological. Hence, this capacity is characteristic and proper of adipocytes and represents a mechanism of protection from the cytotoxicity that free fatty acids (FFA) represent (Trayhurn, 2007). Adipocytes are derived from MSC; these stem cells are able to differentiate into adipocytes, chondrocytes, osteoblasts or myocytes. (Moreno-Navarrete and Fernández-Real, 2012). The subsequent paragraphs explain the process by which these precursors will become a differentiated adipocyte.

2.10.1. Adipocyte differentiation

Both BAT and WAT are developed at different time points during individual growth. Most of the times BAT develops before WAT. In rodents, BAT is developed during fetal period and is activated upon birth due to cold challenge and diet (breastfeeding) (Cannon and Nedergaard, 2004; Symonds *et al*., 2015; Hondares *et al*., 2010). In the case of WAT, its development begins at the last third of gestational period and will continue after birth when it will result favored by the increase in nutrient availability (Gesta *et al*., 2007). Both tissues are originated from mesodermal MSCs in a process denominated as *adipogenesis*. Adipogenesis is a complex and well regulated process which is divided in two phases. In the first phase, or the determination phase, the cell lineage from the MSCs is decided and will be converted into a pre-adipocyte. The second phase involves the signaling cascade in charge of finishing the differentiation process and lipid storage, this is the *adipogenic* phase (where lipids are accumulated inside the cell) and for so is known as terminal differentiation (Cristancho and Lazar, 2011). Both phases are finely regulated by transcription factors and regulatory proteins. In adults, human and rodent, adipogenesis continues to take place but the precursors are more similar to those cells denominated as pericytes in de stroma vascular fraction (SVF). (Ailhaud and Hauner, 1998; Moreno-Navarrete and Fernández- Real, 2012).

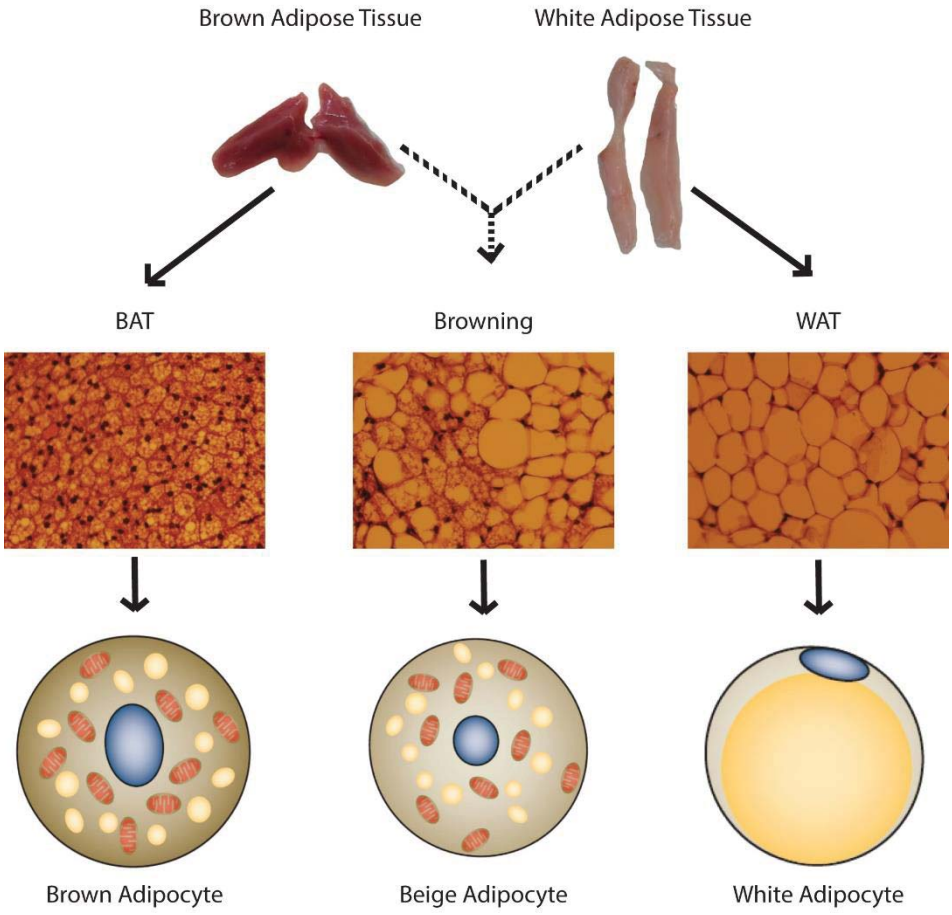

Figure 9. Appearance and morphology of adipose depots and adipocytes. (Information and pictures obtained and modified from Cinti, 1999; and Bartelt and Heeren, 2014).

2.10.2. Lineage determination phase

The result of this phase is the differentiation of precursor cells into pre-adipocytes. This means that this multipotent stem cells won't be able to differentiate into any other specialized cell type after completing this phase. Still, it will be necessary that the pre-adipocyte senses the external stimuli to be able to further complete its differentiation process and reach the end of the terminal differentiation phase.

Accounting for their similarities regarding energy storage, there was a point in time in which the brown and white adipocytes were considered to originate from the same lineage. However, today we know that brown and white adipocytes are originated

from different precursor cells. It was considered that brown precursors were the ones expressing the myogenic factor 5 (*Myf5+*) and the protein Paired-box 7 (*Pax7*), both related to muscle lineage. White adipocytes were believed not to express neither of these markers (and were denominated *Myf5*-). However, it was recently reported that there could be found brown adipocytes lacking the expression of Myf5 and white expressing it (Seale *et al*., 2008). This situation has been explained by the fact that the main differences are due to the localization of the cells independent of the expression of either markers. Cells differentiated from dorsal anterior anatomical region locations express Myf5 and ventral-posterior lack its expression (Sanchez-Gurmaches *et al*., 2012; Sanchez-Gurmaches and Guertin, 2014).

Differentiation will take place thanks to an accumulation of mechanical, physical and chemical signals. In the case of the chemical signals, two main families have been described to take pivotal roles in differentiation, WNT and TGFβ. The first family, WNT, are secretable glycoproteins involved in development. Upon activation of the receptors, they will trigger a signal that recruits transcription factors. It is indeed surprising that this family induced the differentiation of MSCs but not pure white pre-adipocytes. This suggests a close relationship with brown adipocyte differentiation from this type of precursors (Ross *et al.*, 2000; Kanazawa *et al.*, 2005). The second family, TGFβ, has also shown to inhibit the pre-adipocyte differentiation while inducing the differentiation of mesenchymal precursors. It is important to note that, out of this family, some of the members can trigger white adipogenesis (i.e.BMP2) and some others brown adipogenesis (i.e. BMP7 and 9) (Skillington *et al*., 2002; Sottile *et al*., 2000; Tseng *et al*., 2008). Although the members of these families involved in adipocyte differentiation have been very well characterized, it must not be forgotten that several of their members also have the capacity to induce the differentiation of mesenchymal precursors into other specialized cells (i.e. myocytes) (Takada *et al*., 2009; Zamani and Brown, 2011). In addition to this, the expression of some genes is essential for a proper expression of other target genes related to adipogenesis. One example is Pref-1 (Preadipocyte factor -1), a factor that prevents the expression of PPARs (Peroxisome proliferator-activated receptors) which expression is important for adipogenesis as it will be explain later (Smas and Sul, 1993).

As for the mechanical stimuli, it includes extracellular matrix remodeling and cell contact. The rigidity of the area at which the precursor differentiates will modulate the differentiation process. Also, the differentiated cell will contribute to modify the stiffness in the area for the control of future cells' differentiation. Cell contact will increase GTPase activity potentiating WNT signaling and transcription factors' recruitment (Liu *et al*., 2005). This remodeling at the differentiation area will also cause the increase in the protein ECN-1 (Ectodermoneural cortex 1), this protein will bind actin causing a cytoskeleton reorganization. This reorganization will contribute to the modification in the fibroblastic appearance of the cell which will lead to a spherical shaping. This binding of molecules will be important for the second phase of differentiation (Nakajima *et al*., 1998; Gregoire *et al.*, 1998; Zhao *et al*., 2000). At this point, some other proteins and transcription factors make their appearance in the process. One of these factors is ZFP423, this protein potentiates the BMPs family signals and responses while having a role triggering the expression of PPARɣ (later described). Besides this, the arrest of the cell cycle will also contribute to the subsequent maintenance of the adipogenic program. When cells reach confluence (at least during *in vitro* assays), the induction by chemical stimuli will favor mitotic clonal expansion (MCE) (Gupta *et al*., 2010). Type D cyclins will also take part in this process. CDK4/6 orchestrates the point at which the cell passes from G1 in cell cycle to S. Other proteins such as p53 will help in this cell cycle arrest. These last events in collaboration provoke not only the maintenance of the cell in the exact phase to complete the termination phase but also trigger the induction in the expression of master genes for adipocyte differentiation such as C/EBP-β y C/EBP-δ (CCAAT-enhancer-binding protein beta and delta) (Ramji and Foka, 2002; Tang *et al.*, 2004; Farmer, 2006).

2.10.3. Terminal differentiation

As it was mentioned at the description of the previous phase, ECN-1 adhesion and expression is induced in parallel with MCE. As a consequence of these events, plasminogen cascades and the expression of C/EBP-β y C/EBP-δ during the first 24 hours upon induction of the differentiation (described from *in vitro* differentiation) are

initiated. This isoforms of C/EBP are phosphorylated causing the activation of MAPK (mitogen-activated protein kinase) and GSK3β (Glycogen synthase kinase 3 beta). Both kinases, when activated, activated will lead to the induction in the expression of PPARɣ, C/EBP-α and C/EBP-δ, key regulators of adipogenesis. Both genes will start a positive feedback loop in order to maintain their expression and accumulation of the mRNA in order to achieve a proper differentiation (Ramji and Foka, 2002; Tang *et al*., 2005; Farmer, 2006; Lefterova *et al*., 2009). These gene inductions mark the start of the terminal differentiation and will induce the expression of the characteristic adipose genes.

C/EBPs are Basic Leucine Zipper (bZIP) type transcription factors which are expressed widely and have key roles in cell development (at the cells where they are expressed). When still undifferentiated, there are low levels of C/EBP-β in the precursor cells but when the different adipogenic stimulus start to emerge, cAMP will increase its intracellular levels. As a consequence, PKA will be activated and the subsequent phosphorylation of CREB will take place. CREB will bind the response element-binding provoking an induction in C/EBP-β expression (Yeh *et al.*, 1995; Tanaka *et al.*, 1997; Zhang *et al*., 2004). Upon C/EBP-β induction, phosphorylation of the transcription factor will also regulate its function. C/EBP-β will recruit C/EBP-δ, STAT5A (Signal transducer and activator of transcription 5A), GR (glucocorticoid receptor) and RXR (Retinoid Receptor X). This recruitment is essential for the terminal differentiation phase and the reason why C/EBP-β is highly regulated (Tang *et al*., 2004). All three C/EBP members are important for adipogenesis since the loss-of-function models of these transcription factors, especially β and δ, end up in an impaired adipocyte differentiation. In the case of C/EBP-α, it is known to be a target of C/EBP-β and its action is more referred to terminal phases of the differentiation. Also, it has been more related to the cell cycle by phosphorylating D3-cyclin and inhibiting cell proliferation. Likewise, it causes an induction in GLUT4, PEPCK (Phosphoenolpyruvate carboxykinase) and the insulin receptor genes expression during differentiation (Ramji and Foka, 2002; Johnson, 2005; Farmer, 2006).

As mentioned before, the whole C/EBP-β cascade will lead to the induction in the expression of PPARɣ. PPARɣ is a member of the nuclear receptor family that has been described as the master transcription factor in adipogenesis. It has been proven to be essential and sufficient to the termination of differentiation. Although it is sufficient to terminate adipocyte differentiation, C/EBPs will still be necessary for the differentiated adipocytes to be responsive to insulin (Tontonoz *et al*., 1994; Wu *et al*., 1999; Rosen and Spiegelman, 2002). The deletion of this gene is lethal for development and a decrease in its activity leads to metabolism abnormalities of the adipose tissue (i.e. lipodistrophy). There are two isoforms: PPARɣ 1 and PPAR ɣ 2; while the isoform 1 is more related to preadipocytes, the isoform 2 is more prone to be expressed in differentiated adipocytes. During differentiation, the activity of both of them can result in a mature and functional adipocyte (Zhu *et al*. 1995; Chawla *et al*., 2001; Rosen and MacDouglad, 2006). As a heterodimer with RXR, PPARɣ binds the response elements in the sequences of the DNA of the genes to be induced. PPARɣ is a ligand-dependent transcription factor. Despite existing pharmacological activators (glitazones), a physiological agonist has not been fully characterized but some lipid metabolites such as PUFAS and eicosanoids have been proposed (Kim *et al.*, 1996; Fajas *et al.*, 1999). It is important to note that even in the absence of any ligand for PPARɣ, this factor can interact with the target genes causing an induction in their expression. For this reason, these transcription factors need co-activators and finely regulated forms of interaction with the DNA sequences in order to avoid overexpression of some genes at different stages of differentiation (Guan *et al*., 2005).

Another signaling cascade identified in the adipogenesis process is the one that involve KLFs (Kruppel like factors). KLFs are a family of regulatory proteins in several cellular processes, adipogenesis included. Three members of this family (KLF6, KLF9 and KLF15) have been reported to take part in the adipocyte differentiation while other two (KLF2 y KLF7) seen to repress differentiation (Moreno-Navarrete and Fernández- Real, 2012). Multiple other factors may affect and inhibit differentiation such as GATA2 and GATA3 which are union proteins that bind and repress PPARɣ expression (Tong *et al*., 2000).

2.10.4. Differentiated adipocytes

The final stage of adipogenesis is the acquisition of all the typical characteristics of a mature adipocyte. It implies the appearance of lipid droplets and the expression of all those genes and proteins characteristic of each type of adipocyte (Lefterova and Lazar, 2009).

2.10.4.1. Differentiation of the white adipocyte

In this cell type, PPARɣ, C/EBP-α and C/EBP-β are not only important during the differentiation of the cell (as described earlier) but are also necessary to maintain the expression and characteristics of the cell when differentiated. The complex PPARɣ-RXR and C/EBP-α will be necessary to induce and maintain the expression of adipogenic markers. This induction will help maintain the morphology and the assembly of the adipocyte machinery. The proteins which may be of relevance for the proper function of the adipocyte include storage proteins, breakdown proteins and secretable proteins typical of the adipocyte. Some of these proteins include the ones that will help the adipocyte incorporate substrates into the cell (i.e. GLUT4); proteins related to TG synthesis (i.e. FAS, ACC); proteins related to lipid trafficking (i.e. FABP4); those necessary for lipolysis (like HSL) and adipokines (i.e. leptin, adiponectin) important for metabolic regulation by AT (Wu *et al.*, 1999; Tontonoz and Spiegelman, 2008; Maurizi *et al*., 2018).

2.10.4.2. Differentiation of brown adipocyte

Differentiation of both cell types, brown and white, require the signaling cascades triggered by C/EBP-β and PPARɣ, as well as their expression upon differentiation to maintain cell phenotype (Tang *et al*., 2004; Nedergaard *et al*., 2005). It is relevant that, in brown adipocytes, PPARɣ activity is not enough to drive differentiation. In addition, C/EBP-α nullification does not affect brown adipocyte differentiation (contrary to what is observed for white precursors) (Kajimura *et al*., 2010; Carmona *et al*., 2002).

Some slight differences are noted at the beginning of differentiation, during the determination phase. As mentioned, these cells are similar to the muscle cells in the sense that their progenitor cells tend to be *Myf5+* (some studies have also proven some brown adipocytes *Myf5*-). Besides the similar effect of the WNT and TGFβ families in the determination phase and the whole differentiation, there is also an important factor mediating their differentiation, NE. Upon cold exposure, afferent nerves secrete NE that activates the β1-adrenergic receptor promoting cell proliferation and inhibiting apoptosis. β1 receptor activation also inhibits the expression of proteins typical for cell cycle control (i.e. p53) in both pre-adipocytes and MSCs. NE won't induce the expression of thermogenic markers (such as UCP1) in undifferentiated cells but it will promote their differentiation. This promotion of differentiation will contribute to an increase in brown fat mass upon cold exposure. Also, NE will cause an increase in intracellular cAMP; a second messenger that acting through CREB (cAMP response element-binding) will induce the expression of C/EBP-β. This factor is crucial for the induction of thermogenesis, as mentioned earlier (Cannon and Nedergaard, 2004).

A key event for the differentiation of these precursor cells to brown adipocytes is the expression of PRDM16 (PRD1-BF-RIZ1 homologous domain containing protein-16) as a consequence of PPARɣ activity (Kajimura *et al.*, 2009). PRDM16 is a zinc finger protein which was found by screening genes with high expression in BAT compared to WAT. Its induction promotes the expression of thermogenic machinery genes (i.e. *UCP1, Dio2, PGC-1α*) while inducing mitochondrial biogenesis and cell respiration (typical of brown adipocytes) (Seale *et al.*, 2007). The absence of PRMD16 in precursor cells impairs brown adipocyte differentiation while inducing muscle-like phenotypes in differentiated adipocytes. Both effects prove the importance of this gene in the maintenance of brown adipocyte phenotype (Seale *et al.*, 2007; Kajimura *et al.*, 2010).

During brown adipocyte differentiation, C/EBP-α activity is reported earlier than C/EBP-β. Nevertheless, the complex formed by PRDM16 and C/EBP-β is believed to be sufficient for brown adipocyte differentiation and to induce PPARɣ. At the same time, parallel to the interaction with PPARɣ-RXR complex, PRDM16 can induce the expression of thermogenic machinery genes. PRDM16–C/EBP-β complex induces the expression of

PGC-1α, key factor in the induction of the thermogenic program (including the mitochondrial biogenesis and oxidative metabolism) and in the regulation of those genes that could inhibit adipogenesis (Puigserver *et al*. 1998; Barbera *et al*., 2001; Villarroya *et al*., 2007).

PGC-1α is a factor liked to β-adrenergic stimuli and cold response. Its expression is regulated by ATF2. The gene encoding this factor is a target gene of p38 MAPK which is phosphorylated as part of the thermogenic activation response. PGC-1α induces the expression of UCP1 and other thermogenic markers as part of BAT response (Cao *et al.*, 2004). It also has the ability to bind several transcription factors and receptors crucial for the activation of thermogenesis. Some of these interactions include PPARɣ, PPARα, the thyroid hormones' receptor (TR). This causes its own recruitment to the gene promoters of those genes involved in the thermogenic program. Also, PRDM16 is able to bind directly to this co-activator potentiating its activity and provoking a positive feedback on its expression in brown and white ATs (Hondares *et al.*, 2006; Wulf *et al.*, 2008; Seale *et al.*, 2011).

Also relevant to PGC-1α activity is PPARα. As mentioned before, PPARα is regulated by endogenous FA and is an important activator of thermogenesis which acts synergically with PRDM16. It induces the expression of UCP1 while also increasing the expression of PGC-1α and PRDM16 (Hondares *et al*., 2011). Together, these factors provoke the increased expression of thermogenic markers, electron transport chain uncoupling and even enhanced fatty acid oxidation (Giralt *et al.*, 2011).

2.10.4.3. Differentiation of beige adipocyte

Long periods of time at cold temperatures or β-adrenergic agonists stimulation will result in the appearance of mixed-phenotype adipocytes in WAT depots (not white and yet not brown). This process is called '*browning'*. The origins and explanation of the appearance of these cells has resulted controversial thus giving rise to a cumulus of theories. Here are describe the two main ones more which are more likely to explain the phenomenon. The first one proposes that the white adipocytes have the ability to

undergo a transdifferentiation process in response to the adrenergic stimuli (Barbatelli *et al*., 2010). The second one denies any capacity of transdifferentiation and proposes the presence of beige progenitors (probably *Myf5*-) in the tissue. These precursors will undergo a *de novo* differentiation into brown adipocytes favored by noradrenergic stimuli (Lee *et al*., 2012a; Wang *et al*., 2013). Now, it is considered that both theories are excluding and that it may occur that the phenomenon is presented as a consequence of both processes. However, in the case of transdifferentiation it may only occur in adipocytes coming from specific precursor cells (Harms and Seale, 2013).

The ***de novo* differentiation** theory proposes that the white adipose tissue possesses subpopulations of cells that are bipotent. This means that they are able to differentiate into a white or a beige adipocyte. In the presence of noradrenergic stimuli, these cells will increase their proliferation capacity and induce brown-like adipocyte. On the other hand, when exposed to a high fat diet (HFD), these cells will differentiate into a white adipocytes committed to the synthesis and harvest of TGs (Lee *et al*., 2012a; Wang *et al*., 2013). These information gives a clue on how this browning achieved. *De novo differentiation* also gives a hint on the dynamics of the tissue for the possible transdifferentiation depending on the metabolic, feeding and thermal status of the individual (Bartelt and Heeren, 2014).

The second theory is **transdifferentiation,** or the capacity of a quiescent differentiated cell to convert to another cell type. Following this theory, the idea is that upon cold exposure or noradrenergic stimulation, the unilocular white adipocyte is capable of a genetic and epigenetic reprograming. This process will result in the acquisition of a beige phenotype expressing thermogenic markers and producing heat (Rosenwald and Wolfrum, 2014). Evidence of this event was the discovery of paucilocular adipocytes, *UCP1+* white fat cells with intermediate locularity phenotype. These cells are believed to be an intermediate phase between white and beige (Barbatelli *et al*., 2010). Likewise, a recent *in vivo* approach employing marked adipocytes proved a high WAT plasticity since they observed an acquisition beige phenotype upon cold exposure and that once the animal is put back into warmer temperatures the cells will recover a white phenotype and vice versa (Rosselwald *et al.*,

2013). This is not the only example of the high plasticity of WAT, there is another example not related to browning but to nurturing. At the breast zone of mammals, it has been observed that white adipocytes are able to transdifferentiate in a cell type not only multilocular but able to produce milk. When these cells are observed under the microscope, they show an appearance similar to the endothelial cells and for that reason they were named **pink adipocytes** (not to be described profoundly in this dissertation) (Morroni *et al*., 2004).

As for the signaling cascade, it is not as profoundly studied as for white or brown adipocytes. However, it is believed to follow a similar pathway. The differentiation process is very likely to be started by C/EBP-β followed by an induction of PPARɣ and C/EBP-α. C/EBP- β will stay in-transcribed due to the expression of HOXC8 (Homeobox C8). Noradrenergic stimuli (and maybe other stimuli able to trigger browning) will cause the expression of mi-R196a. This microRNA will repress HOXC8 expression resulting in an induction of C/EBP-β. These events will trigger the expression of the subsequent differentiation players (i.e. PRDM16) and the maintenance of the differentiation status. PRDM16 plays a key role during terminal differentiation in these cells while the activation or response to noradrenergic will be mainly mediated by PGC-1α. In addition to this, the maintenance of the phenotype and adipogenesis will be favored by the transcription factors forkhead box C2 (FOXC2) and T-box transcription factor 15 (TBX15). These factors will be necessary for the induction of genes like UCP1 and PGC-1α (Cederberg *et al*., 2001; Gburcik *et al*., 2012; Harms and Seale, 2013). Figure 10 illustrates the differentiation processes followed by precursor cells in order to achieve specialization.

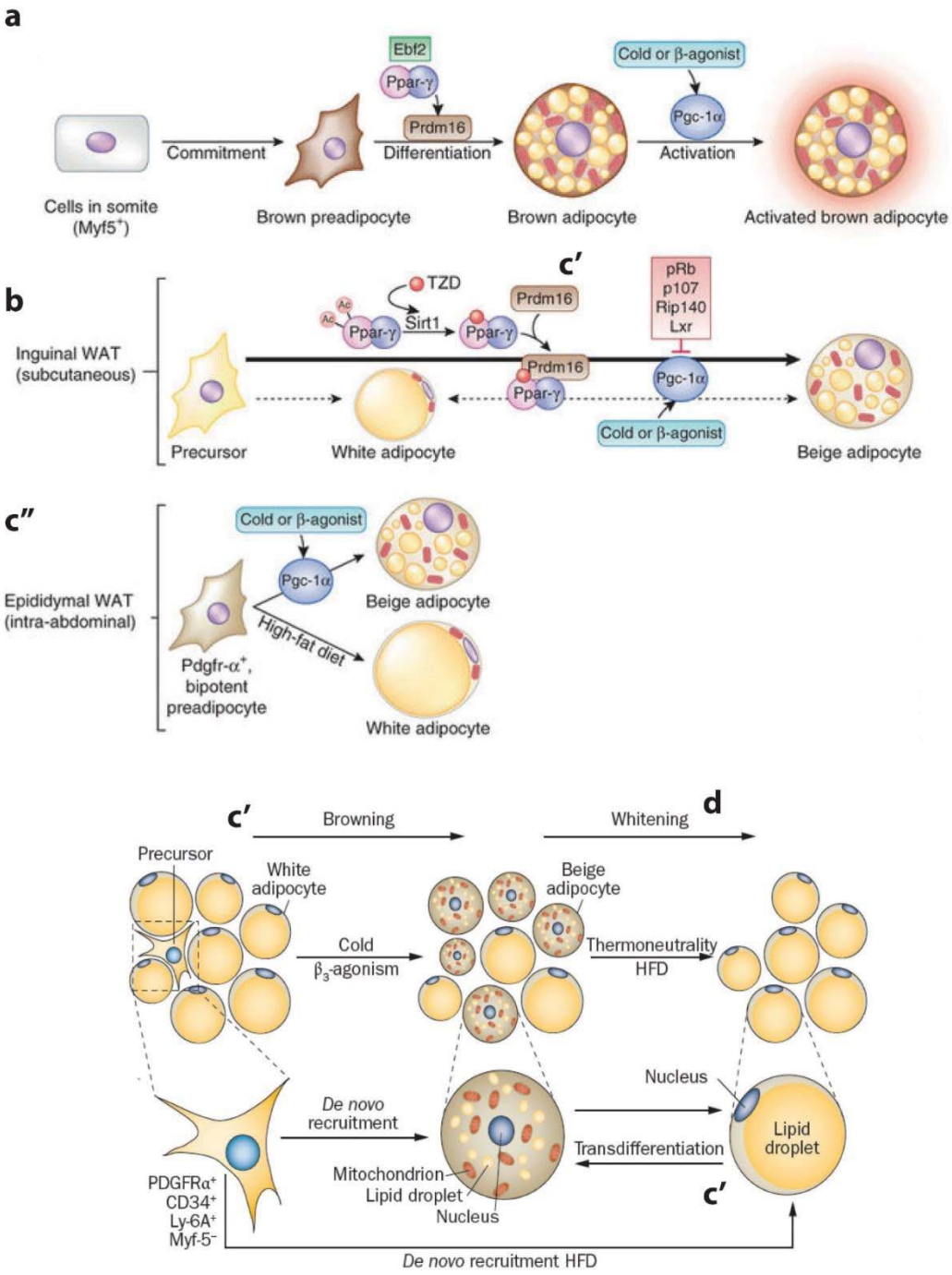

Figure 10. Schematic diagram of brown, beige and white adipocyte differentiation. Main cascades for brown adipocyte differentiation (a), white adipocyte differentiation (b) and the processes proposed to be part of browning: transdifferentiation (c') and *de novo* adipogenesis (c''). Also, the process denominated as whitening, where brown adipocytes acquire white-fat cell characteristics (d) (Image obtained and modified from Harms and Seale, 2013; and Bartelt and Heeren, 2014)

3. The G-protein coupled receptors superfamily

3.1. General description

In order to appropriately sustain survival, cells receive and process environmental signals. Most of the occasions, the cells have to process and respond to several signals at the same time (O'Connor and Adams, 2012). Fat cells are not the exception since mammals' AT is in charge of maintaining energy homeostasis. To be able to perform these functions, AT has to sense, process and respond to the hormonal and metabolic status of the organism.

The signal transduction of external stimuli is driven by several membrane proteins. The G protein-coupled receptors (GPCRs) are the largest protein superfamily in mammalian genomes (encoding more than 800 genes (comprise 3-5% of the human genome)) (Doze and Perez, 2013; Venkatakrishnan *et al*., 2013). They are the most physiologically important membrane protein family since GPCRs are key specific targets for a variety of physiological functions and therapeutic approaches. These functions include blood pressure control, allergic response, kidney function, hormonal responses and some other mechanical and sensory signals (Lagerstrom and Schiöth, 2008; O'Connor and Adams, 2012; Tang *et al.*, 2012). Their discovery and the understanding of their function, activation and signal transduction has modified the biomedical and pharmaceutical field. Nowadays, more than 30% of the commercialized drugs target a GPCR. These pharmacological approaches go beyond just discovering agonists and antagonists mainly due to the higher degree of complexity in these receptors' signaling (Katritch *et al.*, 2013, Doze and Perez, 2013; Zhang *et al.*, 2015).

3.2. GPCR structure and division

GPCRs are enclosed in a type of receptors also denominated seven-transmembrane receptors (7TM-receptors). As the name indicates, they have seven transmembrane-spanning α-helices (helices I–VII, TM 1-7), an extracellular N terminus, an intracellular C terminus, three inter-helical loops on each side of the membrane (ECL1-3, extracellular and ICL1-3, intracellular) and an intracellular amphipathic helix (H8) (Oldham and Hamm, 2008; Venkatakrishnan *et al.*, 2013; Lu and Wu, 2016). While some regions of the protein seem to be important for the maintenance of the structure (i.e.TM3), some others are crucial for the specificity and the response (i.e. TM6, TM7 and H8) (Venkatakrishnan *et al.*, 2013; Lu and Wu, 2016). Another characteristic they share, which also gives rise to the name of the family is their ability to modulate G-protein activity.

The now available structural information on these receptors gives us evidence of the diverse and ample differences in the family. For their classification, there was just considered that there were 3 classes of GPCRs (A, B and C). However, Fredriksson and co-workers (2003) made a great and extent identification and classification of GPCRs giving rise to the GRAFS families (standing for the initials to Glutamate, Rhodopsin, Adhesion, Frizzled and Secretin families) based on phylogeny. This division in families does not mean they share big sequence identities (SI) since they barely reach a 20% of the SI in the transmembrane domain and they show few similarities in the extracellular N-terminus (especially regarding ligand binding structures). It is important to note that there were around 20 GPCRs that were not fitting to any of this families and are denominated as "other 7TM receptors" (Schiöth and Fredriksson, 2004; Katritch *et al*., 2013). GRAFS families are divided as follows:

- ***Rhodopsin (Class A)***

The Rhodopsin family is the largest family of receptors accounting for nearly 700 (241 non-olfactory). As a fingerprint they contain several distinctive motifs. A NSXXNPXXY motif in TM7 and a DRY motif at the cytoplasmic border of TM3, important

for protein stabilization and/or G protein activation, allow the conservation of the inactive structure and favor the formation of TM6-CWxP “toggle switch” upon activation. The ligand can bind at the N terminus (which length is <100 residues, except glycoprotein hormones’ receptors) or within a cavity between the TM regions (most commonly) (Baldwin, 1994; Karnik *et al.*, 2003; Bhattacharya *et al*., 2008a). This class of receptors can be devided into α, β, ƹ and ɣ based on a phylogenetic analysis (Kochman, 2014; Schiöth and Fredriksson, 2004; Katritch *et al.*, 2013).

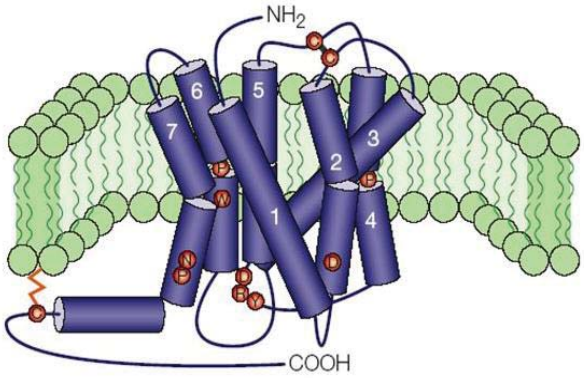

Figure 11. Proposed structure of the Rhodopsin family (Class A) of the GPCRs (Obtained and modified from Ellis, 2004).

- ***Adhesion (Class B)***

It is the second largest GPCR family, often described as a marriage between two receptor families (EGFs and 7TMs). These receptors contain a segment for adhesion, an integrin binding motif, a mucin-like segment and Cysteine residues in the extracellular loops causing N-terminus of 200 to 2800 amino acids long (Fredriksson *et al*., 2003; Karnik *et al*., 2003). These elements bring structure stability while contributing to activation of the receptor upon agonist adhesion (Hayflick, 2000; Bjarnadóttir *et al*., 2004).

- ***Secretin (Class B)***

These receptors bind large peptides which act in a paracrine manner. Usually, they contain long N terminus of ~60–80 amino acids in length with multiple conserved

disulfide bonds (Cysteine bridges) that bind large peptide hormones (Schiöth and Fredriksson 2004).

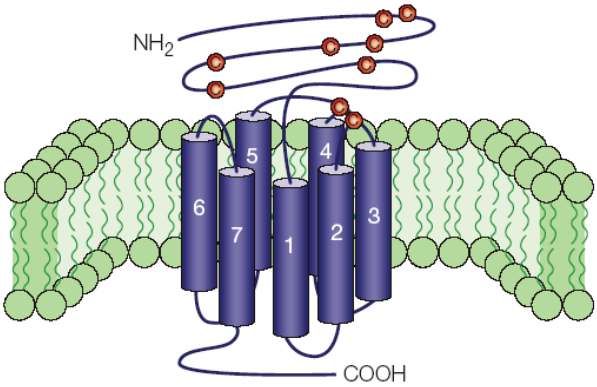

Figure 12. Proposed structure of the Adhesion and Secretin families (Class B) of the GPCRs (Obtained and modified from Ellis, 2004)

- ***Glutamate (Class C)***

Contain the ligand recognition at the N terminus (280–580 residues) where it forms two lobes where the ligand can bind and close around in a structure ('Venus flytrap'). They may also present a Cysteine-rich domains which may play a role in Ca^{2+} signal. Some members of this class are not GPCRs but ion channels (Pin and Acher, 2002).

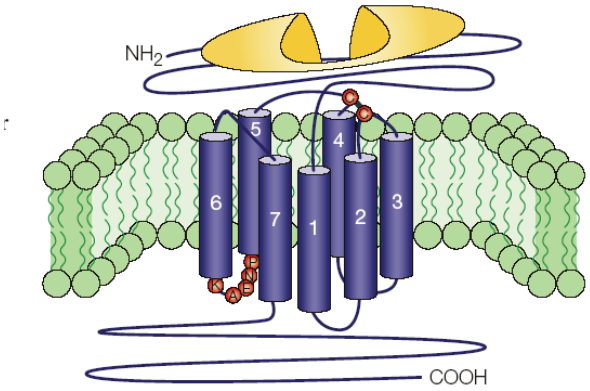

Figure 13. Proposed structure of the glutamate family (Class C) of the GPCRs (Obtained and modified from Ellis, 2004).

- ***Frizzled/Taste2***

This family encloses taste receptors commonly found in tongue and other parts of the intestine and the frizzled receptors (~10 in vertebrates). The Taste2 receptors are

in charge of sensing flavors while Frizzled receptors control cell fate, proliferation, and polarity during metazoan development. They were originally identified from *Drosophila* and the name refers to the curled and twisted WNT ligand (Schiöth and Frederiksson, 2004).

3.3. Activation and signal transduction

3.3.1. Conformation is important

Even though there are a lot of new techniques to explore the structures of GPCRs (such as x-ray crystallography, fluorescence or bioluminescence resonance energy transfer (FRET or BRET), etc.), barely 20 members have their structure disclosed (Venkatakrishnan *et al*., 2013). The conformational plasticity of GPCRs make them a challenging target for structural and functional study. Still, their biological function underlies in this finely regulated plasticity (inactive and active states) (Mangle and Kruse, 2017). The chemical nature of the endogenous ligands is very diverse. Among them, we may find biogenic amines, peptides, glycoproteins, lipids, nucleotides, ions, and proteases without leaving behind the signals from exogenous stimuli (light, odor and taste). Small molecular weight ligands bind the receptors in the hydrophobic core in between the α-helices while peptides and protein agonists bind at the N terminus and extracellular hydrophilic loops joining the transmembrane domains (Gather and Kabila, 1998). In any case, the signals are prone to provoke a response in the cell that they are approaching.

The response that is to be triggered by either of these 'potential activating molecules' will depend on the structure of the GPCR and the conformational changes that it will drive (Lu and Wu, 2016). Although they are thought to have similar signal transduction pathways, it turns out that the activation follows a complex cascade that depends on the receptor, the ligand and modulators (Hang *et al.*, 2013). So, regarding the first steps to receptor activation, structure is important for receptor specificity and gives room for orthosteric and allosteric ligands. The binding sites for orthosteric ligands are commonly found within the 7TM helical bundle and close to the extracellular surface

while allosteric ligand-binding sites are less conserved. ECL2 and the TM3 have been importantly described in this matter. (Cherezov *et al*., 2007; Warne *et al*., 2008; Kruse *et al*., 2012; Lu and Wu, 2016).

On the other hand, particularly for class A receptors, it has been described an important role of the TMs, especially TM3. These regions form of a scaffold structure for ligand recognition and interaction while allowing structure and charge maintenance (TM1-4) and mobility for signal transduction (TM5-7). (Patel *et al*., 2005; Cherezov *et al*., 2007; Venkatakrishnan *et al*., 2013; Manglik and Kruse, 2017). These structural changes will be essential for activation and inactivation. The ability of the agonists or inverse agonists to stabilize the whole GPCR structure (ECLs, TMs, ICLs and H8) will dictate the overall activation of the receptor (Gether *et al*., 1995). Simultaneous conformational changes will occur upon binding. An adequate activation will be achieved by specific interactions of some of the transmembrane regions (TM3, TM5, TM6 and TM7) while other interactions will favor an intracellular-face conformational rearrangement essential for signal transduction (TM3, TM6 and H8). (Patel *et al*., 2005; Cai *et al*., 1999; Bhattacharya *et al*., 2008b; Katritch *et al*., 2013; Manglik and Kruse, 2017). The resulting conformation will make ICL2 and ICL3 available for **β-arrestin** interactions or TM3, 6 and 7 for **G-protein** binding (Marion *et al*., 2006; Nygaard *et al*., 2009; Cherezov *et al*., 2007; Park *et al*., 2008; Manglik and Kruse, 2017). Thus, the mechanism of GPCR activation involves the relaxation of constraining intramolecular interactions and the formation of new ones (Karnik *et al*., 2003). Cysteine residues will be crucial for disulfide bonds formation and the maintenance active/inactive structures (Sheikh *et al*., 1999).

3.3.2. G-protein dependent activation

Once the pertinent conformational changes have occurred, GPCR activation occurs. GPCRs were given their name due to the classical signaling pathway described upon their activation. In this signal transduction, they recruit and regulate the activity of heterotrimeric G-proteins inside the cell. (Hamm, 1998; Gether, 2000; Wang *et al*.,

2018). Upon GPCR activation, these G proteins play an important role in the transduction of the signal and in determining the magnitude and the duration of such signal (while maintaining specificity). Two main models of G-protein interaction with the GPCR are known. The first one suggests that the G-protein is already bound to the receptor before activation, *pre-coupling model*. The second one suggests that ligand binding is necessary for the recruitment of the G-protein, *collisional model* (Gales *et al*., 2006; Hein *et al*., 2005). GPCRs also achieve several responses by acting through second messengers in order to produce a variety of cell responses (described afterwards in this section) (Wang *et al.*, 2018).

Heterotrimeric G-proteins are constituted by the α, β and ɣ subunits product of more than 2 gene codifications (listed in table 6). There have been reported 4 main classes of G proteins (G_s, $G_{i/o}$, $G_{q/11}$ and $G_{12/13}$, listed in table 7) apparently from 16 individual genes (Hilger *et al*., 2018). Gα subunit and Gβɣ subunits-dimer are bound together when Gα is bound to GDP in the inactive state of the heterotrimeric G-protein. Upon activation of the receptor, GDP is released and GTP is bound to the Gα subunit. The heterotrimeric protein is compromised and the GDP dissociation from the alpha subunit is accelerated. The high GTP ratio in the cell causes a fast exchange of nucleotide and becomes a rate-limiting step in G-protein activation. Once GTP is bound to the alpha subunit, it causes the dissociation of the Gβɣ-dimer. Both subunits, Gβɣ-dimer and Gα, have proven to modulate different downstream signaling (a summarized scheme is presented in figure 14) (Karnik *et al*., 2003; Hilger *et al.*, 2018).

For its part, Gα can modulate the activity of adenylyl cyclases, cGMP phosphodiesterases, phospholipase C and RhoGEFs. On the other hand, Gβɣ-dimer can interact with GPCR kinases (GRKs) and arrestins in order to modulate the GPCR itself and Potassium and Calcium channels. The dimer can also impact adenylyl cyclases, phospholipase C, phosphoinosite 3 kinase and mitogen-activated protein kinases activities. There is an important and fine regulation of the activation of this proteins. GTPase-activating proteins (GAPs, such RGS proteins), could increase the GTP hydrolysis

in Gα causing important increase or decrease in the duration and intensity of the GPCR signaling (Lu and Wu, 2016; Hilger *at al.*, 2018). This is the feature that gave rise to the new paradigms and orientations on GPCR studies since they are not receptors that just switch on and off. They can have agonists, antagonists and inverse agonists with different modulations (Samama *et al*., 1993).

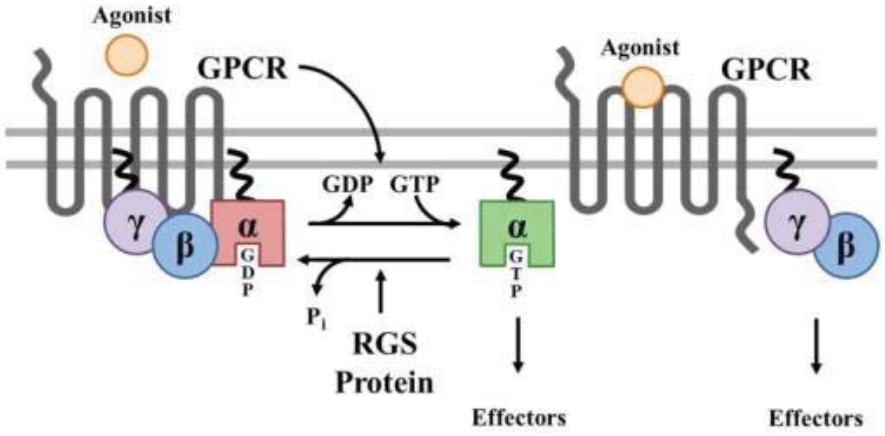

Figure 14. Summarized scheme of GPCRs' G-protein activation (Image obtained from Stewart *et al*., 2012).

GPCRs exist in dynamic equilibrium between active and inactive states, or different signaling states. The ligand free receptors can have very different basal activity that can fluctuate from inactive to a partial activity. Inverse agonists can produce the decrease in the active state while antagonist do not modify the basal activity (Katritch *et al*., 2013). In an attempt to describe this, the ternary complex was described. The complex considers the agonist (A), the receptor (R) and the G protein (G). When activated, the receptor forms a low affinity complex between the agonist and the receptor (AR complex). This complex attracts and couples the G protein causing a high affinity complex between the three elements (ARG-complex). An appropriate or specific agonist will cause this high-affinity complex; in other situations a complex between the receptor and the G protein will be formed spontaneously (describing mutations or even constitutively active forms). An extended theory established that there are activated and inactivated receptors bound to the agonists and only the active ones will interact

with the G-protein. Constitutively active, receptors will be kept active and giving the opportunity of inverse agonists to modulate the activity (Samama *et al*., 1993).

Table 6. Classification of Gα subunits

	Isoform	Gene	Effector	Active state effect
Gs	$G\alpha_{s(s),s(l)}$	GNAS	+ Adenylyl cyclase	↑cAMP
	$G\alpha_{s(xl),s(xxl)}$	GNAS		
	$G\alpha_{olf}$	GNAL		
Go	$G\alpha_{t(r)}$	GNAT1	- Adenylyl cyclase + phospholipase Cβ	↓cAMP ↑Ca
	$G\alpha_{t(c)}$	GNAT2		
	$G\alpha_{gust}$	GNAT3		
	$G\alpha_{i1}$	GNAI1		
	$G\alpha_{i2}$	GNAI2		
	$G\alpha_{i3}$	GNAI3		
	$G\alpha_{o1,o2,o3}$	GNAO		
	$G\alpha_{z}$	GNAZ		
Gq	$G\alpha_{q}$	GNAQ	+ phospholipase Cβ → cleavage $PIP_2 = IP_3$, DAG	↑DAG (PKC) ↑IP3 ↑$[Ca^{2+}]$
	$G\alpha_{11}$	GNA11		
	$G\alpha_{14}$	GNA14		
	$G\alpha_{15/16}$	GNA15		
G12	$G\alpha_{12}$	GNA12	+ RhoGEF = + small monomeric GTPase RhoA	↑RhoA (ATP)
	$G\alpha_{13}$	GNA13		

Obtained and modified from Ellis 2004 and Heng *et al*., 2013

Table 7. Gβ and Gɣ subunits diversity

Isoform	Gene
Gβ subunits	
$G\beta_1$	GNB1
$G\beta_2$	GNB2
$G\beta_3$	GNB3
$G\beta_4$	GNB4
$G\beta_5$	GNB5
Gɣ subunits	
$G\gamma_1(G\gamma_{rod})$	GNGT1
$G\gamma_2(G\gamma_6)$	GNG2
$G\gamma_3$	GNG3
$G\gamma_4$	GNG4
$G\gamma_5$	GNG5
$G\gamma_7$	GNG7
$G\gamma_8(G\gamma_{olf})$	GNG8
$G\gamma_9(G\gamma_{cone}, G\gamma_{14})$	GNGT2
$G\gamma_{10}$	GNG10
$G\gamma_{11}$	GNG11
$G\gamma_{12}$	GNG12
$G\gamma_{13}$	GNG13
Ellis 2004	

3.3.3. G protein targets

Once activated, G-proteins follow different signaling pathways (main effectors can be observed in table 6). $G_{\alpha s}$ stimulates the adenylyl cyclase which will cause an increase in the production and concentration of cAMP. The cAMP increase will promote PKA activity. At the same time, in an attempt to control the signal, $G_{\alpha i}$ inhibits this same adenylyl cyclase to control cAMP production; PKA on its part will activate some phosphodiesterases (PDE) to breakdown some of the already available cAMP. Some

Gβɣ-dimer have also been suggested to modulate adenylyl cyclases dependent on the G protein and the type of enzyme (Simonds, 1999). In the case of $G_{\alpha q/11}$, the effects are different. It activates phospholipase C (PLC) β producing inositol 1, 4, 5-trisphosphate (IP3) and diacylglycerol (DAG) from phosphatidylinositol 4, 5-bisphosphate (PIP2). At the endoplasmic reticulum (ER) surface, this IP3 will promote calcium release while DAG will take advantage of this calcium increase to activate PKC. PKC will regulate PLC activity to modulate a downstream signaling (Vanderheyden *et al*., 2009; Litosch, 2012).

3.3.4. β-arrestins and the concept of desensitization

Other effector proteins that have been gaining fame are arrestins. Arrestins were mainly described as responsible for switching off the GPCR, maybe due to the fact that they promote internalization and, in some cases, degradation of the receptors. Today we know differential functions important for signaling pathways besides desensitization (Kong *et al*., 1994).

β-arrestins are a family of proteins important for regulating signal transduction at G protein-coupled receptors. They were described to modulate the response upon GPCR activation by a process named *desensitization*. For this mechanism to occur, the activated receptors needs to be phosphorylated by GPCR related kinases (GRKs). Once this phosphorylation is achieved, the arrestin is recruited to the plasma membrane where it binds the receptor. These events result in the inhibition of the association with the G-protein and the G-protein mediated downstream signaling pathways previously described (Kong *et al*., 1994; Barak *et al*., 1997; Krilov *et al*., 2011). This desensitization is denominated homologous desensitization. There is another type of desensitization which occurs in the absence of arrestins (and of an agonist). Heterologous desensitization is characterized by the phosphorylation of the receptor causing the activation of kinases, such as PKA and PKC. This activation eventually leads to a prevention in the coupling of the G-protein to the GPCR. The phosphorylation of the receptor is achieved by interactions with the ICLs, TM3 and H8. When there is a mutation

in the SI the result can be either a constitutive activation or an impaired desensitization (Valiquette *et al*., 1995; Montiel *et al*., 2004; Venkatakrishnan *et al.*, 2013).

After binding to the receptor, the arrestins work as scaffolds for the GPCR to interact with those proteins that will enable its internalization (i.e. clathrin, adaptor protein-2 (AP-2) and dynamin. Always mediated by clathrin-coated vesicles the receptors will be internalized and targeted to early endosomes or to lysosomal compartments (Goodman *et al*., 1996; Kang *et al.*, 2009). The final destination upon internalization will depend on the proteins responsible for internalization and on whether the internalization is dependent of β-arrestins or kinases. When they are internalized to be recycled back, they target the early endosomes where they become dephosphorylated by protein phosphatase 2A (PP2A) and then it is recycled back to the membrane (Pitcher *et al*., 1995; Iwata *et al*., 1999). On the other hand, an internalization aimed for a down regulation of the signal will target lysosomes. Ubiquitination (mediated by E3 ligases) has been described to play role in targeting the receptor to lysosomes for degradation. This will contribute to a decreased expression in the cell surface and a longer tolerance upon stimulation (Pippig *et al*., 1995; Shenoy *et al*., 2009; Pierce *et al*., 2002). In addition to this trafficking regulation mediated by internalization, the SI in carboxyl tails of the receptors may include multiple clustered phosphorylation sites causing a slower recycling of the receptor and with this a modulation in the signaling of the GPCR (Oakley *et al*., 2000). An illustrated summary of the internalization mediated by arrestins can be observed in figure 16.

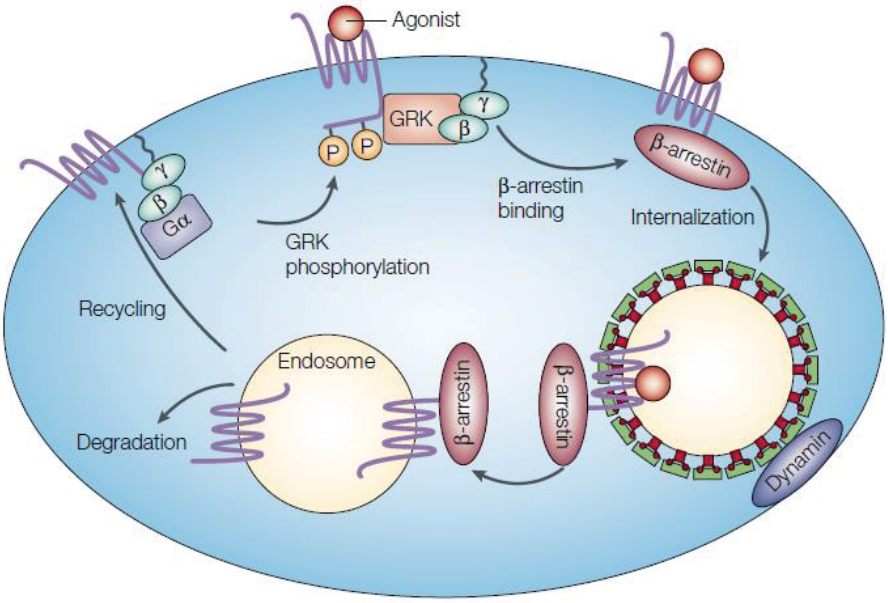

Figure 15. Arrestin mediated internalization of GPCRs (Image obtained from Pierce *et al*., 2002).

3.3.5. β-arrestin mediated signaling of GPCRs

As mentioned earlier in this section, nowadays we know that β-arrestin are not just important due to their role in desensitization of the GPCRs. Lately, it has been described that there can occur an alternative ternary complex of agonist, receptor and β-arrestin. This complex is also able to transduce important signals acting as a scaffold protein to recruit signal components (i.e. ERK, other MAPKs phosphorylation) (Shenoy and Lefkowitz, 2003).

3.3.5.1. ERK signaling mediated by β-arrestins

Although it was mentioned earlier as part of the signaling cascade for G-proteins, it has been lately identified that the ERK pathway can be either activated by G-proteins or by arrestins. Both will have their goals since the G-protein mediated activation will result in a faster activation while the arrestin activation will be slower and enduring. When the response needs to be rapidly targeted to the nucleus, the G-protein will be

activated causing a transient activation of ERK and placing it at the nucleus. On the other way, a longer lasting activation will cause arrestin-mediated activation of ERK placing it in endosomes at the cytosol of the cell (Ahn *et al*., 2004). This pathway can be mediated by Src scaffolding during cell proliferation, for example, where it regulates the Rb-Raf1 pathway (Charest *et al*., 2007).

3.3.5.2. Akt scaffolding mediated by β-arrestins

GPCRs can mediate a recruitment of PP2A to Akt promoting a reduction on its activity. Akt is a player in the signaling pathway P13K → Akt → mammalian target of rapamycin (mTOR) signaling pathway. Such pathway is involved in apoptosis, cell proliferation and migration. Although it has not been profoundly studied, it has been identified an important interaction of protein phosphatase 2A (PP2A), Akt and arrestin. Arrestin brings them both together in a signaling scaffold leading to important effects on metabolism upon GCPR activation targeting this pathway (Morgensztern and McLeod, 2005).

3.3.5.3. Phosphodiesterases complexes with β-arrestins

Also interesting regarding GPCR signaling, complexes formed with phosphodiesterases and β-arrestins modulating cAMP-dependent signaling have been reported in cardiomyocytes. These complexes will cause the degradation of cAMP and alter PKA regulation modifying the overall response to GPCR activation (i.e. β2AR) (Baillie *et al*., 2003). Figure 16 describes the mechanisms of G-protein dependent and G-protein independent GPCR activation.

3.3.6. The concept of biased signaling

Approximately 10 years ago, the multifunctional adaptor β-arrestins were found to be able to initiate parallel G protein-independent signaling pathways. The distinct b-arrestin mediated signaling defined a new GPCR activation mode called 'biased activation'. In this type of activation, a receptor may show preference for signaling through a particular effector dependent on the ligand that bounded it. Initiation of biased GPCR signaling is conveyed by GPCR conformational changes and a 'phospho-barcode' by the receptor and GRKs (or sometimes PKA) (Venkatakrishnan *et al.*, 2013; Zhang *et al.,* 2015; Wang *et al*., 2018).

The fully active state of the receptor will become the dominant state only after binding of a G protein, arrestin or conformation- specific antibodies. There may not be a single active state and ligands could be able to stabilize distinct conformations. These conclusions regarding the stabilization of different conformations give rise to diverse downstream responses. In this context, modifications in the conformation of those helices that have not been linked to the recruitment or interaction with G proteins may possibly mediate biased signaling (Azzi *et al*., 2003; Katritch *et al.*, 2013). So, different ligands that can activate the same receptor thus producing different conformational chances. Different agonists will cause unusual conformations with features intermediate between fully active and inactive states. Which may be representative of an arrestin-preferring signaling conformation. This 'promiscuity' of the receptor will be given by the sequence and structural diversity in the extracellular region. These SIs will allow GPCRs to recognize a wide range of agonists which may stabilize similar conformational changes on the intracellular side of the receptors. These structure stabilizations will converge on the activation of a small number of effector G proteins, arrestins, and kinases. And this is precisely how the signal transduction starts. Depending on the activator, the GPCR can drive either one or another conformational change favoring a different transduction. The internal configuration adopted by the helixes will be important for the transduction and will depend on the receptor and on the ligand (i.e. In the structure of β2AR in complex with Gs protein, the C terminus of the Gα subunit

interacts with the intracellular parts of TM3,5 and 7 well as ICL2). Moreover, this reconfiguration of the receptor will provoke a reorganization of the cytoplasmic side of the receptor exposing or enclosing the intracellular sequences of the receptor. The display of such sequences will engage the corresponding downstream signaling. These effects have led us to categorize some GPCR ligands as biased ligands since they selectively activate certain receptor-associated pathways at the expense of others (Kenakin, 2001; Katritch *et al.*, 2013; Hilger *et al*., 2018). It is important to mention that identification of specific ligand-receptor interactions, or triggers, that control the equilibrium between receptor functional states is critical for understanding and potentially designing efficient agonists (including agonists with desired functional selectivity) (Katritch *et al.*, 2013; Manglik and Kruse, 2017). Also, we shall remember that the knowledge in GPCR signaling is still increasing, these are some of the basic data known until know. Recent findings suggest different interactions with G proteins, even suggesting that there are no Gα and Gβɣ-dimer dissociations during activation but rather a reorganization in the structure able to transduce the signal (Frank *et al*., 2005).

3.3.7. GPCR dimerization role on activation

Numerous studies have suggested the existence of homodimers, heterodimers, and higher oligomers important for many GPCRs' activities. Further, it has been proposed their role in the regulation of GPCR function and cross talk. This matter has been kept under doubt due to the controverted results, some of the techniques make specialists consider this structures as an artifact, especially regarding *in vitro* studies (Kenakin, 2001; Katritch *et al.*, 2013). Besides these opinions, the amount of studies which face the occurrence of these dimers are increasing and seem important for the future understanding of GPCR signaling.

Dimerization activation of GPCRs has been proposed to be important for certain signaling pathways, as well as for the function of receptors. The receptors assume different states as monomers or dimers and their signals and functions are also different.

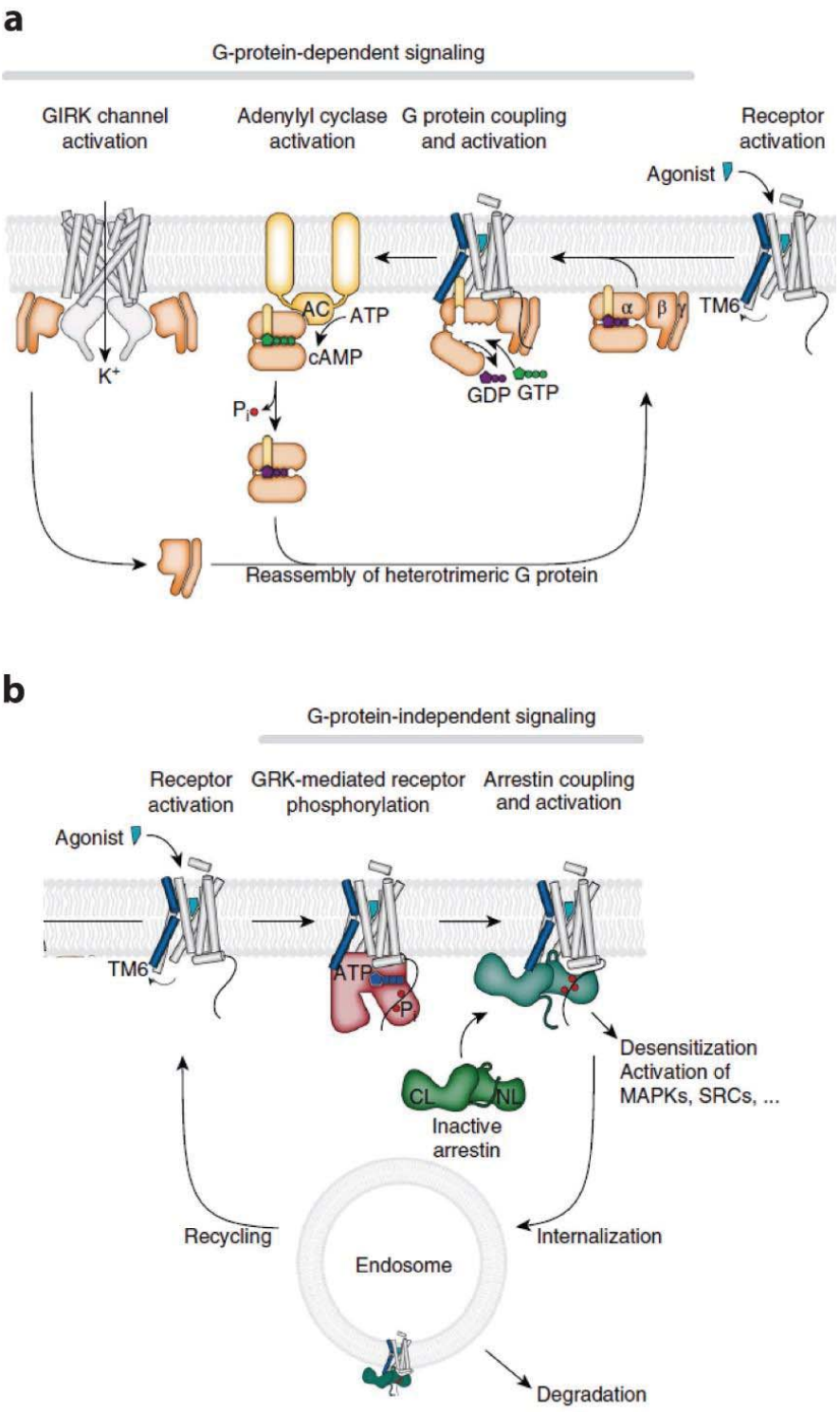

Figure 16. G-protein dependent and β-arrestin dependent activation of GPCRs (Image obtained and modified from Hilger *et al*., 2018)

Some receptors' differential activation precise dimerization in order to give a certain response. This means that a certain response by the GPCR composing the dimer will only be produced in the presence of the other and never as monomers. Besides, it has been detected that the components are able to exchange the signal from a G-protein dependent transduction to an arrestin-dependent one. As dimers, GPCRs are as well able experience a ***transactivation of the receptor***. This transactivation consist of a signal transduction combination with another type of receptor (i.e. tyrosine kinase receptors (RTKs)). The obtained signal of the transactivation will also be conditioned to the presence of both components. Thought-provoking to this type of signal is the idea of a ligand-dependent and a ligand-independent signal given by both receptors. Finally, a ***biphasic activation*** is another unique activation pattern of GPCRs where there are two different phases of activation for one type of receptor; an early phase detected within the first 5 to 10 minutes and late phase observed past 90 to 120 minutes. Both phases may have different effectors and responses. Altogether, these types of activation expand the repertoire of GPCR signaling and function (Wang *et al*., 2018). A summarized scheme of GPCR signaling responses is illustrated in figure 17.

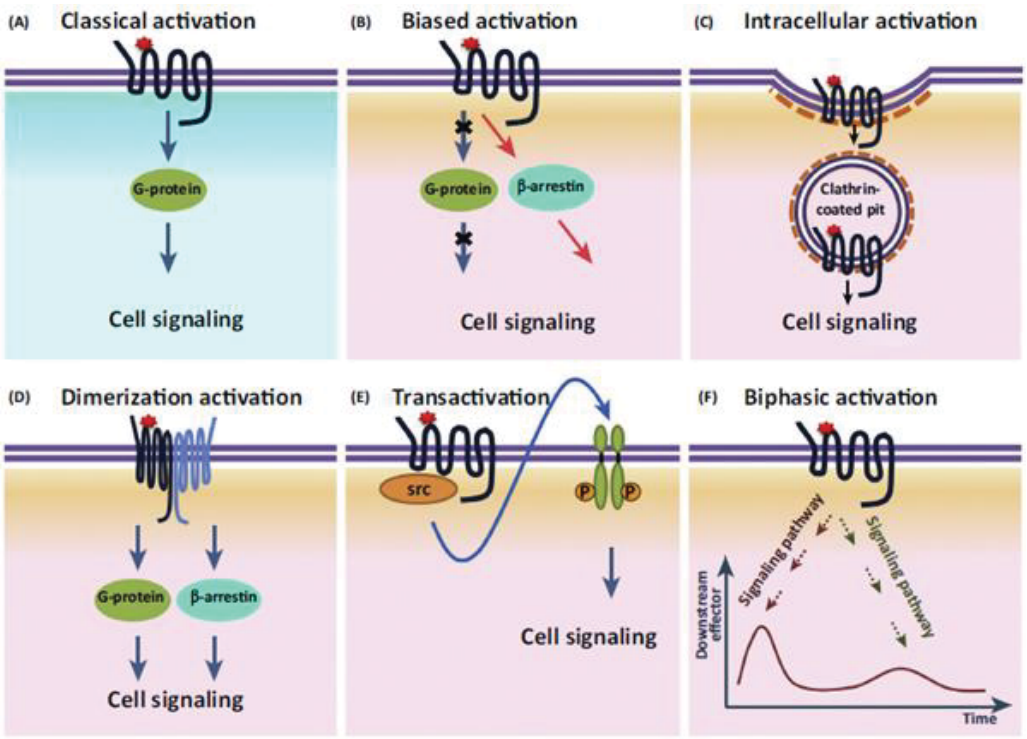

Figure 17. Models of GPCR activation (Image obtained from Wang *et al*., 2018)

3.4. GPCRs activated by circulating metabolites and energy substrates

Earlier in this dissertation, it was mentioned the great variety of molecules that can target a GPCR. One type of molecules that have been gaining attention in the past few years regarding these receptors' activation are circulating metabolites and energy substrates. GPCRs are able to sense changes in extracellular metabolites that fluctuate in between specific ranges of concentrations. The changes are very well identified by the specific GPCRs that are to be signaled and as so, they tend to modulate metabolism with specific responses (Recio *et al*., 2018). Since the development of new technologies that are able to deorphanize GPCRs, scientists have found a large group of metabolite-sensing GPCRs. Furthermore, these metabolite-sensing GPCRs have been found to be expressed in cell types important for metabolism and immune response (i.e. adipocytes, hepatocytes, β-cells and macrophages). Given these findings, recent works aiming to target these receptor in order to better understand their biochemistry have proven their important roles in metabolism, physiology and the progression of metabolic abnormalities associated with obesity (Alvarez-Curto and Milligan, 2016; Yonezawa *et al*., 2013).

Hence, metabolites possess a dual role in the coordination of metabolism since they are a source of energy (that will also modulate metabolism at the point of electron transport) and they are able activate GPCRs resembling a hormonal molecule. This mechanism of metabolite sensing-GPCRs gives them a quality to modulate metabolism and gives an opportunity to develop new therapies for the treatment of metabolic disorders (Blad *et al*., 2012). A large number of GPCRs have been reported to be activated by intermediates of energy metabolism, including free fatty acids (FFAs), lactate, succinate, and ketone bodies (among others); table 8 shows a compilation of some of the metabolite-sensing GPCRs and their described roles.

Table 8. Summary of the currently recognized and potential metabolite-sensing GPCRs (ligands, associated G protein(s), expression profile and effects)				
Receptor	**Ligand(s)**	**G proteins**	**Expression**	**Effects**
Carbohydrates				
TAS1R2–TAS1R3 (T1R2/T1R3)	Glucose, lactose, fructose, maltose and sucrose	Gustducin, G_i	Type II taste cells Enteroendocrine Cells Pancreatic islets	Sweet taste, glucose metabolism (Murovets *et al*., 2015)
Lipids and derivatives				
Short-chain fatty acids (SCFA)				
FFAR2 (GPR43)	Short-chain fatty acids C2=C3≥C4≥C5 (formate, acetate, propionate, butyrate, valerate, caproate, heptanoic acid)	G_q/G_{11}, G_i β-Arrestin 2	Enteroendocrine cells Adipocytes Neutrophils Eosinophils Pancreatic islets	Regulation of energy balance, regulation of insulin-mediated fat accumulation, gut homeostasis, anti-inflammatory, GLP1 secretion, neutrophil chemotaxis
FFAR3 (GPR41)	Short-chain fatty acids C3=C4=C5>C2 (acetate, propionate, butyrate, valerate, caproate, heptanoic acid)	G_i β-Arrestin 2	Enteroendocrine cells, pancreatic islets and sympathetic ganglia	Regulation of energy balance, leptin production, anti-inflammatory, expression of PYY
GPR65	FA derived protons (H+) ← SCFAs Psychosine	G_s	Blood leukocytes Spleen Lymph Nodes Thymus Lung Small intestine	Ulcerative colitis genetic risk (Tan *et al*., 2017)
GPR132	FA derived protons (H+) ← SCFAs Oxidized derivatives of linoleic and arachidonic acids	G_i, G_q	Immune cells Spleen Lung Heart	Regulate intestinal inflammation, chemotaxis, atherosclerosis
Medium-chain fatty acids (MCFA)				
GPR84 (EX33)	MCFAs (C2–C6): capric acid, decanoic acid, and undecanoic acid.	G_i	Adipocytes Immune cells (macrophages, neutrophils) Leukocytes, Microglia cells	LPS-stimulated IL-12 production

Long-chain fatty acids (LCFA)				
FFAR1 (GPR40)	Long-chain fatty acids C8–C22, saturated and unsaturated	G_q/G_{11}	β-cells of pancreas Enteroendocrine cells Immune Cells Taste buds CNS	Enhanced glucose-stimulated insulin secretion; GLP1 and GIP secretion. Inflammation.
FFAR4 (GPR120)	Long-chain fatty acids C14–C18 (saturated); C16–C22 (unsaturated) Specially, n-3 PUFAs and PAHSAs	G_q/G_{11}	Intestinal epithelium (enteroendocrine cells) Adipocytes Type II taste cells Macrophages Colon cells Pancreatic cells	Secretion of GLP1 and GIP; inhibition of inflammatory signaling in macrophages regulation of insulin secretion by GLP-1 (Role in diabetes?) Adipogenesis
GPR32	Resolvins (derived from docosahexaenoic acid)	G_q β-Arrestin	Neutrophils Macrophages	Anti-inflammatory
GPR119	Oleoylethanolamide lysophosphatidylcholine (derived from oxidation of omega-6 fatty acids)	G_s	Pancreas Full gastrointestinal Tract Neutrophils Macrophages	Stimulates insulin and glucagon secretion, stimulates GLP-1 and GIP secretion
TGR5**	Bile acids: lithocholic acid, deoxycholic acid, chenodeoxycholic acid, cholic acid	G_s	Immune cells Adipocytes Enteroendocrine cells Liver Gallbladder	Anti-inflammatory, stimulates gut hormone Secretion, inhibits Hepatosteatosis, modulates secretion
Hydroxycarboxylic acids				
HCA1 (GPR81; GPR104)	Lactate	G_i	Adipose tissue Liver Skeletal muscle Kidney	Mediates anti-lipolytic effects of insulin

HCA2 (GPR109A; HM74A; PUMA-G; NIACR1)	3-hydroxybutyrate **Butyrate (Mielenz, 2017) **Niacin (tryptophan metabolite) (Thorburn et al., 2014)	G_i	Adipose tissue Immune cells Keratinocytes Intestinal and retinal epithelium	Mediates anti-lipolytic effects of ketone bodies; activation of immune cells
HCA3 (GPR109B; HM74; NIACR2)	3-hydroxyoctanoate	G_i	Adipose tissue Immune cells Colon epithelium	Anti-lipolytic effects, activation of immune cells
Citric acid cycle intermediate receptors				
SUCNR1 (GPR91)	Succinate	G_i, $G_{q/11}$	Adipocytes Liver Heart Retinal neurons Intestine Spleen Dendritic cells Kidney Platelets	Sensing of cell stress and hypoxia, proinflammatory, migration of Langerhans cells, hematopoiesis, angiogenesis
OXGR1 (GPR80; GPR99)	α-ketoglutarate	$G_{q/11}$	Kidney Smooth muscle Testis	Inflammation, changes in the mucosal epithelium, and an increase in fluid behind the eardrum
Aminoacids (or aminoacid intermediates)				
GPR35	Kynurenic acid	G_q, G_i, G_{13}	Duodenum Colon Small intestine Stomach Gall bladder Spleen Appendix Bone marrow Adipose tissue	Stimulates lipid metabolism, thermogenic, and anti-inflammatory gene expression in adipose tissue (Agudelo *et al.*, 2018) Anti-inflammatory properties Ulcerative colitis genetic risk and inflammatory bowel disease (Tan *et al.*, 2017)

GPR142	Tryptophan	G_i/G_q	Enteroendocrine cells Endocrine pancreas Immune cells	Stimulates gut hormone secretion, stimulates insulin secretion
CasR	Phenylalanine	G_i/G_q	Parathyroid Kidney Immune cells Enteroendocrine cells Endocrine pancreas	PTH synthesis and secretion, controls divalent cation flux, anti inflammatory, stimulate GLP-1 secretion
Taar1	Tyramine	G_s*	Neurologic system Blood cell Immunologic functions	Immunomodulation Cancer (Miller, 2011)
FPR1/2	N-formyl-methionine	G_i/G_q	Innate immune cells Leukocytes Hepatocytes	Phagocytosis
These table is a compilation of information from several sources taking as basis: Blad *et al*., 2012; Thurnburn *et al*., 2014; Tan *et al*., 2017; Husted *et al*., 2017; Milenz, 2017; Recio *et al*., 2018) **Bile acids receptor is considered in this table. ***Some assays report these metabolites as activators.				

3.4.1. GPCRs activated by fatty acids

Lipids were not recognized as important ligands of GPCRs until not so long ago. Actually, it was not until early 90's when the first cannabinoid receptor was cloned as the first lipid-activated GPCR (Matsuda *et al.*, 1990). In present days, we know that lipids are important for GPCR structure and stability and that lipid species can exert certain effects on cell performance through GPCRs. The structure of these lipid-signaling GPCRs will also be special due to the fact that the N-terminus and the ECLs need to form an hydrophobic pocket for them be able to bind to the receptor. (Im, 2004; Obinata *et al*., 2005; Alemany *et al*., 2007; Lu and Wu, 2016; Miyamoto *et al*., 2016).

Out of the group of lipids, FFAs have revealed to be not only important nutrients from dietary fat (since they provide high amounts of energy) but also important for the composition of the cellular/structural lipids (i.e. lipid bilayer phospholipids). Moreover, they also play a key part as signaling molecules that mediate critical biological functions (Recio *et al*., 2018). They comprise a carboxylic acid attached to an aliphatic tail of different chain dimensions. These dimensions are the basis of FFA classification into short chain fatty acids (SCFAs), with 6 or less carbon chains; medium chain fatty acids (MCFAs), with 7−12 carbon chains; and long chain fatty acids (LCFAs) with ≥13 carbon chains. Also, these LCFAs are able to contain unsaturations, giving rise to a second classification of these FAs into the saturated (SFA), monounsaturated (MUFA), and polyunsaturated (PUFA) fatty acids (Milligan *et al*., 2017). As mentioned, lipid-mediated GPCR signaling is recent to our knowledge. Previous data on the metabolic and signaling roles of lipids were mostly oriented to the activation of PPARs and FABPs (Hara *et* al., 2011; Michalik *et al*., 2006). Out of this list, the recognized GPCRs known to be activated by FFAs are GPR40 (FFAR1), GPR41 (FFAR3), GPR43 (FFAR2), GPR84 (EX33) and GPR120 (FFAR4). GPR40, GPR41 and GPR43 are found in a cluster present on chromosome 19q13.1, GPR84 is located on chromosome 12q13.13 and GPR120 is located on chromosome 10q23.33 (Ichimura *et* al., 2009). Their tissue preferential expression and their activation effects are listed on table 8. Out of this subgroup, we can point out a pair of GPCRs that have been studied with emphasis in current scientific works

(especially regarding inflammation and obesity related comorbidities). This is due to the fact that in the recent years, a subgroup of FFA has been described to exert beneficial effects on the physiology of the individuals, the polyunsaturated fatty acids (Kuda *et al*., 2018).

3.4.2. GPCRs activated by polyunsaturated fatty acids

It was detailed that FAs are able to contain unsaturations, these unsaturations may be present in several positions which are also important. They are defined by how far from the terminal carbon the first unsaturation occurs. Out of this characteristic we can have 3 main types of unsaturated FAs (figure 19), omega-3 (n-3), omega-6 (n-6) and omega-9 (n-9, mainly MUFAs) (Milligan *et al.*, 2017). PUFAs include two subgroups of FA: n-3 and n-6. They started to become popular due to the fact that Eskimos had lower cardiovascular diseases-related mortality and this was linked to a diet rich in this type of FA (Wiktorowska-Owczarek *et al*., 2015). While n-6 FAs are more related to the formation of prostanoids with a proinflammatory activity, n-3 FAs have shown to have potent anti-inflammatory effects (Oh *et al*., 2010; Nowak, 2009).

The most abundant and important, considering dietary intake, n-3 FAs are α-linolenic acid (ALA), eicosapentaenoic acid (EPA) and docosahexaenoic acid (DHA) (illustrated in figure 18). The effects observed after the consumption of these n-3 FAs are the maintenance of the cell-membrane fluidity, inhibition of inflammatory processes, decrease the secretion of pro-inflammatory cytokines by monocytes/macrophages, decrease in the susceptibility to ventricular rhythm disorders of the heart, improvement of vascular endothelial cells function, inhibition of blood platelet aggregation and decrease in hepatic lipogenesis (Nowak, 2009). Still, there are some studies that show evidence against the healthy effects of increasing n-3 consumption (Yip *et al*., 2013). So, it is essential to better understand the biochemical effects that n-3 FAs exert. In that context, we step in the fact and new evidence revealing a subgroup in the lipid-activated GPCRs, the GPCRs activated by PUFAS.

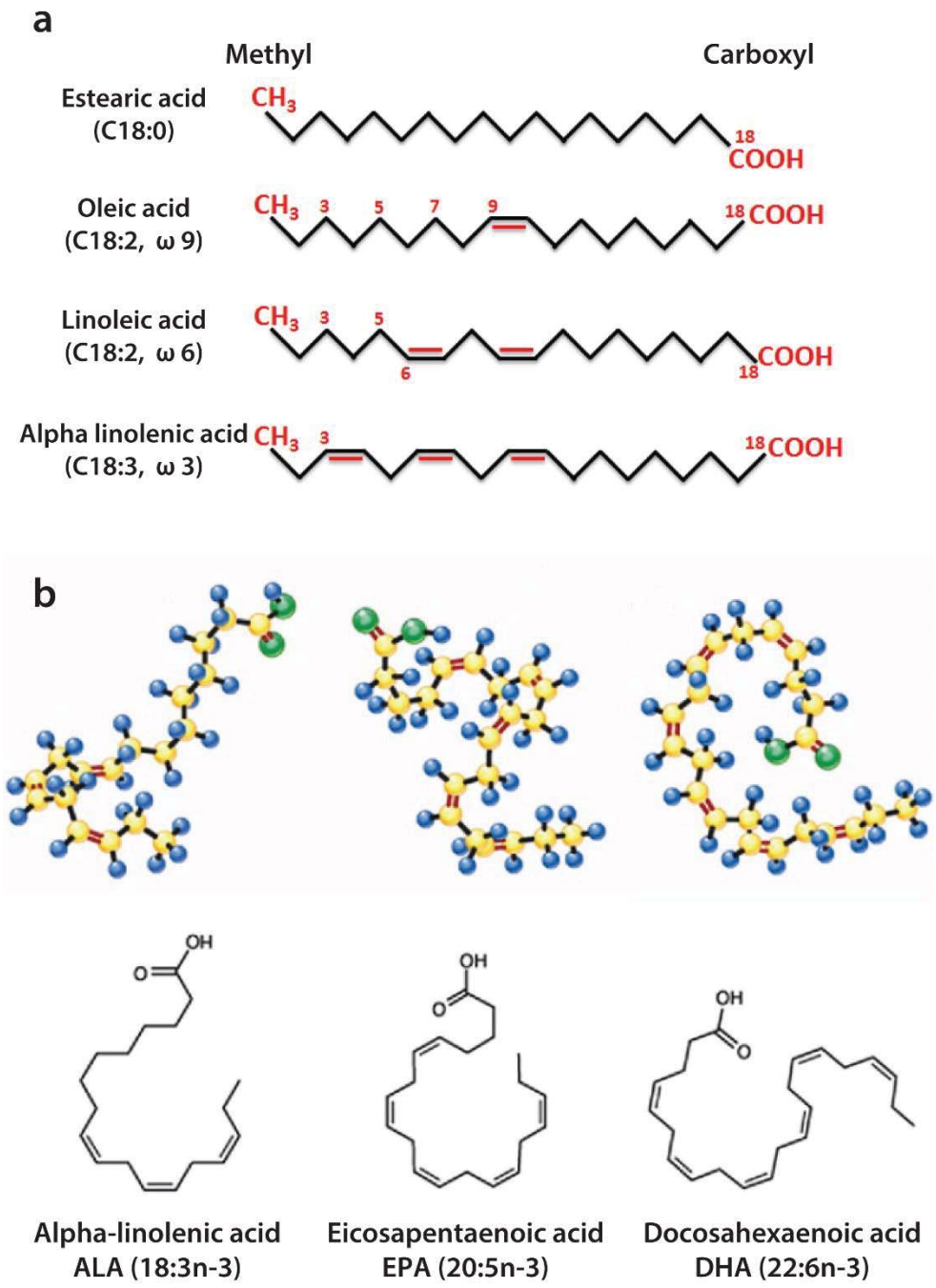

Figure 18. Fatty acid examples. A saturated fatty acid, a MUFA (n-9) and two PUFAs (n-6 and n-3) (**a**); and the structures of the n-3 FAs ALA, EPA and DHA (**b**) are shown. (Image obtained and modified from Valenzuela and Valenzuela, 2013 and Mozaffarian and Wu, 2011).

The GPCRs activated by PUFAs are GPR40 and GPR120 (figure 19). Both receptors have multiple reports on contributing to an improvement of the metabolic conditions upon activation. Yet, their distribution and biological response are not even. This suggests they both have specific and complementary roles. While GPR120 is found importantly expressed in ileum, colon, adipocytes, macrophages and lung (as the main sites of expression), GPR40 is mostly found in pancreatic beta cells and liver. So GPR120 has been linked to metabolic regulation and immune response (anti-inflammatory effects) while GPR40 has been more attached to insulin secretion (Itoh *et al*., 2003; Hirasawa *et al*., 2005; Cornall *et al*., 2014; Hara *et al*., 2011).

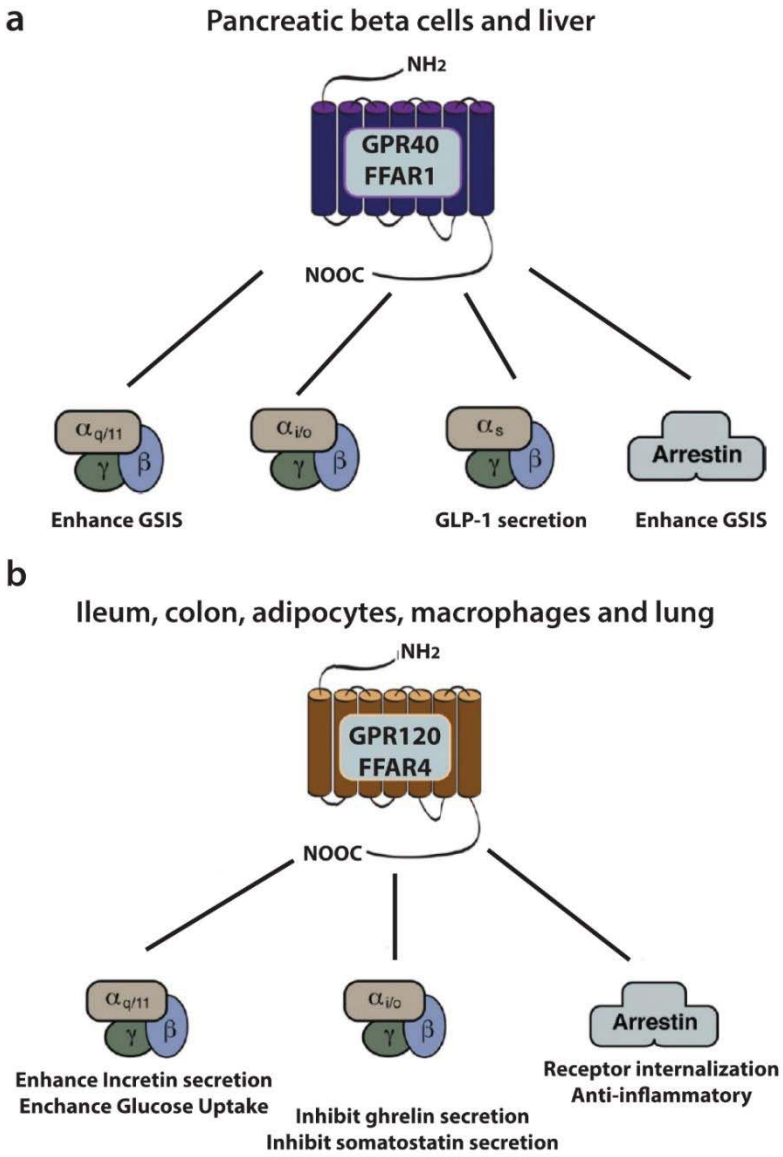

Figure 19. GPR40 (a) and GPR120 (b) expression, G-protein or arrestin interactions and effects (image obtained and modified from Milligan *el at.*, 2017).

3.4.3. GPR120 or Free fatty acid receptor 4

GPR120, also known as FFAR4, is a GPCR member of the Rhodopsin family. At a very first sight, GPR120 has a different sequence homology to the rest of the free fatty acid receptors (FFARs). For this reason, it resulted awkward to classify it in this group of receptors for the first research group that achieved its deorphanization (Hirasawa *et al*., 2005; Davenport *et al*. 2013). Hirasawa and co-workers (2005) identified this receptor to be responsive to PUFAs and from them on, the receptor was considered a FFAR. In the present, several synthetic agonists and antagonists have been developed. These compounds have helped elucidate mechanism of action, roles and also therapeutic effects of GPR120 activation. Table 9 lists the main agonists and antagonists reported for GPR120.

Table 9. Main agonists and antagonists reported for GPR120

Agonists	**Antagonists**
Natural	
Alpha-linolenic acid	
Docosahexaenoic acid	
Eicosapentaenoic acid	
Grifolic acid	
Branched Fatty Acid Esters of Hydroxy Fatty Acids (FAFHAs)	AH 7614
Synthetic	
GW9508	
TUG-891	
Compound A	
NCG-21	

Data obtained from Oh *et al*., 2010 and Milligan *et al*., 2017.

3.4.4. Structural characteristics and polymorphisms

Depending on the species where it is studied, GPR120 (or FFAR4) can exist in multiple splice variants. For the purpose of this dissertation we will focus on human (*Homo sapiens*) and mice (*Mus musculus*) (Watson *et al*., 2012). Humans have shown to

express two variants, a long and a short isoform. While the short isoform corresponds to the one found in mice (species only expressing the short isoform), the long is characterized by a 16 amino acid insertion in the third intracellular loop of the short variant. It results interesting that this former variant seems only present in colon and the ability to cause an increase in intracellular calcium [Ca^{2+}] (and a signal transduction) remains unclear (Moore *et al*., 2009; Watson *et al*., 2012). In relation to human variants, there have been reported a couple of polymorphisms. Both classified as rare in the European populations. One is $R254H^{IL3}$, a single-nucleotide polymorphism in the short isoform of FFA4; the second is $R270H^{IL3}$ variant which is observed in the long isoform. Both polymorphisms have been linked to obesity and possibly to increased fasting glucose in both, human and mice. This polymorphisms were mainly related to the signal mediated by G-proteins (where there was observed either a decreased or none transduction of the signal) but not in arrestin mediated signaling (Ichimura *et al*., 2012). Although, Vestmar and co-workers (2016) failed to reproduce this correlations.

3.4.5. Distinctiveness in the signaling mediated by GPR120

As explained in the previous sections, GPCRs are given their name due to the fact that they interact with G proteins. In the case of GPR120, the G-proteins described (so far) to mediate signal transduction pathways are Gαq/11 and Gαi (Briscoe *et al*., 2006; Engelstoft *et al*., 2013). However, and also explained earlier in this text, there are alternative mechanisms for the signal transduction of this receptors. In this case, and also reported by Hirasawa and coworkers in 2005, it was observed that the activation of this receptor caused a fast internalization. This rapid internalization of the receptor is mainly due to the interactions of the C-terminus of the receptor with β-arrestins 2 and 3 (Watson *et al*., 2012; Hudson *et al*., 2013). The internalization response has been attributed to the activity of kinases (i.e. GRKs, also described earlier) and are presumably dependent on the cell type and the agonist. What remains to be elucidated are the mechanisms and specificity of this response (Burns *et al*., 2014).

3.4.6. Tissue expression and roles

GPR120 was initially described to be a GPCR characteristic of the intestinal cells. Indeed, **lower intestine** shows an increased expression of this receptor and it also seems to be regulated by diet and microbiota. In intestine there is an increase in GPR120 expression upon diet induced obesity (DIO) (*Homo sapiens*, *Ratus norvericus*) (Duca *et al*., 2013; Paulsen *et al*., 2014). Also, *in vitro* studies demonstrate that different species of microbiota show differential expressions of the receptors in CaCo2 intestinal cells (Fredborg *et al*., 2012). Activation of GPR120 in enteroendocrine cells has proven its capacity to induce the secretion of 'gut hormones' from these cells. Glucagon-like peptide-1 (GLP-1) (Hirasawa *et al*., 2005), cholecystokinin (CCK) (Tanaka *et al*., 2008), Gastric inhibitory polypeptide (GIP) (Iwasaki *et al*., 2015) and ghrelin (Lu *et al*., 2012) have been proposed to be regulated by enteroendocrine cells in response to GPR120 activation by LCFAs. These effects were lost for GIP in the GPR120-/- *in vivo* models but not affected in the case of GLP-1, CCK and ghrelin (Xiong *et al*., 2013; Liou *et al*., 2011; Engelstoft *et al*., 2013).

On the other side, it is now well established that there is a high presence of metabolite-sensing GPCRs in adipocytes and other **adipose tissue** cells (Blad *et al*., 2012). GPR120 is part of this nutrient-sensing squadron at the AT. Adipocytes and AT express GPR120 importantly as reported by various groups (including ours) and it is expressed in greater quantity in brown adipose tissue (Gotoh *et al*., 2007; Miyauchi *et al*., 2009; Blad *et al*., 2012; Rosell *et al*., 2014). The specific effects concerning **WAT and white adipocyte** include a requirement of this receptor for an appropriate cell differentiation and a marked regulation of lipolytic enzymes thus controlling circulating levels of TG (Gotoh *et al*., 2007). GPR120 activation *in vitro* also showed $G\alpha_{q/11}$-dependent translocation of Glut4 to the membrane consistent with an increase in the expression of glucose metabolism genes in 3T3 L1 cells. These results suggest a role in glucose oxidation in white adipocytes (Oh *et al*., 2010; Liu *et al*., 2012). Likewise, the activation of the receptor in these cells caused a decrease in the expression and release

of inflammatory factors such as MCP-1 and IL-6 as provoked by TNFα treatment *in vitro* (Cranmer-Byng *et al*., 2015).

Few reports were available at the beginning of this project in relation to **BAT and brown adipocytes**. What was known at the moment was that these tissue expressed high levels of this receptor. Likewise, upon cold exposure, BAT increases GPR120 gene expression levels which suggested a role in thermogenesis (Rossel *et al*., 2014). Opposite to what was found on intestine, it is still unclear whether obesity induces an up-regulation or a down-regulation of the expression of this receptor in this tissue (Ichimura *et al*., 2012; Rodriguez-Pacheco *et al*., 2014).

Also important to this tissue, and in relation to other tissues' metabolic behavior, is the expression of this receptor in **macrophages**. It was previously mentioned that GPR120 showed an increased expression in cells typical of the immune system, however, not all of these cells' responses upon activation of GPR120 have been explored. Macrophages are one of these cells enclosed in the group of immune system response. Their name is derived from the greek and meaning ''large eat-ers''. They are a type of white blood cells which are able to phagocyte strange cells or substances not expressing marker proteins in the surface (similar to those expressed by typical and healthy cells on the environment they are to monitor). So, their role is critical for the control of the healthy status of the organism as a whole but is crucial on tissue specific control of populations. (Ovchinnikov, 2008). Regarding their role in the AT, it has been reported that these cells have an increased expression of this particular receptor and, surprisingly, macrophage derived secretions are able to induce the expression of GPR120 in adipocytes (Trayhurn and Denyer, 2012). The precise role in macrophage inhibition of inflammation has been more widely explored. In this cell type, it is well recognized that β-arrestin 3 plays a central role in the signal transduction upon activation. Once the ligand, mainly the n-3 DHA in this case, is bound to the receptor, β-arrestin 3 is recruited to the GPCR. This event causes β-arrestin 3 to interact with a TAK1 binding protein (TAB1). This sequestration of TAB1 prevents it from binding TAK1. By preventing

TAB1/TAK1 interaction, GPR120 blunts NFκB activation and also the release of inflammatory cytokines such as TNFα and IL-6. Other groups have argued whether this signal also produced a down-regulation in cyclooxygenase 2 (COX2) preventing, with this, the production of prostaglandin E_2 (PGE_2). However, opposing results keep this theory to be better explored. What is true is that the effects over inflammation caused by the activation of the receptor in these cells (specifically being activated with DHA) lead to an overall improvement of the metabolic conditions (Oh *et al*., 2010; Trayhurn *et al*., 2012; Li *et al*., 2013; Liu *et al*., 2013; Frolov *et al*., 2013).

We mentioned earlier that the impaired activation of the receptor or its absence led to the development of obesity and to an increase in fasting plasma glucose (human polymorphisms or loss-of-function animal models). This observation gave rise to a series of investigations regarding the effects of GPR120 activation, especially considering the healthy effects of n-3 PUFAs on the overall metabolic status. Despite all these supporting information and results with GPR120-deficient animal models, it remains unclear the exact role of GPR120 on the improvement of systemic insulin sensitivity due to PUFAs supplementation (Oh *et al*., 2010; Ichimura *et al*., 2012; Suckow *et al*., 2014; Bjursell *et al*., 2014).

Smooth muscle lung cells, pancreatic islets' cells, taste buds monocytes and other immune cells have also been reported to express the receptor. The mechanisms and effects of the activation of the receptor in these cells has not been elucidated. Relevant to metabolism and as a therapeutic target of another important pathologies like cancer, the expression of GPR120 seems to be regulated (enhanced or reduced) in different cancer cells lines. The mechanisms remain unclear, compared to the actual knowledge regarding the mechanisms in inflammation. However they continue to be promising in the treatment of cancer due to several data proposing chemotherapy resistance. Some other authors have found contradictory data, though (Wu *et al*., 2013: Liu *et al*., 2015; Houthuijzen *et* al., 2017; Zhu *et al*., 2017; Zhu *et al*., 2018; Senatorov and Moniri, 2018).

The current knowledge regarding the expression of GPR120 gives a promising landscape of the pharmacological opportunities targeting the receptor. An increased research concerning other mechanisms by which the activation of this type of receptors achieve a general improvement in the metabolic status is necessary. The generated knowledge would help elucidate their physiological role. In this context, the work presented in this dissertation directed strategies to better understand a possible modulation of a hormone-like batokine, FGF21, by the activation of GPR120.

4. Fibroblast growth factors family

The FGFs (Fibroblast Growth Factors) were initially described almost 8 decades ago (Trowell and Willmer, 1939). They are a highly conserved family among the animal kingdom and have shown to be ubiquitously expressed in metazoans. The aminoacid sequence homology they share oscillates from 13 to 71 %. Regarding the size of the polypeptide, it varies from 17 to 34 KDa but despite the size differences they all contain a conserved central domain formed by a 120-130 aminoacid sequence. Concretely in vertebrates, 22 members have been described. These members are highly conserved in function and structure, even regarding isoforms. Besides this, they also share a high affinity for HSGAG (heparan sulphate glycosaminoglycans) necessary for FGFs (with the exception of FGF11-14) to appropriately activate the four types FGF receptors (FGFR) (Goetz *et al*., 2007; Maddaluno *et al*., 2017; Porta *et al*., 2017).

FGFRs are high-affinity single-pass transmembrane tyrosine kinase receptors. There are four main types FGFR1, FGFR2, FGFR3 and FGFR4. Recently, a receptor named FGFRL1 (fibroblast growth factor receptor like 1) which lacks the intracellular tyrosine kinase domain and antagonizes some of the functions has been described. Regarding special mechanism of signaling, the traditional FGFs require heparan sulfate as a co-factor in order to trigger a signal transduction. However, a subfamily of FGFs (FGF19) display endocrine characteristics, this subfamily requires another protein that will act as a co-receptor, the proteins that will act as co-receptor on this process are proteins named klotho (Kurosu *et al.*, 2007; Trueb, 2011; Kyrou *et al.,* 2017). The relevance of these proteins can vary depending on the stage of life at which the organism is. As an embryo, FGFs will play central part in the regulation, proliferation, migration and cell differentiation to proper achieve development. Once the organism reaches adulthood, FGFs take part in tissue repair, cell damage and are crucial for homeostasis achievement (Ornitz and Itoh, 2015; Li *et al*., 2016). These last characteristics helped to describe some FGFs, identifying them due to their role as growth or mitogenic factors. Some others, like FGF21, were firstly described and then corroborated as a member of the family (Ornitz and Itoh, 2001; Itoh and Ornitz, 2011).

Since 2012, FGFs have been classified in seven subfamilies (depicted in figure 21) based on the aminoacid sequence similarity (Oulion *et al*., 2012). Besides this similarity, they also share functionality during the organism development or other biochemical properties. The fact that the numbers sum up to 23 when it was mentioned that 22 have been described is because FGF19 has an orthologous in mice, FGF15. This has also been reported for some other FGFs in other vertebrates which suggests that none FGF has been acquired after the division of mammals form the rest of vertebrates (Itoh and Ornitz, 2008). Regarding the distribution of the FGFs in the genome, they are at multiple localizations suggesting duplications and translocation during the evolution. Mice (*Mus musculus*) and humans (*Homo sapiens*) share the seven identical families (previously mentioned), this makes this specie a good model for studying these proteins (Itoh and Ornitz, 2008; Li *et al*., 2016).

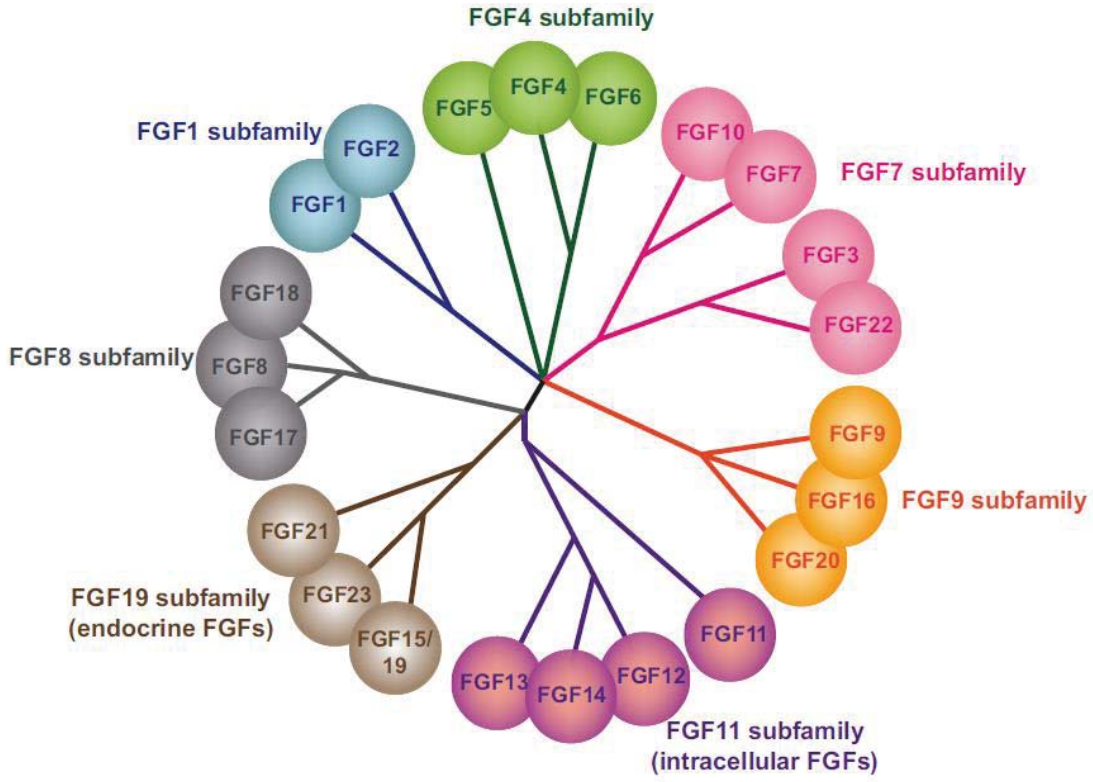

Figure 20. FGF family phylogeny (image obtained from Maddaluno *et al*., 2017).

4.1. The structure of a FGF

FGFs contain a sequence of 120-130 aminoacids which form a β- trefoil structure. Paracrine FGFs contain 12 β- folds while endocrine just contain 11. The central structure is escorted by aminoacid sequences, N- or C- terminal, which confer them their special functions including heparan sulfate interaction. (Goetz *et al*., 2007; Goetz and Mohammadi, 2013). Regarding FGF21 structure, it also possesses a β- trefoil structure and contains a 14 aminoacid-long C-terminus domain necessary for β-klotho interaction (co-receptor for its signal transduction). This C-terminus determines FGF affinity to the receptor. Endocrine factors' C-terminus shows a reduced affinity to the receptor which is the essential characteristic for their endocrine activity (Yie *et al*., 2009; Micanovic *et al*., 2009; Li *et al*., 2016).

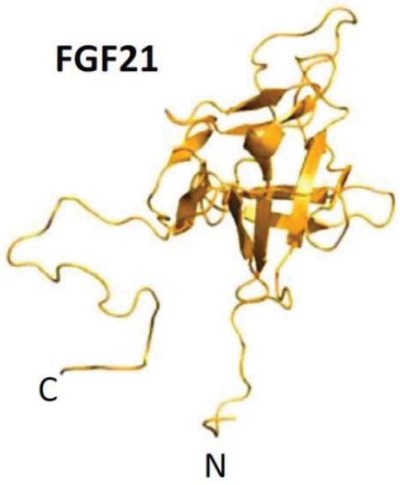

Figure 21. FGF21 structure (image obtained from Gimeno and Moller, 2014).

4.2. FGFs classification by functional characteristics

Besides the classification by phylogeny, they can also be classified by their functionality. The 22 members of the FGF family, and their receptors, can be expressed in all or many of the tissues in an organism. Considering their mechanism of action, FGFs can be categorized into intracrine, autocrine/paracrine and endocrine subgroups (Itoh and Ornitz, 2011; Kyrou *et al*., 2017).

4.2.1. Intracrine FGFs

This group of FGFs are not secreted from the cell, this means that their mechanism of action and targets are situated inside. This also means that an FGFR won't be necessary for them to activate a signal transduction. Instead, they are able to interact with the intracellular domains of sodium voltage-dependent channels and other neuronal MAPK. The described members as part of this family are FGF11, FGF12, FGF13 and FGF14 and have been studied for their role in electrical excitability of neurons (Kyrou *et al*., 2017).

4.2.2. Autocrine/paracrine FGFs

This FGFs have an N-terminus peptide that acts like a signal in order to be able to be secreted from the cell. This peptide is also the site of interaction with the heparan sulfate proteoglycans for the adequate interaction with the FGFRs and a co-receptor in order to trigger a signal transduction. When these FGFs interact with the FGFR and co-receptor, it allows a receptor dimerization, phosphorylation and the activation of the signal transduction. Heparan sulfate in these molecules also works as a strap which maintains the molecule within the same tissue of production making them able to activate either the same cell that secreted them or the neighbor cells. Most of the FGFs subfamilies are in this category: FGF1/2/5, FGF3/4/6, FGF7/10/22, FGF8/17/18 and FGF9/16/20. Interesting for this group is the ability of some factors to translocate to the nucleus and act in an intracrine manner (Kyrou *et al*., 2017).

4.2.3. Endocrine FGFs

The low affinity for heparan sulfate makes this FGFs able to circulate freely through blood in the organism activating cells in other tissues. The low affinity for the heparan sulfate forces them to require another co-receptor to achieve the activation of

the receptor. This co-receptor is often a klotho protein (with several forms later described). They act mostly as differentiation factors in embryos and as hormones in adult organisms. Part of this group are FGF15/19, FGF21 and FGF23.

4.3. FGFs receptors (FGFRs)

As it was briefly mentioned, FGFs exert their effects upon the binding to receptors present in the cell membranes. The FGFRs, possess a canonical tyrosine kinase receptor structure of an approximate of 800 aminoacids. They are conformed by three extracellular Immunoglobulin (Ig)-type domains (IgI, IgII, IgIII), two of them, IgII and IgIII, forming the FGF-binding site structure. They also present acidic residues between IgI and IgII (apparently related to a self-inhibition process), a single pass transmembrane domain and an intracellular tyrosine kinase domain (Wang *et al*., 1995; Powers *et al*., 2000).

The FGFRs are codified by four genes: FGFR1-4. These genes can be subject of exonic splicing generating a receptor with no IgI or without the acidic residues at IgIII. As a result of these splicing, there can be obtained two isoforms of each receptor (except for FGFR4), the isoforms will have different characteristics in the binding on the ligand and possibly modulating the response upon activation. The splicing causes and increase in the functionality of the FGFs since isoforms b are more present in epithelial cells wile isoforms c will be present in mesenchymal stem cells (MSCs) (Johnson *et al*., 1991; Itoh and Ornitz, 2004; Beenken and Mohammadi, 2009). Table 10 shows the affinity for the FGFRs established by the Baf3 cell mitogenicity assay for the members of the FGF19 sub-family, which are the endocrine FGFs like FGF21.

Table 10. Specificity of FGFRs for the FGF19 subfamily (endocrine factors)

	FGFR1b	**FGFR1c**	**FGFR2b**	**FGFR2c**	**FGFR3b**	**FGFR3c**	**FGFR4**
FGF15/19	-	+++	++	++++++	+	++++	++++++++
FGF21	+	+	+++	+++	+	+	++++
FGF23	-	+	++	+++	+	++	++++++
Information obtained from Mason, 2007							

4.4. Co-receptors mediating FGFs behavior and activity

Dictated by their aminoacid sequence, the FGFs will be able to interact with two main types of co-receptors. This will modulate their migration and stability outside the cell and will determine the magnitude and specificity of their signal.

4.4.1. Proteoglycans

Part of the receptor interaction and important for these factors is their ability to interact with the proteoglycans heparin or heparan sulfate. Both are proteoglycans abundant in the cell surface and in the cellular matrix, making it important for protein stability and retention in the tissue they are to target (especially for the paracrine/autocrine subfamilies). Once activated, the FGFRs targeted by paracrine FGFs cause a complex formation composed by the FGF, FGFR and HSGAG. The relation of the components should be in a strict dimer (2:2:2) due to a better stability compared to 1:1:1. This complex is also important because it increases the affinity between the ligands and the heparan sulfate causing a sequestration of the ligand and keeping it close to the area of activation. This dimerization causes an autophosphorylation of the substrates. Some examples of these substrates are FGFS2α (FGFR 2α substrate), PLC (Phospholipase C) or MAPKs (i.e. ERK1/2, relevant to FGF21 signaling) (Itoh and Ornitz, 2004; Kharitonenkov *et al*., 2008; Itoh and Ornitz, 2011; Goetz and Mohammadi, 2013). In the case of the endocrine factors, their low affinity for heparan sulfate helps them escape from the tissue they were produced and then put in circulation to target other tissues. This means that whenever they target a potential cell to activate they will need other type of proteins to help them interact and activate their receptors. These require co-receptors, the klotho proteins (Itoh, 2010, Tiseo *et al*., 2015).

4.4.2. Co-receptor β klotho

As mentioned, endocrine receptors precise a protein that facilitates their interaction with the FGFR, klotho proteins cover this role. There are 3 klotho proteins: α, β and lactase-like (LCTL) or ɣ. Klotho co-receptors are members of the 1β-glycosidase.

α and β Klotho, contain two β-glycosidase-like domains while ɣ-klotho just contains one. The three of them contain a transmembrane domain and a short cytoplasmic tail. While α-klotho has been reported to mediate FGF23 signaling, β-Klotho has been described for the downstream signaling of FGF21 and FGF15/19. Less is known about ɣ-klotho just being described as an additional co-receptor for FGF19 (Fon Tacer *et al*., 2010; Long and Kharitonenkov, 2011). In the case of endocrine FGFs, they require the formation of a ternary complex in the presence of the Klotho protein preserving a relation 1:2:1 in order to have an appropriate signal transduction. As endocrine factors, these FGFs are able to target most of the tissues, the presence of all the FGFRs in the tissues may imply the potential activation of all of them by the FGFs. However the activation of the signals in different tissues will be regulated by the expression of the co-receptors in the tissues. α-klotho expression will mark the activation of FGF23 and is mainly expressed in cerebellum, kidney and the reproductive organs. β-klotho (KLB), on its part, is predominantly expressed in metabolically active tissues (i.e. liver, pancreas, CNS, heart and adipose tissues) (Kurosu *et al*., 2007; Fon Tacer *et al*., 2010; Planavila *et al*., 2015). The abundance of the co-receptors and the isoforms of the FGFRs present in the tissue will also modulate the given response and interaction (i.e. c-isoforms have shown increased affinity for α and β-klotho cofactors) (Koruso *et al*., 2007; Goetz and Mohammadi, 2013).

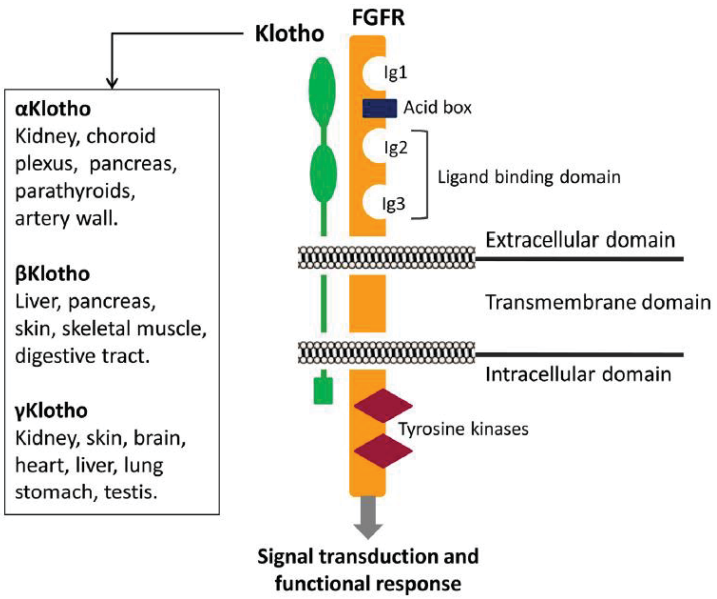

Figure 22. FGFR and β-Klotho structure (image obtained and modified from Donate-Correa *et al*., 2016).

4.5. Endocrine FGFs subfamily

Sub-family FGF19 has been reported to have important roles on homeostasis and their receptors are importantly expressed in a great variety of tissues. They differ from the canonical FGFs as they act as circulating hormones (Degirolamo *et al*., 2016). As for circulation levels, in humans the amount of circulating proteins of this nature may vary. This is mainly due to the fact that they are highly bioactive molecules with a half-life of approximately 30 minutes (Kharitonenkov *et al*., 2007; Angelin *et al*., 2012). In the past decade, FGF15/19, FGF21 and FGF23 have been the focus of attention due to their participation in inter-organ endocrine signaling axes. Their participation has been described important for maintaining whole-body homeostasis, as they govern bile acid, glucose and lipid metabolism, modulate vitamin D and phosphate homeostasis, and assist the metabolic adaptation in response to fasting. More importantly, marked modifications in circulating endocrine FGFs have been associated with human chronic diseases (i.e. obesity, T2DM, coronary artery disease and cancer). Thus, they have been explored due to their potential roles not only as biomarkers of the diseases' progression but also a therapeutic targets for the treatment of those diseases (Degirolamo *et al*., 2016; Donate-Correa *et al*., 2016; Kyrou *et al*., 2017). Table 11 summarizes the current knowledge on endocrine FGFs roles and their signaling in several diseases.

Table 11. Endocrine FGF physiological roles and signaling disorders

Endocrine FGFs	Physiological roles	Changes in signaling with disease
FGF15/19	↓ Bile acid synthesis ↓ Gluconeogenesis ↑ Protein and glycogen Synthesis	Increased in: extrahepatic cholestasis and chronic hemodialysis Decreased in: Inflammatory bowel disease, primary bile acid malabsorption NAFLD and obesity
FGF21	↑ Hepatic fatty acid oxidation ↑ Ketogenesis ↑ Gluconeogenesis ↑ Thermogenesis ↑ WAT browning ↑ Growth hormone resistance ↑ Weight loss ↓ Ovulation ↓ Growth hormone signaling	Increased in: T2DM, MS, NAFLD and coronary heart disease Decreased in: anorexia nervosa

FGF23	↓ Renal phosphate absorption ↓ Bone and renal calcium reabsorption ↓ Vitamin D synthesis ↓ PTH secretion ↑ Calcium secretion ↑ Life span	Increased in: rickets, tumor-induced osteomalacia and cardiac hypertrophy Decreased in: familial tumoral calcinosis and hemodialysis
Information obtained from Degirolamo *et al*., 2016		

As it can be observed in the above table, FGF21 is important for metabolic regulation and fat mass activation or inhibition under dietary stimulus. For this reason and the possible implications in adipose tissue metabolism, it will be the central endocrine FGF to be described in this dissertation.

4.5.1. FGF21

In an attempt to perform a screen for new FGFs, in 2000 a cDNA library from a mouse embryo was created. It was then when Fgf21 was isolated (Nishimura *et al*. 2000). After five years of determining that Fgf21 was highly expressed in mouse liver, it was proven that it has an important effect inducing the glucose transporter 1 (Glut1) thus promoting glucose uptake in adipocytes (murine and human) and an anti-diabetic role for FGF21 was proposed. It was then when it started to be linked to a possible role in metabolism and then classified as an endocrine FGF. A confirming fact of this classification was its description in humans as a circulating protein. (Kharitonenkov *et al*., 2005; Potthoff *et al*.,2012; Chen *et al*., 2008; Gälman *et al*., 2008; Kharitonenkov *et al*., 2008)

Regarding the structure of this protein, human FGF21 is a 181 aminoacid-long polypeptide. Mice's orthologous has a homology of 81%. As described previously for the endocrine FGFs, FGF21 nucleus has a forming the β- trefoil which contains 11 folds, this site comprehends the domains for co-receptor and receptor binding. As a member of FGF15/19 family it is catalogued as a hormone-like molecule being able to flow freely

through circulation due to its low affinity for heparan sulfate (Kharitonenkov *et al*., 2008; Kharitonenkov and Larsen, 2011).

Although it is a protein that has been under the scope for almost 20 years now, the truth is that most of the research has been performed in animals (mainly *Mus musculus*) and still has to be confirmed in humans. From the available research in mice we know that it is mainly expressed in liver (Nishimura *et al*., 2000), pancreatic β-cells, testis (Wente *et al*., 2006), brown and white adipose tissues (Muise *et al*., 2008; Hondares *et al*., 2011) and in a less magnitude (but still important for physiological responses) in muscle (Ribas *et al*., 2014) and heart (Planavila *et al*., 2015a; Planavila, *et al*., 2015b).

Being a highly bioactive molecule and described to have a half-life of 30 minutes, the circulating levels of this hormone are very dynamic. The tendency is to have higher levels of FGF21 at the morning which gradually decrease as the day passes. Also, their low molecular weight (between 32 to 36 KDa, due to the levels of glycosylation) allows them to pass through glomerular barriers and to be eliminated by the kidneys. (Kharitonenkov *et al*., 2007; Angelin *et al.*, 2012; Galman *et al*., 2008; Yu *et al.*, 2011; Lee *et al*., 2012b).

4.5.2. FGF21 mechanism of action

FGF21 has shown more affinity to FGFR1, FGFR2 and FGFR3, resulting in a difficult signal trough FGFR4. On this field, the very special FGFRs to be reported are the c-type (FGFR1c, FGFR2c, FGFR3c) due to the potent interaction observed between the receptors, β-Klotho and FGF21. (Ogawa *et al*., 2007; Kurosu *et al*., 2007; Kharitonenkov *et al*., 2008). The complex FGF21-FGFR-β-Klotho must be formed at the target tissues and is necessary for the factor function (as illustrated in figure 23). So, FGF21 will be unable to signal on those tissues lacking the adequate expression of the co-receptor β-Klotho due to IgI inhibiting domain in the structure of the FGFR. Once the complex FGF21

and klotho are bound, they are able to achieve an interaction with IgII and IgII provoking the phosphorylation of the tyrosine kinases in the receptors (Ding *et al*., 2012; Owen *et al*., 2015). In fact, the mere decrease in the expression of β-Klotho due to inflammation or due to a pharmacological intervention will lead to a decreased FGF21 signaling. Some studies, for example, have proven that in the models of KLB nullification via siRNAs, the signal of FGF21 is blunted (Díaz-Delfín *et al*., 2012; Adams *et al*., 2012; Ding *et al*., 2012). In addition to these details, pharmacological approaches increasing the levels of KLB, such as PPARɣ agonists' treatments, are able to reestablish FGF21 effects under inflammatory profiles (Díaz-Delfín *et al*., 2012). Once activated, the kinase residues are phosphorylated and a signal transduction through ERK1/2, Akt or p38 MAPK can be observed (Potthoff *et al*., 2012).

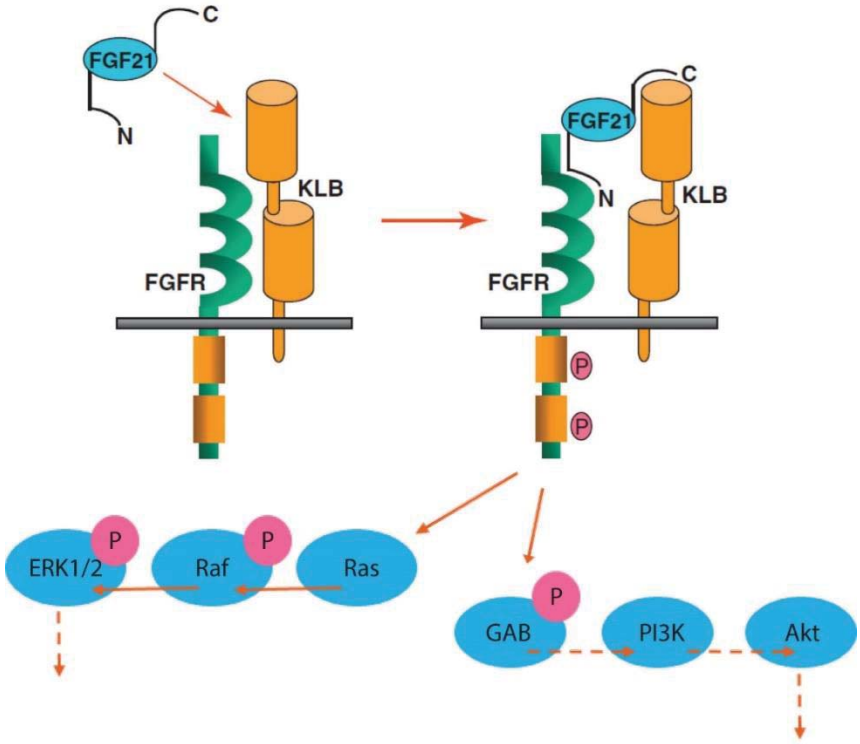

Figure 23. FGF21 model of activation (image obtained and modified from Kharitonenkov and Larsen, 2011; and Minard *et al*., 2016).

4.5.3. FGF21 regulation

The roles of this factor as a hepatokine, adipokine and myokine and their importance to metabolism can be explained by its transcriptional regulation. Conditions

such as fasting, ketogenic or high-carbohydrate diets and FFAs are some of the main transcriptional inducers of FGF21 suggesting its crucial role in the regulation in fuel utilization (Giralt *et al*., 2015; Degirolamo e*t al*., 2016). Therefore, each tissue may present differential regulation in the expression of the protein and also a great variety of effects and signal transduction pathways.

4.5.3.1. Liver

Rodents have been the animal species more frequently used for metabolism studies regarding FGF21 signaling during fasting. An important difference between mice and humans induction of FGF21 is the timing. While mice fasting causes an induction of FGF21 after only 12 h, it takes 7 days to cause the same level of induction in humans (Fazeli *et al*., 2015). Although the difference in the induction of upon fasting in mice and humans has not been cleared yet, it has been well established that FGF21 regulates the fasting response. This trigger on FGF21 expression is mainly present in liver, in this dietary condition, and is mainly mediated by PPARα FA receptor. As a consequence of fasting, the levels of FFAs increase in circulation, when these FFAs reach the liver they interact with the FA receptor PPARα. Upon binding of the FFA and PPARα, they are translocated to the nucleus where they are to interact with the RXR forming the PPARα-FFA-RXR complex able to bind the PPRE (PPARs response element) and thus activating FGF21 transcription. (Badman *et al*., 2007; Inagaki *et al*., 2007; Lundåsen *et al*., 2007). In situations of prolonged fasting, FGF21 controls gluconeogenesis mediated by PGC-1α. Apparently not all the induction of gluconeogenic genes is mediated by PGC-1α since experiment of loss of function for PGC-1α have also shown to induce the expression of gluconeogenic marker genes. PPARα role on these effects has been corroborated since they can be mimicked by the administration of fenofibrates, PPARα synthetic ligands (Badman *et al*., 2007; Iizuka *et al*., 2009; Potthoff *et al*., 2009; Fisher *et al*., 2011). Besides this activation pathway, there has been described another signaling pathway mediated by glucagon and the activation of PKA (Iizuka *et al*., 2009).

In relation to the control by the circulating levels of certain metabolic substrates metabolic substrates, there have been reports on carbohydrates, FFA and even aminoacids. The opposing dietary circumstance described above, meaning an overfeeding, has also proven to induce the expression of FGF21. This induction is mediated by another response element but this time for another dietary substrate, ***carbohydrates***. Increased circulating levels of glucose targeting liver cause their binding to ChREBP (Carbohydrate-responsive element-binding protein) and consequently moving to the nucleus where it will act through the Carbohydrates Response Element (ChRE) in order to induce FGF21 expression (Iizuka *et al*., 2009). Also, an increase in ***fatty acids*** either by ingestion or injection in experimental conditions causes an increase in the circulating levels of FGF21 (Mai *et al*., 2009). Post-prandial decreases in the circulating levels of FGF21 have been related to fat load which may result opposing to the effect observed to the circulating FFA in a fasting situation. Both observations and effects over the circulating levels of the hormone are to be regulated by PPARα. (Uebanso *et al*., 2011). In relation to the fasting situation, another circumstance that increases the circulating levels of FGF21 is the ***aminoacid*** depravation. Situations where diets show deficiencies of certain aminoacids showed an increase in ATF4, (Activating transcription factor 4). The increase in ATF4 would eventually cause an induction in the expression of FGF21 in liver and release to the blood stream. This role in metabolic adaptation is critical for a decrease in body weight, the amelioration of metabolic disturbances and the expression of lipogenic genes in adipocytes (thus increasing the lipolytic ones in BAT and WAT) (De Sousa-Coelho *et al*., 2013).

In experimental situations where obese rodents (either ob/ob or diet induced) are chronically administered FGF21, it has been observed that there is a tendency to decrease the circulating levels of glucose. This effect is due to an improvement on glucose uptake by the liver and thus improving insulin sensitivity. Besides this, there seems to be an inhibition of SREBP-1 (Sterol regulatory element binding protein-1), key factor on lipogenesis. The inhibition of this factor leads to an improvement in fatty liver condition linked to obesity. Also, FGF21 causes an induction in FA oxidation genes and

ketogenesis, while decreasing glucose secretion and gluconeogenesis happening in the liver (Xu *et al*., 2009; Sarruf *et al*., 2010).

On the other hand, the effects of FGF21 over carbohydrate and lipid metabolism require PPARα in liver and PPARɣ in adipocytes. Obese mice treated with FGF21 induce hepatic FA oxidation reducing circulating TG levels and inhibiting AT lipolysis. Systemic and hepatic insulin resistance is also improved by FGF21 (Woo *et al*., 2013). Thus, FGF21 effects over adipose tissue will also contribute to an adequate control of metabolism.

4.5.3.2. Adipose tissues

FGF21 has been described as an important factor in the control of metabolism and function of AT. BAT and WAT are some of the main targets of FGF21. While the tissue mainly attributed for the maintenance of FGF21 circulating levels remains to be the liver, ATs have also proven to be able to produce and secrete the factor. This observations have been mainly performed in rodent *in vivo* models and corroborated by human *in vitro* assays. Human AT production remains to be unclear due to the fact that an almost null expression has been detected in human biopsies. In both tissues, BAT and WAT, as briefly described above, FGF21 expression is stimulated by the PPARɣ receptor and its agonists (natural, like FA; or synthetic, like rosiglitazone) nevertheless the effects over both types may differ in some situations. In general, FGF21 produced by WAT, and possibly also by BAT, has mostly autocrine effects (as described below).

White Adipose tissue

The main effect of FGF21 action over AT is glucose uptake stimulation, actually it was the first effect described in 3T3 L1 adipocytes. Upon an insulin stimulation, a translocation of Glut4-containing vesicles to the membrane is observed. This translocation will allow the entrance of glucose. As on the first observations made for this molecule effects, FGF21 causes and induction in the expression of Glut1. Binding of FGF21 to β-klotho and FGFR1c receptor provokes the phosphorylation of ERK1/2.

ERK1/2 phosphorylation triggers phosphorylation of SRF (serum response transcription factor) and Ets-like protein-1 (Elk-1). Both proteins bind the serum response element and E-26 motifs at the promoter region of Glut1 thus inducing its expression (Ge *et al*., 2011). Glut1 is another member of the glucose transporters family which is able to translocate to the membrane independently of insulin action. Nevertheless, and promising for the metabolic effects of this molecule, the induction in glucose uptake under FGF21 stimulus didn't just affect Glut1 but also Glut4 insulin-dependent glucose uptake (Kharitonenkov *et al*., 2005). Therefore, these effects over both glucose transporters suggest it as a promising molecule for the treatment of T2DM. Nonetheless, under obese conditions the FGF21 effect over ERK1/2 and SRF/Elk1 activity is impaired in AT, this has been related to a FGF21 resistance in obesity. (He *et al*., 2004; Zhang *et al*., 2008; Fisher *et al*., 2010; Ge *et al*., 2011).

In relation to other substrate' metabolism, FGF21 was initially described to elicit lipolysis in the AT (Inagaki *et al*., 2007) and subsequently proven an inhibition on human adipocytes (Arner *et al*., 2008) This contradictory observations make it unclear to conclude whether FGF21 induces or inhibits lipolysis in AT. In other studies combining recombinant FGF21 and rosiglitazone it can be observed that PPARɣ transcriptional activity is increased causing a parallel induction in the expression of β-klotho contributing to a TG breakdown. However, upon feeding PPARɣ induces FGF21 expression in adipocytes (while not in hepatocytes) that will act in an autocrine manner to favor the synthesis of TG without any extra circulating hormone modifications (Cuevas-Ramos *et al*, 2012; Dutchak *et al*., 2012; Qiang and Accili, 2012). In assays of loss-of-function, the absence of FGF21 resulted in a PPARɣ-deficient signaling. This impaired signaling has as a consequence an impaired induction of lipolytic enzymes which contributed to a poor weight loss in this animals. This effect is not related to the protein itself but to a post-translational modification, sumoylation, which causes an increase in PPARɣ activity, (Dutchak *et al*., 2012). On the other hand, *in vivo* or *in vitro* administration of FGF21 caused an increase lipolysis (Inagaki *et al*. 2007; Potthoff *et al*., 2012). In summary, FGF21 effects over AT turn out to be more complex than expected and depend a lot on the physiological context (i.e. dietary and hormonal status). Though,

it is clear that FGF21 is an AT autocrine factor and has been related to an interaction and the activity of PPARɣ (Arner *et al*., 2008; Potthoff *et al*., 2012; Woo *et al*., 2013). Surprisingly, *in vivo* (murine and human derived cells) approaches of a chronic administration of FGF21 attenuated lipolysis upon norepinephrine and forskolin treatment (Arner *et al*., 2008). Human data, however, have correlated FFA concentrations in circulation with FGF21 protein levels. These results were obtained on a 24h tracing in which it was observed that there exists a positive association between the peak concentrations of circulating FFAs and FGF21 during day and nighttime. FFA circulating peak was showed to precede that of FGF21 by approximately 3–4h probably linked to a circadian rhythm (Yu *et al*., 2011).

Regarding its role as a metabolic signal, FGF21 will help the nutritional status information to achieve adipocytes. When it reaches these cells, it will help secrete the pertinent ***adipokines*** to trigger an adequate response. Some studies have linked FGF21 activity to the status and release of factors such as leptin and adiponenctin, decreasing and increasing them respectively. Recombinant FGF21 administration has shown to induce the expression and secretion of adiponectin and this may contribute to its beneficial metabolic effects. Besides this, several therapeutic effects upon FGF21 injection to obese mice (i.e. lowering the glucose levels, increase insulin sensitivity and decreasing the fat content in the liver) are lost in the absence of adiponectin (*AdipoQ -/-*) (Lin *et al*., 2013). Antidiabetic therapies (PPARɣ-targeted) seem to be mediated by FGF21 and a regulation of AT adipokines (Kubota *et al*., 2006; Nawrocki *et al*., 2006) (regarding the effects not related to an improvement in glucose homeostasis). For example, FGF21 increases leptin receptors expression in peripheral tissues (i.e. liver) contributing to a decrease in total body weight (Veniant *et al*., 2012; Holland *et al*., 2013), while adiponectin levels are increased helping in the insulin and glucose sensitivity (Holland *et al*., 2013; Lin *et al*., 2013).

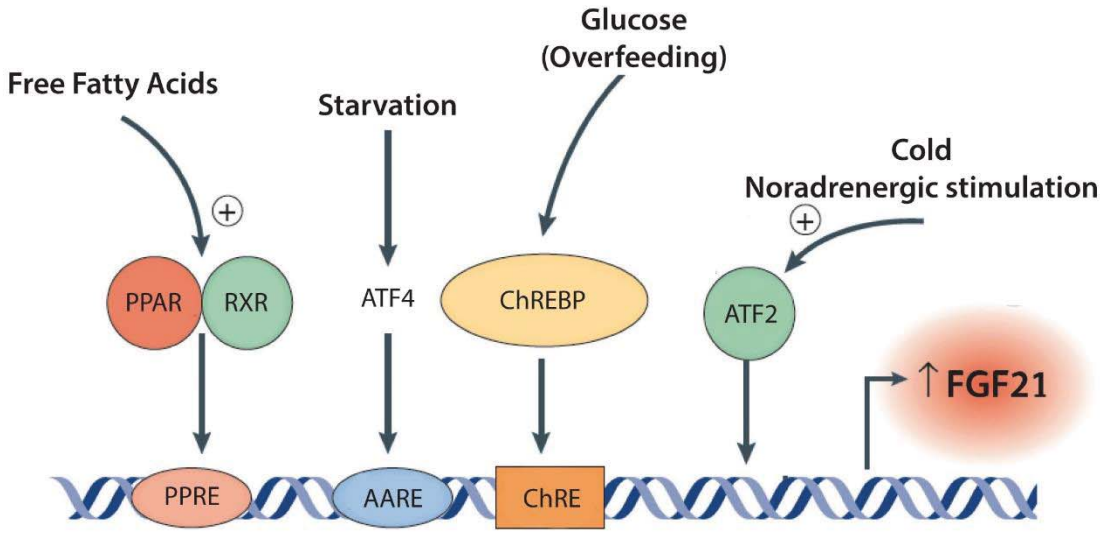

Figure 24. Examples of FGF21 transcriptional regulation (Image obtained and modified from Degiloramo *et al*., 2016 and Uebanso *et al*., 2011).

Brown adipose tissue, thermogenesis and WAT browning

Those effects described for glucose and lipid metabolism in WAT are also observed in BAT (i.e. induction of glucose uptake and increase in lipolysis). Several other effects over this tissue and its main function will be observed. As mentioned earlier, BAT is able to produce and secrete this FGF. FGF21 has been described as an important batokine in this tissue, due to its autocrine role involved in the activation of thermogenesis (Cereijo *et al*., 2015). *In vivo* and *in vitro* models for the study of thermogenesis activation have proven to induce the expression and release of FGF21 in brown adipocytes and BAT. Described in the first section, noradrenergic stimuli activates a signaling pathway mediated by cAMP. This increase in the intracellular concentrations of cAMP leads to a regulation of FGF21 gene expression in two ways. The first one is due to the binding of CREB to the CRE on the FGF21 promoter region. The second is a cAMP-dependent phosphorylation of PKA and p38 MAPK leading to an interaction with an ATF2 binding site in the proximal region of the FGF21 gene promoter. (Chartoumpekis *et al*., 2011; Hondares *et al*., 2011). FGF21 induction in this type of cells upon NE stimuli has a role in thermogenesis activation and the browning of AT (Fisher *et al*., 2012), doubts on whether this effect is performed in an autocrine manner or via CNS are still

not clarified. This is due to knowledge regarding sympathetic control over the induction of the thermogenic machinery and, as described before, the CNS is also a target of FGF21. (Owen *et al*., 2014).

It was explained previously that upon certain conditions WAT is able to recruit cells with an intermediate phenotype between brown and white, beige adipocytes. This browning is characterized by an induction in the expression of thermogenesis related genes in WAT (i.e. *UCP1 and PGC-1α*) upon a chronic exposition to cold. FGF21 seems to have a critical role in the recruitment of these cells to WAT (Fisher *et al.*, 2012). A better explanation of a possible autocrine role or a possible mediation by the CNS is still needed to account all these effects on FGF21 local actions. Regarding this doubt, a cumulus of results in this dissertation describe a possible autocrine role of FGF21 in the acquisition of a brown-like phenotype in adipose cells in the absence of noradrenergic stimuli, and in a cell-autonomous manner in the brown adipocyte.

It was previously mentioned that a physiological condition where the induction of thermogenesis is critical for the maintenance of life is birth. Upon birth, animals pass from a controlled environment where temperature never drops from 37°C to a challenging environment barely reaching 22°C. FGF21 has been described as a key player in cold adaptation at this age. Also, upon breast-feeding an increase in the circulating levels of FFA contribute to an increase in hepatic PPARα expression in liver. This induction in PPARα will cause an induction in FGF21 expression in liver and an increase in the circulating levels. This effect may contribute to a hepatic-based regulation of BAT thermogenic program in rodents upon feeding (Hondares *et al*., 2010).

Another example of FGF21 regulation in BAT is the stimulation of corticotrophin-releasing factor (CRF) in obese rodents. This factor showed to stimulate FGF21 secretion triggering lipolysis and glucose uptake in BAT. Also, FGF21 effects on glucose uptake in BAT have been attributed to FGFR1c since obese mice lacking this receptor showed a loss in the effects of expenditure-promotion (Adams *et al*., 2012b).

4.5.3.3. FGF21 in other tissues

Skeletal muscle

Regarding skeletal muscle metabolism regulation via FGF21, it is known that FGF21 expression is induced with myogenic differentiation and that its expression in myogenic cells is controlled by MyoD (Ribas *et al*., 2014). Even though β-klotho expression in this tissue is really low, FGF21 has been described to have important effects in this tissue. The main roles known are related to glucose metabolism. This factor has been described to decrease the endogenous production of glucose mediated by insulin and insulin-dependent glucose uptake in diet-induced obese mice (Xu *et al*., 2009). Insulin shows a role in FGF21 expression in this tissue since it triggers FGF21 release from skeletal muscle through PI3K/Akt1 signaling pathway. This induction has also been observed upon physical training suggesting FGF21 as a factor contributing to an amelioration of metabolic parameters in obese patients (Izumiya *et al*., 2008). Opposing to what is deduced from liver and AT, muscle expression of FGF21 is not an indicator of the energetic status but of a mitochondrial dysfunction (Tyynismaa *et al*., 2010). A phenomenon also observed in studies from HIV (Human immunodeficiency virus) patients with antiretroviral treatments which cause mitochondrial dysfunction (Gallego-Escuredo *et al*., 2017). The relationship between FGF21 levels and mitochondrial stress are also observed upon HFD feeding to mice or in insulin resistant obese patients (Hojman *et al*., 2009; Vienberg *et al*., 2012). This mitochondrial dysfunction induction of FGF21 has shown to be mediated by ROS production and the activation of p38 MAPK. p38 MAPK phosphorylation provokes the activation of ATF2 at the promoter regulatory region of FGF21 gene (Ribas *et al*., 2014). Other studies have proposed a mechanism where the inhibition of autophagy, under mitochondrial stress conditions, triggers an ER stress response which would result in the binding of ATF4 to the FGF21 promoter region. This ATF4 binding would induce FGF21 transcription. (Kim *et al*., 2013). Besides these proposed pathways, a recent report suggested an autocrine effect of muscle-produced lactate in the induction of FGF21. Pathological situations (mitochondrial dysfunction) that would lead to an increased glycolytic flux result in increased lactate production. Lactate would induce FGF21 expression through p38 MAPK in muscle cells as it occurs with ROS (Villarroya *et al*., 2018). Regarding muscle

contribution to systemic levels, there have been reported increased levels of FGF21 in plasma from patients with mitochondrial diseases (particularly neuromuscular diseases caused by primary mitochondrial DNA mutations). These behavior has suggested FGF21 as a biomarker of such diseases and could be responsible for some of the systemic metabolic alterations in these patients. However, muscle is not considered a substantial source of FGF21 in physiological conditions and the relative contribution of muscle-derived FGF21 to systemic levels still needs to be established (Villarroya *et al*., 2018). The importance of FGF21 in muscle is more related to local metabolism of substrates and to respond to signals targeted to muscle coming from other tissues (Lindegaard *et al*., 2013).

Heart

Several studies have shown that, besides skeletal muscle, heart is also an important target and producer of FGF21 (Planavila *et al*., 2013). Both roles have also been the focus of attention due to approaches attempting to prove FGF21 as a cardioprotective hormone (Liu *et al*., 2011; Planavila *et al*., 2015b). Results from our laboratory and some other study groups have found that in conditions of cardiac hypertrophy there is an induction of FGF21. Also, models of loss-of-function for FGF21 show cardiac abnormalities (such as hypertrophy and cardiac dysfunction) and decreased expression of antioxidant genes (Planavila *et al*., 2013). It is believed that, like occurring with other molecules, FGF21 is released upon a stress situation in heart (i.e. ischemia) in order to assist the early local damage in this tissue and probably assisted by other tissues, like liver. Besides this role, FGF21 has also been proposed to act in an autocrine way to try to achieve an endogenous feedback mechanism. This feedback would work as a compensatory mechanism to mitigate the initial damage (Liu *et al*., 2011; Planavila *et al*., 2015b). To further complete the panorama of FGF21 as a cardioprotective hormone, either an injection or the overexpression of this factor were able to attenuate the extension of an infarction and showed to improve the cardiac activity. Also, recent studies prove an autocrine regulation of antioxidant genes mediated by FGF21 in heart. This regulation modulates ROS production under

inflammatory or hypertrophic conditions thus preventing pro-oxidative responses in the cardiac tissue. (Liu *et al*., 2013; Planavila *et al*., 2015b).

Pancreas

Regarding pancreas, it is known to express the protein and its receptor suggesting it as a producer and also as a target (Nishimura *et al*., 2000). Isolated islets from rodent showed that FGF21 induced a phosphorylation ERK1/2 and Akt in these cells. This kinases' phosphorylation caused an inhibition of glucagon secretion and an increase in insulin production. The administration of glucose in the presence of FGF21 also provoked an increase in islet number and insulin staining in pancreas from diabetic mice (Wente *et al*., 2006)

Brain (CNS)

FGF21 is able to cross the blood brain barrier by simple diffusion. FGF21 has been detected in human and rodent cerebrospinal fluid (Hsuchou *et al*. 2007; Tan *et al*. 2011). In this tissue, the expression of β-klotho and FGFR1c are detected in areas of the brain involved in the hypothalamic-pituitary-adrenal axis and the hypothalamic pituitary-gonadal axis (Bookout *et al*. 2013; Fon Tacer *et al*. 2010; Liang *et al*. 2014). FGF21 increased levels in brain activate the receptor at the hypothalamus, leading to the phosphorylation of ERK1/2. ERK1/2 phosphorylation will unleash the secretion of several other hormones (i.e. corticotrophin releasing hormone (CRH)) (Liang *et al*. 2014). The release of hormones from the hypothalamus will cause subsequent releases of other hormones and factors at other brain localizations (i.e. Adrenocorticotrophic hormone (ACTH) by the pituitary gland). These 'second hormones' will target peripheral tissues to trigger physiological responses (i.e. a production and secretion of corticosterone from the adrenal cortex). A great variety of roles are very well-known to be controlled by the hypothalamus, this tissue is not to the subject of study of the present dissertation. However, it is important to mention that it has been found that FGF21 is able to act in the brain stimulating sympathetic activity thus increasing thermogenesis and metabolic rate (effects also proposed to be present after prolonged periods of cold exposure) (Coskun *et al*., 2008; Sarruf *et al*. 2010; Tan *et al*., 2011; Sa-

nguanmoo *et al*., 2016). Figure 25 illustrates the previously described metabolic regulation mediated by FGF21 in several tissues and the possible cross-talk between them.

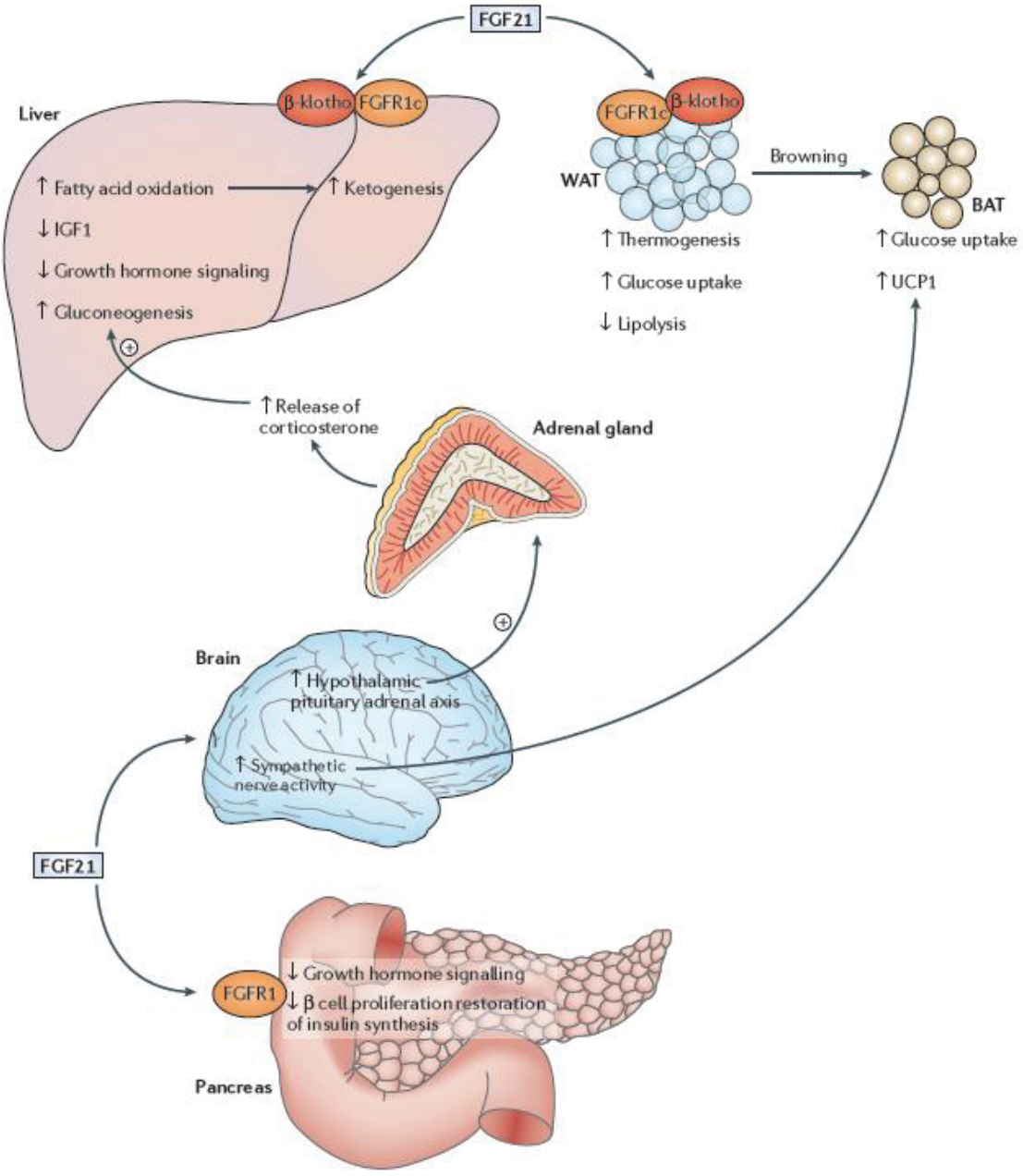

Figure 25. FGF21 actions. FGF21 is an endocrine factor able to act centrally and peripherally. This diagram shows and overview of the interactions between tissues and how FGF21 is able to mediate them (Image obtained from Degirolamo *et al*., 2016).

4.5.3.4. Other functions

FGF21 circulates freely around the organism. Although research has focused on metabolism and its effects on those tissues principally affecting circulating metabolites, other important processes are to be influenced by this hormonal factor. Table 12 describes some of them.

Table 12. Other physiological processes influenced by FGF21	
Growth	It is known that under fasting conditions, the effects of FGF21 induction cause an estate of growth hormone resistance. This resistance is achieved by reducing the expression of STAT5 (Signal transducer and activator of transcription 5), key for GH metabolism. This decreased expression will cause a fall in the induction of those genes target of this signaling cascade (i.e. Igf-1). Also, FGF21 caused an increase in proteins able to de-phosphorylate STAT5 (i.e. SOCS2 (Suppressor of cytokine signaling 2)). This effects are consistent with the fact that FGF21-/- mice show smaller body size in some experimental settings. (Potthoff *et al*., 2012).
Aging	FGF21 has been linked to an increase in lifespan. This increase is similar to what has been observed in situations of calorie restriction prolonging life 30-40% with no differences in diet ingestion or differences in FGF21 circulatory levels. What has been proposed is that this increase is also associated to the STAT5/Igf-1 signaling pathway (Zhang *et al*., 2012; Turturro *et al*., 1999).
Reproduction	Some reports have suggested that the increase in FGF21 circulating levels after a long period of calorie restriction mark importantly the performance of reproduction in female mice. Mice over expression of FGF21 show a delayed onset of puberty and remain infertile through adulthood. This effect has been linked to the effects of FGF21 on CNS where it suppresses vasopressin (AVP) production provoking a reduction of kisspeptin-1 (Kiss-1), an important regulator of fertility (Owen *et al*., 2013).
Bone metabolism	*In vitro* approaches employing BMMSCs (Bone marrow mesenchymal stem cells) have shown an inhibition of osteoblastogenesis by FGF21. This inhibition causes, on the other side, adipogenesis in this precursor cells by activation PPARɣ. As described previously, the induction of PPARɣ by FGF21 will cause a loop in the induction of FGF21 itself and β-klotho contributing to the maintenance of adipogenesis process (Galman *et al*., 2008; Christodoulides *et al*., 2009; Dushay *et al*., 2010; Schoenberg *et al*., 2011). A confirmatory detail of this finding it the fact that FGF21-/- mice show increased bone mass. This is a clinical concern in developing therapies involving FGF21 since a compromised differentiation of BMMSCs in to bone could be observed. Human studies have shown that increased levels of FGF21 does not correlate with bone loss or they do depending on the cohort of human patients and the type of metabolic alterations (Wei *et al*. 2012; Lee *et al*., 2013; Gallego-Escuredo et al., 2017). Further analysis of this observations should be done.

4.5.4.5. FGF21 in Humans and its potential role as a therapeutic target for metabolic abnormalities

Since the very early research reports, several differences between human and rodent data regarding FGF21 regulation have been found. In humans, for example, there are required around 7 days of fasting in order to achieve an increase in FGF21 circulating levels (mice require only 12h of fasting). Other examples of dietary conditions increasing FGF21 circulating levels in humans are lactation, ketogenic diets and HFD (Galman *et al*., 2008; Christodoulides *et al*., 2009; Dushay *et al*., 2010; Schoenberg *et al*., 2011). In relation to the metabolic conditions modifying circulatory levels of the hormone, it is known that FGF21 levels correlate positively with an increased body weight and the presence of metabolic syndrome, glucose intolerance, T2DM, NAFLD and cardiovascular events (Zhang *et al*., 2008; Chavez *et al*., 2009; Chen *et al*., 2008; Cuevas-Ramos *et al*., 2010; Dushay *et al*., 2010; Yang *et al*., 2011; An *et al*., 2012). Some reports show correlations between FGF21 and MS in adult humans, not been observed in infants. Still, FGF21 levels seem to correlate with adiposity and FFA in plasma (Zhang *et al*., 2008; Mai *et al*., 2009; Gallego-Escuredo *et al*., 2012; Reinehr *et al*., 2012) while inversely correlate with HDL-cholesterol. On the other hand physical activity in subjects with metabolic disturbances seems to correlate with an increase in FGF21 levels (Cuevas-Ramos *et al*., 2010). The systemic roles seem to be complex to clarify and depend in a great measure to the physiological or pathological context. An explanation to an increase in FGF21 under metabolic conditions is still required. While some study groups report that obesity and insulin resistance contribute to its up-regulation depending on circadian rhythms (due to increased levels observed during the night) (Yu *et al*., 2011; Reinehr *et al*., 2012) others consider this up-regulation as a compensatory effect (Fisher *et al*., 2010; Hale *et al*., 2012). Whether it is one or the other it seems like FGF21 could mediate an increase in FA oxidation and glucose utilization in order to battle lipotoxicity and glucotoxicity (Cuevas-Ramos *et al*., 2012).

Further research on human responses and effects of FGF21 are needed, especially due to the fact that there are few studies regarding receptors and co-

receptors. One disadvantage, and setback, in these studies is the fact that human adipocytes and adipose tissue show little or no expression of FGF21 (Dushay *et al*., 2010; Gallego-Escuredo *et al*., 2012) Few studies have been conducted in the understanding of their modulation in pathological conditions (receptors and coreceptors). Nevertheless, data from our laboratory suggests that obesity triggers a proinflammatory status in the individual (also in HIV patients with lipodystrophy). This proinflammatory profile leads to a reduction in expression β-Klotho-mediated by TNFα. TNFα will activate JNK1 (c-Jun N-terminal kinase 1) signaling pathway and will cause a reduction to FGF21 response in adipocytes (Diaz-Delfin *et al*., 2012; Gallego-Escuredo *et al.*, 2012). This reduction in the response to FGF21 observed with obesity and metabolic conditions is now well defined as a resistance condition which could be similar to what is observed with other circulating hormones (i.e. insulin). After no response to the hormone, secretory tissues will continue to produce and secrete it not triggering any response due to a poor signal (or none) at the target cells (Fisher *et al*., 2010). Interestingly, a pharmacological treatment with FGF21 or synthetic analogs in obese humans (and rodents) has beneficial effects (i.e. improved glucose uptake) which will not be compatible to a full resistance to FGF21 (Hale *et al*., 2012; Reinehr *et al*., 2012; Gaich *et al*., 2013).

Due to this last detail, and the fact that it has been suggested that FGF21 could play a role in improving the metabolic abnormalities while promoting thermogenic activation, efforts have been directed to employ FGF21 as a therapeutic molecule. Several *in vivo* studies have proven that the administration of recombinant or analogs of FGF21 can decrease circulating levels of glucose, improve insulin sensitivity, reverse NAFLD, improve T2DM condition, improve in pancreatic β-cells functions; suppression of glucagon secretion, and probably mediate a decrease in total body weight due to an induction in ***thermogenesis*** (Kharitonenkov *et al*., 2005; Kharitonenkov *et al*., 2007; Coskun *et al*., 2008; Berglund *et al*., 2009 Fisher *et al*., 2012). However, studies targeting any part of FGF21 signaling should be further explored due to the great variety of processes mediated by this hormone (i.e. osteogenesis, fertility and food intake).

So far, we know that the observed effects will totally depend on the background of the individual. This background will be affected not just by the genetic context but also by the diet by which the metabolic conditions were developed. One of the problems regarding FGF21 as a treating molecule is its short half-life in circulation, physiologically synthesized or pharmacologically administered. In this context, the seek for other molecules or signaling pathways maintaining an increased circulation –or a local concentration, depending on the tissue- in order to achieve a metabolic effect would be necessary. The assays developed in this project helped elucidate a pathway mediated by a FFAR in the activation of FGF21 and its effects over AT, and adipocytes, performance regarding thermogenesis and substrate utilization. Figure 26 summarizes the effects of FGF21 administration to obese mice and humans observed data.

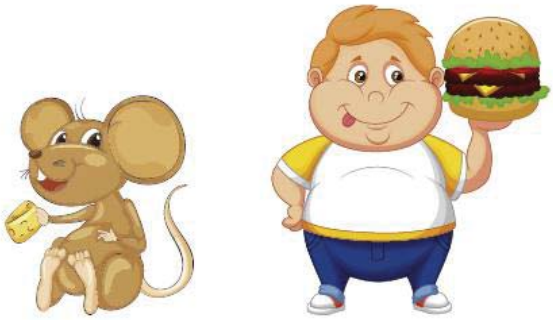

Glucose ↓	✔	✗
Body weight ↓	✔	✔
Insulin ↓	✔	✔
Triglycerides ↓	✔	✔
LDLc ↓, HDLc ↑	N/A	✔
Fatty liver ↓	✔	N/D

Figure 26. FGF21 pharmacological actions. FGF21 supplementation metabolic effects in mice and humans are highlighted. (Image obtained from Kharitonenkov and DiMarchi, 2015).

OBJECTIVES

Objectives

Efforts have been oriented to develop new treatments for obesity and related metabolic diseases. In this context, FGF21 is an endocrine factor proven to mediate thermogenic activation and ameliorate metabolic abnormalities. Likewise, the consumption of n-3 PUFAs has been related to a healthy metabolic profile. GPR120 is a membrane receptor sensible to PUFAs which activation has also proven to have beneficial effects on pathological conditions and is induced upon cold exposure in adipose tissues. With this background, the main objective of this project was to determine the effects of GPR120 activation on BAT and WAT and in FGF21 regulation in these tissues.

Therefore, the following objectives were established in order to:

1. Characterize GPR120 expression in adipose tissues and adipocytes.

2. Determine the effects of GPR120 activation in rodent adipose tissues.

3. Evaluate cell-autonomous responses upon the activation of GPR120 in adipocytes.

4. Determine the implication of the hormonal factor FGF21 on GPR120 activation-mediated effects.

5. Characterize the role of GPR120 in neonatal brown adipose tissue.

DIRECTORS' REPORT ON THE PUBLISHED ARTICLES

INFORME DELS CO-DIRECTORS EN RELACIÓ A LA TESI DOCTORAL DE TANIA PALOMA QUESADA LÓPEZ (PUBLICACIONS I PAPERS DE LA DOCTORANDA):

En tant que codirectors de la Tesi Doctoral de Tania Paloma Quesada López, fem constar que els treballs corresponents a la memòria científica s'estructuren en base als següents articles científics:

1. **Quesada-López T**, Cereijo R, Turatsinze JV, Planavila A, Cairó M, Gavaldà-Navarro A, Peyrou M, Moure R, Iglesias R, Giralt M, Eizirik DL, Villarroya F

The lipid sensor GPR120 promotes brown fat activation and FGF21 release from adipocytes.

Nat Commun. 2016 Nov 17;7:13479.

IF: 12.124 MULTIDISCIPLINARY SCIENCES 3 de 64 (1er Decil)

2. **Quesada-López T**, Gavaldà-Navarro A, Morón-Ros S, Campderrós L, Iglesias R, Giralt M, Villarroya F.

GPR120 is essential for perinatal thermogenic adaptations and brown fat function.

Molecular Metabolism (Submitted).

IF: 6.799 ENDOCRINOLOGY & METABOLISM 11 DE 138 (1er Decil)

La doctoranda, primer autora de les dues publicacions anteriors, ha tingut tot el protagonisme en l'obtenció experimental de les dades així com en l'evolució i progressió dels estudis, i ha participat de manera essencial en la discussió científica dels resultats. El paper dels altres coautors ha estat el donar suport a aspectes experimentals (suport als cultius cel·lulars i alguns aspectes analítics específics) així com la participació dels co-directors i altres autors sènior que han participat en aspectes intel·lectuals, d'elaboració i contextualització de les dades.

3. Gavaldà-Navarro A, Moreno-Navarrete JM, **Quesada-López T**, Cairó M, Giralt M, Fernández-Real JM, Villarroya F.

Lipopolysaccharide-binding protein is a negative regulator of adipose tissue browning in mice and humans.

Diabetologia. 2016 Oct;59(10):2208-18.

IF: 6.080 ENDOCRINOLOGY & METABOLISM 15 DE 138 (1er Tercil),

En aquest treball, la doctoranda realitzà els estudis en cultius primaris d'adipocits marrons i beix dels efectes de LBP en processos adipogènics, aspecte clau en aquesta publicació, a més de participar en la elaboració del conjunt del treball i la seva discussió.

Juntament amb els articles anteriors, que formen el nucli temàtic essencial de la Tesi, durant el període de realització del seu doctorat T. Quesada-López ha desenvolupat treballs relacionats que han resultat en altres publicacions, que es detallen al final de la memòria de Tesi com a Annex.

4. Zarei M, Barroso E, Leiva R, Barniol-Xicota M, Pujol E, Escolano C, Vázquez S, Palomer X, Pardo V, González-Rodríguez Á, Valverde ÁM, **Quesada-López T**, Villarroya F, Wahli W, Vázquez-Carrera M.

Heme-Regulated eIF2α Kinase Modulates Hepatic FGF21 and Is Activated by PPARβ/δ Deficiency.

Diabetes. 2016 Oct;65(10):3185-99.

IF: 8.684 ENDOCRINOLOGY & METABOLISM 9 DE 138 (1er Decil)

5. Zarei M, Barroso E, Palomer X, Dai J, Rada P, **Quesada-López T**, Escolà-Gil JC, Cedó L, Zali MR, Molaei M, Dabiri R, Vázquez S, Pujol E, Valverde ÁM, Villarroya F, Liu Y, Wahli W, Vázquez-Carrera M.

Hepatic regulation of VLDL receptor by PPARβ/δ and FGF21 modulates non-alcoholic fatty liver disease.

Mol Metab. 2018 Feb;8:117-131.

IF: 6.799 ENDOCRINOLOGY & METABOLISM 11 DE 138 (1er Decil)

6. Moure R, Domingo P, Villarroya J, Gasa L, Gallego-Escuredo JM, **Quesada-López T**, Morón-Ros S, Maroto AF, Mateo GM, Domingo JC, Villarroya F, Giralt M.

Reciprocal effects of antiretroviral drugs used to treat HIV infection on the fibroblast growth factor-21/β-Klotho system.

Antimicrob Agents Chemother. 2018 Apr 16. pii: AAC.00029-18.

IF: 4.302 PHARMACOLOGY & PHARMACY 36 DE 257 (1er Quartil)

En aquests altres treballs, T.Quesada-López ha realitzat els estudis que impliquen la utilització del model de ratolins knock-out per a FGF21 i la seva caracterització metabòlica. En el tercer treball annex T. Quesada-López ha desenvolupat les tècniques de cultius primaris d'adipòcits beix i la seva diferenciació, així com altres procediments analítics que han estat bàsics per a la publicació en què consta com a coautor. Les temàtiques estan estretament relacionades amb els estudis de regulació de FGF21 i del teixit adipós marró i beix, per la qual cosa T. Quesada-López ha contribuït també des del punt de vista d'anàlisi i interpretació global de les dades.

A Barcelona, el 15 de maig de 2018

Signat:

_____ _____

Dr. Francesc Villarroya Gombau **Dra. Marta Giralt Oms**

Director Directora

PUBLICATIONS

The lipid sensor GPR120 promotes brown fat activation and FGF21 release from adipocytes

Journal: Nature Communications 2016 Nov 17; 7: 13479.

IF: 12.124 MULTIDISCIPLINARY SCIENCES 3 de 64 (1st Decile)

Abstract:

The thermogenic activity of brown adipose tissue (BAT) and browning of white adipose tissue are important components of energy expenditure. Here we show that GPR120, a receptor for polyunsaturated fatty acids, promotes brown fat activation. Using RNA-seq to analyse mouse BAT transcriptome, we find that the gene encoding GPR120 is induced by thermogenic activation. We further show that GPR120 activation induces BAT activity and promotes the browning of white fat in mice, whereas GRP120-null mice show impaired cold-induced browning. Omega-3 polyunsaturated fatty acids induce brown and beige adipocyte differentiation and thermogenic activation, and these effects require GPR120. GPR120 activation induces the release of fibroblast growth factor-21 (FGF21) by brown and beige adipocytes, and increases blood FGF21 levels. The effects of GPR120 activation on BAT activation and browning are impaired in FGF21-null mice and cells. Thus, the lipid sensor GPR120 activates brown fat via a mechanism that involves induction of FGF21.

nature COMMUNICATIONS

ARTICLE

Received 15 Feb 2016 | Accepted 7 Oct 2016 | Published 17 Nov 2016

DOI: 10.1038/ncomms13479 OPEN

The lipid sensor GPR120 promotes brown fat activation and FGF21 release from adipocytes

Tania Quesada-López[1], Rubén Cereijo[1], Jean-Valery Turatsinze[2], Anna Planavila[1], Montserrat Cairó[1], Aleix Gavaldà-Navarro[1], Marion Peyrou[1], Ricardo Moure[1], Roser Iglesias[1], Marta Giralt[1], Decio L. Eizirik[2] & Francesc Villarroya[1]

The thermogenic activity of brown adipose tissue (BAT) and browning of white adipose tissue are important components of energy expenditure. Here we show that GPR120, a receptor for polyunsaturated fatty acids, promotes brown fat activation. Using RNA-seq to analyse mouse BAT transcriptome, we find that the gene encoding GPR120 is induced by thermogenic activation. We further show that GPR120 activation induces BAT activity and promotes the browning of white fat in mice, whereas GRP120-null mice show impaired cold-induced browning. Omega-3 polyunsaturated fatty acids induce brown and beige adipocyte differentiation and thermogenic activation, and these effects require GPR120. GPR120 activation induces the release of fibroblast growth factor-21 (FGF21) by brown and beige adipocytes, and increases blood FGF21 levels. The effects of GPR120 activation on BAT activation and browning are impaired in FGF21-null mice and cells. Thus, the lipid sensor GPR120 activates brown fat via a mechanism that involves induction of FGF21.

[1] Departament de Bioquímica i Biomedicina Molecular, Institut de Biomedicina, Universitat de Barcelona (IBUB) and CIBER Fisiopatologia de la Obesidad y Nutrición, Avda Diagonal 643, 08028 Barcelona, Spain. [2] ULB Center for Diabetes Research, Medical Faculty, Université Libre de Bruxelles, Avenue Franklin Roosevelt 50, 1050 Brussels, Belgium. Correspondence and requests for materials should be addressed to F.V. (email: fvillarroya@ub.edu).

Brown adipose tissue (BAT) is the main site of non-shivering thermogenesis in mammals. It confers a unique mechanism for energy expenditure and heat production in response to cold and provides a protective mechanism against excessive body weight accumulation in response to overfeeding[1,2].The interest in brown fat activity as a mechanism of protection against the obesity and metabolic diseases has been renewed by the recent recognition that adult humans possess active BAT, and its activity is negatively associated with obesity and type II diabetes[3]. Many aspects of the molecular mechanisms underlying the function of BAT are known, but we do not comprehensively understand how BAT activity is controlled and integrated with whole organism metabolism to ensure that metabolic substrates are burned and heat is provided. Recent studies unravelled an additional BAT-related means to control energy expenditure, wherein white adipose tissue (WAT) has the capacity to acquire BAT-like properties via the so-called 'browning' process. During this process, sustained thermogenic activation leads to the appearance of the so-called beige or brite adipocytes in WAT depots, which, like classical brown adipocytes, express uncoupling protein-1 (UCP1) and perform uncoupled mitochondrial respiration[4,5]. Several lines of evidence suggest that the browning process is especially relevant in controlling whole-body energy balance[4]. This may reflect its high inducibility in response to environmental factors and the ability of beige cells to use additional, non-UCP1-mediated energy expending mechanisms[6].

Studies aimed at assessing how BAT responds to cold can improve our understanding of the processes that mediate BAT activation. Transcriptomic profiling of BAT from cold-exposed mice can provide a snapshot of how BAT responds to the thermogenic activation and may offer an unbiased look at novel BAT activity-related actors. Recently, RNA sequencing (RNA-seq) has emerged as the best tool for transcriptomic studies, as it does not require *a priori* knowledge of targets, and shows both high reproducibility and a low frequency of false positives[7–9]. Moreover, RNA-seq can identify 25–75% more genes than complementary DNA (cDNA) microarrays, and it allows assessment of both whole genes and splice variants[10,11].

Here we used RNA-seq to analyse the responsiveness of BAT to the cold-induced thermogenic activation. Departing from these data set, we identified a novel pathway through which thermogenic activation of BAT and the browning of WAT occur via the activation of GPR120 (*FFAR4*). GPR120 is a G-protein-coupled receptor that binds unsaturated long-chain fatty acids and their derivatives[12]. GPR120 is known to contribute to mediating the anti-inflammatory actions of polyunsaturated fatty acids (PUFAs) and in protecting against obesity and type II diabetes[13,14]. Here we identify a novel pathway of thermogenic regulation through that PUFA-mediated GPR120 activation induces BAT activity and WAT browning via the hormonal factor fibroblast growth factor-21 (FGF21).

Results

Effect of cold exposure on BAT transcriptome. RNA-seq data were obtained from BAT samples obtained from mice housed under thermoneutral conditions or following a 24-h exposure to 4 °C. Among the 21,391 genes detected by the RNA-seq as being 'expressed' (RPKM > 0) a total of 3,470 (16.2%) were significantly modified under the cold condition: 2,498 and 972 were upregulated and downregulated, respectively. To validate our analysis and identify novel candidate genes related to the thermogenic activation in BAT, the top 10% most cold-induced genes were arbitrarily selected for manually curated analysis. Most were already known to be upregulated by cold; these included key components of mitochondrial uncoupling (*UCP1*, 4.5-fold induction), lipid metabolism (*Elovl3*, 9.9-fold induction; and *glycerokinase*, 5.4-fold induction), intracellular regulation (*Dio2*, 4.8-fold induction; and *PGC-1α*, 3.3-fold induction) and extracellular regulation (*Bmp8b* and *FGF21*, > 10-fold inductions). Among the top-induced genes that had not been previously studied, we focused on *FFAR4* (GPR120). This G-protein-coupled receptor binds unsaturated long-chain fatty acids and their derivatives, and has been proposed to mediate multiple metabolic effects, including anti-inflammation and amelioration of insulin resistance[12,13]. Allelic variants causing loss-of-function put human individuals at risk to develop obesity[14]. A comparison of our RNA-seq data with two microarray-based data sets[7,8] and a digital gene expression profiling[15] revealed that GPR120 was consistently and strongly upregulated in BAT following cold exposure. Here we set out to assess the regulation and function of GPR120 in relation to BAT activation.

Thermogenic activation upregulates GPR120 in fat depots. The expression of *GPR120* transcript was determined in adipose depots from mice reared at 21 °C in comparison with small intestine and colon that express functional levels of *GPR120* (refs 16,17). The highest expression was found in interscapular BAT (iBAT), while specific WAT depots (inguinal, iWAT; epididymal, eWAT; and mesenteric WAT) showed lower but still relevant expression (Fig. 1a; Supplementary Fig. 1). The expression of *GPR120* messenger RNA (mRNA) was strongly induced in BAT of mice subjected to either short- or long-term cold exposure (Fig. 1b). Cold also induced *GPR120* mRNA expression in iWAT. GPR120 protein levels were increased in both BAT and iWAT after cold exposure (Fig. 1b).

Similar to markers of brown adipocyte thermogenic activity (for example, *UCP1*), *GPR120* was preferentially expressed in mature, differentiated, brown adipocytes rather than in the stromal vascular fraction (Fig. 1c).

In cultured precursor cells from iBAT, *GPR120* expression was low at the pre-adipocyte stage, increased progressively during brown adipocyte differentiation and peaked at full differentiation (day 10, maximal expression of *UCP1*; (Fig. 1d). Norepinephrine or cyclic AMP (cAMP), the major mediators of thermogenic induction, significantly upregulated GPR120 transcript (Fig. 1e) and protein levels (Fig. 1f) in brown adipocytes. The effects of norepinephrine (NE) and cAMP were blunted by the p38 MAPK inhibitor SB202190, but not by the protein kinase-A (PKA) inhibitor H89 (Fig. 1g). This contrasts with *UCP1* mRNA whose induction by NE and cAMP was partially blunted both by SB202190 and H89, in accordance with the dual involvement of p38 MAPK and PKA in the control of *UCP1* gene expression[18] (Supplementary Fig. 1). GW7647, a peroxisome proliferator-activated receptor alpha (PPARα) activator, did not significantly alter *GPR120* expression (Fig. 1g).

In summary, we herein identified GPR120 as a novel component of the acquisition of the differentiated phenotype of brown adipocytes and showed that it is induced *in vivo* and *in vitro* in BAT by noradrenergic regulators of thermogenic activation.

GW9508 increases the thermogenic activity of BAT and WAT. Mice were treated with GW9508, an activator of GPR120, via their food during 7 days. This treatment did not significantly modify body weight or food intake. Metabolic profiling revealed unaltered glycaemia and triglyceridemia, but GW9508 induced a reduction in insulin levels (Supplementary Table 1), which could reflect improvement in insulin sensitivity. The other tested hormone levels were unaltered following GW9508 treatment

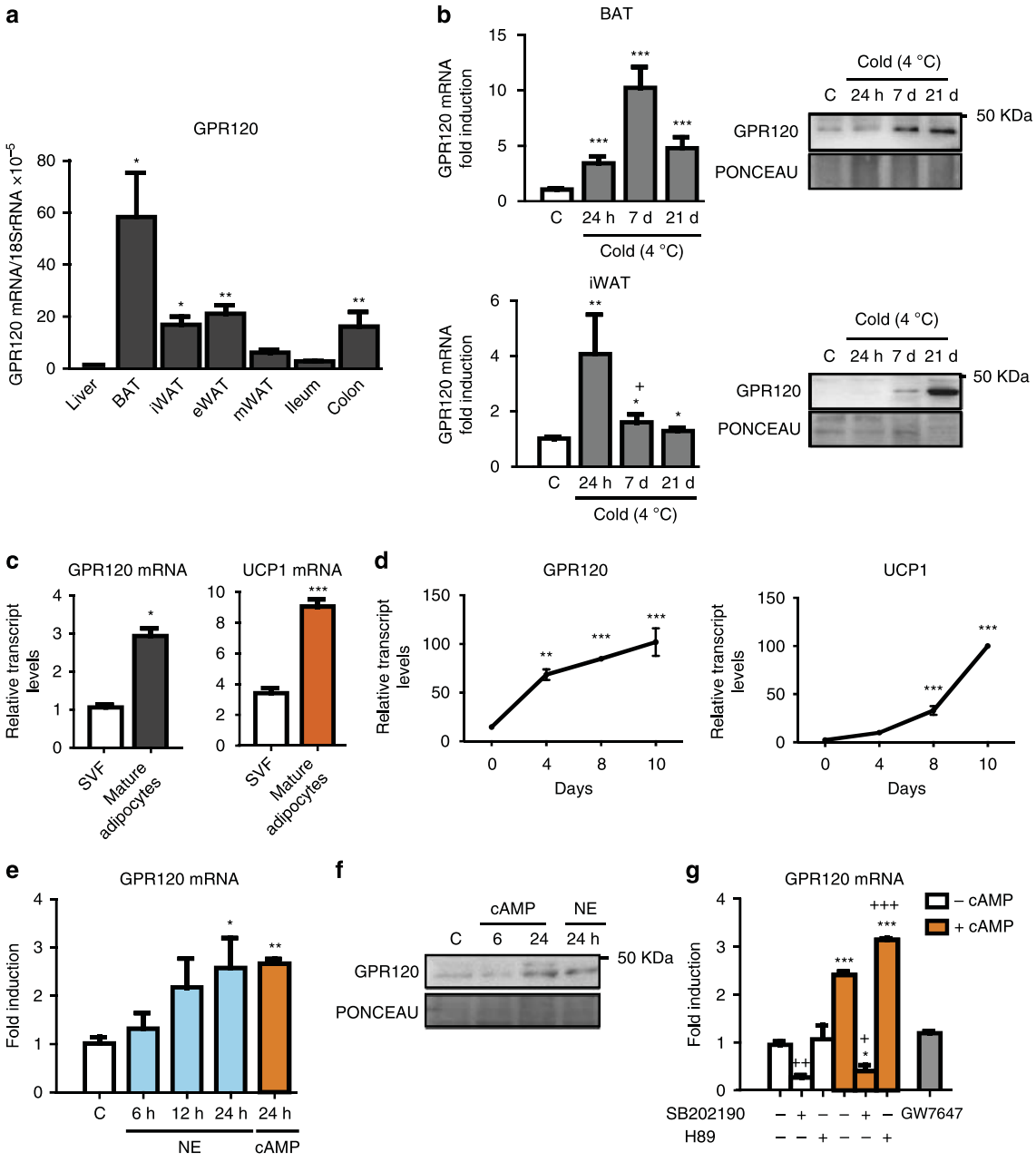

Figure 1 | Regulation of GPR120 gene expression in BAT and brown adipocytes. For **a**, **b**, tissues from adult mice were analysed. (**a**) Relative expression of *GPR120* mRNA in liver, BAT, iWAT, eWAT, mWAT, ileum and colon ($n=4$) was quantified. (**b**) *GPR120* mRNA expression in BAT and iWAT from adult mice maintained at thermoneutrality (29 °C) or exposed to cold (4 °C) for 24 h, 7 days and 21 days ($n=5$) in the left, representative immunoblot of three independent assays of the relative changes of GPR120 protein, in the right. (**c**) mRNA levels of *GPR120* and *UCP1* in the stromal vascular fraction (SVF) and mature adipocytes obtained from iBAT ($n=3$). For d-g, BAT precursor cells were differentiated. (**d**) mRNA expression patterns for *GPR120* and *UCP1* during brown adipocyte differentiation in primary cultures, as assessed at days 0 (pre-adipocytes) 4, 8, and 10 ($n=3$). (**e**) *GPR120* mRNA levels in differentiated brown adipocytes treated with 0.5 μM norepinephrine (NE) for 6, 12 and 24 h (blue bars) or with 1 mM dibutyryl-cAMP for 24 h (orange bars; $n=4$). (**f**) Representative immunoblot of three independent assays of the relative changes of GPR120 protein levels in response to the indicated NE and cAMP treatments. (**g**) Effects of 10 μM SB202190 (a p38 MAPK inhibitor), or 20 μM H89 (a PKA inhibitor) on the upregulation of *GPR120* mRNA in response to 1 mM dibutyryl-cAMP (orange bars), and effects of 1 μM GW7647 (PPARα agonist, grey bar; $n=4$). Bars are means + s.e.m. ($^*P<0.05$, $^{**}P<0.01$ and $^{***}P<0.001$ compared with corresponding controls, or ileum; $+P<0.05$, $++P<0.01$, $+++P<0.001$ for the effects of SB202190 or H89; for **a**, **b**, **e** and **g** analysis of variance with Tukey's *post hoc* test was used; for **c** and **d** two-tailed unpaired Student's *t*-test was performed).

(Supplementary Table 1) with the exception of FGF21 levels, which were markedly induced (see below). The 1-week exposure to GW9508 treatment did not significantly modify the gross masses of iBAT, iWAT, eWAT or mesenteric WAT (Supplementary Table 1). Gene expression analysis revealed significant upregulations among markers of thermogenic activation in BAT, such as *UCP1*, *PGC-1α*, *CoxIV* and *Sirt3*, as well as *Glut1*, but no change in overall adipogenesis. (Fig. 2a). UCP1 protein levels in the iBAT depot were also significantly increased (Fig. 2a). Microscopy examination of iBAT did not reveal major changes (Fig. 2a). In iWAT, we observed strong evidence of GW9508-induced browning, including upregulation of markers of brown-

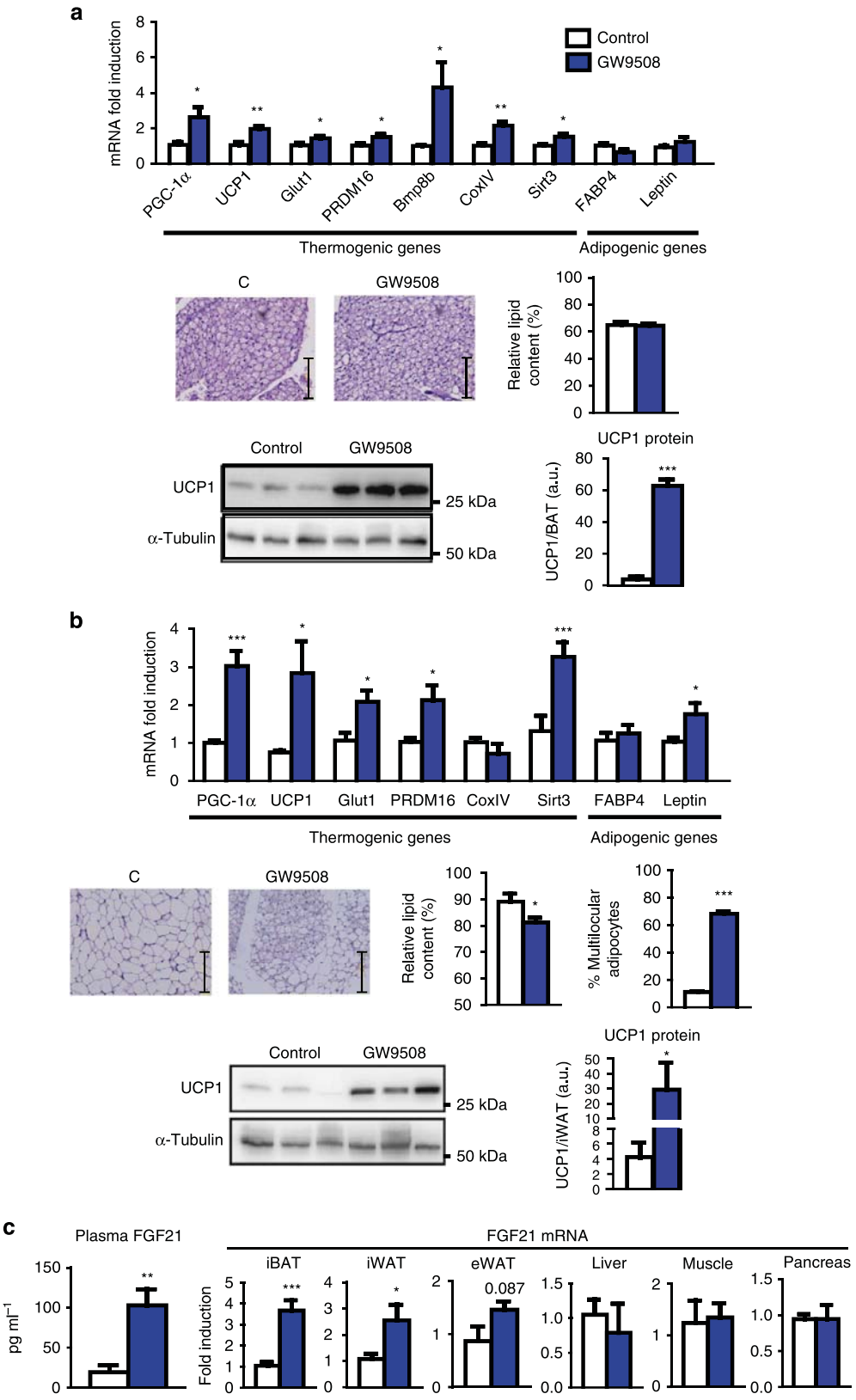

Figure 2 | GW9508 upregulates thermogenic genes in iBAT and browning in iWAT while inducing FGF21 expression and release. Adult mice were fed for 7 days a control diet (white bars) or a diet supplemented with GW9508 (blue bars; $n=6$). (**a**) Relative expression levels of thermogenic and adipogenic genes in iBAT, representative optical microscopy images from H&E-stained iBAT (scale bar, 125 μm), relative lipid content, UCP1 protein levels and representative UCP1 immunoblot. (**b**) Relative expression levels of thermogenic and adipogenic genes in iWAT, representative optical microscopy from H&E-stained iWAT (scale bar, 125 μm), relative lipid content, percentage of multilocular adipocytes, UCP1 protein levels and representative UCP1 immunoblot. (**c**) Circulating levels of FGF21 protein and *FGF21* mRNA expression levels in iBAT, iWAT, eWAT, liver, skeletal muscle and pancreas. Bars are means + s.e.m. (*$P<0.05$, **$P<0.01$ and ***$P<0.001$ relative to untreated control mice; two-tailed unpaired Student's *t*-test).

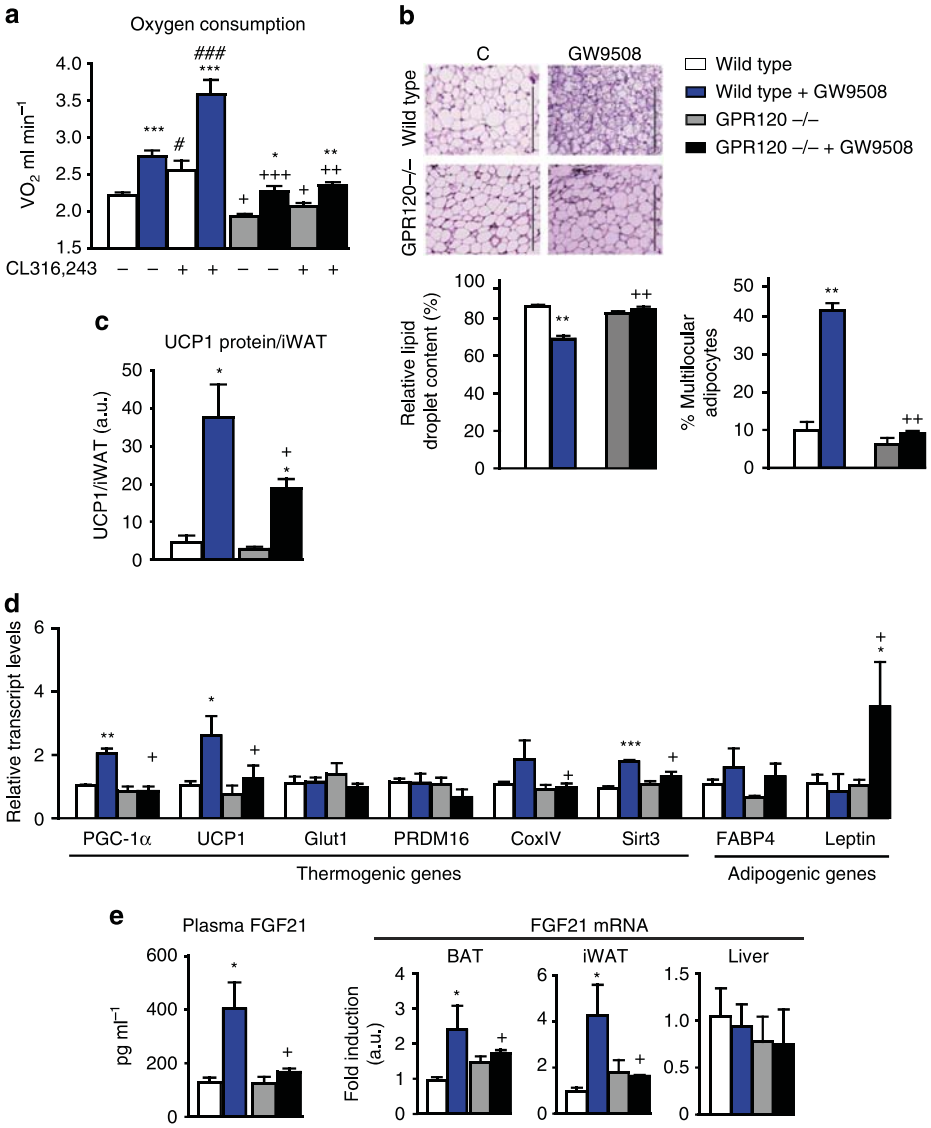

Figure 3 | GPR120 gene invalidation blunts the effects of GW9508 on adipose tissues and systemic FGF21 levels. Wild-type and *GPR120* −/− mice were fed a control diet (white and grey bars, respectively) or a diet supplemented with GW9508 (blue and black bars, respectively) for 7 days ($n=5$ per group). (**a**) Oxygen consumption in basal conditions and after CL316,243 injection. (**b**) Representative optical microscopy from H&E-stained iWAT (scale bar, 200 μm), relative lipid content and percentage of multilocular adipocytes. (**c**) UCP1 protein levels in iWAT. (**d**) Relative expression levels of thermogenic and adipogenic genes in iWAT. (**e**) Circulating levels of FGF21 protein and *FGF21* mRNA expression levels in iBAT, iWAT and liver. Bars are means + s.e.m. (*$P<0.05$, **$P<0.01$ and ***$P<0.001$ relative to untreated control mice of each genotype; +$P<0.05$, ++$P<0.01$ and +++$P<0.001$ for the comparisons between genotypes under same GW9508 treatment status; #$P<0.05$, ###$P<0.001$ for the effects of GW9508 treatment; analysis of variance with Tukey's *post hoc* test).

related thermogenesis (*UCP1*, *PGC-1α* and *Sirt3*), and the beige adipogenesis-related gene *PRDM16* (Fig. 2b). Consistent with these data, GW9508-treated mice exhibited multiple multilocular adipocytes in iWAT, which are typically associated with the browning process (Fig. 2b). UCP1 protein levels in iWAT were significantly induced by GW9508 (Fig. 2b). Epididymal WAT showed some signs of browning, such as upregulation of *UCP1*, *PGC-1α* and *Sirt3*, but no multilocular beige adipocytes (Supplementary Fig. 2).

As FGF21 is induced in association with the thermogenic activation of BAT and browning of WAT[19,20], we examined FGF21 in treated mice. We found that circulating levels of FGF21 were strongly increased in GW9508-treated mice, as were the *FGF21* mRNA expression levels in BAT and iWAT (Fig. 2c), but not in other tissues such as liver, skeletal muscle or pancreas. The lack of effects of GW9508 treatment on hepatic *FGF21* gene expression suggested that the upregulation of circulatory FGF21, following GW9508 treatment was not due to a hepatic effect. In addition to activating GPR120, GW9508 can activate another G-protein-coupled receptor, GPR40, which is expressed in the intestine[21] but absent in adipose tissues and minimally expressed in hepatic cells[17,22]. Accordingly, GPR40 transcript expression was undetectable in BAT and most WAT depots (Supplementary Fig. 3a). Moreover, the intestine does not express FGF21 under basal conditions[23] or following GW9508 treatment (Supplementary Fig. 3b). The glucagon gene (encoding glucagon-like peptide (GLP)-1), a target of GPR120 in the intestine[21], was not altered by GW9508 treatment (Supplementary Fig 3b). These results indicate that GW9508 treatment has only minor intestinal effects under this experimental setting.

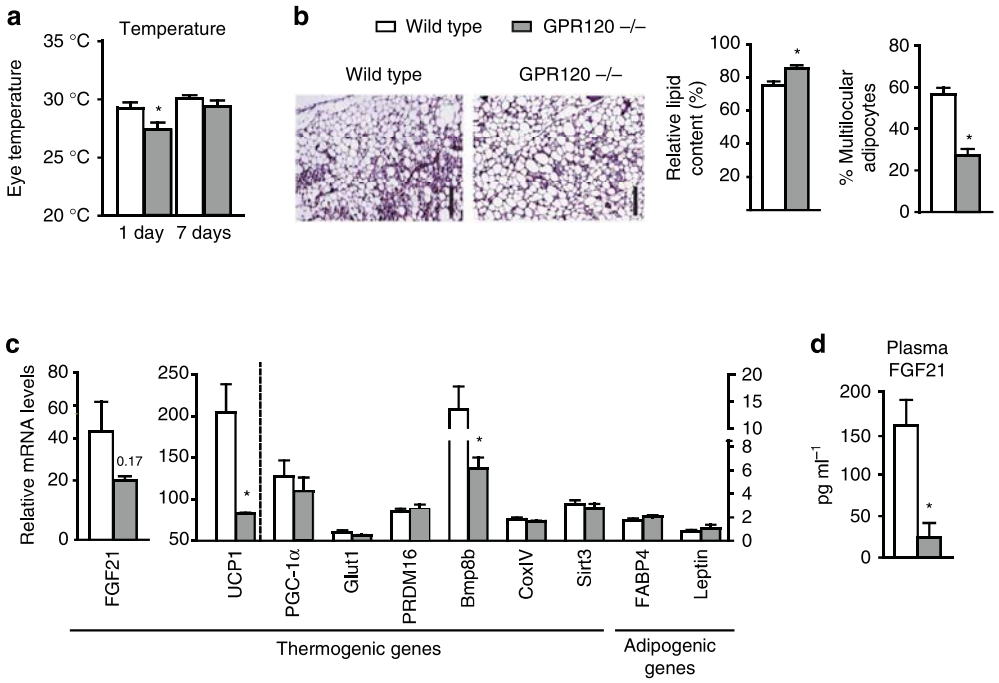

Figure 4 | GPR120 gene invalidation compromises thermoregulation and iWAT browning in association with a reduction in FGF21 levels. Wild-type (Wt, white bars) mice and *GPR120* −/− mice (grey bars) mice were exposed to cold (4 °C) for 7 days ($n=5$). (**a**) Body temperature on days 1 and 7 of cold exposure. (**b**) Representative images of H&E-stained iWAT (scale bar, 200 μm), the relative lipid droplet content, and the percentage of multilocular adipocytes. (**c**) Relative expression levels of thermogenic and adipogenic genes in iWAT. (**d**) Circulating levels of FGF21. Bars are means + s.e.m. (*$P<0.05$, **$P<0.01$ and ***$P<0.001$ relative to wild-type animals exposed to cold; two-tailed unpaired Student's *t*-test).

Impaired action of GW9508 in *GPR120-null* mice. To directly assess the role of GPR120 for the effects of GW9508, we analysed *GPR120*-null mice. Under basal conditions, *GPR120*-null mice did not show any significant change in body weight or in the main metabolic parameters evaluated (for example, glycaemia or triglyceridemia; Supplementary Table 2). This agrees with previous reports[13,14]. To examine the contribution of GPR120 to the actions of GW9508, we treated wild-type and *GPR120*-null mice with the drug for 7 days. The treatment with the drug did not alter glycaemia, triglyceridemia and insulinaemia in *GPR120*-null mice (Supplementary Table. 2). GW9508-treated wild-type mice showed increased oxygen consumption both under basal conditions and following the injection with the β3-adrenergic agonist CL316,243 (Fig. 3a), consistent with the enhanced iWAT browning and signs of BAT activation shown previously. In contrast, *GPR120*-null mice showed a reduction in basal and CL316,243-triggered oxygen consumption. GW9508 treatment increased oxygen consumption in *GPR120*-null mice, but the attained levels were lower in *GPR120*-null versus wild-type mice. Moreover, the capacity of CL316,243 to induce oxygen consumption was strongly impaired in GW9508-treated *GPR120*-null mice (Fig. 3a). *GPR120*-null mice treated with GW9508 exhibited iBAT with larger lipid droplets, which is reminiscent of decreased thermogenic activity (Supplementary Fig. 4). Expression levels of thermogenesis-related transcripts was significantly altered in *GPR120*-null mice for *PGC-1α* and, especially, for *Bmp8b*, with decreased GW9508-triggered upregulations in *GPR120*-null versus wild-type mice. Total levels of UCP1 protein were unaltered in *GPR120*-null mice (Supplementary Fig. 4).

Browning, identified by the presence of numerous multilocular adipocytes and the induction of several brown-versus-white-related genes (for example, *PGC-1α*, *UCP1* and *Sirt3*) was enhanced in the iWAT of GW9508-treated wild-type mice, but this induction was markedly impaired in *GPR120*-null mice (Fig. 3b,d). UCP1 protein levels in iWAT were strongly increased in wild-type mice in response to GW9508 treatment, whereas GW9508-treated *GPR120*-null showed significantly lower levels of UCP1 protein (Fig. 3c).

GPR120 invalidation had especially marked effects on circulating FGF21 levels and *FGF21* expression in the iBAT and iWAT of GW9508-treated mice. The increase of plasma FGF21 observed in GW9508-treated wild-type mice was abrogated in *GPR120*-null mice, as was the significant induction of FGF21 transcript levels elicited by GW9508 in BAT and iWAT (Fig. 3e). There was no alteration of *FGF21* gene expression in the liver, regardless of the treatment or mouse genotype.

These data indicate that GPR120 is largely required for the effects of GW9508 in BAT and iWAT '*in vivo*', although the additional involvement of GPR40 cannot be ruled out in light of the dual agonist properties of GW9508.

Impaired thermogenesis and browning in *GPR120*-null mice. We next tested the effects of cold exposure on *GPR120*-null mice. Most *GPR120*-null mice tolerated exposure to cold (4 °C), but ~20% developed hypothermia (a 10 °C or more drop in body temperature) within the first 24 h of cold exposure; none of the wild-type mice developed similar hypothermia. The estimated core temperature was significantly lower in *GPR120*-null mice than in wild-type mice after 1 day of cold exposure and tended to remain lower after 7 days of cold exposure (Fig. 4a). The microscopic morphology of iBAT did not show major alterations in cold-exposed *GPR120*-null mice and thermogenic gene expression pattern was essentially unaltered in *GPR120*-null mice relative to wild-type controls after 7 days of cold (Supplementary Fig. 5). However, *leptin* expression was increased in *GPR120*-null mice, which is consistent with some extent of 'whitening' in

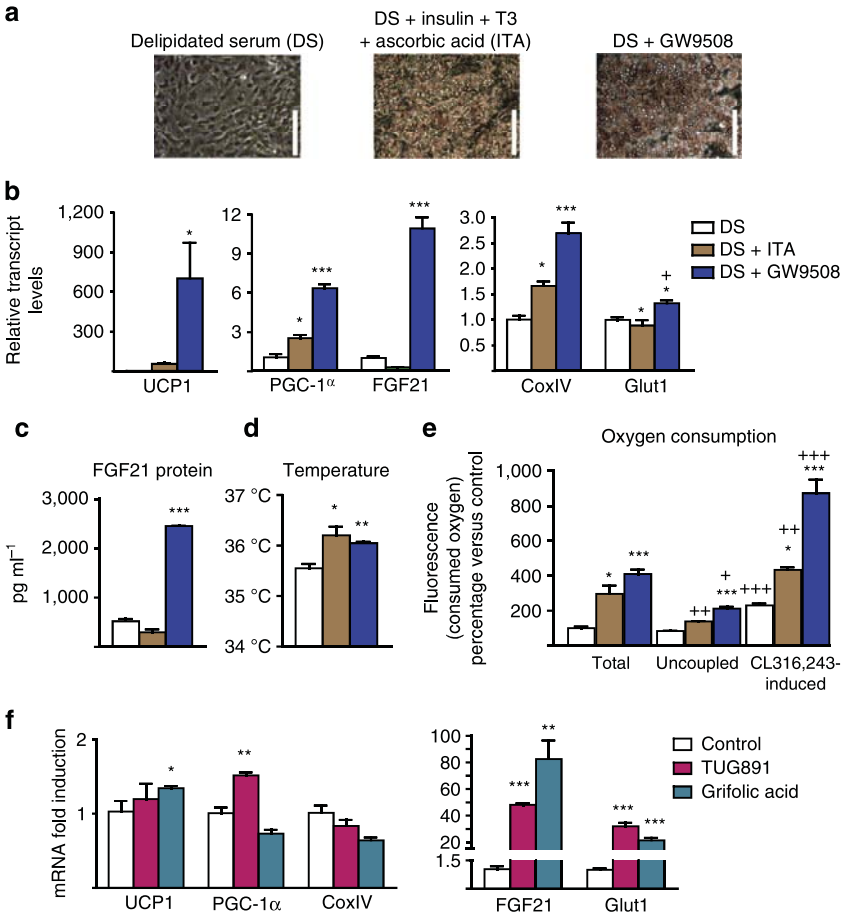

Figure 5 | GPR120 activation induces brown adipocyte differentiation and increases FGF21 expression and release. For **a–e**, iBAT precursors were differentiated in the presence of standard culture medium supplemented as follows: with 10% delipidated serum (DS, white bars; $n=4$); with DS plus insulin, triiodothyronine and ascorbic acid (DS + ITA, brown bars; $n=5$); or with DS plus 100 μM GW9508 (blue bars; $n=4$). (**a**) Representative optical microscopy images from cells at the end of the differentiation (day 9) (scale bars, 200 μm). (**b**) Relative mRNA expression levels of *UCP1*, *PGC-1α*, *COXIV*, *FGF21* and *Glut1*. (**c**) FGF21 protein levels in cell culture media (4 day accumulation). (**d**) Cell culture temperature. (**e**) Total and uncoupled (oligomycin-resistant) respiration, and respiration after CL316,243 treatment (**f**) iBAT precursors from mice were differentiated with DS + ITA, mRNA expression levels of *UCP1*, *PGC-1α*, *CoxIV*, *FGF21* and *Glut1* after 24 h treatment with TUG-891 (200 μM, pink bars) or grifolic acid (100 μM, turquoise bars). Bars are means + s.e.m. (*P* values: $^{*}P<0.05$, $^{**}P<0.01$ and $^{***}P<0.001$ versus DS (**b–e**) or versus controls (**f**); $+P<0.05$, $++P<0.01$ and $+++P<0.001$ for uncoupled respiration or induction in respiration upon CL316,243 versus total respiration; analysis of variance with Tukey's *post hoc* test).

BAT (Supplementary Fig. 5). iWAT browning was significantly impaired in cold-exposed *GPR120*-null mice. There were far fewer clusters of multilocular adipocytes in the iWAT of *GPR120*-null mice compared with wild-type controls (Fig. 4b), whereas the relative lipid content was higher. The expression levels of the thermogenic genes *UCP1* and *Bmp8b* were reduced, and *FGF21* gene expression tended to be lower (Fig. 4c). Circulating FGF21 levels were significantly reduced in cold-exposed *GPR120*-null mice (Fig. 4d), whereas FGF21 transcript expression in the liver and skeletal muscle was unaltered (Supplementary Fig. 5).

GPR120 activation induces brown adipocyte thermogenesis. We next used cell culture systems of brown and beige adipocytes to assess whether the abilities of GPR120 activation to promote BAT activation, WAT browning and FGF21 induction were cell autonomous. GW9508 was used to determine the specific effects of GPR120 activation as brown adipocytes (similar to white adipocytes) lack detectable levels of *GPR40* transcript and thus the actions of GW9508 are only attributable to GPR120 activation[13,24].

First, we determined whether GPR120 activation targets brown adipocyte differentiation. Precursor cells were obtained from iBAT stromal vascular fractions and cultured as previously reported[25]. On day 4 of culture, regular medium was replaced to contain 10% delipidated serum, which does not allow differentiation (Fig. 5a)[26]. The addition of insulin, triiodothyronine and ascorbic acid (ITA) to the culture was sufficient to induce differentiation. Notably, the addition of GW9508 instead of ITA also yielded a robust differentiation of brown adipocytes (Fig. 5a). Analysis of brown differentiation marker genes (for example, *UCP1*, *PGC-1α*, *COXIV* and *Glut1*) indicated that GW9508 triggered a stronger induction compared with ITA (Fig. 5b). Among the tested genes, the highest GW9508-induced upregulation was seen for FGF21 (Fig. 5b). These effects on *FGF21* gene expression were associated with a strong release of FGF21 to the media of GW9508-treated cultures (Fig. 5c). Highly sensitive thermography[27,28] showed that GW9508 treatment increased the cell cultures temperature (Fig. 5d). Moreover, oxygen consumption in brown adipocytes differentiated in the presence of GW9508 was as high as in ITA-differentiated cells (Fig. 5e). GW9508-induced differentiation also enhanced the oxygen consumption triggered by the β3-adrenergic agonist CL316,243 (Fig. 5e).

We next analysed the effects of GPR120 activation on mature, differentiated, brown adipocytes (day 9 of culture). Treatment

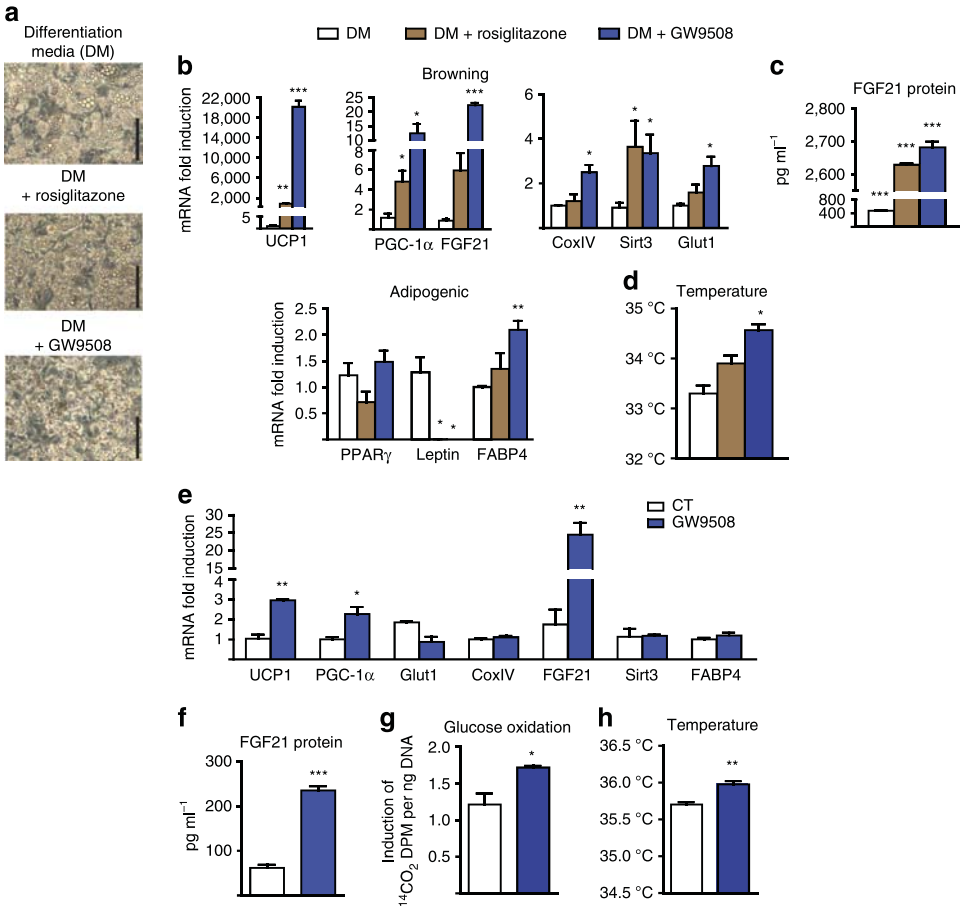

Figure 6 | GPR120 activation promotes beige adipocyte differentiation and increases FGF21 expression and release. For **a–d**, iWAT precursors from mice were differentiated in the presence of the differentiation media (DM, white bars), supplemented with rosiglitazone to drive beige differentiation (DM + rosiglitazone, brown bars; $n=4$) or treated with GW9508 instead of rosiglitazone (DM + GW9508, blue bars; $n=5$; see the Methods section). (**a**) Representative optical microscopy images at the end of differentiation (day 7; scale bar, 200 μm). (**b**) Relative mRNA expression levels of browning-related and general adipogenic genes. (**c**) FGF21 protein levels in the cell culture medium (4 day accumulation). (**d**) Cell culture temperature. For **e–h**, iWAT precursors were differentiated and treated during 24 h with GW9508 (100 μM, blue bars; $n=5$) or nor treated ($n=3$). (**e**) mRNA expression levels of *UCP1*, *PGC-1α*, *Glut1*, *COXIV*, *FGF21*, *Sirt3* and *FABP4*. (**f**) FGF21 protein levels in culture media (24 h accumulation). (**g**) Glucose oxidation rate. (**h**) Cell culture temperature. Bars are means + s.e.m. (*$P<0.05$, **$P<0.01$ and ***$P<0.001$ versus DM (**b–d**) or versus controls (**e–h**); for **b–d**, analysis of variance with Tukey's *post hoc* test was performed; for **e–h**, two-tailed unpaired Student's *t*-test).

with GW9508 for 24 h led to a marked induction of *UCP1*, *Glut1* and *FGF21* expression, as well as a strong increase in the secretion of FGF21 protein (Supplementary Fig 6). Moreover, GW9508 significantly induced the glucose oxidation and tended to increase the cell culture temperature (Supplementary Fig. 6).

To examine whether drugs that also activate GPR120 specifically cause similar effects, we tested TUG-891[29] and grifolic acid[30]. Indeed 0.2 mM TUG-891 and 0.1 mM grifolic acid strongly upregulated *FGF21* and *Glut1*, and had milder effects on *UCP1* and *PGC-1α* (Fig. 5f).

Collectively, these results indicate that GPR120 activation has cell-autonomous effects on brown adipocytes, including a strong effect in promoting brown adipocyte differentiation and a particularly strong activation of FGF21 expression and release associated with signs of the enhanced oxygen consumption, glucose oxidation and thermogenesis.

GPR120 activation induces beige adipocyte thermogenesis. To analyse the cell-autonomous effects of GPR120 activation on the WAT browning process, primary cultures of precursor cells obtained from iWAT were cultured in regular differentiation medium and exposed to rosiglitazone to promote acquisition of the beige phenotype[31]. Rosiglitazone treatment did not alter the morphology of differentiating cells or the lipid droplet accumulation, but did tend to decrease the lipid droplet size (Fig. 6a). Rosiglitazone did not alter the expression of general adipogenic marker genes in differentiating adipocytes; instead it downregulated leptin (a marker of the WAT versus BAT phenotype) and strongly upregulated the beige markers *UCP1* and *PGC-1α* (Fig. 6b). Supplementation with GW9508 instead of rosiglitazone caused a similar, even stronger, induction of browning, as evidenced by upregulation of the beige marker genes (*UCP1*, *PGC-1α* and *Sirt3*; Fig. 6b) and downregulation of leptin, while leaving most general adipogenic genes unaltered. Rosiglitazone-induced and especially GW9508-induced beige differentiation strongly upregulated the expression (Fig. 6b) and release of FGF21 (Fig. 6c). Consistent with the gene expression data, the heat production was significantly higher in GW9508-treated beige cells (Fig. 6d).

We next questioned whether the effects of the GPR120 activation also occurred in adipocytes that had differentiated to a beige phenotype. Indeed, GW9508 treatment of differentiated

beige adipocytes for 24 h triggered a moderate but significant upregulation of thermogenic marker genes (*UCP1* and *PGC-1α*), and a stronger induction of FGF21 expression (Fig. 6e) and release (Fig. 6f). GW9508 also increased the glucose oxidation rate (Fig. 6g) and cellular heat production (Fig. 6h) in beige adipocytes.

Compared with iWAT precursors, eWAT precursors yielded similar results with GW9508 inducing even stronger browning than rosiglitazone (as shown by gene expression analysis) and powerfully inducing FGF21 expression and release in differentiated adipocytes (Supplementary Fig. 7).

n-3 PUFAs promote brown fat activation through GPR120. GPR120 is assumed to interact with unsaturated fatty acids—or derivatives—at the cell surface and trigger subsequent intracellular effects[12]. Since omega-3 PUFAs are more potent than omega-6 or omega-9 PUFAs in eliciting GRP120-mediated effects[12,13], we analysed the effects of α-linolenic (ALA), eicosapentaenoic (EPA) and docosahexaenoic (DHA) acids.

Supplementation of delipidated cell culture medium with EPA or ALA markedly promoted the morphological adipogenic differentiation of brown pre-adipocytes obtained from iBAT, to a degree similar to that elicited by ITA (Fig. 7a). In contrast, DHA had barely significant effects. The thermogenic genes, especially *UCP1* and *FGF21*, were markedly induced by EPA and ALA, relative to ITA. Some induction of general adipogenic genes was also observed, especially in response to EPA (Fig. 7b). EPA and ALA also enhanced FGF21 protein secretion relative to ITA (Fig. 7c). The cellular temperature was increased by EPA relative to cells cultured in delipidated medium, but there was no significant temperature difference relative to ITA-differentiated cells (Fig. 7d). EPA treatment increased oxygen consumption to an extent similar to that elicited by ITA, under both basal and CL316,243-treated conditions (Fig. 7e).

EPA and ALA treatment of beige adipocytes undergoing differentiation from iWAT precursors promoted their morphological differentiation (Fig. 7f), significantly upregulated the tested thermogenic-related genes (with the exception of a non-significant effect of ALA on *UCP1* and *PGC-1α*), and downregulated leptin (Fig. 7g). EPA and ALA increased FGF21 gene expression and release (Fig. 7h), but only EPA significantly increased cell temperature. Overall, in both, the brown and beige experimental settings, EPA tended to be more powerful than ALA.

As PPARα is known to mediate transcriptional effects of fatty acids in brown adipocytes[25] and regulates FGF21 expression in the liver[32,33], we determined the effects of EPA on primary cultures of precursor cells from the iBAT of *PPARα*-null mice. As expected, the absence of PPARα did not alter the responsiveness of brown adipocytes to GW9508 (Supplementary Fig 8a). EPA still promoted brown adipocyte differentiation and strongly induced FGF21 in cells devoid of PPARα, although the levels of FGF21 expression attained were smaller (Supplementary Fig 8a). We also determined whether the effects of EPA could involve PPARγ. Exposure of differentiating brown adipocytes to the PPARγ inhibitor, GW9662, did not significantly alter the effects of EPA or GW9508 on the morphological differentiation; the significant upregulation of the *FGF21* gene in response to EPA was maintained, but the levels achieved were significantly less than those observed in the absence of the PPARγ inhibitor (Supplementary Fig 8b). These results indicate that although PPARs are not necessary for the ability of EPA to induce FGF21, they may contribute to some of the effects of EPA.

We further determined the involvement of GPR120 in mediating the effects of EPA on the brown and beige differentiation of pre-adipocytes. For this purpose, we analysed precursor cells cultures from the iBAT and iWAT of *GPR120*-null mice and wild-type controls. Precursor cells from *GPR120*-null iBAT showed much less differentiation into brown adipocytes, as evidenced by decreased acquisition of brown adipocyte morphology (Fig. 8a), impaired expression of thermogenic marker genes (*UCP1* and *FGF21*; Fig. 8b), and signs of reduced expression of general adipogenesis marker genes. EPA treatment significantly induced *FGF21* mRNA expression (Fig. 8c) and FGF21 protein secretion (Fig. 8d) in wild-type brown adipocytes, but not in *GPR120*-null cells that were totally insensitive to EPA. Precursor cells from *GPR120*-null iWAT showed a delayed differentiation (Fig. 8e; see microscopic morphology on day 3 of culture), but ultimately reached similar levels of thermogenic and adipogenic gene expression by day 7. The abilities of EPA to induce *FGF21* mRNA expression and FGF21 protein release were significantly reduced in *GPR120*-null beige adipocytes (Fig. 8f).

Next, we used two independent approaches to determine whether EPA affects *FGF21* expression and release by previously differentiated brown or beige adipocytes, and whether GPR120 mediated these effects. First, we treated differentiated cells with the GPR120 antagonist, AH7614 (ref. 34). As expected, AH7614 significantly inhibited the capacity of GW9508 to induce *FGF21* expression and release in brown and beige adipocytes (Fig. 8g). AH7614 also inhibited the effects of EPA on FGF21 expression and release, indicating that these effects involve GPR120 in brown and beige adipocytes.

Second, we performed short interfering RNA (siRNA)-driven knockdown of GPR120 in brown adipocytes subjected to *in vitro* differentiation. In these cells, we obtained an 80% reduction in the mRNA expression of the GPR120 as compared with controls (Fig. 8h, left). Under these conditions of GPR120 knocking down, the abilities of GW9508 and EPA to induce *FGF21* gene expression were also strongly impaired (Fig. 8h). GPR120 knocking down also impaired the induction of *UCP1* and *PGC-1α* by EPA.

Collectively, these findings indicate that EPA induces brown and beige differentiation, and enhances *FGF21* gene expression and FGF21 protein secretion mostly via GPR120 activation.

GPR120-mediated induction of FGF21 involves p38 MAPkinase. To further explore the mechanisms through which GPR120 activation induces *FGF21* gene expression, differentiated brown adipocytes were treated with GW9508 in the presence or not of intracellular kinase inhibitors. U-0128 and wortmannin significantly reduced the upregulation of *FGF21* gene expression in response to GW9508 or EPA (Supplementary Fig 9a), confirming the previously reported involvement of ERK1/2 and PI3kinase, respectively, in the intracellular actions following GPR120 activation in other cell systems, such as white adipocytes[13]. In contrast, the inhibitors of PKA or AMP kinase had no effect (Supplementary Fig 9a). Interestingly, the p38 MAPK inhibitor, SB202190, strongly impaired GW9508- or EPA-induced *FGF21* gene expression. Treatment of brown adipocytes with GW9508 or EPA induced the phosphorylations of p38 MAPK and (as expected) ERK1/2, but not of other regulatory proteins such as CREB (Supplementary Fig 9b). As p38 MAPK mediates the regulation of FGF21 in response to noradrenergic stimuli in BAT[19], we determined the effects of GW9598 and EPA on the transcriptional regulation of the *FGF21* gene promoter. We found that these agents significantly induced the activity of the FGF21 promoter (Supplementary Fig 9c). Conversely, a version of the promoter devoid of the p38 MAPK-responsive site failed to respond to GW9508 or EPA. Moreover, transfection of an expression vector for MKK6 (MKK6-K82A), which acts as dominant negative for p38 MAPK-dependent activation[35], blunted the effects of GW9508 and EPA on the *FGF21* gene promoter activity. These findings suggest that GPR120-induced

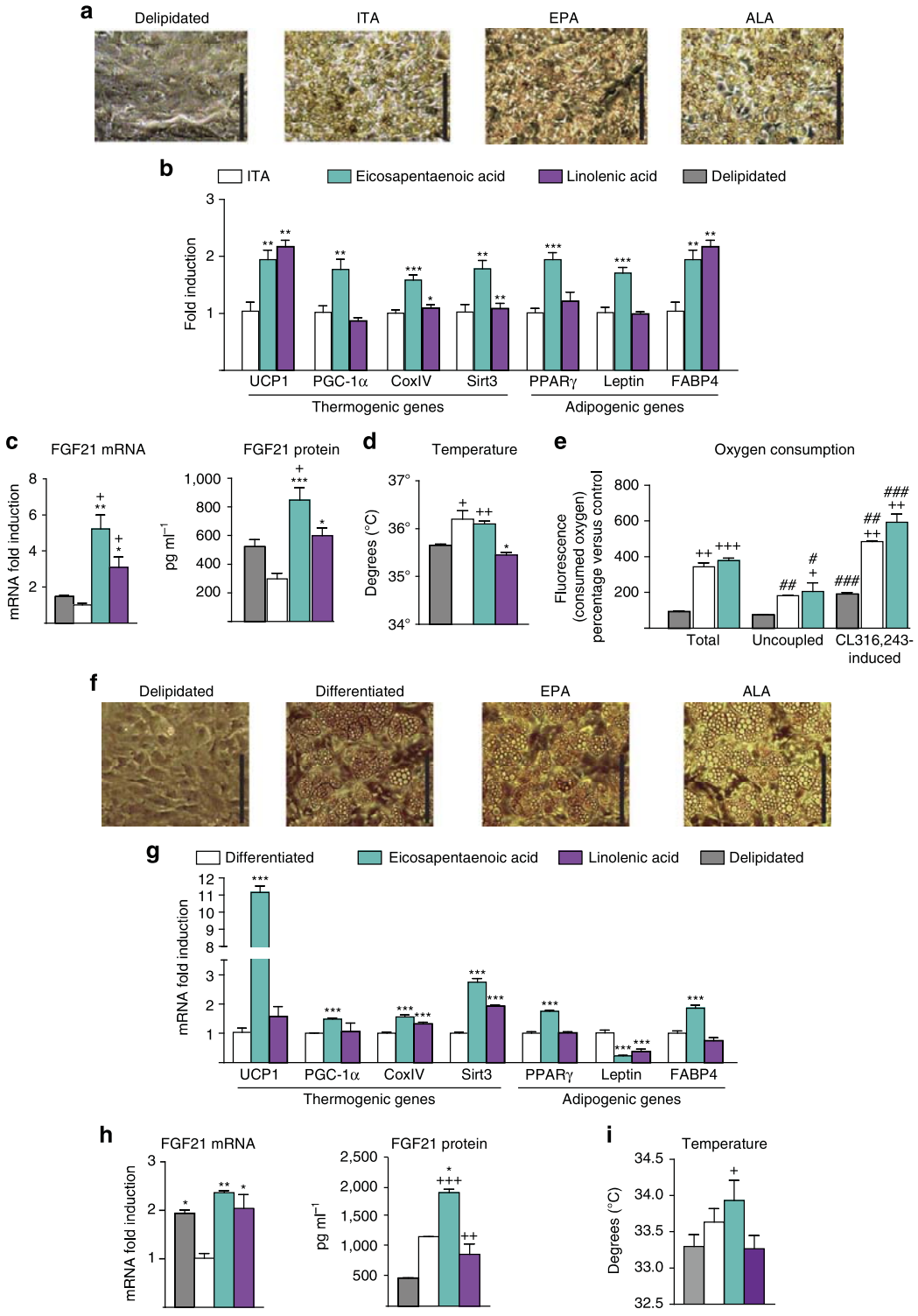

Figure 7 | n-3 PUFAs upregulate thermogenic genes expression and FGF21 expression and release. For **a–d**, iBAT precursors were cultured in media containing only delipidated serum (grey bars), or in the presence of insulin, T3 and ascorbic acid (ITA, white bars) or supplemented with eicosapentaenoic acid (EPA, tourquoise bars) or linolenic acid (ALA, purple bars). (**a**) Representative optical microscopy images of cultured brown precursors after the treatment (scale bar, 200 μm). (**b**) Relative mRNA expression of thermogenesis-related and general adipogenesis-related genes. (**c**) *FGF21* mRNA in adipocytes and protein levels in culture media. (**d**) Cell culture temperature. (**e**) Total and uncoupled respiration after differentiation and after treatment with CL316,243. For **f–i**, iWAT precursors were cultured in media containing only delipidated serum (grey bars), adipogenic cocktail (see the Methods section, white bars), or supplemented with EPA (turquoise bars) or ALA (purple bars). (**f**) Representative optical microscopy images of cultured beige precursors after the treatment (scale bar, 200 μm). (**g**) Relative mRNA expression of thermogenesis-related and general adipogenesis-related genes. (**h**) *FGF21* mRNA in adipocytes, protein levels in culture media and (**i**) cell temperature at the end of the treatment. Bars are means + s.e.m.(*$P<0.05$, **$P<0.01$ and ***$P<0.001$ versus differentiated ITA, +$P<0.05$, ++$P<0.01$ and +++$P<0.001$ versus delipidated, $^{\#}P<0.05$, $^{\#\#}P<0.01$ and $^{\#\#\#}P<0.001$ relative to total respiration; analysis of variance with Tukey's *post hoc* test).

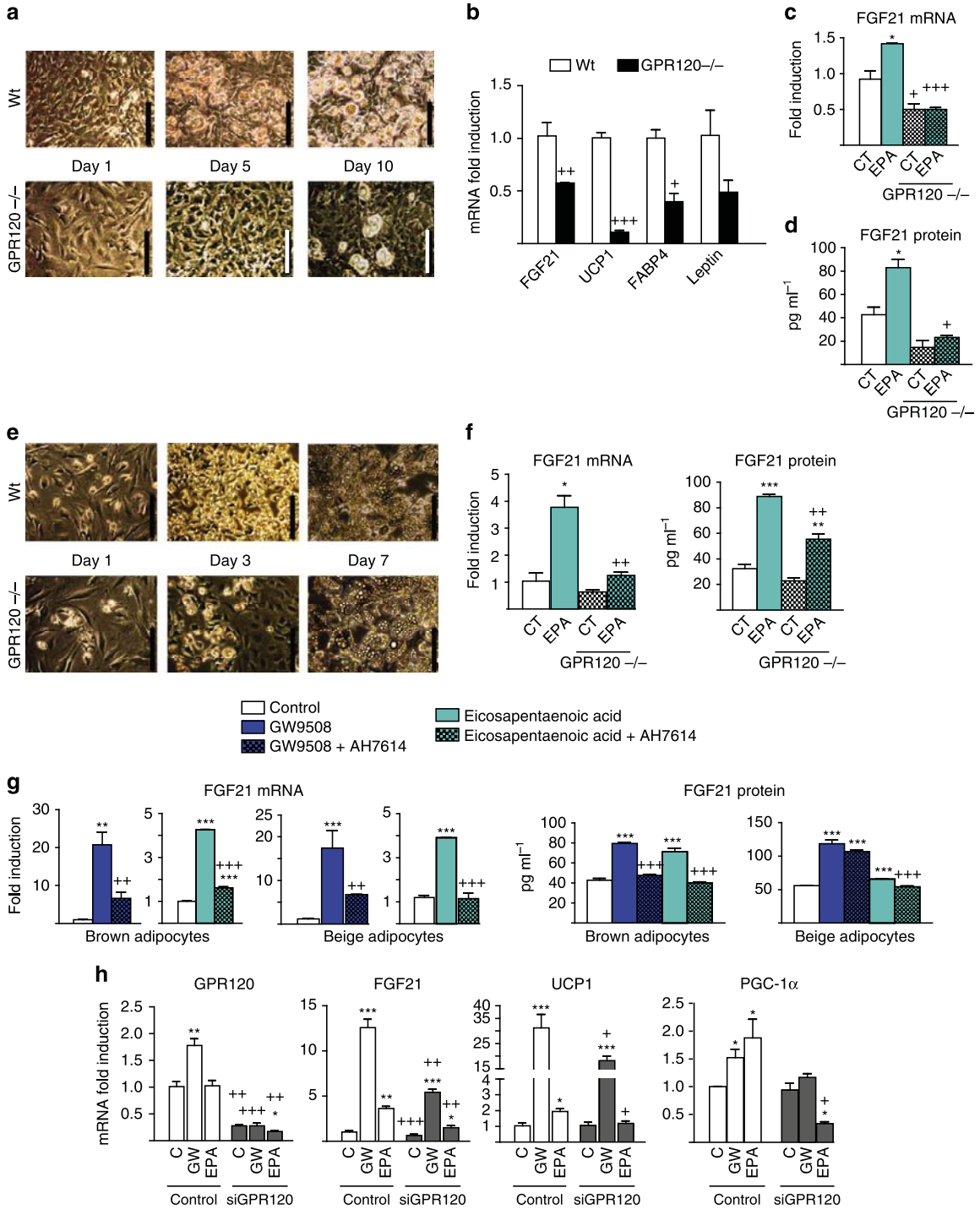

Figure 8 | GPR120 is required for the effects of EPA on adipocytes and FGF21 induction and release. For **a–d**, iBAT precursors from wild-type ($n=3$, white) and *GPR120*-null ($n=5$, black) mice were differentiated. (**a**) Representative optical microscopy images (scale bar, 200 μm). (**b**) Relative mRNA expression levels of *FGF21*, *UCP1*, *FABP4* and *leptin*. (**c**,**d**) Effects of EPA on *FGF21* mRNA expression and FGF21 secretion. For **e** and **f**, iWAT precursors from wild-type ($n=3$) and *GPR120*-null ($n=5$) mice were differentiated into beige adipocytes. (**e**) Representative optical microscopic images (scale bar, 200 μm). (**f**) Effects of EPA on *FGF21* mRNA expression and FGF21 protein secretion. (**g**) Differentiated brown and beige adipocytes were treated with GW9508 (blue bars) or EPA (turquoise bars) in the presence or absence of AH7614 (a GPR120 antagonist, patterned bars) for 24 h ($n=3$). *FGF21* mRNA expression and FGF21 protein levels in culture medium. (**h**) Differentiated brown adipocytes were subjected to siRNA-mediated knockdown of GPR120 (see the Methods section) and treated with GW9508 or EPA. mRNA expression levels of *GPR120*, *FGF21*, *PGC-1α* and *UCP1* ($n=3$). Bars are means + s.e.m. ($^*P<0.05$, $^{**}P<0.01$ and $^{***}P<0.001$ relative to controls, and $+P<0.05$, $++P<0.01$ and $+++P<0.001$ for comparisons between wild-type and *GPR120*-null cells (**a–f**), the effects due to AH7614 (**g**), and the effects due to siRNA-GPR120 (**h**). For **b**, two-tailed unpaired Student's *t*-test was performed; for **c–h**, analysis of variance with Tukey's *post hoc* test).

FGF21 expression in brown adipocytes involves the activation of p38 MAPK and its downstream induction of FGF21 gene transcription.

FGF21 is involved in the effects of GPR120 activation. FGF21, which is a hormonal factor expressed and released by brown and beige cells[19,20], has strong autocrine/endocrine effects on BAT activation and WAT browning[36,37]. Thus, we next explored the involvement of FGF21 in the biological response to GPR120 activation.

FGF21-null mice were treated with GW9508 in their diet for 1 week. The absence of FGF21 strongly impaired the capacity of GW9508 to induce BAT thermogenic activation, as evidenced by decreased induction of thermogenic genes (for example, *UCP1*, *PGC-1α* and *Bmp8b*) and *Glut1*, whereas markers of general adipogenesis (for example, *FABP4*) were unaltered (Fig. 9a). *FGF21*-null mice kept under basal conditions exhibited increased lipid content, indicative of impaired activity and 'whitening' of BAT (Fig. 9b). GW9508 treatment of *FGF21*-null mice, in contrast with wild-type mice, even increased the signs of impaired thermogenic activity and 'whitening' of BAT as evidenced by increased lipid content and enhanced leptin gene expression. Moreover, GW9508 failed to increase UCP1 protein levels in BAT from *FGF21*-null mice (Fig. 9b).

FGF21-null mice also showed strong impairment of iWAT browning in response to GW9508. The clusters of multilocular, beige adipocytes, seen in GW9508-treated wild-type mice were largely absent in GW9508-treated *FGF21*-null mice (Fig. 9d), and there were strong reductions in the GW9508-mediated upregulation of the thermogenic, beige phenotype-related, genes (for example, *PGC-1α*, *UCP1* and *Sirt3*; Fig. 9c). GW9508 treatment increased UCP1 protein levels in iWAT from wild-type mice and the extent of induction of UCP1 protein levels in *FGF21*-null mice was significantly lower. Although the response of eWAT to GW9508-induced browning was less marked than that in iWAT of wild-type mice, the mild upregulation observed among browning-associated genes was blunted in GW9508-treated *FGF21*-null mice (Supplementary Fig 10).

We further explored the cell-autonomous functions of FGF21 in the responsiveness to GPR120 activation. Brown adipocytes from *FGF21*-null mice differentiated normally *in vitro*, and GPR120 expression was not altered by the lack of FGF21. GW9508 was able to activate the expressions of thermogenic genes (*UCP1*, *PGC-1α*, *COXIV* and *Sirt3*) in cultured brown adipocytes, but the extent of these inductions were significantly less in *FGF21*-null cells than in control cells (Fig. 10a). When previously differentiated brown adipocytes from *FGF21*-null mice were treated with GW9508 for 24 h, we observed reductions in the upregulations of some thermogenic genes (Fig. 10b) and glucose oxidation (Fig. 10d). In beige adipocytes differentiated from iWAT, the lack of FGF21 reduced the GW9508-induced upregulations of beige markers (*UCP1* and *PGC-1α*; Fig. 10c) and blocked the ability of GW9508 to induce glucose oxidation (Fig. 10d).

Collectively, these results indicate that at least some of the effects of GPR120 activation on the thermogenic activations of brown and beige adipocytes involve FGF21, potentially via the autocrine/endocrine actions of FGF21 secreted downstream of GPR120 activation.

Discussion

The identification of novel regulators that promote energy expenditure and the capacity of BAT activity to oxidize metabolic substrates may provide key therapeutic targets in obesity, diabetes and dyslipidemias. Attempts to promote energy expenditure by the use of sympathomimetics, which take advantage of the classical adrenergic pathway for controlling of BAT activity, have failed due to the important side effects[38].

We presently identified a novel pathway regulated by the fatty acid receptor GPR120 that controls BAT activity and WAT browning. Our data indicate that GPR120 activation plays a dual role, namely: (1) it promotes the differentiation of pre-adipocytes into the brown and beige lineages; and (2) it promotes thermogenic activation in differentiated brown and beige adipocytes. Previous reports showed that GPR120 activation increases the energy expenditure and ameliorates insulin resistance[13,14]. Given that BAT activity and WAT browning have major impacts on energy expenditure and glucose homoeostasis, our current data provide a biological basis and mechanistic explanation for these observations. This adds a new function for GPR120, in addition to its ability to decrease chronic inflammation, in association with the improved insulin resistance[13,39]. Modifications in the pro- and anti-inflammatory profiles of immune cells were recently reported to influence BAT activation and especially WAT browning[40,41]. Further research is warranted to determine the role of GPR120-mediated regulation of immune cells on BAT and browning of WAT *in vivo*; however, our current findings establish a direct, cell-autonomous effect, of GPR120 in the promotion of brown and beige cell differentiation and activation.

The effects of GPR120 activation on BAT activity and WAT browning appear to mediate the actions of omega-3 PUFAs, which are physiological activators of the GPR120 receptor, on these processes. Dietary enrichment with omega-3 PUFAs have beneficial effects on metabolic health in healthy lean individuals, whereas in experimental rodent models, omega-3 PUFA have been shown to prevent the development of obesity, and decrease hyperglycaemia and dyslipidemia[42]. Several reports agreed that dietary supplementation with PUFAs promote BAT recruitment and WAT browning as reflected by enhanced mitochondrial oxidative capacity and, in some reports, increased UCP1 content[43–47]. Single dietary supplementation with EPA (but not DHA) has reportedly had the most significant effects[43], and recent data show an especially active effect of EPA in the promotion of browning *in vitro*[48]. The molecular mechanisms underlying these effects remained to be clarified. Our current data indicate that omega-3 PUFAs have cell-autonomous GPR120-mediated effects directly stimulating the differentiation and activation of brown and beige adipocytes. This strongly supports the notion that GPR120 activation is involved in the actions of dietary omega-3 PUFAs on BAT activation, WAT browning and metabolic consequences, and may provide a molecular explanation for some of the beneficial effects of PUFAs.

Our study also shows that some of the effects triggered by GPR120 activation are mediated via the GPR120-induced expression and release of FGF21 in brown and beige adipose tissues. Fatty acids stimulate the expression of FGF21 in hepatic cells, which are devoid of GPR120, in a PPARα-mediated manner[32]. However, this pathway does not mediate FGF21 gene expression in BAT[19]. Our present data indicate that GPR120 activation is part of a highly tissue-specific pathway that regulates FGF21 expression via the p38 MAPK-mediated activation of *FGF21* gene transcription in brown and beige cell lineages. Moreover, the effects of GPR120 activation to promote BAT activity and WAT browning are mediated at least in part by FGF21. FGF21 promotes thermogenic activation of BAT, and the browning of WAT in association with increased glucose uptake and oxidation[36,37]. Similar effects were seen following GPR120 activation, and these effects were reduced in FGF21-inactivated animal and cell models. Thus, we herein report that autocrine and (perhaps) endocrine actions of FGF21 are relevant to the GPR120 activation-mediated induction of BAT differentiation and WAT

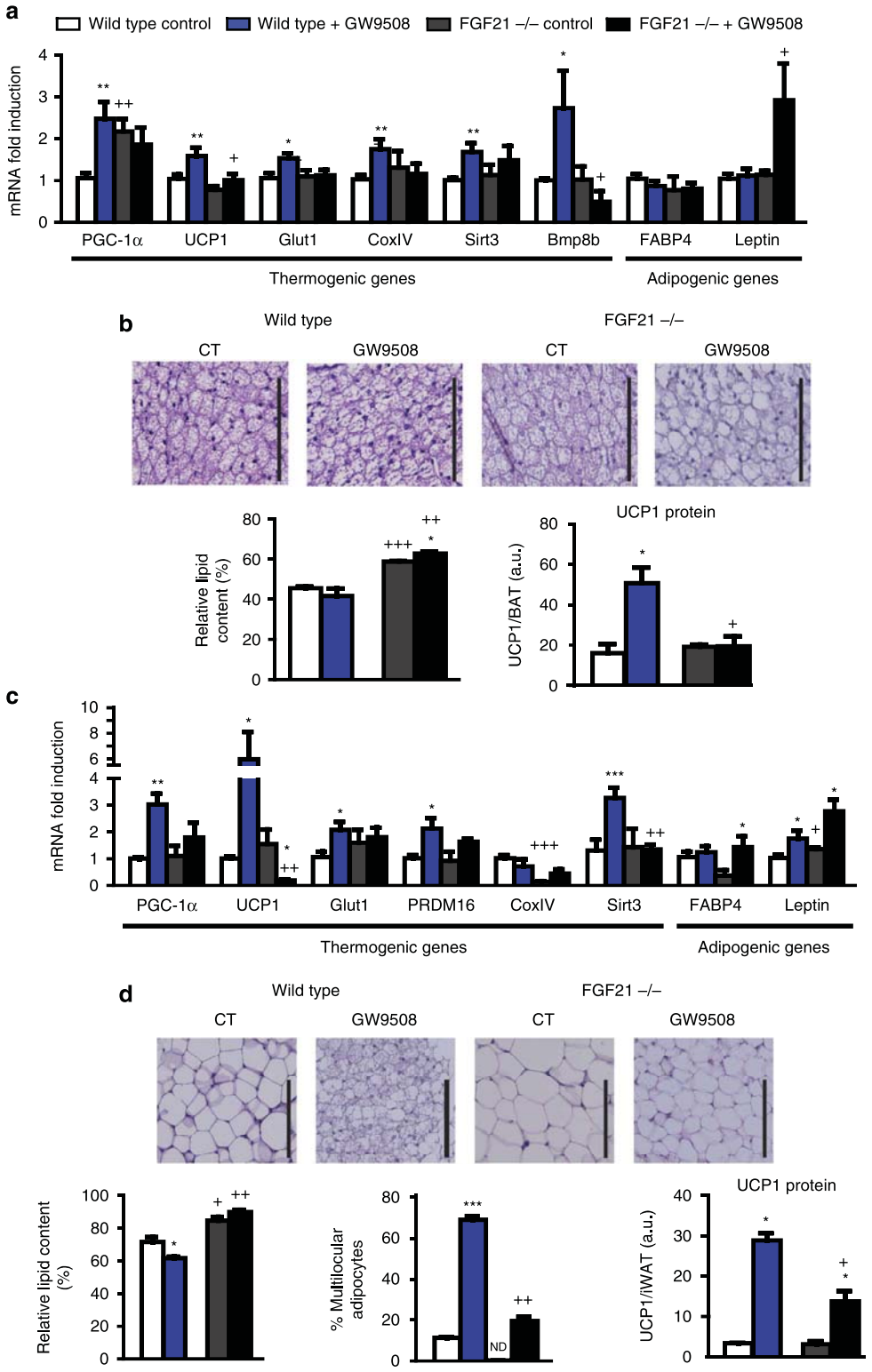

Figure 9 | FGF21 gene invalidation reduces the effects of GW9508 treatment in mice. Wild-type and *FGF21*-null mice were fed a control diet (white and grey bars, respectively) or supplemented with GW9508 (blue and black bars, respectively) for 7 days ($n=5$). (**a**) Relative mRNA levels of thermogenesis-related and adipogenic genes in iBAT (**c**) and iWAT. Representative optical microscopy images of H&E staining (scale bar, 125 μm), the relative lipid content and UCP1 protein levels in iBAT (**b**) and iWAT (**d**), and the percentage of multilocular adipocytes in iWAT. Bars are means + s.e.m. (*$P<0.05$, **$P<0.01$ and ***$P<0.001$ relative to untreated control mice of each genotype; +$P<0.05$, ++$P<0.01$ and +++$P<0.001$ relative to same treatment of the wild-type group; analysis of variance with Tukey's *post hoc* test).

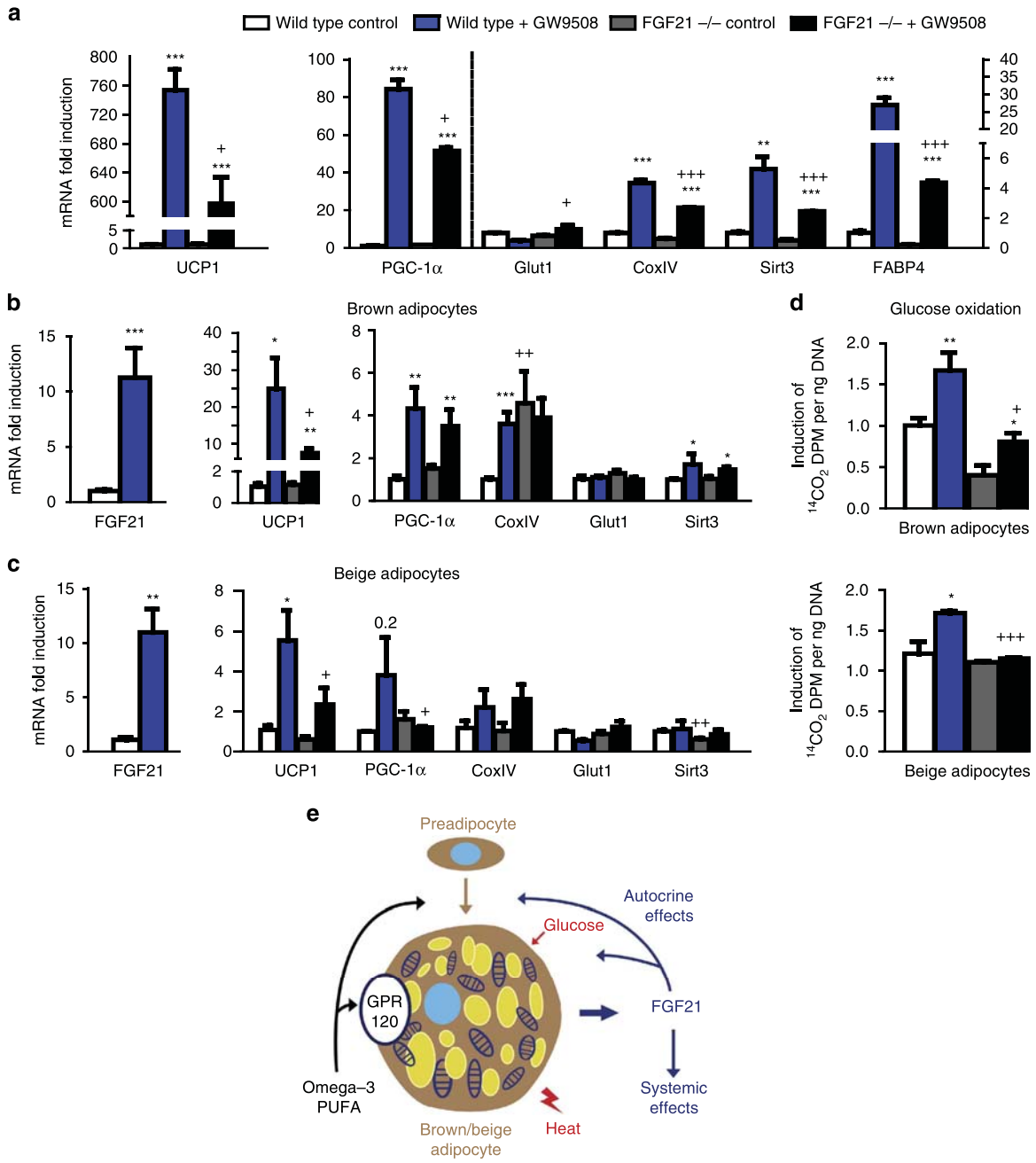

Figure 10 | Impaired effects of GW9508 on FGF21-null brown and beige adipocytes. (**a**) iBAT precursors from wild-type and FGF21-null mice ($n=5$) were treated with GW9508 during differentiation, relative transcript levels of *UCP1*, *PGC-1α*, *Glut1*, *CoxIV*, *Sirt3* and *FABP4*. (**b**) iBAT precursors from wild-type and *FGF21*-null mice ($n=5$) were differentiated and acutely treated with GW9508 (24 h), mRNA expression levels of *FGF21*, *UCP1*, *PGC-1α*, *CoxIV*, *Glut1* and *Sirt3*. (**c**) iWAT precursors from wild-type and *FGF21*-null mice ($n=5$) were differentiated and acutely treated with GW9508 (24 h), mRNA expression levels of *FGF21*, *UCP1*, *PGC-1α*, *CoxIV*, *Glut1* and *Sirt3*. (**d**) Glucose oxidation in iBAT and iWAT-derived adipocytes from wild-type and *FGF21*-null mice after 24 h treatment with GW9508. Bars are means + s.e.m. (*$P<0.05$, **$P<0.01$ and ***$P<0.001$ for the effects of GW9508; and +$P<0.05$, ++$P<0.01$ +++$P<0.001$ for comparisons between wild-type and *FGF21*-null cells; and analysis of variance with Tukey's *post hoc* test). (**e**) Schematic representation of the effects of GPR120 activation by n-3 PUFAs on brown and beige adipocytes. FGF21 is involved in the GPR120 activation-mediated thermogenic activation of BAT and WAT via autocrine/endocrine mechanisms.

browning (Fig. 10e). Of note, the capacity of GPR120 activation to modify intracellular kinases (for example, p38 MAPK) suggests that GPR120 may have additional and direct effects on BAT activity and WAT browning.

In conclusion, we identified a novel pathway of BAT activation and browning of WAT based on a strong, cell autonomous, capacity of the lipid sensor GPR120 to trigger these processes. This pathway is expected to contribute to the systemic metabolic benefits occurring after GPR120 activation. Our present findings reinforce the current interest in the potential of GPR120-activating drugs or dietary molecules for treating metabolic diseases.

Methods

RNA-seq and RNA-seq data analysis. Total RNA was isolated using the RNeasy Mini Kit (Qiagen), which favours purification of RNA molecules longer than 200

nucleotides. Further sample preparation was done as described by the manufacturer (Illumina, Eindhoven, The Netherlands). Briefly, mRNA was purified from 2 μg total RNA using oligo (dT) beads, and then fragmented and randomly primed for reverse transcription followed by second-strand synthesis to create double-stranded cDNA fragments. The generated cDNA had undergone paired-end repair to convert overhangs into blunt ends. After 3′-monoadenylation and adaptor ligation, the cDNAs were purified by 2% agarose gel electrophoresis and 200-bp products were excised from the gel. Following gel digestion, the purified cDNA was amplified by PCR using primers specific for the ligated adaptors. Before sequencing, the generated libraries were submitted to a quality control assessment with an Agilent bioanalyzer 2100 (Agilent Technologies, Wokingham, UK). The RNA integrity number values for all samples were at least 7.5. To verify the cDNA quality and quantity, 1 μl cDNA was loaded on an Agilent DNA chip (DNA-1000, Agilent Technologies). Only libraries that yielded satisfactory results from the quality control studies were sequenced on an Illumina HiSeq 2,000 sequencer (DNAvision, Charleroi, Belgium) with an average of 45 million reads per sample. This level of coverage was previously shown to provide sufficient sequencing depth for the quantification of gene expression and detection of transcripts[49] and has been used in our previous studies[50,51].The obtained 100 nucleotide paired-end reads were mapped to the mouse genome (version GRCm38) using the Tophat mapper. Using this approach, we were able to map 87% of the raw reads on average. Sequencing reads were mapped to the mouse genome (*Mus musculus* version GRCm38) using Tophat version 2.02 (ref. 52) under default options for paired-end read mapping. Mapped reads were used to quantify transcripts from the Ensembl version 73 gene annotation data set (http://www.ensembl.org) using the Flux Capacitor approach. This strategy deconvolutes reads mapping to exonic regions shared by multiple transcripts by optimizing a system of linear equations, and thus specifically assigns some reads to each alternative splice form (http://flux.sammeth.net)[53]. All genes and transcripts were assigned relative coverage rates as measured in RPKM units ('reads per kilobase per million mapped reads')[54]. Lists of differentially expressed genes and transcripts were generated from the Flux Capacitor output using scripts in Perl or R. The 88,346 transcripts annotated in Ensembl 73 corresponded to 33,358 genes. Mice kept under the thermoneutral temperature were found to express a median of 18,494 genes. Of them, 15,971 genes were found in all tested individuals.

To define the genes that were upregulated or downregulated by cold, the fold change was calculated as the proportion between the sum of the RPKM for all gene transcripts under the cold condition and the same sum in control condition. Significance was tested using a Fisher's exact test (the number of reads mapped to a given gene and number of reads mapped to all other genes in the cold condition versus the control condition) and corrected by the Benjamini–Hochberg method (taking for each gene the four samples as independent tests). A difference in gene expression was considered significant if the corrected P value was <0.05. As additional criteria, a gene was considered to be 'modified by cold' only if its expression changed significantly in the same direction—that is, 'up' or 'down'—in at least three out of four samples per group and no significant change in the opposite direction was observed, as in previous studies[50,51].

Animals and treatments *in vivo*. For RNA-seq analysis, eight adult (5 months old at the moment of the experiment) male C57BL6 mice were obtained from Harlan Laboratories and were maintained at thermoneutral temperature (29 °C). After 2 weeks, four mice randomly were placed at an environment temperature of 4 °C for 24 h. Cold-exposed mice and thermoneutral controls were killed by decapitation, iBAT was dissected and frozen for further analysis. *Fgf21*$^{-/-}$ mice (B6N;129S5-*Fgf21*^{tm1Lex}/Mmcd) were obtained from the Mutant Mouse Regional Resource Center (MMRRC), an NCRR-NIH-funded strain repository, having been donated to the MMRRC by Genentech, Inc. *Pparα*-null mice (B6.129S4-*Ppara*^{tm1Gonz}/J) were obtained from Jackson Laboratory (Bar Harbor, ME, USA). *GPR120* −/− mice (Ffar4$^{tm1(KOMP)Vlcg}$) were purchased from MMRRC. Adult (5 months old) male wild-type littermates were used as controls for all experiments with *Fgf21*-null mice, *Pparα*-null mice and *GPR120*-null mice. When indicated, mice were injected intraperitonneal with 1 mg kg^{-1} CL316,243.

GW9508 (Cayman Chemical) was administered to adult (5 months old) male C57BL6 mice through the diet at a dose calculated to yield an intake of 50 μg g^{-1} body weight per day GW9508 intake[55] for 1 week. The diet was prepared as previously described[56] by soaking diet pellets in an acetone solution of the drug; the control diet in was also soaked in acetone and dried. For cold-exposure treatments, *GPR120*-null, *FGF21*-null and the corresponding wild-type littermates were exposed to 4 °C ambient temperature during the indicated timing. Mice were subjected to non-invasive measurements (see below), and then they were killed, and blood and tissues were collected. Tissue samples were frozen for further RNA and/or protein analysis, or placed in 10% buffered formalin overnight and processed for hematoxylin and eosin (H&E) staining and optical microscopy using standard procedures. The relative lipid content and percentage of multilocular adipocytes were measured from optical microscopy images using ImageJ and CellProfiler software, with at least five independent preparations quantified for each experimental group. Data of the relative lipid content and the area occupied by multilocular adipocytes were expressed as percentages relative to total image area.

The volume of consumed oxygen, the volume of produced carbon dioxide and the respiratory quotient were determined (Harvard Apparatus). Rectal temperature was determined using an electronic thermistor equipped with a rectal probe. Body temperature was non-invasively estimated by measuring the eye-surface temperature using a high-sensitivity infrared thermography camera (FLIR T335), as previously reported[57,58].

All experiments were performed in accordance with European Community Council directive 86/609/EEC and experiments, as well as the number of animals to be used were approved by the Institutional Animal Care and Use Committee at the University of Barcelona based on the expected effects size.

Serum biochemistry. Glucose and triglyceride levels were measured using Accutrend Technology (Roche Diagnostics, Basel, Switzerland). FGF21 levels were quantified with ELISA (RD291108200R, Biovendor). Insulin, adipokines and cytokines were quantified using a Multiplex system (MADKMAG-HK, Millipore).

Brown and beige adipocyte cell cultures. Stromal vascular cells were obtained from iBAT and iWAT excised from 3-week-old C57BL6 mice (males and females), primary cultures were generated and the cells were induced to differentiate into brown and beige adipocytes, respectively, following the previously reported procedures[25,26]. Brown adipocyte differentiation was achieved by exposing confluent precursor cells from iBAT in DMEM/F12 medium containing 10% foetal bovine serum (FBS) and supplemented with 20 nM insulin, 2 nM T3 and 0.1 mM ascorbic acid (ITA).

For beige cell differentiation, confluent precursor cells from iWAT and eWAT were maintained in DMEM/F12 containing 10% newborn calf serum (NCS). For differentiarion, 850 nM insulin, 3 μM T3, 35 nM dexamethasone and 10 μM rosiglitazone were added. When indicated, pre-adipocytes were cultured in the presence of delipidated serum (Charcoal Stripped Serum-GIBCO) instead of FBS/NCS

Cells were treated either across the differentiation process or were treated acutely (24 h), when already differentiated. Treatments included TUG-891 (200 μM), grifolic acid (100 μM), GW9508 (100 μM), ALA (100 μM), EPA (100 μM), NE (0.5 μM), dibutyryl-cAMP (1 mM), SB202190 (10 μM), H89 (20 μM), GW7647 (1 μM), GW9662 (30 μM), AH-7614 (100 μM), U-0128 (10 μM), compound C (10 μM), wortmannin (2 μM) and CL316,243 (1 μM). All reagents were obtained from Sigma with the exception of TUG-891, AH-7614, GW9662 (from Tocris), GW9508 (from Cayman Chemical), compound C (Calbiochem) and U-0128 (Enzo). When indicated, cells were subjected to dynamic measurements (see below) and/or further collected for RNA extraction.

Dynamic measurements of adipocytes in culture. Glucose oxidation rates were determined in cultured adipocytes. Cells were incubated for 60 min in the appropriate cell culture medium containing [^{14}C]-glucose after which trapped ^{14}C-CO_2 was measured. Cellular heat production was measured by infrared thermography in accordance with an initial report[59] further developed for application to brown adipocytes[27,28]. Basically, brown or beige adipocytes were grown in a 12-well plate and placed on a 37 °C heat block in a polystyrene box coated with black paper to optimize insulation. Images were acquired by an infrared camera (FLIR systems T335, Wilsonville, OR, USA), which detects a 7.5–13 μm spectral response with a thermal sensitivity of 0.1 °C, and analysed using the FLIR Quick Report software (Wilsonville, OR, USA). Supplementary Figure 11 shows an example of thermographic recording of brown adipocytes in culture. Oxygen consumption of cells was recorded using the Oxygen Biosensor System (BD) in the absence or presence (uncoupled respiration) of 10 μg ml^{-1} oligomycin, and also after exposure of cells to CL316,243 for 24 h, as previoulsy described[36].

siRNA-mediated interference. Reverse transfection of differentiated adipocytes was performed using the Lipofectamine RNAiMAX (InvitroGene) and Optimem (Life Technologies) reagents, random duplexes or two independent siRNA duplexes designed to silence GPR120 (67928017 and 67928014, final concentration 10 μM), all from Integrated DNA Technologies-TriFECTA. One day after transfection, the cells were exposed to various treatments and then collected for analysis of extracted RNA and conditioned media.

Transient transfection of promoter constructs. Reverse transfection of differentiated brown adipocytes with the plasmid −1497-FGF21-Luc, containing the 5′ region of the mouse FGF21 gene linked to the luciferase reporter gene, and the deleted form 69-FGF21-Luc[19] was performed using Lipofectamine. Where indicated, an expression plasmid for a dominant-negative form of MKK6 (MKK6-K82A, Addgene plasmid 13,519) was co-transfected (0.06 μg per well). The pRL-CMV expression plasmid for the sea pansy (Renilla reniformis) luciferase was used as an internal transfection control (Promega, Madison, WI, USA). Cells were incubated for 48 h after transfection, and where indicated, they were treated with 100 μM GW9508 or 100 μM EPA for 24 h before collecting. Firefly luciferase activity elicited by FGF21 promoter constructs was normalized for variation in transfection efficiency using Renilla luciferase as an internal standard, all measured in a Turner Designs luminometer (TD 20/20) using the Dual-Luciferase Reporter Assay system (Promega).

Quantitative PCR with reverse transcription. Reverse transcription was performed, using random hexamers primers (Applied Biosystems, Foster City, CA, USA)

and 0.5 µg RNA in a total reaction volume of 20 µl. For PCR, Taqman Gene Expression Assay probes were used (Supplementary Table 3), with reaction mixtures containing 1 µl cDNA, 10 µl TaqMan Universal PCR Master Mix (Applied Biosystems), 250 nM probes and 900 nM of primers from the Assays-on-Demand Gene Expression Assay Mix. The 18S rRNA was measured as the housekeeping reference gene. The mRNA level of the gene of interest in each sample was normalized to that of the reference control using the comparative $(2-\Delta CT)$ method, according to the manufacturer's instructions. A transcript was considered to be non-detectable when $CT \geq 40$.

Immunoblots and multiplex protein assays. Western blot analysis of tissue and cell culture extracts was performed following standard procedures, using primary anti-UCP1 (1:1,000 ab10983, Abcam, Cambridge, UK) and anti-GPR120 (1:150sc-99105, Santa Cruz, USA). Specificity of GPR120 detection was checked using BAT extracts from male C57BL6 *GPR120*-null mice (Supplementary Fig. 12). Loading controls were established using α-tubulin immunoblots (T9026, Sigma-Aldrich) or Ponceau staining of membranes. Immunoreactive proteins were detected using an ECL (enhanced chemiluminescence) system (GE Healthcare). Signal intensities were quantified by scanning densitometry (Phoretics 1D Software). Uncropped scans of western blots and corresponding Ponceau-stained membranes, including scale markers are shown in Supplementary Fig. 13. Quantitative measurements of changes in phosphorylated ERK1/2, CREB and p38 MAPK were performed using multiplex-based technology (48–680MAG and 48–681MAG kits, Millipore, Billerica, MA, USA) by determining the ratio of the corresponding phosphoproteins relative to total specific proteins.

Statistics. Two-tailed unpaired Student's *t*-test or one-way analysis of variance were used to test for the statistical significance of differences between two experimental conditions. Welch's correction was applied when unequal variances were detected by *F*-test, using the GraphPad statistical software (GraphPad Software Inc., San Diego, CA, USA). Statistical significance was set with an α-value of $P<0.05$, and underlying assumptions for validity of all tests were assessed. Data are shown as means ± s.e.m.

Data availability. The raw data generated during the RNA-seq procedure is deposited in Gene Expression Omnibus (GEO) under accession number GSE77534. The complete list of cold-modulated genes in BAT after RNA-seq data analysis is available at http://lmedex.ulb.ac.be/data.php.

References

1. Lowell, B. B. *et al.* Development of obesity in transgenic mice after genetic ablation of brown adipose tissue. *Nature* **366,** 740–742 (1993).
2. Feldmann, H. M., Golozoubova, V., Cannon, B. & Nedergaard, J. UCP1 ablation induces obesity and abolishes diet-induced thermogenesis in mice exempt from thermal stress by living at thermoneutrality. *Cell Metab.* **9,** 203–209 (2009).
3. Betz, M. J. & Enerbäck, S. Human brown adipose tissue: what we have learned so far. *Diabetes* **64,** 2352–2412 (2015).
4. Giralt, M. & Villarroya, F. White, brown, beige/brite: different adipose cells for different functions? *Endocrinology* **154,** 2992–3000 (2013).
5. Shabalina, I. G. *et al.* UCP1 in brite/beige adipose tissue mitochondria is functionally thermogenic. *Cell. Rep.* **5,** 1196–1399 (2013).
6. Kazak, L. *et al.* A creatine-driven substrate cycle enhances energy expenditure and thermogenesis in beige fat. *Cell* **163,** 643–698 (2015).
7. Plaisier, C. L. *et al.* Zbtb16 has a role in brown adipocyte bioenergetics. *Nutr. Diabetes* **2,** e46 (2012).
8. Rosell, M. *et al.* Brown and white adipose tissues: intrinsic differences in gene expression and response to cold exposure in mice. *Am. J. Physiol. Endocrinol. Metab.* **306,** E945–E964 (2014).
9. Sultan, M. *et al.* A global view of gene activity and alternative splicing by deep sequencing of the human transcriptome. *Science* **321,** 956–1016 (2008).
10. Tang, F. *et al.* RNA-Seq analysis to capture the transcriptome landscape of a single cell. *Nat. Protoc.* **5,** 516–551 (2010).
11. van Bakel, H., Nislow, C., Blencowe, B. J. & Hughes, T. R. Most 'dark matter' transcripts are associated with known genes. *PLoS Biol.* **8,** e1000371 (2010).
12. Ulven, T. & Christiansen, E. Dietary fatty acids and their potential for controlling metabolic diseases through activation of FFA4/GPR120. *Annu. Rev. Nutr.* **35,** 239–263 (2015).
13. Oh, D. Y. *et al.* GPR120 is an omega-3 fatty acid receptor mediating potent anti-inflammatory and insulin-sensitizing effects. *Cell* **142,** 687–785 (2010).
14. Ichimura, A. *et al.* Dysfunction of lipid sensor GPR120 leads to obesity in both mouse and human. *Nature* **483,** 350–354 (2012).
15. Hao, Q. *et al.* Transcriptome profiling of brown adipose tissue during cold exposure reveals extensive regulation of glucose metabolism. *Am. J. Physiol. Endocrinol. Metab.* **308,** E380–E392 (2015).
16. Iwasaki, K. *et al.* Free fatty acid receptor GPR120 is highly expressed in enteroendocrine K cells of the upper small intestine and has a critical role in GIP secretion after fat ingestion. *Endocrinology* **156,** 837–883 (2015).
17. Gotoh, C. *et al.* The regulation of adipogenesis through GPR120. *Biochem. Biophys. Res. Commun.* **354,** 591–597 (2007).
18. Cao, W., Medvedev, A. V., Daniel, K. W. & Collins, S. beta-Adrenergic activation of p38 MAP kinase in adipocytes: cAMP induction of the uncoupling protein 1 (UCP1) gene requires p38 MAP kinase. *J. Biol. Chem.* **276,** 27077–27082 (2001).
19. Hondares, E. *et al.* Thermogenic activation induces FGF21 expression and release in brown adipose tissue. *J. Biol. Chem.* **286,** 12983–12990 (2011).
20. Wu, J. *et al.* Beige adipocytes are a distinct type of thermogenic fat cell in mouse and human. *Cell* **150,** 366–442 (2012).
21. Hirasawa, A. *et al.* Free fatty acids regulate gut incretin glucagon-like peptide-1 secretion through GPR120. *Nat. Med.* **11,** 90–94 (2005).
22. Suh, H. N., Huong, H. T., Song, C. H., Lee, J. H. & Han, H. J. Linoleic acid stimulates gluconeogenesis via Ca2 + /PLC, cPLA2, and PPAR pathways through GPR40 in primary cultured chicken hepatocytes. *Am. J. Physiol. Cell Physiol.* **295,** 1518–1545 (2008).
23. Gavaldà-Navarro, A. *et al.* Fibroblast growth factor 21 in breast milk controls neonatal intestine function. *Sci. Rep.* **5,** 13717 (2015).
24. Wu, Q. *et al.* Identification of G-protein-coupled receptor 120 as a tumor-promoting receptor that induces angiogenesis and migration in human colorectal carcinoma. *Oncogene* **32,** 5541–5550 (2013).
25. Barbera, M. J. *et al.* Peroxisome proliferator-activated receptor alpha activates transcription of the brown fat uncoupling protein-1 gene. A link between regulation of the thermogenic and lipid oxidation pathways in the brown fat cell. *J. Biol. Chem.* **276,** 1486–1579 (2001).
26. Schlüter, A., Barberá, M. J., Iglesias, R., Giralt, M. & Villarroya, F. Phytanic acid, a novel activator of uncoupling protein-1 gene transcription and brown adipocyte differentiation. *Biochem. J.* **362,** 61–70 (2002).
27. Lee, P., Werner, C. D., Kebebew, E. & Celi, F. S. Functional thermogenic beige adipogenesis is inducible in human neck fat. *Int. J. Obes. (Lond)* **38,** 170–176 (2014).
28. Lee, P. *et al.* Irisin and FGF21 are cold-induced endocrine activators of brown fat function in humans. *Cell Metab.* **19,** 302–309 (2014).
29. Hudson, B. D. *et al.* The pharmacology of TUG-891, a potent and selective agonist of the free fatty acid receptor 4 (FFA4/GPR120), demonstrates both potential opportunity and possible challenges to therapeutic agonism *Mol. Pharmacol.* **84,** 710–735 (2013).
30. Hara, T. *et al.* Novel selective ligands for free fatty acid receptors GPR120 and GPR40. *Naunyn Schmiedebergs Arch. Pharmacol.* **380,** 247–302 (2009).
31. Aune, U. L., Ruiz, L. & Kajimura, S. Isolation and differentiation of stromal vascular cells to beige/brite cells. *J. Vis. Exp.* **73,** 50191 (2013).
32. Badman, M. K. *et al.* Hepatic fibroblast growth factor 21 is regulated by PPARalpha and is a key mediator of hepatic lipid metabolism in ketotic states. *Cell Metab.* **5,** 426–437 (2007).
33. Inagaki, T. *et al.* Endocrine regulation of the fasting response by PPARalpha-mediated induction of fibroblast growth factor 21. *Cell Metab.* **5,** 415–425 (2007).
34. Sparks, S. M. *et al.* Identification of diarylsulfonamides as agonists of the free fatty acid receptor 4 (FFA4/GPR120). *Bioorg. Med. Chem. Lett.* **24,** 3100–3103 (2014).
35. Raingeaud, J. *et al.* MKK3- and MKK6-regulated gene expression is mediated by the p38 mitogen-activated protein kinase signal transduction pathway. *Mol Cell Biol.* **16,** 1247–1255 (1996).
36. Hondares, E. *et al.* Hepatic FGF21 expression is induced at birth via PPARalpha in response to milk intake and contributes to thermogenic activation of neonatal brown fat. *Cell Metab.* **11,** 206–212 (2010).
37. Fisher, F. M. *et al.* FGF21 regulates PGC-1alpha and browning of white adipose tissues in adaptive thermogenesis. *Genes Dev.* **26,** 271–281 (2012).
38. Villarroya, F. & Vidal-Puig, A. Beyond the sympathetic tone: the new brown fat activators. *Cell Metab.* **17,** 638–643 (2013).
39. Oh, D. L. *et al.* A Gpr120-selective agonist improves insulin resistance and chronic inflammation in obese mice. *Nat. Med.* **20,** 942–949 (2014).
40. Qiu, Y. *et al.* Eosinophils and type 2 cytokine signaling in macrophages orchestrate development of functional beige fat. *Cell* **157,** 1292–1308 (2014).
41. Rao, R. R. *et al.* Meteorin-like is a hormone that regulates immune-adipose interactions to increase beige fat thermogenesis. *Cell* **157,** 1279–1291 (2014).
42. Flachs, P., Rossmeisl, M. & Kopecky, J. The effect of n-3 fatty acids on glucose homeostasis and insulin sensitivity. *Physiol. Res.* **63,** S93–S118 (2014).
43. Oudart, H. *et al.* Brown fat thermogenesis in rats fed high-fat diets enriched with omega polyunsaturated fatty acids. *Int. J. Obes. Relat. Metab. Disord.* **21,** 955–1017 (1997).
44. Sadurskis, A., Dicker, A., Cannon, B. & Nedergaard, J. Polyunsaturated fatty acids recruit brown adipose tissue: increased UCP content and NST capacity. *Am. J. Physiol.* **269,** e351–e411 (1995).

45. Takahashi, Y. & Ide, T. Dietary omega fatty acids affect mRNA level of brown adipose tissue uncoupling protein 1, and white adipose tissue leptin and glucose transporter 4 in the rat. *Br. J. Nutr.* **84,** 175–259 (2000).
46. Flachs, P. *et al.* Synergistic induction of lipid catabolism and anti-inflammatory lipids in white at of dietary obese mice in response to calorie restriction and omega fatty acids. *Diabetologia* **54,** 2626–2664 (2011).
47. Villarroya, J. *et al.* Fibroblast growth factor-21 and the beneficial effects of long-chain omega polyunsaturated fatty acids. *Lipids* **49,** 1081–1090 (2014).
48. Fleckenstein-Elsen, M. *et al.* Eicosapentaenoic acid and arachidonic acid differentially regulate adipogenesis, acquisition of a brite phenotype and mitochondrial function in primary human adipocytes. *Mol. Nutr. Food Res.* **60,** 2065–2075 (2016).
49. Wang, Z., Gerstein, M. & Snyder, M. RNA-Seq: a revolutionary tool for transcriptomics. *Nat. Rev. Genet.* **10,** 57–63 (2009).
50. Eizirik, D. L. *et al.* The human pancreatic islet transcriptome: expression of candidate genes for type 1 diabetes and the impact of pro-inflammatory cytokines. *PLoS Genet.* **8,** e1002552 (2012).
51. Cnop, M. *et al.* RNA sequencing identifies dysregulation of the human pancreatic islet transcriptome by the saturated fatty acid palmitate. *Diabetes* **63,** 1978–1993 (2014).
52. Trapnell, C. *et al.* Transcript assembly and quantification by RNA-Seq reveals unannotated transcripts and isoform switching during cell differentiation. *Nat. Biotechnol.* **28,** 511–516 (2010).
53. Montgomery, S. B. *et al.* Transcriptome genetics using second generation sequencing in a Caucasian population. *Nature* **464,** 773–780 (2010).
54. Mortazavi, A., Williams, B. A., McCue, K., Schaeffer, L. & Wold, B. Mapping and quantifying mammalian transcriptomes by RNA-Seq. *Nat. Methods* **5,** 621–628 (2008).
55. Ou, H. Y. *et al.* Multiple mechanisms of GW-9508, a selective G protein-coupled receptor 40 agonist, in the regulation of glucose homeostasis and insulin sensitivity. *Am. J. Physiol. Endocrinol. Metab.* **304,** E668–E676 (2013).
56. Cabrero, A. *et al.* Bezafibrate reduces mRNA levels of adipocyte markers and increases fatty acid oxidation in primary culture of adipocytes. *Diabetes* **50,** 1883–1890 (2001).
57. Johnson, S., Rao, S., Hussey, S. B., Morley, P. S. & Traub-Dargatz, J. L. Thermographic eye temperature as an index to body temperature in ponies. *J. Equine. Vet. Sci.* **31,** 63–66 (2011).
58. Purslow, C. & Wolffsohn, J. S. The relation between physical properties of the anterior eye and ocular surface temperature. *Optom. Vis. Sci.* **84,** 197–201 (2007).
59. Paulik, M. A. *et al.* Development of infrared imaging to measure thermogenesis in cell culture: thermogenic effects of uncoupling protein-2, troglitazone, and beta-adrenoceptor agonists. *Pharm. Res.* **15,** 944–949 (1998).

Acknowledgements

We thank A. Peró and M. Morales for technical support. Scientific and technical advice by Dr C. Wolfrum and M. Christian is acknowledged. This work has been supported by Grants SAF2014-55725 and PI14/00063 from the Ministerio de Economia y Competitividad (MINECO), Spain, and co-financed by the European Regional Development Fund (ERDF), and by the European Community's Seventh Framework Program (FP7 BetaBat for F.V. and D.L.E.) and the Horizon 2020 Program (T2Dsystems (GA667191)) to D.L.E. T.Q.-L. was supported by a CONACyT (National Council for Science and Technology in Mexico) Ph. D. scholarship. R.M. and M.C were supported by PhD scholarships from MINECO, Spain.

Authors contributions

The experiments were conceived and designed by T.Q.-L., D.L.E. and F.V.; RNA-seq data were obtained and analysed by J.-V.T., R.C. and D.L.E.; experiments with mice were performed by T.Q.-L., R.M., A.P. and R.I.; cell culture experiments were performed by T.Q.-L., M.G., M.P. and A.G.-N., analysis of microscopy images was performed by M.C. and M.G.; overall data were analysed by T.Q.-L., M.G., D.L.E. and F.V. The paper was written by F.V. and revised/approved by all contributors.

Additional information

Supplementary Information accompanies this paper at http://www.nature.com/naturecommunications

Competing financial interests: The authors declare no competing financial interests.

Reprints and permission information is available online at http://npg.nature.com/reprintsandpermissions/

How to cite this article: Quesada-López, T. *et al.* The lipid sensor GPR120 promotes brown fat activation and FGF21 release from adipocytes. *Nat. Commun.* **7,** 13479 doi: 10.1038/ncomms13479 (2016).

Publisher's note: Springer Nature remains neutral with regard to jurisdictional claims in published maps and institutional affiliations.

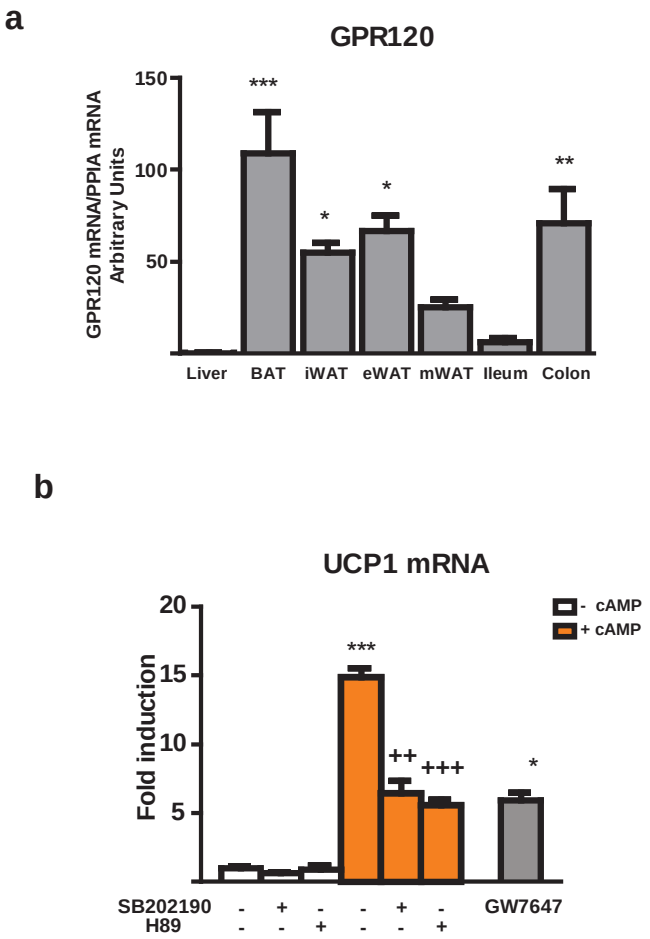

Supplementary Figure 1. GPR120 expression and effects of p38 MAPK and PKA inhibitors and PPARα agonist on UCP1 mRNA levels. (a) *GPR120* mRNA expression in mouse tissues using cyclophilin mRNA as housekeeping reference gene. Bars are means + s.e.m. (*P <0.05, **P <0.01, ***P <0.001 compared with ileum; two-tailed unpaired student t-test). **(b)** Effects of 10 μM SB202190 (a p38 MAPK inhibitor), or 20 μM H89 (a PKA inhibitor) on the up-regulation of *UCP1* mRNA in response to 1mM dibutyryl-cAMP, and effects of 1 μM GW7647 (PPARα agonist) in brown adipocytes differentiated in primary culture (n = 4). Bars are means + s.e.m. (*P <0.05, ***P <0.001 compared with controls; ++P<0.01, +++ P<0.001 for the effects of SB202190 or H89; ANOVA with Tukey's post hoc test).

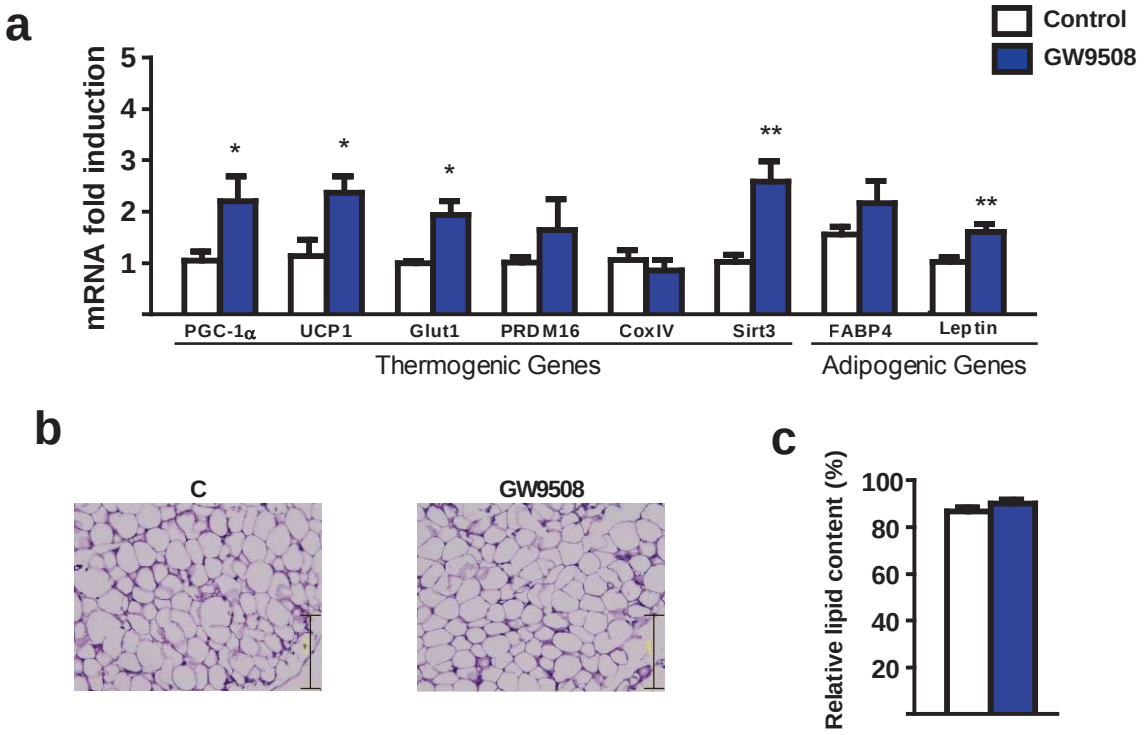

Supplementary Figure 2. Effects of GW9508 on thermogenic genes in epididymal WAT. Adult mice were fed for 7 days a control diet (white bars) or a diet supplemented with GW9508 (blue bars) (n = 6). **(a)** Relative expression levels of thermogenic and adipogenic genes in eWAT, **(b)** representative optical microscopy images from H&E-stained eWAT (scale, 125µm), **(c)** relative lipid content. Bars are means + s.e.m. (*P<0.05 and **P<0.01relative to untreated control mice; two-tailed unpaired student t-test).

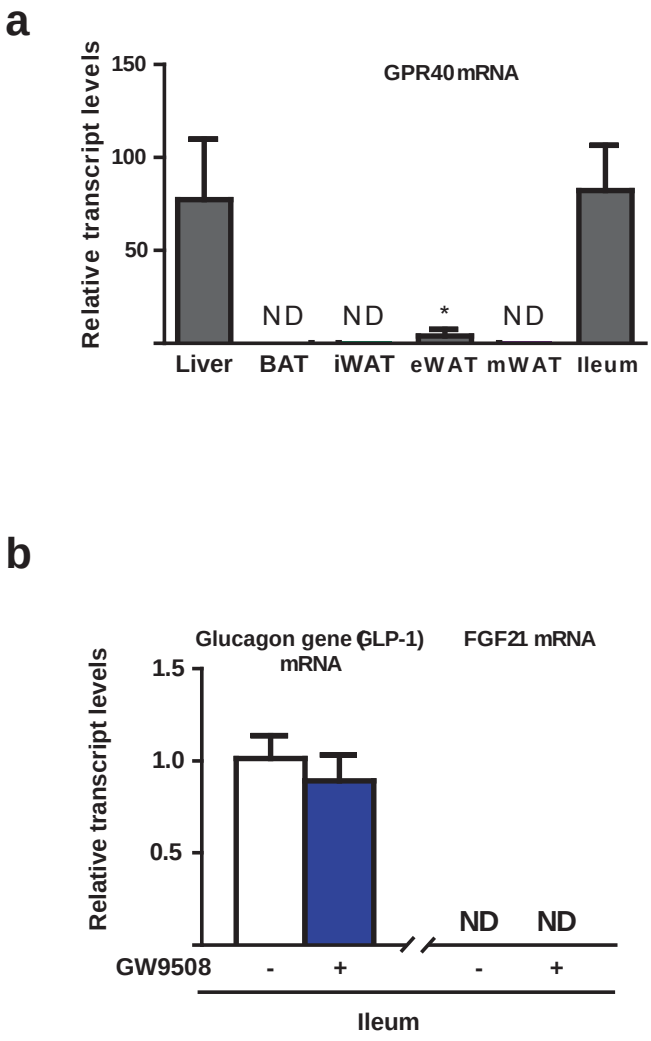

Supplementary Figure 3. GPR40 mRNA expression levels in adipose depots and GW9508 effect on intestinal cells. (a) *GPR40* mRNA expression levels in mouse tissues (n = 4). **(b)** Relative expression levels of *GLP-1* and *FGF21* in Ileum from adult mice fed for 7 days a control diet (white bars) or a diet supplemented with GW9508 (blue bars). Bars are means + s.e.m. (*P<0.05 relative to liver GPR40 mRNA expression; two-tailed unpaired student t-test).

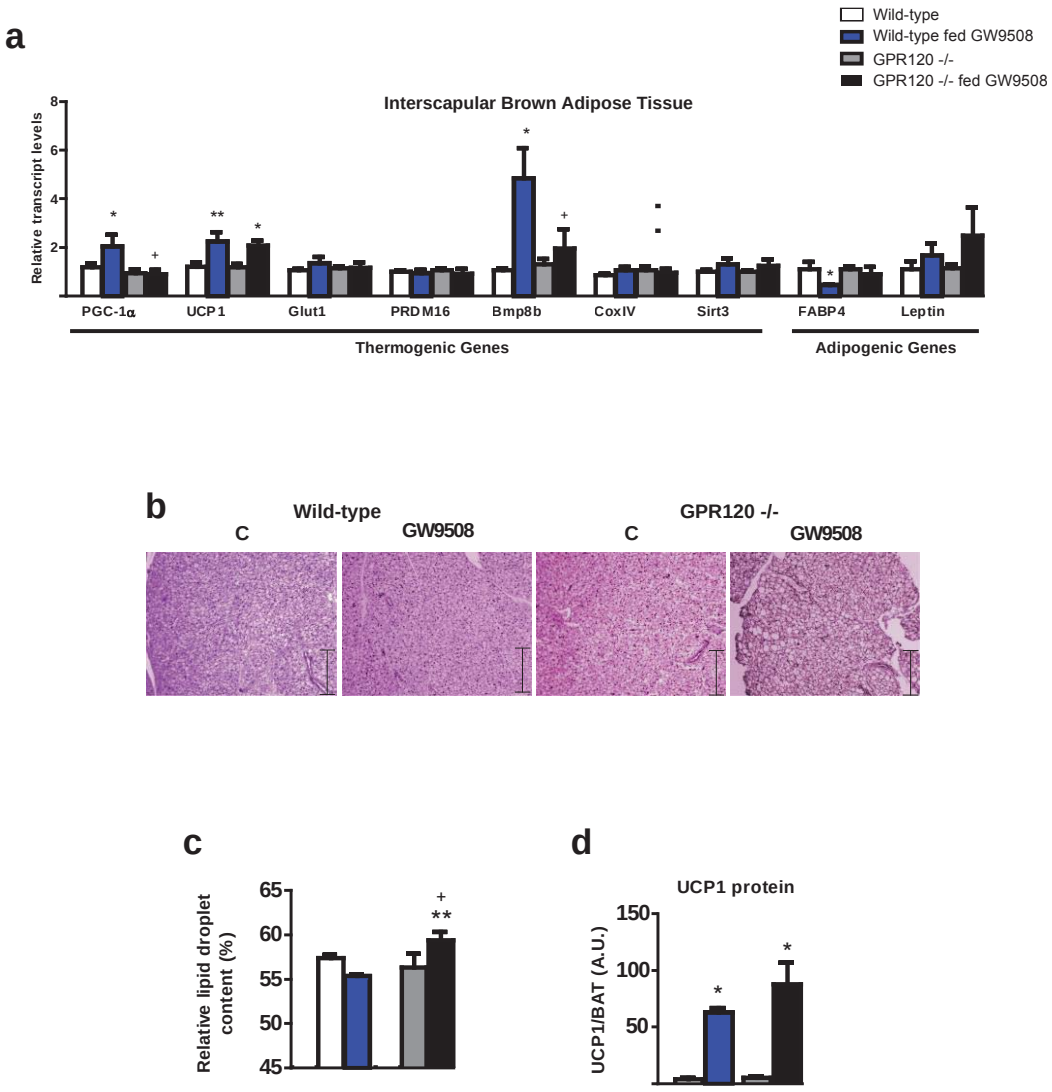

Supplementary Figure 4. Effects of GPR120 gene invalidation on the response to GW9508 treatment in iBAT. *Wild-type* and *GPR120-/-* mice (n = 5) were fed for 7 days a control diet (white and grey bars, respectively) or a diet supplemented with GW9508 (blue and black bars, respectively). **(a)** Relative expression levels of thermogenic and adipogenic genes in iBAT. **(b)** Representative optical microscopy from H&E-stained iBAT (scale, 200µm), **(c)** relative lipid content, **(d)** UCP1 protein levels. Bars are means + s.e.m. (*P<0.05, **P<0.01, and ***P<0.001 relative to untreated mice of each genotype; +P<0.05, ++P<0.01 relative to the effects of the genotype in mice under the same treatment; ANOVA with Tukey's post hoc test).

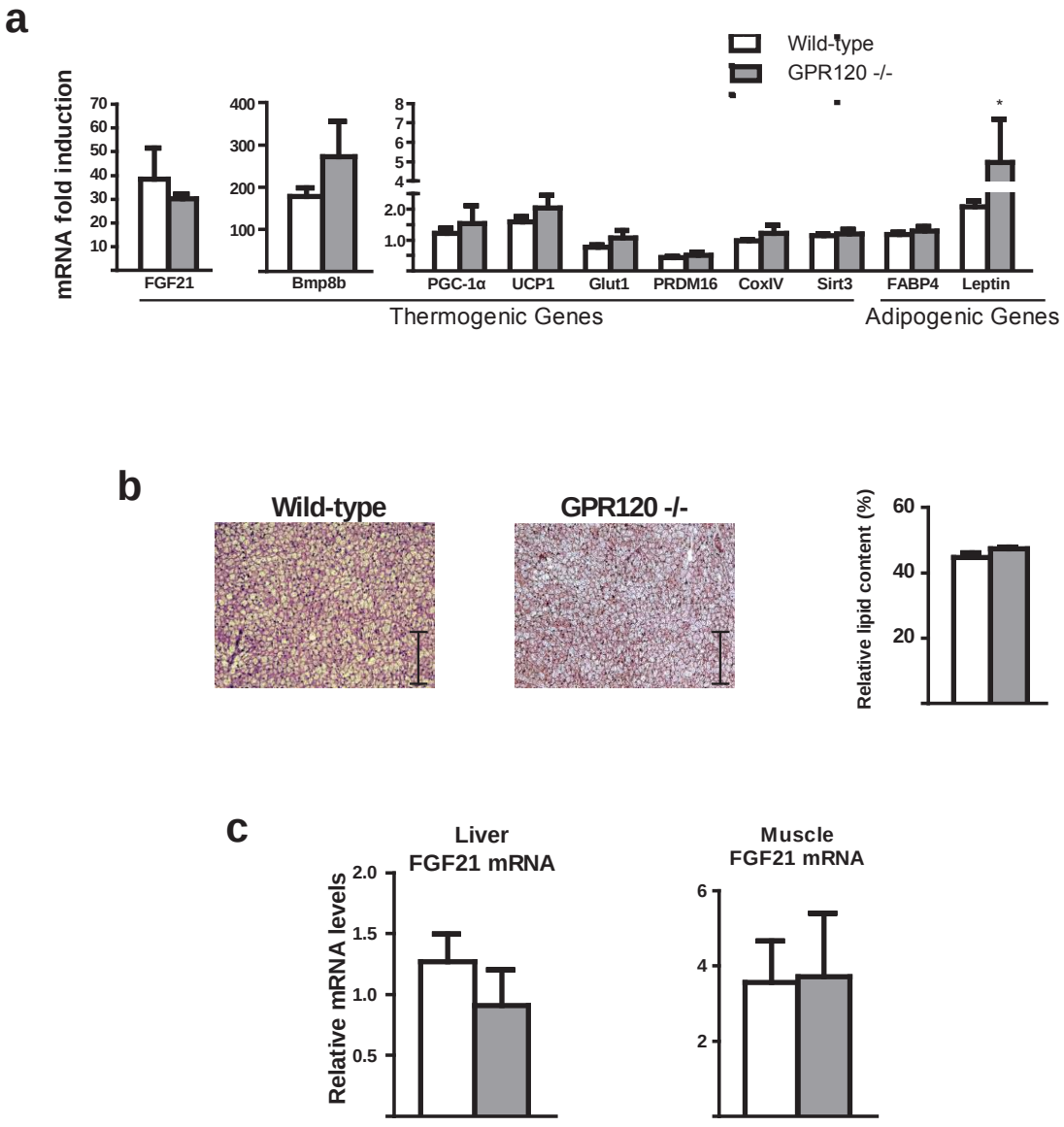

Supplementary Figure 5. Effects of GPR120 invalidation on iBAT from mice exposed to cold. *Wild-type* (white bars) and *GPR120-/-* (grey bars) mice were exposed to cold (4ºC) for 7 days (n=5). **(a)** Relative expression levels of thermogenic and adipogenic genes in iBAT. **(b)** Representative images of H&E-stained iBAT (scale, 125µm) and the relative lipid droplet content. **(c)** *FGF21* mRNA expression levels in liver and skeletal muscle. Bars are means + s.e.m. (*P<0.05, relative to wild-type control mice; two-tailed unpaired student t-test).

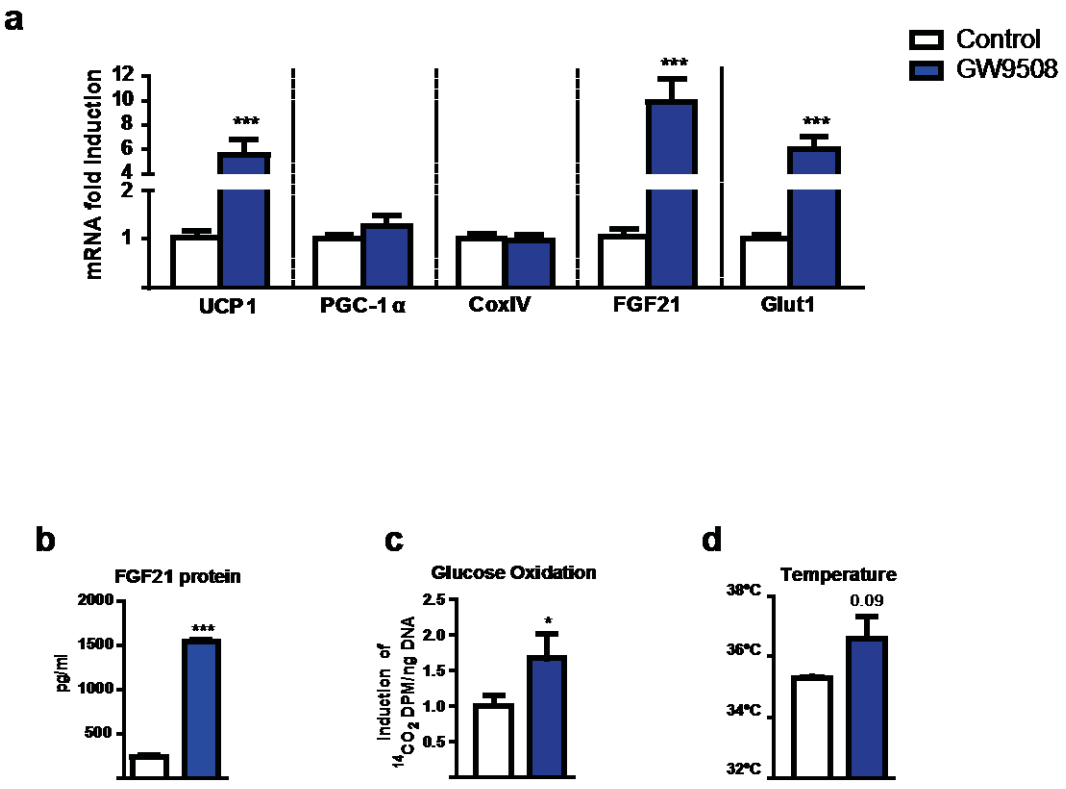

Supplementary Figure 6. GPR120 activation induces thermogenesis-related genes expression, glucose oxidation and FGF21 protein release in brown adipocytes. iBAT precursors were differentiated and treated for 24h with 100µM GW9508 (n = 5) **(a)** Relative expression levels of *UCP1*, *PGC-1α*, *CoxIV*, *FGF21* and *Glut1*. **(b)** FGF21 protein in supernatant (24h accumulation). **(c)** Glucose oxidation rate. **(d)** Cell culture temperature. Bars are means + s.e.m. (*P<0.05, **P<0.01, and ***P<0.001 relative to untreated control cells; two-tailed unpaired student t-test).

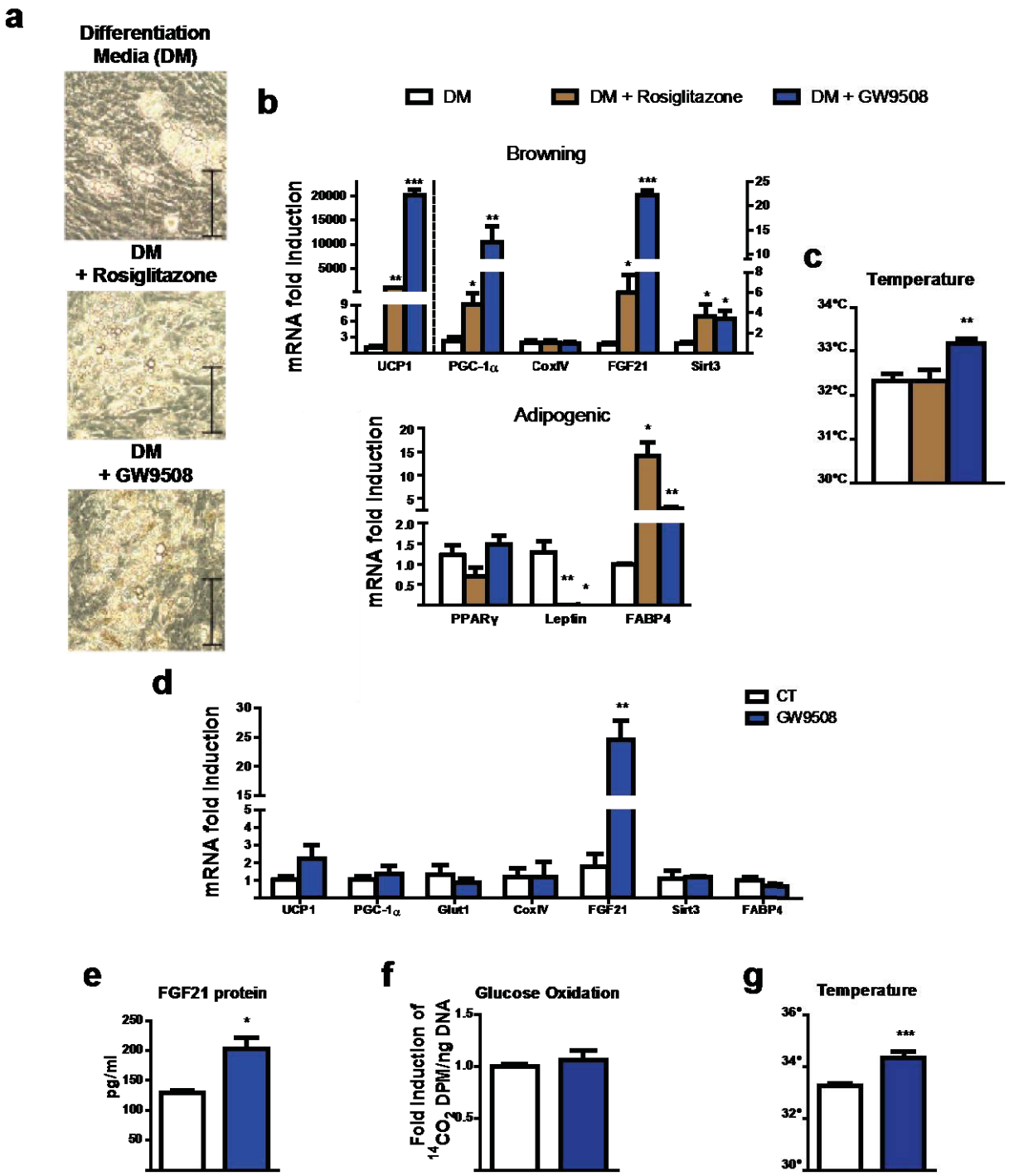

Supplementary Figure 7. GPR120 activation promotes eWAT derived beige adipocyte differentiation and increases FGF21 expression and release. For a-c, eWAT precursors from wild-type mice were differentiated (n=3-5) in the presence of the differentiation media (DM) (n=3), supplemented with rosiglitazone to drive beige differentiation (DM + Rosiglitazone)(n=5), or treated with GW9508 instead of rosiglitazone (DM + GW9508) (n=5) (see Methods section). **(a)** Representative optical microscopy images at the end of differentiation (day 7) (scale bar, 200µm). **(b)** Relative mRNA expression levels of browning-related and general adipogenic genes. **(c)** Cell culture temperature. For d-g, eWAT precursors from *wild-type* mice were differentiated and treated during 24h with GW9508 (100µM) (n=5). **(d)** mRNA expression levels of *UCP1*, *PGC-1α*, *Glut1*, *COXIV*, *FGF21*, *Sirt3*, and *FABP4*. **(e)** FGF21 protein levels in culture media (24h accumulation). **(f)** Glucose oxidation rate. **(g)** Cell culture temperature. Bars are means + s.e.m. (*P<0.05, **p<0.01, and ***p<0.001 versus controls; two-tailed unpaired student t-test).

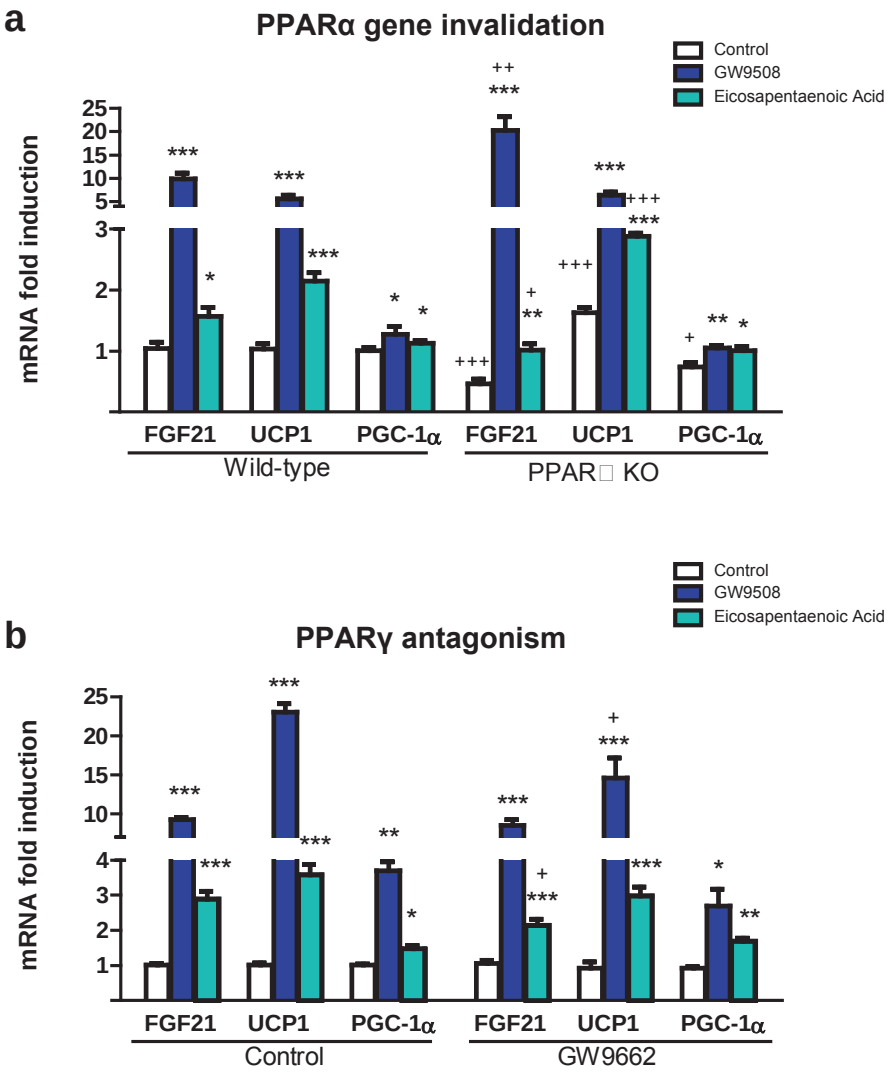

Supplementary Figure 8. Involvement of the PPARα and PPARγ pathways in the FGF21 induction elicited by activation of GPR120. (a) iBAT precursors from *wild-type* and *PPARα–null* mice were differentiated and treated during 24h with GW9508 (100µM) or EPA (100µM). Relative mRNA expression for *FGF21*, *UCP1* and *PGC-1α* is shown (n = 3). **(b)** iBAT precursors from wild-type mice were differentiated and treated with GW9508 or EPA and the PPARγ antagonist (GW9662). Relative mRNA expression for *FGF21*, *UCP1* and *PGC-1α* is shown (n = 3). Bars are means + s.e.m. (*P<0.05, **p<0.01, and ***p<0.001 versus controls; +P<0.05, ++p<0.01, and +++p<0.001 PPARα-null cells or GW9662 treated cells; ANOVA with Tukey's post hoc test).

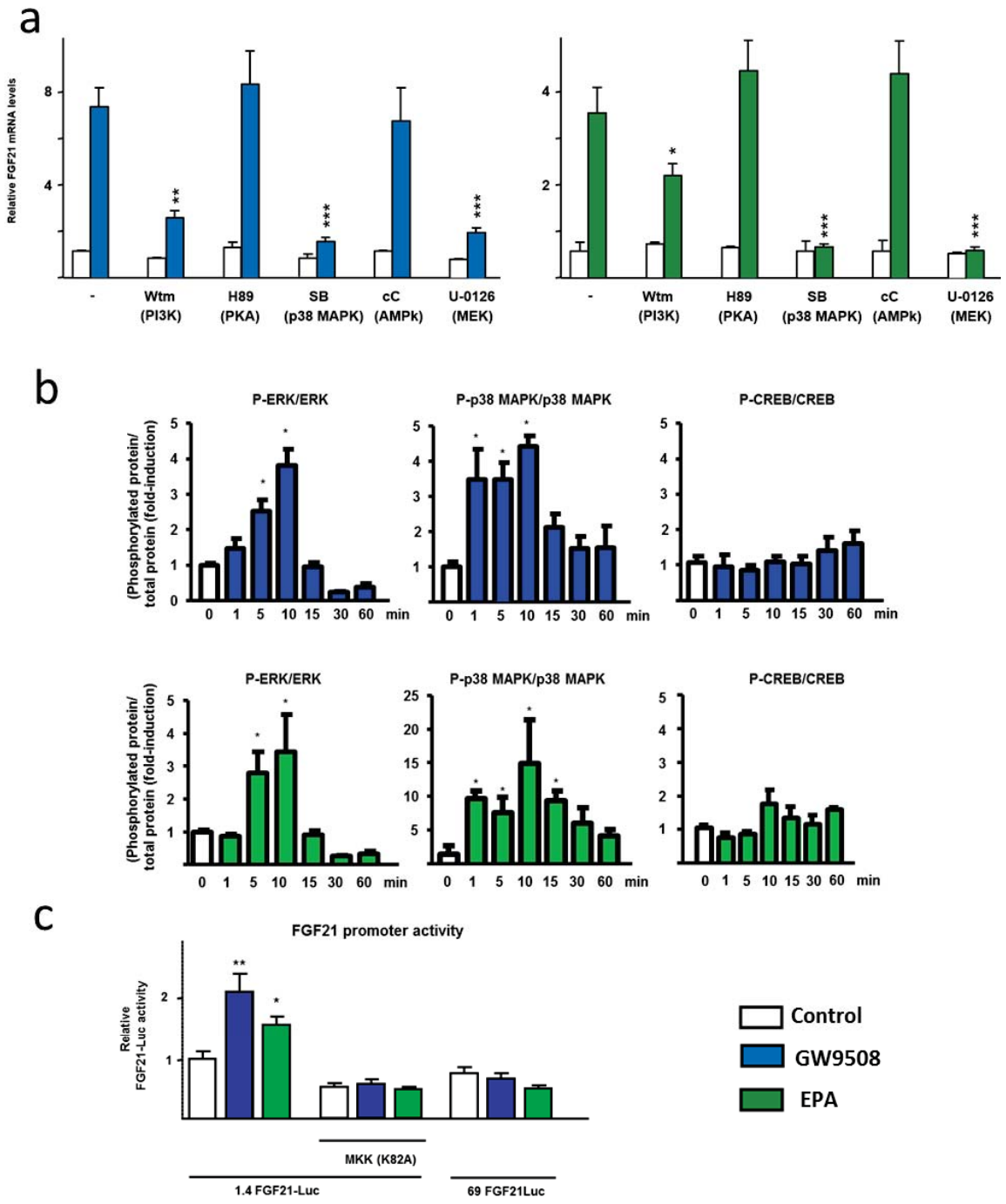

Supplementary Figure 9. Effects of GW9508 or EPA on FGF21 mRNA expression in the presence of kinases inhibitors, phosphorylation of regulatory kinases, and FGF21 gene promoter activity. Brown adipocytes in culture were used. **(a)** *FGF21* mRNA expression after 24h treatment with GW9508 (100μM) or EPA (100μM) in the presence of 2 μM wortmannin (PI3K inhibitor), 10 μM compound C (AMP kinase inhibitor),10 μM SB202190 (p38 MAPK inhibitor), 20 μM H89 (PKA inhibitor), 10 μM U-0128 (ERK inhibitor) (n = 4). **(b)** Relative levels of phosphorylated versus total kinases in response to GW9508 or EPA at the indicated times of treatment (n = 3). **(c)** *Wild-type* (1.4 FGF21-Luc) and deleted (69-FGF21-Luc) FGF21 gene promoter activity in transfected brown adipocytes in response to GW9508 or EPA. Effects of co-transfection with the dominant negative form of MKK6 (K82A) (n = 4). Bars are means + s.e.m. (*P<0.05, versus controls in the absence of inhibitors in (a), and versus non-treated cells in (b) and (c); for a, Student's t test was used and for b and c, ANOVA and Tukey post-hoc tests.

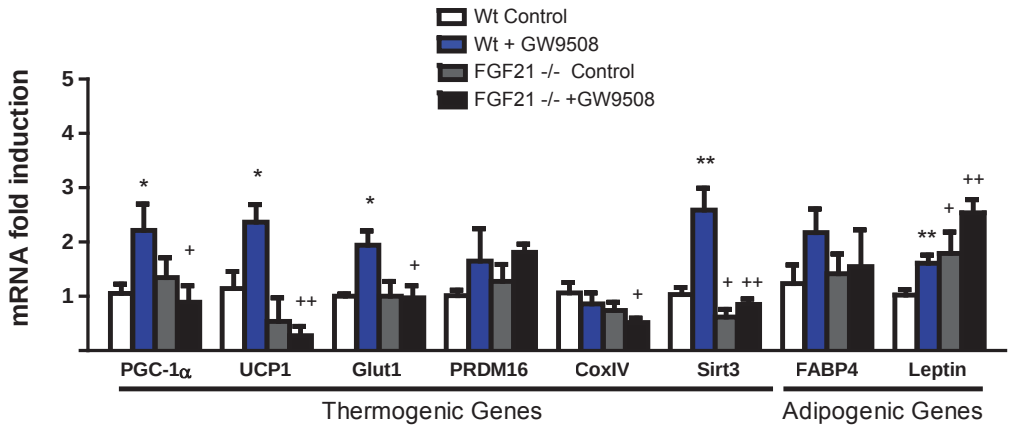

Supplementary Figure 10. Impaired effects of GW9508 on FGF21-null beige adipocytes derived from eWAT. eWAT precursors from *wild-type* and *FGF21-null* mice were differentiated and treated with GW9508 (24h) (n = 5), mRNA expression levels of thermogenic and adipogenic genes are shown. Bars are means + s.e.m. (*P<0.05, **P<0.01, for the effects of GW9508; and +P<0.05, ++P<0.01, for comparisons between *wild-type* and *FGF21-null* cells; ANOVA with Tukey's post hoc test).

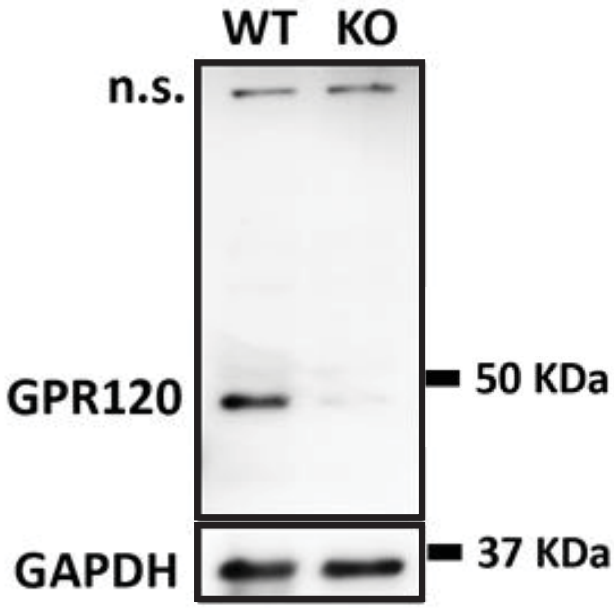

Supplementary Figure 11. Validation of specificity of GPR120 detection by immunoblot using BAT from GPR120-null mice. The Figure shows a representative western blot of 20 µg of protein extracts from mouse iBAT from *wild-type* (WT) and *GPR120-null* (KO) mice probed with the sc-99105 rabbit anti-GPR120 antibody (1:150) (Santa Cruz, USA). N.s., non-pecific. GAPDH, probing of the membrane with the leading control GAPDH (1:3000) to ensure equal loading of lanes.

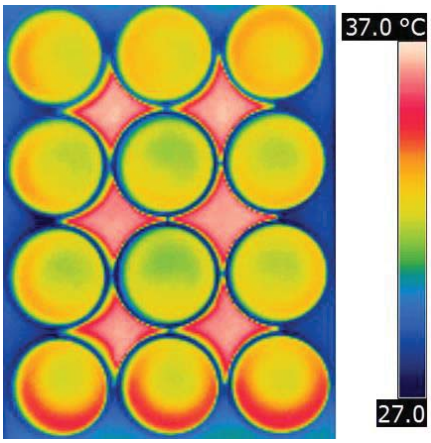

Supplementary Figure 12. Methodology for infrared thermography of brown adipocytes in culture. Example of thermographic recording of brown adipocytes in culture as described in Methods.

Western blot figure 1 b:

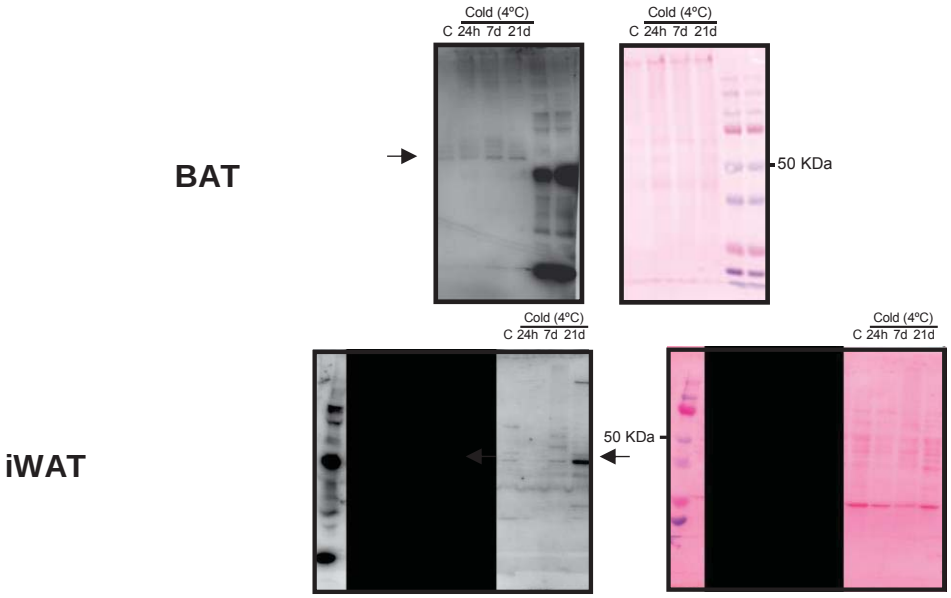

Western blot figure 1 f:

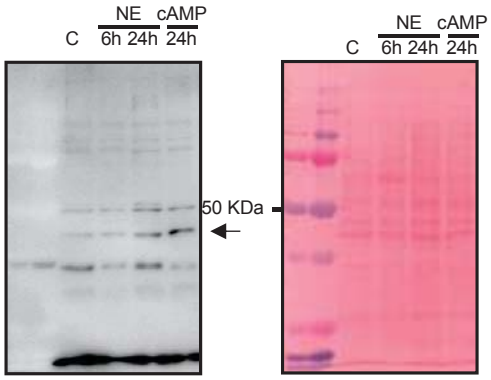

Western blot figure 2:

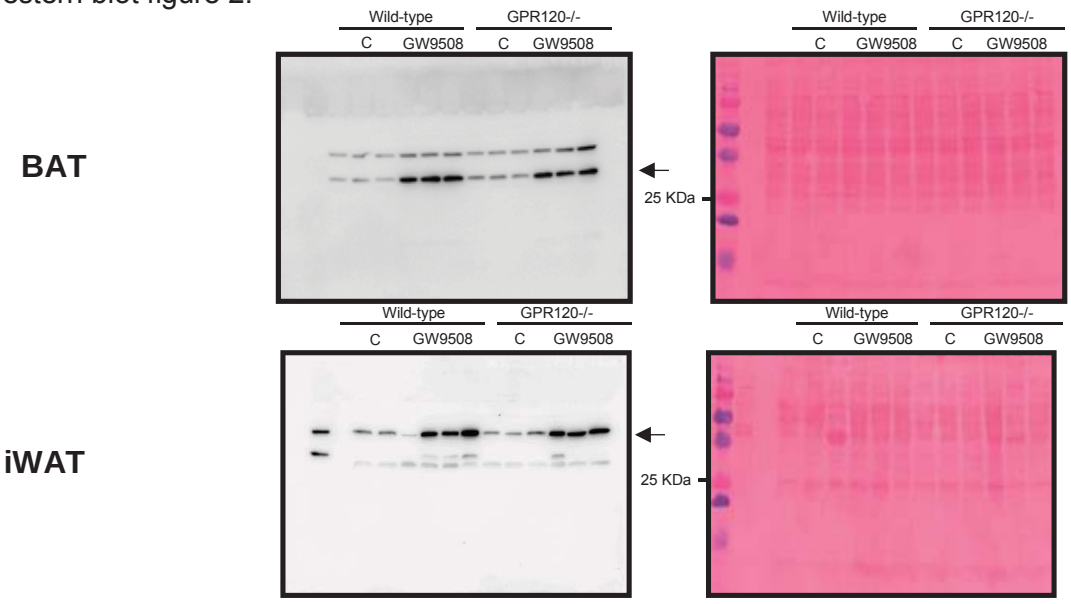

Supplementary Figure 13. Uncropped western blots and markers. Immunoblots (left) and Ponceau-stained membranes showing weight markers (right). Arrow, specific immunoblot signal. Black areas, lanes unrelated to current study.

Supplementary Table 1. Tissue weight, body temperature and circulating metabolic and hormonal parameters in mice treated with dietary GW9508 for 7 days Adult mice were fed a standard chow diet supplemented with or without GW9508 for 7 days. Data are means ± s.e.m. (*P<0.05 relative to untreated control mice; two-tailed unpaired student t-test).

	Control (n=5)	GW9508(n=6)
Body Weight (g)	29.0 ± 0.8	27,6 ± 0.6
Food intake (g)	6.4 ± 0.7	4.8 ± 0.6
iBAT (mg)	99.4 ± 7.8	96.0 ± 3.1
iWAT (mg)	95.4 ± 14	100.2 ± 11.8
eWAT (mg)	180.0 ± 24.7	181.1 ± 25.9
mWAT (mg)	169.1 ± 27.5	133.4 ± 13.0
Rectal temperature (ºC)	35.7 ± 0.4	35.8 ± 0.4
Core temperature (eye) (ºC)	35.9 ± 0.5	35.6 ± 0.3
Glucose (mg/dL)	183 ± 10	157 ± 14
Triglycerides (mg/dL)	140 ± 14	169 ± 12
Insulin (pg/dL)	966 ± 99	633 ± 62 *
IL-6 (pg/dL)	54 ± 39	27 ± 11
Leptin (pg/dL)	1090 ± 382	1374 ± 324
PAI1 (pg/dL)	1168 ± 334	1579 ± 329
Resistin (pg/dL)	1930 ± 130	1971 ± 171

Supplementary Table 2. Tissue weight, body temperature and circulating metabolic and hormonal parameters in wild-type mice and GPR120-null mice treated with dietary GW9508 for 7 days Adult mice were fed a standard chow diet supplemented with or without GW9508 for 7 days. Data are means ± s.e.m. (*P<0.05 relative to untreated control mice; ANOVA with Tukey's post hoc test).

	Wild-type		GPR120-/-	
	Control	GW9508	Control	GW9508
Body weight (g)	27.7 ± 0.6	27.0 ± 0.6	26.9 ± 0.5	27.4 ± 0.3
Food intake (g)	4.0 ± 0.2	4.5 ± 0.1	4.3 ± 0.1	4.1 ± 0.21
iBAT (mg)	83.7 ± 1.8	97.4 ± 15.5	90.6 ± 5.4	91.6 ± 7.4
iWAT (mg)	147.6 ± 10.0	205.5 ± 3.0	133.4 ± 7.3	204.0 ± 31.9
eWAT(mg)	264.6 ± 15.3	440.5 ± 143.5	228.8 ± 21.5	433.8 ± 50.0
Core temperature (eye) (ºC)	35.8 ± 0,5	35.6 ± 0,3	36.2 ± 0,18	36.0 ± 0.2
Glucose (mg/dL)	195 ± 11	185 ± 8	170 ± 9	174 ± 17
Triglycerides (mg/dL)	159 ± 13	138 ± 7	157 ± 9	160 ± 19
Insulin (pg/dL)	1520 ± 45	996 ± 96 *	1110 ± 350	1200 ± 180

Supplementary Table 3. TaqMan probes (Applied Biosystems) used for RT-PCR quantification of gene transcripts.

Gene	Reference
18S rRNA	Hs99999901_s1
FGF21	Mm00840165_g1
PGC-1alpha	Mm447183_m1
UCP1	Mm00494069_m1
Glut1	Mm00441480_m1
PRDM16	Mm00712556_m1
Bmp8b	Mm00432115_g1
CoxIV	Mm00438289_g1
Sirt3	Mm00452129_m1
PPARg	Mm440945_m1
FABP4	Mm00445880_m1
GPR120	Mm00725193_m1
GPR40	Mm00809442_s2
Leptin	Mm00434759_m1
PPIA(cyclophillin)	Mm02342430_g1

GPR120 controls neonatal thermogenic adaptation and brown fat function

Journal: Molecular Metabolism (Submitted).

IF: 6.799 ENDOCRINOLOGY & METABOLISM 11 DE 138 (1st Decile)

Abstract:

Objectives: The present study aimed to elucidate the possible role of GPR120 in adaptive thermogenesis and FGF21 regulation in new born mice. Methods: Heterozygous mice for GPR120 (Ffar4-/+) were mated. Pup deliveries were monitored and the animals were sampled at embryonic age 19, and at 6, 12 and 24 hours after birth. To examine the possible role of GPR120 on neonatal brown adipose tissue (BAT) thermogenic activation, new-born BAT indirect calorimetry was assessed by thermographic images. Also, BAT from these animals was dissected and analyzed for RNA and protein expression. Finally, BAT from 1 day old pups was dissected to determine the substrate oxidation capacity of these tissues (14C-glucose and 14Cpalmitate).

Results: Ffar4 (GPR120), Ucp1 and Fgf21 genes were up-regulated in neonates product of thermal stress. Mice with a targeted disruption of the GPR120 gene (Ffar4) show an increased mortality during the first 24 hours of life under 21°C housing temperatures. Analysis on BAT from these animals show that the induction of Ucp1 mRNA and protein expression upon birth is reduced in GPR120-null mice. In addition, GPR120-null pups showed a reduced BAT temperature and decreased fatty acid oxidation capacity.

Conclusions: GPR120 expression in BAT is induced in pups after birth due to thermal stress. The lipid receptor expression and activity is essential for new-born adequate thermogenic adaptations. GPR120 deficiency leads to a decrease in FGF21 circulating levels during the first 24 hours post-partum which seems to correlate with decreased expression of UCP1 and fatty acid oxidation in BAT.

GPR120 controls neonatal thermogenic adaptation and brown fat function

Quesada-López T [1,2], Gavaldà-Navarro A[1, 2], Morón-Ros S[1, 2], Campderrós L[1, 2], Iglesias R[1, 2], Giralt M[1, 2], Villarroya F[1, 2].

[1] Department of Biochemistry and Molecular Biomedicine and Institut de Biomedicina (IBUB), University of Barcelona, Barcelona, Catalonia, Spain.

[2] CIBER Fisiopatología de la Obesidad y Nutrición, Spain.

Abstract

Objectives: The present study aimed to elucidate the possible role of GPR120 in adaptive thermogenesis and FGF21 regulation in new born mice.

Methods: Heterozygous mice for GPR120 (*Ffar4*-/+) were mated. Pup deliveries were monitored and the animals were sampled at embryonic age 19, and at 6, 12 and 24 hours after birth. To examine the possible role of GPR120 on neonatal brown adipose tissue (BAT) thermogenic activation, newborn BAT indirect calorimetry was assessed by thermographic images. Also, BAT from these animals was dissected and analyzed for RNA and protein expression. Finally, BAT from 1 day old pups was dissected to determine the substrate oxidation capacity of these tissues (^{14}C-glucose and ^{14}C-palmitate).

Results: *Ffar4* (GPR120), *Ucp1* and *Fgf21* genes were upregulated in neonates product of thermal stress. Mice with a targeted disruption of the GPR120 gene (*Ffar4*) show an increased mortality during the first 24 hours of life under 21°C housing temperatures. Analysis on BAT from these animals show that the induction of *Ucp1* mRNA and protein expression upon birth is reduced in GPR120-null mice. In addition, GPR120-null pups showed a reduced BAT temperature and decreased fatty acid oxidation capacity.

Conclusions: GPR120 expression in BAT is induced in pups after birth due to thermal stress. The lipid receptor expression and activity is essential for newborn adequate thermogenic adaptations. GPR120 deficiency leads to a decrease in FGF21 circulating levels during the first 24 hours post-partum which seems to correlate with decreased expression of UCP1 and fatty acid oxidation in BAT.

1. Introduction

Fetal life is a stable period of time at which fetus' temperature is intimately linked to the maternal temperature. It is estimated that the fetal temperature can reach temperatures up to one degree higher than there of the mother[1, 2]. Heat production for maintaining body temperature is suppressed in the fetus. However, it is in this period that brown adipose tissue (BAT), the main site responsible for thermal adaptations, begins its maturation. Brown fat is the main tissue specialized for adaptive

thermogenesis[1]. Upon delivery, the newborn temperature drops dramatically and it must rapidly adapt from the warm uterine environment (close to 37°C) to a cool extra-uterine life. The achievement of this adaptation is crucial since newborn hypothermia can be lethal[3]. Thermogenic activation in the newborn begins within minutes after birth and continues for many hours. Temperature maintenance will be mainly achieved by non-shivering thermogenesis (NST) [1, 4]. The capacity of BAT to endure NST depends in great measure on the amount of uncoupling protein-1 (UCP1) present in the tissue[1, 5] due to its capacity for uncoupling the respiratory chain and producing heat[1]. Thus, an adequate control of UCP1 expression upon delivery is essential for thermogenic adaptations in the neonate. Expression of UCP1 gene in BAT is turned on in late fetal life and, after birth, UCP1 gene expression is dramatically induced. Mitochondrial biogenesis and overall BAT hypertrophy also develops after birth to cope with the postnatal thermogenic challenge.

Sympathetic activation is believed to induce neonatal BAT thermogenesis, in a manner similar to cold-induced BAT activation in adults. However, additional factors have been proposed to be necessary for neonatal BAT induction. Accordingly, high levels of the fibroblast growth factor 21 (FGF21) in neonatal plasma, originating in liver in response to the initiation of milk intake, have been proposed to regulate neonatal BAT thermogenesis[6]. FGF21 is known to favor NST and promote browning of white adipose tissue in adults[7]. FGF21 is presumed to be expressed and secreted not only in liver but also by BAT in conditions of thermogenic activation. However, its local role in neonatal BAT thermogenesis is unknown. Recently, another pathway of thermogenic regulation of BAT and WAT has been identified involving the activation of the G-protein coupled receptor 120 (GPR120), a fatty acid receptor also called FFAR4[8]. Activation of GPR120 in BAT and WAT appears to promote adaptive thermogenesis through the induction of FGF21 expression. Here we report a key role of the GPR120/FGF21 axis in relation to thermogenic adaptation and regulation of BAT activity in neonatal life.

2. Materials and methods

2.1 Animals

All animal experiments were performed in accordance with European Community Council directive 86/609/EEC, as well as the number of animals to be used were approved by the Institutional Animal Care and Use Committee at the University of Barcelona based on the expected effects size. Swiss wild-type (purchased from Envigo) and C57/BL6 GPR120-heterozygote mice (Ffar4tm1 (KOMP) Vlcg, purchased from MMRRC) were used. C57/BL6 GPR120-heterozygote mice were mated and experiments were performed on GPR120-null, heterozygous and wild-type littermates. For studies in fetuses, cesarean sections were performed on Swiss or C57/BL6 mice on day 19 of gestation (Fetus-E19). Pups were studied starting at the time at which all pups had been born but had not yet started suckling (0 hr) and at 6 (P0.25), 12 (P0.5) and 24 (P1) hours

after birth. For ontogeny expression studies in Swiss mice ages: 7 (P7), 14 (P14), 21 (P21), and 70 days (adult) after birth were also sampled.

For studies on postnatal starvation, wild-type Swiss pups were separated from mothers prior to initiation of suckling, and placed in a humidified thermostatically controlled chamber (21°C or 37°C) for 8 hours.

BAT temperature was non-invasively estimated by measuring the iBAT skin-surface temperature using a high-sensitivity infrared thermography camera (FLIR T335), as previously reported[8].

Mice were killed by decapitation. Liver, interscapular BAT, duodenum, jejunum, ileum and colon were dissected. Blood was collected and glucose levels were determined using Accutrend (Roche) or centrifuged to obtain plasma.

2.2 Optical microscopy

Tissue samples were placed in 10% buffered formalin overnight and processed for hematoxylin and eosin (H&E) staining using standard procedures, previously described[8].

2.3 Transmission Electron Microscopy

BAT samples were fixed in 2.5% glutaraldehyde and 2% paraformaldehyde in 0.1 M phosphate buffer (pH 7.4) and post-fixed in 1% osmium tetroxide and 0.8% FeCNK in phosphate buffer. After dehydration in a graded acetone series, tissue samples were embedded in Spurr resin. Ultrathin sections were stained with uranyl acetate and lead citrate and examined with a Jeol 1010 transmission electron microscope (Izasa Scientific, Barcelona, Spain), as described previously[9].

2.4 Glucose and palmitate oxidation

Interscapular BAT from one day old (P1) wild-type and GPR120-/- pups was dissected. Two pieces of interscapular BAT were separated and weighted. Subsequently, both pieces of tissue were placed in DMEM no glucose (Gibco) for 1 hour. In these explants, ^{14}C-glucose and ^{14}C-palmitate oxidation (Perkin Elmer, NEC043X050UC and NEC534050UC) was quantified by the assessment of $^{14}CO_2$ production from the substrates added to the culture plate where BAT explants were incubated.

2.5 RNA extraction and quantitative PCR with reverse transcription

RNA from the tissue samples was extracted with the kit NucleoSpin® RNA (Macherey-Nagel, Düren, Germany). Reverse transcription was performed, using random hexamers primers (Applied Biosystems, Foster City, CA, USA) and 0.5 µg RNA in a total reaction volume of 20 µl. For PCR, Taqman Gene Expression Assay probes were used, with reaction mixtures containing 1 µl cDNA, 10 µl TaqMan Universal PCR Master Mix (Applied Biosystems), 250 nM probes and 900 nM of primers from the Assays-on-Demand Gene Expression Assay Mix. The 18S rRNA was measured as the housekeeping reference gene. The mRNA level of the gene of interest in each sample was normalized

to that of the reference control using the comparative (2−ΔCT) method, according to the manufacturer's instructions. A transcript was considered to be non-detectable when CT≥40. Supplementary table 1 shows the reference numbers for the TaqMan probes used during these studies.

2.6 Western blot and ELISA

Western blot analysis of tissue extracts was performed following standard procedures, using primary anti-UCP1 (1:1000 Abcam, Cambridge, UK), and anti-GPR120 (1:150 sc-390752, Santa Cruz, USA). Loading controls were established using α-tubulin immunoblots (T9026, Sigma-Aldrich) or Ponceau staining of membranes. Immunoreactive proteins were detected using an ECL (enhanced chemiluminescence) system (GE Healthcare). Signal intensities were quantified by scanning densitometry (Multi Gauge V3.0, Fujifilm). Plasma FGF21 levels were quantified with ELISA (RD291108200R, Biovendor).

2.7 Statistics

Results are expressed as mean ± SEM. Statistical analyses were performed using GraphPad Prism 6 (La Jolla, CA, USA). The statistical significance of differences was assessed using unpaired Student's t tests, one-way ANOVA with Tukey's multiple comparison test, or two-way ANOVA with Bonferroni post-testing, as appropriate.

3. Results

3.1 GPR120 expression in BAT is induced after birth, as a consequence of thermal stress.

All animal experiments were performed in accordance with European Community Council directive 86/609/EEC, as well as the number of animals to be used were approved by the Institutional Animal Care and Use Committee at the University of Barcelona based on the expected effects size. Developmental regulation of *GPR120* gene expression in mouse BAT, in comparison with known GPR120-expressing tissues (intestine sections) and with a tissue minimally expressing GPR120 (liver)[10, 11, 12, 13, 14, 15] is shown in figure 1a. In adults, the expression of the GPR120 transcript in BAT is significantly higher than in any other GPR120-expressing tissue (such as the distinct intestine sections), in accordance with previous data[8, 16]. GPR120 mRNA expression was low in fetal BAT but, after birth, *GPR120* mRNA levels increased dramatically; just 6 hours post-partum, *GPR120* mRNA levels were even much higher than those in adult BAT. High levels of *GPR120* mRNA expression in BAT were maintained during the first days of life and declined progressively thereafter to reach adult levels. In the other GPR120-expressing tissues, GPR120 expression was higher in adults than in neonates, and *GPR120* mRNA levels trended to follow a progressive increase throughout development. Only *GPR120* mRNA expression in colon showed early postnatal induction of *GPR120* gene expression, always to an extent much lower than that in BAT.

Assessment of GPR120 protein levels confirmed these trends and indicated the highest abundance of GPR120 in neonatal BAT (figure 1b).

Given that GPR120 is a lipid sensor, we tested whether the early postnatal induction in the expression of this gene in BAT could be due to the initiation of suckling or to other events associated with delivery-associated stress. For this purpose, mouse pups were studied at four different conditions: just after birth but before initiating sucking (0h), and 8 hours after birth being maintained with the mother (and confirmed to have suckled) or having been separated from the mother before initiation of sucking and maintained in non-feeding conditions either at 21°C or 37°C of environment temperature. Results showed the induction in the expression of *GPR120* mRNA in BAT 8h after delivery in feeding conditions, a behavior shared by other BAT thermogenesis-related genes such as *Ucp1* and *Fgf21* (figure 1c). The induction of *GPR120* expression occurred also in pups not allowed to suckle and maintained at 21°C, whereas it was totally blunted in non-fed pups maintained at 37°C, the same temperature as in the intrauterine environment. Again, the behavior of GPR120 gene expression under these conditions was similar to that of thermogenesis-related genes *Ucp1* and *Fgf21,* and revealed that, like those genes, the neonatal induction of GPR120 gene expression in BAT is mostly elicited by the postnatal thermogenic stress rather than nutritional-mediated events.

3.2 **GPR120 deficiency increases neonatal mouse mortality, which is influenced by the environment temperature.**

Results above showing an intense regulation of the GPR120-coding gene in neonatal BAT were suggestive of a role for GPR120 in neonatal thermogenic adaptations. To analyze this, GPR120-null mouse neonates were studied. Male and female C57/BL6 heterozygous mice for GPR120 gene invalidation (*Ffar4*) were mated and females were maintained at 21°C housing temperature during pregnancy and deliveries. At this temperature, the mortality GPR120-null pups one day after birth was significantly high relative to wild-type littermates, whereas GPR120-heterozygote pups showed intermediate rates of mortality (Table 1). Increasing the environment temperature at delivery by 4°C (25°C) suppressed the enhanced mortality of GPR120-null pups, which became indistinguishable from the anecdotical mortality rates of wild-type pup littermates. Wild-type and GPR120-null littermates maintained at 25°C were further studied.

3.3 The neonatal augmentation of plasma FGF21 levels and FGF21 gene expression in BAT are impaired in GPR120-null mice.

Wild-type mice and GPR120-null littermates were studied at E19, P0.25, P0.5 and P1 stages of neonatal life. No significant differences were observed in total body weight or BAT and liver tissue weights in GPR120-null pups compared with wild-type pups. Blood glucose levels didn't show either major differences according to the genotype, and only 24 h-old GPR120-deficient pups showed decreased blood glucose levels (table 2). The postnatal induction of *GPR120* mRNA in wild-type littermates of GPR120-null mice

(C57/BL6 strain) occurred similarly to that was observed in Swiss mice (Figure 2a). Previous reports showed that FGF21 plasma levels were increased during the first days of life[6], and we had previously found that GPR120-deficient adult mice show reduced FGF21 circulating levels upon cold exposure[8]. Induction of FGF21 levels after birth is considered a relevant adaptation to the neonatal period, contributing to BAT thermogenesis[6]. We found that pups deficient for GPR120 show impaired postnatal induction of plasma FGF21 levels at 12 and 24 hours of age (figure 2b). Neonatal FGF21 in blood is considered to have a main hepatic origin[6], although it is known that adult BAT expresses and releases significant amounts of FGF21 when thermogenesis is activated[17]. We found that *Fgf21* mRNA expression is markedly induced in BAT in the first hours of life, and such induction is strongly impaired in GPR120-deficient pups. The postnatal increase in *Fgf21* mRNA expression in liver was not affected by GPR120 gene invalidation (figure 2c) nor the expression of several FGF21 target genes (Supplemental figure 1).

3.4 GPR120 is required for the adaptive thermogenic activation of BAT in the neonatal period.

Heat production by BAT was determined using infrared thermography at the interscapular site of mouse pups where the most prominent BAT depot is present. Data indicated a significant reduction in BAT heat production in one day-old GPR120-null pups in comparison with wild-type control neonates (figure 3c). The postnatal induction of *UCP1* mRNA gene expression and UCP1 protein was significantly reduced in BAT from GPR120-null mice at distinct neonatal ages. In fact, the GPR120-null genotype determined a statistically significant reduction of *UCP1* mRNA ($P \leq 0.05$) and UCP1 protein (P $P \leq 0.05$) when distinctly aged neonates were analyzed as a whole, according to two-way ANOVA factor analysis. The analysis of the oxidative activity of BAT explants from one day-old pups revealed that GPR120-invalidation did not alter glucose oxidation rate but resulted in a dramatic reduction of fatty acid oxidation activity (figure 3d). However, no significant differences in the expression of adipogenic gene markers was observed (figure 4). Also, neither optical nor electronic microscopy assessments of cellular morphology at BAT revealed massive alterations due to GPR120 invalidation (Supplemental figure 2).

4. Discussion

GPR120 is a fatty acid receptor that has proven to mediate thermogenic activation in adipose tissues[8, 18, and 19]. Besides this activation effects over thermogenesis, GPR120-deficient animals have proven to be sensible to cold exposure[8]. Consistent with the former detail, GPR120-deficient pups show a compromised mortality during the first hours of life at 21°C housing temperatures. Here we show that thermal stress causes an induction in the expression of GPR120 and that this induction is lost when animals are

born at a temperature similar to that experienced at the mother's womb. Alike to this, the expression of other thermogenic markers showed similar behaviors not just regarding temperature but also to the feeding status of the pups which seemed to have mild effects over this induction, as observed for UCP1 in other studies[5, 6]. This suggests that the induction in GPR120 in BAT upon delivery is due to the thermal challenge and not to other events related with delivery-associated stress.

Previous reports from our laboratory have proven that the activation of GPR120 *in vivo* leads to increased circulating levels of FGF21 and *FGF21* mRNA expression in the adipose depots[8]. Likewise, diet supplementation with EPA, a well-known natural occurring agonist of GPR120, results in increased in FGF21 expression in BAT[20]. Consistent with this, and regarding GPR120 signaling, we have previously proven that GPR120-deficient mice show decreased plasma FGF21 levels upon cold exposure[8]. FGF21 was previously described to be markedly induced in the postnatal period. At first day of life, feeding promotes FGF21 expression in liver and its release to the circulation contributing to BAT thermogenesis[6]. However, liver is not the only tissue expressing FGF21 and contributing to FGF21 plasma levels. Brown adipose tissue has also proven to be an important producer and target of FGF21[17]. Whilst, it has been linked to an appropriate induction of thermogenesis in the adipose tissues upon cold exposure[7, 21]. Observed in this study, FGF21 plasma levels were importantly induced since 6 hours of life in wild-type animals. Nonetheless, this effect in FGF21 induction is not observed in GPR120-null pups. While no differences were observed in the expression of *Fgf21* gene in liver, BAT showed an impairment in *Fgf21* expression, especially during the first 12 hours after birth.

Several studies have found different components important for the development and activation of the thermogenic machinery in the perinatal period (i.e. iodothyronine 5'-deiodinase activity, insulin-like growth factor-2 (IGF-2), interleukin-33 (IL-33)) [5, 22, 23]. On these bases, here we show a BAT-mediated regulation of FGF21 in neonates intervened by GPR120. This regulation may show an effect over BAT thermogenic activation. Although in this study we found no important differences in morphology in BAT (i.e. lipid accumulation) or differential expression of OXPHOS proteins (data not shown), we did found an important blunt in the induction of Ucp1 mRNA and protein in GPR120-null neonates. Consistent with this observations, we found that indirect temperature estimation of BAT from animals deficient of the receptor showed decreased temperatures. Likewise, despite no important differences in glucose oxidation were reported, fatty acids oxidation seemed to be impaired in GPR120-deficient pups, important energy substrates at this age. Other studies where FGF21 levels were decreased in newborns have also shown reduced expression in BAT thermogenic machinery which were restored upon FGF21 administration to the animals[6]. This suggests that the effects observed in GPR120-null mice could be explained by the reduced expression of FGF21. In this study, the effects observed over UCP1 were sufficient to compromise thermogenic adaptation in perinatal period. Together, these

data suggest that the increased mortality under standard housing temperatures (21°C) could be due to an inadequate thermogenic adaptation in GPR120-deficient pups. This conclusion is also supported by the improvement in pup mortality by the increase in the environmental temperature (25°C) where the pup deliveries took place.

5. Conclusion

The lipid sensor GPR120 has an important role in mediating neonatal thermogenic adaptation. This role could be mediated through the regulation of FGF21 in BAT by this receptor and thus having an impact in the induction of BAT thermogenic machinery genes (i.e.UCP1) and fatty acid oxidation.

6. Highlights

6.1 GPR120 expression in BAT is enhanced in neonatal period.
6.2 GPR120 is necessary to achieve appropriate plasma FGF21 levels in the neonate.
6.3 The absence of GPR120 causes a decreased expression of UCP1 and heat production during the first hours of life.
6.4 GPR120 deficiency causes an impaired FA oxidation in BAT.

Authors' contributions

TQL, SMR and LC performed the animal experiments and monitoring of the pup deliveries. RI, AGN and TQL performed the C-sections for fasting tests, differential temperature exposures and substrates' oxidation. MG, FV and TQL performed the data analysis and statistics; also cooperated in the writing of the article. All authors revised and accepted the manuscript details.

Conflict of interest

The authors declare that no conflicts of interest exist.

Acknowledgments

We thank Merche Morales and Albert Peró for their help with the sample management. We also thank the University of Barcelona TEM microscopy technical service and the animal facility service for the animal care. This research was supported by grants from Ministerio de Economía y Competitividad (SAF2017-85722) and Fondo de Investigaciones Sanitarias, Instituto de Salud Carlos III (PI17/00420), co-financed by the European Regional Development Fund (ERDF). Finally, TQL thanks CONACyT (Consejo Nacional de Ciencia y Tecnología, México) for her PhD scholarship.

References

1. Cannon B and Nedeergard , 2004. Brown adipose tissue: function and physiological significance. Physiol Rev.; 84(1): 277-359.
2. Blackburn S, 2011. Brown adipose tissue. J Perinat Neonatal Nurs.; 25(3): 222-3.
3. Gunn TR, Gluckman PD, 1995. Perinatal thermogenesis. Early Hum Dev.; 42(3): 169-83.
4. Asakura H, 2004. Fetal and neonatal thermoregulation. J Nippon Med Sch.; 71(6): 360-70.
5. Giralt M, Martin I, Iglesias R, Viñas O, Villarroya F, Mampel T, 1990. Ontogeny and perinatal modulation of gene expression in rat brown adipose tissue. Unaltered iodothyronine 5'-deiodinase activity is necessary for the response to environmental temperature at birth. Eur J Biochem.; 193(1): 297-302.
6. Hondares E, Rosell M, Gonzalez FJ, Giralt M, Iglesias R, Villarroya F, 2010. Hepatic FGF21 expression is induced at birth via PPARalpha in response to milk intake and contributes to thermogenic activation of neonatal brown fat. Cell Metab.; 11(3): 206-12.
7. Fisher FM, Kleiner S, Douris N, Fox EC, Mepani RJ, Verdeguer F, *et al.* 2012. FGF21 regulates PGC-1α and browning of white adipose tissues in adaptive thermogenesis. Genes Dev. 26(3):271-81.
8. Quesada-López T, Cereijo R, Turatsinze JV, Planavila A, Cairó M, Gavaldà-Navarro A, *et al*., 2016. The lipid sensor GPR120 promotes brown fat activation and FGF21 release from adipocytes. Nat Commun.; 7: 13479.
9. Cairó M, Villarroya J, Cereijo R, Campderrós L, Giralt M, Villarroya F, 2016. Thermogenic activation represses autophagy in brown adipose tissue. Int J Obes (Lond).; 40(10): 1591-1599.
10. Hirasawa A, Tsumaya K, Awaji T, Katsuma S, Adachi T, Yamada M, *et al*., 2005. Free fatty acids regulate gut incretin glucagon-like peptide-1 secretion through GPR120. Nat Med.; 11(1): 90-4.
11. Tanaka, T.; Yano, T.; Adachi, T.; Koshimizu, T. A.; Hirasawa, A.; Tsujimoto, G, 2008. Cloning and Characterization of the Rat Free Fatty Acid Receptor GPR120: In Vivo Effect of the Natural Ligand on GLP-1 Secretion and Proliferation of Pancreatic Beta Cells. Naunyn- Schmiedeberg's Arch. Pharmacol., 377, 515−522.
12. Lu, X.; Zhao, X.; Feng, J.; Liou, A. P.; Anthony, S.; Pechhold, S.; Sun, Y.; Lu, H.; Wank, S. (2012). Postprandial Inhibition of Gastric Ghrelin Secretion by Long-Chain Fatty Acid through GPR120 in Isolated Gastric Ghrelin Cells and Mice. Am. J. Physiol. Gastrointest. Liver Physiol., 303, G367−376.
13. Duca, F. A.; Swartz, T. D.; Sakar, Y.; Covasa, M, 2013. Decreased Intestinal Nutrient Response in Diet-Induced Obese Rats: Role of Gut Peptides and Nutrient Receptors. Int. J. Obes., 37, 375−381.
14. Paulsen, S. J.; Larsen, L. K.; Hansen, G.; Chelur, S.; Larsen, P. J.; Vrang, N. (2014). Expression of the Fatty Acid Receptor GPR120 in the Gut of Diet-Induced-Obese Rats and Its Role in GLP-1 Secretion. PLoS One, 9, e88227.

15. Iwasaki K, Harada N, Sasaki K, Yamane S, Iida K, Suzuki K, *et al*., 2015. Free Fatty Acid Receptor GPR120 Is Highly Expressed in Enteroendocrine K Cells of the Upper Small Intestine and Has a Critical Role in Gip Secretion after Fat Ingestion. Endocrinology, 156, 837−846.
16. Rosell M, Kaforou M, Frontini A, Okolo A, Chan YW, Nikolopoulou E, *et al*., 2014. Brown and white adipose tissues: intrinsic differences in gene expression and response to cold exposure in mice. Am J Physiol Endocrinol Metab; 306 (8):E945-64.
17. Hondares E, Iglesias R, Giralt A, Gonzalez FJ, Giralt M, *et al*., 2011. Thermogenic activation induces FGF21 expression and release in brown adipose tissue. J Biol Chem 286, 12983-12990.
18. Kim J, Okla M, Erickson A, Carr T, Natarajan SK, Chung S, 2016. Eicosapentaenoic Acid Potentiates Brown Thermogenesis through FFAR4-dependent Up-regulation of miR-30b and miR-378. J Biol Chem.; 291(39): 20551-62.
19. Schilperoort M, van Dam AD, Hoeke G, Shabalina IG, Okolo A, Hanyaloglu AC, *et al*., 2018. The GPR120 agonist TUG-891 promotes metabolic health by stimulating mitochondrial respiration in brown fat. EMBO Mol Med. pii: e8047.
20. Pahlavani M, Razafimanjato F, Ramalingam L, Kalupahana NS, Moussa H, Scoggin S, *et al*, 2017. Eicosapentaenoic acid regulates brown adipose tissue metabolism in high-fat-fed mice and in clonal brown adipocytes. J Nutr Biochem.; 39: 101-109.
21. Cereijo R, Villarroya J, Villarroya F, 2015. Non-sympathetic control of brown adipose tissue. Int J Obes Suppl.; 5(Suppl 1):S40-4.
22. Viengchareun S, Servel N, Fève B, Freemark M, Lombès M, Binart N, 2008. Prolactin receptor signaling is essential for perinatal brown adipocyte function: a role for insulin-like growth factor-2. PLoS One.; 3(2): e1535.
23. Odegaard JI, Lee MW, Sogawa Y, Bertholet AM, Locksley RM, Weinberg DE, *et al*., 2017. Perinatal Licensing of Thermogenesis by IL-33 and ST2. Cell. 171(7): 1707.

Table 1. One day old (24h) pups' mortality		
Genotype	**Mortality at 21°C**	**Mortality at 25°C**
GPR120 +/+	5%	5%
GPR120 +/-	16%	5%
GPR120 -/-	27.3%	5%
C57/BL6 GPR120+/- mice were mated. Pup deliveries were monitored and mortality of the three genotype littermates (GPR120+/+, GPR120+/- and GPR120-/-) is presented in this table.		

Table 2. Body weight, BAT and liver weights and circulating glucose								
	Fetus (E19)		**6 h (P 0.25)**		**12 h (P 0.5)**		**24h (P 1)**	
	Wild-type	**GPR120 - null**	**Wild-type**	**GPR120 - null**	**Wild-type**	**GPR120 - null**	**Wild-type**	**GPR120 - null**
Body Weight (BW) (g)	1.1 ± 0.05	1 ± 0.05	1.3 ± 0.03	1.3 ± 0.06	1.4 ± 0.05**	1.3 ± 0.07	1.4 ± 0.07**	1.4 ± 0.04*
BAT Weight (mg/gBW)	9 ± 0.5	9.3 ± 1.2	7.2 ± 0.5*	6.6 ± 0.6	7.2 ± 0.6*	7.6 ± 0.75	6.3 ± 0.4***	6.2 ± 0.3**
Liver Weight (mg/gBW)	55.1 ± 1.9	46 ± 4.1	37.8 ± 1.3***	42.9 ± 1.5 +	37 ± 1.1***	37.6 ± 1.6	33.8 ± 1.3***	31.7 ± 2.4**
Glucose (mg/dL)	52.8 ± 10.6	48 ± 5	60 ± 2.6	63.6 ± 10.5	63.7 ± 5.2	62.9 ± 4.9	81 ± 4.1***	63.8 ± 4.9 +
C57/BL6 GPR120+/- mice were mated. Pup deliveries were monitored and sampled at day 19 of embryonic age (E19), 6 hours (P0.25), 12 hours (P0.5) or 24 hours (P1). Blood was collected and interscapular BAT (BAT) and liver were dissected. Body weight, tissue weights and blood and glucose at the moment of sacrifice is presented in this table. Two-way ANOVA analysis was employed for determining developmental and genotype differences (*P<0.05, **P<0.01 and ***P<0.001 compared with corresponding controls (E19); +P<0.05 for genotype differences).								

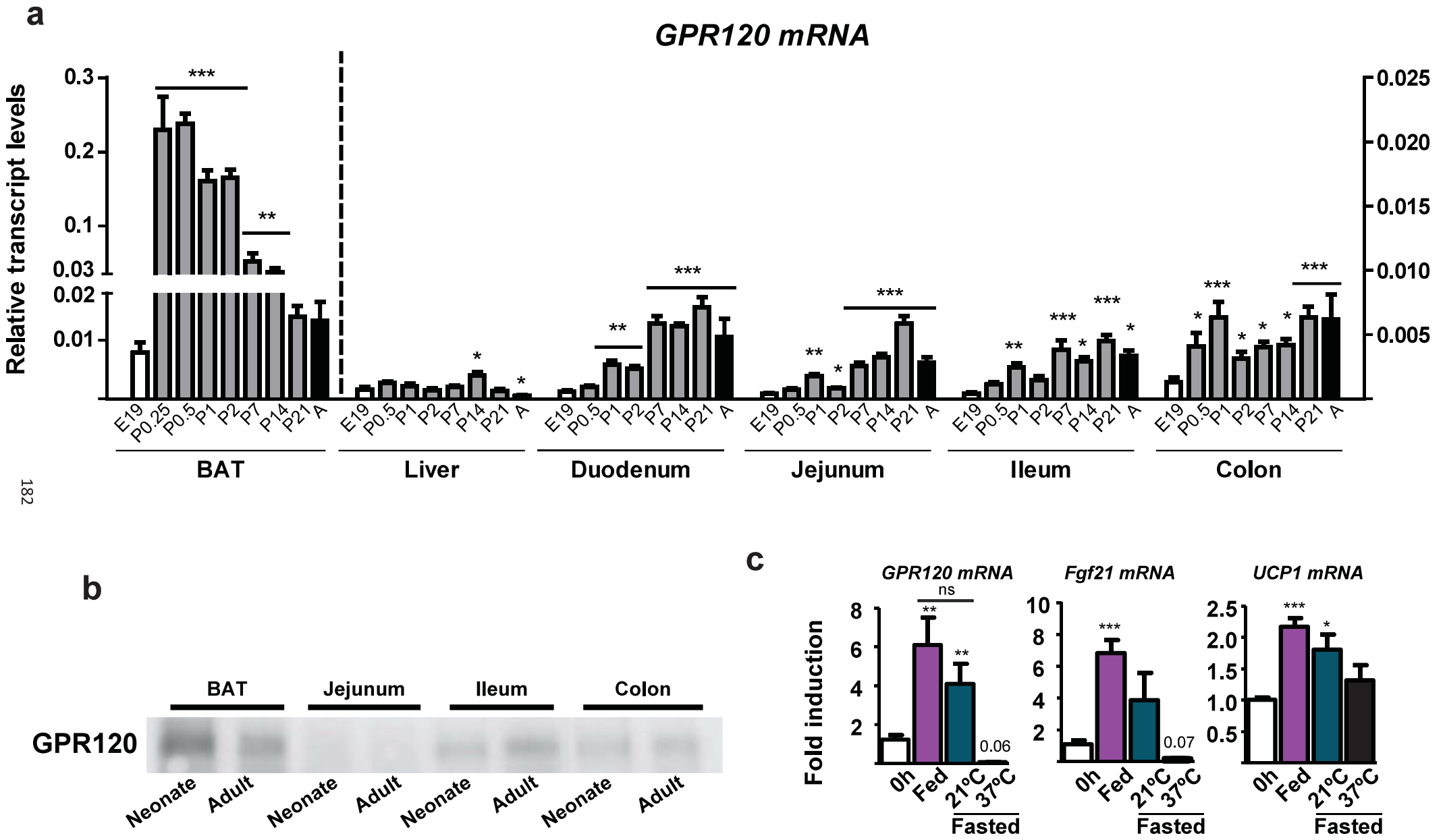
a
GPR120 mRNA
Relative transcript levels
0.3
0.2
0.1
0.03
0.02
0.01
0.025
0.020
0.015
0.010
0.005
***
**
*
E19 P0.25 P0.5 P1 P2 P7 P14 P21 A
E19 P0.5 P1 P2 P7 P14 P21 A
BAT
Liver
Duodenum
Jejunum
Ileum
Colon
182
b
BAT
Jejunum
Ileum
Colon
GPR120
Neonate
Adult
c
GPR120 mRNA
Fgf21 mRNA
UCP1 mRNA
Fold induction
ns
0.06
0.07
0h
Fed
21°C
37°C
Fasted

Figure 1. Developmental regulation of GPR120 gene expression. Swiss wild-type animals were mated. Pup deliveries were monitored and sampled at day 19 of embryonic age (E19), 6 hours (P0.25), 12 hours (P0.5), 24 hours (P1), 48 hours (P2), 7 days (P7), 14 days (P14), and 21 days (P21) after birth, and in 70-day-old (adult) mice. Interscapular BAT (BAT), liver, duodenum, jejunum, ileum and colon tissues were dissected. (**a**) Relative transcript levels of GPR120 (*Ffar4*) were quantified by real-time PCR, n=4-6. (**b**) Representative GPR120 protein levels in BAT from P0.5 (Neonate) and 70-day-old (Adult) mice are depicted in the blot. (**c**) Swiss wild-type animals were mated. On embryonic day 19 (0h), caesarean sections were performed. Pups were kept for 8 hours at room temperature (21°C), either fed or fasted, or at 37°C. BAT mRNA expression of *UCP1*, *Fgf21* and *GPR120* were quantified by real-time PCR, n=4-10. One-way ANOVA analysis of variance was performed for differences during the different times after birth (*P<0.05, **P<0.01 and ***P<0.001 compared with corresponding controls, E19 or 0h).

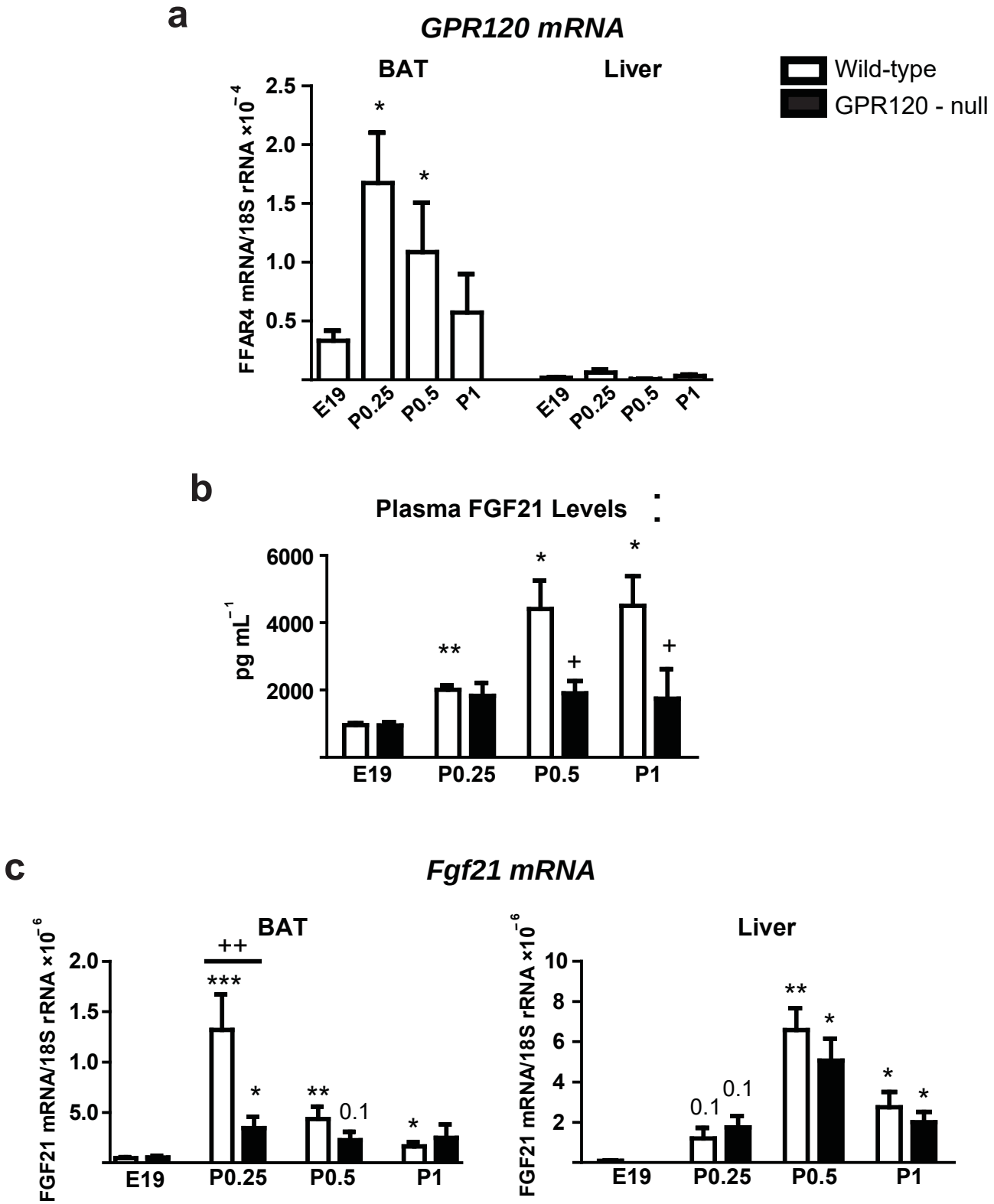
a
GPR120 mRNA
BAT
Liver
Wild-type
GPR120 - null
FFAR4 mRNA/18S rRNA ×10⁻⁴
2.5
2.0
1.5
1.0
0.5
E19
P0.25
P0.5
P1
b
Plasma FGF21 Levels
pg mL⁻¹
6000
4000
2000
c
Fgf21 mRNA
BAT
Liver
FGF21 mRNA/18S rRNA ×10⁻⁶
++
0.1

Figure 2. Developmental regulation of FGF21 gene expression in GPR120-null mice. C57/BL6 GPR120+/- mice were mated. Pup deliveries were monitored and sampled at day 19 of embryonic age (E19), 6 hours (P0.25), 12 hours (P0.5) or 24 hours (P1). Blood was collected and interscapular BAT (BAT) and liver were dissected. (**a**) Wild-type animals' gene expression of GPR120 (Ffar4) in BAT and liver were quantified by real-time PCR, n=5-9. (**b**) Circulating levels of FGF21 in wild-type and GPR120-/- offspring were measured by ELISA, n=4-6. (**c**) *Fgf21* mRNA transcript was measured by qPCR in BAT and liver from wild-type and GPR120 -/- perinatal mice, n=5-9. One-way ANOVA analysis of variance was performed for differences over time for the same genotype during the different times after birth. Two-way ANOVA was employed for determining differences between genotypes (*P<0.05, **P<0.01 and ***P<0.001 compared with the corresponding controls at E19; +P<0.05, ++P<0.01 for genotype differences).

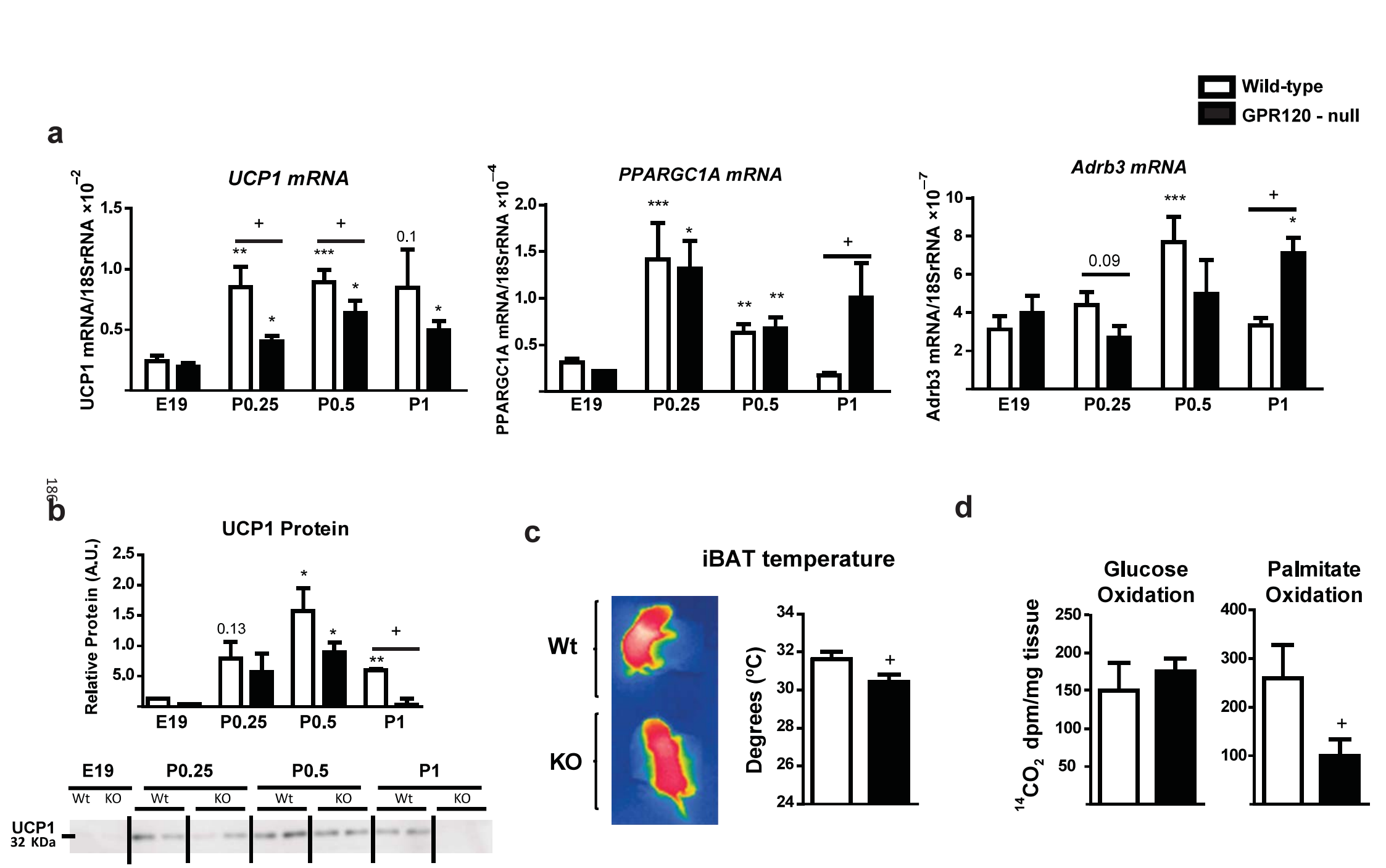
Wild-type
GPR120 - null
a
UCP1 mRNA
UCP1 mRNA/18SrRNA ×10−2
PPARGC1A mRNA
PPARGC1A mRNA/18SrRNA ×10−4
Adrb3 mRNA
Adrb3 mRNA/18SrRNA ×10−7
E19
P0.25
P0.5
P1
0.1
0.09
b
UCP1 Protein
Relative Protein (A.U.)
0.13
Wt
KO
UCP1
32 KDa
c
iBAT temperature
Degrees (ºC)
d
Glucose Oxidation
Palmitate Oxidation
14CO2 dpm/mg tissue

Figure 3. Effects of GPR120 gene invalidation in BAT thermogenic activation during the perinatal period. C57/BL6 GPR120+/- mice were mated. Pup deliveries were monitored and sampled at day 19 of embryonic age (E19), 6 hours (P0.25), 12 hours (P0.5) or 24 hours (P1). (**a**) Wild-type and GPR120 -/- animals' interscapular BAT (BAT) was dissected and gene expression of *Ucp1*, *Ppargc1a* and *Adrb3* was quantified by real-time PCR, n=5-9. (**b**) UCP1 protein levels were determined by western-blot at the mentioned time-points, quantified and corrected by α-tubulin (ATUB). (**c**) Representative thermographic images (left) and surface temperature quantification of BAT-area back skin (right) of one-day-old (P1) wild-type and GPR120-/- pups. (**d**) Quantification of ^{14}C-Glucose and ^{14}C-Palmitate oxidation in BAT explants from 1-day-old pups, n=7-14. Two-way ANOVA analysis was performed for determining differences in gene expression. Two-tailed unpaired Student's t-test was performed for differences in substrate oxidation (*P<0.05, **P<0.01 and ***P<0.001 compared with corresponding controls at E19; +P<0.05 for genotype differences).

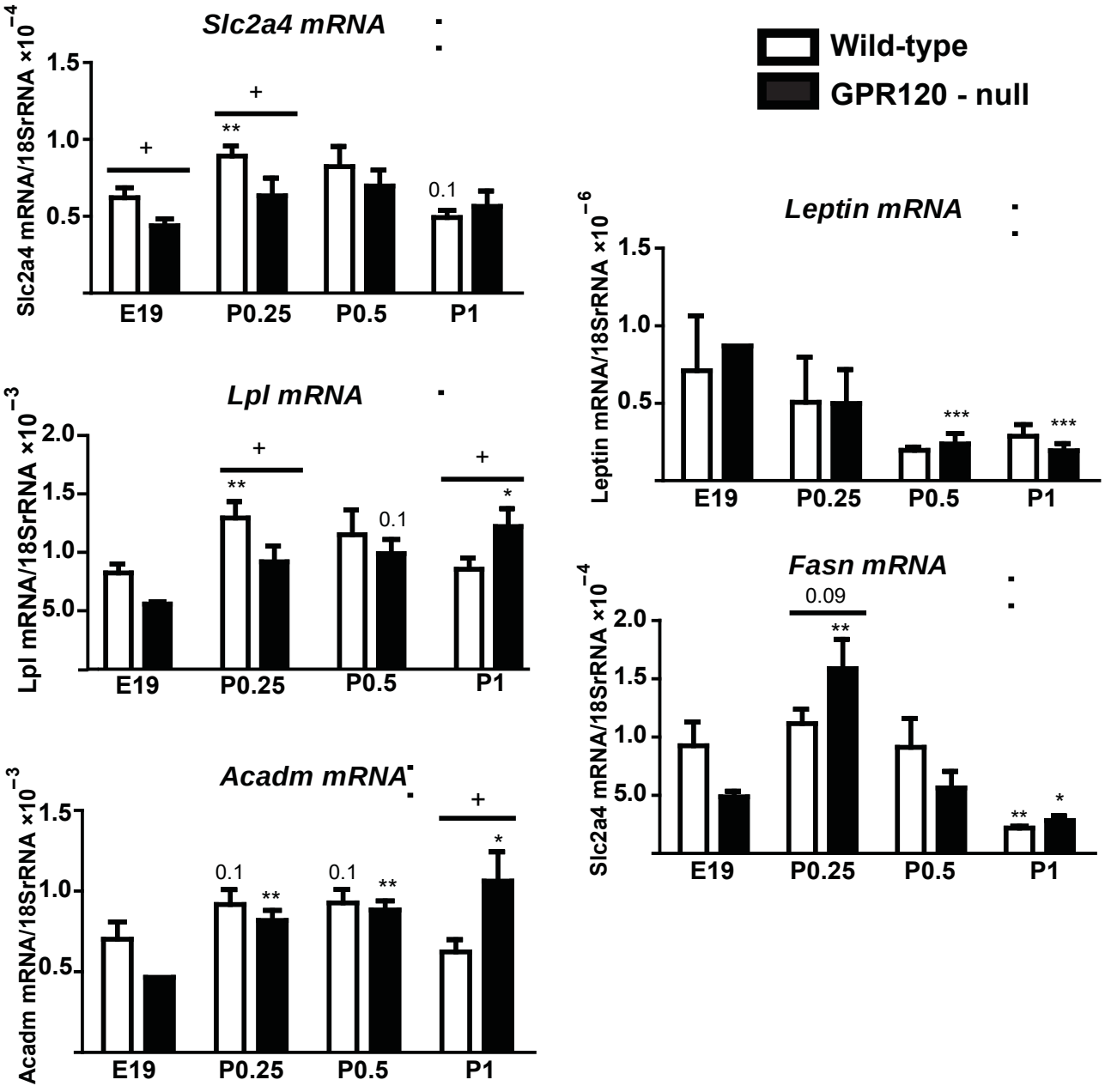
Wild-type
GPR120 - null
Slc2a4 mRNA
Slc2a4 mRNA/18SrRNA ×10−4
1.5
1.0
0.5
+
+
**
0.1
E19
P0.25
P0.5
P1
Lpl mRNA
Lpl mRNA/18SrRNA ×10−3
2.0
1.5
1.0
5.0
+
+
**
0.1
*
E19
P0.25
P0.5
P1
Acadm mRNA
Acadm mRNA/18SrRNA ×10−3
1.5
1.0
0.5
0.1
**
0.1
**
+
*
E19
P0.25
P0.5
P1
Leptin mRNA
Leptin mRNA/18SrRNA ×10−6
1.5
1.0
0.5
***
***
E19
P0.25
P0.5
P1
Fasn mRNA
Slc2a4 mRNA/18SrRNA ×10−4
2.0
1.5
1.0
5.0
0.09
**
**
*
E19
P0.25
P0.5
P1

Figure 4. Effects of GPR120 gene invalidation in BAT metabolic gene expression during the perinatal period. C57/BL6 GPR120+/- mice were mated. Pup deliveries were monitored and sampled at day 19 of embryonic age (E19), 6 hours (P0.25), 12 hours (P0.5) or 24 hours (P1). Interscapular BAT (BAT) was dissected from wild-type and GPR120 -/- mice and gene expression of adipogenic and lipogenic machinery markers was determined by real-time PCR. *Slc2a4*, *Leptin*, *Fasn*, *Lpl* and *Acadm* mRNA expressions are shown, n=5-9. Two-way ANOVA was performed for determining differences in gene expression (*P<0.05, **P<0.01 and ***P<0.001 compared with corresponding controls at E19; +P<0.05 for genotype differences).

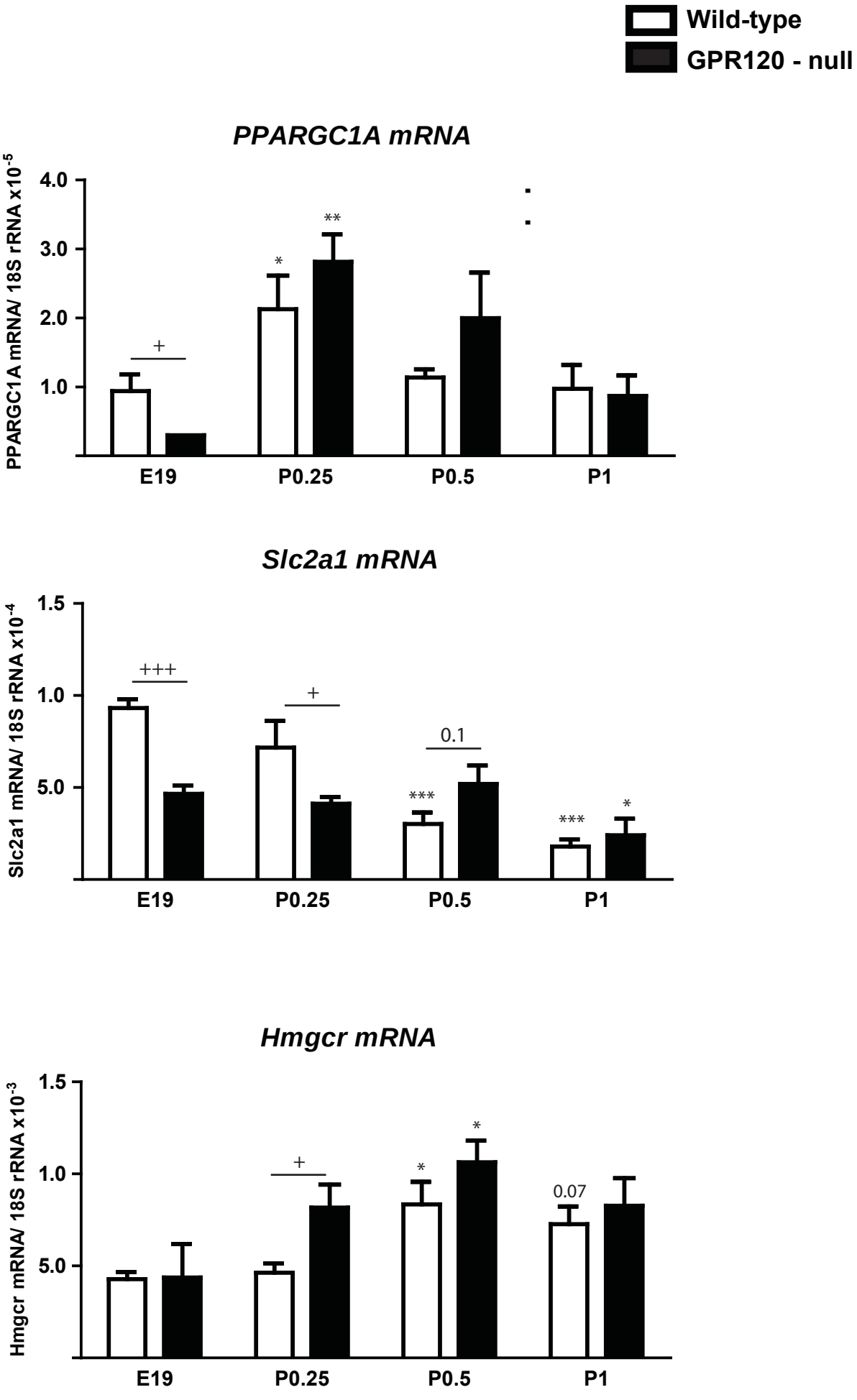
Wild-type
GPR120 - null
PPARGC1A mRNA
PPARGC1A mRNA/ 18S rRNA x10-5
4.0
3.0
2.0
1.0
+
*
**
E19
P0.25
P0.5
P1
Slc2a1 mRNA
Slc2a1 mRNA/ 18S rRNA x10-4
1.5
1.0
5.0
+++
+
0.1
***
***
*
E19
P0.25
P0.5
P1
Hmgcr mRNA
Hmgcr mRNA/ 18S rRNA x10-3
1.5
1.0
5.0
+
*
*
0.07
E19
P0.25
P0.5
P1

Supplementary figure 1. Effects of GPR120 gene invalidation in perinatal liver. Expression of FGF21 target genes in liver from wild-type and GPR120-/- pups, n=5-9. Two-way ANOVA was employed for determining genotype differences in gene expression (*P<0.05, **P<0.01 and ***P<0.001 compared with corresponding controls at E19; +P<0.05, +++P<0.001 for genotype differences).

iBAT Optical Microscopy Images

iBAT Transmission Electron Microscopy Images

	Wild-type	GPR120-/-	Wild-type	GPR120-/-
P0.25	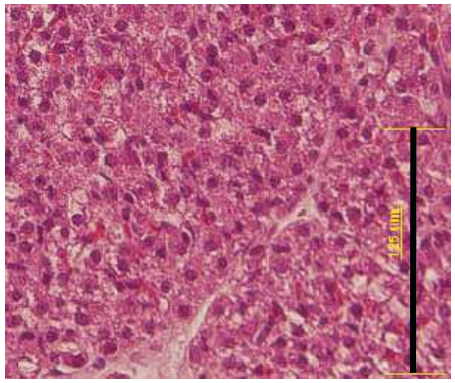	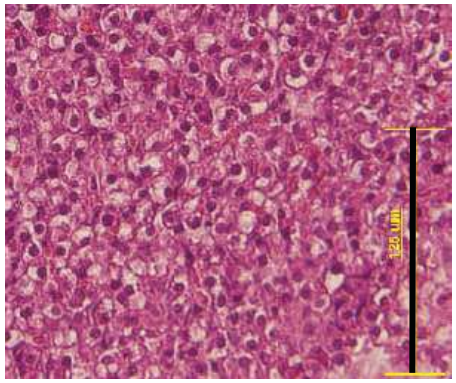	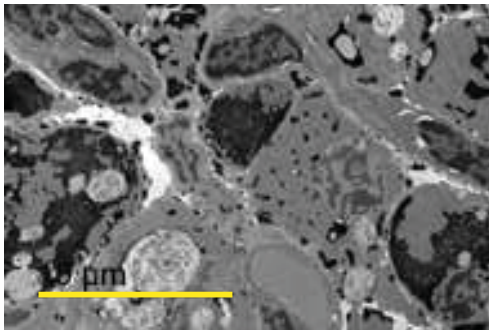	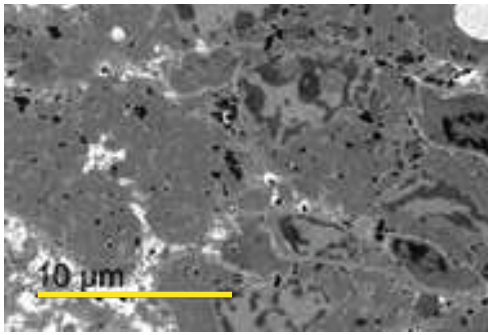
P0.5	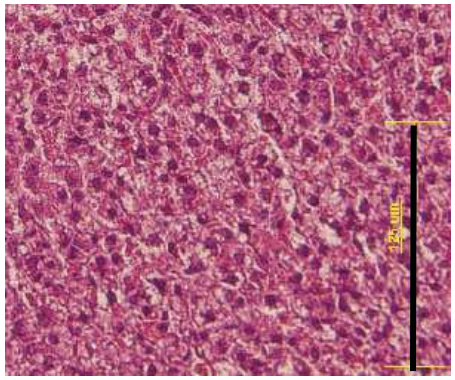	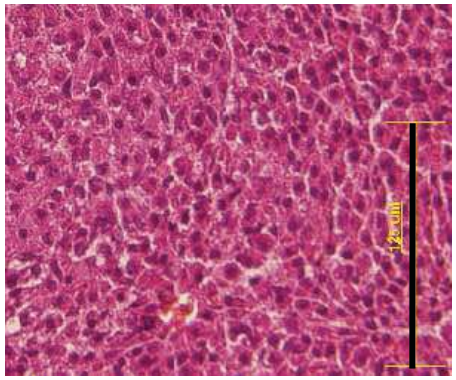	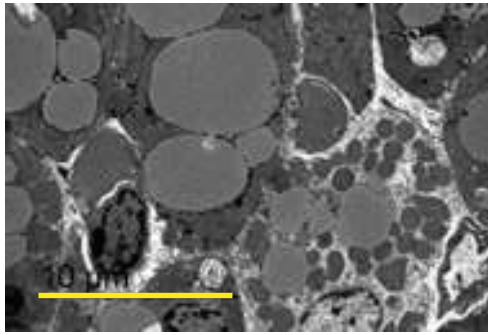	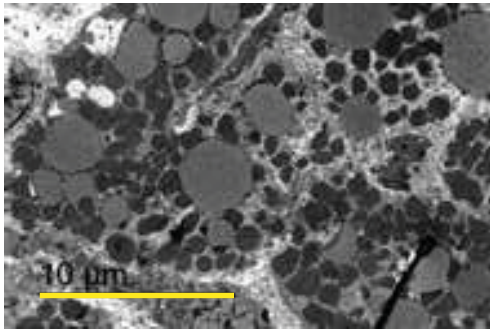
P1	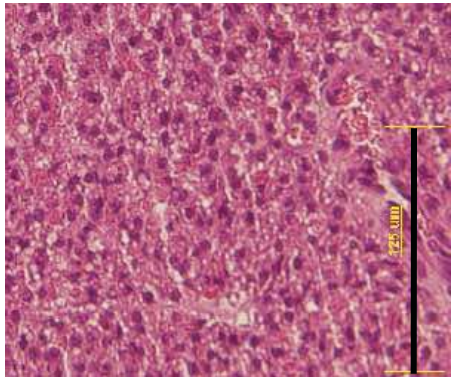	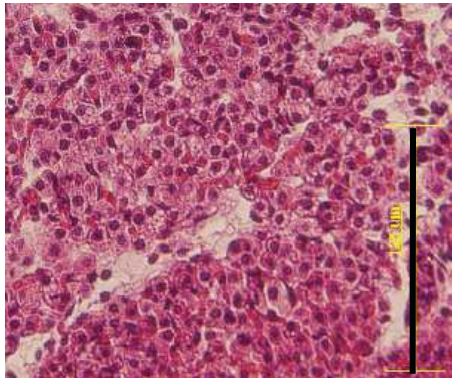	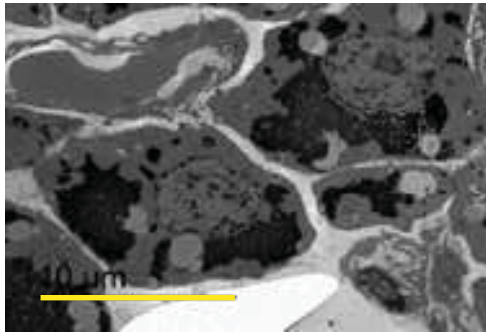	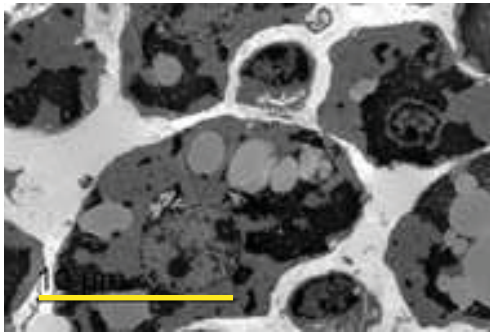

Supplementary figure 2. Effects of GPR120 gene invalidation in perinatal BAT histology and cell morphology. Representative optical microscopy (scale bar: 125µM) and transmission electron microscopy (scale bar: 10µM) images of interscapular BAT from wild-type and GPR120-/- mice at ages P0.25, P0.5 and P1 are shown.

Supplementary table 1. Taqman Probes (Applied Biotechnologies)	
Gene	Reference
18S	Hs99999901_s1
GPR120 (Ffar4)	Mm00725193_m1
UCP1	Mm00494069_m1
Fgf21	Mm00840165_g1
Ppargc1a	Mm447183_m1
Adrb3	Mm02601819_g1
Slc2a4	Mm00436615_m1
Leptin	Mm00434759_m1
Fasn	Mm00662319_m1
Lpl	Mm00434764_m1
Acadm	Mm00431611_m1
Hmgcs2	Mm00550050_m1
Slc2a1	Mm00441480_m1

Lipopolysaccharide-binding protein is a negative regulator of adipose tissue browning in mice and humans

Journal: Diabetologia. 2016 Oct; 59(10): 2208-18.

IF: 6.080 ENDOCRINOLOGY & METABOLISM 15 DE 138 (1st Tercile)

Abstract:

Aims/hypothesis: Adipocyte lipopolysaccharide-binding protein (LBP) biosynthesis is associated with obesity-induced adipose tissue dysfunction. Our purpose was to study the role of LBP in regulating the browning of adipose tissue.

Methods: Adult mice were maintained at 4°C for 3 weeks or treated with the β3-adrenergic agonist, CL316,243, for 1 week to induce the browning of white fat. Precursor cells from brown and white adipose tissues were cultured under differentiation-inducing conditions to yield brown and beige/ brite adipocytes, respectively. In vitro, Lbp was knocked down in 3T3-L1 adipocytes, and cells were treated with recombinant LBP or co-cultured in transwells with control 3T3-L1 adipocytes. Wild-type and Lbp-null mice, fed a standard or high fat diet (HFD) for 15 weeks, were also used in investigations. In humans, subcutaneous and visceral adipose tissue samples were obtained from a cohort of morbidly obese participants.

Results: The induction of white fat browning by exposure of mice to cold or CL316,243 treatment was strongly associated with decreased Lbp mRNA expression in white adipose tissue. The acquisition of the beige/brite phenotype in cultured cells was associated with downregulation of Lbp. Moreover, silencing of Lbp induced the expression of brown fat-related genes in adipocytes, whereas LBP treatment reversed this effect. Lbp-null mice exhibited the spontaneous induction of subcutaneous adipose tissue browning, as evidenced by a remarkable increase in Ucp1 and Dio2 gene expression and the appearance of multivacuolar adipocyte clusters. The amount of brown adipose tissue, and brown adipose tissue activity were also increased in Lbp-null mice. These changes were associated with decreased weight gain in Lbp-null mice and protection against HFD-induced inflammatory responses, as shown by reduced IL-6 levels. However, rather than improving glucose homeostasis, these effects led to glucose intolerance and insulin resistance.

Conclusions/interpretation: LBP is identified as a negative regulator of the browning process, which is likely to contribute to the obesity-promoting action of LBP. The deleterious metabolic effects of LBP deletion are compatible with the concept that the appropriate regulation of inflammatory pathways is necessary for a healthy systemic metabolic profile, regardless of body weight regulation.

Diabetologia (2016) 59:2208–2218
DOI 10.1007/s00125-016-4028-y

ARTICLE

Lipopolysaccharide-binding protein is a negative regulator of adipose tissue browning in mice and humans

Aleix Gavaldà-Navarro[1,2,3,4] · **José M. Moreno-Navarrete**[4,5] · **Tania Quesada-López**[1,2,3,4] · **Montserrat Cairó**[1,2,3,4] · **Marta Giralt**[1,2,3,4] · **José M. Fernández-Real**[4,5] · **Francesc Villarroya**[1,2,3,4]

Received: 5 January 2016 / Accepted: 25 May 2016 / Published online: 25 June 2016

Abstract
Aims/hypothesis Adipocyte lipopolysaccharide-binding protein (LBP) biosynthesis is associated with obesity-induced adipose tissue dysfunction. Our purpose was to study the role of LBP in regulating the browning of adipose tissue.
Methods Adult mice were maintained at 4°C for 3 weeks or treated with the β_3-adrenergic agonist, CL316,243, for 1 week to induce the browning of white fat. Precursor cells from brown and white adipose tissues were cultured under differentiation-inducing conditions to yield brown and beige/brite adipocytes, respectively. In vitro, *Lbp* was knocked down in 3T3-L1 adipocytes, and cells were treated with recombinant LBP or co-cultured in transwells with control 3T3-L1 adipocytes. Wild-type and *Lbp*-null mice, fed a standard or high fat diet (HFD) for 15 weeks, were also used in investigations. In humans, subcutaneous and visceral adipose tissue samples were obtained from a cohort of morbidly obese participants.
Results The induction of white fat browning by exposure of mice to cold or CL316,243 treatment was strongly associated with decreased *Lbp* mRNA expression in white adipose tissue. The acquisition of the beige/brite phenotype in cultured cells was associated with downregulation of *Lbp*. Moreover, silencing of *Lbp* induced the expression of brown fat-related genes in adipocytes, whereas LBP treatment reversed this effect. *Lbp*-null mice exhibited the spontaneous induction of subcutaneous adipose tissue browning, as evidenced by a remarkable increase in *Ucp1* and *Dio2* gene expression and the appearance of multivacuolar adipocyte clusters. The amount of brown adipose tissue, and brown adipose tissue activity were also increased in *Lbp*-null mice. These changes were associated with decreased weight gain in *Lbp*-null mice and protection against HFD-induced inflammatory responses, as shown by reduced IL-6 levels. However, rather than improving glucose homeostasis, these effects led to glucose intolerance and insulin resistance.
Conclusions/interpretation LBP is identified as a negative regulator of the browning process, which is likely to contribute to the obesity-promoting action of LBP. The deleterious metabolic effects of LBP deletion are compatible with the concept that the appropriate regulation of inflammatory pathways is necessary for a healthy systemic metabolic profile, regardless of body weight regulation.

Keywords Brown adipose tissue · Browning · High-fat diet · Lipopolysaccharide-binding protein · Obesity

Abbreviations

BAT	Brown adipose tissue
eWAT	Epididymal white adipose tissue
HFD	High fat diet

Electronic supplementary material The online version of this article (doi:10.1007/s00125-016-4028-y) contains peer-reviewed but unedited supplementary material, which is available to authorised users.

✉ Francesc Villarroya
fvillarroya@ub.edu

1 Department of Biochemistry and Molecular Biology, University of Barcelona, Av. Diagonal 643, 08028 Barcelona, Catalonia, Spain

2 The Institute of Biomedicine of the University of Barcelona (IBUB), Barcelona, Spain

3 Institut de Recerca Pediàtrica Hospital Sant Joan de Déu, Barcelona, Spain

4 Centro de Investigación Biomédica en Red de Fisiopatología de la Obesidad y Nutrición (CIBEROBN), Spain
http://www.ciberobn.es/en

5 Section of Diabetes, Endocrinology and Nutrition, Institut d'Investigació Biomèdica de Girona (IdIBGi), Hospital of Girona "Dr Josep Trueta", Girona, Spain

iBAT	Interscapular brown adipose tissue
ITT	Insulin tolerance test
iWAT	Inguinal white adipose tissue
LBP	Lipopolysaccharide-binding protein
LPS	Lipopolysaccharide
SAT	Subcutaneous adipose tissue
shControl	Control small hairpin RNA
shLBP	Small hairpin RNA-mediated LBP knockdown
shRNA	Small hairpin RNA
UCP1	Uncoupling protein 1
VAT	Visceral adipose tissue
WAT	White adipose tissue
WT	Wild-type

Introduction

Obesity is characterised by lipid accumulation in white adipose tissue (WAT) as a consequence of a disturbed energy balance due to increased food energy intake and/or lowered energy expenditure. Importantly, it is associated with an increased incidence of metabolic disorders, especially type 2 diabetes mellitus [1].

Brown adipose tissue (BAT) is characterised by the presence of multivacuolar adipocytes with a thermogenic capacity that reflects the natural uncoupling of their mitochondria, as mediated by uncoupling protein 1 (UCP1). BAT is the main site of adaptive energy expenditure in response to cold and possibly to diet [2]. In experimental models, enhanced BAT activity is associated with protection against obesity, whereas impaired BAT activity favours an obese phenotype. Moreover, BAT is a major site of lipid breakdown and glucose uptake; therefore, BAT activation is associated with improvements in hyperlipidaemia and hyperglycaemia [3, 4]. In humans, it was previously thought that BAT is only present in neonates. However, more recent research has established that adult humans retain substantial BAT activity [5, 6]. In addition to the presence of BAT at defined anatomical locations, recent studies have attached special relevance to the WAT browning process [7]. This phenomenon consists of the appearance of functionally thermogenic brown adipocyte-like cells (so-called beige or brite adipocytes) in WAT depots. Several studies in mice have indicated that the capacity to activate this process may protect against diet-induced obesity and systemic metabolic disturbances [8, 9], although the actual relevance of adipose tissue browning to metabolism is still a matter of debate [10, 11].

Lipopolysaccharide (LPS)-binding protein (LBP) is a type I acute-phase reactant protein, thought to be mainly produced by the liver [12]. LBP facilitates the binding of the lipid A component of LPS to CD14 and toll-like receptor 4 (TLR4) [13], thus modulating the immunostimulatory capacity of LPS in bacterial infections [14]. LBP is also present in adipose tissues and high levels of LBP synthesis in white adipocytes are associated with WAT dysfunction in obesity [15]. LBP expression is associated with inflammatory markers and is increased with metabolic deterioration and insulin resistance in obese patients [16]. Here, we sought to establish the role of LBP in the browning of WAT. We investigated the association of *Lbp* expression with browning and studied alterations in browning and metabolism in *Lbp*-null mice.

Methods

Exposure of mice to chronic cold and treatment with CL316,243 The care and use of mice was carried out in accordance with the European Community Council Directive 86/609/EEC and approved by the Institutional Animal Care Committee of the University of Barcelona. C57BL/6 mice (Harlan Laboratories; Indianapolis, IN, USA) were maintained under standard conditions (12 h light/12 h dark cycle, 21 ± 1°C). Where indicated, 3-month-old mice were exposed to 4°C for 3 weeks, or 2-month-old mice received daily i.p injections with 1 mg/kg CL316,243 for 8 days (see electronic supplementary material [ESM] Methods; exposure of mice to chronic cold, and treatment of mice with CL316,243, for further details).

Adipocyte culture For primary adipocyte cultures, the stromal–vascular fraction was isolated from the inguinal WAT (iWAT) and interscapular BAT (iBAT) depots of 1-month-old mice. Pre-adipocytes were induced to differentiate into beige/brite and brown adipocytes, respectively, as previously reported [17, 18]. Differentiated beige/brite and brown adipocytes were treated with 0.5 μmol/l noradrenaline (norepinephrine) for 6 h. Differentiation of 3T3-L1 fibroblasts (ATCC; LGC Standards, Barcelona, Spain) was induced by treatment with 0.86 μmol/l insulin, 0.5 μmol/l dexamethasone and 0.5 mmol/l 3-isobutyl-1-methylxanthine (IBMX) for 2 days, followed by 0.86 μmol/l insulin alone for 5 days. See ESM Methods for further details.

LBP knockdown and co-culture experiments Stable silencing of *Lbp* was achieved by transfecting 3T3-L1 fibroblasts with small hairpin (interfering) RNA (shRNA) targeting mouse *Lbp* (shLBP)or control shRNA (shControl) (Sigma Mission shRNA; Sigma-Aldrich, St Louis, MO, USA) as previously reported [16], generating transfected cells described in this paper as shRNA-mediated LBP knockdown (shLBP) or control (shControl) cells, respectively. Where indicated, shLBP adipocytes were incubated with 10 ng/ml LBP (R&D Systems; Minneapolis, MN, USA) during differentiation. Differentiated shLBP or shControl 3T3-L1 adipocytes were placed on one side of a Transwell plate (VWR-

International Eurolab, Barcelona, Spain) and co-cultured with shLBP adipocytes on the other side. See ESM Methods for further details.

***Lbp*-null mouse studies** *Lbp*-knockout mice (C.129P2-Lbptm1Jack/J, Balb strain background; obtained from The Jackson Laboratory, Bar Harbor, ME, USA) were maintained at 21 ± 1°C. Five-week-old male *Lbp*-null and wild-type (WT) littermate mice were fed standard chow (CTRL) or a high fat diet (HFD) for 15 weeks. For GTTs, 2.5 g glucose/kg was administered i.p. to mice starved for 6 h. For insulin tolerance tests (ITTs), 0.75 IU/kg insulin (Actrapid; Novo Nordisk, Bagsvaerd, Denmark) was administered i.p. Plasma glucose (Accutrend; Roche Diagnostics, Mannheim, Germany), plasma insulin (BioVendor, Brno, Czech Republic); adiponectin (Life Technologies, Foster City, CA, USA); leptin, resistin and IL-6 (Millipore; Billerica, MA, USA); NEFA and 3-hydroxybutyrate (Wako Chemicals; Neuss, Germany); and triacylglycerols (Sigma-Aldrich) were assessed. Samples of iBAT or iWAT (25–50 mg) were incubated with 55.5 kBq/ml [U-^{14}C]D-glucose (Hartmann Analytic, Braunschweig, Germany) for 3 h. Disintegrations per minute (DPM) from $^{14}CO_2$ retained in a CO_2 trap and [^{14}C]tissue lipid extracts [19] were measured (Packard Instrument Company, Meriden, CT, USA). See ESM Methods for further details.

Human study Paired subcutaneous and visceral adipose tissue (VAT) samples (n = 38) from a cohort of morbidly obese (BMI >35 kg/m^2) participants were studied. These participants were recruited, gave written informed consent, and were validated and approved by the ethical committee at the Hospital of Girona 'Dr Josep Trueta'. Samples were obtained from subcutaneous adipose tissue (SAT) and VAT depots during elective surgical procedures. See ESM Methods for further details.

RNA isolation, cDNA synthesis and real-time PCR Total RNA was isolated (Macherey-Nagel, Düren, Germany) from BAT, iWAT, eWAT and liver samples from mice, and SAT and VAT samples from humans and retrotranscribed using TaqMan Reverse Transcription Reagents (Life Technologies). For the quantitative analysis of mRNA, TaqMan quantitative real-time PCR was performed on a 7500 Real-Time PCR System (Life Technologies) using the specific primer pair/probe sets, as described in ESM Table 1. See ESM Methods for further details.

Western blot assays Western blot analysis was performed on BAT and iWAT samples following standard procedures, using primary anti-UCP1 (1:1000; Abcam, Cambridge, UK) and anti-β-actin (1:5000; Sigma-Aldrich) antibodies. Both antibodies were diluted in 1× PBS containing 0.1% Tween-20, as per manufacturer's instructions. See ESM Methods for further details.

Statistical methods Results are expressed as mean ± SEM. Statistical analyses were performed using GraphPad Prism 6 (La Jolla, CA, USA). The statistical significance of differences was assessed using unpaired Student's t tests, one-way ANOVA with Tukey's multiple comparison test, or two-way ANOVA with Bonferroni post-testing, as appropriate.

Results

Induction of browning in subcutaneous WAT is associated with reduced *Lbp* expression We subjected mice to long-term cold exposure (4°C for 3 weeks) and then examined *Lbp* gene expression in adipose tissue depots. As expected, cold exposure increased expression of the thermogenesis-related genes *Ucp1*, *Sirt3*, *Fgf21* and *Ppargc1a* in subcutaneous WAT (i.e. iWAT; Fig. 1d–h); it also induced the browning process, indicated by the appearance of large amounts of multilocular adipocytes (Fig. 1a,b). These changes were associated with a marked reduction in *Lbp* expression (Fig. 1c). *Lbp* expression in visceral WAT (i.e. epididymal WAT [eWAT]), a WAT site less prone to browning, was also decreased in mice exposed to chronic cold, albeit to lesser extent (ESM Fig. 1a). In contrast, chronic cold exposure did not modify *Lbp* expression in iBAT (ESM Fig. 1h), even though we observed significant induction of thermogenesis-related genes in this tissue (ESM Fig. 1i–n).

Chronic treatment of mice with the β_3-adrenergic agonist CL316,243 (a model of induction of browning in iWAT and eWAT [20]), triggered the appearance of multilocular adipocytes (Fig. 1l, m), induced thermogenesis-related gene expression (Fig. 1o–v) and strongly repressed *Lbp* gene expression (Fig. 1n) in iWAT and eWAT (ESM Fig. 2a–i). Although iBAT also showed signs of activation following CL316,243 treatment (e.g. the induction of *Dio2* and *Bmp8b*), *Lbp* expression was not significantly altered in this tissue (ESM Fig. 2l–r). Overall, our results suggest that the downregulation of LBP is more strongly associated with WAT browning than with the induction of thermogenesis in iBAT.

***Lbp* expression is involved in the repression of browning in adipocytes** In order to determine whether the inverse relationship between *Lbp* expression and browning is a cell-autonomous phenomenon, we used rosiglitazone-induced browning (i.e. acquisition of the beige/brite phenotype) in precursor cells obtained from iWAT [17, 21]. Incubation of iWAT precursor cells with rosiglitazone during differentiation induced the expression of several marker genes for browning (Fig. 2b–f), and repressed *Lbp* expression (Fig. 2a), without

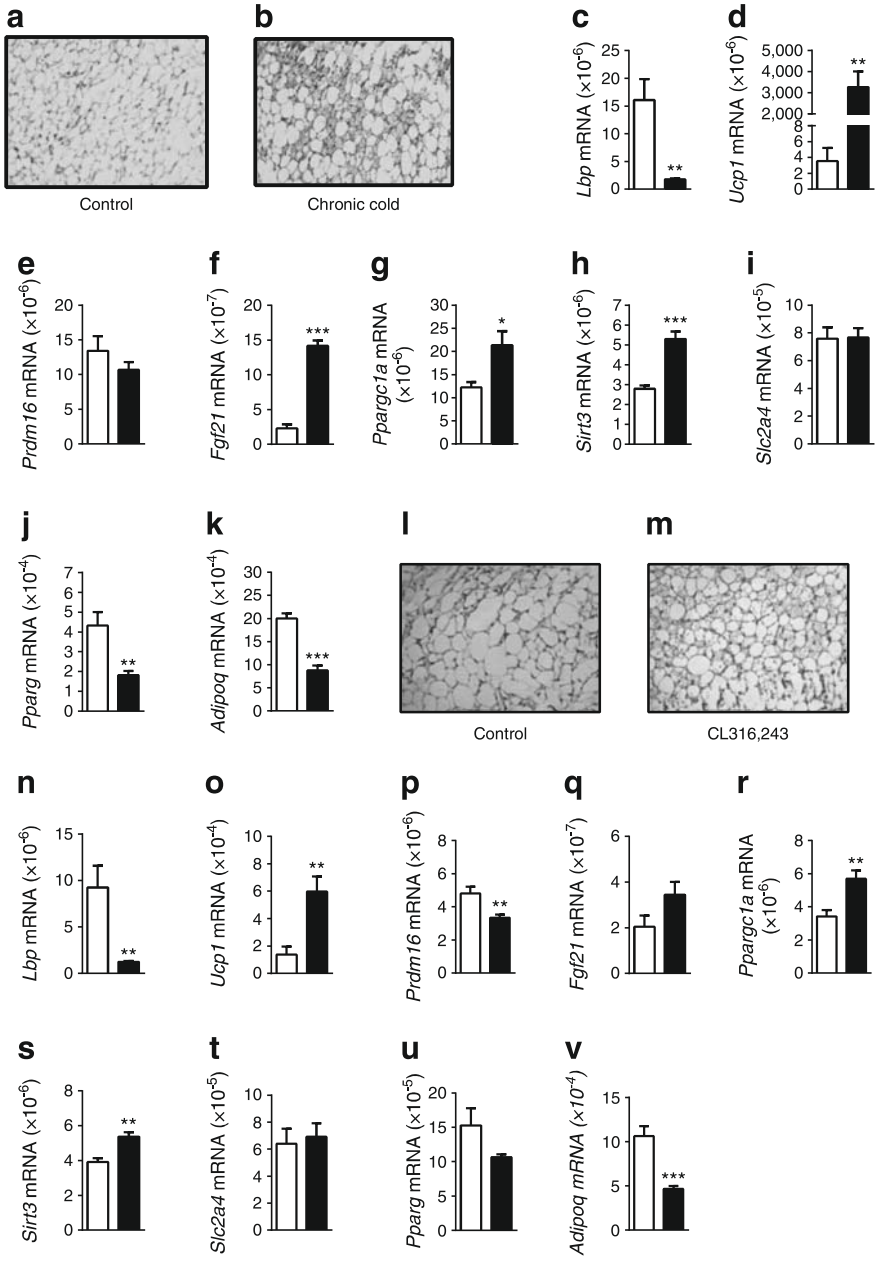

Fig. 1 Cold and β_3-adrenergic induction of iWAT browning is associated with reduced *Lbp* expression. (**a**, **b**) Micrographs (magnification × 20) of iWAT from (**a**) control mice or (**b**) mice maintained at 4°C for 3 weeks (chronic cold). (**c**–**k**) Transcript levels of (**c**) *Lbp*, (**d**) *Ucp1*, (**e**) *Prdm16*, (**f**) *Fgf21*, (**g**) *Ppargc1a*, (**h**) *Sirt3*, (**i**) *Slc2a4*, (**j**) *Pparg* and (**k**) *Adipoq* from control mice (white bars) or mice maintained at 4°C for 3 weeks (black bars). (**l**, **m**) Micrographs (magnification × 20) of iWAT from (**l**) control mice or (**m**) mice injected daily with 1 mg/kg CL316,243 for 8 days. (**n**–**v**) Transcript levels of (**n**) *Lbp*, (**o**) *Ucp1*, (**p**) *Prdm16*, (**q**) *Fgf21*, (**r**) *Ppargc1a*, (**s**) *Sirt3*, (**t**) *Slc2a4*, (**u**) *Pparg* and (**v**) *Adipoq* from control mice (white bars) or mice injected with CL316,243 (black bars). mRNA levels are normalised to 18S rRNA levels. Data are presented as mean ± SEM of six independent samples per group. *$p < 0.05$, **$p < 0.01$, and ***$p < 0.001$

affecting the expression of the general adipogenesis-related genes *Slc2a4* (also known as *Glut4*), *Adiponectin* (*Adipoq*) and *Pparg* (Fig. 2g–i). These data confirm that negative regulation of LBP expression is associated with the adipocyte browning. Moreover, treatment of differentiated beige/brite adipocytes with noradrenaline repressed *Lbp* and induced *Ucp1* gene expression (ESM Fig. 3a,b); however, noradrenaline did not modify *Lbp* expression in brown adipocytes (ESM Fig. 3c).

To investigate whether LBP has a direct role in the browning process, we studied the effects of shRNA-mediated LBP knockdown in 3T3-L1 adipocytes. After 7 days of differentiation, shLBP exhibited increased mRNA levels of several thermogenesis-related genes, including *Ucp1*, *Ppargc1a* and *Sirt3* (Fig. 2k–o). Treatment of shLBP cells with recombinant LBP rescued the induction of *Ucp1* mRNA expression induced by loss of *Lbp* (Fig. 2s). Moreover, shLBP adipocytes subjected to transwell co-culture with control adipocytes showed lower levels of *Ucp1* mRNA expression compared with those co-cultured with shLBP cells (Fig. 2t). Overall, these data suggest that the downregulation of *Lbp* represses browning in a cell-autonomous manner.

***Lbp*-null mice exhibit reduced body weight gain accompanied by an induction of the browning process in iWAT** To study the role of LBP in vivo, *Lbp*-null mice and WT littermate controls were fed standard chow (CTRL) or an

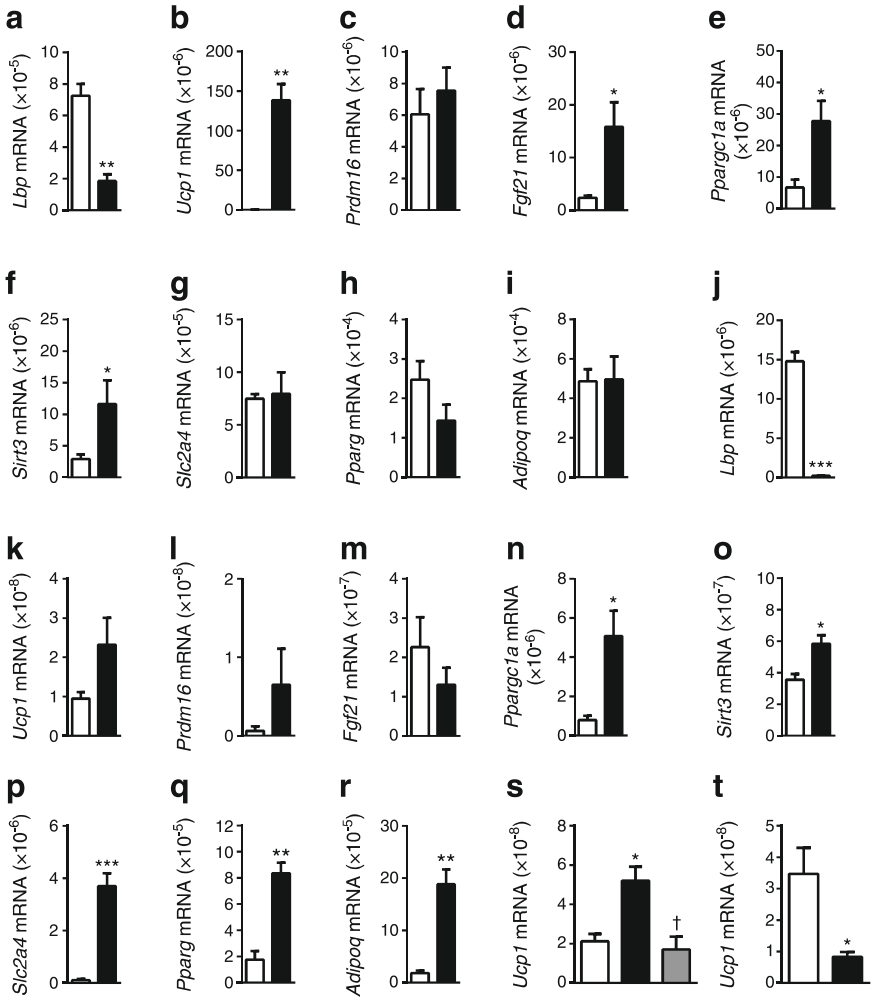

Fig. 2 *Lbp* and the expression of browning-related genes are inversely regulated in a cell-autonomous manner. (**a**–**i**) Transcript levels of (**a**) *Lbp*, (**b**) *Ucp1*, (**c**) *Prdm16*, (**d**) *Fgf21*, (**e**) *Ppargc1a*, (**f**) *Sirt3*, (**g**) *Slc2a4*, (**h**) *Pparg* and (**i**) *Adipoq*, in WAT-derived primary white adipocytes (white bars) or rosiglitazone-induced beige/brite adipocytes (black bars). (**j**–**r**) Transcript levels of (**j**) *Lbp*, (**k**) *Ucp1*, (**l**) *Prdm16*, (**m**) *Fgf21*, (**n**) *Ppargc1a*, (**o**) *Sirt3*, (**p**) *Slc2a4*, (**q**) *Pparg* and (**r**) *Adipoq* in 3T3-L1 adipocytes transfected with a control shRNA (shControl; white bars) or an shRNA targeting LBP (black bars). (**s**) Transcript levels of *Ucp1* in control 3T3-L1 adipocytes (white bars) or LBP-knockdown adipocytes untreated (black bar) or treated (grey bar) with 10 ng/ml LBP. (**t**) Transcript levels of *Ucp1* in LBP-knockdown 3T3-L1 adipocytes co-cultured with LBP-knockdown (white bar) or control 3T3-L1 adipocytes (black bar). mRNA levels are normalised to 18S rRNA levels. Data are presented as mean ± SEM of 4–7 independent samples per group. *$p < 0.05$, **$p < 0.01$ and ***$p < 0.001$ vs control $^{\dagger}p < 0.05$ for treated vs non-treated LBP-knockdown)

HFD for 15 weeks. At the start of the experiment (5-week-old mice), body weight was similar between WT and *Lbp*-null mice. The body weight of WT mice increased to 144% of the initial weight under standard feeding conditions and to 162% when fed an HFD (Fig. 3a,b). When fed a standard (CTRL) diet, the increase in body weight was significantly lower in *Lbp*-null mice (135%) than in WT mice on the same diet. On an HFD, the body weight of *Lbp*-null mice increased to only 145% of their initial weight; this increase was not significantly different from the body weight increase in *Lbp*-null mice on a standard diet. *Lbp*-null mice did not show significant changes in food intake relative to WT mice under standard diet (105 ± 4% kJ/day in *Lbp*-null vs WT) or HFD (112 ± 8% kJ/day in *Lbp*-null vs WT) conditions. Oxygen consumption was not significantly different among the different experimental groups (Fig. 3c).

The RQ was significantly decreased in WT mice fed HFD (Fig. 3d). In *Lbp*-null mice, RQ did not change significantly in response to an HFD, indicating a somewhat altered metabolic flexibility to adapt to HFD as a consequence of *Lbp* invalidation.

Lbp-null mice showed no statistically significant alterations in blood glucose levels (Fig. 3e), whereas *Lbp*-null mice had higher plasma triacyclglycerol levels when maintained on an HFD diet (Fig. 3f). Insulinaemia was strongly increased in *Lbp*-null mice relative to WT mice on an HFD (Fig. 3g). There were no differences in plasma NEFA, 3-hydroxybutyrate, leptin, adiponectin or resistin levels between WT and *Lbp*-null

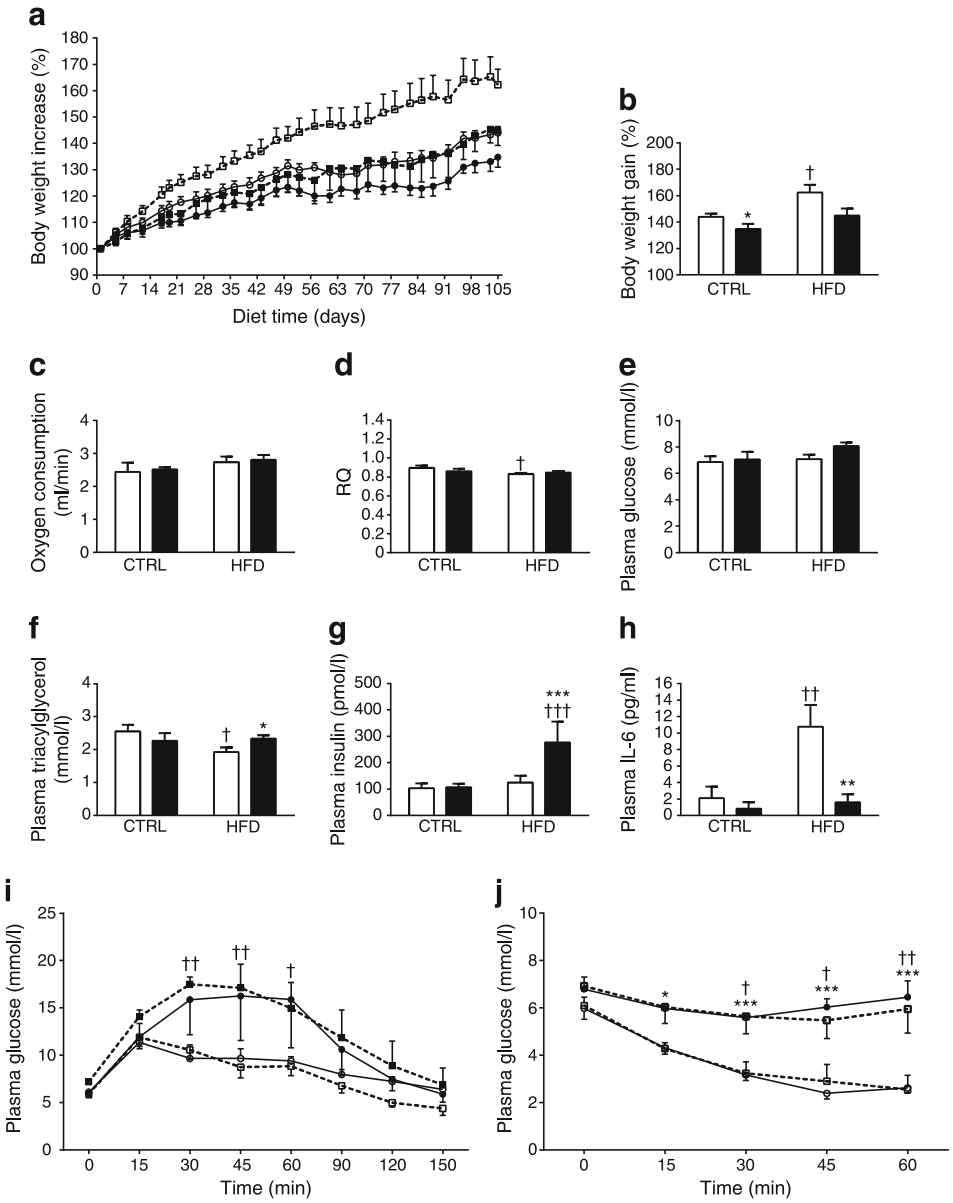

Fig. 3 *Lbp*-null mice have diminished body weight gain, with impaired glucose homeostasis. (**a**) Time course of mouse body weight, (**b**) final body weight gain, (**c**) oxygen consumption and (**d**) RQ. (**e**–**h**) Plasma levels of (**e**) glucose, (**f**) triacylglycerols, (**g**) insulin and (**h**) IL-6. White bars, WT mice; black bars, *Lbp*-null mice. (**i**) Glucose tolerance and (**j**) insulin tolerance tests in WT and *Lbp*-null mice after 15 weeks on a standard diet (CTRL) or HFD. White circles, WT mice, standard diet; White squares, WT mice, HFD; black circles, *Lbp*-null mice, standard diet; black squares, *Lbp*-null mice, HFD. Data are presented as mean ± SEM of 6–7 mice per group. *$p < 0.05$, **$p < 0.01$ and ***$p < 0.001$, WT vs LBP-null mice; $^{\dagger}p < 0.05$, $^{\dagger\dagger}p < 0.01$ and $^{\dagger\dagger\dagger}p < 0.001$, CTRL vs HFD

mice under CTRL or HFD conditions (ESM Table 2). Of the proinflammatory factors, HFD strongly induced circulating IL-6 levels in WT mice; this effect was totally ablated in *Lbp*-null mice (Fig. 3h). Consistent with the Balb genetic background of these mice, HFD did not affect glucose tolerance or the insulin response of WT mice, as determined by GTTs and ITTs (Fig. 3i,j) [22]. However, *Lbp*-null mice exhibited marked glucose intolerance and reduced insulin sensitivity on both a standard diet and HFD.

Under both standard diet and HFD conditions, *Lbp*-null mice showed a marked induction of the browning phenotype markers *Ucp1* and *Dio2* in iWAT (Fig. 4a,b). Other marker genes, including *Prdm16*, *Fgf21* and *Ppargc1a* (Fig. 4c–e), showed a similar trend that did not reach statistical significance between groups, although multifactorial ANOVA analysis revealed a significant increase in *Fgf21* ($p = 0.03$) for the *Lbp*-null factor. iWAT depots showed clusters of multivacuolar adipocytes (with beige/brite morphology) in *Lbp*-null mice, consistent with the gene expression data (Fig. 4j–m). Expression of genes involved in overall adipogenesis (*Pparg*, *Leptin* [*Lep*], and *Adipoq*) did not change (Fig. 4g–i), whereas multifactorial ANOVA analysis revealed a significant increase in *Slc2a4* ($p = 0.04$) for the *Lbp*-null factor. The amount of UCP1 protein per iWAT depot was higher in *Lbp*-null mice than in WT mice under both standard diet and HFD conditions (Fig 4p). Under conditions that promoted the highest browning, the amount of UCP1 protein in iWAT was around 8% of the levels observed in iBAT. Explants of iWAT from *Lbp*-null mice had an increased rate of glucose oxidation (Fig. 4q), but no change

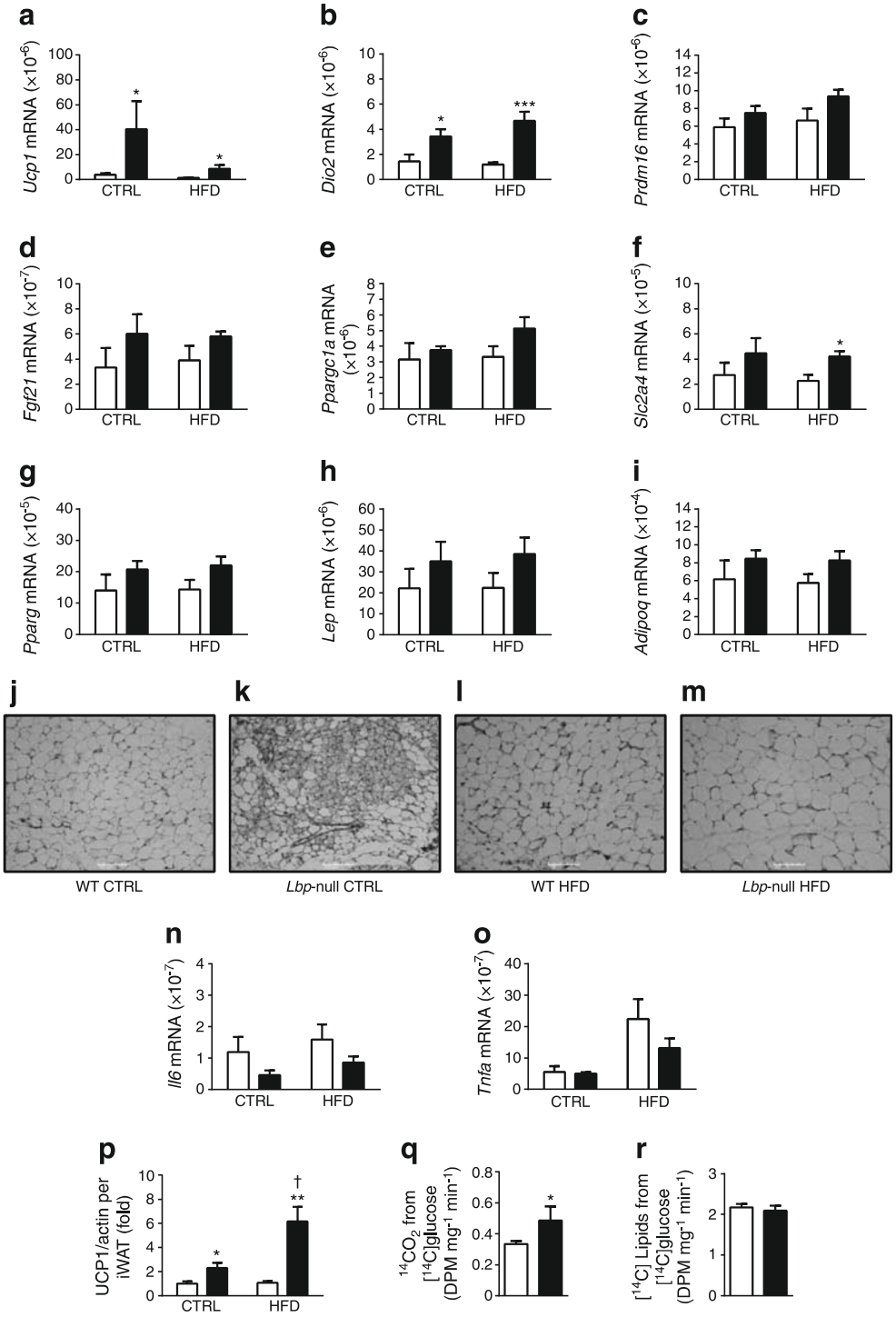

Fig. 4 *Lbp*-null mice exhibit induction of iWAT browning. (**a**–**i**, **n**, **o**) Transcript levels of (**a**) *Ucp1*, (**b**) *Dio2*, (**c**) *Prdm16*, (**d**) *Fgf21*, (**e**) *Ppargc1a*, (**f**) *Slc2a4*, (**g**) *Pparg*, (**h**) *Lep*, (**i**) *Adipoq*, (**n**) *Il6* and (**o**) *Tnfa* in iWAT from WT (white bars) and *Lbp*-null (black bars) mice fed a standard diet (CTRL) or an HFD for 15 weeks. (**j**–**m**) Micrographs (magnification × 20) of iWAT sections. (**p**) UCP1 protein per iWAT depot. (**q**) Glucose oxidation and (**r**) glucose incorporation into lipids in iWAT explants from WT (white bars) and *Lbp*-null (black bars) mice. mRNA levels are normalised to 18S rRNA levels. Data are presented as mean ± SEM of 4–6 independent samples per group. *$p < 0.05$, **$p < 0.01$ and ***$p < 0.001$, WT vs *Lbp*-null mice; †$p < 0.05$, CTRL vs HFD. DPM, disintegrations per minute

in the incorporation of glucose into lipids (Fig. 4r). This result indicates that oxidative pathways are enhanced in iWAT from *Lbp*-null mice, which is consistent with the molecular and morphological signs of browning in iWAT.

No evidence of significant browning due to *Lbp* gene ablation was detected in eWAT under any feeding condition, whether determined by gene expression analysis (with the exception of *Dio2*; ESM Fig. 4) or microscopic examination (data not shown).

iBAT in *Lbp*-null mice iBAT weight tended to be higher in *Lbp*-null mice relative to controls (Fig. 5a) and total iBAT protein content was significantly higher in *Lbp*-null mice (Fig. 5b), indicating functional hypertrophy of iBAT in

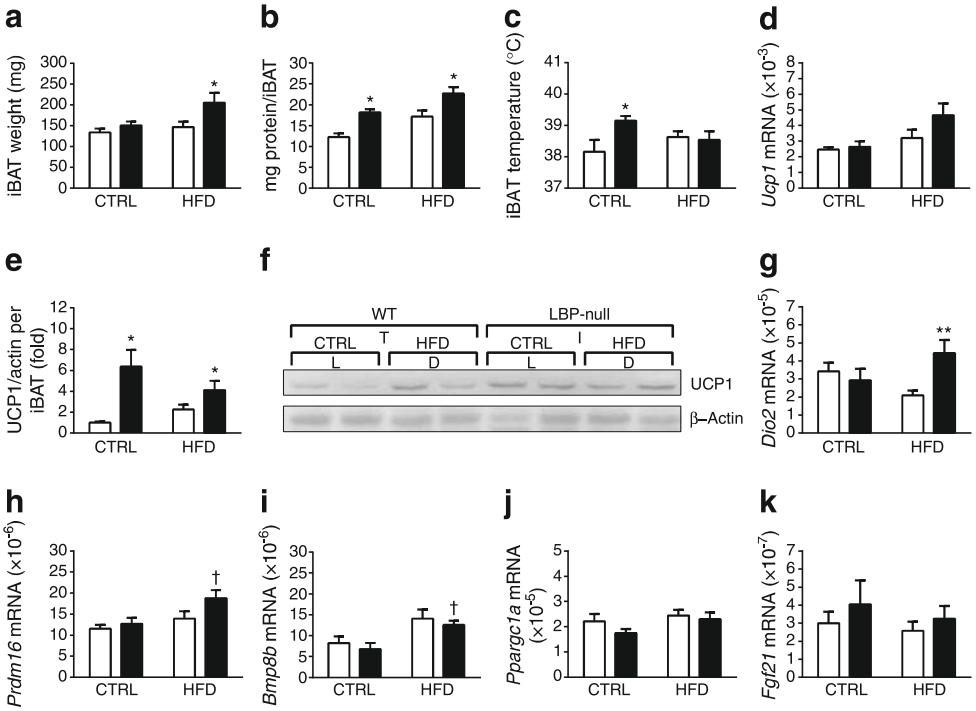

Fig. 5 iBAT in *Lbp*-null mice. (**a**) iBAT weight, (**b**) iBAT protein content and (**c**) surface temperature at the iBAT site in WT (white bars) and *Lbp*-null (black bars) mice fed a standard diet (CTRL) or an HFD. (**d**) *Ucp1* transcript levels and (**e**) UCP1 protein content per iBAT depot. (**f**) Representative immunoblot showing UCP1 protein levels in iBAT (40 μg protein/lane). (**g**–**k**) Transcript levels of (**g**) *Dio2*, (**h**) *Prdm16*, (**i**) *Bmp8b*, (**j**) *Ppargc1a* and (**k**) *Fgf21* in iBAT. mRNA levels are normalised to 18S rRNA levels. Data are presented as mean ± SEM of 4–6 independent samples per group. *$p < 0.05$ and **$p < 0.01$, WT vs *Lbp*-null mice; †$p < 0.05$, CTRL vs HFD

response to the lack of LBP. Consistent with this, the local temperature in the iBAT region was higher in *Lbp*-null mice than in WT mice, at least under standard diet conditions (Fig. 5c).

Total UCP1 per iBAT depot was increased in *Lbp*-null mice (Fig. 5e,f), although relative *Ucp1* transcript levels were not significantly altered (Fig. 5d). This scenario is consistent with a long-term BAT recruitment process [23]. Transcript levels for other thermogenesis-related genes showed no major changes due to LBP ablation, except for a significant induction of *Dio2* in the HFD group (Fig. 5g–k).

Hepatic alterations in *Lbp*-null mice Liver size and hepatic triacylglycerol content were unaltered in *Lbp*-null mice (data not shown). Expression of genes encoding gluconeogenesis-related enzymes (*G6pase* and *Pepck*) tended to be lower in *Lbp*-null mice (ESM Fig. 5a,b). The hepatic expression of *Srebp*, a master regulator of lipid synthesis, as well as *Fas*, *Scd1* and *Acaca*, was significantly reduced in *Lbp*-null mice under CTRL conditions (ESM Fig. 5c–f). *Il6* gene expression was undetectable under CTRL conditions in both WT and *Lbp*-null mice, but was strongly induced under HFD. This induction was impaired in *Lbp*-null mice, a profile that paralleled circulating IL-6 levels (ESM Fig. 5i).

LBP expression negatively correlates with the expression of browning marker genes in human subcutaneous adipose tissue We analysed the expression of *LBP* and browning marker genes in SAT and VAT biopsies from morbidly obese patients. Anthropometrical and clinical variables included age (48.3 ± 9.1 years), BMI (43.8 ± 6.9 kg/m^2), percentage fat mass (56.1 ± 10.1%), fasting glucose (5.33 ± 0.67 mmol/l) and *M* value (23.5 ± 13.3 μmol kg^{-1} min^{-1}). We found significant negative correlations between *LBP* transcript levels and the levels of transcripts for the browning marker genes *UCP1*, *PRDM16*, *PPARGC1A* and *TMEM26* (the latter being a putative marker of beige/brite adipocytes [24]) in SAT (Table 1). No such correlation was found between *LBP* expression and general markers of WAT such as *PLIN1*, *LEP* or *DGAT1*. In VAT, *LBP* mRNA levels negatively correlated with *TMEM26* mRNA levels and positively correlated with *LEP* mRNA levels (Table 1).

Table 1 Bivariate correlations between *LBP* gene expression and the expression of browning marker genes in SAT and VAT from obese individuals ($n = 38$)

Gene	SAT	VAT
PRDM16	−0.32*	−0.21
PPARGC1A	−0.51**	−0.28
UCP1	−0.35*	−0.08
TMEM26	−0.33*	−0.49**
PLIN1	−0.06	−0.22
LEP	0.21	0.55***
DGAT1	0.22	0.27

Data are Spearman's *r* coefficients

*$p < 0.05$, **$p < 0.01$ and ***$p < 0.001$

Discussion

In addition to its immunostimulatory functions [14], LBP has been identified as an adipokine associated with obesity-induced metabolic and proinflammatory disorders [15, 16]. The promotion of BAT activity and, especially, of WAT browning are active research areas that hold promise for strategies aimed at protecting against obesity and associated metabolic abnormalities (e.g. hyperglycaemia and hyperlipidaemia) [24, 25]. Here, we report that both cold exposure and chronic treatment with a β_3-adrenergic agonist (two validated models for inducing WAT browning [20, 26]) were associated with dramatic decreases in *Lbp* gene expression in iWAT. This phenomenon occurred in a cell-autonomous manner: *Lbp* expression was strongly repressed in cultures of adipocytes induced to acquire a beige/brite phenotype. Moreover, silencing of *Lbp* expression in adipocytes enhanced the expression of browning marker genes, whereas LBP treatment reversed this effect. As LBP is secreted by adipocytes, these data suggest that LBP may negatively regulate browning, apparently in an autocrine manner.

We observed that *Lbp*-null mice were protected against body weight increases, which is consistent with the relationship observed between obesity and *Lbp* expression in the adipose tissues of human patients and mouse models [15]. In rodents, the thermogenic activity in BAT accounts for a significant proportion of whole body energy expenditure [27]; therefore, the observed activation of BAT in *Lbp*-null mice may be involved in reducing weight gain. Moreover, although the estimated total thermogenic capacity of 'browned' WAT is much lower than that of BAT [23], browning of WAT is proposed to be relevant to protection against HFD-induced obesity [8, 9]. Our results indicate that a lack of LBP in mice strongly enhances the browning of WAT, thus indicating that the in vitro function of LBP as negative regulator of browning also occurs in vivo. These findings support the concept that LBP, possibly acting in an autocrine manner, negatively regulates the browning process. The negative correlation between *Lbp* expression and marker genes of browning in human adipose samples is consistent with this scenario. The signs of BAT activation in mice lacking LBP appear to contrast with the minor association of BAT activation with *Lbp* downregulation in iBAT. It is possible that the effects of LBP deficiency on body weight in mice occur through alterations in *Lbp* expression in other tissues (e.g. nervous system) that indirectly contribute to regulation of BAT activity, and that the cell-autonomous effects of LBP deficiency are minor in the context of the whole animal. Furthermore, the lack of an overt increase in oxygen consumption (despite activated BAT and WAT browning) and unchanged food intake in *Lbp*-null mice could be due to changes in these variables that are too small to be measurable but have long-term consequences on body weight. In any case, these observations warrant further research to determine whether impaired absorption of food might be different in *Lbp*-null mice than in WT mice, given evidence for a role for LBP in gut biology [28]. In summary, the *Lbp*-null model supports a role for LBP in the browning process, but the pleiotropic phenotype in these mice (see below) precludes definitive conclusions on the impact of browning induction on whole-body energy balance.

The obesity resistance, promotion of browning and increased BAT activity observed in *Lbp*-null mice were accompanied by glucose intolerance and insulin insensitivity. Although seemingly unexpected, these findings can be viewed in relation to our current understanding that complex relationships exist between inflammatory pathways (*Lbp*-null mice also showed a decrease in systemic and local inflammatory markers, such as IL-6) and metabolic regulation. Numerous studies have demonstrated a positive association between serum LBP concentration and obesity-associated metabolic disturbances, including insulin resistance, in humans [29–33]. However, a discrepancy between circulating concentrations of innate immune system proteins in obese patients and the metabolic phenotype of the corresponding knockout mice has also been reported for lipocalin-2 [34, 35] and IL-6 [4, 36]. Other mouse models with loss of function of proinflammatory factors leading to impaired inflammation, such as the dominant-negative *Tnfa* transgenic mouse [37] and *Fsp27*-deficient mice [38], show reduced inflammation in adipose tissue associated with weight loss, but also insulin resistance. In fact, mice lacking LPS-binding capacity due to *Cd14* knockout show reduced proinflammatory responses to LPS, but with significantly impaired glucose tolerance [39]. Thus, although current concepts tend to support the hypothesis that adipose tissue expansion in obesity is associated with local inflammation, which contributes to insulin resistance, recent research indicates that a certain degree of inflammatory response is essential for healthy adipose tissue expansion [37]. Our findings suggest the possibility that total impairment of the LPS signalling pathway limits an appropriate inflammatory response, abolishing the improvement in glucose tolerance that might be expected as a consequence of protection against obesity.

In conclusion, LBP appears to be a negative regulator of WAT browning and possibly of BAT activation. This action of LBP may be relevant to its role in favouring obesity and fat accretion. However, a total lack of LBP, even if protective against obesity, does not result in a systemic healthy phenotype. The complexities of homeostatic vs deleterious roles of inflammatory pathways in metabolic regulation are highlighted in the mouse model of *Lbp* gene ablation. Fine-tuning LBP levels should be considered a part of any prospective use of this factor in promoting healthy metabolism.

Funding This work was partly supported by research grants from the Ministerio de Economía y Competitividad (PI11–00214, PI12/02631, SAF2014–55725 and BFU2015–70454-REDT) and FONDOS FEDER. CIBEROBN Fisiopatología de la Obesidad y Nutrición is an initiative of the Instituto de Salud Carlos III, Spain.

Duality of interest The authors declare that there is no duality of interest associated with this manuscript.

Contribution statement AG-N, TQ-L and MC performed experiments in rodent models; JMM-N and JMF-R performed the studies involving human tissue; AG-N, TQ-L, MG and JMM-N performed the cell culture experiments; all authors contributed to the study design and participated in data analysis; AG-N and FV wrote the manuscript; all authors contributed to drafting the manuscript or revised it critically for intellectual content; and all authors gave final approval of the version to be published. FV is the guarantor of this work.

References

1. Erdmann J, Kallabis B, Oppel U, Sypchenko O, Wagenpfeil S, Schusdziarra V (2008) Development of hyperinsulinaemia and insulin resistance during the early stage of weight gain. Am J Physiol Endocrinol Metab 294:E568–E575
2. Saito M (2013) Brown adipose tissue as a regulator of energy expenditure and body fat in humans. Diabetes Metab J 37:22–29
3. Bartelt A, Bruns OT, Reimer R et al (2011) Brown adipose tissue activity controls triglyceride clearance. Nat Med 17:200–205
4. Stanford KI, Middelbeek RJ, Townsend KL et al (2013) Brown adipose tissue regulates glucose homeostasis and insulin sensitivity. J Clin Invest 123:215–223
5. Virtanen KA, Lidell ME, Orava J et al (2009) Functional brown adipose tissue in healthy adults. N Engl J Med 360:1518–1525
6. Cypess AM, White AP, Vernochet C et al (2013) Anatomical localization, gene expression profiling and functional characterization of adult human neck brown fat. Nat Med 19:635–639
7. Young P, Arch JR, Ashwell M (1984) Brown adipose tissue in the parametrial fat pad of the mouse. FEBS Lett 167:10–14
8. Guerra C, Koza RA, Yamashita H, Walsh K, Kozak LP (1998) Emergence of brown adipocytes in white fat in mice is under genetic control. Effects on body weight and adiposity. J Clin Invest 102:412–420
9. Seale P, Conroe HM, Estall J et al (2011) Prdm16 determines the thermogenic program of subcutaneous white adipose tissue in mice. J Clin Invest 121:96–105
10. Bartelt A, Heeren J (2014) Adipose tissue browning and metabolic health. Nat Rev Endocrinol 10:24–36
11. Nedergaard J, Cannon B (2014) The browning of white adipose tissue: some burning issues. Cell Metab 20:396–407
12. Grube BJ, Cochane CG, Ye RD et al (1994) Lipopolysaccharide binding protein expression in primary human hepatocytes and HepG2 hepatoma cells. J Biol Chem 269:8477–8482
13. Hailman E, Lichenstein HS, Wurfel MM et al (1994) Lipopolysaccharide (LPS)-binding protein accelerates the binding of LPS to CD14. J Exp Med 179:269–277
14. Tobias PS, Soldau K, Ulevitch RJ (1989) Identification of a lipid A binding site in the acute phase reactant lipopolysaccharide binding protein. J Biol Chem 264:10867–10871
15. Moreno-Navarrete JM, Escote X, Ortega F et al (2013) A role for adipocyte-derived lipopolysaccharide-binding protein in inflammation-and obesity-associated adipose tissue dysfunction. Diabetologia 56:2524–2537
16. Moreno-Navarrete JM, Escote X, Ortega F et al (2015) Lipopolysaccharide binding protein is an adipokine involved in the resilience of the mouse adipocyte to inflammation. Diabetologia 58:2424–2434
17. Aune UL, Ruiz L, Kajimura S (2013) Isolation and differentiation of stromal vascular cells to beige/brite cells. J Vis Exp 73:50191
18. Barbera MJ, Schluter A, Pedraza N, Iglesias R, Villarroya F, Giralt M (2001) Peroxisome proliferator-activated receptor alpha activates transcription of the Brown fat uncoupling protein-1 gene. A link between regulation of the thermogenic and lipid oxidation pathways in the brown fat cell. J Biol Chem 276:1486–1493
19. Folch J, Lees M, Sloane Stanley GH (1957) A simple method for the isolation and purification of total lipids from animal tissues. J Biol Chem 226:497–509
20. Lee YH, Petkova AP, Mottillo EP, Granneman JG (2012) In vivo identification of bipotential adipocyte progenitors recruited by β3-adrenoceptor activation and high-fat feeding. Cell Metab 15:480–491
21. Petrovic N, Walden TB, Shabalina IG, Timmons JA, Cannon B, Nedergaard J (2010) Chronic peroxisome proliferator-activated receptor gamma (PPARgamma) activation of epididymally derived white adipocyte cultures reveals a population of thermogenically competent, UCP1-containing adipocytes molecularly distinct from classic brown adipocytes. J Biol Chem 285:7153–7164
22. Montgomery MK, Hallahan NL, Brown SH et al (2013) Mouse strain-dependent variation in obesity and glucose homeostasis in response to high-fat feeding. Diabetologia 56:1129–1139
23. Nedergaard J, Cannon B (1831) UCP1 mRNA does not produce heat. Biochim Biophys Acta 2013:943–949
24. Jespersen NZ, Larsen TJ, Peijs L et al (2013) A classical brown adipose tissue mRNA signature partly overlaps with brite in the supraclavicular region of adult humans. Cell Metab 17:798–805
25. Lichtenbelt W, Kingma B, van der Lans A, Schellen L (2014) Cold exposure–an approach to increasing energy expenditure in humans. Trends Endocrinol Metab 25:165–167
26. Lee P, Greenfield JR (2015) Non-pharmacological and pharmacological strategies of brown adipose tissue recruitment in humans. Mol Cell Endocrinol 418:184–190
27. Cannon B, Nedergaard J (2004) Brown adipose tissue: function and physiological significance. Physiol Rev 84:277–359
28. Vreugdenhil AC, Snoek AM, Greve JW, Buurman WA (2000) Lipopolysaccharide binding protein is vectorially secreted and transported by cultured intestinal epithelial cells and is present in the intestinal mucus of mice. J Immunol 165:4561–4566
29. Sun L, Yu Z, Ye X et al (2010) A marker of endotoxemia is associated with obesity and related metabolic disorders in apparently healthy Chinese. Diabetes Care 33:1925–1932
30. Moreno-Navarrete JM, Ortega F, Serino M et al (2012) Circulating lipopolysaccharide-binding protein (LBP) as a marker of obesity-related insulin resistance. Int J Obes (Lond) 36:1442–1449
31. Serrano M, Moreno-Navarrete JM, Puig J et al (2013) Serum lipopolysaccharide-binding protein as a marker of atherosclerosis. Atherosclerosis 230:223–227
32. Gonzalez-Quintela A, Alonso M, Campos J, Vizcaino L, Loidi L, Gude F (2013) Determinants of serum concentrations of lipopolysaccharide-binding protein (LBP) in the adult population: the role of obesity. PLoS One 8:e54600
33. Liu X, Lu L, Yao P et al (2014) Lipopolysaccharide binding protein, obesity status and incidence of metabolic syndrome: a prospective study among middle-aged and older Chinese. Diabetologia 57:1834–1841

34. Moreno-Navarrete JM, Manco M, Ibanez J et al (2010) Metabolic endotoxemia and saturated fat contribute to circulating NGAL concentrations in subjects with insulin resistance. Int J Obes (Lond) 34: 240–249
35. Guo H, Jin D, Zhang Y et al (2010) Lipocalin-2 deficiency impairs thermogenesis and potentiates diet-induced insulin resistance in mice. Diabetes 59:1376–1385
36. Matthews VB, Allen TL, Risis S et al (2010) Interleukin-6-deficient mice develop hepatic inflammation and systemic insulin resistance. Diabetologia 53:2431–2441
37. Wernstedt AI, Tao C, Morley TS et al (2014) Adipocyte inflammation is essential for healthy adipose tissue expansion and remodeling. Cell Metab 20:103–118
38. Zhou L, Park SY, Xu L et al (2015) Insulin resistance and white adipose tissue inflammation are uncoupled in energetically challenged Fsp27-deficient mice. Nat Commun 6:5949
39. Young JL, Mora A, Cerny A et al (2012) CD14 deficiency impacts glucose homeostasis in mice through altered adrenal tone. PLoS One 7:e29688

ESM Methods

Exposure of mice to chronic cold

The care and use of mice was in accordance with the European Community Council Directive 86/609/EEC and all experimental procedures were approved by the Institutional Animal Care and Use Committee of the University of Barcelona. Three-month-old C57BL/6 mice, obtained from Harlan Laboratories (Indianapolis, IN, USA), were maintained under standard conditions of light (12-hour light/12-hour dark cycle) and temperature (21±1°C) (Control) or at 4ºC (Chronic cold) for 3 weeks. Mice were killed by decapitation, and tissues were removed, weighed, immediately frozen in liquid nitrogen, and stored at -80ºC until processing. A portion of each tissue was fixed with 4% formalin for 24 h and then stored in 70% ethanol at 4ºC until paraffin infiltration was performed. Paraffin-embedded tissues were sectioned, mounted on glass slides, stained with hematoxylin-eosin, and photographed under a light microscope (20x magnification).

Treatment of mice with CL 316,243

The care and use of mice was in accordance with the European Community Council Directive 86/609/EEC and all experimental procedures were approved by the Institutional Animal Care and Use Committee of the University of Barcelona. Two-month-old C57BL/6 mice, obtained from Harlan Laboratories (Indianapolis, IN, USA), were maintained under standard conditions of light (12-hour light/12-hour dark cycle) and temperature (21±1°C). Mice were injected daily with 1 mg/kg CL 316,243 (β_3-adrenergic receptor agonist) during 8 days. Mice were killed by decapitation, and tissues were removed, weighed, immediately frozen in liquid nitrogen, and stored at -

80ºC until processing. A portion of each tissue was fixed with 4% formalin for 24 h and then stored in 70% ethanol at 4ºC until paraffin infiltration was performed. Paraffin-embedded tissues were sectioned, mounted on glass slides, stained with hematoxylin-eosin, and photographed under a light microscope (20x magnification).

Adipocyte cultures

For primary adipocyte cultures, the stromal-vascular fraction was isolated from the inguinal WAT (iWAT) and interscapular BAT (iBAT) depots of one-month-old mice, and pre-adipocytes were cultured as previously reported [1, 2]. Once preadipocytes reached confluence, differentiation was induced by maintaining cells with DMEM/F-12 medium supplemented with 10% NCS (Gibco Life Technologies, Foster City, CA, USA), 0.86 µmols/l insulin, 33 nmols/l dexamethasone, 1 µg/ml transferrin, and 2 ng/ml T3 (Sigma-Aldrich, St. Louis, MO, USA) for 1 week. Where indicated, 10 µmols/l rosiglitazone was included in differentiation medium. Brown adipocyte differentiation was achieved by exposing confluent precursor cells from iBAT in DMEM/F12 medium containing 10% FBS and supplemented with 20 nmols/l insulin, 2 nmols/l T3 and 0.1 mmols/l ascorbic acid (ITA), as previously reported. Where indicated, beige and brown adipocytes were treated with 0.5 µmols/l noradrenaline during 6 h.

Embryonic mouse fibroblast 3T3-L1 cells (ATCC; LGC Standards, Barcelona, Spain) were maintained in a humidified atmosphere of 5% CO2 at 37°C in DMEM containing 20 mmol/l glucose, 10% FBS, 100 U/ml penicillin, and 100 µg/ml streptomycin. Two days after cells reached confluence, 0.86 µmols/l insulin, 0.5 µmol/l dexamethasone and 0.5 mmol/l IBMX were added for 2 days, followed by 0.86 µmols/l insulin alone for 5 days.

LBP knockdown and co-culture experiments

The small (interfering) hairpin RNA (shRNA)-mediated knockdown protocol has been described previously [3]. Briefly, five plasmids containing mouse Lbp-targeting shRNA (Sigma-Aldrich Mission RNA shRNA) were cloned into pLKO.1-puro shRNA vector. LBP knockdown was achieved by stably expressing shRNA against LBP in 3T3-L1 fibroblasts. Cells stably transfected with a non-targeting shRNA plasmid were used as a control. Where indicated, shLBP adipocytes were incubated with 10 ng/ml LBP during differentiation.

Coculture was performed using shLBP and shControl 3T3-L1 adipocytes during all the differentiation process in Transwell® plates (VWR International Eurolab S.L., Barcelona, Spain). The experiment was compared with a coculture of shLBP adipocytes at both sides of the transwell.

LBP-null mouse studies

LBP-knockout mice (C.129P2-Lbptm1Jack/J, Balb strain background), obtained from The Jackson Laboratory (Bar Harbor, ME, USA) were maintained under standard conditions of light (12-hour light/12-hour dark cycle) and temperature (21±1°C). Five-week-old male LBP-null and wild-type (WT) littermate control mice were fed a standard chow diet (CTRL) or HFD for 15 weeks. Body weight increases and energy intake were calculated by weighing animals and food every 3-4 days, assuming that the energy density of a standard diet and HFD are 13 and 19.8 kJ/g, respectively. The volume of consumed oxygen (VO2) and produced carbon dioxide (VCO2), as well as respiratory quotient were determined (Harvard Apparatus). Skin temperature at the site of interscapular BAT was recorded using a high-sensitivity thermal imaging camera (FLIR® T335) following previously established procedures [4].

For glucose tolerance tests, glucose in aqueous solution was administered intraperitoneally (2.5 g glucose/kg) to 6 hour-starved mice, and glycaemia in blood obtained from the tail was measured 15, 30, 45, 60, 90, 120 and 150 minutes after glucose injection. For insulin tolerance tests, insulin (Actrapid; Novo Nordisk Pharma A/S, Bagsvaerd, Denmark) in saline solution was administered intraperitoneally (0.75 UI/kg) to mice, and glycaemia in blood obtained from the tail was measured 15, 30, 45 and 60 minutes after glucose injection.

After killing mice by decapitation, blood was collected in heparinized tubes for preparation of plasma, and subcutaneous (inguinal depot) and visceral (epididymal depot) WAT, interscapular BAT and liver were removed, weighed, immediately frozen in liquid nitrogen, and stored at -80ºC until processing.

Plasma glucose was determined using an Accutrend system (Roche Diagnostics GmbH, Mannheim, Germany). Commercially available kits were used to assess plasma insulin (RSHAKRIN031R; BioVendor R&D, Brno, Czech Republic); adiponectin (KMP0041; Life Technologies); leptin, resistin and IL-6 (MADKMAG-71K Milliplex; Millipore, Billerica, MA, USA); NEFA (434-91795, 436-91995; Wako Chemicals GmbH, Neuss, Germany); 3-hydroxybutyrate (417-73501, 413-73601; Wako); and triglycerides (TR0100; Sigma-Aldrich).

For glucose oxidation assay, interscapular BAT, inguinal WAT (iWAT) and epididymal WAT depots were obtained from wild-type and LBP-null mice (as described above) and 100-150 mg tissue fragments were incubated with DMEM (without D-glucose) supplemented with 3 mmols/l D-glucose and 55.5 kBq/ml [^{14}C(U)]-D-glucose (Hartmann Analytic GmbH, Braunschweig, Germany) for 3 h at 37°C in a 5% (v/v) CO_2 atmosphere. Labeled $^{14}CO_2$ was then released from the medium by acidification with 3 mols/l $HClO_4$ and retained in a CO_2 trap consisting of Whatman 3MM Chr paper (Whatman, GE Healthcare, Little Chalfont, UK) impregnated with B-phenylethylamine

(Sigma) and positioned over the wells inside the sealed plates. After 1 h, CO_2 traps were placed in scintillation vials containing 4 ml of scintillation fluid, and the samples were counted using a Packard 2100TR TriCarb Liquid Scintillation Counter (Packard Instrument Company Inc., Meriden, CT). Decays per minute were normalized to tissue fragment weight. For [^{14}C(U)]-D-glucose incorporation to lipids assay, lipids were extracted from tissue fragments used in glucose oxidation assay using Folch's chloroform:methanol method [5]. Choloform phase containing labeled lipids was evaporated in scintillation vials and dessecated lipids were dissolved with 10 ml of scintillation fluid and counted using a Packard 2100TR TriCarb Liquid Scintillation Counter. Decays per minute were normalized to tissue fragment weight.

Human study

Paired subcutaneous and visceral adipose tissue samples (n = 38) from a cohort of morbidly obese (BMI > 35 kg/m^2) subjects were studied. Anthropometrical and clinical parameters of these patients include age (48.29±9.1 years), BMI (43.8±6.9 kg/m2), percent fat mass (56.1±10.1 %), fasting glucose (96.03±12.01 mg/dL) and M-value (23.5±13.3 µmol kg^{-1} min^{-1}). These subjects were recruited at the Endocrinology Service of the Hospital of Girona "Dr Josep Trueta". All subjects were of Caucasian origin with no systemic disease other than obesity. All subjects gave written informed consent, validated and approved by the ethical committee of the Hospital of Girona "Dr Josep Trueta", after the purpose of the study was explained to them. Adipose tissue samples were obtained from SAT and VAT depots during elective surgical procedures (cholecystectomy, surgery of abdominal hernia, and gastric by-pass surgery), immediately frozen in liquid nitrogen, and stored at -80ºC until processing.

RNA isolation, cDNA synthesis, and real-time PCR

Dissected tissues (BAT, iWAT, eWAT and liver from mice, and SAT and VAT from humans) were homogenized using an IKA T25 digital ULTRA-TURRAX homogenizer (Staufen, Germany). Total RNA from homogenized tissues and cultured cells was isolated using a column affinity-based method (NucleoSpin RNA II; Macherey-Nagel, Düren, Germany). Total RNA (500 ng) was transcribed into cDNA using TaqMan Reverse Transcription Reagents (Applied Biosystems/Life Technologies, Foster City, CA, USA). For quantitative analysis of mRNA expression, TaqMan quantitative real-time polymerase chain reaction (qPCR) was performed on a 7500 Real-Time PCR System (Applied Biosystems) using the specific primer pair/probe sets described in ESM Table 1. Relative mRNA levels of target genes were normalized with respect to that of 18S rRNA in mice and PPIA in humans, using the comparative (2-ΔCT) method. Transcript levels were considered undetectable in cases where the CT value was >40 under our experimental conditions.

Western blot analysis

Dissected tissues (BAT and iWAT) were homogenized using an IKA T25 digital ULTRA-TURRAX homogenizer in lysis buffer (50 mmols/l Tris-HCl pH 7.4, 150 mmols/l NaCl, 1.5 mmols/l $MgCl_2$, 1 mmols/l EDTA, 1 mmols/l EGTA, 40 mmols/l β-glycerophosphate, 2 mmols/l Na_3VO_4, 1 mmols/l PMSF, 1 mmols/l DTT) containing complete protease inhibitor cocktail (Roche Applied Science). Lysates were centrifuged at 1,500 x g for 5 minutes at 4°C to remove intact cells, and protein content was quantified using the Bradford method. For Western blotting, proteins (40 µg) were resolved by SDS-PAGE and transferred to a PVDF membrane (Immobilon; Millipore). Membranes were exposed to primary 1/1000 anti-UCP1 (ab10983, Abcam Plc, Cambridge, UK) and 1/5000 anti-β-actin (A5441, Sigma-Aldrich) antibodies, diluted in 1x PBS containing 0.1% Tween-20, following the recommendations of the

manufacturer. Signals were detected using enhanced chemiluminescence HRP substrate (Millipore) and analyzed with a Luminescent Image Analyzer LAS-3000 (Fujifilm Life Science, Tokyo, Japan). Signal intensities were quantified using Multi Gauge software (Fujifilm).

Statistical methods

All results are expressed as means ± SEM. Statistical analyses were performed using Prism 6 software (GraphPad Software Inc., La Jolla, CA, USA) Differences were tested for statistical significance using unpaired t-test, one-way analysis of variance (ANOVA) with Tukey's Multiple Comparison Test, or two-way ANOVA with Bonferroni post-test, as appropriate.

1. Aune UL, Ruiz L, Kajimura S. Isolation and differentiation of stromal vascular cells to beige/brite cells. *J Vis Exp* 2013; **73**: 50191.

2. Barbera MJ, Schluter A, Pedraza N, Iglesias R, Villarroya F, Giralt M. Peroxisome proliferator-activated receptor alpha activates transcription of the Brown fat uncoupling protein-1 gene. A link between regulation of the thermogenic and lipid oxidation pathways in the brown fat cell. *J Biol Chem* 2001; **276**: 1486-1493.

3. Moreno-Navarrete JM, Escote X, Ortega F, Camps M, Ricart W, Zorzano A et al. Lipopolysaccharide binding protein is an adipokine involved in the resilience of the mouse adipocyte to inflammation. *Diabetologia* 2015; **58**:2424-2434.

4. Beiroa D, Imbernon M, Gallego R, Senra A, Herranz D, Villarroya F et al. GLP-1 agonism stimulates brown adipose tissue thermogenesis and browning through hypothalamic AMPK. *Diabetes* 2014; **63**: 3346-3358.

5. Folch J, Lees M, Sloane Stanley GH. A simple method for the isolation and purification of total lipides from animal tissues. *J Biol Chem* 1957; **226**:497-509.

ESM Table 1. Specific probe sets of TaqMan Gene Expression Assays (Applied Biosystems) used to perform the quantitative real-time polymerase chain reactions (qPCR).

Gene	Product number
Mice	
Acaca (Acetyl-CoA carboxylase 1)	Mm01304257_m1
Acadm (Medium-chain acyl-CoA dehydrogenase)	Mm00431611_m1
Adipoq (Adiponectin)	Mm00456425_m1
Bmp8b (Bone morphogenetic protein 8b)	Mm00432115_g1
Dio2 (Deiodinase 2)	Mm00515664_m1
Fasn (Fatty acid synthase)	Mm00662319_m1
Fgf21 (Fibroblast growth factor 21)	Mm00840165_g1
G6pc3 (Glucose-6-phosphatase)	Mm00616234_m1
Hmgcs2 (3-hydroxy-3-methylglutaryl-CoA synthase 2)	Mm00550050_m1
Il6 (Interleukine 6)	Mm00446191_m1
Lbp (Lipopolysaccharide binding protein)	Mm00493139_m1
Lep (Leptin)	Mm00434759_m1
Pck1 (Phosphoenolpyruvate kinase 1)	Mm00440636_m1
Pparg (Peroxisome proliferator-activated receptor gamma)	Mm00440945_m1
Ppargc1a (Peroxisome proliferative activated receptor, gamma, coactivator 1 alpha)	Mm00447183_m1
Prdm16 (PR domain containing 16)	Mm00712556_m1
Scd1 (Stearoyl-CoA desaturase 1)	Mm01197142_m1
Sirt3 (Sirtuin 3)	Mm00452131_m1
Slc2a4 (Glucose transporter type 4)	Mm00436615_m1
Srebf1 (Sterol regulatory element-binding protein)	Mm00550338_m1
Tnf (Tumor necrosis factor α)	Mm00443258_m1
Ucp1 (Uncoupling protein 1)	Mm00494069_m1
Humans	
LBP (Lipopolysaccharide binding protein)	Hs01084628_m1
PRDM16 (PR domain containing 16)	Hs00922674_m1
PPARGC1A (Peroxisome proliferative activated receptor, gamma, coactivator 1 alpha)	Hs01016719_m1
UCP1 (Uncoupling protein 1)	Hs00222453_m1
TMEM26 (Transmembrane protein 26)	Hs00415619_m1
PLIN1 (Perilipin 1)	Hs00160173_m1
LEP (Leptin)	Hs00174877_m1
DGAT1 (Diacylglycerol O-acyltransferase 1)	Hs01017541_m1
18S rRNA (Eukaryotic 18S rRNA)	Hs99999901_s1
PPIA (Peptidylprolyl isomerase A [Cyclophilin A])	Hs99999904_m1

ESM Figure 1

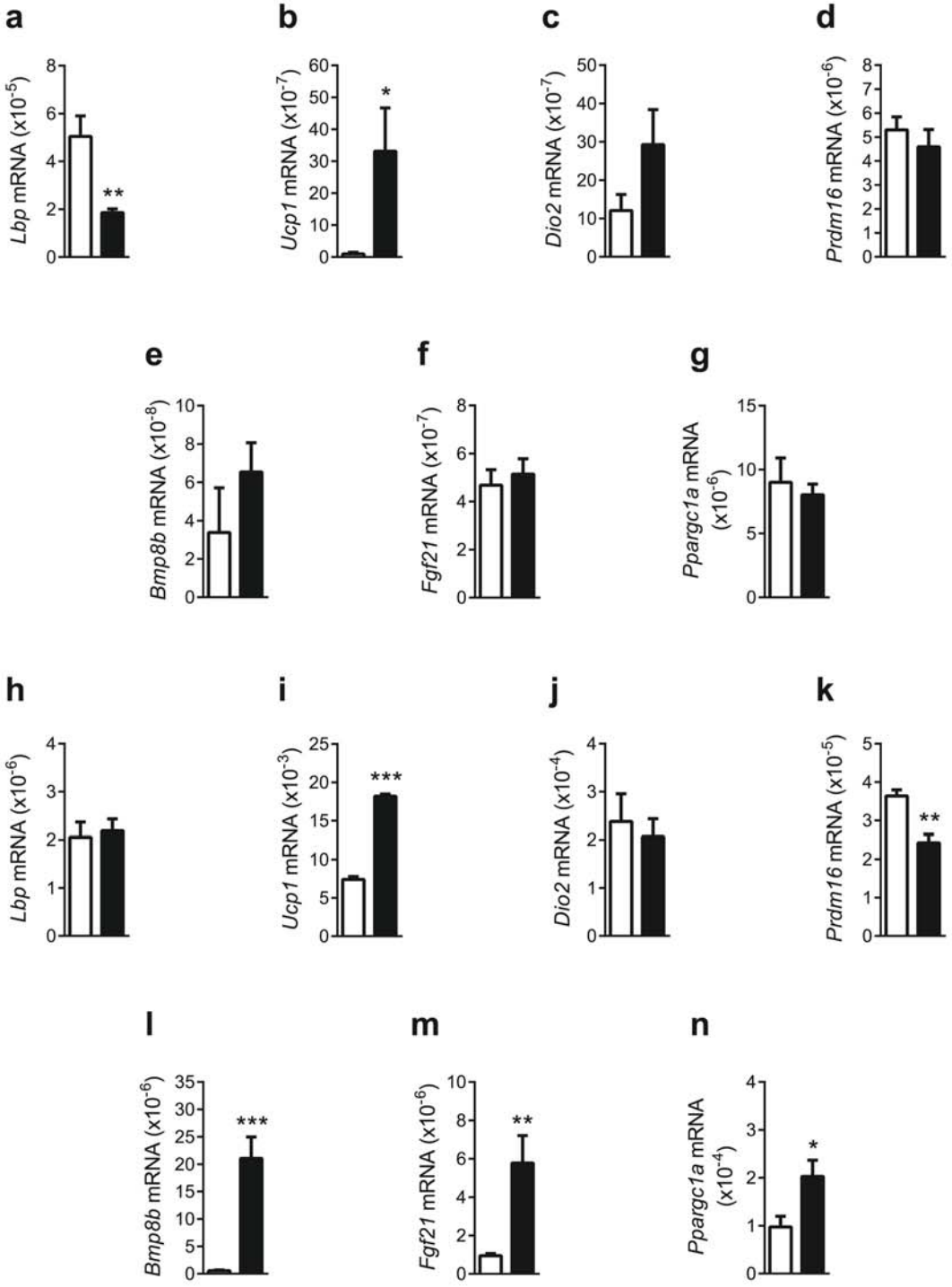

ESM Fig. 1 Expression of *Lbp* and thermogenesis-related genes in visceral WAT and BAT. Transcript levels of *Lbp* (a) and the thermogenesis-related genes *Ucp1* (e), *Dio2* (e), *Prdm16* (e), *Bmp8b* (e), *Fgf21* (e) and *Pgc-1α* (e) in visceral WAT (epididymal depot, eWAT) from WT mice maintained at 22ºC (white bars) or 4ºC (black bars) for 3 weeks. Transcript levels of *Lbp*(h), *Ucp1* (i), *Dio2* (j), *Prdm16* (k), *Bmp8b* (l), *Fgf21* (m) and *Pgc-1α* (n) in interscapular BAT (iBAT) from WT mice maintained at 22ºC (white bars) or 4ºC (black bars) for 3 weeks. mRNA levels are normalised to 18S rRNA. Data are means ± SEM of 6 independent samples per group (*P < 0.05, **P < 0.01 and ***P < 0.001).

ESM Table 2. Plasma metabolic profile of wild-type (WT) and LBP-null mice maintained with control or high fat diet during 15 weeks. Data shown are means ± SEM of 4-6 independent samples per group. [a] represents statistically significant changes between control and high fat diet.

	Control diet		High fat diet	
	WT	***Lbp*-null**	**WT**	***Lbp*-null**
NEFA (mg/dl)	42.4 ± 1.6	34.5 ± 1.3	26.3 ± 2.0[a]	32.1 ± 1.9
3-hydroxybutyrate (µM)	252.4 ± 28.8	240.6 ± 12.3	383.4 ± 42.8	404.1 ± 43.5
Leptin (pg/ml)	693.5 ± 231.7	875.3 ± 193.6	720.2 ± 149.8	1415.1 ± 501.0
Adiponectin (µg/ml)	25.8 ± 1.3	24.3 ± 1.4	22.8 ± 1.3	25.8 ± 1.5
Resistin (pg/ml)	945.0 ± 265.1	1070.3 ± 65.2	1017.8 ± 94.1	1199.8 ± 167.1
MCP-1 (pg/ml)	6.2 ± 4.0	ND	2.2 ± 1.4	4.6 ± 4.6
PAI-1 (pg/ml)	1678.6 ± 545.4	1627.5 ± 536.6	2046.3 ± 356.7	1371.8 ± 478.6

ESM Figure 2

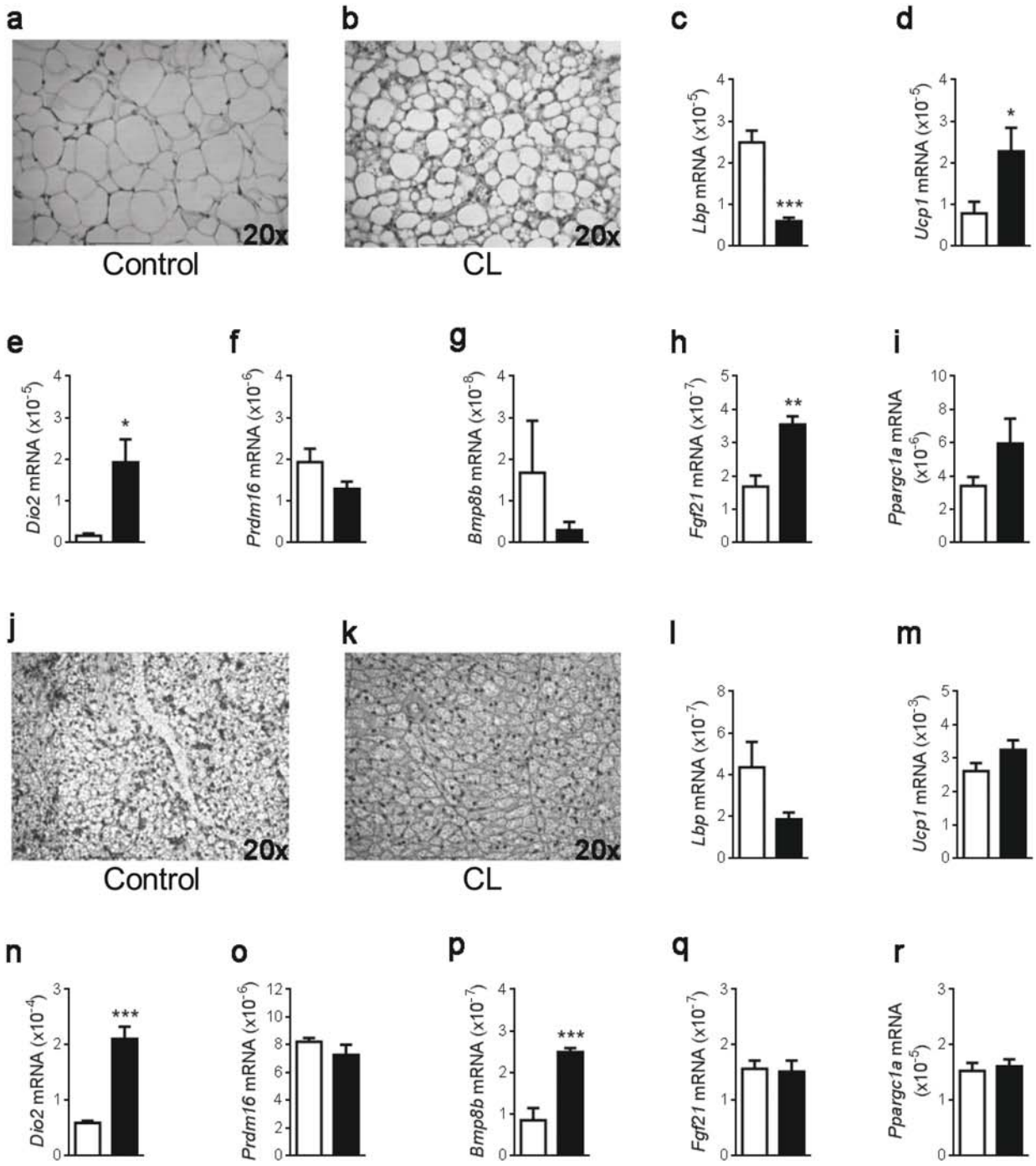

ESM Fig. 2 Effects of β_3-adrenergic stimulation on visceral WAT and BAT. Micrographs of visceral WAT (eWAT) from control mice (**a**) or mice daily injected with 1 mg/kg CL316,243 for 8 days (**b**). Transcript levels of *Lbp* (**c**), *Ucp1* (**d**), *Dio2* (**e**), *Prdm16* (**f**), *Bmp8b* (**g**), *Fgf21* (**h**) and *Pgc-1α* (**i**) in eWAT from control mice (white bars) or mice daily injected with 1 mg/kg CL316,243 for 8 days (black bars). Micrographs of interscapular BAT (iBAT) from control mice (**j**) or mice daily injected with 1 mg/kg CL316,243 for 8 days (**k**). Transcript levels of *Lbp* (**l**), *Ucp1* (**m**), *Dio2* (**n**), *Prdm16* (**o**), *Bmp8b* (**p**), *Fgf21* (**q**) and *Pgc-1α* (**r**) in iBAT from control mice (white bars) or mice daily injected with 1 mg/kg CL316,243 for 8 days (black bars). mRNA levels are normalised to 18S rRNA. Data are means ± SEM of 6 independent samples per group (*P < 0.05, **P < 0.01, and ***P < 0.001).

ESM Figure 3

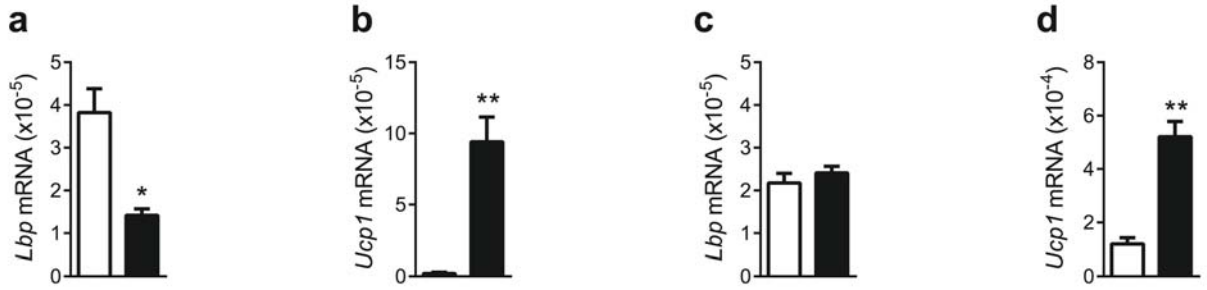

ESM Fig. 3 Effects of noradrenaline on *Lbp* and *Ucp1* gene expression in beige or brown adipocytes. Transcript levels of *Lbp* (a) and *Ucp1* (b) in control (white bars) or beige adipocytes treated with 0.5 µmols/l noradrenaline during 6h (black bars). Transcript levels of *Lbp* (c) and *Ucp1* (d) in control brown adipocytes (white bars) or brown adipocytes treated with 0.5 µmols/l noradrenaline during 6h. mRNA levels are normalised to 18S rRNA. Data are means ± SEM of 6 independent samples per group (*P < 0.05 and **P < 0.01).

ESM Figure 4

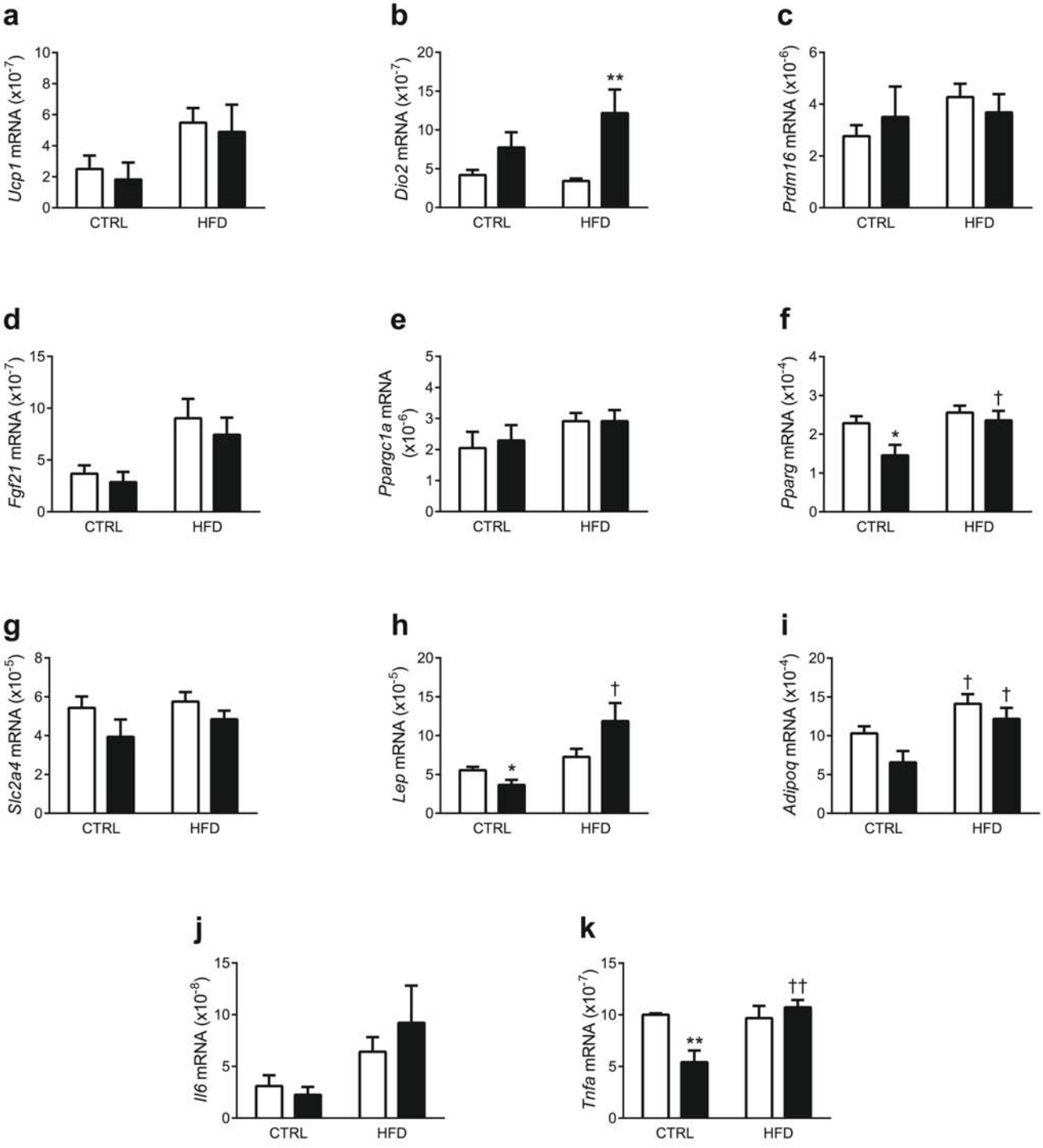

ESM Fig. 4 Gene expression in visceral WAT from *Lbp*-null mice. Transcript levels of thermogenesis-related genes *Ucp1* (a), *Dio2* (b), *Prdm16* (c), *Fgf21* (d) and *Pgc-1α* (e); adipogenesis-related genes *Ppar-γ* (f), *Glut4* (g), *Leptin* (h) and *Adiponectin* (i); and inflammatory markers *Il-6* (j) and *Tnf-α* (k) in visceral WAT (epididymal depot, eWAT) from WT (white bars) and *Lbp*-null (black bars) mice after 15 weeks on a standard chow diet (CTRL) or HFD. mRNA levels are normalised to 18S rRNA. Data are means ± SEM of 4-6 independent samples per group (*P < 0.05 and **P < 0.01, WT vs. *Lbp*-null mice; †P < 0.05 and ††P < 0.01, CTRL vs. HFD).

ESM Figure 5

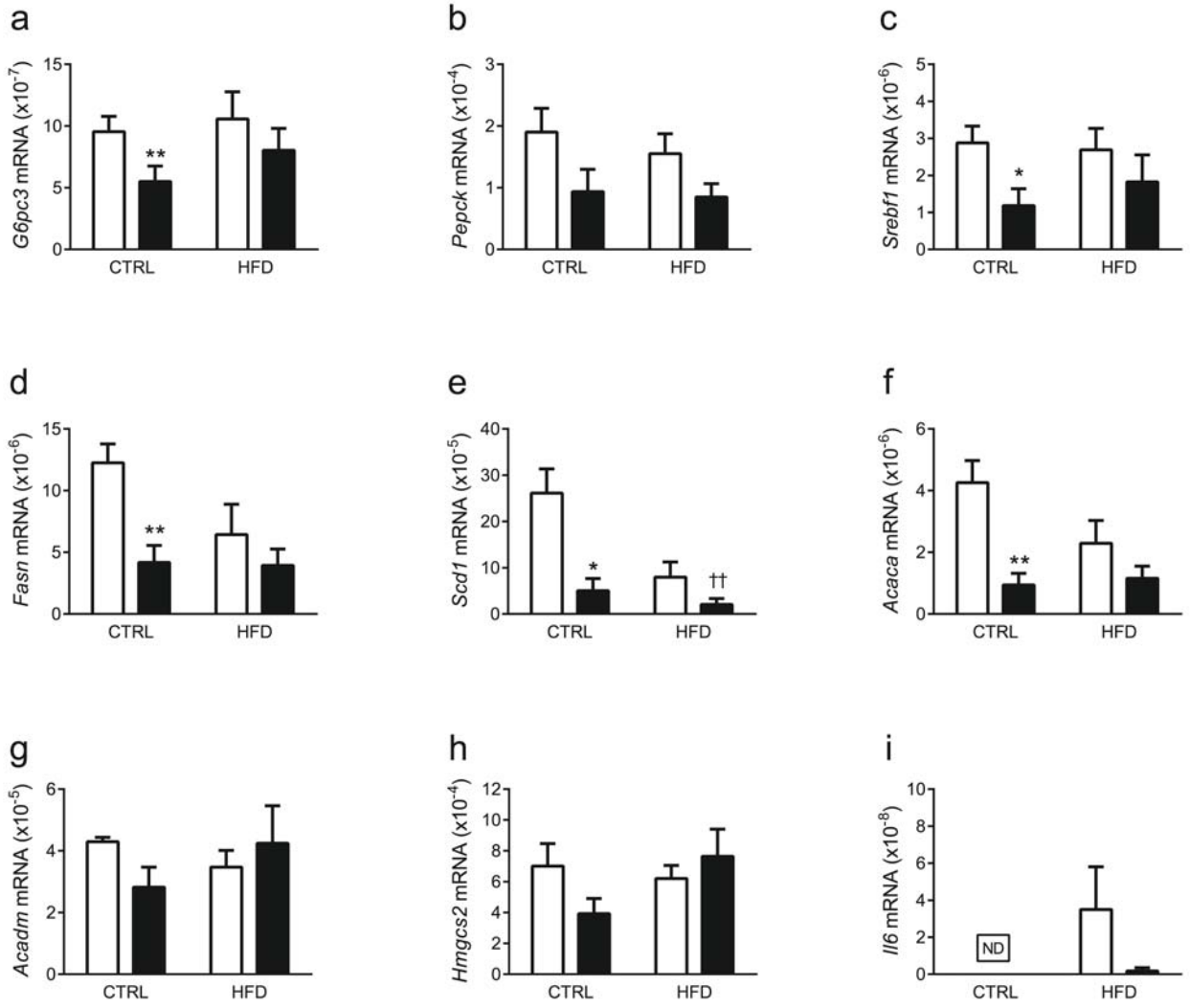

ESM Fig. 5 Hepatic gene expression in *Lbp*-null mice. Transcript levels of the gluconeogenesis pathway-related genes *G6pase* (a) and *Pepck* (b); the fatty acid synthesis pathway-related genes *Srebp* (c), *Fas* (d), *Scd* (e) and *Acc-*α (f); the fatty acid oxidation-related gene *Mcad* (g); the ketogenesis-related gene *Hmgcs2* (h); and the inflammatory gene *Il-6* (i) in liver from WT (white bars) and *Lbp*-null (black bars) mice after 15 weeks on a standard chow diet (CTRL) or HFD. mRNA levels are normalised to 18S rRNA. Data are means ± SEM of 4-6 independent samples per group (*P < 0.05 and **P < 0.01, WT vs. LBP-null mice; ††P < 0.01, CTRL vs. HFD). ND, not detectable.

SUMMARY RESULTS AND DISCUSSION

Summary results and discussion

Humanity is found submerged in a health crisis worldwide. This crisis is characterized by a cumulus of metabolic abnormalities that are found indistinctively in the world population. Unfortunately, these disturbances start to be present in young individuals which compromises their development and wellness. With this in mind, scientific research has oriented efforts in understanding the mechanisms in the development of those pathologies related to obesity and metabolic syndrome. The main tissue acknowledged for the storage of the excess of energy that characterizes the development of these abnormalities is the adipose tissue. This tissue has been found not to be only an energy reservoir, on the contrary it is now well known that the fat depots have a great variety of roles and functions for the achievement of homeostasis and integration of responses to demanding stimuli (i.e. cold exposure).

Adipose tissue is highly sensitive organ for the metabolic status of an organism. Thus, its physiology during the different stages of life is important for an adequate metabolic performance. To accomplish this role, AT needs to be able to sense the incoming signals from other tissues in the organism. These signals not only include hormones, they also comprise the great variety of energy substrates and metabolic intermediates that are found in circulation and cellular matrix. Recently, the largest class of membrane proteins in the human genome, the GPCRs, is being subject of attention due to the deorphanization of several of its members. These members have been found to be activated by circulating metabolites and other signals. GPCRs mediate an important number of physiological responses to hormones, neurotransmitters, environmental stimulants, and, recently considered, energetic metabolites. Whilst, metabolites have a dual role in the coordination of metabolism. They are a source of energy able to modulate metabolism at the stage of electron transport, for example, while they are able activate certain nuclear receptors and also membrane receptors which helps them act like hormonal molecules (Blad *et al*., 2012).

In this sense, the expression of those membrane receptors able to detect extracellular and circulating levels of energy metabolites are proposed be important for AT. These molecules and their receptors have proven to trigger responses inside the adipocyte and other cell-types characteristic of the AT. Also, they are able to modify the biochemistry of the different cell populations thus contributing to the establishment of a metabolic profile in an individual. For this reason, metabolite sensing GPCRs have been intensively studied in health and during the development of certain pathologies. The work on this receptors have proposed some of them as potential therapeutic targets for the treatment of obesity and associated metabolic alterations. In this context, the observations made during this work helped us elucidate the role of one of these receptors on AT, GPR120, and its possible contribution to an improvement in the overall metabolic performance.

At the beginning of this project, as mentioned earlier, few information regarding possible roles of this receptor in brown adipose tissue and thermogenesis were known. In the past four years, increasing information on this receptor, regarding BAT activity and WAT browning, has been emerging. This knowledge has been emerging in parallel with the development of new synthetic agonists for GPR120 to be used as therapeutic molecules for the treatment of metabolic diseases. GPR120 is a lipid sensor, initially described to be activated by n-3 PUFAs (Hirasawa *et al*., 2005; Milligan *et al*., 2017). These type of lipids have been profoundly studied since they possess a great variety of beneficial effects regarding inflammation and amelioration of the metabolic conditions (Novak, 2009). On these basis, and in an attempt to elucidate a bit more on its role on adipose tissues, several research groups around the world, including ours, have been exploring the possible roles of GPR120 in the activation on the AT. As for this dissertation, here I describe the information that was obtained through the experimental work performed.

GPR120 is a distinctive receptor of the brown adipose tissue and important for brown adipocyte biology and function.

As described earlier, BAT thermogenic activation and WAT browning have been the subject of attention due to the increased demand of energy they imply. Moreover, consistent data has been found on the association between active BAT and beige adipose tissue recruitment with a healthy metabolic status. In the presence of extra weight or obesity, fat activation could lead to a decrease in fat depots' size and contributing to an amelioration of the metabolic conditions. New techniques for the study of messenger RNA dynamics allow us to identify differential expression of several genes upon a given stimulus, one of these techniques is the whole transcriptome shotgun sequencing (WTSS) or RNA-sequencing (RNA-seq) (Wang *et al*., 2009). Following this idea, an RNA-seq analysis was performed on BAT samples from mice at thermoneutrality (30°C) and at 4°C during 24 hours. This approach helped identify those genes significantly induced or decreased in expression upon activation of BAT. Out of this analysis, a list of around 3,500 genes differentially regulated was obtained, 2,498 of these genes showed to be up-regulated. A validation of the results was necessary so a comparison between different data bases and well-known up-regulated genes was performed. Hence, it was decided to check for unreported genes that were also among the top-induced genes. Due to their relevance as therapeutic targets, a GPCR called our attention, GPR120. G protein-coupled receptors (GPCRs) are the largest protein superfamily in mammalian genomes (Doze and Perez, 2013; Venkatakrishnan *et al*., 2013). They are the most physiologically important membrane protein family due to their role as key specific targets for a variety of physiological functions and therapeutic approaches. (Lagerstrom and Schiöth, 2008; O'Connor and Adams, 2012; Tang *et al.*, 2012). Therefore GPR120 appeared to be as possible metabolic regulator for adipose tissue and subsequent experiments focused on understanding its role on BAT thermogenesis and WAT browning.

In order to asses GPR120 importance and expression in BAT, the patterns of expression of GPR120 in different tissues were characterized. The results of this analysis showed that the adipose depots, especially BAT, were the tissues to mainly express GPR120. Then, we proceeded to confirm the induction of its expression on both, BAT and WAT, during different timings of cold exposure. Our results show that acute and chronic exposure to cold caused an increase in GPR120 expression in adipose depots, and this was also observed by Rosell and co-workers (2014). Concerning adipocyte biology, we quantified the expression of the receptor in the SVF obtained from interscapular BAT and from differentiated adipocytes. It was evident that the differentiated adipocytes showed increased expression of the receptor. Also, an approach determining the expression levels during the differentiation process *in vitro* showed a parallel induction with differentiation as observed for Ucp1 mRNA, the main thermogenic marker for brown adipocytes. On the other side, assays of GPR120-nullification resulted in a compromised adipogenesis, explained latter. In addition to these *in vitro* observations, the treatment of differentiated adipocytes with norepinephrine, a β-adrenergic agonist, and cyclic-AMP caused an increase in GPR120 expression. This induction was blunted when the adipocytes were pretreated with SB202190, a p38 MAPK inhibitor. Both observations, under differentiation and upon adrenergic stimulation, in the induction of GPR120 were later confirmed by Schilperoort and co-workers (2018).

Altogether, these findings suggested a putative role of this fatty acid receptor in adipocyte biology and noradrenergic stimulation (which mimics the effects of cold exposure). Besides this, at beginning of this project, it was known that the R270H variant for the gene coding for FFAR4 (GPR120) in the human genome caused a decreased signaling of the receptor upon activation and it correlated with an increased risk of obesity in European populations (Ichimura *et al*., 2012), correlation that was reproduced in the rodent models. Hence, we hypothesized that the receptor could play a major role in energy homeostasis modulation by the AT and so we directed the following experiments to understand the effects of its activation.

GPR120 activation induces the expression of thermogenic machinery in BAT and WAT.

Once it was suggested that GPR120 plays a major role in adipocyte biology, we decided to test the effects of GPR120 activation on the adipose tissues. For this, we supplemented chow diet of adult C57/Bl6 mice with the available synthetic agonist for GPR120, GW9508, during seven days. Our first results showed no significant differences in the circulating levels of metabolites nor in total body weight or specific tissue weights. However, it is important to mention that this experiment was performed in healthy adult mice under a chow diet and not in diet induced obesity like other researchers have done. These other studies performed under diet induced obesity and administering natural or synthetic agonists for GPR120 did found significant decreases in body or AT weights upon the agonist administration (Oh *et al*., 2014; Kim *et al*., 2016; Pahlavani *et al*., 2016; Schilperoort *et al*., 2018). Even when no important effects on adiposity nor circulating metabolites were detected, two hormones showed important modifications. While insulin plasma levels showed a reduction after 7 days of diet supplementation (previously observed with other GPR120 agonists, Oh *et al*., 2014), the star result that oriented the subsequent analysis of this project was a marked induction in FGF21 plasma levels.

FGF21 is an endocrine factor which has been described as a metabolic regulator contributing to glucose homeostasis, insulin sensitivity and ketogenesis while it is also linked to thermogenic activation of the adipose tissues (Badman *et al*., 2007; Gälman *et al*., 2008; Fischer *et al*., 2012). It was mentioned in the introduction of this dissertation that the main site of production and secretion of FGF21 is liver; however the factor is also importantly regulated by BAT (affecting its expression and release) (Hondares *et al*., 2010). Thus, we decided to measure the expression of FGF21 in these tissues. Surprisingly, GW9508 administration did not affect FGF21 expression in liver. Conversely, the adipose depots, specially brown and inguinal white, showed an induction in the expression of this factor. Even though, none other experiments have

reported this effect in FGF21 induction in the presence of a GPR120 synthetic agonist, a similar effect was achieved by Pahlavani and co-workers (2016). In her assay, she administered HFD alone or supplemented with EPA, a natural occurring agonist of GPR120. The results on EPA supplementation, during DIO in mice resulted in an increased expression of FGF21 in BAT but none results are shown for circulating levels in these animals. Extended discussion on these results will be held in the next pages. Given that FGF21 has been proposed as an important batokine able to induce thermogenesis (Hondares *et al*., 2010; Fischer *et al*., 2012) in the adipose depots, we decided to measure the possible effects of its expression over the thermogenic activation in AT.

Our first *in vivo* results on GPR120 activation effects, upon GW9508 feeding, over the AT showed an induction in the expression of thermogenic machinery genes (i.e. *Ucp1*, *PGC-1α*, *and Bmp8b*) and an increase in Ucp1 protein expression in both, BAT and inguinal WAT. These results were consistent with smaller adipocytes and visible browning observed in optical microscopy images from haematoxylin and eosin (H&E) stained tissues (BAT and iWAT). Epipidymal WAT also showed a tendency to achieve this activation, however less pronounced. Albeit the induction of the thermogenic machinery seemed conclusive, it is known that GW9508 is not a selective agonist for GPR120, it can also activate GPR40. We decided to check if the effects over FGF21 expression and the thermogenic activation were indeed mediated by GPR120. A second diet-supplemented experiment was performed. This time, animals deficient of the gene FFAR4 (coding for GPR120) and wild-type controls were used. In this experiment, we first decided to measure oxygen consumption in these animals. The results indicated that GW9508 diet supplementation caused an increase in oxygen consumption under basal conditions and upon noradrenergic stimuli compared to their wild-type controls. However, GPR120-deficient animals showed a decreased respiration under a non-supplemented diet and after diet supplementation. In addition, the increase in respiration upon GW9508 supplementation or CL316, 243 (a β3-adrenergic activator) injection was significantly lower in the knock-out animals. A similar result on oxygen consumption in GPR120-deficient animals was further obtained by Schilperoort et al

(2018) on observations made during a high-fat diet induced obesity and the supplementation of TUG-891, another GPR120 agonist. Since oxygen consumption in the GW9508-fed animals gave a good prognostic of our experiment, the effects over FGF21 were checked. FGF21 plasma levels of wild-type animals fed with GW9508-supplemented diet were also increased in this second assay, however no induction was observed in the GPR120 knock-out animals. Moreover, the effects in the induction of FGF21 mRNA expression by GW9508 in the adipose depots was blunted in the absence of GPR120. This led to conclude that the induction in the expression of FGF21 in the adipose depots and in plasma levels were mediated by GPR120 activation. After determining the effects of the loss-of-function of GPR120 over FGF21 regulation, the effects over the adipose tissues were assessed. BAT seemed slightly affected by the genotype. No important differences were detected but a tendency to accumulate fat and a decrease in the induction of some thermogenic markers was observed. Conversely, WAT browning observed upon GW9508 administration was importantly impaired in the GPR120-KO animals. The induction in the thermogenic machinery genes was lost and Ucp1 protein expression was decreased in WAT. In addition, the microscopy images from the H&E stained tissues showed no browning acquisition in the knockout iWAT from the animals supplemented with GW9508. So, these results conducted a hypothesis of GPR120 being important for the thermogenic activation of the tissues. Hence, it was decided to test what would occur in GPR120-deficient animals under a condition where thermogenesis and browning was crucial for homeostasis maintenance.

GPR120 is necessary for an appropriate activation of thermogenesis and browning of WAT.

Cold exposure is a classic experiment for studying the activation of the thermogenic machinery of the adipose depots (Cannon and Nedeergard, 2004). After determining that GPR120 may be necessary for an appropriate induction of thermogenesis through mechanisms not involving noradrenergic stimulus, it resulted

interesting to test how the deficiency of the receptor would affect noradrenergic stimulated thermogenesis. Adult animals, wild-type or deficient of GPR120, were maintained at room temperature or at 4°C during 7 days. The first relevant observation was acquired after 24 when 20% of the knock-out animals experienced hypothermia and had to be put back to room temperature conditions (21°C). Indirect thermographic images of the eye, to measure body temperature, helped us identify a decrease in the core temperature in the knockout animals under an acute cold exposure. However, at the end of the experiment, the knock-out animals recovered the decrease in temperature (while still a showing a tendency to stay below the wild-types, but unsignificant). Interestingly, the GPR120-deficient animals showed decreased FGF21 plasma levels. Considering the adipose tissues, BAT expression of FGF21 seemed unaltered while iWAT expression showed a tendency to be reduced. Regarding the thermogenic machinery, GPR120-deficient BAT reflected minor differences in thermogenic machinery genes' expression. Yet, BAT from knockout animals showed a tendency to have increased lipid accumulation (as observed from H&E-stained tissues) and an increased expression of leptin. On the other hand, inguinal WAT did show marked impairment on thermogenesis, some thermogenic markers genes expressions (i.e. *Ucp1, Bmp8b*) were reduced and this was consistent with a decreased multilocularity and increased cell size in iWAT depots from knock-out animals. These led to think that GPR120 deficiency caused an impairment in thermogenesis activation and browning.

To date, no other results on noradrenergic stimulation of GPR120 knock-out animals have been reported. However, an interesting experiment regarding thermogenic activation of BAT can be found in the literature. Kim and co-workers (2016) performed an experiment where animals were fed a low-fat diet or three different types of HFD; the first one containing 15% of palm oil; the second one 15% of olive oil; and the third contained 15% of fish oil (well-known for the high EPA content, GPR120 natural occurring agonist). All diets were administered for 12 weeks. At the end of the experiment, these animals were put in cold for 45 minutes. Interestingly, diets with palm and olive oil showed reduced BAT temperatures compared to low fat diet. However, the diet supplemented with fish oil caused an increased BAT temperature under this acute

cold stimulation (as assessed by thermographic camera images and rectal temperatures). These results were consistent with a decreased AT tissue weight in fish-oil supplemented animals and increased expression of thermogenic markers (*Ucp1*, *Prdm16* and *Cidea*) and Ucp1 protein compared to control low-fat diet. These effects were not observed in the case of palm and olive oil diets. These results could be explained with some data presented by other research group which suggested that different models of obesity in rodents caused a decrease in GPR120 expression in adipose depots (BAT, iWAT and eWAT from mice and rats) (Satapati *et al*., 2017). However a greater elucidation on the effects of different diet-compositions on GPR120-mediated effects of HFD is necessary, especially regarding the induction of thermogenic markers that are observed under some types of HFDs (Pahlavani *et al*., 2016; Villarroya *et al*., 2014).

GPR120 activation induces brown and beige adipocyte differentiation and thermogenic activation

In order to clarify cell-autonomous effects of the activation of GPR120, primary cultures were performed. The SVF from interscapular BAT, inguinal WAT and epididymal WAT was obtained from wild-type animals. In the case of BAT precursors they were maintained in the conventional media (insulin, T3 and ascorbic acid) or in the presence of a GPR120 agonist (GW9508, EPA or ALA). On the other hand, white precursors were maintained under basal media, the conventional differentiation cocktails (+/- rosiglitazone) or just GPR120 agonists. The results show that the treatment of adipocyte precursors with GPR120 agonists trigger brown and beige adipocyte differentiation (marked by increased expression of thermogenic markers such as *Ucp1* or *PGC-1α*). In addition, these cells showed increased temperatures and respiration. When comparing the effects of rosiglitazone, a PPARɣ agonist known to induce adipogenic differentiation, and GPR120 agonists, it is important to note that the agonists caused a similar and even stronger induction of browning, as evidenced by the up-regulation of the beige marker genes (*Ucp1*, *PGC-1α*) and a down-regulation of leptin. Most general adipogenic genes

were unaltered. These effects of GPR120 agonists, natural and synthetic (i.e. EPA and TUG-891), on adipocyte differentiation were further reproduced by other laboratories. These experiments showed adipocyte differentiation in the presence of these agonists and increased expression of thermogenic markers (i.e. Ucp1) (Fleckenstein-Elsen *et al*., 2016; Kim *et al*., 2016). Furthermore, and consistent with what was observed *in vivo*, adipogenesis in the presence of GPR120 agonists caused an induction in FGF21 mRNA expression and release to the culture media.

Then, the question was whether these effects on inducing thermogenic machinery could also be achieved acutely in already differentiated brown/beige adipocytes. To test this, differentiated adipocytes were treated with natural and synthetic agonists. GW9508, TUG-891, grifolic acid (another GPR120 agonist), EPA and ALA (n-3 PUFAs expected to act as GPR120 agonists) were administered during 24 hours to the cell cultures. Results showed that both types of adipocytes increased the expression of thermogenic markers upon GPR120 activation by the distinct agonists. This induction was consistent with an increased temperature (as assessed by thermographic images of the cultures) and an increase in glucose oxidation in those cells treated with GPR120 agonists. In addition, 24 hours of treatment in these cells was sufficient to trigger FGF21 mRNA expression and release. Similar results upon acute treatments with GPR120 agonists were observed later by other study groups where EPA prove to increase the expression of thermogenic markers (i.e. *Ucp1*, *Prdm16* and *Cidea*) while increasing respiration and mitochondrial content (Kim *et al*., 2016; Pahlavani *et al*., 2016). Also, studies in the presence of GW9508 and TUG-891 showed to cause an increase in respiration, Ucp1 expression and Ca^{2+}-mediated mitochondrial depolarization and fission in adipocytes (Kim *et al*., 2016; Schilperoort *et al*., 2018). In the case of natural occurring agonists, Pahlavani et al (2016) reported that the treatment of human adipocytes with EPA resulted in increased expression of thermogenic markers and an increase in mitochondrial content.

Given these results, and considering that n-3 fatty acids are also able to activate GPR40, cell-autonomous effects of GPR120 activation were analyzed on GPR120-null precursors and adipocytes.

n-3 induction of FGF21 occurs via GPR120.

GPR120-deficient cells were employed to confirm that the cell-autonomous effects upon agonist administration were due to GPR120 activation. Primary cultures of BAT and iWAT obtained from GPR120-deficient mice were performed. The first outstanding observation was that GPR120-null precursor cells failed to achieve a proper differentiation. This result has been recently confirmed by Schilperoort and collaborators (2018) in brown precursors and by Gotoh's group in white precursors (2007). The cultures of GPR120-null cells showed decreased expression of thermogenic machinery and, upon GPR120 activation, they failed to induce FGF21 mRNA expression and release. Since these cells did not achieve a proper differentiation, two separate assays were perform to confirm these results. The first one consisted in pre-treating the cells with AH7614, a GPR120 antagonist, before adding GW9508 or EPA. This experiment showed that the antagonist caused a reduction in the expression of FGF21 mRNA and its release from the adipocytes. This effect was blunted in the case of EPA-mediated FGF21 induction upon GPR120 activation. The second one consisted in knocking-down GPR120 expression (siGPR120) in differentiated brown adipocytes which allowed us to determine the effects of GPR120 signaling impairment in adipocytes when already differentiated. This assay evidenced an impaired induction of FGF21 upon agonist administration to the cultures in GPR120-knockdown cells, while also a decrease in the effects over the induction of thermogenic markers. Kim and co-workers (2016) reproduced this effect of loss-of-function in an assay where GPR120 knock-down cells were treated with EPA. While control cells also reported an induction on thermogenic markers (i.e. *Ucp1, Cidea*), GPR120-knockdown cells showed no induction upon EPA treatment.

As depicted in the introduction of this dissertation, GPCR signaling has become a complicated field. We know from the literature that GPR120 is able to act through Gαq/11 in enteroendocrine cells and adipocytes, Gαi in enteroendocrine cells and β-arrestins in macrophages. All of these mechanisms of action have been revealed in the presence of different GPR120 agonists. Surprisingly, taking as an example PUFAs, natural agonists for GPR120, it is observed that the activation of the receptor is different depending on the tissue and the agonist. In this work, there were examined the effects upon GPR120 activation on FGF21 and thermogenesis regulation in AT. What was found in these results was that the activation of GPR120 caused phosphorylation of p38-MAPK and ERK1/2. Both kinases have been related to FGF21 regulation and activity. p38 MAPK has been reported to be activated upon noradrenergic stimuli leading to an increased transcription of several genes such as FGF21 in brown adipocytes (Hondares *et al*., 2011). To confirm the direct effects of GPR120 activation over FGF21 expression, an experiment transfecting differentiated brown adipocytes with the plasmid −1497-FGF21-Lu containing the 5' region of the mouse FGF21 gene linked to the luciferase reporter gene was assessed. Both GPR120 agonists, GW9508 and EPA, significantly induced the activity of the transfected FGF21 promoter. This effect was not observed in the presence of a transfected construct missing p38 MAPK-responsive site nor with a transfected dominant negative p38 MAPK-dependent activation vector (MKK6-K82A). This result was subsequently confirmed with an *in vitro* assay where brown adipocytes were pre-treated with SB202190, a p38 MAPK inhibitor, before the administration of GW9508 or EPA. The kinase inhibitor caused a reduction in FGF21 expression in adipocytes. In relation to ERK1/2, the other kinase reported to be phosphorylated upon GPR120 activation with GW9508 or EPA, the pretreatment of the cells with U-0126, an ERK1/2 inhibitor, caused the reduction in FGF21 mRNA expression in brown adipocytes. ERK1/2 has been described as part of the signaling pathway upon FGF21 treatment and is considered the main kinase responsible for the intracellular responses to FGF21 (Ogawa *et al*., 2007).These findings suggest that GPR120-induced FGF21 expression in brown adipocytes is different to FGF21 regulation in liver. While hepatic induction of

FGF21 is mediated by PPARα (Purushotham *et al*., 2009), induction of FGF21 in BAT involves the activation of p38 MAPK. Likewise, ERK1/2 phosphorylation may induce a positive feedback loop in response to the whole GPR120 mechanism of activation in the brown/beige adipocyte. Thus, contributing to FGF21 expression and its intracellular effects. FGF21 is also able to activate FGFR1, the main FGF receptor in the adipose tissues. FGFR1 results, out of several other responses, in the phosphorylation of CREB. It is known that one target of CREB phosphorylation is PGC-1α (Ventura-Clapier *et al*., 2008). We did not observe a phosphorylation of CREB in our experiments, however we did observe an increase in PGC-1α expression. This induction of PGC-1α may be induced by other signal transduction pathway upon GPR120 activation, such as p38 MAPK. PGC-1α induction is key due to its role on metabolic regulation and mitochondrial biogenesis in AT (Aubert *et al*., 2013).

As for other reports on the signal transduction pathway mediated by GPR120 activation in brown adipocytes, Kim and co-workers (2016) observed an increase in intracellular levels of cAMP, a second messenger identified for $G_{\alpha s}$. However, this increase in intracellular cAMP upon the activation of GPR120 was not observed by Schilperoort and co-workers (2018). While no results on thermogenic machinery effects upon the inhibition of ERK1/2 or other kinases were shown, the former group showed results suggesting that the increase in respiration is mediated via $G_{\alpha q/11}$ effects over intracellular Ca^{2+}. This increase in calcium would provoke mitochondria depolarization and fission while increasing respiration without altering cAMP intracellular levels. (Hou et al., 2017; Schilperoort et al., 2018). Effects of the Gq family on brown differentiation and thermogenic activation remain to be controversial due to results found by Klepac and co-workers (2016). This group employed a Gαq-null (*GNAQ*) animal model and *in vitro* assays. They observed that Gq signaling is a crucial inhibitor of adipocyte differentiation through activation of Rho/ROCK signaling cascade, a major regulator of brown adipocyte differentiation (Klepac *et al*., 2016). While the inhibition of Rho in their experiments caused the potentiation of brown adipocytes differentiation, no reports in this work are presented for PLC, IP3 or intracellular calcium. Also, it should be mentioned that Gα11 and Gαq are members of the Gq-family in the classification of the α-subunits

but are coded by different genes (*GNA11* and *GNAQ*, respectively). Their downstream signaling may result different and also their agonist-mediated activation pathways. Further experiments regarding differences between Gq and G11 roles on brown adipocytes should be performed to better understand G-protein dynamics in adipocyte biochemistry.

At the introduction of this dissertation it was mentioned that a GPCR may show preference to signal through a particular effector depending on the ligand that activates the receptor, this is known as *biases signaling*. It has been reported that other GPR120 agonists (i.e. DHA) have mild or no effects over thermogenic or adipogenic markers nor in oxygen consumption (Fleckenstein-Elsen *et al*., 2016). *Biased signaling* may result depending on the agonist activating the receptor in adipocytes triggering different effects. Current available data, including the one presented here, show that adipocyte differentiation and thermogenic markers induction in brown adipocytes are induced upon GPR120 activation with some synthetic agonists (like GW9508 and TUG-891) and EPA. Also, these effects are blunted in experiments of loss-of-function of GPR120, as confirmed by other groups (Kim *et al*., 2016; Schilperoort *et al*., 2018). What comes intriguing is how and why this induction is preferentially accomplished by EPA-mediated activation of GPR120. It still needs to be clarified why the effects observed upon activation of GPR120 with a certain natural agonist in a specific cell-type are not reproduced with other known occurring agonists. For example, EPA effects over adipogenesis and thermogenic activation are not reproduced by DHA (Fleckenstein-Elsen *et al*., 2016 and unpublished data from our laboratory). On the other hand, DHA effects over macrophages have not been intimately linked to EPA (Oh *et al*., 2010; Oh *et al*., 2014). Also, it shall not be forgotten that this work focused on the effects of GPR120 activation on adipocytes and its role on thermogenic activation. Other effects regarding GPR120 activation (i.e. glucose uptake and anti-inflammatory or stress responses) were not explored with the same detail, yet. It could also occur that different allosteric agonists, inverse agonists and antagonists play different roles in the same cell at different time-points to respond to distinct stimulus, as the concept of *biased signaling* suggests. One example is glucose uptake. DHA has failed to achieve any induction on

thermogenic machinery in our and Fleckenstein-Elsen's groups experiments (2016). However, Oh and co-workers (2010) reported that DHA stimulation of GPR120 in 3T3-L1 adipocytes increased GLUT4 translocation to the cell surface with a subsequent increase in glucose transport into the cells. It is also important to bring to the scope findings regarding effects of n-6 PUFAs, ARA (arachidonic acid, an n-6 PUFA) and EPA induced adipogenesis in precursor cells. However, while EPA increased beige markers at the end of differentiation, ARA showed no effects over thermogenic marker genes' expression but instead increased white gene markers expression (Fleckenstein-Elsen *et al*., 2016). Whether these type of PUFAs may interact or affect GPR120 activation remains to be elucidated and results important to be clarified in order to understand mechanism of activation in DIO. Likewise, it should be interesting to test whether these 'whitening' effects are impaired in the presence of n-3 PUFAs.

GPR120 effects through FGF21 in brown and beige adipocytes and the induction of thermogenesis.

As described during these data sets of results, FGF21 is importantly induced and released from adipocytes and adipose tissue upon GPR120 activation. FGF21 is an endocrine factor which has been linked to a great variety of beneficial effects for metabolism. Some of them include glucose uptake in white adipocytes by inducing Glut1 expression (Kharitonenkov *et al*., 2005), thermogenic activation in brown adipose tissue (Hondares *et al*., 2010; Wu *et al*., 2012) and inducing browning in depots characteristic of white fat (Hondares *et al*., 2011; Fisher *et al*., 2012). The analysis of these results and other groups' reports show that GPR120 activation induced the expression of the thermogenic machinery (Kim *et al*., 2016; Schilperoort *et al*., 2018). The results here described show that GPR120-activation caused an induction in FGF21. Hence, the FGF21-dependent effects after the activation of GPR120 were further explored. For this reason, another *in vivo* experiment in wild-type and FGF21-deficient animals was performed. Chow diet of these animals was supplemented with GW9508 and after 7 days animals were sacrificed. The effects over FGF21 were reproduced in

wild-type animals, so the analysis focused on the knock-out effects. In the case of BAT, we observed that there was an important impairment of thermogenic activation upon GW9508 administration in mice lacking FGF21. The induction in thermogenic marker genes (i.e. *Ucp1, CoxIV, and Bmp8b*) was unaffected or even decreased upon GPR120 activation in FGF21-knockout animals. In addition, Ucp1 protein expression in the FGF21-deficient adipose tissues showed no induction upon GW9508 supplementation; conversely, they showed increased lipid accumulation and leptin expression. Regarding WAT and the induction of browning by GPR120 agonists, we observed that the FGF21-knockout tissues showed increased lipid content. Also, the induction in the expression of thermogenic markers was blunted in the absence of FGF21. This effect was consistent with a decreased effect on Ucp1 protein expression and fewer multilocular adipocytes in the iWAT depots from FGF21-null animals.

To verify if cell-autonomous effects that were reported before were also dependent on FGF21, three main *in vitro* approaches were performed. It was verified if the absence of FGF21 resulted in adipocyte differentiation upon GPR120 activation. Precursor cells from interscapular BAT from wild-type and FGF21-deficient animals were obtained. As in the previous experiments, the cells were maintained in the basal media or supplemented with GW9508. While no significant impairment in differentiation was observed in the FGF21-null cells, the induction in the expression of thermogenic markers upon GW9508 administration during differentiation did show an impairment. Likewise, when differentiated adipocytes obtained from iBAT or iWAT of wild-type and FGF21-deficient mice were treated with GW9508 during 24 hours, the induction in the thermogenic markers gene expression was impaired. Glucose oxidation was measured in this experiments showing that GPR120 activation caused an increase in glucose oxidation in wild-type animals and that the absence of FGF21 resulted in a reduced oxidation capacity upon activation. These results are consistent with what is known of FGF21 effects on BAT and WAT where it promotes thermogenic activation and browning, respectively, and is associated with glucose uptake and oxidation (Hondares *et al*., 2010; Fisher *et al*., 2012). Altogether, these approaches help clarify that effects

observed on thermogenic activation upon GPR120 activation are mediated by FGF21 in an autocrine (and potentially endocrine) manner.

GPR120 role on neonatal BAT thermogenesis.

Our results together with other recent reports (Kim *et al*., 2016; Schilperoort *et al*., 2018) reveled that GPR120 mediates thermogenic activation in adipose tissues and that GPR120-deficient animals have proven to be sensible to cold exposure. Consistent with the former detail, GPR120-deficient pups show a compromised survival during the first hours of life at standard housing temperatures (21°C) this was ameliorated by raising environmental temperature to 25°C. Thermal stress post-partum induced the expression of GPR120 in BAT from wild-type animals. The expression of other thermogenic markers (*Ucp1* and *Fgf21*) showed similar behaviors not just regarding temperature but also the initiation of suckling, which seemed to have mild effects over this post-natal induction (and similar to what is observed for Ucp1). Neonatal GPR120 activation in BAT showed to be accompanied by an increase in FGF21 circulating levels and mRNA expression in brown fat. Likewise, HFD supplementation with EPA, a well-known natural occurring agonist of GPR120, shows an increase in FGF21 mRNA expression in BAT (Pahlavani *et al*., 2017). In a previous section, it was described that upon cold exposure, GPR120-deficient mice show decreased levels of FGF21 compared to wild-type animals. FGF21 was previously described to be markedly induced in the postnatal period (Hondares *et al*., 2010). Pup initiation of suckling causes an increase in FA plasma levels and promotes FGF21 expression in liver and its release to the circulation. This FGF21 contributes to BAT thermogenic activity (Hondares *et al*., 2010 and 2011). While liver has been described as the main tissue to express and contribute to plasma levels of FGF21, it is also known that brown adipose tissue is an important producer of FGF21. Therefore, and after several previous reports on its role on thermogenesis, it is presumed to be linked to BAT adequate activation (Fischer *et al*., 2012; Cereijo *et al*., 2015). Consistent with what was previously reported, data in this set of experiments showed an important increase in plasma FGF21 levels since 6 hours

of life. This induction observed in the wild-type animals was impaired in GPR120-null pups. No effects of GPR120 loss-of-function were observed in liver. Conversely, BAT showed an impairment in *Fgf21* expression, especially during the first 12 hours after birth. This observation conducted the idea that BAT-mediates neonatal levels of FGF21 through GPR120. The final effect seems to be thermogenic activation of BAT due to an important decrease observed in the induction of *Ucp1* mRNA and protein in neonates deficient of GPR120. FGF21 levels in the neonatal period have previously been reported to be essential for BAT thermogenic machinery induction in newborns (Hondares *et al*., 2010). Also supportive to this idea were the indirect temperature estimations of BAT performed. Thermographic images show decreased temperatures during the first hours of life. In addition, fatty acids (important energy substrates at this age) oxidation seemed to be impaired in GPR120-deficient pups. On the other hand, no important differences were observed for glucose oxidation. Together, these data suggests decreased pup survival under 21°C of housing temperatures could be due to an inadequate thermogenic adaptation in GPR120-deficient pups. This conclusion is also supported by the improvement in pup survival with the increase in the environmental temperature by four degrees at the place where pup deliveries took place (25°C).

GPR120 activation as a therapeutic target for the induction of thermogenesis through FGF21 and perspectives in the field.

The results presented here describe GPR120 activation as a potential target for the treatment of obesity. They propose a GPR120-mediated induction of adipose tissue thermogenesis mediated by FGF21. FGF21 has previously been reported to mediate thermogenic activation and substrate oxidation in WAT (Markan *et al*., 2014). Other effects of GRP120 activation in adipose tissue have been described such as an improvement in glucose utilization and a decrease in inflammatory markers (Oh *et al*., 2010; Oh *et al*., 2014). However, there are still no concluding reports regarding modifications to GPR120 activation or expression in obesity. Some studies report an overexpression of the receptor in the presence of obesity while others report a

reduction in the expression of GPR120 in DIO models (Ichimura *et al*., 2012; Rodriguez-Pacheco *et al*., 2014; Satapati *et al*., 2017). It could occur that the effects over the expression of the receptor rely on the type of diet that is employed (regarding lipid composition). Also, the increased expression of the receptor could also imply a type of resistance to the physiological signals that are to target GPR120, something similar to what has been described for FGF21 or insulin (Fisher *et al*,. 2010).

GPR120 activation and its role on FGF21 regulation in obesity results challenging to clarify due to different phenotypes observed in studies of loss-of-function for both proteins. Ichimura and co-workers (2012) have reported that GPR120 deficiency leads to increased body and fat mass weight. However, this phenotype has failed to be reproduced by other study groups including ours (Oh *et al*., 2014; Schilperoort *et al*., 2018). The situation is similar for FGF21 where some studies show an increase in adiposity (Hotta *et al*. 2009) while others report a decrease in fat accumulation related to a decreased PPARɣ activity (Dutchak *et al*. 2012). Further analysis considering other parameters such as age or diet composition should be done to clarify these panorama. Also, while no impairment in adipogenesis is observed in the absence of FGF21, there is a strong impairment in adipogenesis on GPR120-null precursors as observed in these results.

This work focused on the effects of GPR120 activation *in vivo* under healthy conditions. GPR120 showed to induce thermogenesis through FGF21. For considering GPR120 a therapeutic target modulating FGF21 system it should be taken into account that several studies have revealed that HFD itself induces an increase in FGF21 expression (Villarroya *et al*., 2014; Pahlavani *et al*., 2017; Zhang *et al*. 2008). This induction seems to be dependent on the composition of the diet that is administered to the animals and also to the stress status of the tissues (ER and oxidative). In addition, it remains unclear that some experimental treatments for obesity have no effects over FGF21 expression (in some or all adipose depots). Likewise, several DIO experiments have shown that some HFDs are able to increase thermogenic activity in BAT, as

described by Kim and co-workers (2016). So, to drive appropriate conclusions and direct further experiments, diet composition should be chosen appropriately. In the case of those HFDs showing no induction of FGF21 or BAT thermogenesis, the activation of GPR120 should be explored in order to test a possible recovery in FGF21 signaling or FGF21 expression. Subsequent analysis, should consider the effects over the adipose tissue receptor (FGFR1) and the co-receptor β-klotho (KLB), both previously described to be essential for FGF21 response in the tissues targeted by this endocrine factor (Kurosu *et al*., 2007; Kharitonenkov *et al*., 2008; Ding *et al*., 2012; Owen *et al*., 2015). Also, long-term effects of GPR120 agonists administration in DIO models over different physiological and cell specific responses (i.e. oxidative and ER-stress, mitochondrial regulation) and the interaction with other cell populations (especially regarding the immune system) should be covered. Furthermore, some of the effects observed could be related to FGF21 effects in brain. FGF21 has the ability to activate its receptor in the hypothalamus resulting in CNS stimulation. This effect over CNS could lead to thermogenic activation of BAT (and WAT) (Owen *et* al., 2014). Therefore, possible mechanisms of BAT regulation mediated by the CNS could also be found.

While these experiments' results show a relation in GPR120 activation-mediated increase in FGF21 plasma levels and thermogenic activation of the adipose depots, there are several studies suggesting that an increase in plasma FGF21 levels are related to adipose tissue dysregulation (i.e. obesity and T2DM or lipodystrophy) (Zhang *et al*., 2008; Gallego-Escuredo *et al*., 2015; Miehle *et al*., 2016). During the development of this project, three collaborations were performed where it was determined that FGF21 modulated stress responses. FGF21 showed to be increased in situations leading to ER stress in liver (Zarei *et al*., 2016; Zarei *et al*., 2018). These studies propose FGF21 as a protective molecule in the progression of ER stress and the development of NAFLD. This protective role has also been described for the heart (Planavila *et al*., 2013). On the other hand, increases in FGF21 levels were also observed under the administration of antiretroviral drugs in several cell-types. These treatments were described to mediate a type of FGF21 resistance under ER-stress conditions which leads to a decreased expression of KLB in different cell-types (Moure et al., 2018). However, the recovery of

KLB levels was not observed in all situations that inhibited ER stress nor oxidative stress. KLB expression is crucial for FGF21 signaling and its downstream effects, GPR120 activation has shown to induce the expression of FGF21 however it remains unexplored whether this activation could impact KLB expression (previously reported to be determinant FGF21 resistance). GPR120 activation possible effects over AT dysfunction should include those effects over KLB and the stress status of the tissue. It could be of interest whether GPR120 activation could have a positive effect over the stress response in other metabolic situations (NAFLD or even treatments with antiretroviral drugs). Even if liver and other tissues do not express significant amounts of GPR120, the induction of FGF21 and the activation of GPR120 in immune cells could result in a positive impact on the metabolic status of the tissue.

Important for the information acquired in the development of targets is the fact that GPR120 activation induced adipocyte differentiation. This could imply that GPR120 activation effects over FGF21 induction in expression and release could have an adverse effect on osteogenic differentiation resulting in a compromised bone homeostasis. Previous reports have shown that GPR120 activation can induce adipogenic before osteogenic differentiation. Similarly, increased expression of FGF21 has been linked to a compromised osteogenic differentiation (Wei et al., 2012; Gao *et al*., 2015; Gallego-Escuredo *et al*., 2017). The possible effects over bone homeostasis should be checked in subsequent experimental approaches in order to discard any accelerated bone loss or other bone effects.

As for the immune system, macrophages have been found to express GPR120 and are also able to trigger responses with beneficial effects upon GPR120 activation (Oh *et al*., 2010). As mentioned, GPR120 is not expressed in all tissues, several effects over metabolic active organs (i.e. liver) could also occur due to a possible global inflammatory modulation. Studies revealed that the inflammatory processes driven by LPS were ameliorated in the presence of GPR120 agonists on macrophages. Given that inflammatory processes are also observed in AT as a consequence of obesity, the effects

over the inhibition/modification in the induction of several marker genes known to decrease the activation of thermogenesis or browning (i.e. LBP) could be explored. Previous results by Oh and co-workers (2010) have shown to inhibit the expression of inflammatory markers upon GPR120 activation. During the development of this thesis a collaboration on the role of LBP, a protein mediating immune-stimulation to LPS (lipopolysaccharide), was performed (Gavaldà-Navarro *et al*., 2016). LBP mediates the immunostimulatory capacity of LPS in bacterial infections by enabling the binding of the lipid A component of LPS to CD14 and toll-like receptor 4 (TLR4). While it is mainly expressed in liver, adipose tissues also expresses LBP. Its expression is associated with inflammatory markers and shows an up-regulation in situations of metabolic syndrome and insulin resistance in obese patients (Moreno-Navarrete *et al*., 2015). GPR120 activation by natural or synthetic agonists has proven to repress the ability of TLR4 to bind LPS thus inhibiting inflammatory responses in macrophages. Since LBP has been observed to be increased on WAT in obesity and given that GPR120 activation causes an induction in browning and glucose uptake from adipocytes, it could be of interest to investigate a possible effect over the inflammatory profile in WAT (like, for example, LBP expression) in hypertrophic conditions.

GPR120 activation comprises a wide variety of responses depending on the agonist and the cell target. So far, activation of the receptor has resulted beneficial for the treatment of metabolic conditions by improving insulin sensitivity, reducing the inflammatory profile and inducing thermogenic activation in adipose depots. Still, treatment doses and timings need to be defined in order to achieve the desired effects without leaving any chances for adverse effects (i.e. bone homeostasis dysregulation).

CONCLUSIONS

Conclusions

1. The G protein-coupled receptor GPR120 (also known as FFAR4) is highly expressed in brown adipose tissue in response to thermogenic stimuli (cold), and in brown adipocytes in culture in response to noradrenergic activation.

2. GPR120 is required for the browning of white adipose tissue, the stimulation of the hormonal factor FGF21, and optimal physiological responses to a thermogenic challenge (cold).

3. Pharmacological activation of GPR120 causes browning of white adipose tissue, promotes thermogenic/oxidative activity, and induces the expression of FGF21 in adipose tissues. This effect is mimicked in brown and beige adipocytes in culture.

4. n-3 PUFAS (especially eicosapentaenoic acid) induce differentiation of brown and beige adipocytes, promote thermogenic/oxidative activity, and enhance FGF21 gene transcription and FGF21 release through a GPR120-dependent mechanism.

5. The action of GPR120 activation on brown adipocytes involves activation of p38 MAP kinase and ERK1/2.

6. The effects of GPR120 activation stimulating white adipose tissue browning require FGF21.

7. GPR120 is dramatically induced after birth in brown adipose tissue, and is required for the postnatal induction of FGF21 and neonatal adaptive thermogenesis.

REFERENCES

References

A

Adams, A.C., Cheng, C.C., Coskun, T., Kharitonenkov, A. (2012). FGF21 Requires βklotho to Act In Vivo. PLoS ONE 7(11).

Adams AC, Yang C, Coskun T, Cheng CC, Gimeno RE, Luo Y, Kharitonenkov A. (2012b). The breadth of FGF21's metabolic actions are governed by FGFR1 in adipose tissue. Mol. Metab. 2, 31–37.

Agudelo LZ, Ferreira DMS, Cervenka I, Bryzgalova G, Dadvar S, Jannig PR, Pettersson-Klein AT, Lakshmikanth T, Sustarsic EG, Porsmyr-Palmertz M, Correia JC, Izadi M, Martínez-Redondo V, Ueland PM, Midttun Ø, Gerhart-Hines Z, Brodin P, Pereira T, Berggren PO, Ruas JL. (2018). Kynurenic Acid and Gpr35 Regulate Adipose Tissue Energy Homeostasis and Inflammation. Cell Metab.; 27(2):378-392.e5.

Ahn S, Shenoy SK, Wei H and Lefkowitz RJ (2004) Differential kinetic and spatial patterns of beta-arrestin and G protein-mediated ERK activation by the angiotensin II receptor. J Biol Chem 279(34): 35518-35525.

Ailhaud G. (2001). Adipose Tissue Protocols. Vol. 155. Humana Press. Totowa NJ. 1-6.

Ailhaud G., Hauner H. Development of white adipose tissue. (1998). En: GA. Bray, Claude Bouchard, W.P.T. James, editores. Handbook of Obesity. New York: Marcel Dekker Inc., pp. 359-378.

Albrink MJ, Meigs JW. (1965). The relationship between serum triglycerides and skinfold thickness in obese subjects. Ann N Y Acad Sci.; 131(1): 673-83.

Alemany R, Perona JS, Sánchez-Dominguez JM, Montero E, Cañizares J, Bressani R, Escribá PV, Ruiz-Gutierrez V. (2007). G protein-coupled receptor systems and their lipid environment in health disorders during aging. Biochim Biophys Acta.; 1768 (4): 964-75.

Altarejos JY, Montminy M. (2011). CREB and the CRTC co-activators: sensors for hormonal and metabolic signals. Nat Rev Mol Cell Biol.; 12(3):141-51.

Alvarez R, de Andrés J, Yubero P, Viñas O, Mampel T, Iglesias R, Giralt M, Villarroya F. (1995). A novel regulatory pathway of brown fat thermogenesis. Retinoic acid is a transcriptional activator of the mitochondrial uncoupling protein gene. J Biol Chem 270, 5666-5673.

Alvarez-Curto E and Milligan G. (2016). Metabolism meets immunity: the role of free fatty acid receptors in the immune system. Biochem Pharmacol 114: 3–13.

An SY, Lee MS, Yi SA, Ha ES, Han SJ, Kim HJ, Kim DJ, Lee KW. (2012). Serum fibroblast growth factor 21 was elevated in subjects with type 2 diabetes mellitus and was associated with the presence of carotid artery plaques. Diabetes Res Clin Pract.; 96(2): 196-203.

Anagnostis P, Katsiki N, Adamidou F, Athyros VG, Karagiannis A, Kita M, Mikhailidis DP. (2013). 11beta-Hydroxysteroid dehydrogenase type 1 inhibitors: novel agents for the treatment of metabolic syndrome and obesity-related disorders? Metabolism; 62(1):21-33.

Andrews M.T., Squire T.L., Bowen C.M., and Rollins M.B. (1998). Low-temperature carbon utilization is regulated by novel gene activity in the heart of a hibernating mammal. Proc. Natl. Acad. Sci. U. S. A 95, 8392-8397.

Angelin B., Larsson T.E., and Rudling M. (2012). Circulating fibroblast growth factors as metabolic regulators a critical appraisal. Cell Metab. 16, 693-705.

Antuna-Puente B, Feve B, Fellahi S, Bastard JP. (2008). Adipokines: the missing link between insulin resistance and obesity. Diabetes Metab.; 34(1):2-11.

Arner P, Pettersson A, Mitchell PJ, Dunbar JD, Kharitonenkov A, Ryden M. (2008) FGF21 attenuates lipolysis in human adipocytes—a possible link to improved insulin sensitivity. FEBS Lett; 582: 1725–30.

Aubert G, Vega RB, Kelly DP. (2013). Perturbations in the gene regulatory pathways controlling mitochondrial energy production in the failing heart. Biochim Biophys Acta.; 1833(4): 840-7.

Azzi M, Charest PG, Angers S, Rousseau G, Kohout T, Bouvier M and Pineyro G (2003) Beta arrestin-mediated activation of MAPK by inverse agonists reveals distinct active conformations for G protein-coupled receptors. Proc Natl Acad Sci U S A 100(20): 11406-11411.

B

Badman MK, Pissios P, Kennedy AR, Koukos G, Flier JS, Maratos-Flier E. (2007). Hepatic fibroblast growth factor 21 is regulated by PPARalpha and is a key mediator of hepatic lipid metabolism in ketotic states. Cell Metab.; 5(6): 426-37.

Baillie GS, Sood A, McPhee I, Gall I, Perry SJ, Lefkowitz RJ and Houslay MD (2003) beta-Arrestin-mediated PDE4 cAMP phosphodiesterase recruitment regulates beta-adrenoceptor switching from Gs to Gi. Proc Natl Acad Sci U S A 100(3): 940-945.

Baldwin JM (1994) Structure and function of receptors coupled to G proteins. Curr Opin Cell Biol 6:180–190.

Ballinger MA, Andrews MT. (2018). Nature's fat-burning machine: brown adipose tissue in a hibernating mammal. J Exp Biol.; 221(Pt Suppl 1). pii: jeb162586.

Barak LS, Ferguson SS, Zhang J and Caron MG. (1997). A beta-arrestin/green fluorescent protein biosensor for detecting G protein-coupled receptor activation. J Biol Chem 272(44): 27497-27500.

Barbatelli G, Murano I, Madsen L, Hao Q, Jimenez M, Kristiansen K, Giacobino JP, De Matteis R, Cinti S. (2010). The emergence of cold-induced brown adipocytes in mouse

white fat depots is determined predominantly by white to brown adipocyte transdifferentiation. Am J Physiol Endocrinol Metab 298, E1244-1253.

Barbera MJ, Schluter A, Pedraza N, Iglesias R, Villarroya F, Giralt M. (2001). Peroxisome proliferator-activated receptor alpha activates transcription of the brown fat uncoupling protein-1 gene. A link between regulation of the thermogenic and lipid oxidation pathways in the brown fat cell. J Biol Chem 276, 1486-1493.

Bartelt, A., Heeren, J. (2014). Adipose tissue browning and metabolic health. Nature reviews. Endocrinology, 10(1), pp. 24–36.

Bays, H. E. (2011).Adiposopathy is "sick fat" a cardiovascular disease? J Am Coll Cardiol 57, 2461-2473.

Beenken,A. and Mohammadi,M. (2009). The FGF family: biology, pathophysiology and therapy. Nat. Rev. Drug Discov. 8, 235-253.

Berglund ED, Li CY, Bina HA, Lynes SE, Michael MD, Shanafelt AB, Kharitonenkov A, Wasserman DH. (2009). Fibroblast growth factor 21 controls glycemia via regulation of hepatic glucose flux and insulin sensitivity. Endocrinology.; 150(9): 4084-93.

Bhattacharya S, Hall SE and Vaidehi N (2008a) Agonist-induced conformational changes in bovine rhodopsin: insight into activation of G-protein-coupled receptors. J Mol Biol 382(2): 539-555.

Bhattacharya S, Hall SE, Li H and Vaidehi N (2008b) Ligand-stabilized conformational states of human beta(2) adrenergic receptor: insight into G-protein-coupled receptor activation. Biophys J 94(6): 2027-2042.

Bjarnadottir TK, Fredriksson R, Hoglund PJ, Gloriam DE, Lagerstrom MC and Schioth HB (2004). The human and mouse repertoire of the adhesion family of G-protein-coupled receptors. Genomics 84(1): 23-33.

Bjarnadóttir TK, Fredriksson R, Schiöth HB. (2007). The adhesion GPCRs: a unique family of G protein-coupled receptors with important roles in both central and peripheral tissues. Cell Mol Life Sci.; 64(16):2104-19.

Bjursell M, Xu X, Admyre T, Böttcher G, Lundin S, Nilsson R, Stone VM, Morgan NG, Lam YY, Storlien LH, Lindén D, Smith DM, Bohlooly-Y M, Oscarsson J. (2014). The Beneficial Effects of N-3 Polyunsaturated Fatty Acids on Diet Induced Obesity and Impaired Glucose Control Do Not Require GPR120. PLoS One, 9, e114942.

Blad CC, Tang C, Offermanns S. (2012). G protein-coupled receptors for energy metabolites as new therapeutic targets. Nat Rev Drug Discov.; 11 (8):603-19.

Betz MJ, Enerbäck S. (2018). Targeting thermogenesis in brown fat and muscle to treat obesity and metabolic disease. Nat Rev Endocrinol.; 14(2): 77-87.

Bonet, M. L., Oliver, P. & Palou, A. (2013). Pharmacological and nutritional agents promoting browning of white adipose tissue. Biochim Biophys Acta 1831, 969-985.

Bookout AL, de Groot MH, Owen BM, Lee S, Gautron L, Lawrence HL, Ding X, Elmquist JK, Takahashi JS, Mangelsdorf DJ, Kliewer SA. (2013). FGF21 regulates metabolism and circadian behavior by acting on the nervous system. Nat Med.; 19(9): 1147-52.

Brasaemle, D. L. (2007).Thematic review series: adipocyte biology. The perilipin family of structural lipid droplet proteins: stabilization of lipid droplets and control of lipolysis. J Lipid Res 48, 2547-2559.

Briscoe CP, Peat AJ, McKeown SC, Corbett DF, Goetz AS, Littleton TR, McCoy DC, Kenakin TP, Andrews JL, Ammala C, Fornwald JA, Ignar DM, Jenkinson S. (2006). Pharmacological Regulation of Insulin Secretion in Min6 Cells through the Fatty Acid Receptor GPR40: Identification of Agonist and Antagonist Small Molecules. Br. J. Pharmacol., 148, 619−628.

Burns, R. N.; Singh, M.; Senatorov, I. S.; Moniri, N. H. (2014). Mechanisms of Homologous and Heterologous Phosphorylation of FFA Receptor 4 (GPR120): GRK6 and PKC Mediated Phosphorylation of Thr347, Ser350, and Ser357 in the C-terminal Tail. Biochem Pharmacol., 87, 650−659.

C

Cai K, Klein-Seetharaman J, Hwa J, Hubbell WL and Khorana HG. (1999). Structure and function in rhodopsin: effects of disulfide cross-links in the cytoplasmic face of rhodopsin on transducin activation and phosphorylation by rhodopsin kinase. Biochemistry 38(39): 12893-12898.

Cairó M, Villarroya J, Cereijo R, Campderrós L, Giralt M, Villarroya F. (2016). Thermogenic activation represses autophagy in brown adipose tissue. Int J Obes(Lond).; 40(10): 1591-1599.

Cannon B, Connoley E, Obregon M-J, Nedergaard J. (1988). Perinatal activation of brown adipose tissue. In The Endocrine Control of the Fetus, ed.WKunzel, A Jesen, pp. 306–20.

Cannon, B., Nedergaard, J. (2004). Brown adipose tissue: function and physiological significance. Physiol Rev 84, 277-359.

Cao W, Daniel KW, Robidoux J, Puigserver P, Medvedev AV, Bai X, Floering LM, Spiegelman BM, Collins S. (2004). p38 mitogen-activated protein kinase is the central regulator of cyclic AMP-dependenttranscription of the brown fat uncoupling protein 1 gene. Mol Cell Biol 24, 3057-3067.

Carmona MC, Iglesias R, Obregón MJ, Darlington GJ, Villarroya F, Giralt M. (2002). Mitochondrial biogenesis and thyroid status maturation in brown fat require CCAAT/enhancer-binding protein alpha. J Biol Chem 277, 21489-21498.

Cederberg A, Grønning LM, Ahrén B, Taskén K, Carlsson P, Enerbäck S. (2001). FOXC2 is a winged helix gene that counteracts obesity, hypertriglyceridemia, and diet-induced insulin resistance. Cell 106, 563-573.

Cereijo R, Villarroya J, Villarroya F. (2015). Non-sympathetic control of brown adipose tissue. Int J Obes Suppl.; 5(Suppl 1):S40-4.

Chakrabarti P, Kim JY, Singh M, Shin YK, Kim J, Kumbrink J, Wu Y, Lee MJ, Kirsch KH, Fried SK, Kandror KV. (2013). Insulin inhibits lipolysis in adipocytes via the evolutionarily conserved mTORC1-Egr1-ATGL-mediated pathway. Mol Cell Biol.; 33(18): 3659-66.

Charest PG, Oligny-Longpre G, Bonin H, Azzi M and Bouvier M (2007) The V2 vasopressin receptor stimulates ERK1/2 activity independently of heterotrimeric G protein signalling. Cell Signal 19(1): 32-41.

Chartoumpekis DV, Habeos IG, Ziros PG, Psyrogiannis AI, Kyriazopoulou VE, Papavassiliou AG. (2011). Brown adipose tissue responds to cold and adrenergic stimulation by induction of FGF21. Mol Med.; 17(7-8): 736-40.

Chavez AO, Molina-Carrion M, Abdul-Ghani MA, Folli F, Defronzo RA, Tripathy D.(2009). Circulating fibroblast growth factor-21 is elevated in impaired glucose tolerance and type 2 diabetes and correlates with muscle and hepatic insulin resistance. Diabetes Care.; 32(8): 1542-6.

Chawla A, Repa JJ, Evans RM, Mangelsdorf DJ. (2001). Nuclear Receptors and Lipid Physiology: Opening the X.Files. Science Vol 204. 1865- 1870.

Chen WW, Li L, Yang GY, Li K, Qi XY, Zhu W, Tang Y, Liu H, Boden G. (2008). Circulating FGF-21 levels in normal subjects and in newly diagnose patients with Type 2 diabetes mellitus. Exp Clin Endocrinol Diabetes. 2008 Jan;116(1):65-8.

Chen W, Hoo RL, Konishi M, Itoh N, Lee PC, Ye HY, Lam KS, Xu A. (2011). Growth hormone induces hepatic production of fibroblast growth factor 21 through a mechanism dependent on lipolysis in adipocytes. J Biol Chem.; 286(40): 34559-66.

Cherezov V, Rosenbaum DM, Hanson MA, Rasmussen SG, Thian FS, Kobilka TS, Choi HJ, Kuhn P, Weis WI, Kobilka BK and Stevens RC. (2007). High-resolution crystal structure of an engineered human beta2-adrenergic G protein-coupled receptor. Science 318(5854): 1258-1265.

Christodoulides C., Dyson P., Sprecher D., Tsintzas K., and Karpe F. (2009). Circulating fibroblast growth factor 21 is induced by peroxisome proliferator-activated receptor agonists but not ketosis in man. J. Clin. Endocrinol. Metab. 94, 3594-3601.

Choe SS, Huh JY, Hwang IJ, Kim JI, Kim JB. (2016). Adipose Tissue Remodeling: Its Role in Energy Metabolism and Metabolic Disorders. Front Endocrinol (Lausanne).; 7:30.

Chu DT, Tao Y, Son LH, Le DH. (2016). Cell source, differentiation, functional stimulation, and potential application of human thermogenic adipocytes in vitro. J Physiol Biochem.; 73(3):315-321.

Chusyd DE, Wang D, Huffman DM, Nagy TR. (2016).Relationships between Rodent White Adipose Fat Pads and Human White Adipose Fat Depots. Front Nutr.; 3:10.

Cinti S. (2005). The adipose organ. Prostaglandins Leukot Essent Fatty Acids.; 73(1): 9-15. Review.

Cinti, S. (2009). Transdifferentiation properties of adipocytes in the adipose organ. American Journal of Physiology Endocrinology and Metabolism, 297(5), E977–E9E9.

Clarke L, Heasman L, Firth K, Symonds ME. (1997). Influence of route of delivery and ambient temperature on thermoregulation in newborn lambs. Am. J. Physiol. 272:R1931–39.

Commins, S. P., Watson, P. M., Frampton, I. C. & Gettys, T. W. (2001).Leptin selectively reduces white adipose tissue in mice via a UCP1-dependent mechanism in brown adipose tissue. Am J Physiol Endocrinol Metab 280, E372-377.

Cornall LM, Mathai ML, Hryciw DH, McAinch AJ. (2014). GPR120 agonism as a countermeasure against metabolic diseases. Drug Discov Today.; 19 (5):670-9.

Coskun T, Bina HA, Schneider MA, Dunbar JD, Hu CC, Chen Y, Moller DE, Kharitonenkov A. (2008). Fibroblast growth factor 21 corrects obesity in mice. Endocrinology.; 149(12): 6018-27.

Cranmer-Byng, M. M.; Liddle, D. M.; De Boer, A. A.; Monk, J. M.; Robinson, L. E. (2015). Proinflammatory Effects of Arachidonic Acid in a Lipopolysaccharide-Induced Inflammatory Microenvironment in 3T3- L1 Adipocytes in Vitro. Appl. Physiol., Nutr., Metab. 2015, 40, 142−154.

Cristancho, A. G., Lazar, M. A. (2011). Forming functional fat: a growing understanding of adipocyte differentiation. Nat Rev Mol Cell Biol 12, 722-734.

Cuevas-Ramos D, Almeda-Valdes P, Gómez-Pérez FJ, Meza-Arana CE, Cruz-Bautista I, Arellano-Campos O, Navarrete-López M, Aguilar-Salinas CA. (2010). Daily physical activity, fasting glucose, uric acid, and body mass index are independent factors associated with serum fibroblast growth factor 21 levels. Eur J Endocrinol.; 163(3): 469-77.

Cypess AM, Lehman S, Williams G, Tal I, Rodman D, Goldfine AB, Kuo FC, Palmer EL, Tseng YH, Doria A, Kolodny GM, Kahn CR. (2009).Identification and importance of brown adipose tissue in adult humans. N Engl J Med 360, 1509-1517.

D

Dani C, Billon N. (2012). Adipocyte Precursors: Developmental Origins, Self-Renewal, and Plasticity. Adipose Tissue Biology. Springer. New York, NY. pp.1-13.

Davenport AP, Alexander SP, Sharman JL, Pawson AJ, Benson HE, Monaghan AE, Liew WC, Mpamhanga CP, Bonner TI, Neubig RR, Pin JP, Spedding M, Harmar AJ. (2013). International Union of Basic and Clinical Pharmacology. LXXXVIII. G protein-coupled receptor list: recommendations for new pairings with cognate ligands. Pharmacol Rev. 2013 May 17;65(3):967-86.

de Onis M, Blössner M, Borghi E. (2010). Global prevalence and trends of overweight and obesity among preschool children. Am J Clin Nutr.; 92(5):1257-64.

De Sousa-Coelho,A.L., Marrero,P.F., and Haro,D. (2012). Activating transcription factor 4-dependent induction of FGF21 during amino acid deprivation. Biochem. J. 443, 165-171.

Degirolamo C, Sabbà C, Moschetta A. (2016). Therapeutic potential of the endocrine fibroblast growth factors FGF19, FGF21 and FGF23. Nat Rev Drug Discov.; 15(1): 51-69.

Díaz-Delfín, J., Hondares, E., Iglesias, R., Giralt, M., Caelles, C., Villarroya, F. (2012). TNF-α represses β-klotho expression and impairs FGF21 action in adipose cells: Involvement of JNK1 in the FGF21 pathway. Endocrinology 153, 4238–4245.

Ding, X., Boney-Montoya, J., Owen, B. M., Bookout, A. L., Coate, K. C., Mangelsdorf, D. J. and Kliewer, S. A. (2012). B-Klotho Is Required for Fibroblast Growth Factor 21 Effects on Growth and Metabolism', Cell metabolism, 16(3), pp. 387–393.

Donate-Correa J, Martín-Núñez E, Delgado NP, de Fuentes MM, Arduan AO, Mora-Fernández C, Navarro González JF. (2016). Implications of Fibroblast growth factor/Klotho system in glucose metabolism and diabetes. Cytokine Growth Factor Rev.; 28: 71-7.

Doze VA, Perez DM. (2013) GPCRs in stem cell function. Prog Mol Biol Transl Sci.; 115:175-216.

Duca, F. A.; Swartz, T. D.; Sakar, Y.; Covasa, M. (2013). Decreased Intestinal Nutrient Response in Diet-Induced Obese Rats: Role of Gut Peptides and Nutrient Receptors. Int. J. Obes., 37, 375−381.

Dushay J., Chui P.C., Gopalakrishnan G.S., Varela-Rey M., Crawley M., Fisher F.M., Badman M.K., Martinez-Chantar M.L., and Maratos-Flier E. (2010). Increased fibroblast growth factor 21 in obesity and nonalcoholic fatty liver disease. Gastroenterology 139, 456-463.

Dutchak PA, Katafuchi T, Bookout AL, Choi JH, Yu RT, Mangelsdorf DJ, Kliewer SA. (2012). Fibroblast growth factor-21 regulates PPARγ activity and the antidiabetic actions of thiazolidinediones. Cell.; 148(3): 556-67.

E

Ellis (2004) Nature Reviews Drug Discovery GPCR Questionnaire Participants. The state of GPCR research in 2004. Nat Rev Drug Discov.; 3(7): 575, 577-626.

Engelstoft MS, Park WM, Sakata I, Kristensen LV, Husted AS, Osborne-Lawrence S, Piper PK, Walker AK, Pedersen MH, Nøhr MK, Pan J, Sinz CJ, Carrington PE, Akiyama TE, Jones RM, Tang C, Ahmed K, Offermanns S, Egerod KL, Zigman JM, Schwartz TW. (2013). Seven Transmembrane G Protein-Coupled Receptor Repertoire of Gastric Ghrelin Cells. Mol. Metab.; 2, 376−392.

F

Fajas L, Schoonjans K, Gelman L, Kim JB, Najib J, Martin G, Fruchart JC, Briggs M, Spiegelman BM, Auwerx J. (1999). Regulation of peroxisome proliferator-activated receptor gamma expression by adipocyte differentiation and determination factor 1/sterol regulatory element binding protein 1: implications for adipocyte differentiation and metabolism. Mol Cell Biol 19, 5495-5503.

Fantuzzi G, Mazzone T. (2007). Adipose tissue and adipokines in health and disease. Humana Press, Totowa. Pp. 3-19.

Farmer SR. (2006). Transcriptional control of adipocyte formation. Cell Metab 4:263–273.

Fazeli, P. K., Lun, M., Kim, S. M., Bredella, M. A., Wright, S., Zhang, Y., Lee, H., Catana, C., Klibanski, A., Patwari, P. and Steinhauser, M. L. (2015). FGF21 and the late adaptive response to starvation in humans. Journal of Clinical Investigation, 125(12), pp. 4601–4611.

Feldmann, H. M., Golozoubova, V., Cannon, B. and Nedergaard, J. (2009). UCP1 Ablation Induces Obesity and Abolishes Diet-Induced Thermogenesis in Mice Exempt from Thermal Stress by Living at Thermoneutrality. Cell Metabolism, 9(2), pp. 203–209.

Ferrannini E, Haffner SM, Stern MP. (1990) Insulin sensitivity and hypertension. J Hypertens Suppl.; 8(7): S169-74.

Fisher FM, Chui PC, Antonellis PJ, Bina HA, Kharitonenkov A, Flier JS, Maratos-Flier E. (2010) Obesity is a fibroblast growth factor 21 (FGF21)-resistant state. Diabetes; 59: 2781–9.

Fisher, F. M., Estall, J. L., Adams, A. C., Antonellis, P. J., Bina, H. A., Flier, J. S., Kharitonenkov, A., Spiegelman, B. M. and Maratos-Flier, E. (2011). Integrated regulation of hepatic metabolism by fibroblast growth factor 21 (FGF21) in vivo. Endocrinology, 152(8), pp. 2996–3004.

Fisher, F. F., Kleiner, S., Douris, N., Fox, E. C., Mepani, R. J., Verdeguer, F., Wu, J., Kharitonenkov, A., Flier, J. S., Maratos-Flier, E. and Spiegelman, B. M. (2012). FGF21 regulates PGC-1α and browning of white adipose tissues in adaptive thermogenesis. Genes and Development, 26(3), pp. 271–281.

Fleckenstein-Elsen M, Dinnies D, Jelenik T, Roden M, Romacho T, Eckel J. (2016). Eicosapentaenoic acid and arachidonic acid differentially regulate adipogenesis, acquisition of a brite phenotype and mitochondrial function in primary human adipocytes. Mol Nutr Food Res.; 60(9): 2065-75.

Fon Tacer, K., Bookout, A. L., Ding, X., Kurosu, H., John, G. B., Wang, L., Goetz, R., Mohammadi, M., Kuro-o, M., Mangelsdorf, D. J. and Kliewer, S. a (2010) 'Research resource: Comprehensive expression atlas of the fibroblast growth factor system in adult mouse.', Molecular endocrinology (Baltimore, Md.), 24(10), pp. 2050–2064.

Fr ank M, Thumer L, Lohse MJ and Bunemann M (2005) G Protein activation without subunit dissociation depends on a G{alpha}(i)-specific region. J Biol Chem 280(26): 24584- 24590.

Fredborg, M.; Theil, P. K.; Jensen, B. B.; Purup, S. (2012). G Protein- Coupled Receptor120 (GPR120) Transcription in Intestinal Epithelial Cells Is Significantly Affected by Bacteria Belonging to the Bacteroides, Proteobacteria, and Firmicutes Phyla. J. Anim. Sci. , 90 (Suppl 4),10−12.

Fredriksson R., Lagerstrom M.C., Lundin L.G., Schioth H.B. (2003). The G-protein-coupled receptors in the human genome form five main families. Phylogenetic analysis, paralogon groups, and fingerprints. Mol. Pharmacol.; 63: 1256-1272.

Friedman, J. M., Halaas, J. L. (1998). Leptin and the regulation of body weight in mammals. Nature 395, 763-770.

Frolov, A.; Yang, L.; Dong, H.; Hammock, B. D.; Crofford, L. J. (2013). Anti-Inflammatory Properties of Prostaglandin E2: Deletion of Microsomal Prostaglandin E Synthase-1 Exacerbates Non-Immune Inflammatory Arthritis in Mice. Prostaglandins, Leukotrienes Essent. Fatty Acids, 89, 351−358.

Frühbeck, G., Méndez-Giménez, L., Fernández-Formoso, J.-A., Fernández, S. and Rodríguez, A. (2014). Regulation of adipocyte lipolysis. Nutrition Research Reviews, 27(1), pp. 63–93.

G

Gaich G, Chien JY, Fu H, Glass LC, Deeg MA, Holland WL, Kharitonenkov A, Bumol T, Schilske HK, Moller DE. (2013). The effects of LY2405319, an FGF21 analog, in obese human subjects with type 2 diabetes. Cell Metab.; 18(3): 333-40.

Gales C, Van Durm JJ, Schaak S, Pontier S, Percherancier Y, Audet M, Paris H and Bouvier M. (2006). Probing the activation-promoted structural rearrangements in preassembled receptor-G protein complexes. Nat Struct Mol Biol 13(9): 778-786.

Gallego-Escuredo JM, Domingo P, Gutiérrez Mdel M, Mateo MG, Cabeza MC, Fontanet A, Vidal F, Domingo JC, Giralt M, Villarroya F. (2012). Reduced levels of serum FGF19 and impaired expression of receptors for endocrine FGFs in adipose tissue from HIV-infected patients. J Acquir Immune Defic Syndr.; 61(5): 527-34.

Gallego-Escuredo JM, Gómez-Ambrosi J, Catalan V, Domingo P, Giralt M, Frühbeck G, Villarroya F. (2015). Opposite alterations in FGF21 and FGF19 levels and disturbed expression of the receptor machinery for endocrine FGFs in obese patients. Int J Obes (Lond).; 39(1): 121-9.

Gallego-Escuredo JM, Lamarca MK, Villarroya J, Domingo JC, Mateo MG, Gutierrez MDM, Vidal F, Villarroya F, Domingo P, Giralt M. (2017). High FGF21 levels are associated with altered bone homeostasis in HIV-1-infected patients. Metabolism.; 71: 163-170.

Gälman C., Lundasen T., Kharitonenkov A., Bina H.A., Eriksson M., Hafstrom I., Dahlin M., Amark P., Angelin B., and Rudling M. (2008). The circulating metabolic regulator FGF21 is induced by prolonged fasting and PPARalpha activation in man. Cell Metab. 8, 169-174.

Gao B, Huang Q, Jie Q, Lu WG, Wang L, Li XJ, Sun Z, Hu YQ, Chen L, Liu BH, Liu J, Yang L, Luo ZJ. (2015). GPR120: A bi-potential mediator to modulate the osteogenic and adipogenic differentiation of BMMSCs. Sci Rep.; 5: 14080.

García A, Méndez E. (2011). ¿Qué sabe Ud. acerca de… sobrepeso y obesidad? What do you know about … overweight and obesity? Revista Mexicana de Ciencias Farmacéuticas. 42(3): 57-9.

García-García E, De la Llata-Romero M, Kaufer-Horwitz M, Tusié-Luna MT, Calzada-León R, Vázquez-Velázquez V, Barquera-Cervera S, Caballero-Romo AJ, Orozco L, Velásquez-Fernández D, Rosas-Peralta M, Barriguete-Meléndez A, Zacarías-Castillo R, Sotelo-Morales J. (2008). La obesidad y el síndrome metabólico como problema de salud pública. Una reflexión. Salud Pública Méx. 50(6):530-547.

Gavaldà-Navarro A, Moreno-Navarrete JM, Quesada-López T, Cairó M, Giralt M, Fernández-Real JM, Villarroya F. (2016). Lipopolysaccharide-binding protein is a negative regulator of adipose tissue browning in mice and humans. Diabetologia.; 59(10): 2208-18.

Gburcik, V., Cawthorn, W. P., Nedergaard, J., Timmons, J. A. & Cannon, B. (2012). An essential role for Tbx15 in the differentiation of brown and "brite" but not white adipocytes. Am J Physiol Endocrinol Metab 303, E1053-1060.

Ge X, Chen C, Hui X, Wang Y, Lam KS, Xu A. (2011). Fibroblast growth factor 21 induces glucose transporter-1 expression through activation of the serum response factor/Ets like protein-1 in adipocytes. J Biol Chem; 286: 34533–41.

Gesta, S., Tseng, Y. H. & Kahn, C. R. (2007). Developmental origin of fat: tracking obesity to its source. Cell 131, 242-256.

Gesta S y Kahn CR. (2012). White Adipose Tissue. Adipose Tissue Biology. Springer. New York, NY. Pp. 71-89.

Gether U, Lin S and Kobilka BK (1995) Fluorescent labeling of purified beta 2 adrenergic receptor. Evidence for ligand-specific conformational changes. J Biol Chem 270(47): 28268-28275.

Gether U, Kobilka BK. (1998) G protein-coupled receptors. II. Mechanism of agonist activation. J Biol Chem.; 273(29):17979-82.

Gether U (2000). Uncovering molecular mechanisms involved in activation of G protein-coupled receptors. Endocr Rev.; 21(1): 90-113. Review.

Gimble, J. M., & Guilak, F. (2003). Differentiation potential of adipose derived adult stem (ADAS) cells. Current Topics in Developmental Biology, 58, 137–160.

Gimeno RE, Moller DE. (2014). FGF21-based pharmacotherapy--potential utility for metabolic disorders. Trends Endocrinol Metab.; 25(6): 303-11.

Giordano, A., Smorlesi, A., Frontini, A., Barbatelli, G. & Cinti, S. (2014). White, brown and pink adipocytes: the extraordinary plasticity of the adipose organ. Eur J Endocrinol 170, R159-171.

Giralt, M., Domingo, P. and Villarroya, F. (2011). Adipose tissue biology and HIV-infection. Best Practice and Research: Clinical Endocrinology and Metabolism, 25(3), pp. 487–499.

Giralt, M. and Villarroya, F. (2013). White, brown, beige/brite: Different adipose cells for different functions? Endocrinology, pp. 2992–3000.

Giralt, M., Gavaldà-Navarro, A., Villarroya, F., (2015). Fibroblast growth factor- 21, energy balance and obesity. Mol. Cell. Endocrinol. 418, 66–73.

Gnanalingham MG, Giussani DA, Sivathondan P, Forhead AJ, Stephenson T, Symonds ME, Gardner DS. (2005). Chronic umbilical cord compression results in accelerated maturation of lung and brown adipose tissue in the sheep fetus during late gestation. Am. J. Physiol. 289:E456–65.

Goetz,R., Beenken,A., Ibrahimi,O.A., Kalinina,J., Olsen,S.K., Eliseenkova,A.V., Xu,C., Neubert,T.A., Zhang,F., Linhardt,R.J., Yu,X., White,K.E., Inagaki,T., Kliewer,S.A., Yamamoto,M., Kurosu,H., Ogawa,Y., Kuro-o M, Lanske,B., Razzaque,M.S., and Mohammadi,M. (2007). Molecular insights into the klotho dependent, endocrine mode of action of fibroblast growth factor 19 subfamily members. Mol. Cell Biol. 27, 3417-3428.

Goetz R, Mohammadi M. (2013). Exploring mechanisms of FGF signalling through the lens of structural biology. Nat Rev Mol Cell Biol.; 14(3): 166-80.

Goldberg, I. J., Eckel, R. H. & Abumrad, N. A. (2009). Regulation of fatty acid uptake into tissues: lipoprotein lipaseand CD36-mediated pathways. J Lipid Res 50 Suppl, S86-90.

Golozoubova V, Gullberg H, Matthias A, Cannon B, Vennström B, Nedergaard J. (2004).Depressed thermogenesis but competent brown adipose tissue recruitment in mice devoid of all hormone-binding thyroid hormone receptors. Mol Endocrinol 18, 384-401.

Goodman OB, Jr., Krupnick JG, Santini F, Gurevich VV, Penn RB, Gagnon AW, Keen JH and Benovic JL. (1996). Beta-arrestin acts as a clathrin adaptor in endocytosis of the beta2- adrenergic receptor. Nature 383(6599): 447-450.

Gotoh C, Hong YH, Iga T, Hishikawa D, Suzuki Y, Song SH, Choi KC, Adachi T, Hirasawa A, Tsujimoto G, Sasaki S, Roh SG. (2007). The Regulation of Adipogenesis through GPR120. Biochem. Biophys. Res. Commun., 354, 591−597.

Gregoire FM, Smas CM, Sul HS. (1998). Understanding adipocyte differentiation. Physiol Rev 78:783–809.

Guan, H. P., Ishizuka, T., Chui, P. C., Lehrke, M. & Lazar, M. A. (2005). Corepressors selectively control the transcriptional activity of PPARgamma in adipocytes. Genes Dev 19, 453-461.

Gulick A (1922). A study of weight regulation in the adult human body during over-nutrition. Am J Physiol 60: 371–395.

Gupta RK, Arany Z, Seale P, Mepani RJ, Ye L, Conroe HM, Roby YA, Kulaga H, Reed RR, Spiegelman BM. (2010). Transcriptional control of preadipocyte determination by Zfp423. Nature 464, 619-623.

H

Haffner SM, Stern MP, Hazuda HP, Mitchell BD, Patterson JK. (1990). Cardiovascular risk factors in confirmed prediabetic individuals. Does the clock for coronary heart disease start ticking before the onset of clinical diabetes? JAMA. 1990; 263(21):2893-8.

Hale C, Chen MM, Stanislaus S, Chinookoswong N, Hager T, Wang M, Véniant MM, Xu J. (2012). Lack of overt FGF21 resistance in two mouse models of obesity and insulin resistance. Endocrinology.; 153(1): 69-80.

Hall KD, Heymsfield SB, Kemnitz JW, Klein S, Schoeller DA, Speakman JR. (2012).Energy balance and its components: implications for body weight regulation. Am J Clin Nutr 95, 989-994.

Haman F. (2006). Shivering in the cold: from mechanisms of fuel selection to survival. J Appl Physiol (1985).; 100(5):1702-8. Review.

Hamm HE. (1998). The many faces of G protein signaling. J Biol Chem 273(2): 669-672. Han Y, Moreira IS, Urizar E, Weinstein H and Javitch JA (2009) Allosteric communication between protomers of dopamine class A GPCR dimers modulates activation. Nat Chem Biol 5(9): 688-695.

Hara T, Hirasawa A, Ichimura A, Kimura I, Tsujimoto G. (2011). Free fatty acid receptors FFAR1 and GPR120 as novel therapeutic targets for metabolic disorders. J Pharm Sci.; 100(9):3594-601.

Harms, M., Seale, P. (2013). Brown and beige fat: development, function and therapeutic potential. Nat Med 19, 1252-1263.

Harwood, H. J., Jr. (2012). The adipocyte as an endocrine organ in the regulation of metabolic homeostasis. Neuropharmacology 63, 57-75.

Hayflick JS. (2000). A Family of Heptahelical Receptors With Adhesion-Like Domains: A Marriage Between Two Super Families, Journal of Receptors and Signal Transduction, 20:2-3, 119-131.

He Z, Jiang T, Wang Z, Levi M, Li J. (2004). Modulation of carbohydrate response element-binding protein gene expression in 3T3-L1 adipocytes and rat adipose tissue. Am J Physiol Endocrinol Metab.; 287(3): E424-30.

Hein P, Frank M, Hoffmann C, Lohse MJ and Bunemann M (2005) Dynamics of receptor/G protein coupling in living cells. EMBO J 24(23): 4106-4114.

Heng BC, Aubel D, Fussenegger M. (2013) An overview of the diverse roles of G-protein coupled receptors (GPCRs) in the pathophysiology of various human diseases. Biotechnol Adv.; 31(8):1676-94.

Hilger D, Masureel M, Kobilka BK. (2018). Structure and dynamics of GPCR signaling complexes. Nat Struct Mol Biol.; 25(1):4-12.

Himsworth HP. (1939). The mechanism of diabetes mellitus. Lancet I (2): 1–6.

Hirasawa A, Tsumaya K, Awaji T, Katsuma S, Adachi T, Yamada M, Sugimoto Y, Miyazaki S, Tsujimoto G. (2005). Free fatty acids regulate gut incretin glucagon-like peptide-1 secretion through GPR120. Nat Med.; 11(1): 90-4.

Hojman P, Pedersen M, Nielsen AR, Krogh-Madsen R, Yfanti C, Akerstrom T, Nielsen S, Pedersen BK. (2009). Fibroblast growth factor-21 is induced in human skeletal muscles by hyperinsulinemia. Diabetes.; 58(12): 2797-801.

Holland WL, Adams AC, Brozinick JT, Bui HH, Miyauchi Y, Kusminski CM, Bauer SM, Wade M, Singhal E, Cheng CC, Volk K, Kuo MS, Gordillo R, Kharitonenkov A, Scherer PE. (2013). An FGF21-adiponectin-ceramide axis controls energy expenditure and insulin action in mice. Cell Metab.; 17(5): 790-7.

Hondares E, Mora O, Yubero P, Rodriguez de la Concepción M, Iglesias R, Giralt M, Villarroya F. (2006). Thiazolidinediones and rexinoids induce peroxisome proliferator-activated receptorcoactivator (PGC)-1alpha gene transcription: an autoregulatory loop controls PGC-1alpha expression in adipocytes via peroxisome proliferator-activated receptor-gamma coactivation. Endocrinology 147, 2829-2838.

Hondares E, Rosell M, Gonzalez FJ, Giralt M, Iglesias R, Villarroya F. (2010). Hepatic FGF21 expression is induced at birth via PPARalpha in response to milk intake and contributes to thermogenic activation of neonatal brown fat. Cell Metab 11, 206-212.

Hondares E, Rosell M, Díaz-Delfín J, Olmos Y, Monsalve M, Iglesias R, Villarroya F, Giralt M. (2011).Peroxisome proliferator-activated receptor alpha (PPARalpha) induces PPARgamma coactivator 1alpha (PGC-1alpha) gene expression and contributes to thermogenic activation of brown fat: involvement of PRDM16. J Biol Chem 286, 43112-43122.

Hou Y, Kitaguchi T, Kriszt R, Tseng YH, Raghunath M, Suzuki M. (2017). Ca(2+)-associated triphasic pH changes in mitochondria during brown adipocyte activation. Mol Metab.; 6(8): 797-808.

Houthuijzen JM, Oosterom I, Hudson BD, Hirasawa A, Daenen LGM, McLean CM, Hansen SVF, van Jaarsveld MTM, Peeper DS, Jafari Sadatmand S, Roodhart JML, van de Lest CHA, Ulven T, Ishihara K, Milligan G, Voest EE. (2017). Fatty acid 16:4(n-3) stimulates a

GPR120-induced signaling cascade in splenic macrophages to promote chemotherapy resistance. FASEB J.; 31(5): 2195-2209.

Hsuchou H, PanW, Kastin AJ. (2007). The fasting polypeptide FGF21 can enter brain from blood. Peptides 28:2382–2386.

Huang HC, Klein PS. (2004). The Frizzled family: receptors for multiple signal transduction pathways. Genome Biol.; 5(7):234.

Hudson, B. D.; Ulven, T.; Milligan, G. (2013). The Therapeutic Potential of Allosteric Ligands for Free Fatty Acid Sensitive GPCRs. Curr. Top. Med. Chem., 13, 14−25.

Husted AS, Trauelsen M, Rudenko O, Hjorth SA, Schwartz TW. (2017). GPCR-Mediated Signaling of Metabolites. Cell Metab.; 25(4): 777-796.

I

Ichimura, A.; Hirasawa, A.; Poulain-Green, H., Meuth, M. (1974). An established pre-adipose cell line and its differentiation in culture. Cell 3, 127- 133.

Ichimura A, Hirasawa A, Hara T, Tsujimoto G. (2009). Free fatty acid receptors act as nutrient sensors to regulate energy homeostasis. Prostaglandins Other Lipid Mediat.; 89 (3-4):82-8.

Ichimura A, Hirasawa A, Poulain-Godefroy O, Bonnefond A, Hara T, Yengo L, Kimura I, Leloire A, Liu N, Iida K, Choquet H, Besnard P, Lecoeur C, Vivequin S, Ayukawa K, Takeuchi M, Ozawa K, Tauber M, Maffeis C, Morandi A, Buzzetti R, Elliott P, Pouta A, Jarvelin MR, Körner A, Kiess W, Pigeyre M, Caiazzo R, Van Hul W, Van Gaal L, Horber F, Balkau B, Lévy-Marchal C, Rouskas K, Kouvatsi A, Hebebrand J, Hinney A, Scherag A, Pattou F, Meyre D, Koshimizu TA, Wolowczuk I, Tsujimoto G, Froguel P. (2012). Dysfunction of Lipid Sensor GPR120 Leads to Obesity in Both Mouse and Human. Nature, 483, 350−354.

Iizuka, K., Takeda, J. and Horikawa, Y. (2009). Glucose induces FGF21 mRNA expression through ChREBP activation in rat hepatocytes. FEBS Letters, 583(17), pp. 2882–2886.

Im DS. (2004). Discovery of new G protein-coupled receptors for lipid mediators. J Lipid Res.; 45(3): 410-8. Review.

Inagaki T, Dutchak P, Zhao G, Ding X, Gautron L, Parameswara V, Li Y, Goetz R, Mohammadi M, Esser V, Elmquist JK, Gerard RD, Burgess SC, Hammer RE, Mangelsdorf DJ, Kliewer SA. (2007). Endocrine regulation of the fasting response by PPARalpha-mediated induction of fibroblast growth factor 21. Cell Metab.; 5(6): 415-25.

Ishibashi, J., Seale, P. (2010). Beige Can Be Slimming. Science, 328(5982), pp. 1113–1114.

Itoh Y, Kawamata Y, Harada M, Kobayashi M, Fujii R, Fukusumi S, Ogi K, Hosoya M, Tanaka Y, Uejima H, Tanaka H, Maruyama M, Satoh R, Okubo S, Kizawa H, Komatsu H, Matsumura F, Noguchi Y, Shinohara T, Hinuma S, Fujisawa Y, Fujino M. (2003). Free fatty

acids regulate insulin secretion from pancreatic beta cells through GPR40. Nature.; 422 (6928): 173-6.

Itoh,N. and Ornitz,D.M. (2004). Evolution of the Fgf and Fgfr gene families. Trends Genet. 20, 563-569.

Itoh, N. and Ornitz, D. M. (2008). Functional evolutionary history of the mouse Fgf gene family. Developmental Dynamics, pp. 18–27.

Itoh,N. (2010). Hormone-like (endocrine) Fgfs: their evolutionary history and roles in development, metabolism, and disease. Cell Tissue Res. 342, 1-11.

Itoh, N. and Ornitz, D. M. (2011). Fibroblast growth factors: From molecular evolution to roles in development, metabolism and disease. Journal of Biochemistry, pp. 121–130.

Iwata K, Ito K, Fukuzaki A, Inaki K and Haga T (1999) Dynamin and rab5 regulate GRK2-dependent internalization of dopamine D2 receptors. Eur J Biochem 263(2): 596-602.

Iwasaki K, Harada N, Sasaki K, Yamane S, Iida K, Suzuki K, Hamasaki A, Nasteska D, Shibue K, Joo E, Harada T, Hashimoto T, Asakawa Y, Hirasawa A, Inagaki N. (2015). Free Fatty Acid Receptor GPR120 Is Highly Expressed in Enteroendocrine K Cells of the Upper Small Intestine and Has a Critical Role in Gip Secretion after Fat Ingestion. Endocrinology, 156, 837−846.

Izumiya Y., Bina H.A., Ouchi N., Akasaki Y., Kharitonenkov A., and Walsh K. (2008). GF21 is an Aktregulated myokine. FEBS Lett. 582, 3805-3810.

J

Jaworski K, Sarkadi-Nagy E, Duncan RE, Ahmadian M, Sul HS. (2007). Regulation of triglyceride metabolism. IV. Hormonal regulation of lipolysis in adipose tissue. Am J Physiol Gastrointest Liver Physiol 293:G1–G4.

Johnson D.E., Lu J., Chen H., Werner S., and Williams L.T. (1991). The human fibroblast growth factor receptor genes: a common structural arrangement underlies the mechanisms for generating receptor forms that differ in their third immunoglobulin domain. Mol. Cell Biol. 11, 4627-4634.

Johnson, P. F. (2005). Molecular stop signs: regulation of cell-cycle arrest by C/EBP transcription factors. J Cell Sci 118, 2545-2555.

K

Kajimura S, Seale P, Kubota K, Lunsford E, Frangioni JV, Gygi SP, Spiegelman BM. (2009). Initiation of myoblast to brown fat switch by a PRDM16-C/EBP-beta transcriptional complex. Nature 460, 1154-1158.

Kajimura, S., Seale, P. & Spiegelman, B. M. (2010).Transcriptional control of brown fat development. Cell Metab 11, 257-262

Kanazawa A, Tsukada S, Kamiyama M, Yanagimoto T, Nakajima M, Maeda S. (2005). Wnt5b partially inhibits canonical Wnt/beta-catenin signaling pathway and promotes adipogenesis in 3T3-L1 preadipocytes. Biochem Biophys Res Commun 330, 505-510.

Kang DS, Kern RC, Puthenveedu MA, von Zastrow M, Williams JC and Benovic JL (2009) Structure of an arrestin2-clathrin complex reveals a novel clathrin binding domain that modulates receptor trafficking. J Biol Chem 284(43): 29860-29872.

Karnik SS, Gogonea C, Patil S, Saad Y, Takezako T. (2003). Activation of G-protein-coupled receptors: a common molecular mechanism. Trends Endocrinol Metab.; 14(9):431-7.

Katritch V, Cherezov V, Stevens RC. (2013). Structure-function of the G protein-coupled receptor superfamily. Annu Rev Pharmacol Toxicol.; 53: 531-56.

Kawada T. (2018). Food-derived regulatory factors against obesity and metabolic syndrome. Biosci Biotechnol Biochem.: 1-7.

Kenakin T (2001) Inverse, protean, and ligand-selective agonism: matters of receptor conformation. FASEB J 15(3): 598-611.

Kersten, S. (2001). Mechanisms of nutritional and hormonal regulation of lipogenesis. EMBO Reports, pp. 282–286.

Kharitonenkov A., Shiyanova T.L., Koester A., Ford A.M., Micanovic R., Galbreath E.J., Sandusky G.E., Hammond L.J., Moyers J.S., Owens R.A., Gromada J., Brozinick J.T., Hawkins E.D., Wroblewski V.J., Li D.S., Mehrbod F., Jaskunas S.R., and Shanafelt A.B. (2005). FGF-21 as a novel metabolic regulator. J. Clin. Invest. 115, 1627-1635.

Kharitonenkov,A., Wroblewski,V.J., Koester,A., Chen,Y.F., Clutinger,C.K., Tigno,X.T., Hansen,B.C., Shanafelt,A.B., and Etgen,G.J. (2007). The metabolic state of diabetic monkeys is regulated by fibroblast growth factor-21. Endocrinology 148, 774-781 .

Kharitonenkov A., Dunbar J.D., Bina H.A., Bright S., Moyers J.S., Zhang C., Ding L., Micanovic R., Mehrbod S.F., Knierman M.D., Hale J.E., Coskun T. and Shanafelt A.B. (2008). FGF 21/FGF-21 receptor interaction and activation is determined by betaKlotho. J. Cell Physiol. 215, 1-7.

Kharitonenkov,A. and Larsen,P. (2011). FGF21 reloaded: challenges of a rapidly growing field. Trends Endocrinol. Metab. 22 , 81-86.

Kharitonenkov A, DiMarchi R. (2015). FGF21 Revolutions: Recent Advances Illuminating FGF21 Biology and Medicinal Properties. Trends Endocrinol Metab.; 26(11): 608-617.

Kim, J. B. & Spiegelman, B. M. (1996).ADD1/SREBP1 promotes adipocyte differentiation and gene expression linked to fatty acid metabolism. Genes Dev 10, 1096-1107.

Kim KH, Jeong YT, Oh H, Kim SH, Cho JM, Kim YN, Kim SS, Kim DH, Hur KY, Kim HK, Ko T, Han J, Kim HL, Kim J, Back SH, Komatsu M, Chen H, Chan DC, Konishi M, Itoh N, Choi CS, Lee MS. (2013). Autophagy deficiency leads to protection from obesity and insulin resistance by inducing Fgf21 as a mitokine. Nat Med.; 19(1): 83-92.

Kim J, Okla M, Erickson A, Carr T, Natarajan SK, Chung S. (2016). Eicosapentaenoic Acid Potentiates Brown Thermogenesis through FFAR4-dependent Up-regulation of miR-30b and miR-378. J Biol Chem.; 291(39):20551-62.

Klepac K, Kilić A, Gnad T, Brown LM, Herrmann B, Wilderman A, Balkow A, Glöde A, Simon K, Lidell ME, Betz MJ, Enerbäck S, Wess J, Freichel M, Blüher M, König G, Kostenis E, Insel PA, Pfeifer A. (2016). The Gq signalling pathway inhibits brown and beige adipose tissue. Nat Commun.; 7: 10895.

Kochman K. (2014). Superfamily of G-protein coupled receptors (GPCRs)—extraordinary and outstanding success of evolution. Postepy Hig Med Dosw; 68: 1225-37.

Kong G, Penn R and Benovic JL (1994) A beta-adrenergic receptor kinase dominant negative mutant attenuates desensitization of the beta 2-adrenergic receptor. J Biol Chem 269(18): 13084-13087.

Konkar, A. A., Zhai, Y. & Granneman, J. G. (2000). beta1-adrenergic receptors mediate beta3-adrenergicindependent effects of CGP 12177 in brown adipose tissue. Mol Pharmacol 57, 252-258.

Krauss, S., Zhang, C.-Y. and Lowell, B. B. (2005). The mitochondrial uncoupling-protein homologues. Nature Reviews Molecular Cell Biology, 6(3), pp.

Krilov L, Nguyen A, Miyazaki T, Unson CG, Williams R, Lee NH, Ceryak S and Bouscarel B. (2011). Dual mode of glucagon receptor internalization: role of PKC alpha, GRKs and betaarrestins. Exp Cell Res 317(20): 2981-2994.

Kruse AC, Hu J, Pan AC, Arlow DH, Rosenbaum DM, Rosemond E, Green HF, Liu T, Chae PS, Dror RO, Shaw DE, Weis WI, Wess J and Kobilka BK. (2012). Structure and dynamics of the M3 muscarinic acetylcholine receptor. Nature 482(7386): 552-556.

Kubota N, Terauchi Y, Kubota T, Kumagai H, Itoh S, Satoh H, Yano W, Ogata H, Tokuyama K, Takamoto I, Mineyama T, Ishikawa M, Moroi M, Sugi K, Yamauchi T, Ueki K, Tobe K, Noda T, Nagai R, Kadowaki T. (2006). Pioglitazone ameliorates insulin resistance and diabetes by both adiponectin-dependent and -independent pathways. J Biol Chem.; 281(13): 8748-55.

Kuda O, Rossmeisl M, Kopecky J. (2018). Omega-3 fatty acids and adipose tissue biology. Mol Aspects Med. pii: S0098-2997(17)30162-0. Review.

Kurosu H, Choi M, Ogawa Y, Dickson AS, Goetz R, Eliseenkova AV, Mohammadi M, Rosenblatt KP, Kliewer SA, Kuro-o M. (2007). Tissue-specific expression of betaKlotho and fibroblast growth factor (FGF) receptor isoforms determines metabolic activity of FGF19 and FGF21. J. Biol. Chem. 282, 26687–26695.

Kyrou I, Weickert MO, Gharanei S, Randeva HS, Tan BK. (2017). Fibroblast growth factors: new insights, new targets in the management of diabetes. Minerva Endocrinol.; 42(3): 248-270.

L

Lagerstrom MC, Schioth HB. (2008). Structural diversity ofGprotein-coupled receptors and significance for drug discovery. Nat. Rev. Drug Discov. 7:339–57.

Lee, Y. H., Petkova, A. P., Mottillo, E. P. and Granneman, J. G. (2012a). In vivo identification of bipotential adipocyte progenitors recruited by β3- adrenoceptor activation and high-fat feeding. Cell Metabolism, 15(4), pp. 480–491.

Lee,S.A., Jeong,E., Kim,E.H., Shin,M.S., Hwang,J.Y., Koh,E.H., Lee,W.J., Park,J.Y., and Kim,M.S. (2012b). Various oscillation patterns of serum fibroblast growth factor 21 concentrations in healthy volunteers. Diabetes Metab J. 36, 29-36.

Lee P, Linderman J, Smith S, Brychta RJ, Perron R, Idelson C, Werner CD, Chen KY, Celi FS. (2013). Fibroblast growth factor 21 (FGF21) and bone: is there a relationship in humans? Osteoporos Int.; 24(12): 3053-7.

Lefterova, M. I. & Lazar, M. A. (2009). New developments in adipogenesis. Trends Endocrinol Metab 20, 107-114.

Li, X.; Yu, Y.; Funk, C. D. (2013). Cyclooxygenase-2 Induction in Macrophages Is Modulated by Docosahexaenoic Acid Via Interactions with Free Fatty Acid Receptor 4 (FFA4). FASEB J., 27, 4987− 4997.

Li X, Wang C, Xiao J, McKeehan WL, Wang F. (2016). Fibroblast growth factors, old kids on the new block. Semin Cell Dev Biol.; 53: 155-67.

Liang Q, Zhong L, Zhang J, Wang Y, Bornstein SR, Triggle CR, Ding H, Lam KS, Xu A. (2014). FGF21 maintains glucose homeostasis by mediating the cross talk between liver and brain during prolonged fasting. Diabetes.; 63(12): 4064-75.

Lichtenbelt, W., Kingma, B., van der Lans, A. & Schellen, L. (2014). Cold exposure--an approach to increasing energy expenditure in humans. Trends Endocrinol Metab 25, 165-167.

Lin Z., Tian,H., Lam K.S., Lin S., Hoo R.C., Konishi M., Itoh N., Wang Y., Bornstein S.R., Xu A., and Li X. (2013). Adiponectin mediates the metabolic effects of FGF21 on glucose homeostasis and insulin sensitivity in mice. Cell Metab. 17, 779-789.

Lindegaard B, Hvid T, Grøndahl T, Frosig C, Gerstoft J, Hojman P, Pedersen BK. (2013). Expression of fibroblast growth factor-21 in muscle is associated with lipodystrophy, insulin resistance and lipid disturbances in patients with HIV. PLoS One.; 8(3): e55632.

Liou, A. P.; Lu, X.; Sei, Y.; Zhao, X.; Pechhold, S.; Carrero, R. J.; Raybould, H. E.; Wank, S. (2011). The G-Protein-Coupled Receptor GPR40 Directly Mediates Long-Chain Fatty Acid-Induced Secretion of Cholecystokinin. Gastroenterology, 140, 903−912.

Litosch I (2012) Negative feedback regulation of Gq signaling by protein kinase C is disrupted by diacylglycerol kinase zeta in COS-7 cells. Biochem Biophys Res Commun 417(3): 956-960.

Liu, J., DeYoung, S. M., Zhang, M., Cheng, A., Saltiel, A. R. (2005). Changes in integrin expression during adipocyte differentiation. Cell Metab 2, 165-177.

Liu SQ, Wu YH. (2010). Liver cell-mediated alleviation of acute ischemic myocardial injury. Front Biosci (Elite Ed) 2:711–24.

Liu S.Q., Tefft B.J., Zhang D., Roberts D., Schuster D.J., and Wu A. (2011). Cardioprotective mechanisms activated in response to myocardial ischemia. Mol. Cell Biomech. 8, 319-338.

Liu, D.; Wang, L.; Meng, Q.; Kuang, H.; Liu, X. (2012). G-Protein Coupled Receptor 120 Is Involved in Glucose Metabolism in Fat Cells. Cell. Mol. Biol. (Noisy-le-grand) 2012, No. Suppl 58, OL1757−1762.

Liu SQ, Roberts D, Kharitonenkov A, Zhang B, Hanson SM, Li YC, Zhang LQ, Wu YH. (2013). Endocrine protection of ischemic myocardium by FGF21 from the liver and adipose tissue. Sci Rep.; 3: 2767.

Liu, Y.; Chen, L. Y.; Sokolowska, M.; Eberlein, M.; Alsaaty, S.; Martinez-Anton, A.; Logun, C.; Qi, H. Y.; Shelhamer, J. H. (2014). The Fish Oil Ingredient, Docosahexaenoic Acid, Activates Cytosolic Phospholipase a (2) Via GPR120 Receptor to Produce Prostaglandin E(2) and Plays an Anti-Inflammatory Role in Macrophages. Immunology, 143, 81−95.

Liu, Z.; Hopkins, M. M.; Zhang, Z. H.; Quisenberry, C. B.; Fix, L. C.; Galvan, B. M.; Meier, K. E. (2015). Omega-3 Fatty Acids and Other FFA4 Agonists Inhibit Growth Factor Signaling in Human Prostate Cancer Cells. J. Pharmacol. Exp. Ther., 352, 380−394.

Long YC, Kharitonenkov A. (2011). Hormone-like fibroblast growth factors and metabolic regulation. Biochim Biophys Acta.; 1812(7): 791-5.

López M, Varela L, Vázquez MJ, Rodríguez-Cuenca S, González CR, Velagapudi VR, Morgan DA, Schoenmakers E, Agassandian K, Lage R, Martínez de Morentin PB, Tovar S, Nogueiras R, Carling D, Lelliott C, Gallego R, Oresic M, Chatterjee K, Saha AK, Rahmouni K, Diéguez C, Vidal-Puig A. (2010). Hypothalamic AMPK and fatty acid metabolism mediate thyroid regulation of energy balance. Nat Med 16, 1001-1008.

Lu, X.; Zhao, X.; Feng, J.; Liou, A. P.; Anthony, S.; Pechhold, S.; Sun, Y.; Lu, H.; Wank, S. (2012). Postprandial Inhibition of Gastric Ghrelin Secretion by Long-Chain Fatty Acid through GPR120 in Isolated Gastric Ghrelin Cells and Mice. Am. J. Physiol. Gastrointest. Liver Physiol., 303, G367−376.

Lu M, Wu B. (2016) Structural studies of G protein-coupled receptors. IUBMB Life.; 68(11):894-903.

Lundåsen, T., Hunt, M. C., Nilsson, L. M., Sanyal, S., Angelin, B., Alexson, S. E. H. and Rudling, M. (2007). PPARα is a key regulator of hepatic FGF21. Biochemical and Biophysical Research Communications, 360(2), pp. 437–440.

M

Maddaluno L, Urwyler C, Werner S. (2017). Fibroblast growth factors: key players in regeneration and tissue repair. Development.; 144(22): 4047-4060.

Madsen L, Pedersen LM, Lillefosse HH, Fjaere E, Bronstad I, Hao Q, Petersen RK, Hallenborg P, Ma T, De Matteis R, Araujo P, Mercader J, Bonet ML, Hansen JB, Cannon B, Nedergaard J, Wang J, Cinti S, Voshol P, Døskeland SO, Kristiansen K. (2010). UCP1 induction during recruitment of brown adipocytes in white adipose tissue is dependent on cyclooxygenase activity. PLoS One 5, e11391.

Mai K, Andres J, Biedasek K, Weicht J, Bobbert T, Sabath M, Meinus S, Reinecke F, Möhlig M, Weickert MO, Clemenz M, Pfeiffer AF, Kintscher U, Spuler S, Spranger J. (2009). Free fatty acids link metabolism and regulation of the insulin-sensitizing fibroblast growth factor-21. Diabetes. 2009 Jul; 58(7): 1532-8.

Malik VS, Willett WC, Hu FB. (2013). Global obesity: trends, risk factors and policy implications. Nat Rev Endocrinol.; 9(1): 13-27.

Manglik A, Kruse AC. (2017). Structural Basis for G Protein-Coupled Receptor Activation. Biochemistry; 56 (42): 5628-5634.

Marion S, Oakley RH, Kim KM, Caron MG and Barak LS. (2006). A beta-arrestin binding determinant common to the second intracellular loops of rhodopsin family G protein-coupled receptors. J Biol Chem 281(5): 2932-2938.

Markan, K. R., Naber, M. C., Ameka, M. K., Anderegg, M. D., Mangelsdorf, D. J., Kliewer, S. A., Mohammadi, M. and Potthoff, M. J. (2014). Circulating FGF21 Is Liver Derived and Enhances Glucose Uptake During Refeeding and Overfeeding. Diabetes; 63(12); pp. 4057–4063.

Marlatt KL, Ravussin E. (2002). Brown Adipose Tissue: an Update on Recent Findings. Curr Obes Rep. 2017 Dec;6(4):389-396.

Mason I. (2007). Initiation to end point: the multiple roles of fibroblast growth factors in neural development. Nat Rev Neurosci.; 8(8): 583-96. Review.

Matsuda, L. A., S. J. Lolait, M. J. Brownstein, A. C. Young, and T. I. Bonner. (1990). Structure of a cannabinoid receptor and functional expression of the cloned cDNA. Nature. 346: 561–564.

Maurizi G, Petäistö T, Maurizi A, Della Guardia L. (2018). Key-genes regulating the liposecretion process of mature adipocytes. J Cell Physiol; 233(5): 3784-3793.

Meigal, A. (2002). Gross and fine neuromuscular performance at cold shivering. Int J Circumpolar Health 61, 163-172.

Micanovic, R., Raches, D. W., Dunbar, J. D., Driver, D. A., Bina, H. A., Dickinson, C. D., & Kharitonenkov, A. (2009). Different roles of N- and C- termini in the functional activity of FGF21. Journal of Cellular Physiology, 219(2), 227–234.

Michalik L, Auwerx J, Berger JP, Chatterjee VK, Glass CK, Gonzalez FJ, Grimaldi PA, Kadowaki T, Lazar MA, O'Rahilly S, Palmer CN, Plutzky J, Reddy JK, Spiegelman BM, Staels B and Wahli W. (2006). International Union of Pharmacology. LXI. Peroxisome proliferatoractivated receptors. Pharmacol Rev 58(4): 726-741.

Miehle, K., Ebert, T., Kralisch, S., Hoffmann, A., Kratzsch, J., Schlögl, H., Stumvoll, M. and Fasshauer, M. (2016). Serum concentrations of fibroblast growth factor 21 are elevated in patients with congenital or acquired lipodystrophy. Cytokine, 83, pp. 239–244.

Mielenz M. (2017). Invited review: nutrient-sensing receptors for free fatty acids and hydroxycarboxylic acids in farm animals. Animal.; 11(6): 1008-1016.

Miller GM. (2011). The emerging role of trace amine-associated receptor 1 in the functional regulation of monoamine transporters and dopaminergic activity. J Neurochem.; 116(2):164-76.

Milligan G, Shimpukade B, Ulven T, Hudson BD. (2017). Complex Pharmacology of Free Fatty Acid Receptors. Chem Rev.; 117(1): 67-110.

Minard AY, Tan SX, Yang P, Fazakerley DJ, Domanova W, Parker BL, Humphrey SJ, Jothi R, Stöckli J, James DE. (2016). mTORC1 is a Major Regulatory Node in the FGF21 Signaling Network in Adipocytes. Cell Rep.; 17(1): 29-36.

Miyamoto J, Hasegawa S, Kasubuchi M, Ichimura A, Nakajima A, and Kimura I. (2016) Nutritional Signaling via Free Fatty Acid Receptors. Int J Mol Sci 17: 450.

Miyauchi, S.; Hirasawa, A.; Iga, T.; Liu, N.; Itsubo, C.; Sadakane, K.; Hara, T.; Tsujimoto, G. (2009). Distribution and Regulation of Protein Expression of the Free Fatty Acid Receptor GPR120. Naunyn- Schmiedeberg's Arch. Pharmacol., 379, 427−434.

Montiel M, Quesada J and Jimenez E (2004) Activation of second messenger-dependent protein kinases induces muscarinic acetylcholine receptor desensitization in rat thyroid epithelial cells. Mol Cell Endocrinol 223(1-2): 35-41.

Moore, K.; Zhang, Q.; Murgolo, N.; Hosted, T.; Duffy, R. (2009). Cloning, Expression, and Pharmacological Characterization of the GPR120 Free Fatty Acid Receptor from Cynomolgus Monkey: Comparison with Human GPR120 Splice Variants. Comp. Biochem. Physiol., Part B: Biochem. Mol. Biol., 154, 419−426.

Morales-Villegas E. (2006). Síndrome X vs síndrome metabólico: Entendiendo sus coincidencias y sus diferencias hacia una “nueva cardiología”. Archivos de Cardiología de México. 76: 173-188.

Moreno-Navarrete JM, Fernández-Real JM. (2012). Adipocyte Differentiation. Adipose Tissue Biology. Springer. New York, NY. Pp. 17-33.

Moreno-Navarrete JM, Escoté X, Ortega F, Camps M, Ricart W, Zorzano A, Vendrell J, Vidal-Puig A, Fernández-Real JM. (2015). Lipopolysaccharide binding protein is an adipokine involved in the resilience of the mouse adipocyte to inflammation. Diabetologia.; 58(10): 2424-34.

Morgensztern D and McLeod HL (2005) PI3K/Akt/mTOR pathway as a target for cancer therapy. Anticancer Drugs 16(8): 797-803.

Morrison SF, Madden CJ, Tupone D. (2012). Central control of brown adipose tissue thermogenesis. Front Endocrinol (Lausanne). 2012 Jan 24;3(5).

Morrison SF, Madden CJ, Tupone D. (2014). Central neural regulation of brown adipose tissue thermogenesis and energy expenditure. Cell Metab.; 19(5): 741-756.

Morrison SF. (2016). Central control of body temperature. F1000Res.; 5. pii: F1000 Faculty Rev-880.

Morroni M, Giordano A, Zingaretti MC, Boiani R, De Matteis R, Kahn BB, Nisoli E, Tonello C, Pisoschi C, Luchetti MM, Marelli M, Cinti S. (2004). Reversible transdifferentiation of secretory epithelial cells into adipocytes in the mammary gland. Proc Natl Acad Sci U S A 101, 16801-16806.

Mottillo EP, Bloch AE, Leff T, Granneman JG. (2012). Lipolytic products activate peroxisome proliferator-activated receptor (PPAR) α and δ in brown adipocytes to match fatty acid oxidation with supply. J Biol Chem.; 287(30): 25038-48.

Moure R, Domingo P, Villarroya J, Gasa L, Gallego-Escuredo JM, Quesada-López T, Morón-Ros S, Maroto AF, Mateo GM, Domingo JC, Villarroya F, Giralt M. (2018). Reciprocal effects of antiretroviral drugs used to treat HIV infection on the fibroblast growth factor-21/β-Klotho system. Antimicrob Agents Chemother. pii: AAC.00029-18.

Mozaffarian D, Wu JH. (2011). Omega-3 fatty acids and cardiovascular disease: effects on risk factors, molecular pathways, and clinical events. J Am Coll Cardiol.; 58(20):2047-67.

Muise ES, Azzolina B, Kuo DW, El-Sherbeini M, Tan Y, Yuan X, Mu J, Thompson JR, Berger JP, Wong KK. (2008). Adipose fibroblast growth factor 21 is up-regulated by peroxisome proliferator-activated receptor gamma and altered metabolic states. Mol Pharmacol.; 74(2): 403-12.

Murovets VO, Bachmanov AA, Zolotarev VA. (2015). Impaired Glucose Metabolism in Mice Lacking the Tas1r3 Taste Receptor Gene. PLoS One.; 10(6):e0130997.

N

Nakajima, I., Yamaguchi, T., Ozutsumi, K., Aso, H. (1998).Adipose tissue extracellular matrix: newly organized by adipocytes during differentiation. Differentiation 63, 193-200.

Nawrocki AR, Rajala MW, Tomas E, Pajvani UB, Saha AK, Trumbauer ME, Pang Z, Chen AS, Ruderman NB, Chen H, Rossetti L, Scherer PE. (2006). Mice lacking adiponectin show decreased hepatic insulin sensitivity and reduced responsiveness to peroxisome proliferator-activated receptor gamma agonists. J Biol Chem.; 281(5): 2654-60.

NCD Risk Factor Collaboration (NCD-RisC). (2017). Worldwide trends in body-mass index, underweight, overweight, and obesity from 1975 to 2016: a pooled analysis of 2416 population-based measurement studies in 128·9 million children, adolescents, and adults. Lancet; 390 (10113): 2627-2642.

Nedergaard J, Golozoubova V, Matthias A, Asadi A, Jacobsson A, Cannon B. (2001). UCP1: the only protein able to mediate adaptive non-shivering thermogenesis and metabolic inefficiency. Biochim Biophys Acta.; 1504(1):82-106.

Nedergaard, J., Petrovic, N., Lindgren, E. M., Jacobsson, A. & Cannon, B. (2005). PPARgamma in the control of brown adipocyte differentiation. Biochim Biophys Acta 1740, 293-304.

Nedergaard, J., Bengtsson, T. and Cannon, B. (2007) 'Unexpected evidence for active brown adipose tissue in adult humans.', American journal of physiology. Endocrinology and metabolism, 293(2), pp. E444-52.

Neumann RO (1902). Experimental contributions to the science of human daily nutritional needs with particular regard to the necessary amount of protein (author's experiments). Arch Hyg Bakteriol 45:69–78.

Nicholls DG, Locke RM. (1984). Thermogenic mechanisms in brown fat. Physiol Rev 64:1–64

Nishimura,T., Nakatake,Y., Konishi,M., and Itoh,N. (2000). Identification of a novel FGF, FGF-21, preferentially expressed in the liver. Biochim. Biophys. Acta 1492, 203-206.

Nowak JZ. (2009). Wielonienasycone kwasy tłuszczowe omega-3: aspekty biochemiczne, funkcjonalne i praktyczne. Farmakoter Psychiatr Neurol, 3–4, 127–146.

Nygaard R, Frimurer TM, Holst B, Rosenkilde MM and Schwartz TW. (2009). Ligand binding and micro-switches in 7TM receptor structures. Trends Pharmacol Sci 30(5): 249-259.

O

Oakley RH, Laporte SA, Holt JA, Caron MG and Barak LS (2000) Differential affinities of visual arrestin, beta arrestin1, and beta arrestin2 for G protein-coupled receptors delineate two major classes of receptors. J Biol Chem 275(22): 17201-17210.

Obinata H, Hattori T, Nakane S, Tatei K, Izumi T. (2005). Identification of 9-hydroxyoctadecadienoic acid and other oxidized free fatty acids as ligands of the G protein-coupled receptor G2A. J Biol Chem.; 280(49): 40676-83.

O'Connor, C. M. & Adams, J. U. (2012) Essentials of Cell Biology. Cambridge, MA: NPG Education.

Odegaard JI, Lee MW, Sogawa Y, Bertholet AM, Locksley RM, Weinberg DE, Kirichok Y, Deo RC, Chawla A. (2016). Perinatal Licensing of Thermogenesis by IL-33 and ST2. Cell.; 166(4):841-854.

Ogawa Y, Kurosu H, Yamamoto M, Nandi A, Rosenblatt KP, Goetz R, Eliseenkova AV, Mohammadi M, Kuro-o M. (2007). Beta Klotho is required for metabolic activity of fibroblast growth factor 21. Proc Natl Acad Sci U S A.; 104(18): 7432-7.

Oh, D. Y.; Talukdar, S.; Bae, E. J.; Imamura, T.; Morinaga, H.; Fan, W.; Li, P.; Lu, W. J.; Watkins, S. M.; Olefsky, J. M. (2010). GPR120 Is an Omega-3 Fatty Acid Receptor Mediating Potent Anti-Inflammatory and Insulin-Sensitizing Effects. Cell., 142, 687–698.

Oh DY, Walenta E, Akiyama TE, Lagakos WS, Lackey D, Pessentheiner AR, Sasik R, Hah N, Chi TJ, Cox JM, Powels MA, Di Salvo J, Sinz C, Watkins SM, Armando AM, Chung H, Evans RM, Quehenberger O, McNelis J, Bogner-Strauss JG, Olefsky JM. (2014). A Gpr120-selective agonist improves insulin resistance and chronic inflammation in obese mice. Nat Med.; 20(8): 942-7.

Olaiz-Fernández G, Rivera-Dommarco J, Shamah-Levy T, Rojas R, Villalpando-Hernández S, Hernández-Avila M, Sepúlveda-Amor J. (2012). Encuesta Nacional de Salud y Nutrición. Cuernavaca, México: Instituto Nacional de Salud Pública. Pp. 85-102.

Oldham WM, Hamm HE. (2008). Heterotrimeric G protein activation by G-protein-coupled receptors. Nat Rev Mol Cell Biol.; 9(1):60-71. Review.

O'Sullivan C, Dev KK. (2013). The structure and function of the S1P1 receptor. Trends Pharmacol Sci.; 34(7):401-12.

Ornitz, D. M. and Itoh, N. (2001) 'Protein family review Fibroblast growth factors Gene organization and evolutionary history', Genome Biology, 2(reviews), pp. 1–12.

Ornitz, D. M. and Itoh, N. (2015). The Fibroblast Growth Factor signaling pathway. Wiley Interdiscip. Rev. Dev. Biol. 4, 215-266.

Ortiz-Dominguez ME. (2008). NORMA Oficial Mexicana NOM-008-SSA3-2010, Para el tratamiento integral del sobrepeso y la obesidad. Diario Oficial de la Federación, 08 de diciembre de 2008.

Oulion, S., Bertrand, S. and Escriva, H. (2012). Evolution of the FGF gene family. Int. J. Evol. Biol., 298147.

Ovchinnikov DA. (2008). Macrophages in the embryo and beyond: much more than just giant phagocytes. Genesis.; 46(9): 447-62.

Owen BM, Bookout AL, Ding X, Lin VY, Atkin SD, Gautron L, Kliewer SA, Mangelsdorf DJ. (2013). FGF21 contributes to neuroendocrine control of female reproduction. Nat Med.; 19(9): 1153-6.

Owen, B. M., Ding, X., Morgan, D. A., Coate, K. C., Bookout, A. L., Rahmouni, K., Kliewer, S. A. and Mangelsdorf, D. J. (2014). FGF21 acts centrally to induce sympathetic nerve activity, energy expenditure, and weight loss. Cell Metabolism, 20(4), pp. 670–677.

Owen, B. M., Mangelsdorf, D. J. and Kliewer, S. A. (2015) 'Tissue-specific actions of the metabolic hormones FGF15/19 and FGF21.', Trends in endocrinology and metabolism: TEM, 26(1), pp. 22–9.

P

Pahlavani M, Razafimanjato F, Ramalingam L, Kalupahana NS, Moussa H, Scoggin S, Moustaid-Moussa N. (2017). Eicosapentaenoic acid regulates brown adipose tissue metabolism in high-fat-fed mice and in clonal brown adipocytes. J Nutr Biochem.; 39: 101-109.

Park JH, Scheerer P, Hofmann KP, Choe HW and Ernst OP (2008) Crystal structure of the ligand-free G-protein-coupled receptor opsin. Nature 454(7201): 183-187.

Patel AB, Crocker E, Reeves PJ, Getmanova EV, Eilers M, Khorana HG and Smith SO (2005) Changes in interhelical hydrogen bonding upon rhodopsin activation. J Mol Biol 347(4): 803-812.

Paulsen, S. J.; Larsen, L. K.; Hansen, G.; Chelur, S.; Larsen, P. J.; Vrang, N. (2014). Expression of the Fatty Acid Receptor GPR120 in the Gut of Diet-Induced-Obese Rats and Its Role in GLP-1 Secretion. PLoS One, 9, e88227.

Petrovic N, Walden TB, Shabalina IG, Timmons JA, Cannon B, Nedergaard J. (2010). Chronic peroxisome proliferator-activated receptor gamma (PPARgamma) activation of epididymally derived white adipocyte cultures reveals a population of thermogenically competent, UCP1-containing adipocytes molecularly distinct from classic brown adipocytes. J Biol Chem 285, 7153-7164.

Pierce KL, Premont RT, Lefkowitz RJ. (2002). Seven-transmembrane receptors. Nat Rev Mol Cell Biol.; 3(9): 639-50. Review.

Pin JP, Acher F. (2002). The metabotropic glutamate receptors: structure, activation mechanism and pharmacology. Curr Drug Targets CNS Neurol Disord.; 1(3):297-317.

Pippig S, Andexinger S and Lohse MJ (1995) Sequestration and recycling of beta 2-adrenergic receptors permit receptor resensitization. Mol Pharmacol 47(4): 666-676.

Pitcher JA, Payne ES, Csortos C, DePaoli-Roach AA and Lefkowitz RJ (1995) The G-protein coupled receptor phosphatase: a protein phosphatase type 2A with a distinct subcellular distribution and substrate specificity. Proc Natl Acad Sci U S A 92(18): 8343-8347.

Planavila A, Redondo I, Hondares E, Vinciguerra M, Munts C, Iglesias R, Gabrielli LA, Sitges M, Giralt M, van Bilsen M, Villarroya F. (2013). Fibroblast growth factor 21 protects against cardiac hypertrophy in mice. Nat Commun.; 4: 2019.

Planavila, A., Redondo-Angulo, I. and Villarroya, F. (2015a) 'FGF21 and Cardiac Physiopathology', Frontiers in Endocrinology, 6.

Planavila, A., Redondo-Angulo, I., Ribas, F., Garrabou, G., Casademont, J., Giralt, M. and Villarroya, F. (2015b). Fibroblast growth factor 21 protects the heart from oxidative stress. Cardiovascular Research, 106(1), pp. 19–31.

Popkin BM, Adair LS, Ng SW. (2012). Global nutrition transition and the pandemic of obesity in developing countries. Nutr Rev.; 70(1): 3-21.

Porta R, Borea R, Coelho A, Khan S, Araújo A, Reclusa P, Franchina T, Van Der Steen N, Van Dam P, Ferri J, Sirera R, Naing A, Hong D, Rolfo C. (2017). FGFR a promising druggable target in cancer: Molecular biology and new drugs. Crit Rev Oncol Hematol.; 113: 256-267.

Potthoff, M. J., Inagaki, T., Satapati, S., Ding, X., He, T., Goetz, R., Mohammadi, M., Finck, B. N., Mangelsdorf, D. J., Kliewer, S. A. and Burgess, S. C. (2009). FGF21 induces PGC-1alpha and regulates carbohydrate and fatty acid metabolism during the adaptive starvation response. Proc Natl Acad Sci U S A, 106(26), pp. 10853–10858.

Potthoff MJ, Kliewer SA, Mangelsdorf DJ. (2012). Endocrine fibroblast growth factors 15/19 and 21: from feast to famine. Genes Dev.; 26(4): 312-24.

Powers CJ, McLeskey SW, Wellstein A. (2000). Fibroblast growth factors, their receptors and signaling. Endocr Relat Cancer.; 7(3): 165-97. Review.

Puigserver P, Wu Z, Park CW, Graves R, Wright M, Spiegelman BM. (1998). A cold-inducible coactivator of nuclear receptors linked to adaptive thermogenesis. Cell 92, 829-839.

Pyörälä M, Miettinen H, Laakso M, Pyörälä K. (1998). Hyperinsulinemia predicts coronary heart disease risk in healthy middle-aged men: the 22-year follow-up results of the Helsinki Policemen Study. Circulation. ;98(5):398-404.

Q

Qiang L. and Accili D. (2012). FGF21 and the second coming of PPARgamma. Cell 148, 397-398.

R

Ramji DP, Foka P. (2002). CCAAT/enhancer-binding proteins: structure, function and regulation. Biochem J 365:561–575.

Rasmussen, A. T. (1923). The so-called hibernating gland. J. Morphol. 38, 147-205.

Recio C, Lucy D, Iveson P, Iqbal AJ, Valaris S, Wynne G, Russell AJ, Choudhury RP, O'Callaghan C, Monaco C, Greaves DR. (2018). The Role of Metabolite-Sensing G Protein-Coupled Receptors in Inflammation and Metabolic Disease. Antioxid Redox Signal. [Epub ahead of print]

Reinehr T., Woelfle J., Wunsch R., and Roth C.L. (2012). Fibroblast growth factor 21 (FGF-21) and its relation to obesity, metabolic syndrome, and nonalcoholic fatty liver in children: a longitudinal analysis. J. Clin. Endocrinol. Metab. 97, 2143-2150.

Ribas, F., Villarroya, J., Hondares, E., Giralt, M. and Villarroya, F. (2014). FGF21 expression and release in muscle cells: involvement of MyoD and regulation by mitochondria-driven signaling. Biochem J, 199, pp. 191–199.

Rodriguez-Pacheco F, Garcia-Serrano S, Garcia-Escobar E, Gutierrez-Repiso C, Garcia-Arnes J, Valdes S, Gonzalo M, Soriguer F, Moreno-Ruiz FJ, Rodriguez-Cañete A, Gallego-Perales JL, Martinez-Ferriz A, Rojo-Martínez G, Garcia-Fuentes E. (2014). Effects of Obesity/Fatty Acids on the Expression of GPR120. Mol. Nutr. Food Res., 58, 1852−1860.

Ronti T, Lupattelli G, Mannarino E. (2006). The endocrine function of adipose tissue: an update. Clin Endocrinol (Oxf); 64(4):355-65.

Rosell M, Hondares E, Iwamoto S, Gonzalez FJ, Wabitsch M, Staels B, Olmos Y, Monsalve M, Giralt M, Iglesias R, Villarroya F. (2012). Peroxisome proliferator-activated receptors-alpha and -gamma, and cAMP-mediated pathways, control retinol-binding protein-4 gene expression in brown adipose tissue. Endocrinology 153, 1162-1173.

Rosell M, Kaforou M, Frontini A, Okolo A, Chan YW, Nikolopoulou E, Millership S, Fenech ME, MacIntyre D, Turner JO, Moore JD, Blackburn E, Gullick WJ, Cinti S, Montana G, Parker MG, Christian M. (2014). Brown and white adipose tissues: intrinsic differences in gene expression and response to cold exposure in mice. Am J Physiol Endocrinol Metab; 306 (8):E945-64.

Rosen, E. D. & MacDougald, O. A. (2006). Adipocyte differentiation from the inside out. Nat Rev Mol Cell Biol 7, 885-896.

Rosen, E. D. & Spiegelman, B. M. (2014). What we talk about when we talk about fat. Cell 156, 20-44.

Rosenwald, M., Perdikari, A., Rulicke, T. & Wolfrum, C. (2013). Bi-directional interconversion of brite and white adipocytes. Nat Cell Biol 15, 659-667.

Rosenwald, M. and Wolfrum, C. (2014). The origin and definition of brite versus white and classical brown adipocytes. Adipocyte 3, 4-9.

Ross SE, Hemati N, Longo KA, Bennett CN, Lucas PC, Erickson RL, MacDougald OA. (2000). Inhibition of adipogenesis by Wnt signaling. Science 289, 950-953.

Rothwell, N. J., Stock, M. J. (1981)A role for insulin in the diet-induced thermogenesis of cafeteria-fed rats. Metabolism 30, 673-678.

S

Sa-Nguanmoo P, Chattipakorn N, Chattipakorn SC. (2016). Potential roles of fibroblast growth factor 21 in the brain. Metab Brain Dis.; 31(2): 239-48.

Saely CH, Geiger K, Drexel H. (2012).Brown versus white adipose tissue: a ini-review. Gerontology.;58(1):15-23.

Saito, M. et al. (2009). High incidence of metabolically active brown adipose tissue in healthy adult humans: effects of cold exposure and adiposity. Diabetes 58, 1526-1531.

Sam S. (2007).Obesity and Polycystic Ovary Syndrome. Obes Manag. 2007 Apr;3(2):69-73.

Samama P, Cotecchia S, Costa T and Lefkowitz RJ (1993) A mutation-induced activated state of the beta 2-adrenergic receptor. Extending the ternary complex model. J Biol Chem 268(7): 4625-4636.

Sanchez-Gurmaches, J. and Guertin, D. A. (2014). Adipocytes arise from multiple lineages that are heterogeneously and dynamically distributed. Nature Communications, 5.

Sanchez-Gurmaches, J., Hung, C. M., Sparks, C. A., Tang, Y., Li, H., Guertin, D. A. (2012). PTEN loss in the Myf5 lineage redistributes body fat and reveals subsets of white adipocytes that arise from Myf5 278 precursors. Cell Metabolism, 16(3), pp. 348–362.

Sarruf DA, Thaler JP, Morton GJ, German J, Fischer JD, Ogimoto K, Schwartz MW.(2010). Fibroblast growth factor 21 action in the brain increases energy expenditure and insulin sensitivity in obese rats. Diabetes.; 59(7): 1817-24.

Satapati S, Qian Y, Wu MS, Petrov A, Dai G, Wang SP, Zhu Y, Shen X, Muise ES, Chen Y, Zycband E, Weinglass A, Di Salvo J, Debenham JS, Cox JM, Lan P, Shah V, Previs SF, Erion M, Kelley DE, Wang L, Howard AD, Shang J. (2017). GPR120 suppresses adipose tissue lipolysis and synergizes with GPR40 in antidiabetic efficacy. J Lipid Res.; 58(8): 1561-1578.

Schilperoort M, van Dam AD, Hoeke G, Shabalina IG, Okolo A, Hanyaloglu AC, Dib LH, Mol IM, Caengprasath N, Chan YW, Damak S, Miller AR, Coskun T, Shimpukade B, Ulven T, Kooijman S, Rensen PC, Christian M. (2018). The GPR120 agonist TUG-891 promotes metabolic health by stimulating mitochondrial respiration in brown fat. EMBO Mol Med. pii: e8047.

Schiöth HB and Fredriksson R. (2004). The GRAFS classification system of G-protein coupled receptors in comparative perspective. Gen Comp Endocrinol; 142(1–2):94–101.

Schoenberg K.M., Giesy S.L., Harvatine K.J., Waldron M.R., Cheng C., Kharitonenkov A., and Boisclair Y.R. (2011). Plasma FGF21 is elevated by the intense lipid mobilization of lactation. Endocrinology 152, 4652-4661.

Sheikh SP, Vilardarga JP, Baranski TJ, Lichtarge O, Iiri T, Meng EC, Nissenson RA and Bourne HR. (1999). Similar structures and shared switch mechanisms of the beta2-adrenoceptor and the parathyroid hormone receptor. Zn(II) bridges between helices III and VI block activation. J Biol Chem 274(24): 17033-17041.

Shenoy SK and Lefkowitz RJ. (2003). Multifaceted roles of beta-arrestins in the regulation of seven-membrane-spanning receptor trafficking and signalling. Biochem J 375(Pt 3): 503-515.

Shenoy SK, Modi AS, Shukla AK, Xiao K, Berthouze M, Ahn S, Wilkinson KD, Miller WE and Lefkowitz RJ. (2009). Beta-arrestin-dependent signaling and trafficking of 7-transmembrane receptors is reciprocally regulated by the deubiquitinase USP33 and the E3 ligase Mdm2. Proc Natl Acad Sci U S A 106(16): 6650-6655.

Seale P, Kajimura S, Yang W, Chin S, Rohas LM, Uldry M, Tavernier G, Langin D, Spiegelman BM. (2007). Transcriptional control of brown fat determination by PRDM16. Cell Metab 6, 38-54.

Seale P, Bjork B, Yang W, Kajimura S, Chin S, Kuang S, Scimè A, Devarakonda S, Conroe HM, Erdjument-Bromage H, Tempst P, Rudnicki MA, Beier DR, Spiegelman BM. (2008). PRDM16 controls a brown fat/skeletal muscle switch. Nature 454, 961-967.

Seale P, Conroe HM, Estall J, Kajimura S, Frontini A, Ishibashi J, Cohen P, Cinti S, Spiegelman BM. (2011). Prdm16 determines the thermogenic program of subcutaneous white adipose tissue in mice. J Clin Invest 121, 96-105.

Senatorov IS, Moniri NH. (2018). The role of free-fatty acid receptor-4 (FFA4) in human cancers and cancer cell lines. Biochem Pharmacol.; 150: 170-180.

Shukla L, Morrison WA, Shayan R. (2015) Adipose-derived stem cells in radiotherapy injury: a new frontier. Front Surg.; 2: 1.

Simonds WF (1999) G protein regulation of adenylate cyclase. Trends Pharmacol Sci 20(2): 66-73.

Skillington, J., Choy, L. & Derynck, R. (2002).Bone morphogenetic protein and retinoic acid signaling cooperate to induce osteoblast differentiation of preadipocytes. J Cell Biol 159, 135-146.

Smas, C. M., Sul, H. S. (1993). Pref-1, a protein containing EGF-like repeats, inhibits adipocyte differentiation. Cell 73, 725-734.

Sottile, V., Seuwen, K. (2000).Bone morphogenetic protein-2 stimulates adipogenic differentiation of mesenchymal precursor cells in synergy with BRL 49653 (rosiglitazone). FEBS Lett 475, 201-204.

Spalding KL, Arner E, Westermark PO, Bernard S, Buchholz BA, Bergmann O, Blomqvist L, Hoffstedt J, Naslund E, Britton T, Concha H, Hassan M, Ryden M, Frisen J, Arner P. (2008). Dynamics of fat cell turnover in humans. Nature 453:783–787.

Stewart A, Huang J, Fisher RA. (2012). RGS Proteins in Heart: Brakes on the Vagus. Front Physiol.; 3:95.

Strable, M. S., Ntambi, J. M. (2010). Genetic control of de novo lipogenesis: role in diet-induced obesity. Crit Rev Biochem Mol Biol 45, 199-214.

Suckow, A. T.; Polidori, D.; Yan, W.; Chon, S.; Ma, J. Y.; Leonard, J.; Briscoe, C. P. (2014). Alteration of the Glucagon Axis in GPR120 (FFAR4) Knockout Mice a Role for GPR120 in Glucagon Secretion. J. Biol. Chem., 289, 15751−15763.

Symonds ME, Pope M, Budge H. (2015). The Ontogeny of Brown Adipose Tissue. Annu Rev Nutr.; 35: 295-320.

Sztalryd C, Xu G, Dorward H, Tansey JT, Contreras JA, Kimmel AR, Londos C. (2003). Perilipin A is essential for the translocation of hormone-sensitive lipase during lipolytic activation. J Cell Biol 161, 1093-1103.

T

Takada, I., Kouzmenko, A. P. and Kato, S. (2009). Wnt and PPARγ signaling in osteoblastogenesis and adipogenesis. Nature Reviews Rheumatology, 5(8), pp. 442–447.

Tamucci KA, Namwanje M, Fan L, Qiang L. (2018) The dark side of browning. Protein Cell.; 9(2):152-163.

Tan BK, Hallschmid M,Adya R,KernW, Lehnert H, Randeva HS. (2011). Fibroblast growth factor 21 (FGF21) in human cerebrospinal fluid: relationship with plasma FGF21 and body adiposity. Diabetes 60: 2758–2762.

Tan JK, McKenzie C, Mariño E, Macia L, Mackay CR. (2017). Metabolite-Sensing G Protein-Coupled Receptors-Facilitators of Diet-Related Immune Regulation. Annu Rev Immunol.; 35: 371-402.

Tanaka, T., Yoshida, N., Kishimoto, T. and Akira, S. (1997). Defective adipocyte differentiation in mice lacking the C/EBPbeta and/or C/EBPdelta gene. The EMBO journal, 16(24), pp. 7432–43.

Tanaka, T.; Yano, T.; Adachi, T.; Koshimizu, T. A.; Hirasawa, A.; Tsujimoto, G. (2008). Cloning and Characterization of the Rat Free Fatty Acid Receptor GPR120: In Vivo Effect of the Natural Ligand on GLP-1 Secretion and Proliferation of Pancreatic Beta Cells. Naunyn- Schmiedeberg's Arch. Pharmacol., 377, 515−522.

Tang, Q. Q., Zhang, J. W. & Daniel Lane, M. (2004). Sequential gene promoter interactions of C/EBPbeta, C/EBPalpha, and PPARgamma during adipogenesis. Biochem Biophys Res Commun 319, 235-239.

Tang XL, Wang Y, Li DL, Luo J, Liu MY. (2012) Orphan G protein-coupled receptors (GPCRs): biological functions and potential drug targets. Acta Pharmacol Sin.; 33(3):363-71.

Tang Y, Wallace M, Sanchez-Gurmaches J, Hsiao WY, Li H, Lee PL, Vernia S, Metallo CM, Guertin DA. (2016). Adipose tissue mTORC2 regulates ChREBP-driven de novo lipogenesis and hepatic glucose metabolism. Nat Commun.; 7: 11365.

Taube, A., Schlich, R., Sell, H., Eckardt, K. and Eckel, J. (2012). 'Inflammation and metabolic dysfunction: links to cardiovascular diseases', AJP: Heart and Circulatory Physiology, 302(11), pp. H2148–H2165.

Tchkonia T, Giorgadze N, Pirtskhalava T, Thomou T, DePonte M, Koo A, Forse RA, Chinnappan D, Martin-Ruiz C, von Zglinicki T, Kirkland JL. (2006). Fat depot-specific characteristics are retained in strains derived from single human preadipocytes. Diabetes; 55(9): 2571-8.

Terada, H. (1990). Uncouplers of oxidative phosphorylation. Environmental Health Perspectives, 87, 213–218.

Thonberg, H., Fredriksson, J. M., Nedergaard, J. & Cannon, B. (2002). A novel pathway for adrenergic stimulation of cAMP-response-element-binding protein (CREB) phosphorylation: mediation via alpha1- adrenoceptors and protein kinase C activation. Biochem J 364, 73-79.

Thorburn AN, Macia L, Mackay CR. (2014). Diet, metabolites, and "western-lifestyle" inflammatory diseases. Immunity.; 40(6):833-42.

Tiseo M, Gelsomino F, Alfieri R, Cavazzoni A, Bozzetti C, De Giorgi AM, Petronini PG, Ardizzoni A. (2015). FGFR as potential target in the treatment of squamous non small cell lung cancer. Cancer Treat Rev.; 41(6): 527-39.

Tong Q, Dalgin G, Xu H, Ting CN, Leiden JM, Hotamisligil GS. (2000). Function of GATA transcription factors in preadipocyte-adipocyte transition. Science 290, 134-138.

Tontonoz, P. and Spiegelman, B. M. (2008). Fat and Beyond: The Diverse Biology of PPARγ. Annual Review of Biochemistry, 77(1), pp. 289–312.

Trayhurn, P. (2007). Adipocyte biology. Obes Rev 8 Suppl 1, 41-44.

Trayhurn, P.; Denyer, G. (2012). Mining Microarray Datasets in Nutrition: Expression of the GPR120 (n-3 Fatty Acid Receptor/Sensor) Gene Is Down-Regulated in Human Adipocytes by Macrophage Secretions. J. Nutr. Sci., 1, e3.

Trowell A. and Willmer E.N. (1939). Studies on the Growth of Tissues in vitro. The Journal of Experimental Biology 16, 60-70.

Trueb B. (2011). Biology of FGFRL1, the fifth fibroblast growth factor receptor. Cell Mol Life Sci.; 68(6): 951-64.

Tseng YH, Kokkotou E, Schulz TJ, Huang TL, Winnay JN, Taniguchi CM, Tran TT, Suzuki R, Espinoza DO, Yamamoto Y, Ahrens MJ, Dudley AT, Norris AW, Kulkarni RN, Kahn CR. (2008). New role of bone morphogenetic protein 7 in brown adipogenesis and energy expenditure. Nature 454, 1000-1004.

Turturro A., Witt W.W., Lewis S., Hass B.S., Lipman R.D., and Hart R.W. (1999). Growth curves and survival characteristics of the animals used in the Biomarkers of Aging Program. J. Gerontol. A Biol. Sci. Med. Sci. 54, B492-B501.

Tyynismaa H, Carroll CJ, Raimundo N, Ahola-Erkkilä S, Wenz T, Ruhanen H, Guse K, Hemminki A, Peltola-Mjøsund KE, Tulkki V, Oresic M, Moraes CT, Pietiläinen K, Hovatta I, Suomalainen A. (2012). Mitochondrial myopathy induces a starvation-like response. Hum Mol Genet.; 19(20): 3948-58.

U

Uebanso T, Taketani Y, Yamamoto H, Amo K, Ominami H, Arai H, Takei Y, Masuda M, Tanimura A, Harada N, Yamanaka-Okumura H, Takeda E. (2011). Paradoxical regulation of human FGF21 by both fasting and feeding signals: is FGF21 a nutritional adaptation factor? PLoS One.; 6(8): e22976.

V

Vague J. (1956). The degree of masculine differentiation of obesities: a factor determining predisposition to diabetes, atherosclerosis, gout, and uric calculous disease. Am J Clin Nutr. 1956; 4:20–34.

Valenzuela R., Valenzuela A. (2013) Overview About Lipid Structure. Lipid Metabolism. Ch. 01. InTech. Rijeka. http://dx.doi.org/10.5772/52306

Valiquette M, Parent S, Loisel TP and Bouvier M (1995) Mutation of tyrosine-141 inhibits insulin-promoted tyrosine phosphorylation and increased responsiveness of the human beta 2-adrenergic receptor. EMBO J 14(22): 5542-5549.

Valle A, Oliver J, Roca P. (2010). Role of uncoupling proteins in cancer. Cancers (Basel).; 2(2): 567-91.

Vanderheyden V, Devogelaere B, Missiaen L, De Smedt H, Bultynck G and Parys JB (2009). Regulation of inositol 1,4,5-trisphosphate-induced Ca2+ release by reversible phosphorylation and dephosphorylation. Biochim Biophys Acta 1793(6): 959-970.

Vegiopoulos A, Müller-Decker K, Strzoda D, Schmitt I, Chichelnitskiy E, Ostertag A, Berriel Diaz M, Rozman J, Hrabe de Angelis M, Nüsing RM, Meyer CW, Wahli W, Klingenspor M, Herzig S. (2010). Cyclooxygenase-2 controls energy homeostasis in mice by de novo recruitment of brown adipocytes. Science 328, 1158-1161.

Véniant MM, Hale C, Helmering J, Chen MM, Stanislaus S, Busby J, Vonderfecht S, Xu J, Lloyd DJ. (2012). FGF21 promotes metabolic homeostasis via white adipose and leptin in mice. PLoS One.; 7(7): e40164.

Venkatakrishnan AJ, Deupi X, Lebon G, Tate CG, Schertler GF, Babu MM. (2013) Molecular signatures of G-protein-coupled receptors. Nature.;494(7436):185-94.

Ventura-Clapier R, Garnier A, Veksler V. (2008). Transcriptional control of mitochondrial biogenesis: the central role of PGC-1alpha. Cardiovasc Res.; 79(2): 208-17.

Vestmar MA, Andersson EA, Christensen CR, Hauge M, Glümer C, Linneberg A, Witte DR, Jørgensen ME, Christensen C, Brandslund I, Lauritzen T, Pedersen O, Holst B, Grarup N, Schwartz TW, Hansen T. (2016). Functional and genetic epidemiological characterisation

of the FFAR4 (GPR120) p.R270H variant in the Danish population. J Med Genet.; 53(9): 616-23.

Vienberg SG, Brøns C, Nilsson E, Astrup A, Vaag A, Andersen B. (2012). Impact of short-term high-fat feeding and insulin-stimulated FGF21 levels in subjects with low birth weight and controls. Eur J Endocrinol.; 167(1): 49-57.

Villarroya F, Iglesias R, Giralt M. (2007). PPARs in the Control of Uncoupling Proteins Gene Expression. PPAR Res.; 2007: 74364.

Villarroya J, Flachs P, Redondo-Angulo I, Giralt M, Medrikova D, Villarroya F, Kopecky J, Planavila A. (2014). Fibroblast growth factor-21 and the beneficial effects of long-chain n-3 polyunsaturated fatty acids. Lipids.; 49(11): 1081-9.

Villarroya J, Campderros L, Ribas-Aulinas F, Carrière A, Casteilla L, Giralt M, Villarroya F. (2018). Lactate induces expression and secretion of fibroblast growth factor-21 by muscle cells. Endocrine. [Epub ahead of print]

Virtanen, K. A., Lidell, M. E., Orava, J., Heglind, M., Westergren, R., Niemi, T., Taittonen, M., Laine, J., Savisto, N.-J., Enerbäck, S. and Nuutila, P. (2009). 'Functional brown adipose tissue in healthy adults.', The New England journal of medicine, 360(15), pp. 1518–25.

Vitali A, Murano I, Zingaretti MC, Frontini A, Ricquier D, Cinti S. (2012). The adipose organ of obesity-prone C57BL/6J mice is composed of mixed white and brown adipocytes. J Lipid Res 53, 619-629.

von Essen G, Lindsund E, Cannon B, Nedergaard J. (2017). Adaptive facultative diet-induced thermogenesis in wild-type but not in UCP1-ablated mice. Am J Physiol Endocrinol Metab.; 313(5): E515-E527.

W

Wang, F., Kan, M., Yan, G., Xu, J., & McKeehan, W. L. (1995). Alternately spliced NH2-terminal immunoglobulin-like Loop I in the ectodomain of the fibroblast growth factor (FGF) receptor 1 lowers affinity for both heparin and FGF-1. The Journal of Biological Chemistry, 270(17), 10231–5.

Wang Z, Gerstein M, Snyder M. (2009). RNA-Seq: a revolutionary tool for transcriptomics. Nat Rev Genet.; 10(1): 57-63.

Wang, H., Iakova, P., Wilde, M., Welm, A., Goode, T., Roesler, W. J., & Timchenko Wang, Q. A., Tao, C., Gupta, R. K. and Scherer, P. E. (2013). Tracking adipogenesis during white adipose tissue development, expansion and regeneration. Nature Medicine, 19(10), pp. 1338–1344.

Wang W, Qiao Y, Li Z. New Insights into Modes of GPCR Activation. (2018). Trends Pharmacol Sci.; 39(4):367-386.

Warne T, Serrano-Vega MJ, Baker JG, Moukhametzianov R, Edwards PC, Henderson R, Leslie AG, Tate CG and Schertler GF. (2008). Structure of a beta1-adrenergic G-proteincoupled receptor. Nature 454(7203): 486-491.

Watanabe M, Houten SM, Mataki C, Christoffolete MA, Kim BW, Sato H, Messaddeq N, Harney JW, Ezaki O, Kodama T, Schoonjans K, Bianco AC, Auwerx J. (2006). Bile acids induce energy expenditure by promoting intracellular thyroid hormone activation. Nature 439, 484-489.

Watson, S. J.; Brown, A. J. (2012). Holliday, N. D. Differential Signaling by Splice Variants of the Human Free Fatty Acid Receptor GPR120. Mol. Pharmacol., 81, 631−642.

Wei W, Dutchak PA, Wang X, Ding X, Wang X, Bookout AL, Goetz R, Mohammadi M, Gerard RD, Dechow PC, Mangelsdorf DJ, Kliewer SA, Wan Y. (2012) Fibroblast growth actor 21 promotes bone loss by potentiating the effects of peroxisome proliferator-activated receptor γ. Proc Natl Acad Sci U S A.; 109(8): 3143-8.

Wente W, Efanov AM, Brenner M, Kharitonenkov A, Köster A, Sandusky GE, Sewing S, Treinies I, Zitzer H, Gromada J. (2006). Fibroblast growth factor-21 improves pancreatic beta-cell function and survival by activation of extracellular signal-regulated kinase 1/2 and Akt signaling pathways. Diabetes.; 55(9): 2470-8.

Whittle AJ, Carobbio S, Martins L, Slawik M, Hondares E, Vázquez MJ, Morgan D, Csikasz RI, Gallego R, Rodriguez-Cuenca S, Dale M, Virtue S, Villarroya F, Cannon B, Rahmouni K, López M, Vidal-Puig A. (2012). BMP8B increases brown adipose tissue thermogenesis through both central and peripheral actions. Cell 149, 871-885.

Wiktorowska-Owczarek A, Berezińska M, Nowak JZ. (2015). PUFAs: Structures, Metabolism and Functions. Adv Clin Exp Med.; 24(6): 931-41.

Woo YC, Xu A, Wang Y, Lam KS. (2013). Fibroblast growth factor 21 as an emerging metabolic regulator: clinical perspectives. Clin Endocrinol (Oxf).; 78(4): 489-96.

World Health Organization (WHO). (2018). Obesity and overweight. http://www.who.int/mediacentre/factsheets/fs311/en/ consulted on January 22th, 2018.

Wu, Z., Rosen, E. D., Brun, R., Hauser, S., Adelmant, G., Troy, A. E., McKeon, C., Darlington, G. J. and Spiegelman, B. M. (1999). Cross-regulation of C/EBPα and PPARγ controls the transcriptional pathway of adipogenesis and insulin sensitivity. Molecular Cell, 3(2), pp. 151–158.

Wu, J., Boström, P., Sparks, L. M., Ye, L., Choi, J. H., Giang, A. H., Khandekar, M., Virtanen, K. A., Nuutila, P., Schaart, G., Huang, K., Tu, H., Van Marken Lichtenbelt, W. D., Hoeks, J., Enerbäck, S., Schrauwen, P. and Spiegelman, B. M. (2012). Beige adipocytes are a distinct type of thermogenic fat cell in mouse and human. Cell, 150(2), pp. 366–376.

Wu, Q.; Wang, H.; Zhao, X.; Shi, Y.; Jin, M.; Wan, B.; Xu, H.; Cheng, Y.; Ge, H.; Zhang, Y. (2013). Identification of G-Protein-Coupled Receptor 120 as a Tumor-Promoting

Receptor That Induces Angiogenesis and Migration in Human Colorectal Carcinoma. Oncogene, 32, 5541−5550.

Wulf A, Harneit A, Kröger M, Kebenko M, Wetzel MG, Weitzel JM. (2008). T3-mediated expression of PGC-1alpha via a far upstream located thyroid hormone response element. Mol Cell Endocrinol 287, 90-95.

X

Xiong Y, Swaminath G, Cao Q, Yang L, Guo Q, Salomonis H, Lu J, Houze JB, Dransfield PJ, Wang Y, Liu JJ, Wong S, Schwandner R, Steger F, Baribault H, Liu L, Coberly S, Miao L, Zhang J, Lin DC, Schwarz M. (2013). Activation of FFA1 Mediates GLP-1 Secretion in Mice. Evidence for Allosterism at FFA1. Mol. Cell. Endocrinol., 369, 119−129.

Xu J, Stanislaus S, Chinookoswong N, Lau YY, Hager T, Patel J, Ge H, Weiszmann J, Lu SC, Graham M, Busby J, Hecht R, Li YS, Li Y, Lindberg R, Véniant MM. (2009). Acute glucose-lowering and insulin-sensitizing action of FGF21 in insulin-resistant mouse models--association with liver and adipose tissue effects. Am J Physiol Endocrinol Metab.; 297(5): E1105-14.

Y

Yang SJ, Hong HC, Choi HY, Yoo HJ, Cho GJ, Hwang TG, Baik SH, Choi DS, Kim SM, Choi KM. (2011). Effects of a three-month combined exercise programme on fibroblast growth factor 21 and fetuin-A levels and arterial stiffness in obese women. Clin Endocrinol (Oxf).; 75(4): 464-9.

Yeh, W. C., Cao, Z., Classon, M., McKnight, S. L. (1995). Cascade regulation of terminal adipocyte differentiation by three members of the C/EBP family of leucine zipper proteins. Genes Dev 9, 168-181.

Yiannikouris F, Gupte M, Putnam K, Cassis L. (2010). Adipokines and blood pressure control. Curr Opin Nephrol Hypertens.; 19(2):195-200.

Yie J, Hecht R, Patel J, Stevens J, Wang W, Hawkins N, Steavenson S, Smith S, Winters D, Fisher S, Cai L, Belouski E, Chen C, Michaels ML, Li YS, Lindberg R, Wang M, Véniant M, Xu J. (2009). FGF21 N- and C-termini play different roles in receptor interaction and activation. FEBS Lett.; 583(1): 19-24.

Yip PK, Pizzasegola C, Gladman S, Biggio ML, Marino M, Jayasinghe M, Ullah F, Dyall SC, Malaspina A, Bendotti C and Michael-Titus A. (2013). The omega-3 Fatty Acid eicosapentaenoic Acid accelerates disease progression in a model of amyotrophic lateral sclerosis. PLoS One 8(4): e61626.

Yonezawa T, Kurata R, Yoshida K, Murayama MA, Cui X, and Hasegawa A. (2013). Free fatty acids-sensing G proteincoupled receptors in drug targeting and therapeutics. Curr Med Chem 20: 3855–3871.

Yore MM, Syed I, Moraes-Vieira PM, Zhang T, Herman MA, Homan EA, Patel RT, Lee J, Chen S, Peroni OD, Dhaneshwar AS, Hammarstedt A, Smith U, McGraw TE, Saghatelian A, Kahn BB. (2014). Discovery of a class of endogenous mammalian lipids with anti-diabetic and anti-inflammatory effects. Cell. ;159(2):318-32.

Yu H., Xia F., Lam K.S., Wang Y., Bao Y., Zhang J., Gu Y., Zhou P., Lu J., Jia W., and Xu A. (2011). Circadian rhythm of circulating fibroblast growth factor 21 is related to diurnal changes in fatty acids in humans. Clin. Chem. 57, 691-700.

Z

Zamani, N. and Brown, C. W. (2011). Emerging roles for the transforming growth factor-{beta} superfamily in regulating adiposity and energy expenditure. Endocrine reviews, 32(3), pp. 387–403.

Zapata ME, Bibiloni MD, Tur JA. (2016). Prevalence of overweight, obesity, abdominal-obesity and short stature of adult population of Rosario, Argentina. Nutr Hosp.20; 33(5): 580.

Zarei M, Barroso E, Leiva R, Barniol-Xicota M, Pujol E, Escolano C, Vázquez S, Palomer X, Pardo V, González-Rodríguez Á, Valverde ÁM, Quesada-López T, Villarroya F, Wahli W, Vázquez-Carrera M. (2016). Heme-Regulated eIF2α Kinase Modulates Hepatic FGF21 and Is Activated by PPARβ/δ Deficiency. Diabetes.; 65(10): 3185-99.

Zarei M, Barroso E, Palomer X, Dai J, Rada P, Quesada-López T, Escolà-Gil JC, Cedó L, Zali MR, Molaei M, Dabiri R, Vázquez S, Pujol E, Valverde ÁM, Villarroya F, Liu Y, Wahli W, Vázquez-Carrera M. (2018). Hepatic regulation of VLDL receptor by PPARβ/δ and FGF21 modulates non-alcoholic fatty liver disease. Mol Metab.; 8: 117-131.

Zhang J., Kaasik K., Blackburn M.R., and Lee C.C. (2006). Constant darkness is a circadian metabolic signal in mammals. Nature 439, 340-343.

Zhang X, Yeung DC, Karpisek M, Stejskal D, Zhou ZG, Liu F, Wong RL, Chow WS, Tso AW, Lam KS, Xu A. (2008). Serum FGF21 levels are increased in obesity and are independently associated with the metabolic syndrome in humans. Diabetes.; 57(5): 1246-53.

Zhang Y, Xie Y, Berglund ED, Coate KC, He TT, Katafuchi T, Xiao G, Potthoff MJ, Wei W, Wan Y, Yu RT, Evans RM, Kliewer SA, Mangelsdorf DJ. (2012). The starvation hormone, fibroblast growth factor-21, extends lifespan in mice. Elife.;1 : e00065.

Zhang D, Zhao Q, Wu B. (2015) Structural Studies of G Protein-Coupled Receptors. Mol Cells.; 38(10):836-42.

Zhao L, Gregoire F, Sook Sul H. (2000). Transient induction of ENC-1, a Kelch-related actinbinding protein, is required for adipocyte differentiation. J Biol Chem 275:16845–16850.

Zhu Y, Qi C, Korenberg JR, Chen XN, Noya D, Rao MS, Reddy JK. (1995) Structural organization of mouse peroxisome proliferator-activated receptor gamma (mPPAR

gamma) gene: alternative promoter use and different splicing yield two mPPAR gamma isoforms. Proc Natl Acad Sci U S A 92, 7921-7925.

Zhu S, Lin G, Song C, Wu Y, Feng N, Chen W, He Z, Chen YQ. (2017). RA and ω-3 PUFA co-treatment activates autophagy in cancer cells. Oncotarget.; 8(65): 109135-109150.

Zhu S, Jiang X, Jiang S, Lin G, Gong J, Chen W, He Z, Chen YQ. (2018). GPR120 is not required for ω-3 PUFAs-induced cell growth inhibition and apoptosis in breast cancer cells. Cell Biol Int.; 42(2): 180-186.

Zingaretti MC, Crosta F, Vitali A, Guerrieri M, Frontini A, Cannon B, Nedergaard J, Cinti S. (2009).The presence of UCP1 demonstrates that metabolically active adipose tissue in the neck of adult humans truly represents brown adipose tissue. FASEB J 23, 3113-3120.

Zwick RK, Guerrero-Juarez CF, Horsley V, Plikus MV. (2018). Anatomical, Physiological, and Functional Diversity of Adipose Tissue. Cell Metab.; 27(1): 68-83.

APPENDIX

Effects of FGF21 gene invalidation on brown and white adipose tissue pathophysiology

Congress: European Congress on Obesity 2015

****Awarded best poster in the category of adipose tissue biology

Journal: Obesity Facts

Abstract:

Introduction. Experimental increases in the endocrine factor FGF21 protect against diabetes and obesity in rodents. However, obese patients and rodent models of obesity show a paradoxical increase in blood FGF21. We undertook a “loss-of-function” approach to get insight in the role of FGF21 on adiposity.

Methods: Male FGF21-KO and wild-type mice were sacrificed. Interscapular BAT, inguinal and epididymal WAT were collected. Metabolites, hormones and cytokines were determined by spectrophotometry, ELISA or Multiplex. Gene expression was determined by qRT-PCR. Cell morphology was assessed by optical microscopy. Cell precursors from fat depots were differentiated to adipocytes in culture, and 14C-glucose oxidation was determined.

Results. FGF21-KO mice did not show major changes in adipose depots size; glycemia and insulinemia were increased, and adiponectin levels were reduced. The expression of marker genes of carbohydrate and lipid metabolism, adipogenesis and “browning” was essentially unaltered in adipose depots. Increased expression of inflammation and macrophage infiltration markers (e.g. Nos2, TNFa, Arg1) was found in BAT from FGF21-KO mice; opposite changes were found in inguinal WAT. Morphological differentiation “in vitro” of brown and white adipocytes lacking FGF21 was unaltered, whereas the expression of marker genes of “browning” (e.g. UCP1, Sirt3, Bmp8b, UCP3) was reduced. Glucose oxidation in FGF21-KO brown and white adipocytes was significantly reduced.

Conclusions. In vivo, the lack of FGF21 causes minor effects in adipose tissues, with the exception of altered local inflammation status. However, the impaired glucose oxidation due to the lack of FGF21 found in adipocytes support the notion of an autocrine role of adipose tissue FGF21 on glucose homeostasis.

EFFECTS OF FGF21 GENE INVALIDATION ON BROWN AND WHITE ADIPOSE TISSUE PATHOPHYSIOLOGY

Quesada T.[1], Planavila A.[1], Ribas F.[1], Cairó M.[1], Iglesias R.[1], Giralt M.[1], Villarroya F.[1]

[1]Department of Biochemistry and Molecular Biology, and Institute of Biomedicine (IBUB). University of Barcelona, and CIBERobn. Barcelona. Catalonia. Spain.

INTRODUCTION

FGF21, an endocrine member of the FGF family, has been described to **promote glucose oxidation** in multiple tissues including the **adipose depots**. In addition to this, several experimental increases in the endocrine factor FGF21 have shown to **protect against diabetes and obesity** in rodents. Under basal conditions the liver is the main site of production of this hormone; however, recent findings have proven that the activation of the adipose tissues, specially Brown Adipose Tissue, can induce the secretion of this hormone. Despite the promising findings, some groups have found **a paradoxical increase in blood FGF21 from obese patients** and rodent models of obesity. The aim of the present work was to **clarify the role of FGF21 on adiposity**; with this purpose we analyzed the alterations in metabolism and adiposity in mice with targeted invalidation of the FGF21 gene (FGF21-null mice).

1 FGF21 null mice show increased circulating glucose and a tendency to decrease circulating insulin and adiponectin

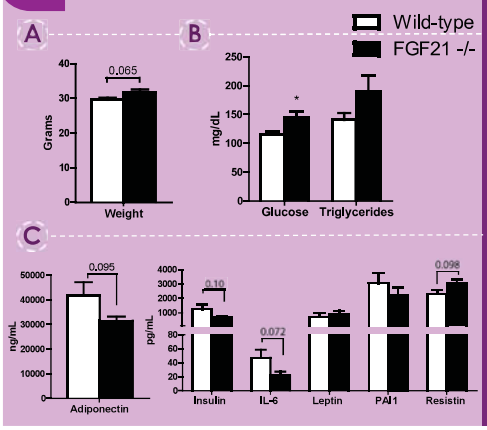

Wild-type and FGF21-/- male adult mice fed standard chow were sacrificed. Weights are expressed in grams for both groups **(A)**. Circulating metabolites, glucose and triglycerides, are expressed in mg/dL **(B)** and both profiles of circulating hormones and cytokines (ng and pg/mL) are shown **(C)**. Assessed by spectrophotometry or milliplex (MADKMAG-71K, Luminex equipment). Bars represent the mean ± SEM. * *P* <0.05 n=5.

2 Adipose depots from FGF21 null mice did not show massive alterations but a tendency to modify macrophage activation profile

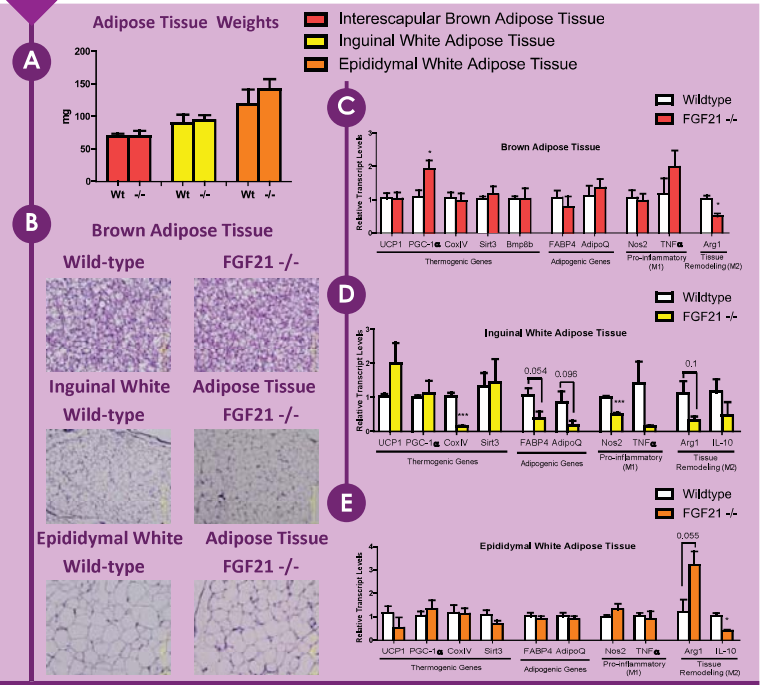

Wild-type and FGF21-/- male adult mice fed standard chow were sacrificed. Interescapular brown adipose tissue (BAT), inguinal white adipose tissue (iWAT) and epididymal white adipose tissue (eWAT) were dissected and weighted (mg) **(A)**. Tissues were fixed to perform optical microscopy, the six representative images are for BAT, iWAT and eWAT from both genotypes **(B)**. Relative transcript levels of thermogenic genes, adipogenic genes, pro-inflammatory (M1) macrophage-related genes and tissue remodeling (M2) macrophage-related genes were quantified by qRT-PCR for BAT **(C)**, iWAT **(D)** and eWAT **(E)** from Wt and FGF21 **-/-** animals. Bars represent the mean ± SEM. * *P* <0.05; *** *P* <0.001 n=5.

3 Differentiated FGF21-/- adipocytes show reduced glucose oxidation and decrease expression of thermogenic genes

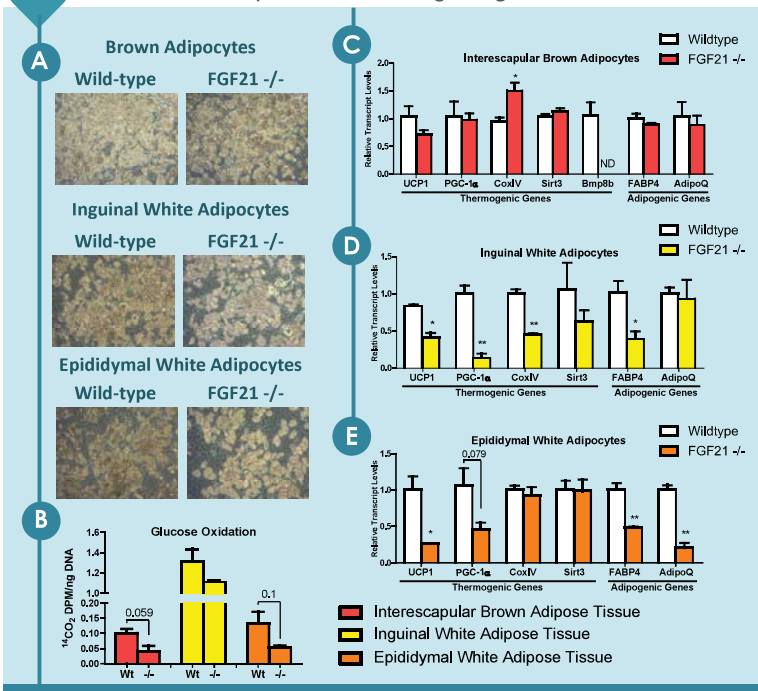

Stromal vascular fraction from interescapular BAT, inguinal WAT and epididymal WAT were obtained from wild-type and FGF21 **-/-** mice, the obtained cells were differentiated to adipocytes following a standard procedure. Optical microscopy from the differentiated cells for BAT, iWAT and eWAT (wt and **-/-**) are shown **(A)**. ^{14}C glucose oxidation capacity was performed in the differentiated adipocytes **(B)**. Relative transcript levels of thermogenic and adipogenic genes from Wt and FGF21 **-/-** differentiated adipocytes were quantified by qRT-PCR **(C)**. Bars represent the mean ± SEM. * *P* <0.05 ; ** *P* <0.01 n=3.

CONCLUSIONS

The present work has found that the loss of FGF21 *in vivo* causes an increase in circulating glucose levels but has no major effects on circulating hormones. Also, mice lacking FGF21 show signs of altered inflammation status in the adipose tissues. However, the adipose depots from these mice show minor alterations. Besides these data, differentiated adipocytes from the SVF of the FGF21 **-/-** mice showed a decreased expression of thermogenic and adipogenic genes and a trend to lowered glucose oxidation. These findings may support the notion of an autocrine role of adipose tissue FGF21 on glucose homeostasis.

Acknowledgement: Supported by MINECO-ISCIII (Grant PI14/00063) and FP7-Health (BetaBat project). T.Q. is recipient of an international PhD scholarship by CONACyT.México.

Heme-Regulated eIF2α Kinase Modulates Hepatic FGF21 and Is Activated by PPARβ/δ Deficiency

Journal: Diabetes. 2016 Oct; 65(10): 3185-99.

IF: 8.684 ENDOCRINOLOGY & METABOLISM 9 DE 138 (1st Decile)

Abstract:

Fibroblast growth factor 21 (FGF21), a peptide hormone with pleiotropic effects on carbohydrate and lipid metabolism, is considered a target for the treatment of diabetes. We investigated the role of peroxisome proliferator–activated receptor (PPAR) β/δ deficiency in hepatic FGF21 regulation. Increased Fgf21 expression was observed in the livers of PPARb/d-null mice and in mouse primary hepatocytes when this receptor was knocked down by small interfering RNA (siRNA). Increased Fgf21 was associated with enhanced protein levels in the heme-regulated eukaryotic translation initiation factor 2a (eIF2a) kinase (HRI). This increase caused enhanced levels of phosphorylated eIF2a and activating transcription factor (ATF) 4, which is essential for Fgf21-induced expression. siRNA analysis demonstrated that HRI regulates Fgf21 expression in primary hepatocytes. Enhanced Fgf21 expression attenuated tunicamycin-induced endoplasmic reticulum stress, as demonstrated by using a neutralizing antibody against FGF21. Of note, increased Fgf21 expression in mice fed a high-fat diet or hepatocytes exposed to palmitate was accompanied by reduced PPAR β/δ and activation of the HRI-eIF2a-ATF4 pathway. Moreover, pharmacological activation of HRI increased Fgf21 expression and reduced lipid-induced hepatic steatosis and glucose intolerance, but these effects were not observed in Fgf21-null mice. Overall, these findings suggest that HRI is a potential target for regulating hepatic FGF21 levels.

Mohammad Zarei,[1,2,3] Emma Barroso,[1,2,3] Rosana Leiva,[1] Marta Barniol-Xicota,[1] Eugènia Pujol,[1] Carmen Escolano,[1] Santiago Vázquez,[1] Xavier Palomer,[1,2,3] Virginia Pardo,[2,4] Águeda González-Rodríguez,[2,4] Ángela M. Valverde,[2,4] Tania Quesada-López,[3,5,6] Francesc Villarroya,[3,5,6] Walter Wahli,[7,8,9] and Manuel Vázquez-Carrera[1,2,3]

Heme-Regulated eIF2α Kinase Modulates Hepatic FGF21 and Is Activated by PPARβ/δ Deficiency

Diabetes 2016;65:3185–3199 | DOI: 10.2337/db16-0155

Fibroblast growth factor 21 (FGF21), a peptide hormone with pleiotropic effects on carbohydrate and lipid metabolism, is considered a target for the treatment of diabetes. We investigated the role of peroxisome proliferator–activated receptor (PPAR) β/δ deficiency in hepatic FGF21 regulation. Increased *Fgf21* expression was observed in the livers of PPARβ/δ-null mice and in mouse primary hepatocytes when this receptor was knocked down by small interfering RNA (siRNA). Increased *Fgf21* was associated with enhanced protein levels in the heme-regulated eukaryotic translation initiation factor 2α (eIF2α) kinase (HRI). This increase caused enhanced levels of phosphorylated eIF2α and activating transcription factor (ATF) 4, which is essential for *Fgf21*-induced expression. siRNA analysis demonstrated that HRI regulates *Fgf21* expression in primary hepatocytes. Enhanced *Fgf21* expression attenuated tunicamycin-induced endoplasmic reticulum stress, as demonstrated by using a neutralizing antibody against FGF21. Of note, increased *Fgf21* expression in mice fed a high-fat diet or hepatocytes exposed to palmitate was accompanied by reduced PPARβ/δ and activation of the HRI-eIF2α-ATF4 pathway. Moreover, pharmacological activation of HRI increased *Fgf21* expression and reduced lipid-induced hepatic steatosis and glucose intolerance, but these effects were not observed in *Fgf21*-null mice. Overall, these findings suggest that HRI is a potential target for regulating hepatic FGF21 levels.

Fibroblast growth factor 21 (FGF21), a member of the FGF family, is a hormone with a wide range of endocrine and autocrine actions on carbohydrate and lipid metabolism (1) and is considered a novel therapeutic target for the treatment of nonalcoholic fatty liver disease (NAFLD), insulin resistance, and type 2 diabetes. Several studies in genetic and diet-induced models of obesity have demonstrated that FGF21 administration ameliorates a large number of metabolic parameters (2–5), including plasma glucose and triglyceride levels and hepatic steatosis. However, despite these beneficial effects of administered FGF21, serum FGF21 levels are paradoxically increased in animal models of obesity (6). Likewise, circulating FGF21 levels are elevated in patients with obesity, hypertriglyceridemia, type 2 diabetes, or NAFLD (7–9).

The pleiotropic effects of FGF21 on target tissues, including adipose tissue, β-cells, and liver (1,2,10), are mediated by its binding to FGF receptors in a β-klotho–dependent manner (11–13). β-Klotho is almost exclusively expressed in liver, adipose tissue, and pancreas (13), which might explain why these specific tissues are the predominant sites of action of FGF21. Circulating

[1]Department of Pharmacology, Toxicology and Therapeutic Chemistry, Faculty of Pharmacy and Institute of Biomedicine of the University of Barcelona, Barcelona, Spain
[2]CIBERDEM, Instituto de Salud Carlos III, Madrid, Spain
[3]Pediatric Research Institute, Hospital Sant Joan de Déu, Barcelona, Spain
[4]Instituto de Investigaciones Biomédicas Alberto Sols (CSIC/UAM), Madrid, Spain
[5]Department of Biochemistry and Molecular Biology and Institute of Biomedicine of the University of Barcelona, Barcelona, Spain
[6]CIBEROBN, Instituto de Salud Carlos III, Madrid, Spain
[7]Center for Integrative Genomics, University of Lausanne, Lausanne, Switzerland
[8]Lee Kong Chian School of Medicine, Nanyang Technological University, Singapore, Singapore
[9]INRA ToxAlim, UMR1331, Chemin de Tournefeuille, Toulouse Cedex, France
Corresponding author: Manuel Vázquez-Carrera, mvazquezcarrera@ub.edu.
Received 10 February 2016 and accepted 12 July 2016.
This article contains Supplementary Data online at http://diabetes.diabetesjournals.org/lookup/suppl/doi:10.2337/db16-0155/-/DC1.

FGF21 is liver derived (14), and hepatic *FGF21* expression is upregulated, following extended periods of fasting, by peroxisome proliferator–activated receptor (PPAR) α, a nuclear receptor that induces the expression of numerous genes involved in mitochondrial fatty acid (FA) oxidation (15). In recent years, FGF21 has been reported to be regulated by additional transcription factors, including CREBPH (16) and retinoic acid receptor–related orphan receptor (ROR) α (17). Moreover, hepatic FGF21 is negatively regulated by the PPARγ coactivator 1α (PGC-1α) by modulating the heme-sensing nuclear receptor REV-ERBα, which acts as a transcriptional repressor through its binding to ROR response elements (18). Impaired mitochondrial oxidative phosphorylation (mtOXPHOS) is also responsible for *Fgf21* induction by activating transcription factor (ATF) 4. ATF4 is a transcriptional effector of the protein kinase R–like endoplasmic reticulum (ER) kinase branch of the ER stress/unfolded protein response pathway, which is essential for *Fgf21*-induced expression (19). However, although circulating FGF21 has been reported to be increased following treatment with PPARβ/δ agonists (20), little is known about the effects of PPARβ/δ on FGF21 regulation in liver. PPARβ/δ is a ligand-activated transcription factor involved in the regulation of glucose and lipid homeostasis (21) and has been proposed as a therapeutic target for the treatment of the metabolic syndrome (22). Thus, genetic manipulations of PPARβ/δ as well as it activation by agonists attenuates dyslipidemia and hyperglycemia, improves whole-body insulin sensitivity, and prevents diet-induced obesity (23).

In this study, we examined the effects of PPARβ/δ deficiency on hepatic *Fgf21* expression. *Pparβ/δ*-null mice showed enhanced hepatic *Fgf21* expression, which appears to depend on a reduction in PGC-1α levels and the subsequent reduction in hemin levels that finally activate the heme-regulated eukaryotic translation initiation factor 2α (eIF2α) kinase (HRI). This kinase phosphorylates eIF2α, which in turn increases ATF4 levels, resulting in enhanced *Fgf21* expression. Overall, the findings point to HRI as a new therapeutic target for regulating *Fgf21* expression and metabolic dysregulation.

RESEARCH DESIGN AND METHODS

Reagents

N,N′-diarylureas 1-(benzo[d][1,2,3]thiadiazol-6-yl)-3-(3,4-dichlorophenyl)urea (BTdCPU) or 1-(benzo[d][1,2,3]thiadiazol-6-yl)-3-(4-chloro-3-[trifluoromethyl]phenyl)urea (BTCtFPU), were synthesized as previously described (Supplementary Data) (24).

Mice and Cell Culture

Male *Pparβ/δ* knockout (*Pparβ/δ*$^{-/-}$) mice and their wild-type littermates (*Pparβ/δ*$^{+/+}$) with the same genetic background (C57BL/6 × 129/SV) (25) and initial weight of 20–25 g were fed a standard diet. Lipid-containing media were prepared by conjugation of palmitic acid with FA-free BSA as previously described (26). Primary mouse hepatocytes were isolated from nonfasting male C57BL/6 mice (10–12 weeks old) by perfusion with collagenase as described elsewhere (27).

Male mice (Harlan Ibérica SA, Barcelona, Spain) were randomly distributed into three experimental groups (n = 8 each): standard diet, Western-type high-fat diet (HFD) (35% fat by weight, 58% kcal from fat; Harlan Ibérica SA) plus one daily oral gavage of vehicle (0.5% weight for volume carboxymethylcellulose), and HFD plus one daily oral dose of 3 mg · kg^{-1} · day^{-1} of the PPARβ/δ agonist GW501516 dissolved in the vehicle (volume administered 1 mL · kg^{-1}). In a second study, male mice received one daily intraperitoneal administration of DMSO (vehicle) or BTdCPU (70 mg · kg^{-1} · day^{-1}) for 7 days. In a third study, male mice were randomly distributed into two experimental groups: standard chow (n = 8) or HFD (n = 16) for 3 weeks. Mice fed standard chow and one-half of the mice fed the HFD received one daily intraperitoneal administration of DMSO (vehicle) for the last week. The rest of the mice fed the HFD received one daily intraperitoneal administration of BTdCPU (70 mg · kg^{-1} · day^{-1}) for the last week. In a fourth study, male knockout (*Fgf21*$^{-/-}$) mice (B6N;129S5-*Fgf21*^{tm1Lex}/Mmcd obtained from the Mutant Mouse Regional Resource Centre) and their wild-type littermates (*Fgf21*$^{+/+}$) were treated as described in the third study.

RNA Preparation and Quantitative RT-PCR

The relative levels of specific mRNAs were assessed by real-time RT-PCR as previously described (26). Primer sequences used for real-time RT-PCR are displayed in Supplementary Table 1.

Immunoblotting

Western blot analyses were performed as previously indicated (26).

Heme Protein Content Quantification

Heme content in liver was quantified by measuring the oxidized version of the protein hemin by using an enzymatic assay kit (Hemin Assay Kit; Sigma-Aldrich).

Oil Red O Staining

Lipid accumulation in hepatocytes was assessed by Oil Red O (ORO) staining as previously reported (28).

Statistical Analyses

Results are expressed as mean ± SD. Significant differences were established by one-way ANOVA by using the GraphPad Instat program (GraphPad version 5.01; GraphPad Software, La Jolla, CA). When significant variations were found by one-way ANOVA, the Tukey-Kramer multiple comparison posttest was performed. Differences were considered significant at $P < 0.05$.

RESULTS

Pparβ/δ$^{-/-}$ Mice Show Increased Hepatic *Fgf21* Expression and Plasma Levels

PPARβ/δ$^{-/-}$ mice displayed higher hepatic *Fgf21* mRNA levels than wild-type littermates (threefold induction, $P <$ 0.001) (Fig. 1*A*). Consistent with circulating FGF21 being

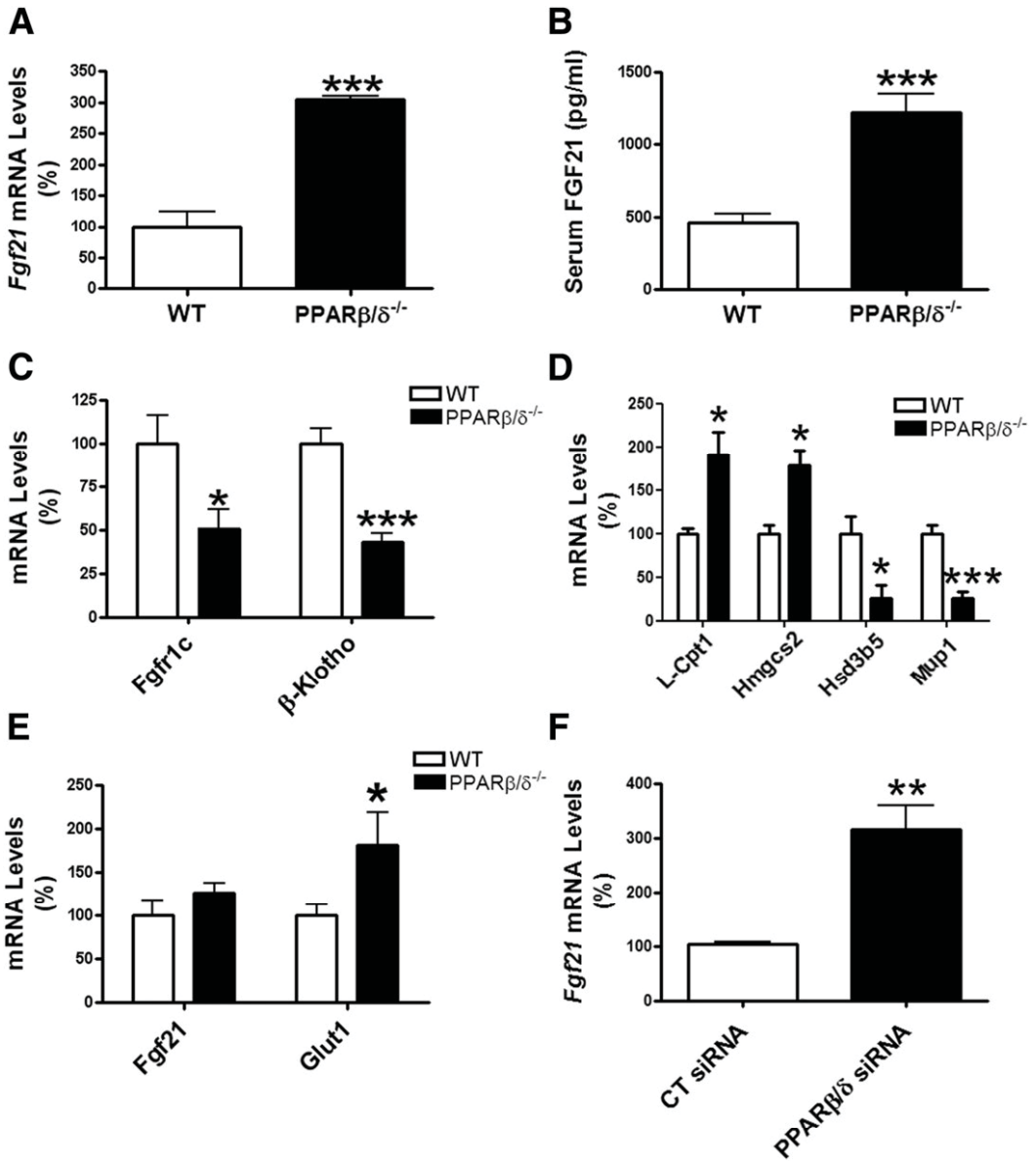

Figure 1—*Fgf21* expression is increased in liver of *Pparβ/δ*-null mice and in primary hepatocytes following knockdown of *Pparβ/δ*. Liver and epididymal white adipose tissue from male wild-type (WT) and *Pparβ/δ*-null mice were used (n = 6/group). *A*: Assessment by quantitative real-time RT-PCR of hepatic *Fgf21*. *B*: Serum FGF21 levels. Data are the mean ± SD (n = 6/group) relative to WT mice. *C*: mRNA abundance of hepatic *Fgfr1c* and *β-klotho*. *D*: mRNA abundance of hepatic *L-Cpt-1*, *Hmgcs2*, *Hsd3b5*, and *Mup1*. *E*: mRNA abundance of epididymal white adipose tissue *Fgf21* and *Glut1*. *F*: *Fgf21* mRNA abundance in primary hepatocytes transfected with control (CT) siRNA or *Pparβ/δ* siRNA for 24 h. mRNA levels are mean ± SD (n = 6/group). *$P < 0.05$, **$P < 0.01$, ***$P < 0.001$ vs. WT mice or CT siRNA.

liver derived (14), we found increased plasma FGF21 levels in *Pparβ/δ*-deficient mice (2.6-fold increase, $P < 0.001$) (Fig. 1*B*) and reduced expression of one of the receptor and coreceptor pairs used by FGF21, *Fgfr1c* (49% reduction, $P < 0.05$) and *β-klotho* (57% reduction, $P < 0.001$) (Fig. 1*C*). Carnitine palmitoyltransferase 1A (*Cpt-1a*), 3-hydroxy-3-methylglutaryl-CoA synthase 2 (*Hmgcs2*) (29), 3-β-hydroxysteroid dehydrogenase type 5 (*Hsd3b5*) (30), and major urinary protein 1 (*Mup1*) (30) are FGF21-responsive genes. In accordance with increased FGF21 plasma levels, hepatic expression of *Cpt-1a* and *Hmgcs2* was increased, whereas the expression of *Hsd3b5* and the mRNA and protein levels of MUP1 were decreased in *Pparβ/δ*$^{-/-}$ mice (Fig. 1*D* and Supplementary Fig. 1*A*). In agreement with the reported observation of increased glucose uptake in adipocytes through enhanced Glut1 expression by FGF21 secreted by the liver (31), the expression of this glucose transporter was higher in white adipose tissue of *Pparβ/δ*$^{-/-}$ mice than in the wild-type animals (Fig. 1*E*). In contrast to the liver, the

expression of *Fgf21* in white adipose tissue was not significantly increased in *Pparβ/δ*-deficient mice (Fig. 1*E*), pointing to a tissue-specific effect. Because increased serum free fatty acids (32) and glucose levels (33) are two important stimuli that upregulate *Fgf21* expression in liver, we measured their levels in serum of *Pparβ/δ*$^{-/-}$ and wild-type mice. No differences were observed in serum free fatty acids and glucose levels (Supplementary Fig. 1*B* and *C*), suggesting that they were not involved in the reported increase in *Fgf21* expression. In addition, the expression levels of *Pparα* and its target genes *Acox* and *Mcad* were not significantly increased, rendering it unlikely that PPARα is involved in the increase in *Fgf21* expression in these mice (Supplementary Fig. 1*D*). *Pparβ/δ*-null mice did not present upregulation of *Chop*, *Orp150*, or *Atf3* expression (Supplementary Fig. 1*E*) or phosphorylated (phospho)-IRE1α and BiP levels (Supplementary Fig. 1*F*), suggesting that ER stress was not the stimulus responsible for the increase in *Fgf21* expression. Primary hepatocytes transfected with either control small interfering RNA (siRNA) or *Pparβ/δ* siRNA showed a significant reduction (71%, $P < 0.001$) in this transcription factor (Supplementary Fig. 1*G*) and a significant increase in *Fgf21* gene expression (Fig. 1*F*), confirming that downregulation of *Pparβ/δ* in hepatocytes raises *Fgf21* expression.

Because AMPK (34) and SIRT1 (35) stimulate *Fgf21* expression, we explored the levels of these proteins in *Pparβ/δ*$^{-/-}$ mice. No changes were observed either in phosphorylated or total AMPK protein levels in *Pparβ/δ*-deficient mice compared with wild-type animals, whereas in accordance with the reported regulation of SIRT1 by PPARβ/δ (36), the protein levels of SIRT1 were reduced in *Pparβ/δ*$^{-/-}$ mice (Fig. 2*A*). Next, we focused on PGC-1α because this transcriptional coactivator negatively regulates hepatic levels of *Fgf21* (18). *Pparβ/δ*-null mice showed reduced nuclear PGC-1α protein levels compared with wild-type mice (Fig. 2*B*). Because the reduction in PGC-1α upregulates *Fgf21* mRNA levels by decreasing the expression of the transcriptional repressor *Rev-Erbα* (18), we measured its mRNA and protein levels. *Pparβ/δ*$^{-/-}$ mice exhibited lower *Rev-Erbα* expression and protein levels than wild-type mice (Fig. 2*B* and *C*), which is consistent with the upregulation of Rev-Erbα–repressed *Bmal1* in *Pparβ/δ*-null mice (Fig. 2*C*). Because PGC-1α stimulates the expression of the *Nrf-1* gene (37), its reduction was in accordance with the reduction in hepatic PGC-1α (Fig. 2*B*). mtOXPHOS is regulated by both PGC-1α (38) and REV-ERBα (39), and their decrease is consistent with the reduction observed in the protein levels of several members of mtOXPHOS in the livers of *Pparβ/δ*$^{-/-}$ mice (Fig. 2*D*). Impaired mtOXPHOS is reportedly responsible for FGF21 induction through activation of the eIF2α-ATF4 pathway (19). Although this pathway is activated by ER stress, the increase in phosphorylated eIF2α and activation of its downstream ATF4 signaling pathway can occur independently of ER stress because eIF2α can also be phosphorylated by other kinases, including HRI (40). Of note, HRI is activated by heme deprivation (41), and PGC-1α is an important regulator of heme in liver cells because it coactivates NRF-1 and other transcription factors that increase the expression of *Alas1*, the rate-limiting enzyme in heme biosynthesis. In addition, the repressive activity of REV-ERBα on *Fgf21* expression is potentiated by the binding of its ligand heme (18). Given that *Pparβ/δ*$^{-/-}$ mice exhibited reduced PGC-1α and NRF-1 protein levels, we assessed heme content levels by measuring the oxidized form of this protein hemin. *Pparβ/δ*$^{-/-}$ mice showed reduced levels of hemin compared with wild-type mice (Fig. 2*E*) and increased HRI levels in *Pparβ/δ*$^{-/-}$ mice compared with wild-type littermates (Fig. 2*F*). In agreement with the increase in HRI, levels of the downstream proteins of this pathway, phospho-eIF2α and ATF4, were also upregulated (Fig. 2*F*).

In accordance with the findings observed in the livers of *Pparβ/δ*-deficient mice, siRNA knockdown of *Pparβ/δ* in primary hepatocytes led to enhanced protein levels of HRI, phospho-eIF2α, and ATF4 and reduced levels of MUP1 (Fig. 3*A*). Transfection of primary hepatocytes with siRNA against *Hri* caused a significant reduction in hemin levels and in the expression of *Fgf21*, *Atf4*, and *Chop*, the latter being a direct ATF4 transcriptional target (42) used as a marker of the activation of the eIF2α-ATF4 pathway following activation of HRI (Fig. 3*B*–*E*) (24). Likewise, the protein levels of phosphorylated eIF2α, ATF4, and CHOP were decreased, whereas the protein levels of MUP1 were increased (Fig. 3*F*), confirming through a genetic approach that HRI controls *Fgf21* expression in hepatocytes.

PPARβ/δ Regulates ER Stress Through Hepatic *Fgf21* Expression

Hepatic *Fgf21* expression increases in response to ER stressors in liver, where it seems to display an adaptive response to these stimuli (43). In fact, exogenous administration of FGF21 alleviates the tunicamycin-induced eIF2α-ATF4-CHOP pathway, whereas it shows an insignificant effect on the IRE1α-XBP1s pathway (43). We hypothesized that the increase in FGF21 levels in *Pparβ/δ*-deficient mice may protect the liver from ER stress, which is consistent with the fact that in contrast to the liver, skeletal muscle of these mice showed increased expression of ER stress markers (44). To test this, wild-type and *Pparβ/δ*$^{-/-}$ mice were treated with the ER stressor tunicamycin for 24 h. Wild-type mice treated with tunicamycin exhibited a ninefold increase ($P < 0.001$) in *Fgf21* expression, and this increase was higher (~21-fold induction, $P < 0.001$ vs. tunicamycin-treated wild-type mice) in livers of *Pparβ/δ*$^{-/-}$ mice (Fig. 4*A*). A similar effect was observed in plasma FGF21 levels (Fig. 4*B*). The mRNA and protein levels of the ER stress marker BiP were higher in the livers of tunicamycin-treated *Pparβ/δ*-deficient mice than in tunicamycin-treated wild-type mice, suggesting that ER stress is

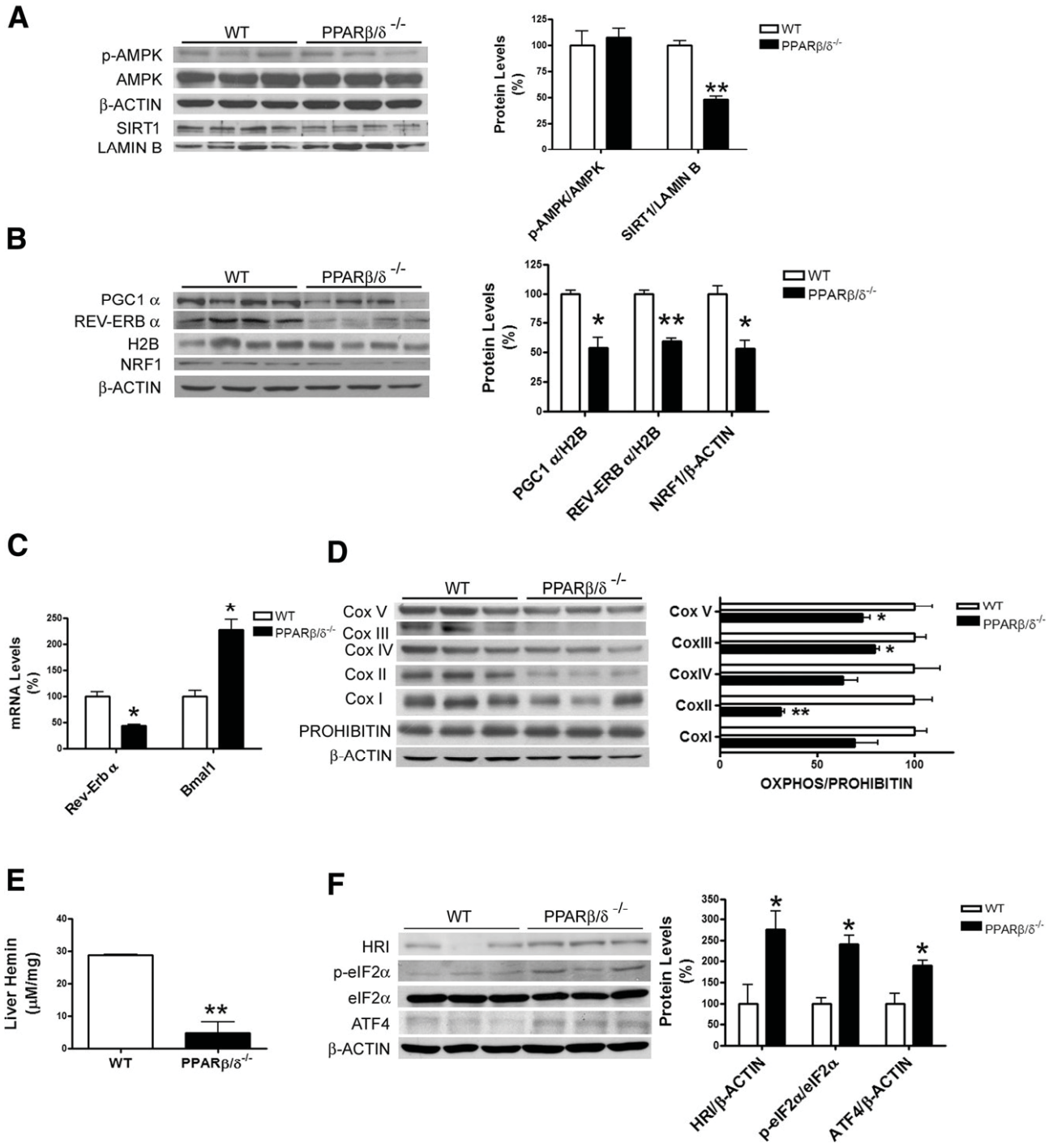

Figure 2—*Pparβ/δ* deficiency decreases PGC-1α and hemin levels and activates the HRI-eIF2α-ATF4 pathway. *A*: Liver cell lysates and nuclear extracts from male wild-type (WT) and *Pparβ/δ*-null mice were assayed for Western blot analysis with antibodies against total and phospho (p)-AMPK and SIRT1. Data are mean ± SD (n = 6/group) relative to WT mice. *B*: Nuclear extracts were assayed by Western blot analysis with antibodies against PGC-1α, REV-ERBα, and NRF-1. *C*: *Rev-Erbα* and *Bmal1* mRNA levels in liver from WT and *Pparβ/δ*-null mice. Data are mean ± SD (n = 6/group) relative to WT mice. *D*: Immunoblot analyses of mtOXPHOS proteins. *E*: Liver hemin levels. Data are mean ± SD (n = 6/group) relative to WT mice. *F*: Immunoblot analyses of HRI, total and p-eIF2α, and ATF4. Data are mean ± SD (n = 6/group) relative to WT mice. *P < 0.05, **P < 0.01 vs. WT mice.

exacerbated in the former (Supplementary Figs. 2*A* and 4*C*) probably as a result of the increase in ER stress pathways, such as the IRE1α-XBP1s, which are not inhibited by FGF21. The higher levels of FGF21 in vehicle-treated *Pparβ/δ*$^{-/-}$ mice compared with vehicle-treated wild-type mice were accompanied by a reduction in phospho-eIF2α protein levels (Fig. 4*C*). This was especially marked in tunicamycin-treated *Pparβ/δ*$^{-/-}$ mice compared with

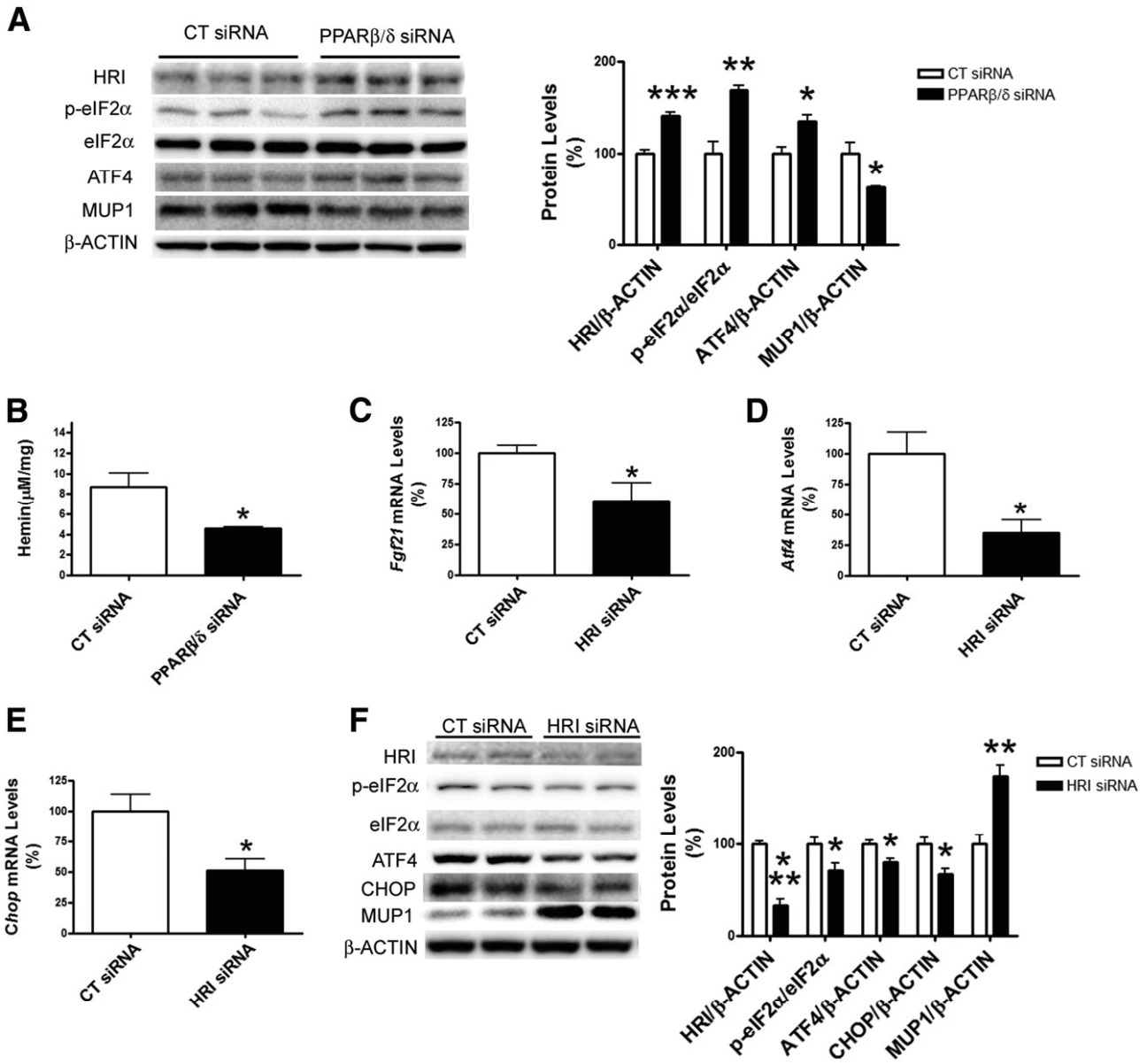

Figure 3—*Hri* knockdown in primary hepatocytes reduces *Fgf21* expression. *A*: Primary hepatocytes were transfected with control (CT) or *Pparβ/δ* siRNA for 24 h, and the protein levels of HRI, phosphorylated (p) and total eIF2α, ATF4, and MUP1 were analyzed by immunoblotting. *B*: Hemin levels. *C–E*: *Fgf21*, *Atf4*, and *Chop* mRNA abundance in primary hepatocytes transfected with CT or *Hri* siRNA for 24 h. *F*: Immunoblot analyses of HRI, total and p-eIF2α, ATF4, CHOP, and MUP1 in primary hepatocytes transfected with CT siRNA or *Hri* siRNA for 24 h. Data are mean ± SD (n = 6/group). *P < 0.05, **P < 0.01, ***P < 0.001 vs. CT siRNA.

tunicamycin-treated wild-type mice (Fig. 4*C*), suggesting that the higher levels of FGF21 in $Pparβ/δ^{-/-}$ mice inhibited the phosphorylation of eIF2α as previously described (43). To demonstrate this more clearly, we used an FGF21-neutralizing antibody. In wild-type mice, treatment with the FGF21-neutralizing antibody for 14 h did not significantly affect eIF2α phosphorylation compared with IgG-treated mice (Supplementary Fig. 2*B*). In contrast, when $Pparβ/δ^{-/-}$ mice were treated with the FGF21-neutralizing antibody for the same amount of time, a significant increase was observed in phospho-eIF2α levels (Fig. 4*D*). $Pparβ/δ^{-/-}$ mice treated for 14 h with tunicamycin and IgG showed a reduction in the levels of phospho-eIF2α, suggesting that the additional increase in FGF21 levels caused by tunicamycin treatment was responsible for this effect. In line with this, injection of the FGF21-neutralizing antibody raised phospho-eIF2α levels (Fig. 4*D*). The protein levels of ATF4 also showed an increase following treatment with the FGF21-neutralizing antibody (Fig. 4*D*). Through its negative action on eIF2α and ATF4, FGF21 can activate a negative feedback loop that reduces *Fgf21* expression (43). Consistently, administration of the FGF21-neutralizing antibody raised the mRNA levels of *Fgf21* (Fig. 4*E*). The increase in *BiP* and

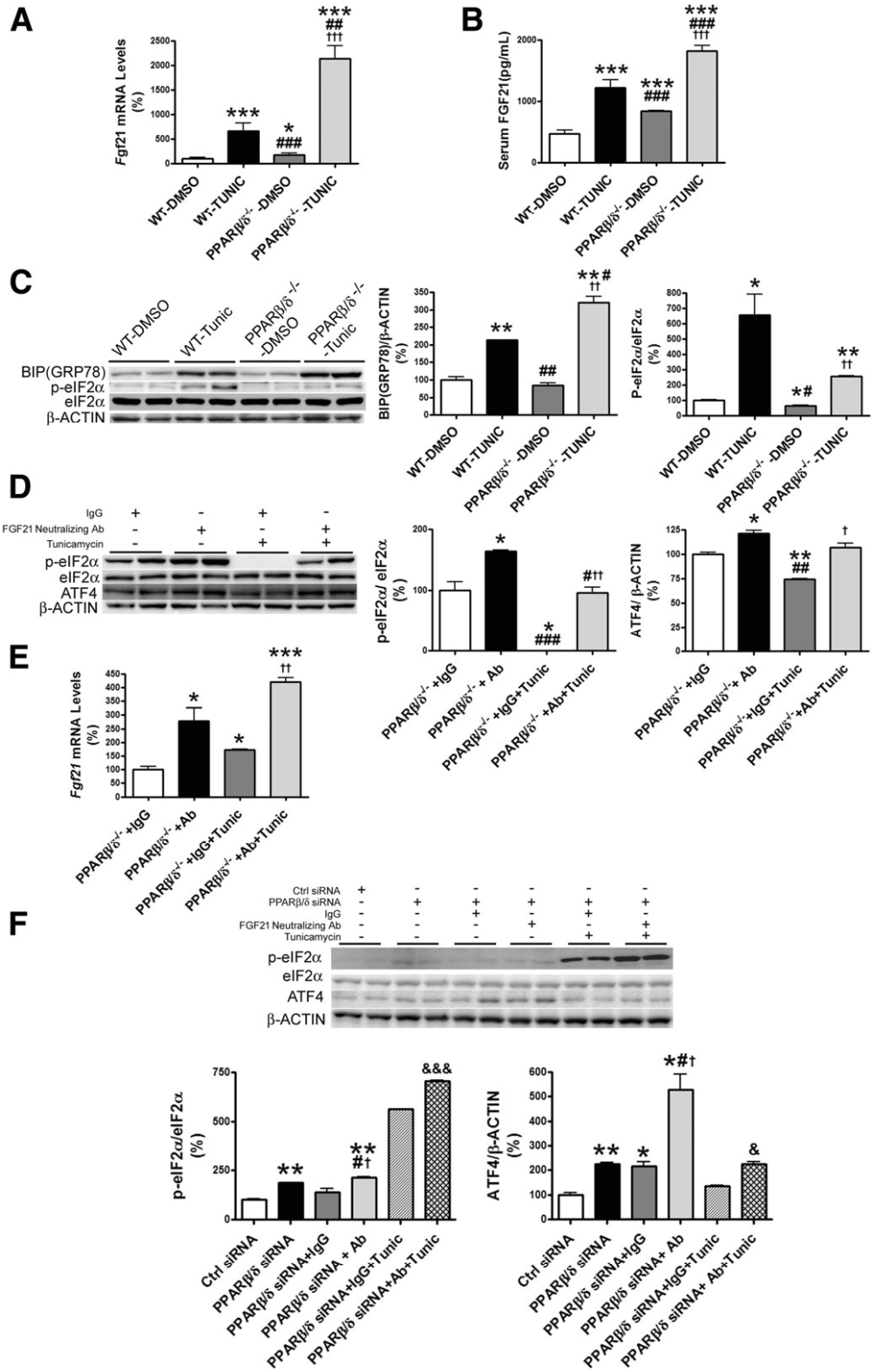

Figure 4— Increased *Fgf21* expression in liver of *Pparβ/δ*-null mice alleviates ER stress. Male wild-type (WT) and *Pparβ/δ*-null mice were treated for 24 h through intraperitoneal injection of DMSO (vehicle) or tunicamycin (Tunic) (3 mg · kg^{-1} body weight), and the mRNA abundance of hepatic *Fgf21* (*A*) and serum levels of FGF21 (*B*) were determined. Data are mean ± SD (n = 6/group). *C*: Immunoblot analyses of BiP and total and phospho (p)-eIF2α. **P* < 0.05, ***P* < 0.01, ****P* < 0.001 vs. WT animals treated with DMSO (vehicle); #*P* < 0.05, ##*P* < 0.01, ###*P* < 0.001 vs. WT animals treated with Tunic; ††*P* < 0.01, †††*P* < 0.001 vs. *Pparβ/δ*-null mice treated with DMSO (vehicle). *D*: Male WT and *Pparβ/δ*-null mice at 12 weeks of age were injected intraperitoneally with IgG (9 μg/mouse) or a neutralizing antibody (Ab) (9 μg/mouse) against FGF21 together with DMSO or Tunic (3 mg · kg^{-1} body weight). Mice were killed 14 h after treatment. Immunoblot analyses of total and p-eIF2α and ATF4 were performed in liver lysates. Data are mean ± SD (n = 4/group). *E*: mRNA

Atf3 expression and BiP protein levels confirmed that tunicamycin treatment for 14 h results in ER stress (Supplementary Fig. 2*C*–*E*).

Next, we explored whether the described mechanisms also operated in human HepG2 cells. Treatment with *Pparβ/δ* siRNA led to a significant increase in phosphorylated eIF2α and ATF4 levels (Fig. 4*F*), confirming that *Pparβ/δ* deficiency activates the eIF2α-ATF4 pathway. In addition, in the presence of the FGF21-neutralizing antibody, the increase in phospho-eIF2α and especially in ATF4 was exacerbated compared with IgG-treated cells. We then examined the effects of the FGF21-neutralizing antibody on tunicamycin-treated cells. In these cells, the FGF21-neutralizing antibody increased the levels of phosho-eIF2α and ATF4 protein compared with IgG-treated cells (Fig. 4*F*). Overall, these findings confirm that an increase in FGF21 levels in *Pparβ/δ*$^{-/-}$ mice prevents an increase in the eIF2α-ATF4 pathway, alleviating part of the ER stress process in liver.

In Liver, PPARβ/δ Activation Prevents the Increase in the HRI-eIF2α-ATF4 Pathway Caused by an HFD

Exposure to an HFD increases *Fgf21* expression (10), and we have previously reported that exposure to an HFD reduces hepatic mRNA levels of *Pgc-1α* (45). This suggests that exposure to an HFD might activate the HRI-eIF2α-ATF4 pathway and contribute to an increase in hepatic *Fgf21* expression. In mice exposed to an HFD for 3 weeks in the presence or absence of the PPARβ/δ activator GW501516, we observed that the HFD increased hepatic *Fgf21* expression by eightfold ($P < 0.05$), whereas this increase was prevented by GW501516 (Fig. 5*A*). Consistent with the changes in *Fgf21* expression, feeding with an HFD reduced MUP1 protein levels, whereas the PPARβ/δ agonist prevented the decrease caused by the HFD (Fig. 5*B*). No change was observed in the protein levels of the ER stress marker BiP (Supplementary Fig. 3*A*), rendering it unlikely that ER stress might be responsible for the increase in *Fgf21* expression caused by an HFD. Of note, the HFD strongly reduced the protein levels of PPARβ/δ, PGC-1α, and REV-ERBα, whereas ATF4 protein levels were increased (Fig. 5*C*). In contrast, these changes were abolished in mice fed the HFD and treated with GW501516. Furthermore, the reduction in PPARβ/δ, PGC-1α, and REV-ERBα was accompanied by a reduction in hemin levels (Supplementary Fig. 3*B*) and an increase in HRI levels in mice fed the HFD, whereas this increase was blunted following drug treatment (Supplementary Fig. 3*B* and Fig. 5*D*). To confirm whether FAs were the HFD component responsible for the changes observed in the in vivo study, we exposed human Huh-7 hepatocytes to the saturated fatty acid (SFA) palmitate. Cells incubated with palmitate showed a huge increase in *FGF21* and *ATF4* expression (Fig. 5*E*). Palmitate also elicited a reduction in PPARβ/δ, PGC-1α, and REV-ERBα and a subsequent increase in HRI, phospho-eIF2α, and ATF4 protein levels (Fig. 5*F*). These findings suggest that by reducing PPARβ/δ and PGC-1α, SFAs lead to activation of the HRI-eIF2α-ATF4 pathway and a subsequent increase in *FGF21* expression.

HRI Is a Pharmacological Target to Modulate Hepatic *Fgf21* Expression

Given that HRI regulates *FGF21*, we next explored its suitability as a pharmacological target to modulate hepatic *FGF21* expression. For this purpose, we used two N,N′-diarylureas, BTdCPU and BTCtFPU, which are HRI activators, thereby causing the phosphorylation of eIF2α and the increased expression of the transcription factor *ATF4* (24). Exposure of human Huh-7 hepatocytes to 10 μmol/L of either BTdCPU or BTCtFPU for 24 h strongly increased *Fgf21* and *Atf4* mRNA levels (Fig. 6*A* and *B*). The increase in the expression of *CHOP* (Fig. 6*C*), a direct ATF4 transcriptional target (42), confirmed that this pathway was activated by the N,N′-diarylureas. These compounds did not increase PPARα, its target genes, *BiP* mRNA (Supplementary Fig. 4*A*–*D*), or BiP protein levels (Fig. 6*D*), suggesting that these mechanisms were not involved in *Fgf21* upregulation. In line with the reported activation of HRI by these N,N′-diarylurea compounds, we observed increased protein levels of phospho-eIF2α and ATF4, especially following treatment with BTdCPU (Fig. 6*D*). Treatment of mice with BTdCPU for 1 week also increased hepatic *Fgf21* expression (Fig. 6*E*) without changes in BiP protein levels, whereas phospho-eIF2α and ATF4 were increased (Fig. 6*F*). Moreover, consistent with the increased expression of *Fgf21*, *Glut1* mRNA levels were higher in the white adipose tissue of mice treated with BTdCPU (Fig. 6*G*).

Next, we explored the effects of BTdCPU on human Huh-7 hepatocytes exposed to the SFA palmitate. Cells exposed to this FA showed increased *FGF21*, *ATF4*, and CHOP mRNA levels, and when cells were coincubated with the FA and BTdCPU, a significantly higher increase was observed in the expression of these three genes (Fig. 7*A*). Of note, when Huh-7 cells were exposed to palmitate, a high accumulation of triglycerides was observed in the cells, as demonstrated by ORO staining, but this accumulation was prevented in the presence of the BTdCPU

abundance of hepatic *Fgf21*. *$P < 0.05$, **$P < 0.01$, ***$P < 0.001$ vs. *Pparβ/δ*-null mice treated with IgG and DMSO; #$P < 0.05$, ##$P < 0.01$, ###$P < 0.001$ vs. *Pparβ/δ*-null mice treated with neutralizing Ab against FGF21 and DMSO; †$P < 0.05$, ††$P < 0.01$ vs. *Pparβ/δ*-null mice treated with IgG and Tunic. *F*: HepG2 cells transfected with control (Ctrl) siRNA or PPARβ/δ siRNA were coincubated with Tunic (2 μg/mL) and IgG (3 μg/mL) or a neutralizing Ab (3 μg/mL) against FGF21 for 24 h. Immunoblot analyses of total and p-eIF2α and ATF4 were performed in cell lysates. *$P < 0.05$, **$P < 0.01$ vs. Ctrl siRNA; #$P < 0.05$ vs. PPARβ/δ siRNA; †$P < 0.05$ vs. cells transfected with *PPARβ/δ* siRNA incubated with IgG; &$P < 0.05$, &&&$P < 0.001$ vs. cells transfected with *PPARβ/δ* siRNA coincubated with IgG and Tunic.

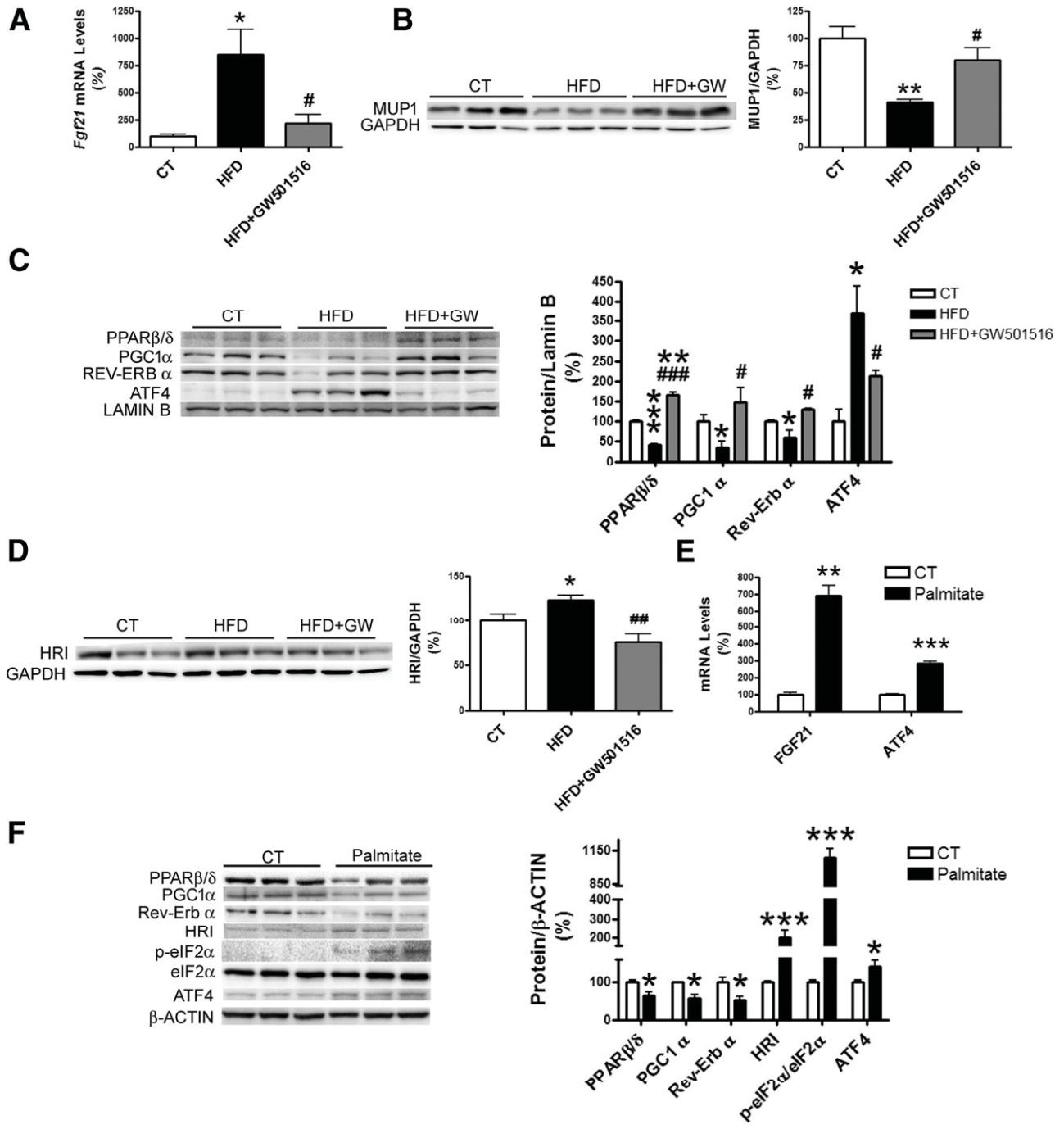

Figure 5—The increase in hepatic *Fgf21* expression caused by feeding an HFD is associated with a reduction in PPARβ/δ and subsequent activation of the HRI-eIF2α-ATF4 pathway. Male mice were fed a standard chow or an HFD with or without GW501516 (GW) (3 mg · kg^{-1} · day^{-1}). Animals were killed after 3 weeks of treatment. *A*: Assessment by quantitative real-time RT-PCR of hepatic *Fgf21*. Data are mean ± SD (n = 6/group) relative to the control (CT) group. *B–D*: Immunoblot analyses are shown for MUP1; PPARβ/δ, PGC-1α, REV-ERBα, and ATF4; and HRI. Data are mean ± SD (n = 6/group). *P < 0.05, **P < 0.01, ***P < 0.001 vs. CT group; #P < 0.05, ##P < 0.01, ###P < 0.001 vs. mice fed an HFD. *E*: Huh-7 hepatocytes were incubated for 16 h in the absence (CT) or presence of 0.5 mmol/L palmitate. mRNA abundance of *FGF21* and *ATF4* was measured. Data are mean ± SD (n = 6 per group). *F*: Immunoblot analyses of PPARβ/δ, PGC-1α, REV-ERBα, HRI, total and phospho (p)-eIF2α, and ATF4. Data are mean ± SD (n = 5/group). *P < 0.05, **P < 0.01, ***P < 0.001 vs. CT group.

compound, and this effect was attenuated in the presence of the FGF21-neutralizing antibody (Fig. 7*B* and Supplementary Fig. 5*A*). Similar effects were observed in mouse Hepa-1c1c7 hepatocytes (Supplementary Fig. 5*B*). Likewise, this compound partially restored the reduction in insulin-stimulated Akt phosphorylation caused by palmitate (Fig. 7*C* and Supplementary Fig. 5*C*), showing that this drug treatment prevents SFA-induced attenuation of

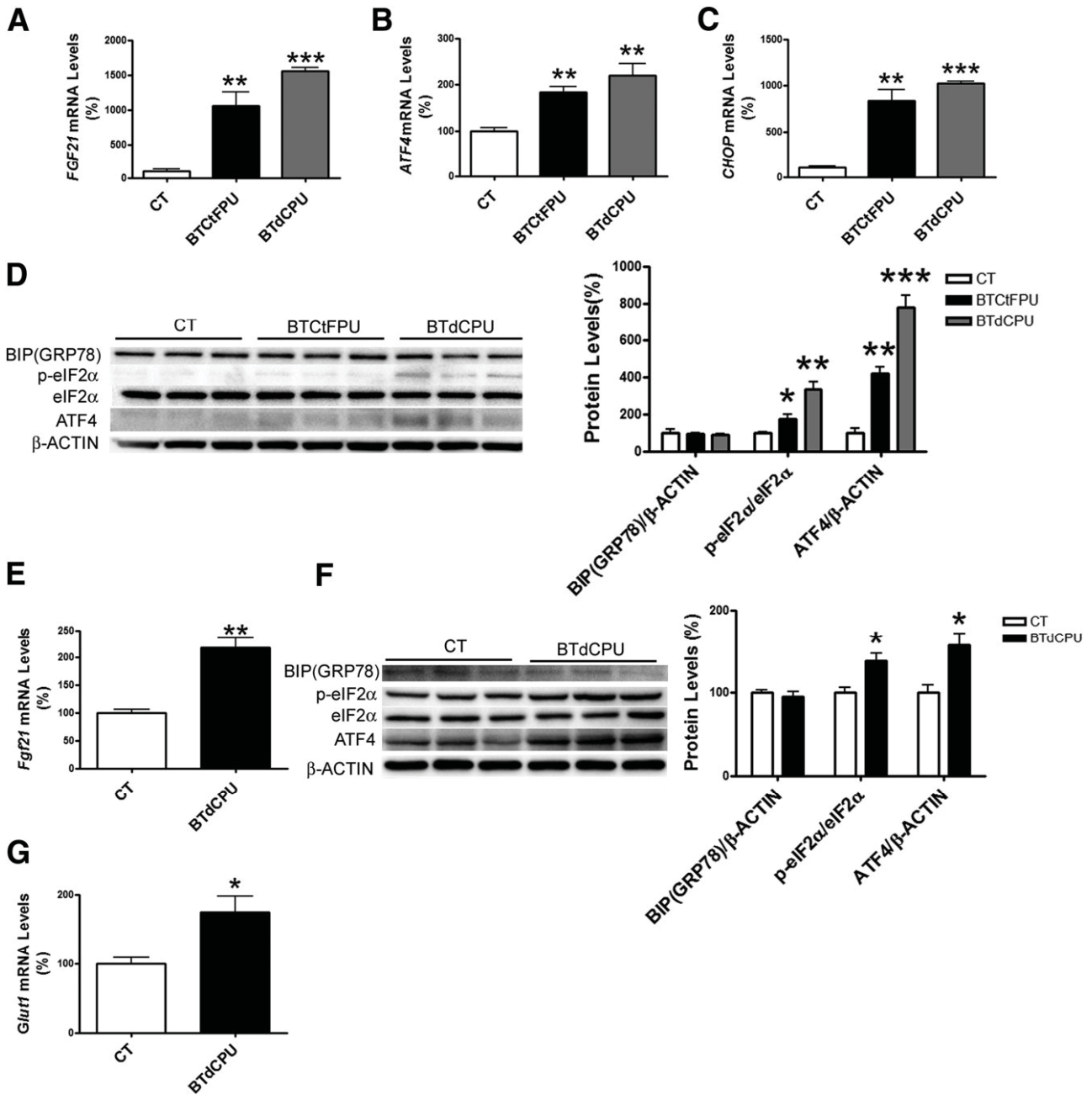

Figure 6—HRI activators increase *FGF21* expression in hepatocytes. Huh-7 hepatocytes were incubated for 16 h in the absence (control [CT]) or presence of 10 μmol/L of either BTdCPU or BTCtFPU. mRNA abundance of *FGF21* (*A*), ATF4 (*B*), and CHOP (*C*). Immunoblot analyses of BiP, total and phospho (p)-eIF2α, and ATF4 (*D*). *Fgf21* mRNA abundance (*E*) and immunoblot analyses (*F*) of BiP total and p-eIF2α and ATF4 in the livers of mice treated with DMSO (vehicle) or BTdCPU (70 mg · kg^{-1} · day^{-1}) for 7 days. *Glut1* mRNA abundance in white adipose tissue of mice treated with DMSO (vehicle) or BTdCPU (70 mg · kg^{-1} · day^{-1}) for 7 days (*G*). Data are mean ± SD (n = 5/group). *P < 0.05, **P < 0.01, ***P < 0.001 vs. CT group.

the insulin signaling pathway. Next, we examined the effects of the BTdCPU compound in mice fed an HFD. BTdCPU administration prevented the glucose intolerance caused by HFD feeding (Fig. 7*D*), increased *Glut1* expression in white adipose tissue (Fig. 7*E*), and prevented hepatic steatosis as demonstrated by ORO and hematoxylin-eosin staining and quantification of hepatic triglyceride levels (Fig. 7*F* and *G*). Drug treatment did not affect the expression of PPARα-target genes (Supplementary Fig. 5*D* and *E*), whereas the expression of the lipogenic gene fatty acid synthase (*Fas*) and stearoyl-CoA desaturase 1 (*Scd1*) was reduced (Supplementary Fig. 5*F* and *G*), which is consistent with the reported reduction of these genes by FGF21 (46).

To demonstrate more clearly that the improvement in glucose tolerance and hepatic steatosis caused by the administration of the HRI activator in mice fed an HFD

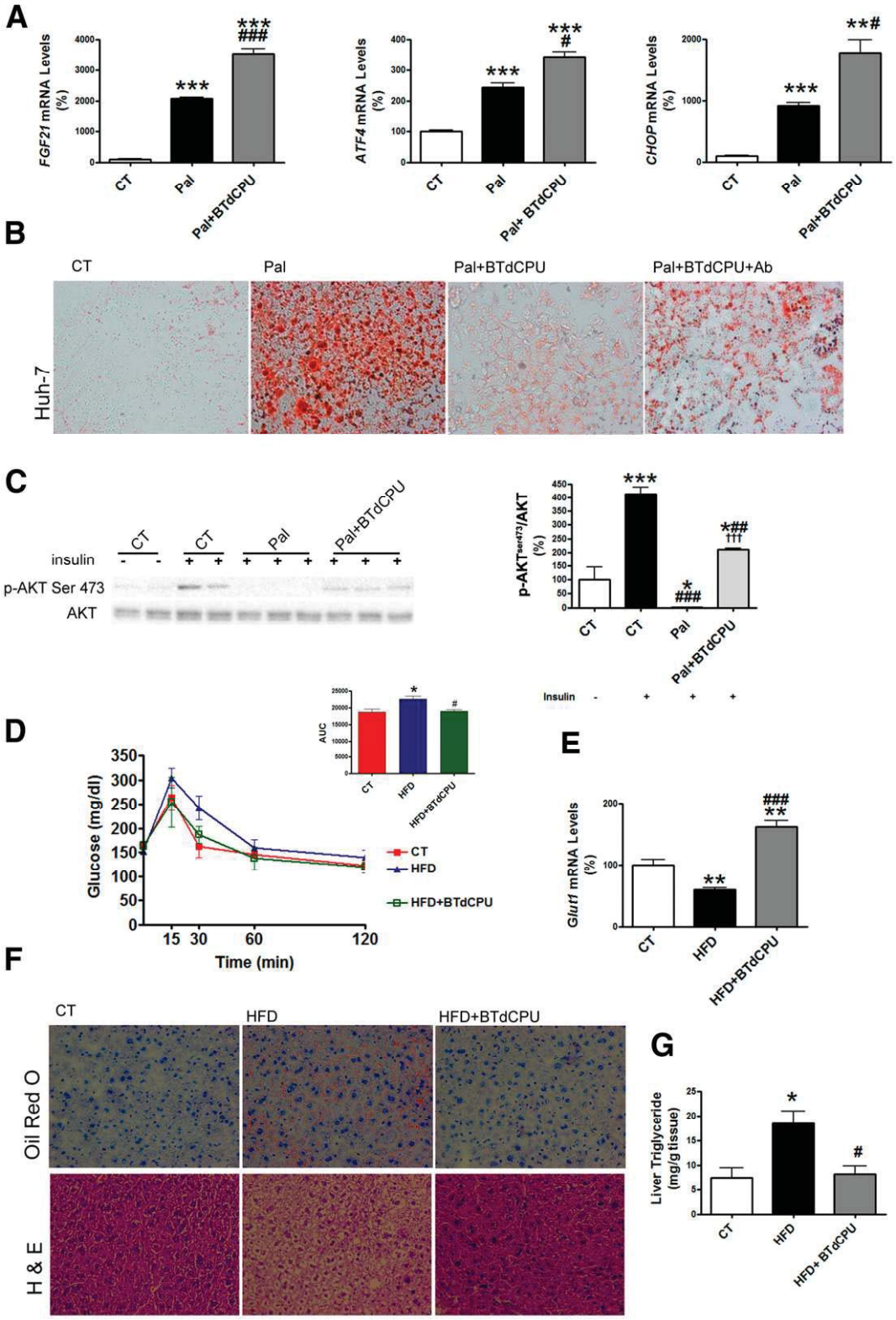

Figure 7—HRI activation prevents HFD-induced glucose intolerance and hepatic steatosis. Huh-7 cells were incubated for 24 h with BSA (control [CT]), 0.75 mmol/L palmitate (Pal) conjugated with BSA, or 0.75 mmol/L Pal plus 10 μmol/L BTdCPU. *A*: mRNA levels of *FGF21*, *ATF4*, and *CHOP*. Data are mean ± SD (n = 5/group). $^{**}P < 0.01$, $^{***}P < 0.001$ vs. CT group; $\#P < 0.05$, $\#\#\#P < 0.001$ vs. Pal-exposed cells. *B*: ORO staining of Huh-7 cells. Huh-7 cells were incubated for 24 h with BSA (CT), 0.75 mmol/L Pal conjugated with BSA, 0.75 mmol/L Pal plus 10 μmol/L BTdCPU, and IgG (3 μg/mL) or 0.75 mmol/L Pal plus 10 μmol/L BTdCPU and an FGF21-neutralizing antibody (Ab) (3 μg/mL). *C*: Immunoblot analyses of total and phosphorylated (p) Akt. When indicated, cells were incubated with 100 nmol/L insulin for the last 10 min. Data are mean ± SD (n = 4/group). $^{*}P < 0.05$, $^{***}P < 0.001$ vs. CT cells not exposed to insulin; $\#\#P < 0.01$, $\#\#\#P < 0.001$ vs. insulin-stimulated CT cells; $\dagger\dagger\dagger P < 0.001$ vs. insulin-stimulated cells incubated with Pal. *D*: Glucose tolerance test and

depends on FGF21, we used wild-type and *Fgf21*-null mice. The reduction in glucose intolerance observed in wild-type mice fed an HFD caused by administration of the HRI activator was completely abolished in *Fgf21*-null mice (Fig. 8*A*), suggesting that in the absence of FGF21, the effect of the HRI activator on glucose tolerance is lost. Similarly, the reduction in hepatic triglyceride accumulation in wild-type mice fed an HFD caused by BTdCPU administration was suppressed in *Fgf21*-null mice, as demonstrated by the analysis of the levels of triglycerides and the ORO and hematoxylin-eosin staining (Fig. 8*B* and *C*).

DISCUSSION

FGF21 has emerged as an important regulator of glucose and lipid metabolism and, hence, is a promising agent for the treatment of obesity, NAFLD, insulin resistance, and type 2 diabetes . Unraveling the mechanisms that regulate *Fgf21* expression in liver may provide pharmacological targets for modulating its expression to prevent metabolic diseases. In this study, we demonstrate that *Pparβ/δ*-null mice show enhanced hepatic *Fgf21* expression and circulating levels of this hormone. *Pparβ/δ* deficiency caused a reduction in transcriptional coactivator PGC-1α levels that resulted in a reduction in hemin levels and the subsequent activation of HRI and the eIF2α-ATF4 pathway, which is essential for *Fgf21*-induced expression (Fig. 8*D*). Likewise, activation of this pathway could be an additional mechanism that contributes to the increase in *Fgf21* expression under lipid overload conditions. The findings reveal HRI as a regulator of *Fgf21* expression and, consistent with this, knockdown of *Hri* or its pharmacological activation regulate *Fgf21* expression in hepatocytes.

The finding that *Pparβ/δ* deficiency upregulates *Fgf21* expression in liver was unexpected because it has previously been reported that pharmacological activation of this nuclear receptor increases FGF21 levels (20). The latter is consistent with the discovery of two putative peroxisome proliferator response elements in the mouse and human *FGF21* promoters (47) and that both PPARα and PPARγ activators increase FGF21 levels in hepatocytes and adipocytes, respectively. However, genetically reduced PGC-1α, a transcriptional coactivator that controls the expression and activity of PPARs and is regulated by these transcription factors, likewise results in increased FGF21 levels (18). In fact, reduced hepatic PGC-1α upregulates *Fgf21* expression by reducing REV-ERBα and the levels of its ligand heme. This alleviated the repressive activity of REV-ERBα on the *Fgf21* promoter, leading to enhanced *Fgf21* expression. In the current study, we show that *Pparβ/δ* deficiency results in a reduction in PGC-1α levels that leads to a reduction in REV-ERBα and hemin, the oxidized form of heme, suggesting that this mechanism can also contribute to an increase in *Fgf21* expression in the liver of *Pparβ/δ*-null mice. In addition, the current findings reveal a new biochemical pathway that can contribute to the enhanced expression of *Fgf21* in the liver of these mice. Indeed, the reduction in heme can increase HRI levels (42), which in turn can activate the eIF2α-ATF4 pathway where the increase in ATF4 is one of the most important transcription factors that upregulate *Fgf21* expression. In fact, overexpression of ATF4 has been reported to induce *Fgf21* expression (19), whereas knockdown of *Atf4* reduces basal and ER stress–induced *Fgf21* expression (48). Therefore, the current findings indicate that *Pparβ/δ* deficiency in liver results in increased levels of ATF4 and a subsequent increase in *Fgf21* expression. The increase in ATF4 levels seems to be a crucial step in *Fgf21* upregulation because this transcription factor is involved in the increase of this hormone in impaired mtOXPHOS induced by autophagy deficiency (19), ER stress (48), metformin-induced inhibition of the mitochondrial respiratory chain (49), and now PPARβ/δ-PGC-1α deficiency as shown in the current study.

As has been demonstrated by injection of recombinant FGF21 (43), the eIF2α-ATF4 pathway is activated by ER stress, which leads to enhanced *Fgf21* expression that in turn alleviates ER stress by suppressing this eIF2α-ATF4 pathway. By using a neutralizing antibody against FGF21, we confirm that this negative feedback is also activated by FGF21.

Of note, the reduction in PPARβ/δ and PGC-1α following exposure to an HFD might also contribute to increased *Fgf21* expression. In fact, livers of mice exposed to an HFD or hepatocytes exposed to the SFA palmitate showed reduced PPARβ/δ and PGC-1α levels, resulting in an increase in the levels of HRI and subsequent activation of the eIF2α-ATF4 pathway. These findings suggest that activation of this pathway could also contribute to the increase in FGF21 in those conditions associated with fat overfeeding, such as obesity, type 2 diabetes, and NAFLD, which show increased levels of this hormone (7–9). In contrast, activation of PPARβ/δ under conditions of lipid overload recovers PGC-1α levels and attenuates the eIF2α-ATF4 pathway, restoring *Fgf21* expression.

The regulation of FGF21 by HRI provides a target for regulation of the levels of this hormone to prevent or treat metabolic diseases, including NAFLD, insulin resistance, and diabetes. N,N′-diarylureas are activators of HRI that cause phosphorylation of eIF2α, which were developed as anticancer drugs (24). Here, we show that these drugs can increase *Fgf21* expression in hepatocytes

area under the curve (AUC) of mice fed a standard chow, an HFD for 3 weeks, or an HFD for 3 weeks plus BTdCPU during the last week. Mice fed a standard chow and one-half of the mice fed the HFD received one daily intraperitoneal administration of DMSO (vehicle) for the last week. The rest of the mice fed the HFD received one daily intraperitoneal administration of BTdCPU (70 mg · kg^{-1} · day^{-1}) for the last week. Data are mean ± SD (n = 6/group). *E*: *Glut1* mRNA abundance in the white adipose tissue. *F*: Hematoxylin-eosin (H & E) and ORO staining of livers. *G*: Liver triglyceride levels. *P < 0.05, **P < 0.01 vs. mice fed a standard diet (CT); #P < 0.05, ###P < 0.001 vs. mice fed an HFD.

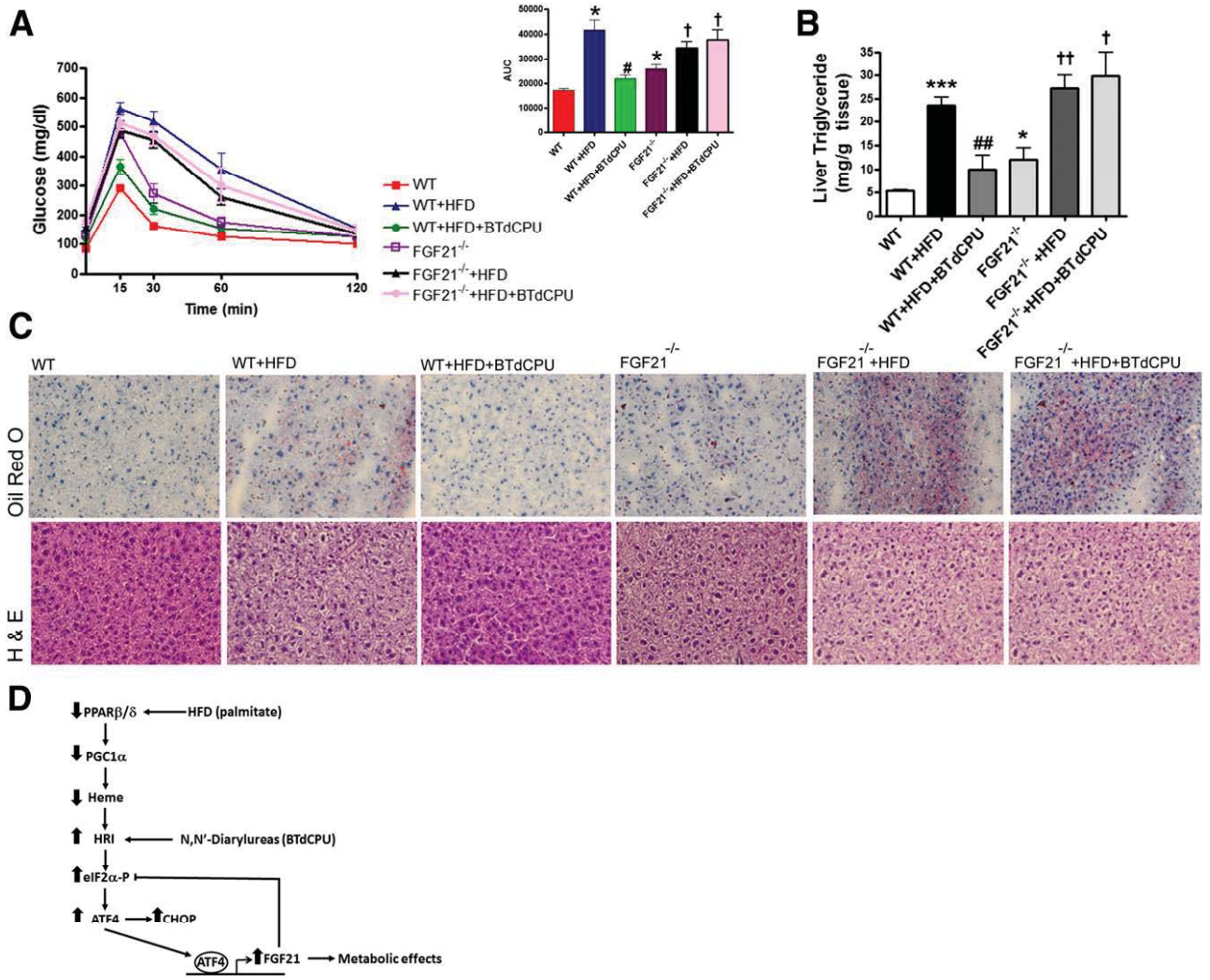

Figure 8—The beneficial effects of HRI pharmacological activation in glucose intolerance and hepatic steatosis depend on FGF21. *A*: Glucose tolerance test and area under the curve (AUC) of wild-type (WT) and *Fgf21*-null mice fed a standard chow diet, an HFD for 3 weeks, or an HFD for 3 weeks plus BTdCPU during the last week. Mice fed a standard chow and one-half of the mice fed the HFD received one daily intraperitoneal administration of DMSO (vehicle) for the last week. The rest of the mice fed the HFD received one daily intraperitoneal administration of BTdCPU (70 mg · kg^{-1} · day^{-1}) for the last week. Data are mean ± SD (n = 5/group). *B*: Liver triglyceride levels. *C*: Hematoxylin-eosin (H & E) and ORO staining of livers. **P* < 0.05, ****P* < 0.001 vs. WT mice fed a standard diet (control); #*P* < 0.05, ##*P* < 0.01 vs. mice fed an HFD; †*P* < 0.05, ††*P* < 0.01 vs. *Fgf21*-null mice fed a standard diet. *D*: Schematic representation of the potential role of *Pparβ/δ* deficiency in the regulation of hepatic *Fgf21* expression through activation of the HRI-eIF2α-ATF4 pathway. *Pparβ/δ* deficiency and overconsumption of HFD can result in the activation of this pathway, contributing to the increase in *Fgf21* expression observed under these conditions.

and that their administration to mice fed an HFD prevents the accumulation of triglycerides in liver and improves glucose intolerance. This is consistent with liver-specific *Fgf21* knockout mice fed an HFD displaying glucose intolerance and increased hepatic lipid accumulation (14). Moreover, we demonstrate that the improvement in glucose tolerance and hepatic steatosis caused by the HRI activator BTdCPU in mice fed an HFD depends on FGF21 because it was not observed in *Fgf21*-null mice.

In summary, we propose that *Pparβ/δ* deficiency results in a reduction in hepatic PGC-1α and hemin levels that in turn increase HRI levels, leading to activation of the eIF2α-ATF4 pathway and a subsequent increase in *Fgf21* expression. Moreover, pharmacological activation of HRI increases *Fgf21* expression, and treatment with a drug that activates HRI prevents glucose intolerance and hepatic triglyceride accumulation in mice fed an HFD. These findings point to HRI as a target for the treatment of metabolic diseases by modulating FGF21 levels.

Acknowledgments. M.Z. thanks Bijan Almassian, Massachusetts College of Pharmacy and Health Sciences. R.L. thanks the Spanish Ministry of Education for a PhD grant (FPU program). M.B.-X. thanks the Institute of Biomedicine of the University de Barcelona for a PhD grant.

Funding. This study was partly supported by funds from the Spanish Ministry of the Economy and Competitiveness (SAF2015-65267-R to Á.M.V.,

SAF2014-55725 to F.V., and SAF2012-30708 and SAF2015-64146-R to M.V.-C.) and the European Union European Regional Development Fund. CIBERDEM and CIBEROBN are Instituto de Salud Carlos III Health Institute projects. T.Q.-L. is supported by a CONACyT (National Council for Science and Technology in Mexico) PhD scholarship. W.W. is supported by start-up grants from the Lee Kong Chian School of Medicine, Nanyang Technological University, and by the Région Midi-Pyrénées, France.

Duality of Interest. No potential conflicts of interest relevant to this article were reported.

Author Contributions. M.Z. contributed to the study design, experiments, review of the results, and editing and final approval of the manuscript. E.B., X.P., V.P., Á.G.-R., Á.M.V., and T.Q.-L. contributed to the experiments and editing and final approval of the manuscript. R.L., M.B.-X., E.P., C.E., and S.V. synthesized the compounds and contributed to the editing and final approval of the manuscript. F.V. and W.W. contributed to the data analysis, review of the results, and editing and final approval of the manuscript. M.V.-C. contributed to the study design, experiments, review of the results, and writing, editing, and final approval of the manuscript. M.V.-C. is the guarantor of this work and, as such, had full access to all the data in the study and takes responsibility for the integrity of the data and the accuracy of the data analysis.

References

1. Potthoff MJ, Kliewer SA, Mangelsdorf DJ. Endocrine fibroblast growth factors 15/19 and 21: from feast to famine. Genes Dev 2012;26:312–324
2. Kharitonenkov A, Shiyanova TL, Koester A, et al. FGF-21 as a novel metabolic regulator. J Clin Invest 2005;115:1627–1635
3. Xu J, Lloyd DJ, Hale C, et al. Fibroblast growth factor 21 reverses hepatic steatosis, increases energy expenditure, and improves insulin sensitivity in diet-induced obese mice. Diabetes 2009;58:250–259
4. Xu J, Stanislaus S, Chinookoswong N, et al. Acute glucose-lowering and insulin-sensitizing action of FGF21 in insulin-resistant mouse models—association with liver and adipose tissue effects. Am J Physiol Endocrinol Metab 2009;297: E1105–E1114
5. Coskun T, Bina HA, Schneider MA, et al. Fibroblast growth factor 21 corrects obesity in mice. Endocrinology 2008;149:6018–6027
6. Badman MK, Kennedy AR, Adams AC, Pissios P, Maratos-Flier E. A very low carbohydrate ketogenic diet improves glucose tolerance in ob/ob mice independently of weight loss. Am J Physiol Endocrinol Metab 2009;297:E1197–E1204
7. Zhang X, Yeung DC, Karpisek M, et al. Serum FGF21 levels are increased in obesity and are independently associated with the metabolic syndrome in humans. Diabetes 2008;57:1246–1253
8. Chavez AO, Molina-Carrion M, Abdul-Ghani MA, Folli F, Defronzo RA, Tripathy D. Circulating fibroblast growth factor-21 is elevated in impaired glucose tolerance and type 2 diabetes and correlates with muscle and hepatic insulin resistance. Diabetes Care 2009;32:1542–1546
9. Li H, Fang Q, Gao F, et al. Fibroblast growth factor 21 levels are increased in nonalcoholic fatty liver disease patients and are correlated with hepatic triglyceride. J Hepatol 2010;53:934–940
10. Kharitonenkov A, Larsen P. FGF21 reloaded: challenges of a rapidly growing field. Trends Endocrinol Metab 2011;22:81–86
11. Kharitonenkov A, Dunbar JD, Bina HA, et al. FGF-21/FGF-21 receptor interaction and activation is determined by betaKlotho. J Cell Physiol 2008;215:1–7
12. Ogawa Y, Kurosu H, Yamamoto M, et al. BetaKlotho is required for metabolic activity of fibroblast growth factor 21. Proc Natl Acad Sci U S A 2007;104: 7432–7437
13. Suzuki M, Uehara Y, Motomura-Matsuzaka K, et al. betaKlotho is required for fibroblast growth factor (FGF) 21 signaling through FGF receptor (FGFR) 1c and FGFR3c. Mol Endocrinol 2008;22:1006–1014
14. Markan KR, Naber MC, Ameka MK, et al. Circulating FGF21 is liver derived and enhances glucose uptake during refeeding and overfeeding. Diabetes 2014; 63:4057–4063
15. Lefebvre P, Chinetti G, Fruchart JC, Staels B. Sorting out the roles of PPAR alpha in energy metabolism and vascular homeostasis. J Clin Invest 2006;116: 571–580
16. Kim H, Mendez R, Zheng Z, et al. Liver-enriched transcription factor CREBH interacts with peroxisome proliferator-activated receptor α to regulate metabolic hormone FGF21. Endocrinology 2014;155:769–782
17. Wang Y, Solt LA, Burris TP. Regulation of FGF21 expression and secretion by retinoic acid receptor-related orphan receptor alpha. J Biol Chem 2010;285: 15668–15673
18. Estall JL, Ruas JL, Choi CS, et al. PGC-1alpha negatively regulates hepatic FGF21 expression by modulating the heme/Rev-Erb(alpha) axis. Proc Natl Acad Sci U S A 2009;106:22510–22515
19. Kim KH, Jeong YT, Oh H, et al. Autophagy deficiency leads to protection from obesity and insulin resistance by inducing Fgf21 as a mitokine. Nat Med 2013;19:83–92
20. Christodoulides C, Dyson P, Sprecher D, Tsintzas K, Karpe F. Circulating fibroblast growth factor 21 is induced by peroxisome proliferator-activated receptor agonists but not ketosis in man. J Clin Endocrinol Metab 2009;94:3594–3601
21. Evans RM, Barish GD, Wang YX. PPARs and the complex journey to obesity. Nat Med 2004;10:355–361
22. Salvadó L, Serrano-Marco L, Barroso E, Palomer X, Vázquez-Carrera M. Targeting PPARβ/δ for the treatment of type 2 diabetes mellitus. Expert Opin Ther Targets 2012;16:209–223
23. Giordano Attianese GM, Desvergne B. Integrative and systemic approaches for evaluating PPARβ/δ (PPARD) function. Nucl Recept Signal 2015;13:e001
24. Chen T, Ozel D, Qiao Y, et al. Chemical genetics identify eIF2α kinase heme-regulated inhibitor as an anticancer target. Nat Chem Biol 2011;7:610–616
25. Nadra K, Anghel SI, Joye E, et al. Differentiation of trophoblast giant cells and their metabolic functions are dependent on peroxisome proliferator-activated receptor beta/delta. Mol Cell Biol 2006;26:3266–3281
26. Salvadó L, Coll T, Gómez-Foix AM, et al. Oleate prevents saturated-fatty-acid-induced ER stress, inflammation and insulin resistance in skeletal muscle cells through an AMPK-dependent mechanism. Diabetologia 2013;56:1372–1382
27. Benveniste R, Danoff TM, Ilekis J, Craig HR. Epidermal growth factor receptor numbers in male and female mouse primary hepatocyte cultures. Cell Biochem Funct 1988;6:231–235
28. Koopman R, Schaart G, Hesselink MKC. Optimisation of oil red O staining permits combination with immunofluorescence and automated quantification of lipids. Histochem Cell Biol 2001;116:63–68
29. Li H, Gao Z, Zhang J, et al. Sodium butyrate stimulates expression of fibroblast growth factor 21 in liver by inhibition of histone deacetylase 3. Diabetes 2012;61:797–806
30. Inagaki T, Lin VY, Goetz R, Mohammadi M, Mangelsdorf DJ, Kliewer SA. Inhibition of growth hormone signaling by the fasting-induced hormone FGF21. Cell Metab 2008;8:77–83
31. Ge X, Chen C, Hui X, Wang Y, Lam KS, Xu A. Fibroblast growth factor 21 induces glucose transporter-1 expression through activation of the serum response factor/Ets-like protein-1 in adipocytes. J Biol Chem 2011;286:34533–34541
32. Badman MK, Pissios P, Kennedy AR, Koukos G, Flier JS, Maratos-Flier E. Hepatic fibroblast growth factor 21 is regulated by PPARalpha and is a key mediator of hepatic lipid metabolism in ketotic states. Cell Metab 2007;5:426–437
33. Iizuka K, Takeda J, Horikawa Y. Glucose induces FGF21 mRNA expression through ChREBP activation in rat hepatocytes. FEBS Lett 2009;583:2882–2886
34. Nygaard EB, Vienberg SG, Ørskov C, Hansen HS, Andersen B. Metformin stimulates FGF21 expression in primary hepatocytes. Exp Diabetes Res 2012; 2012:465282
35. Li Y, Wong K, Giles A, et al. Hepatic SIRT1 attenuates hepatic steatosis and controls energy balance in mice by inducing fibroblast growth factor 21. Gastroenterology 2014;146:539–49.e7

36. Okazaki M, Iwasaki Y, Nishiyama M, et al. PPARbeta/delta regulates the human SIRT1 gene transcription via Sp1. Endocr J 2010;57:403–413
37. Wu Z, Puigserver P, Andersson U, et al. Mechanisms controlling mitochondrial biogenesis and respiration through the thermogenic coactivator PGC-1. Cell 1999;98:115–124
38. St-Pierre J, Lin J, Krauss S, et al. Bioenergetic analysis of peroxisome proliferator-activated receptor gamma coactivators 1alpha and 1beta (PGC-1alpha and PGC-1beta) in muscle cells. J Biol Chem 2003;278:26597–26603
39. Woldt E, Sebti Y, Solt LA, et al. Rev-erb-α modulates skeletal muscle oxidative capacity by regulating mitochondrial biogenesis and autophagy. Nat Med 2013;19:1039–1046
40. Ron D, Walter P. Signal integration in the endoplasmic reticulum unfolded protein response. Nat Rev Mol Cell Biol 2007;8:519–529
41. Chen JJ. Regulation of protein synthesis by the heme-regulated eIF2alpha kinase: relevance to anemias. Blood 2007;109:2693–2699
42. Lu PD, Harding HP, Ron D. Translation reinitiation at alternative open reading frames regulates gene expression in an integrated stress response. J Cell Biol 2004;167:27–33
43. Jiang S, Yan C, Fang QC, et al. Fibroblast growth factor 21 is regulated by the IRE1α-XBP1 branch of the unfolded protein response and counteracts endoplasmic reticulum stress-induced hepatic steatosis. J Biol Chem 2014;289:29751–29765
44. Salvadó L, Barroso E, Gómez-Foix AM, et al. PPARβ/δ prevents endoplasmic reticulum stress-associated inflammation and insulin resistance in skeletal muscle cells through an AMPK-dependent mechanism. Diabetologia 2014;57:2126–2135
45. Barroso E, Rodríguez-Calvo R, Serrano-Marco L, et al. The PPARβ/δ activator GW501516 prevents the down-regulation of AMPK caused by a high-fat diet in liver and amplifies the PGC-1α-Lipin 1-PPARα pathway leading to increased fatty acid oxidation. Endocrinology 2011;152:1848–1859
46. Zhang Y, Lei T, Huang JF, et al. The link between fibroblast growth factor 21 and sterol regulatory element binding protein 1c during lipogenesis in hepatocytes. Mol Cell Endocrinol 2011;342:41–47
47. Lundåsen T, Hunt MC, Nilsson LM, et al. PPARalpha is a key regulator of hepatic FGF21. Biochem Biophys Res Commun 2007;360:437–440
48. Kim SH, Kim KH, Kim HK, et al. Fibroblast growth factor 21 participates in adaptation to endoplasmic reticulum stress and attenuates obesity-induced hepatic metabolic stress. Diabetologia 2015;58:809–818
49. Kim KH, Jeong YT, Kim SH, et al. Metformin-induced inhibition of the mitochondrial respiratory chain increases FGF21 expression via ATF4 activation. Biochem Biophys Res Commun 2013;440:76–81

SUPPLEMENTARY DATA

Supplementary Materials

The research complied with the Guide for the Care and Use of Laboratory Animals published by the US National Institutes of Health (NIH Publication No. 85-23, revised 1996). All procedures were approved by the University of Barcelona Bioethics Committee, as stated in Law 5/21 July 1995 passed by the Generalitat de Catalunya.

Reagents

Control and HRI siRNA were purchased from Santa Cruz (Dallas, TX) and PPARβ/δ siRNA from GE Dharmacon (Lafayette, CO). Human and mouse FGF21 neutralizing antibodies were purchased from Antibody and Immunoassays Services (Hong Kong, China).

Plasma FGF21 was measured using a rat/mouse FGF21 ELISA kit (Millipore, Bedford, MA). Serum glucose (Bayer Iberia, Sant Joan Despí, Spain), triglyceride (Sigma) and free fatty acid (FFA) (Wako, Japan) levels were measured using commercial kits.

Cell culture

Human HepG2 and Huh-7 and mouse Hepa1c1c7 cells were purchased from the ATCC and cultured in DMEM supplemented with 10% serum, at 37°C/5% CO2. siRNA transfections were performed with Lipofectamine 2000 (Life Technologies).

Synthesis of N,N'-diarylureas

Step 1. (2-Amino-5-nitrophenyl) disulphide 2

15 g (83.4 mmol) 6-nitrobenzothiazole 1 was suspended in abs. ethanol (300 mL). Hydrazine hydrate (30 mL, 600 mmol) was added and the mixture was refluxed for 2 h, converting from a yellow mixture to a dark red solution. The reaction was cooled to 30 °C and 50% hydrogen peroxide (16.2 mL) was added in small portions, maintaining the temperature with an ice water bath. On completion, the red color disappeared and a yellow precipitate formed. The suspension was stirred for 1 h, the precipitate was collected, washed with water and diethyl ether, and dried to give 11.71 g of product 2. Yield: 83.5%. 1H-NMR (400 MHz, DMSO) δ: 6.85 (d, J = 9.2 Hz, 2 H, 3-H), 7.21 (b. s., 4 H, NH2), 7.51 (d, J = 2.6 Hz, 2 H, 6-H), 7.99 (dd, J = 9.2 Hz, J' = 2.6 Hz, 2 H, 4-H).

Step 2. 6-Nitro-1,2,3-benzothiadiazole 3

11.68 g (34.5 mmol) (2-amino-5-nitrophenyl) disulphide 2 was dissolved in concentrated sulfuric acid (96 mL), chilled to 0 °C, and 5.45 g (86.3 mmol) sodium nitrite was added in small portions, while the temperature was kept under 10 °C. The reaction was allowed to warm to room temperature and stirred for 18 h. The reaction mixture was poured into a mixture of 650 g ice and water (65 mL), stirred for 1 h, and the pale brown precipitate was collected, then washed with water and diethyl ether. The crude product was taken up in dichloromethane (1 x 300 mL), filtered, and the filtrate was treated with a small amount of charcoal (1 g), filtered, and evaporated to give 5.29 g of a brown solid. Yield: 42.3% NMR: 90%. Column chromatography on alumina (Hexane 95%/Ethyl acetate 5% mixture) gave product 3 as a yellow solid (3.45 g). 1H-NMR (400 MHz, CDCl3) δ: 8.51 (dd, J = 9.2 Hz, J' = 2.0 Hz, 1 H, 5-H), 8.80 (d, J = 9.2 Hz, 1 H, 4-H), 9.04 (d, J = 2.0, 1 H, 7-H). 13C-NMR (100.5 MHz, CDCl3) δ: 115.7 (CH,

C7), 122.0 (CH, C5), 124.8 (CH, C4), 141.1 (C, C3a), 147.7 (C, C7a), 159.5 (C, C6).

Step 3. 6-Amino-1,2,3-thiadiazole 4

2 g (11.0 mmol) 6-nitro-1,2,3-benzothiadiazole 3 was added to a solution of 10.6 g tin (II) chloride in concentrated hydrochloric acid (16 mL) at 55 °C, using a water bath to maintain that temperature. The reaction mixture was heated to 70 °C for 10 min, then cooled to 4 °C and let stand for 18 h. The crystalline precipitate was collected and washed with ice cold water. The solid was dissolved in water (40 mL) and 10 N sodium hydroxide (10 mL) was added followed by ethyl acetate (30 mL) and the mixture was stirred for 15 min. The layers were separated; the aqueous layer was extracted with, then ethyl acetate (1 x 30 mL, 1 x 20 mL). The organic layers were combined, washed with saturated brine (1 x 20 mL), water (1 x 20 mL) and evaporated to give 0.97 g of product 4. Yield: 58%. 1H-NMR (400 MHz, CDCl3) δ: 4.20 (b. s., 2 H, NH2), 6.92 (dd, J = 9.2 Hz, J' = 2.4 Hz, 1 H, 5-H), 7.13 (d, J = 2.4 Hz, 1 H, 7-H), 8.34 (d, J = 9.2, 1 H, 4-H). 13C-NMR (100.5 MHz, CDCl3) δ: 100.4 (CH, C7), 117.0 (CH, C5), 124.5 (CH, C4), 143.8 (C, C3a), 148.1 (C, C7a), 152.9 (C, C6).

1.44 g (7.9 mmol) 6-nitro-1,2,3-benzothiadiazole 3 was added to a solution of 7.6 g tin (II) chloride in concentrated hydrochloric acid (12 mL) at 55 °C, using a water bath to maintain that temperature. The reaction mixture was heated to 70 °C for 10 min, then cooled to 4 °C and let stand for 18 h. The crystalline precipitate was dissolved in water (20 mL) and 10 N sodium hydroxide (5 mL) was added followed by ethyl acetate (20 mL) and the mixture was stirred for 15 min. The layers were separated; the aqueous layer was extracted with, then ethyl acetate (1 x 20 mL, 1 x 10 mL). The organic layers were combined, washed with saturated brine (1 x 20 mL), water (1 x 20 mL) and evaporated to give 0.84 g of product 4. Yield: 70%

Step 4a. 1-(1,2,3-Benzothiadiazol-6-yl)-3-(4-chloro-3-(trifluoromethyl)phenyl)urea 5

0.5 g (3.31 mmol) 6-Amino-1,2,3-thiadiazole 4, and 0.81 g (3.64 mmol) 4-chloro-3-(trifluoromethyl)phenyl isocyanate were dissolved in tetrahydrofuran (13 mL), and stirred at room temperature for 2.5 h; a white precipitate formed. IR (ATR) ν: 659, 679, 720, 749, 782, 812, 840, 863, 875, 910, 949, 1026, 1130, 1173, 1220, 1249, 1268, 1321, 1352, 1403, 1469, 1484, 1545, 1573, 1708, 3094, 3132, 3266, 3302, 3339. 1H-NMR (400 MHz, CDCl3) δ: 7.63-7.67 (c. s., 2 H, 5'-H, 6'-H), 7.69 (dd, J = 9.2 Hz, J' = 2.0 Hz, 1 H, 5-H), 8.17 (d, J = 2.0 Hz, 1 H, 2'-H), 8.59 (d, J = 9.2 Hz, 1 H, 4-H), 8.63 (d, J = 2.0, 1 H, 7-H), 9.38 (b. s., 1 H, NH), 9.52 (b. s., 1 H, NH). 13C-NMR (100.5 MHz, CDCl3) δ: 106.8 (CH, C7), 117.0 (q, J = 6.1 Hz, CH, C2'), 119.8 (CH, C5), 122.76 (q, J = 273.2 Hz, C, CF3), 122.83 (q, J = 2.0 Hz, C, C4'), 123.3 (b. s., CH, C5'), 123.6 (CH, C4), 126.7 (q, J = 31.0 Hz, C, C3'), 132.0 (CH, C6'), 138.9 (C, C1'), 140.8 (C, C3a), 142.2 (C, C7a), 152.2 (C, C6), 153.8 (C, CO). Calcd for C14H8ClF3N4OS · 2/3 H20: C 43.70, H 2.45, N 14.56. Found: C 43.75, H 2.43, N 14.60.

Step 4b. 1-(1,2,3-Benzothiadiazol-6-yl)-3-(3,4-dichlorophenyl)urea 6

0.5 g (3.31 mmol) 6-Amino-1,2,3-thiadiazole 4, and 0.68 g (3.64 mmol) 3,4dichlorophenyl isocyanate were dissolved in tetrahydrofuran (13 mL), and stirred at room temperature for 2.5 h; a white precipitate formed. Methanol (0.3 mL) was added and the mixture was stirred for 15 min, cooled to 0 °C in an ice-water bath, stirred for 30 min, and the precipitate was collected and washed with ice cold tetrahydrofuran to give 0.71 g of product 6 (68% yield), mp 267 – 269 °C (dec). IR (ATR) ν: 685, 731, 746, 805, 856, 881, 910, 1026, 1060, 1129, 1220, 1265, 1304, 1351, 1385, 1417, 1455, 1467, 1531, 1567, 1673, 3098, 3171, 3306. 1H-NMR (400 MHz, CDCl3) δ: 7.38 (dd, J = 9.2 Hz, J' = 2.4 Hz, 1 H,

6’-H), 7.55 (d, J = 9.2 Hz, 1 H, 5’-H), 7.69 (dd, J = 9.2 Hz, 1 H, J’ = 2.0 Hz, 1 H, 5-H), 7.91 (d, J = 2.4 Hz, 1 H, 2’-H), 8.56-8.60 (c. s., 2 H, 4-H, 7-H), 9.20 (b. s., 1 H, NH), 9.47 (b. s., 1 H, NH). 13C-NMR (100.5 MHz, CDCl3) δ: 106.7 (CH, C7), 118.6 (CH, C6’), 119.6 (CH, C2’), 119.7 (CH, C5), 123.58 (C, C4), 123.64 (C, C4’), 130.6 (CH, C6’), 131.1 (C, C3’), 731, 746,139.5 (C, C1’), 140.8 (C, C3a), 142.2 (C, C7a), 152.1 (C, C6), 153.8 (C, CO). Calcd for C13H8Cl2N4OS: C 46.03, H 2.38, N 16.52. Found: C 45.89, H 2.36, N 16.10.

SUPPLEMENTARY DATA

Supplementary Figure 1. A, liver cell lysates from male wild-type and PPARβ/δ-null mice were assayed for Western-blot analysis with antibodies against MUP-1 and β-actin. Data are presented as the mean ± S.D. (n=6 per group) relative to the wild-type mice. Serum free fatty acids (FFA) (B) and glucose (C) levels in wild-type and PPARβ/δ-null mice. D, mRNA levels of hepatic *Pparα*, *Acox1* and *Mcad*. E, mRNA abundance of *Chop*, *Orp150* and *Atf3*. F, immunoblot analyses of total and phospho-IRE1. Data are presented as the mean ± S.D. (n=6 per group). G, *PPARβ/δ* mRNA abundance in primary hepatocytes transfected with control siRNA or PPARβ/δ siRNA for 24 h. ***p<0.001 and **p<0.01 vs. wild-type mice.

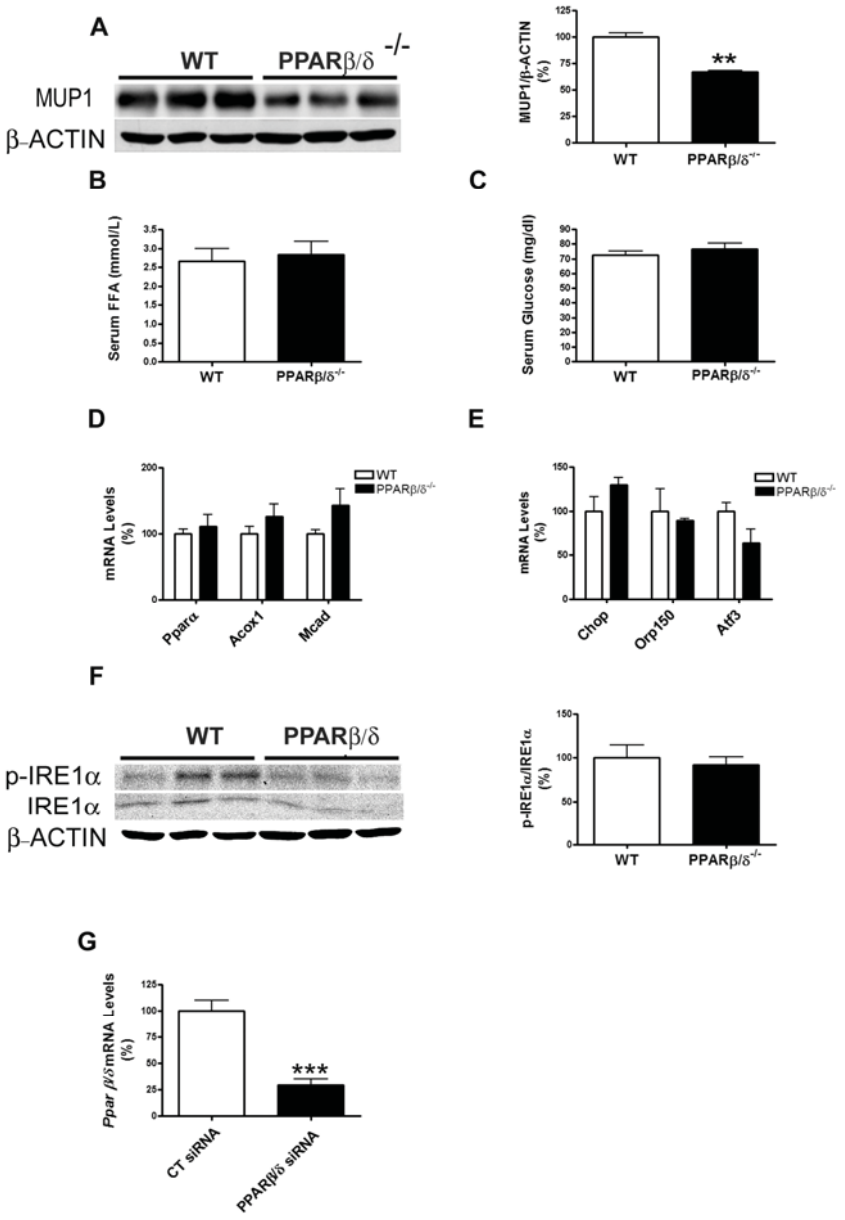

SUPPLEMENTARY DATA

Supplementary Figure 2. A, Male wild-type and PPARβ/δ-null mice at 12 weeks of age were treated for 24 h through intraperitoneal injection with DMSO (vehicle) or tunicamycin (Tunic) (3 mg kg^{-1} body weight) and the mRNA abundance of hepatic *BiP* was determined. B, male wild-type mice were injected intraperitoneally with IgG or a neutralizing antibody (Ab) against FGF21. Immunoblot analyses of total and phospho-eIF2α. Data are presented as the mean ± S.D. (n=6 per group). Male wild-type and PPARβ/δ-null mice were injected intraperitoneally with IgG or a neutralizing antibody (Ab) against FGF21 together with DMSO or tunicamycin (Tunic) (3 mg kg^{-1} body weight). Mice were sacrificed at 14 h after treatment. mRNA abundance of hepatic *BiP* (C) and *Atf3* (D). Data are presented as the mean ± S.D. (n=6 per group). E, immunoblot analyses of hepatic BiP. Data are presented as the mean ± S.D. (n=4 per group). $^{***}p<0.001$, $^{**}p<0.01$ and $^{*}p<0.05$ *vs.* PPARβ/δ-null mice treated with IgG and DMSO. $^{###}p<0.001$, $^{##}p<0.01$ and $^{#}p<0.05$ *vs.* PPARβ/δ-null mice treated with neutralizing antibody against FGF21 and DMSO. $^{†††}p<0.001$ *vs.* PPARβ/δ-null mice treated with IgG and tunicamycine.

SUPPLEMENTARY DATA

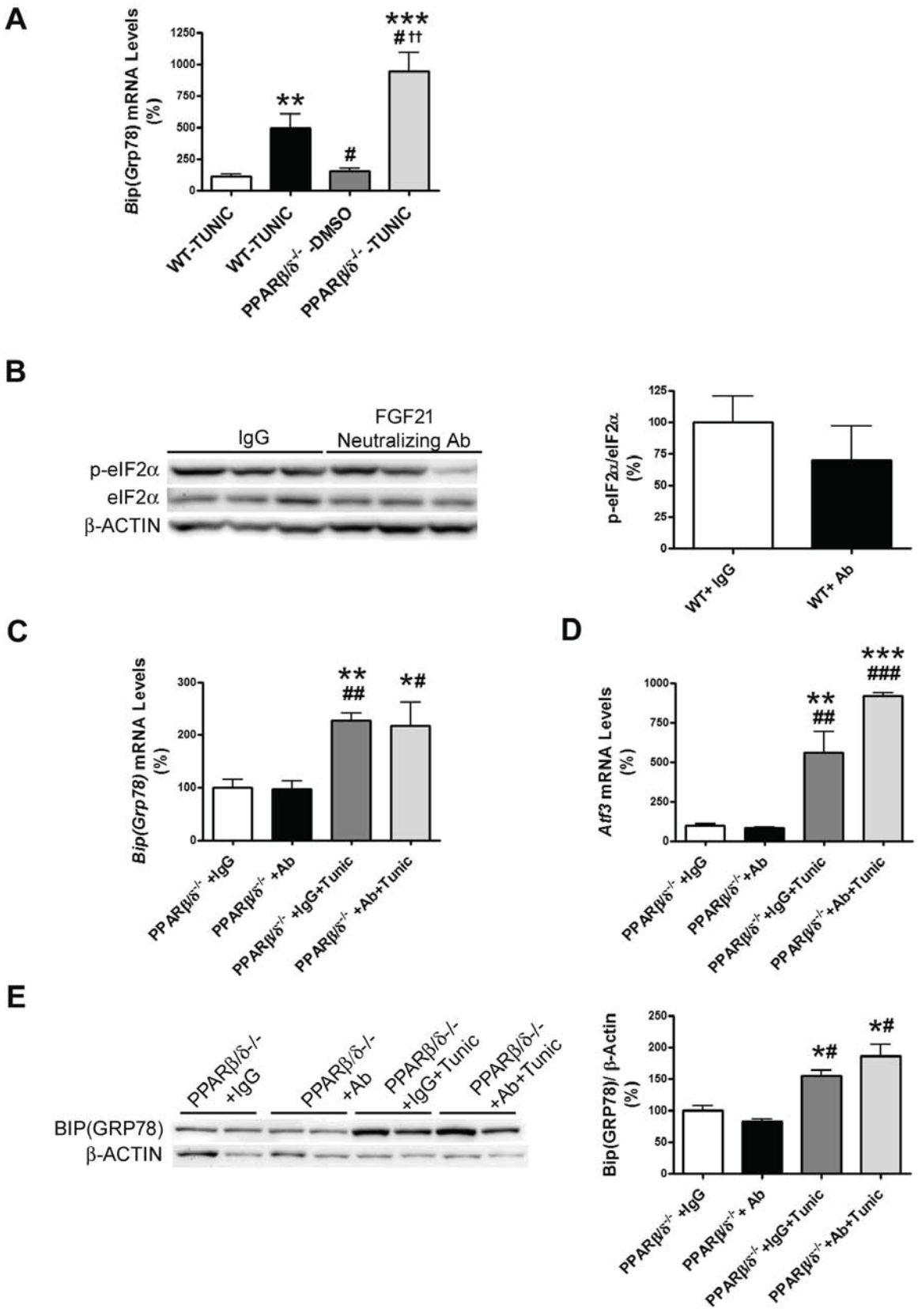

SUPPLEMENTARY DATA

Supplementary Figure 3. Male mice were fed a standard chow or HFD with or without GW501516 (3 mg kg^{-1} day^{-1}). Animals were sacrificed after three weeks of treatment. A, Immunoblot analyses of BiP. B, hemin levels. Data are presented as the mean ± S.D. (n=6 per group).

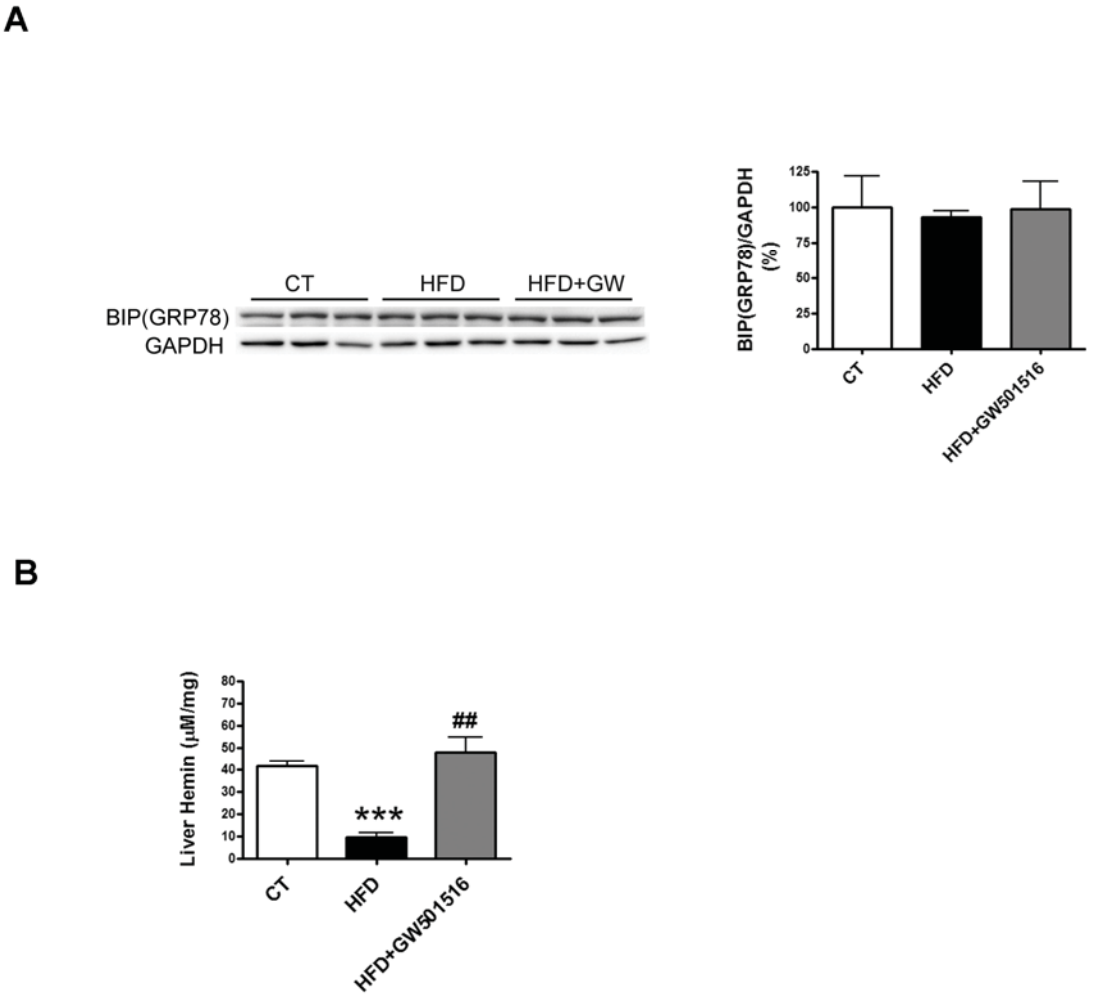

SUPPLEMENTARY DATA

Supplementary Figure 4. Huh-7 hepatocytes were incubated for 24 h in the absence (Control, CT) or in the presence of 10 μmol/L of either BTdCPU or BTCtFPU. mRNA abundance of PPARα (A), ACOX (B), MCAD (C) and BiP (D Data are presented as the mean ± S.D. (n=5 per group).

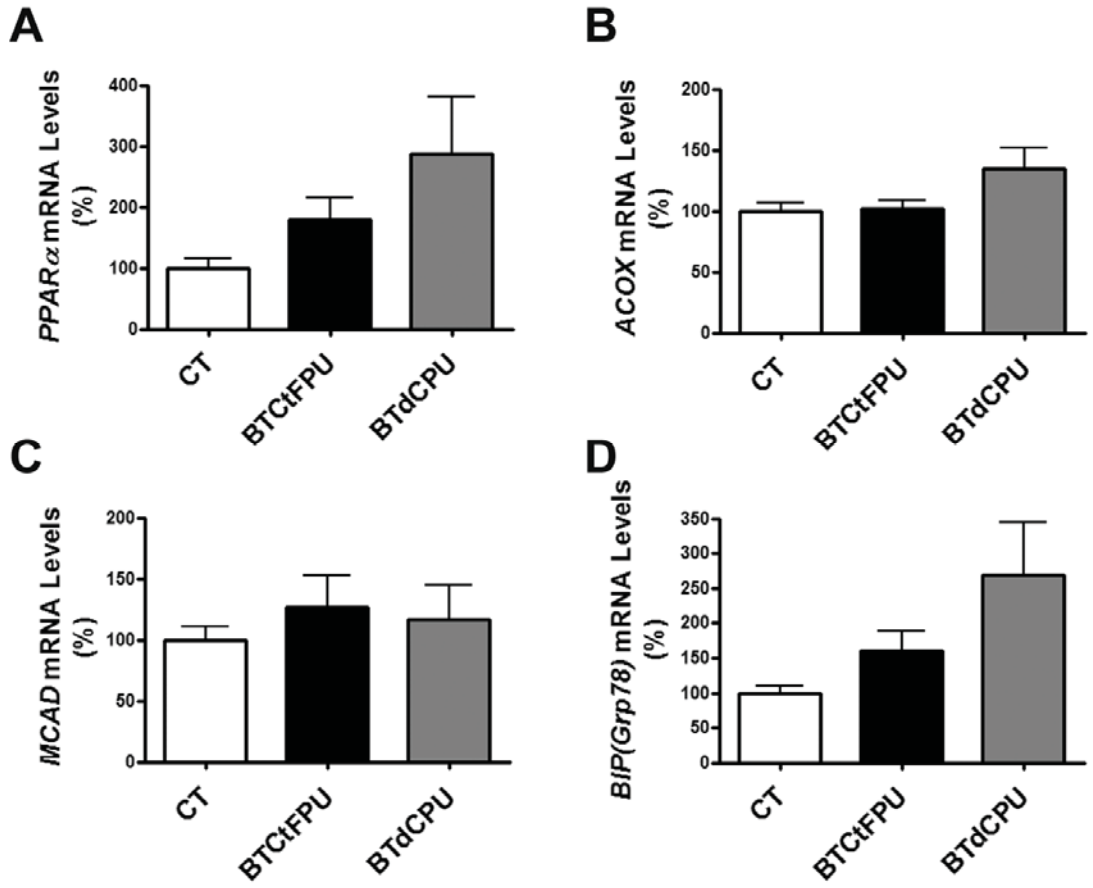

SUPPLEMENTARY DATA

Supplementary Figure 5. Oil Red O staining of Huh-7 (A) and Hepa1c1c7 (B) hepatocytes. Cells were incubated for 24 h with BSA (Control, CT), 0.75 mmol/L palmitate (Pal) conjugated with BSA, 0.75 mmol/L palmitate plus 10 μmol/L BTdCPU and IgG (3 μg/ml) or 0.75 mmol/L palmitate plus 10 μmol/L BTdCPU and a FGF21 neutralizing antibody (Ab) (3 μg/ml). C, immunoblot analyses of total and phosphorylated Akt at Thr^{308}. When indicated, cells were incubated with 100 nmol/L insulin for the last 10 min. Data are presented as the mean ± S.D. (n=4 per group). $^{***}p<0.001$ and $^{**}p<0.01$ vs. control cells not exposed to insulin. $^{###}p<0.001$ and $^{##}p<0.01$ vs. insulin-stimulated control cells. $^{†}p<0.05$ vs. insulin-stimulated cells incubated with palmitate. mRNA abundance of MCAD (D), ACOX (E), FAS (F) and SCD1 (G) in the livers of mice fed a standard chow, a HFD for three weeks or a HFD for three weeks plus BTdCPU during the last week. Mice fed a standard chow and half of the mice fed the HFD received one daily i.p. administration of DMSO (vehicle) for the last week. The rest of the mice fed the HFD received one daily i.p. administration of BTdCPU (70 mg kg-1 day-1) for the last week. Data are presented as the mean ± S.D. (n=5 per group). $^{**}p<0.01$ and $^{*}p<0.05$ vs. mice fed a standard diet (CT). $^{#}p<0.05$ vs. mice fed a HFD.

SUPPLEMENTARY DATA

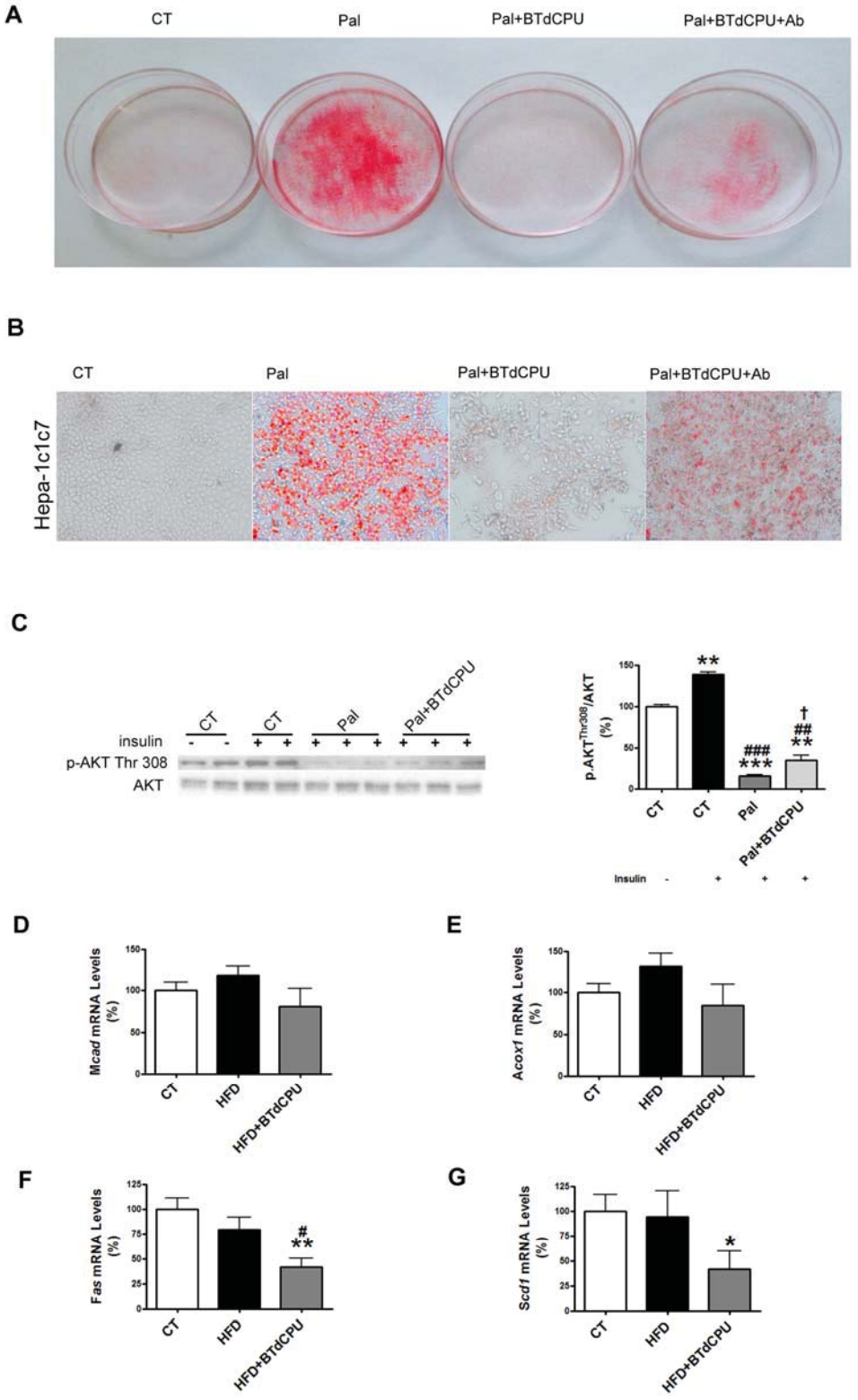

SUPPLEMENTARY DATA

Supplementary Table 1. Primer sequences used for real-time RT- PCR

Gene	Primers	
mAprt	for	5'-CAGCGGCAAGATCGACTACA-3'
	rev	5'-AGCTAGGGAAGGGCCAAACA-3'
mAtf3	for	5'-CTGGAGATGTCAGTCACCAAGTCT-3'
	rev	5'-TTTCTCGCCGCCTCCTTT-3'
mAtf4	for	5'-AGCAAAACAAGACAGCAGCC-3'
	rev	5'-ACTCTCTTCTTCCCCCTTGC-3'
hATF4	for	5'-GCGGGCTCCTCCGAAT-3'
	rev	5'-ATCCTCCTTGCTGTTGTTGGA-3'
mAcox	for	5'-TCTGGAGATCACGGGCACTT-3'
	rev	5'-TTTCCAAGCCTCGAAGATGAG-3'
hACOX	for	5'-GGAAAAAAACTCGGGCAGAAC-3'
	rev	5'-TGGCGAGGAACTCTGACCTT-3'
mβ-Klotho	for	5`-TGGGGTCCCATTGGATAGAG-3`
	rev	5`-ACTCAGGGTAGTCGCCGTC-3`
mBip	for	5`-CAGATCTTCTCCACGGCTTC-3`
	rev	5`-GCAGGAGGAATTCCAGTCAG-3`
hBIP	for	5`-ACTATTGCTGGCCTAAATGTTATGAG-3`
	rev	5`-TTATCCAGGCCATAAGCAATAGC-3`
mBmal1	for	5`-ACGACATAGGACACCTCGCAGA-3`
	rev	5`-CGGGTTCATGAAACTGAACCATC-3`
mChop	for	5`-CGAAGAGGAAGAATCAAAAACCTT-3`
	rev	5`-GCCCTGGCTCCTCTGTCA-3`
hCHOP	for	5`- GGAAATGAAGAGGAAGAATCAAAAAT-3`
	rev	5`-GTTCTGGCTCCTCCTCAGTCA-3`
mFas	for	5`-CATTGGTGGTGTGGACATGGT -3`
	rev	5`-GACCGCTTGGGTAATCCATAGA-3`
hFGF21	for	5`-ACCAGAGCCCCGAAAGTCT-3`
	rev	5`-CTTGACTCCCAAGATTTGAATAACTC-3`
mFgfr1c	for	5`-TGTTTGACCGGATCTACACACA-3`
	rev	5`-CTCCCACAAGAGCACTCCAA-3`
mGlut1	for	5`-GCCCCCAGAAGGTTATTGA-3`
	rev	5`-CGTGGTGAGTGTGGTGGAT-3`
hGAPDH	for	5`-GGCCTCCAAGGAGTAAGACC-3`
	rev	5`-AGGGGTCTACATGGCAACTG-3`
mHmgcs2	for	5`-TCTTTTCATTCCGAGTGTCCA-3`
	rev	5`-ATCTGACACACTAGACACCAGTTTCTC-3`
mHsd3b5	for	5`-GCTCTTGGAAACCACAAGGAAC-3`
	rev	5`-GACAATCCTCTGGCCAAGAAAC-3`
mL-cpt1α	for	5`-GCAGAGCACGGCAAAATGA-3`
	rev	5`-GGCTTTCGACCCGAGAAGAC-3`
mMcad	for	5`-TGACGGAGCAGCCAATGA-3`
	rev	5`-ATGGCCGCCACATCAGA-3`
hMCAD	for	5`-CCCAGTGGCTGCAGAATATGAT-3`

	rev	5`-AAACCAAGTTCCCAGGCTCTTC-3`
mMup1	for	5`-CAAAACAGAAAAGGCTGGTGA-3`
	rev	5`-TTGTGCAAACCTTTCCTTGA-3`
mOrp150	for	5`-CACTGCACAGAACGTCATGTTCT-3`
	rev	5`-GGTGACGATGGTGCACACA-3`
mRev-Erb α	for	5`-GGACAACCAGCCCTCAGTTC-3`
	rev	5`-GCAGCTTCGGACCCATGTT-3`
hREV-ERB α	for	5`-ATGACCAAGTCACCCTGCTTAG-3`
	rev	5`-TCTGGTCCTTCACGTTGAACAA-3`
mPparα	for	5`-CAAGGCCTCAGGGTACCACTAC-3`
	rev	5`-GCCGAATAGTTCGCCGAAA-3`
*h*PPARα	for	5`-TGAAGTTCAATGCACTGGAACTG-3`
	rev	5`-GGACGATCTCCACAGCAAATG-3`
mPparβ/δ	for	5`-GCCACAACGCACCCTTTG-3`
	rev	5`-CCACACCAGGCCCTTCTCT-3`
mScd1	for	5`-CTGTACGGGATCATACTGGTTC-3`
	rev	5`-GCCGTGCCTTGTAAGTTCTG-3`

Hepatic regulation of VLDL receptor by PPARβ/δ and FGF21 modulates non-alcoholic fatty liver disease

Journal: Molecular Metabolism 2018 Feb; 8: 117-131.

IF: 6.799 ENDOCRINOLOGY & METABOLISM 11 DE 138 (1st Decile)

Abstract:

Objective: The very low-density lipoprotein receptor (VLDLR) plays an important role in the development of hepatic steatosis. In this study, we investigated the role of Peroxisome Proliferator-Activated Receptor (PPAR) β/δ and fibroblast growth factor 21 (FGF21) in hepatic VLDLR regulation.

Methods: Studies were conducted in wild-type and Ppar β/δ-null mice, primary mouse hepatocytes, human Huh-7 hepatocytes, and liver biopsies from control subjects and patients with moderate and severe hepatic steatosis.

Results: Increased VLDLR levels were observed in liver of Ppar β/δ-null mice and in Ppar β/δ-knocked down mouse primary hepatocytes through mechanisms involving the heme-regulated eukaryotic translation initiation factor 2a (eIF2a) kinase (HRI), activating transcription factor (ATF) 4 and the oxidative stress-induced nuclear factor (erythroid-derived 2)-like 2 (Nrf2) pathways. Moreover, by using a neutralizing antibody against FGF21, Fgf21-null mice and by treating mice with recombinant FGF21, we show that FGF21 may protect against hepatic steatosis by attenuating endoplasmic reticulum (ER) stress-induced VLDLR upregulation. Finally, in liver biopsies from patients with moderate and severe hepatic steatosis, we observed an increase in VLDLR levels that was accompanied by a reduction in PPAR β/δ mRNA abundance and DNA-binding activity compared with control subjects.

Conclusions: Overall, these findings provide new mechanisms by which PPAR β/δ and FGF21 regulate VLDLR levels and influence hepatic steatosis development.

Original Article

MOLECULAR METABOLISM

Hepatic regulation of VLDL receptor by PPARβ/δ and FGF21 modulates non-alcoholic fatty liver disease

Mohammad Zarei [1,2,3], Emma Barroso [1,2,3], Xavier Palomer [1,2,3], Jianli Dai [4], Patricia Rada [2,5], Tania Quesada-López [3,6,7], Joan Carles Escolà-Gil [2,8,9], Lidia Cedó [2,8], Mohammad Reza Zali [10], Mahsa Molaei [10], Reza Dabiri [11], Santiago Vázquez [1], Eugènia Pujol [1], Ángela M. Valverde [2,5], Francesc Villarroya [3,6,7], Yong Liu [12], Walter Wahli [13,14,15], Manuel Vázquez-Carrera [1,2,3,*]

ABSTRACT

Objective: The very low-density lipoprotein receptor (VLDLR) plays an important role in the development of hepatic steatosis. In this study, we investigated the role of Peroxisome Proliferator-Activated Receptor (PPAR)β/δ and fibroblast growth factor 21 (FGF21) in hepatic VLDLR regulation.

Methods: Studies were conducted in wild-type and *Pparβ/δ*-null mice, primary mouse hepatocytes, human Huh-7 hepatocytes, and liver biopsies from control subjects and patients with moderate and severe hepatic steatosis.

Results: Increased VLDLR levels were observed in liver of *Pparβ/δ*-null mice and in *Pparβ/δ*-knocked down mouse primary hepatocytes through mechanisms involving the heme-regulated eukaryotic translation initiation factor 2α (eIF2α) kinase (HRI), activating transcription factor (ATF) 4 and the oxidative stress-induced nuclear factor (erythroid-derived 2)-like 2 (Nrf2) pathways. Moreover, by using a neutralizing antibody against FGF21, *Fgf21*-null mice and by treating mice with recombinant FGF21, we show that FGF21 may protect against hepatic steatosis by attenuating endoplasmic reticulum (ER) stress-induced VLDLR upregulation. Finally, in liver biopsies from patients with moderate and severe hepatic steatosis, we observed an increase in VLDLR levels that was accompanied by a reduction in *PPARβ/δ* mRNA abundance and DNA-binding activity compared with control subjects.

Conclusions: Overall, these findings provide new mechanisms by which PPARβ/δ and FGF21 regulate VLDLR levels and influence hepatic steatosis development.

Keywords VLDLR; PPAR; FGF21; ATF4; ER stress

1. INTRODUCTION

Non-alcoholic fatty liver disease (NAFLD) is currently the most common liver disorder, and its growing prevalence has increased to reach worldwide epidemic proportions [1]. NAFLD encompasses a spectrum of liver injuries ranging from hepatic steatosis, defined by the excessive accumulation of triglycerides in the liver, to the most severe condition of non-alcoholic steatohepatitis (NASH). In addition, NAFLD is

[1]Department of Pharmacology, Toxicology and Therapeutic Chemistry, Faculty of Pharmacy and Food Sciences, University of Barcelona, Institute of Biomedicine of the University of Barcelona (IBUB), Barcelona, Spain [2]Spanish Biomedical Research Center in Diabetes and Associated Metabolic Diseases (CIBERDEM)-Instituto de Salud Carlos III, Barcelona, Spain [3]Research Institute-Hospital Sant Joan de Déu, Esplugues de Llobregat, Barcelona, Spain [4]Key Laboratory of Nutrition and Metabolism, Institute for Nutritional Sciences, Shanghai Institutes for Biological Sciences, Chinese Academy of Sciences, University of the Chinese Academy of Sciences, Shanghai, China [5]Instituto de Investigaciones Biomédicas Alberto Sols (CSIC/UAM), Madrid, Spain [6]Department of Biochemistry and Molecular Biomedicine and IBUB, University of Barcelona, Barcelona, Spain [7]Spanish Biomedical Research Center in Physiopathology of Obesity and Nutrition (CIBEROBN)-Instituto de Salud Carlos III, Spain [8]Institut d'Investigacions Biomèdiques (IIB) Sant Pau, Barcelona, Spain [9]Departament de Bioquímica i Biología Molecular, Universitat Autònoma de Barcelona, Barcelona, Spain [10]Gastroenterology and Liver Diseases Research Center, Research Institute for Gastroenterology and Liver Diseases, Shahid Beheshti University of Medical Sciences, Tehran, Iran [11]Internal Medicine Department, Semnan University of Medical Sciences, Semnan, Iran [12]Hubei Key Laboratory of Cell Homeostasis, College of Life Sciences, Institute for Advanced Studies, Wuhan University, Wuhan, China [13]Center for Integrative Genomics, University of Lausanne, Lausanne, Switzerland [14]Lee Kong Chian School of Medicine, Nanyang Technological University, 308232, Singapore [15]INRA ToxAlim, UMR1331, Chemin de Tournefeuille, Toulouse Cedex, France

*Corresponding author. Unitat de Farmacologia, Facultat de Farmàcia i Ciències de l'Alimentació, Av. Joan XXIII 27-31, Barcelona E-08028, Spain. Fax: +34 93 4035982. E-mail: mvazquezcarrera@ub.edu (M. Vázquez-Carrera).

Abbreviations: ATF4, activating transcription factor 4; Chop, C/EBP homologous protein; eIF2α, eukaryotic translation initiation factor 2α; FGF21, fibroblast growth factor 21; HFD, high-fat diet; HRI, heme-regulated eIF2α kinase; NAFLD, non-alcoholic fatty liver disease; PPAR, peroxisome proliferator-activated receptor

Received August 23, 2017 • Revision received December 8, 2017 • Accepted December 13, 2017 • Available online 19 December 2017

https://doi.org/10.1016/j.molmet.2017.12.008

an important risk factor for the development of obesity-related pathologies including insulin resistance, type 2 diabetes mellitus (T2DM), and cardiovascular diseases [2].

Hepatic triglyceride levels are regulated by multiple mechanisms such as *de novo* synthesis, fatty acid oxidation, lipolysis, dietary fat consumption, and the secretion and hepatic delivery of lipoprotein particles [3—5]. Recently, it has been reported that very low-density lipoprotein receptor (VLDLR) plays an important role in the development of hepatic steatosis [6]. VLDLR belongs to the low-density lipoprotein (LDL) receptor family and is widely expressed in the brain, heart, skeletal muscle, and adipose tissue, whereas its expression is very low in the liver under normal conditions [7,8]. This receptor binds apolipoprotein E (apoE) triglyceride-rich lipoproteins such as chylomicrons, VLDL, and intermediate density lipoproteins, leading to lipid entry into the cell through lipoprotein lipase (LPL)-dependent lipolysis or receptor-mediated endocytosis [9—12]. As a result, a link has been established between VLDLR levels and plasma triglyceride levels [13]. VLDLR-null mice are leaner, display normal blood lipids [14] and are protected from obesity induced by HFD feeding or leptin deficiency [15]. However, following fasting or exposure to a HFD, these animals show increased plasma triglyceride levels [15,16]. In recent years, it has been reported that VLDLR is regulated by several transcription factors, including Peroxisome Proliferator-Activated Receptor (PPAR) γ in adipose tissue [12] and hypoxia-inducible factor 1α (HIF-1α) in the heart [17], contributing to lipid deposition in both tissues. In liver, the upregulation of VLDLR levels has been reported to be dependent on the activation of oxidative stress-induced nuclear factor (erythroid-derived 2)-like 2 (Nrf2) in alcoholic liver disease [18], whereas stimulation of activating transcription factor 4 (ATF4) signaling during endoplasmic reticulum (ER) stress induces hepatic steatosis via increase VLDLR by enhancing lipoprotein delivery to the liver [6]. In addition, hepatic VLDLR upregulation plays an essential role in the triglyceride-lowering effect of fenofibrate through PPARα activation [19]. However, little is known about the effects of PPARβ/δ on VLDLR regulation in the liver. PPARβ/δ is a ligand-activated transcription factor involved in the regulation of glucose and lipid homeostasis [20], and it has been proposed as a therapeutic target for the treatment of metabolic syndrome [21]. Thus, genetic manipulation of PPARβ/δ as well as its activation by agonists attenuate dyslipidemia and hyperglycemia, improve whole-body insulin sensitivity, and prevent diet-induced obesity [22]. In this study, we show that *Pparβ/δ* deficiency regulates VLDLR levels through Nrf2 and ATF4-dependent mechanisms, whereas fibroblast growth factor 21 (FGF21) deficiency exacerbates ER stress-induced VLDLR levels, contributing to the progression of hepatic steatosis. Finally, our findings show that in humans with severe hepatic steatosis, increased levels of VLDLR accompany a reduction in PPARβ/δ activity.

2. RESEARCH DESIGN AND METHODS

2.1. Reagents

Control, VLDLR, HRI, ATF4, and Nrf2 siRNA were purchased from Santa Cruz (Dallas, TX) and PPARβ/δ siRNA from GE Dharmacon (Lafayette, CO). Mouse FGF21 neutralizing antibody was purchased from Antibody and Immunoassays Services (Hong Kong, China) and human recombinant FGF21 from R&D Systems (Minneapolis, MN). Triglyceride levels were measured using a commercial kit (Sigma, St. Louis, MO).

2.2. Mice

Male (8—9-wk old) *Pparβ/δ* knockout (*Ppar$\beta/\delta^{-/-}$*) mice and their wild-type littermates (*Ppar$\beta/\delta^{+/+}$*) with the same genetic background (C57BL/6X129/SV) [23] and an initial weight of 20—25 g were fed a standard diet. Genotyping was performed as previously described [23]. Wild-type and *Pparβ/δ*-null mice were treated for 24 h through i.p. injection with DMSO (vehicle) or tunicamycin (3 mg kg^{-1} body weight). Likewise, male wild-type and *Pparβ/δ*-null mice at 12 wk. of age were injected intraperitoneally with IgG (9 μg/mouse) or a neutralizing antibody (9 μg/mouse) against FGF21 [24] together with DMSO or tunicamycin (3 mg kg^{-1} body weight) and were sacrificed at 14 h after treatment. In addition, male wild-type and *Pparβ/δ*-null mice were either fed a 30% fructose solution or plain tap water for 12 wk, as previously described [25]. The hepatic content of malondialdehyde (MDA) and hydrogen peroxide (H_2O_2) were determined using the lipid peroxidation (MDA) and Peroxidetect assay kits (Sigma), respectively. Male (10-wk old) knockout (*Fgf21$^{-/-}$*) mice [B6N; 129S5-*Fgf21*^{tm1Lex}/Mmcd] and their wild-type littermates (*Fgf21$^{+/+}$*) were obtained from the Mutant Mouse Regional Resource Center (MMRRC). For examination of the effect of FGF21 on VLDLR levels, male C57BL/6 mice at 12 wk of age were treated with DMSO or tunicamycin (1 mg kg^{-1} body weight), and starting at 6 h before tunicamycin injection, recombinant mouse FGF21 (PeproTech, London, UK) was administered intraperitoneally at 1 mg kg^{-1} body weight for a total of five times every 6 h. Mice were sacrificed at 24 h after tunicamycin treatment. All animals were killed under anesthetic conditions, and livers were snap-frozen in liquid nitrogen immediately after resection and stored at -80 °C. The research complied with the Guide for the Care and Use of Laboratory Animals published by the US National Institutes of Health (NIH Publication No. 85-23, revised 1996). All procedures were approved by the University of Barcelona Bioethics Committee, as stated in Law 5/21 July 1995 passed by the Generalitat de Catalunya.

2.3. Cell culture

Human Huh-7 cells (a kindly gift from Dr. Mayka Sanchez from Josep Carreras Leukaemia Research Institute) were cultured in DMEM supplemented with 10% serum, at 37 °C/5% CO_2. Primary mouse hepatocytes were isolated from non-fasting male C57BL/6 mice (10—12 weeks old) by perfusion with collagenase as described elsewhere [26]. siRNA transfections were performed with Lipofectamine 2000 (Life Technologies).

2.4. Human samples

Subjects were recruited by the Gastroenterology Department at the Shahid Beheshti University of Medical Sciences (Tehran, Iran) with the approval of the Ethical Committee of the University Review Board of the participating Taleghani Hospital. NAFLD subjects (Table S1) were diagnosed according to WHO criteria. Patients were considered as having potential liver steatosis if they had abnormal liver blood tests. Alcohol consumption had to be less than 20 g/day for the past 5 years, as assessed using a standard questionnaire. In addition, liver specimen had to be compatible with NAFLD [27], without any pattern suggestive of other cause. Patients were not included if they had another cause of chronic liver disease, complicated cirrhosis, or received putative antifibrotic treatment in the past 6 months. Liver biopsies were performed at Taleghani Hospital in 2012—2013 using a Meghini 16 swg (1.6 mm) $\times$ 70 mm syringe. The material consisted of 15 needle biopsies from adult patients. Specimens were immediately sent for pathology assessment by routine procedures; two biopsies were required to obtain an acceptable specimen. All the biopsies were reviewed by the pathologist and the presence of steatosis was graded in grade 0 with $<$5% of hepatocytes presenting steatosis (control group) (n $=$ 5), grade 2 with 33—66% of hepatocytes presenting steatosis (n $=$ 4), and grade 3 with more than

66% steatotic hepatocytes (n = 6). Written informed consent was obtained from each patient included in the study and the study protocol conformed to the ethical guidelines of the 2013 Declaration of Helsinki as reflected in a priori approval by the institution's human research committee.

2.5. RNA preparation and quantitative RT-PCR

The relative levels of specific mRNAs were assessed by Real-Time RT-PCR, as previously described [28]. Primer sequences used for Real-Time RT-PCR are displayed in Table S2.

2.6. Immunoblotting

Isolation of total and nuclear extracts was performed as described elsewhere [28]. Proteins (30 μg) were separated by SDS-PAGE on 10% acrylamide separation gels and transferred to Immobilon polyvinylidene difluoride membranes (Millipore). Western blot analysis was performed using antibodies against VLDLR (sc-18824), Nrf2 (sc-722), Nqo1 (sc-393736), ATF4 (sc-200) (Santa Cruz), VLDLR (AF2258) (R&D system), eIF2α (9722), phospho-eIF2α (Ser51) (9721), IgG control (2729S) (Cell Signaling Technology Inc., Danvers, MA), actin (A5441) (Sigma—Aldrich, Madrid, Spain). Detection was achieved using the Western Lightning® Plus-ECL chemiluminescence kit (PerkinElmer, Waltham, MA, USA). The equal loading of proteins was assessed by Ponceau S staining. The size of detected proteins was estimated using protein molecular-mass standards (Bio-Rad).

2.7. Electrophoretic mobility shift assay

The electrophoretic mobility shift assay (EMSA) was performed using double-stranded oligonucleotide for the consensus binding site of PPRE (Santa Cruz Biotechnology). Nuclear extracts (NE) were isolated as previously reported [28]. Oligonucleotides were labeled by incubating the following reaction at 37 °C for 2 h: 2 μL oligonucleotide (1.75 pmol/μL), 2 μL of 5X kinase buffer, 1 μL of T4 polynucleotide kinase (10 U/μL), and 2.5 μL [γ-^{32}P] ATP (3,000 Ci/mmol at 10 mCi/mL). The reaction was stopped by adding 90 μL of TE buffer (10 mmol/L Tris—HCl, pH 7.4, and 1 mmol/L EDTA). To separate the labeled probe from the unbound ATP, the reaction mixture was eluted in a Nick column (GE Healthcare, Barcelona, Spain) according to the manufacturer's instructions. Five micrograms of crude nuclear protein was incubated for 10 min on ice in binding buffer (10 mmol/L Tris—HCl, pH 8.0, 25 mmol/L KCl, 0.5 mmol/L dithiothreitol, 0.1 mmol/L EDTA, pH 8.0, 5% (v:v) glycerol, 5 mg/mL BSA, and 50 μg/ml poly[dI-dC]) in a final volume of 15 μL. Then, specific competitor oligonucleotide or antibody for supershift assays were added and incubated for 15 min on ice. Subsequently, the labeled probe (100,000 cpm) was added and the reaction was incubated for an additional 15 min on ice. Finally, protein-DNA complexes were resolved by electrophoresis at 4 °C on 5% (w:v) polyacrylamide gels in 0.5X Tris-borate-EDTA buffer and subjected to autoradiography.

2.8. Hematoxylin-eosin and Oil Red and staining

We performed hematoxylin-eosin and Oil Red O staining as previously reported [28]. ORO staining was quantified using Image J software.

2.9. Statistical analyses

Results are expressed as means ± S.D. Significant differences were established by two-way ANOVA using the GraphPad Instat program (GraphPad Software V5.01) (GraphPad Software Inc., San Diego, CA). When significant variations were found by two-way ANOVA, the Tukey—Kramer multiple comparison post-test was performed. Differences were considered significant at $p < 0.05$.

3. RESULTS

3.1. Pparβ/δ$^{-/-}$ mice show increased hepatic VLDLR levels

First, we examined whether *Pparβ/δ*-deficiency affected VLDLR levels. VLDLR mRNA and protein levels were increased in the livers of *Pparβ/δ*$^{-/-}$ mice compared with wild-type littermates (Figure 1A and B). This increase in VLDLR was accompanied by the presence of hepatic steatosis in *Pparβ/δ*$^{-/-}$ mice compared to wild-type littermates, as demonstrated by ORO and hematoxylin-eosin staining and hepatic triglyceride quantification (Figure 1C and D), whereas differences in plasma triglyceride levels did not reach statistical significance (data not shown). In accordance with the observations in the liver of *Pparβ/δ*-deficient mice, siRNA knockdown of *Pparβ/δ* in primary hepatocytes (Figure S1B) led to enhanced *Vldlr* mRNA and protein levels (Figure 1E and F). Similarly, transfection of human Huh-7 hepatocytes with siRNA against *PPARβ/δ* caused a significant increase in *VLDLR* mRNA levels (Figure 1G) and in cellular lipid accumulation (Figure 1H). Next, we focused on ATF4 as the potential transcription factor responsible for the increase in VLDLR in *Pparβ/δ*-deficient cells. Although ATF4 is activated by ER stress through eukaryotic translation initiation factor 2α (eIF2α), the increase in phosphorylated eIF2α and activation of its downstream ATF4 signaling pathway can occur independently of ER stress, since eIF2α can also be phosphorylated by other kinases, including the heme-regulated eIF2α kinase (HRI) [29]. Interestingly, *Pparβ/δ*$^{-/-}$ mice showed increased levels of HRI, which in turn activates the eIF2α-ATF4 pathway [28], suggesting that HRI might also regulate VLDLR levels. In agreement with this, siRNA knockdown of *Hri* (Figure S1A) in primary hepatocytes caused a reduction in VLDLR mRNA and protein levels (Figure 2A). Moreover, two well-known HRI activators [30], BTCtFPU and BTdCPU, upregulated VLDLR mRNA and protein levels in human Huh-7 hepatocytes (Figure 2B), and BTdCPU also upregulated VLDLR levels in the liver of mice treated with this compound (Figure 2C).

Next, we checked whether other transcription factors such as Nrf2, known to be involved in the upregulation of hepatic VLDLR [18], might be responsible for the increase in the expression of this gene in the livers of *Pparβ*/δ-null mice. Interestingly, livers of *Pparβ/δ*$^{-/-}$ mice showed increased levels of phosphorylated Nrf2, an indicator of the activity of this transcription factor [31], compared with wild-type littermates (Figure 2D). In agreement with this, the mRNA and protein levels of the Nrf2-target gene NAD(P)H quinone dehydrogenase 1 (*Nqo1*) were also upregulated (Figure 2D and E).

To confirm the involvement of HRI, ATF4, and Nrf2 in the upregulation of *Vldlr* in the context of *Pparβ/δ* deficiency, we performed siRNA studies in primary hepatocytes. Knockdown of *Pparβ/δ* increased the expression of *Vldlr*, but this increase was prevented by siRNA transfection against *Atf4*, *Nrf2*, or *Hri* (Figure 2F). Two ATF4-target genes, *Trb3* [28] and *Fgf21* [32], were upregulated by *Pparβ/δ* knockdown, but this was prevented by transfecting siRNA against either *Atf4* or *Hri* (Figure S1C and D). Similarly, expression of *Nrf2* and two of its target genes, *Nqo1* and *Ho-1*, increased following *Pparβ/δ* knockdown and this was prevented by siRNA transfection against *Nrf2* (Figure S1E—G). These findings indicate that *Pparβ/δ* deficiency increases *Vldlr* expression through the HRI-eIF2α-ATF4 and Nrf2 pathways.

3.2. Pparβ/δ deficiency exacerbates hepatic steatosis and VLDLR upregulation caused by ER stress

Given that ER stress induces hepatic steatosis via increased expression of VLDLR through eIF2α-ATF4 [6], we hypothesized that *Pparβ/δ* deficiency may exacerbate liver steatosis in the context of ER stress by potentiating the increase in VLDLR levels. To test this, wild-type and

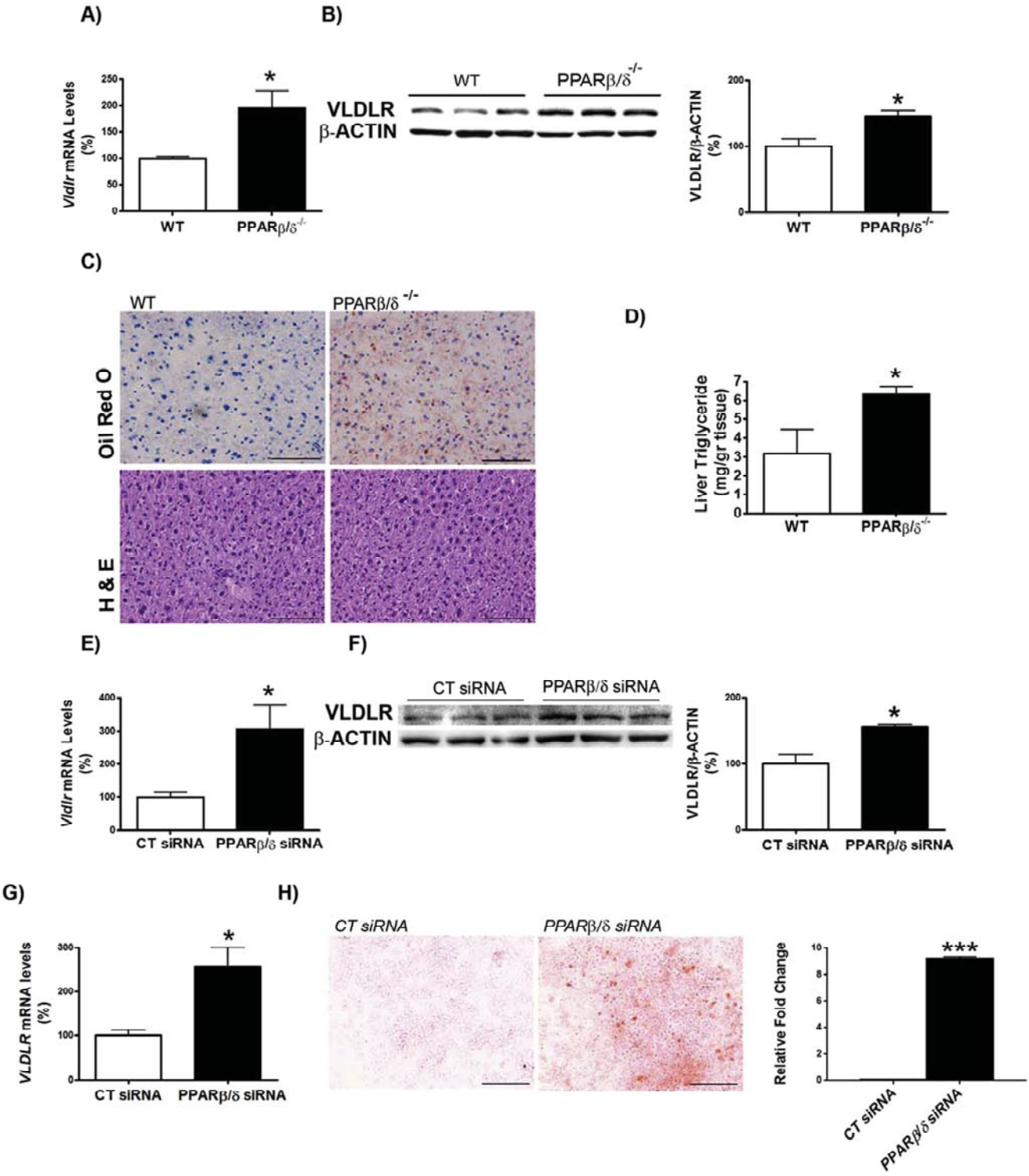

Figure 1: VLDLR abundance is increased in liver of *Pparβ/δ*-null mice and in primary hepatocytes following knockdown of *Pparβ/δ*. Livers from male wild-type (WT) and *Pparβ/δ*-null mice were used (n = 6 per group). A, Assessment by quantitative real-time RT-PCR of hepatic *Vldlr*. B, Immunoblot analysis of liver VLDLR. C, Oil Red O and hematoxylin-eosin staining of livers. Scale bar: 100 μm. D, Liver triglyceride levels. Data are presented as the mean ± S.D. (n = 6 per group) relative to the wild-type mice. *Vldlr* mRNA abundance (E) and protein levels (F) in primary hepatocytes transfected with control siRNA or *Pparβ/δ* siRNA for 24 h. *VLDLR* mRNA levels (G) and Oil Red O staining (H) in Huh-7 hepatocytes transfected with control siRNA or *Pparβ/δ* siRNA for 24 h. Levels are presented as the mean ± S.D. (n = 3–5 per group). *p < 0.05 *vs.* wild-type mice or control siRNA. Scale bar: 100 μm.

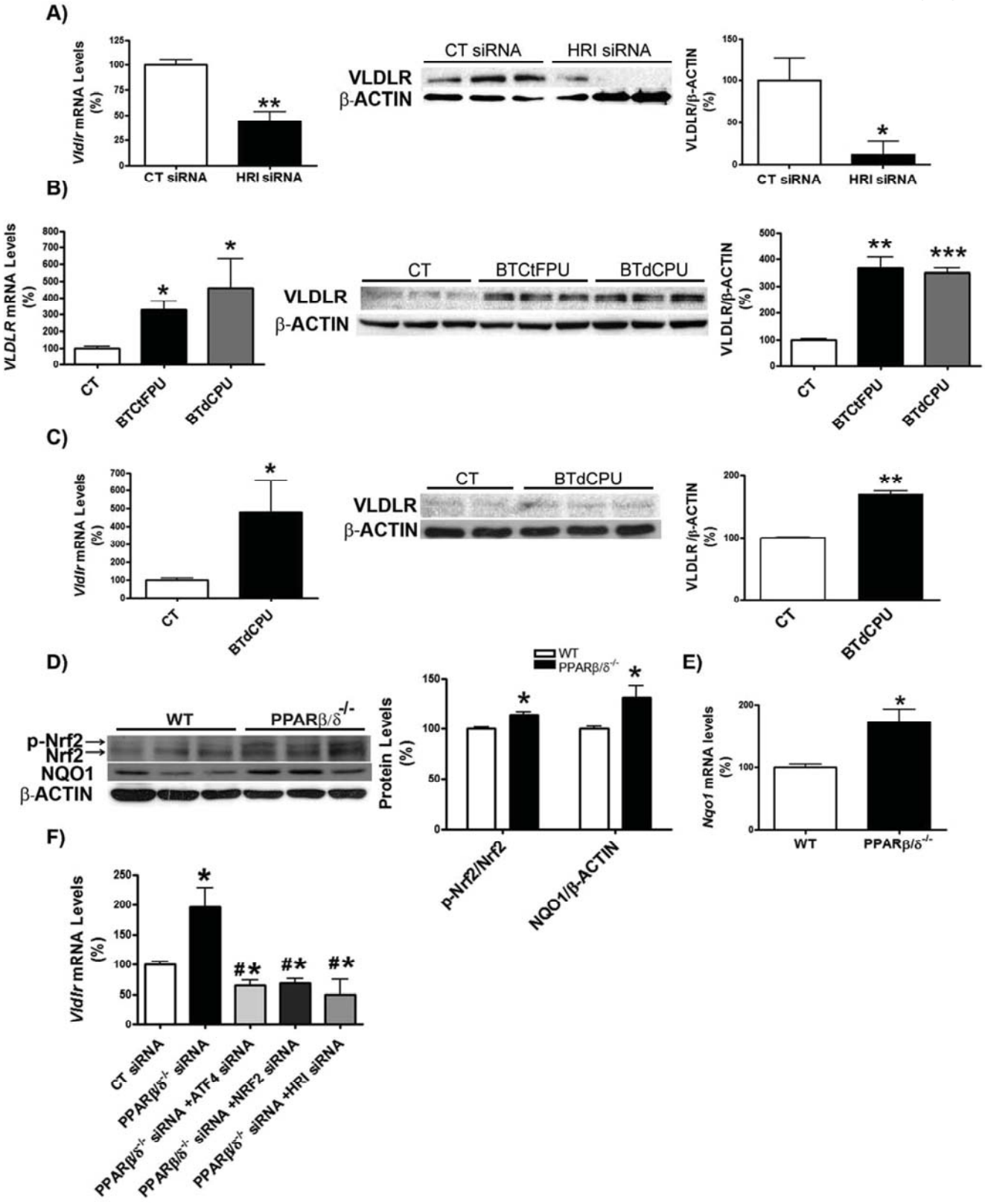

Figure 2: HRI regulates VLDLR abundance in hepatocytes. A, primary hepatocytes were transfected with control or *Hri* siRNA for 24 h, and the mRNA abundance and protein levels of VLDLR were assessed. *$p < 0.05$ and **$p < 0.01$ *vs.* control siRNA. B, Huh-7 hepatocytes were incubated for 16 h in the absence (Control, CT) or presence of 10 μmol/L of either BTdCPU or BTCtFPU and the mRNA abundance and protein levels of VLDLR were analyzed. ***$p < 0.001$, **$p < 0.01$ and *$p < 0.05$ *vs.* control. C, mRNA abundance and protein levels of VLDLR in liver of mice treated with DMSO (vehicle) or BTdCPU (70 mg kg^{-1} day^{-1}) for 7 days ($n = 6$ per group). ***$p < 0.001$, **$p < 0.01$ and *$p < 0.05$ *vs.* control cells or control mice. Immunoblot analyses of total and phospho-Nrf2 and NQO1 (D) and mRNA abundance of *Nqo1* (E) in liver from male wild-type (WT) and *Pparβ/δ*-null mice ($n = 6$ per group). *$p < 0.05$ *vs.* control. F, *VLDLR* mRNA abundance in primary hepatocytes transfected with control, *Pparδ*, *Atf4*, *Nrf2* and *Hri* siRNA for 24 h *$p < 0.05$ *vs.* control siRNA. #$p < 0.05$ *vs. Pparδ* siRNA.

Pparβ/δ$^{-/-}$ mice were treated with the ER stressor tunicamycin for 24 h. Tunicamycin increased hepatic triglyceride accumulation in wild-type mice (approximately 5-fold increase, $p < 0.01$) compared with vehicle-treated animals, but this accumulation was exacerbated in tunicamycin-treated *Pparβ/δ*$^{-/-}$ mice (approximately 8-fold increase, $p < 0.001$ compared with tunicamycin-treated wild-type mice) (Figure 3A—C). In agreement with an increased lipoprotein delivery to the liver through VLDLR as the mechanism responsible for hepatic steatosis, plasma triglyceride levels were reduced in tunicamycin-treated wild-type mice (60% reduction, $p < 0.01$) compared with vehicle-treated wild-type mice. This reduction was exacerbated in tunicamycin-treated *Pparβ/δ*$^{-/-}$ mice (70% reduction, $p < 0.001$) compared with vehicle-treated *Pparβ/δ*$^{-/-}$ mice (Figure 3D), which is consistent with the higher increase in VLDLR protein levels in the livers of tunicamycin-treated *Pparβ/δ*$^{-/-}$ mice (Figure 3E). Likewise, the expression of two additional ATF4-target genes, *Trb3* and *Chop,* was significantly higher in tunicamycin-treated *Pparβ/δ*$^{-/-}$ mice than in tunicamycin-treated wild-type mice, indicating higher ATF4 activity in the former group (Figure 3F and G). Of note, in contrast to *Trb3* expression that was increased in PPARβ/δ-null mice compared to wild-type mice, *Chop* expression was independent of the genotype and it was only increased following tunicamycin treatment.

Since ER stress can also activate Nrf2 [33], we next evaluated whether this antioxidant transcription factor can contribute to the increase in VLDLR in tunicamycin-treated *Pparβ/δ*$^{-/-}$ mice. Tunicamycin administration led to significant changes in hepatic phospho-Nrf2 and NQO1 protein levels in wild-type mice, and the increase in phospho-Nrf2 was exacerbated in *Pparβ/δ*-null mice (Figure 3H). Overall, these findings suggest that ATF4 and Nrf2 activation by tunicamycin in the presence of *Pparβ/δ* deficiency intensifies the increase in hepatic VLDLR.

3.3. FGF21 protects against hepatic steatosis and the upregulation of VLDLR levels caused by ER stress

Since FGF21 suppresses the eIF2α-ATF4 pathway through a negative feedback [34], we hypothesized that the reported increase in FGF21 observed in *Pparβ/δ*-deficient mice [28] might attenuate the increase in the ATF4-target gene *Vldlr*. To check this, we treated *Pparβ/δ*-null mice with an FGF21 neutralizing antibody and tunicamycin. Administration of the FGF21 neutralizing antibody to *Pparβ/δ*$^{-/-}$ mice increased hepatic triglyceride accumulation in both vehicle and tunicamycin-treated mice compared with mice receiving IgG (Figure 4A and B). Consistent with this, *Vldlr* mRNA levels increased in *Pparβ/δ*$^{-/-}$ mice injected FGF21 neutralizing antibody compared with mice treated with IgG, especially in tunicamycin-treated mice (Figure 4C). No changes in these parameters were observed in wild-type mice injected with the neutralizing antibody (Figure S2A and B). VLDLR regulation by FGF21 was confirmed in the livers of *Fgf21*-deficient mice. These mice showed increased hepatic triglyceride accumulation (Figure 4D), a process which has been reported to be age-dependent [35], and *Vldlr* mRNA (Figure 4E) and protein abundance accompanied by enhanced eIF2α phosphorylation and ATF4 protein levels (Figure 4F). Similarly, the expression levels of two *Atf4*-target genes, *Trb3* and *Chop*, were also increased in the livers of *Fgf21*$^{-/-}$ mice compared with wild-type mice (Figure S2C and D), although *Chop* did not reach statistical significance. In contrast, phosphorylated levels of Nrf2 were reduced in *Fgf21*$^{-/-}$ mice (Figure 4G), rendering its involvement in VLDLR upregulation unlikely. Finally, we examined the effects of recombinant FGF21 treatment on ER-stress-induced VLDLR levels. In Huh-7 hepatocytes FGF21 significantly reduced the increase in *VLDLR* and *CHOP* expression (Figure 5A and B) and in VLDLR protein levels caused by tunicamycin, and these reductions were accompanied by a decrease in the levels of phospho-eIF2α (Figure 5C). Similarly, administration of FGF21 reduced the increase in both the expression and the protein levels of VLDR caused by tunicamycin in liver (Figure 5D and E). These findings suggest that FGF21 may protect against hepatic steatosis by limiting the increase in VLDLR levels via attenuation of the eIF2α-ATF4 pathway.

3.4. VLDLR upregulation is intensified by fructose feeding in the liver of Pparβ/δ-null mice

Fructose feeding leads to hepatic steatosis [36]. Consequently, we explored whether VLDLR was involved in the effects of fructose on liver in the context of *Pparβ/δ* deficiency. As previously shown [25], feeding wild-type mice (C57BL/6X129/SV genetic background) with fructose did not result in hepatic steatosis (Figure 6A and B). However, *Pparβ/δ*$^{-/-}$ mice exposed to fructose exhibited a clear and intense steatosis. When hepatic VLDLR mRNA and protein levels were assessed, water-fed *Pparβ/δ*$^{-/-}$ mice showed a significant increase that was intensified by fructose feeding (Figure 6C and D). As previously reported [37], fructose feeding increased *Fgf21* expression in liver of wild-type mice (Figure S3A), indicating that despite the lack of induction of triglyceride accumulation in the liver of wild-type mice, fructose feeding was efficacious. This increase was exacerbated in *Pparβ/δ*-deficient mice. In contrast, expression of the ATF4-target gene *Chop* was unaffected in fructose-fed *Pparβ/δ*$^{-/-}$ mice (Figure S3B), rendering it unlikely that this pathway was involved in the VLDLR upregulation observed in the liver of these mice. Consistent with the trend observed in VLDLR, phospho-Nrf2 levels and the expression of its target gene *Nqo1* were elevated in livers of fructose-fed *Pparβ/δ*$^{-/-}$ mice (Figure 6E and F). The oxidative stress status measured by the lipid peroxidized product MDA and H_2O_2 was significantly increased only in fructose-fed *Pparβ/δ*$^{-/-}$ mice (Figure 6G and H), suggesting that enhanced ROS levels was the stimulus responsible for the increase in the activity of this redox transcription factor. To clearly demonstrate the involvement of Nrf2, the expression of this gene and that of *Pparβ/δ* was knocked down by siRNA transfection in mouse primary hepatocytes. As previously shown, *Pparβ/δ* knockdown increased the expression of *Vldlr* and this increase was intensified by incubation with fructose (Figure 6I). However, *Nrf2* knockdown abrogated the increase caused by the reduction in *Pparβ/δ* expression and incubation with fructose (Figure 6I). The increase in *VLDLR* expression was also observed in human hepatocytes transfected with siRNA against *PPARβ/δ* and this effect was specific for fructose, since it was not observed in hepatocytes exposed to a related carbohydrate such as mannitol (Figure S3C). Overall, these data suggest that in the context of *Pparβ/δ* deficiency, fructose induces ROS production, a well-known activator of Nrf2, which in turn increases VLDLR levels and ultimately produces hepatic steatosis by increasing lipoprotein delivery to the liver.

3.5. VLDLR content is increased in the liver of patients with steatosis

Our findings in *in vitro* and animal models suggest a new potential pathway that might contribute to NAFLD. In this pathway, a reduction in PPARβ/δ levels might result in activation of both ATF4 and Nrf2, which in turn would enhance VLDLR levels, leading to increased VLDL (triglyceride) delivery to the liver. The contribution of this potential pathway was explored in liver biopsies of patients classified into three grades based on the percentage of hepatocytes presenting steatosis: grade 0 (<5%), grade 2 or moderate steatosis (33—66%) and grade 3 or severe steatosis (>66%) (Figure 7A). VLDLR mRNA expression

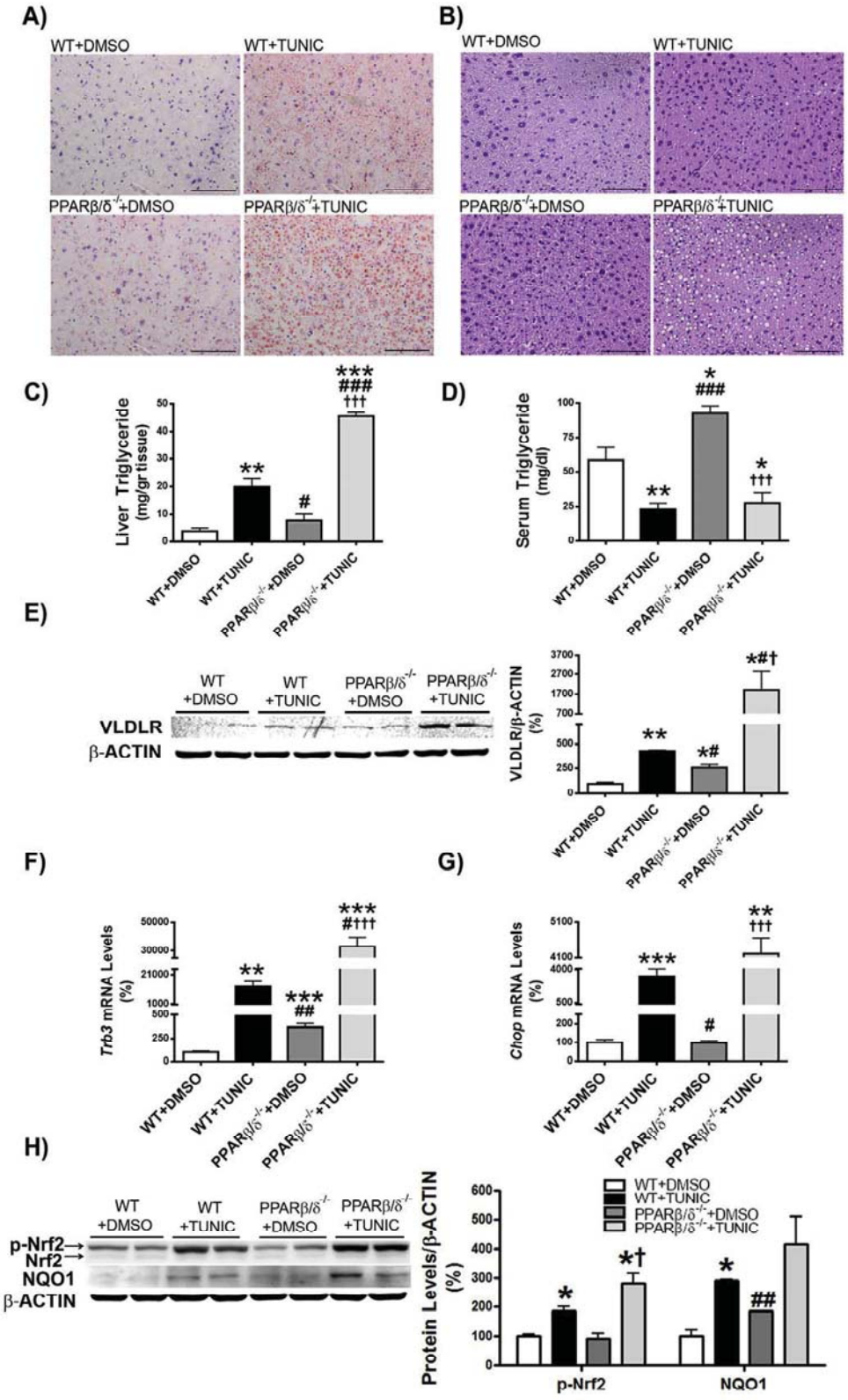

Figure 3: *Pparβ/δ* deficiency exacerbates hepatic steatosis and VLDLR upregulation caused by ER stress. Oil Red O (A) and hematoxylin-eosin (B) staining of livers from male wild-type (WT) and *Pparβ/δ*-null mice treated for 24 h through i.p. injection with DMSO (vehicle) or tunicamycin (Tunic) (3 mg kg^{-1} body weight). Scale bar: 100 μm. C, Liver triglyceride levels. D, Serum triglyceride levels. E, Immunoblot analyses of VLDLR. *Trb3* (F) and *Chop* (G) mRNA abundance. H, immunoblot analyses of total and phospho-Nrf2 and NQO1. Data are presented as the mean ± S.D. (n = 6 per group). ***p < 0.001, **p < 0.01 and *p < 0.05 *vs.* wild-type animals treated with DMSO (vehicle). ###p < 0.001, ##p < 0.01 and #p < 0.05 *vs.* wild-type animals treated with tunicamycin. †††p < 0.001 and †p < 0.05 *vs. Pparβ/δ*-null mice treated with DMSO (vehicle).

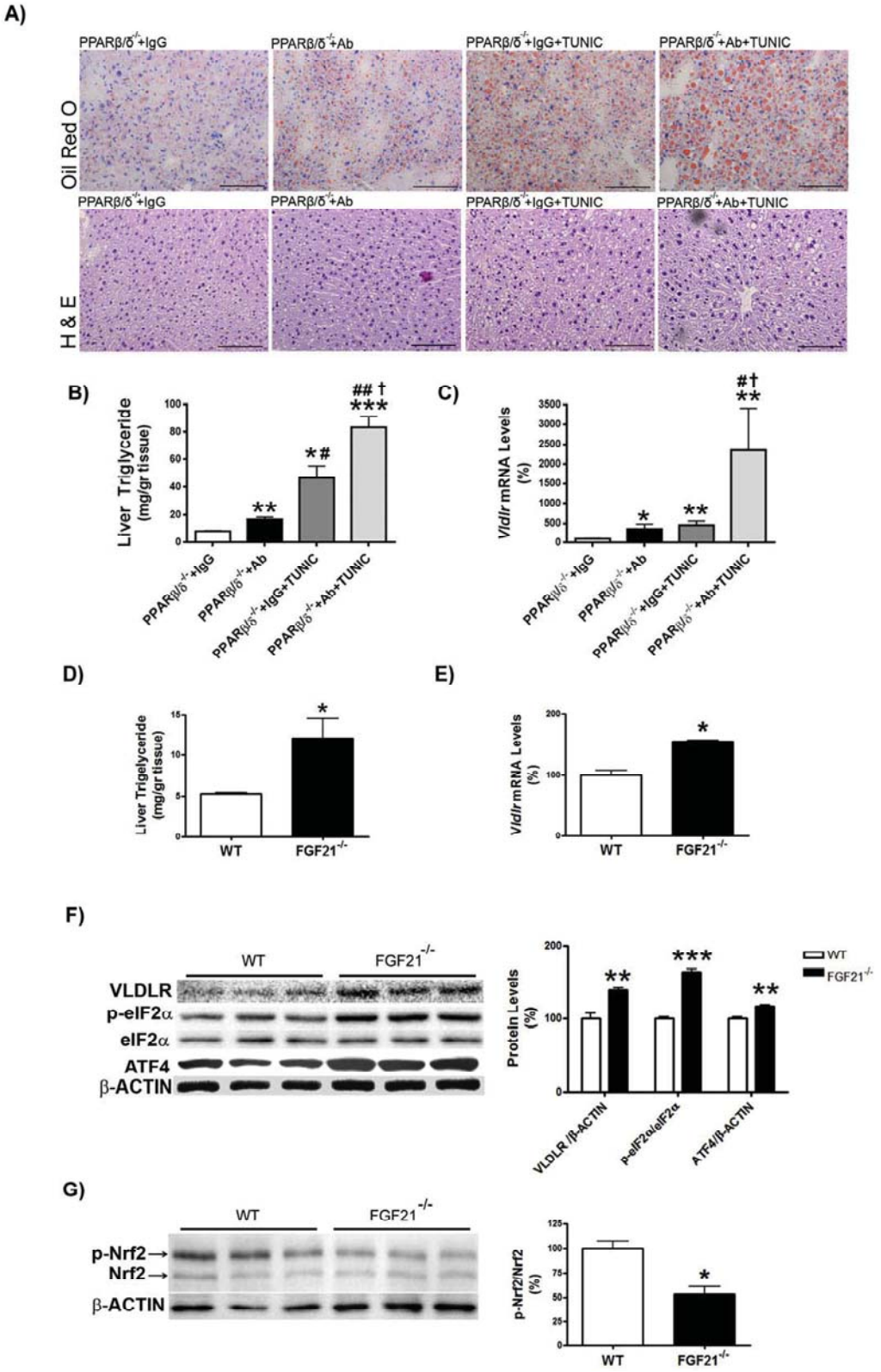

Figure 4: Increased *Fgf21* expression in liver of *Pparβ/δ*-null mice attenuates VLDLR abundance. A, Oil Red O and hematoxylin-eosin staining of livers from male wild-type (WT) and *Pparβ/δ*-null mice injected intraperitoneally with IgG (9 μg/mouse) or a neutralizing antibody (Ab) (9 μg/mouse) against FGF21 together with DMSO or tunicamycin (Tunic) (3 mg kg^{-1} body weight). Scale bar: 100 μm. Mice were sacrificed at 14 h after treatment. B, Liver triglyceride levels. C, *Vldlr* mRNA abundance. ***$p < 0.001$, **$p < 0.01$ and *$p < 0.05$ *vs. Pparβ/δ*-null mice treated with IgG and DMSO. ##$p < 0.01$ and #$p < 0.05$ *vs. Pparβ/δ*-null mice treated with neutralizing antibody against FGF21 and DMSO. †$p < 0.05$ *vs. Pparβ/δ*-null mice treated with IgG and tunicamycin. Liver triglyceride levels (D) and *Vldlr* mRNA abundance (E) in the liver from WT and *Fgf21*$^{-/-}$ mice. Data are presented as the mean ± S.D. ($n = 5$ per group). ***$p < 0.001$, **$p < 0.01$ and *$p < 0.05$ *vs.* wild-type mice. Immunoblot analyses of VLDLR, total and phospho-eIF2α and ATF4 (F) and total and phospho-Nrf2 (G) were performed in liver lysates. Data are presented as the mean ± S.D. ($n = 5$ per group). ***$p < 0.001$, **$p < 0.01$ and *$p < 0.05$ *vs.* wild-type mice.

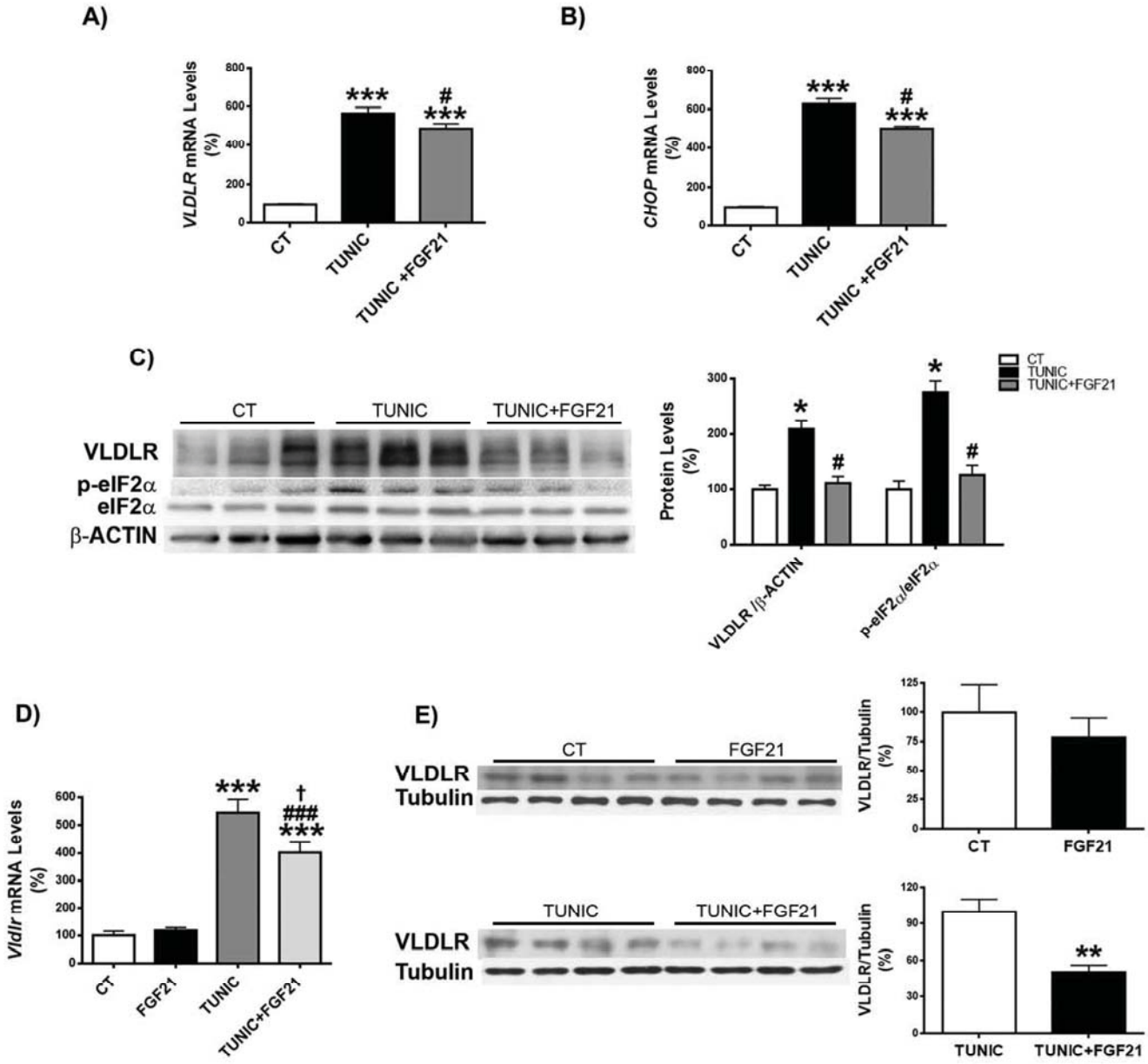

Figure 5: Recombinant FGF21 protein attenuates the increase in VLDLR levels caused by ER stress. Human Huh-7 hepatocytes were incubated with DMSO (vehicle, control, CT), tunicamycin (TUNIC) (1 μg/ml) or tunicamycin plus recombinant human FGF21 (1 μg/ml) and the mRNA abundance of VLDLR (A) and CHOP (B) and the protein levels of VLDLR and total and phospho-eIF2α (C) were assessed (n = 3 independent experiments). ***$p < 0.001$ *vs.* CT cells. $^{\#}p < 0.05$ *vs.* tunicamycin-treated cells. Analysis of the hepatic levels of VLDLR in mice injected intraperitoneally with vehicle or recombinant mouse FGF21 together with DMSO or tunicamycin. Data are presented as the mean ± S.D. (n = 5 per group). C, *Vldlr* and *Chop* mRNA abundance. D, Immunoblot analyses of hepatic VLDLR. ***$p < 0.001$, **$p < 0.01$ and *$p < 0.05$.

(Figure 7B) and protein levels (Figure 7C) were increased in patients suffering hepatic steatosis. The increase in VLDLR levels was accompanied by a reduction in *PPARβ/δ* mRNA abundance that only reached statistical significance in livers of patients with severe hepatic steatosis (Figure 7D). The expression of the PPARβ/δ-target genes involved in fatty acid oxidation, *PDK4* and *CPT-1α,* was reduced in the livers of patients with steatosis (Figure 7D). Consistent with the reduced levels of PPARβ/δ, the DNA-binding activity of this transcription factor assessed by EMSA showed a reduction in patients with hepatic steatosis, especially in those with severe hepatic steatosis (Figure 7E). The reduction in PPARβ/δ expression and activity in patients with severe hepatic steatosis was accompanied by an increase in *HRI*, *TRB3,* and *NQO1* expression (Figure 7F), suggesting that the increase in VLDLR levels in humans with severe hepatic steatosis in the context of reduced PPARβ/δ levels might be the result of activation of the HRI-eIF2α-ATF4 and Nrf2 pathways. Expression of ATF4-target gene *FGF21* was significantly increased only in the patients with severe steatosis (Figure 7G), whereas expression of its receptors, β-klotho and *FGFR1c,* was reduced, although the reduction of the receptor did not reach significance, suggesting that the effect of this hormone might be attenuated (Figure 7G).

4. DISCUSSION

Here we present evidence that VLDLR is regulated by PPARβ/δ and FGF21. The reported increase in VLDLR in *Pparβ/δ* null macrophages

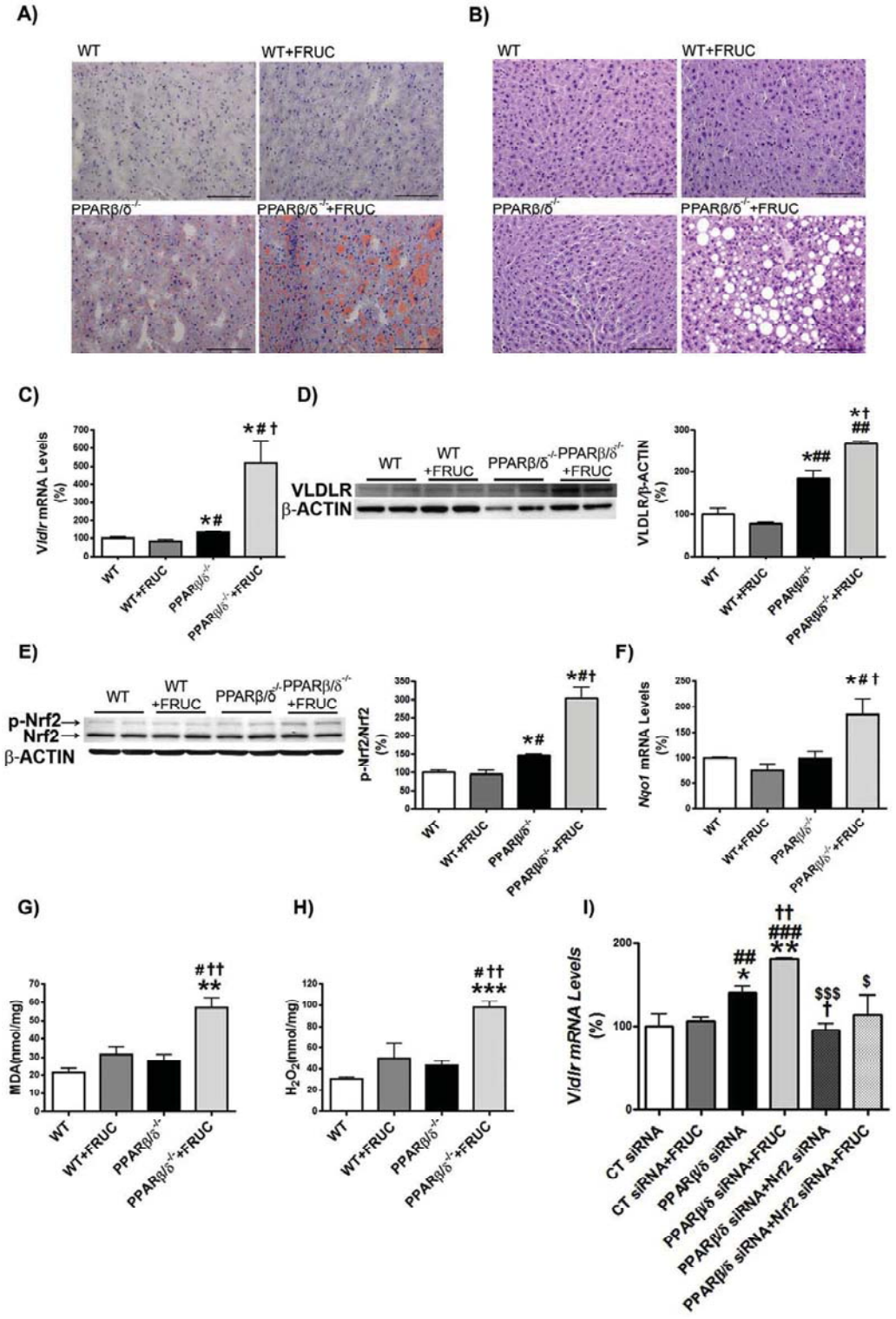

Figure 6: VLDLR upregulation is intensified by fructose feeding in the liver of *Pparβ/δ*-null mice. Oil Red O (A) and hematoxylin-eosin (B) staining of livers from male wild-type (WT) and *Pparβ/δ*-deficient mice (PPARβ/$\delta^{-/-}$) fed with either water or water containing 30% fructose for eight weeks. Scale bar: 100 μm. C, Hepatic *Vldlr* mRNA abundance. Immunoblot analyses of hepatic VLDLR (D) and total and phospho-Nrf2 (E). F, *Nqo1* mRNA abundance. MDA (G) and H_2O_2 (H) levels from liver of wild-type (WT) and *Pparβ/δ*-deficient mice fed with either water or water containing 30% fructose. Data are presented as the mean ± S.D. (n = 6 per group). $^{**}p < 0.01$ and $^{*}p < 0.05$ *vs.* water-fed WT mice. $^{\#\#}p < 0.01$ and $^{\#}p < 0.05$ *vs.* fructose-fed WT mice. $^{\dagger\dagger}p < 0.01$ and $^{\dagger}p < 0.05$ *vs.* water-fed *Pparβ/δ*$^{-/-}$ mice. I, *Vldlr* mRNA abundance in primary hepatocytes transfected with control, *Pparδ* and *Nrf2* siRNA for 24 h in the presence or absence of 25 mM fructose. $^{*}p < 0.05$ *vs.* control siRNA. $^{\#}p < 0.05$ *vs. Pparδ* siRNA.

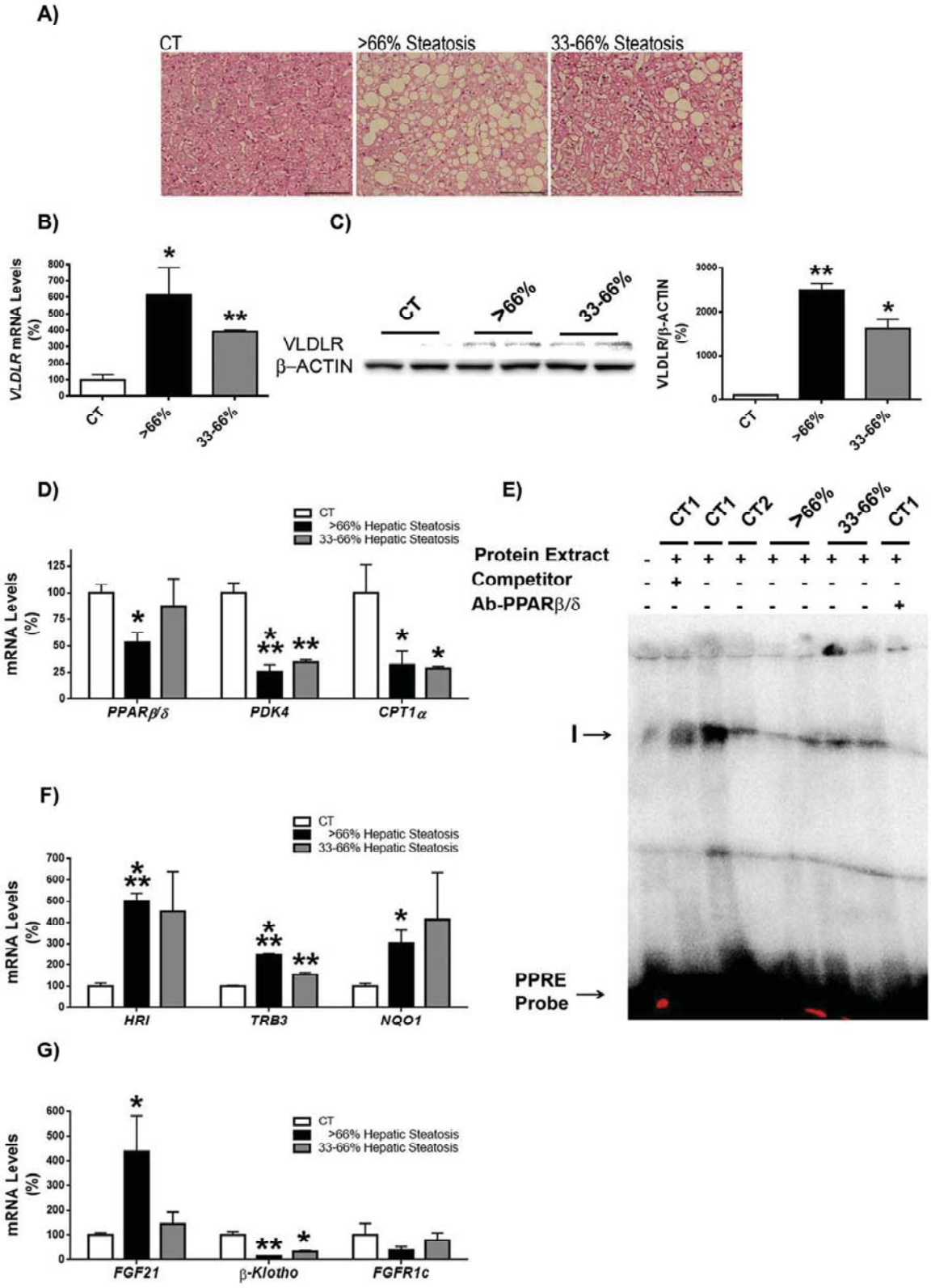

Figure 7: Liver of patients with steatosis show increased VLDLR content. A, Hematoxylin-eosin staining of liver biopsies from control subjects (Control, CT) and patients with moderate (30–66% of hepatocytes presenting steatosis) and severe (>66%) hepatic steatosis. Scale bar: 100 μm. Hepatic *VLDLR* mRNA (B) and protein (C) abundance. D, mRNA abundance of *PPARβ/δ*, *PDK4* and *CPT1α*. E, autoradiograph of EMSA performed with a ^{32}P-labeled PPRE and crude nuclear protein extract (NE) from liver biopsies. One main specific complex (I) based on competition with a molar excess of unlabeled probe is shown. The supershift assay performed by incubating NE with an antibody (Ab) directed against PPARβ/δ shows a reduction in the band. F, mRNA abundance of *HRI*, *TRB3* and *NQO1*. G, mRNA abundance of *FGF21*, *β-KLOTHO* and *FGFR1c*. Data are presented as the mean ± S.D. (n = 4 per group) relative to the control (CT) group. ***p < 0.001, **p < 0.01 and *p < 0.05 *vs.* CT group.

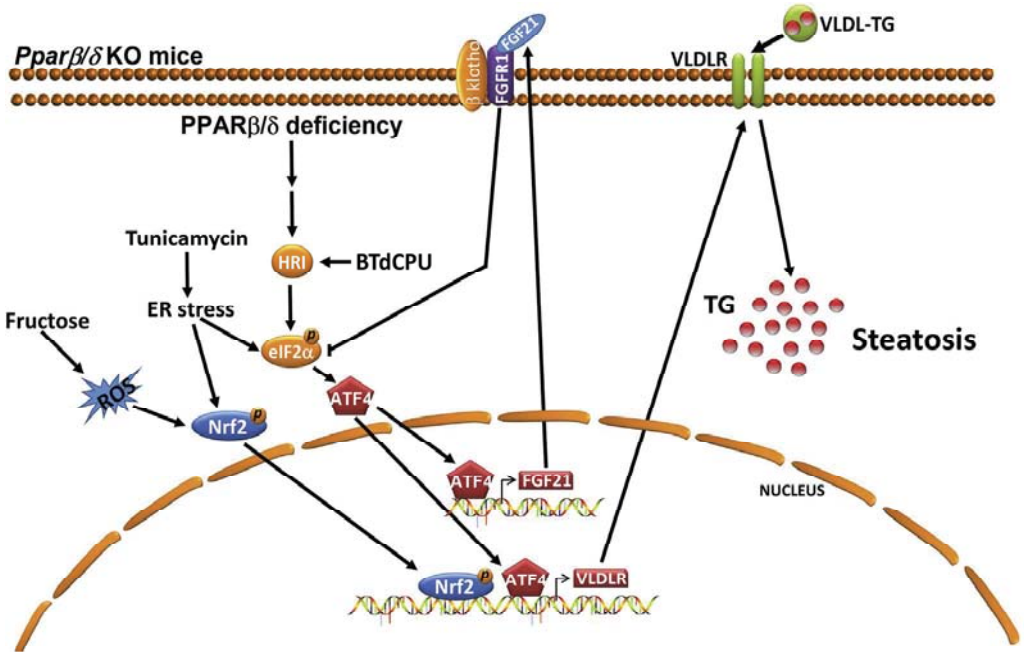

Figure 8: Proposed mechanisms by which PPARβ/δ regulates VLDLR levels and hepatic steatosis. *Pparβ/δ* deficiency may result in an increase in VLDLR levels and hepatic steatosis through several mechanisms. The activation of HRI caused by *Pparβ/δ* deficiency (reference [28]) and by activators of this kinase (BTdCPU) may increase the levels of VLDLR through the eIF2α-ATF4 pathway. ER stress can also activate the eIF2α-ATF4 pathway leading to an increase in the expression of VLDLR and FGF21. This hormone suppresses the eIF2α-ATF4 pathway through a negative feedback mechanism and thereby it also regulates the levels of VLDLR. ER stress also enhances the activity of Nrf2, a transcription factor reported to upregulate the expression of Fgf21 (reference [19]). Fructose feeding increases the levels of ROS and the activity of Nrf2 providing a mechanism for the increase of the levels of VLDLR. All these mechanisms may result in an increase in the levels of VLDLR causing hepatic steatosis. TG: triglyceride.

[38], prompted us to examine whether *Pparβ/δ*-null mice showed increased VLDLR levels and determine its contribution to NAFLD and the mechanisms involved. Our findings indicate that in *Pparβ/δ*-null mice, HRI activation in liver increases VLDLR levels through the eIF2α-ATF4 pathway (Figure 8). Despite this, HRI activators do not increase hepatic steatosis; on the contrary, these compounds also increased FGF21 levels and this hormonal factor improved glucose intolerance and hepatic triglyceride accumulation induced by feeding a HFD [28]. In addition, *Pparβ/δ*-deficiency also results in the activation of Nrf2, another transcription factor that contributes to increase VLDLR levels [18]. Under conditions of *Pparβ/δ*-deficiency, the increase in VLDLR levels would contribute to hepatic steatosis. In addition, stimulation of ER stress induces hepatic steatosis through VLDLR [6], and this process might be exacerbated in *Pparβ/δ*-null mice through a higher activation of both ATF4 and Nrf2, suggesting that the absence of PPARβ/δ contributes to intensify ER stress-induced fatty liver.

It has previously been reported that the PPARβ/δ agonist GW501516 promotes glucose flux to the pentose phosphate pathway and fatty acid synthesis in liver [39], establishing a discrepancy with the findings of this manuscript. However, a time-course study demonstrated that GW501516 induces accumulation of liver lipids following 4 wk of treatment, but this turned into a reduction in the content of hepatic lipids after 8 wk. of GW501516 treatment [40], probably as the result of an increase in fatty acid oxidation. Therefore, long treatments with GW501516 reduce hepatic lipids, which is consistent with the increase in liver lipids observed in *Pparβ/δ*-null mice.

FGF21 has emerged as an important regulator of glucose and lipid metabolism and hence is a promising agent for the treatment of obesity, NAFLD, insulin resistance, and type 2 diabetes mellitus [41]. This study also suggests that the reported enhanced FGF21 levels in *Pparβ/δ*-deficient mice [28] prevent a higher increase in VLDLR levels and hepatic triglyceride accumulation. This effect of FGF21 is the result of a negative feedback loop by which this hormone suppresses the eIF2α-ATF4 pathway [28,34]. In fact, we show here that blocking FGF21 increases VLDLR levels and hepatic steatosis. In agreement with this, *Fgf21*$^{-/-}$ mice showed increased hepatic activation of the eIF2α-ATF4 pathway and VLDLR levels, suggesting that this receptor may account for part of the hepatic steatosis observed in these mice. Thus, FGF21 can prevent NAFLD by increasing hepatic fatty acid oxidation and reducing lipid synthesis [41], and our findings indicate that this hormone may also prevent NAFLD by downregulating VLDLR levels.

Fructose feeding increases hepatic steatosis, but this process is influenced by the genetic background of the mice. In our study, feeding wild-type mice (C57BL/6X129/SV genetic background) with fructose did not result in hepatic steatosis, although fructose feeding was successful, as demonstrated by the increase in *Fgf21* expression, probably through carbohydrate response element binding protein (ChREBP)-mediated mechanisms, as previously reported [37]. However, *Pparβ/δ*-null mice of the same genetic background fed with fructose showed hepatic steatosis, and this was accompanied by higher hepatic VLDLR levels. Our findings demonstrate that in the context of *Pparβ/δ* deficiency, fructose induces ROS production, leading to an increase in phospho-Nrf2 levels and therefore in its activity. A step further, our siRNA studies demonstrated that this transcription factor was responsible for fructose-induced *Vldlr* expression in primary hepatocytes.

An analysis of human samples from patients with hepatic steatosis showed an increase in the liver protein content of VLDLR compared with control subjects. Interestingly, a reduction in PPARβ/δ levels and/or activity, as demonstrated by EMSA and the expression of its target genes, was also observed in the liver of these patients, suggesting that

the relationship between PPARβ/δ and VLDLR observed in mice might also operate in humans with hepatic steatosis.

Targeting PPAR isotypes for the treatment of fatty liver disease has been extensively studied, mainly in the case of PPARα [42,43]. However, although the beneficial effect of activating PPARα for NAFLD has been proven in several mouse models [42,43], fibrates, which are PPARα agonists, do not correct NAFLD in humans [44]. In contrast, long-term activation of PPARβ/δ can improve hepatic steatosis by activating fatty acid oxidation in different mouse models [45,46], whereas clinical studies have also demonstrated a reduction of hepatic fat content in humans upon treatment with PPARβ/δ agonists [47,48]. Our findings show that in patients with hepatic steatosis the reduction in PPARβ/δ activity is accompanied by an increase in VLDLR levels. It remains to be studied whether in the clinical setting PPARβ/δ agonists improve hepatic steatosis by regulating VLDLR abundance. Moreover, since we have reported that PPARβ/δ activation in mice increases PPARα expression and activity and enhances the hepatic levels of the endogenous PPARα ligand 16:0/18:1-phosphatidylcholine [49], we cannot discard that the reduction of PPARβ/δ activity may also affect the activity of PPARα. Consistent with this, drugs combining PPARα and PPARβ/δ isotype agonism are a promising treatment for NAFLD. In fact, the dual PPARα/β(δ) agonist elafibranor (GFT505) shows anti-steaotic effects in rodent models [50], and, in abdominally obese subjects, it improves hepatic and peripheral insulin sensitivity and probably NAFLD, although liver fat content was not measured [51].

On the other hand, the increase in hepatic *FGF21* expression in patients suffering hepatic steatosis is in agreement with previous studies [52], and it has been considered to be the result of a resistance to this hormone [53], implying that the lack of FGF21 activity may also contribute to increase VLDLR levels in hepatic steatosis. It is important to point out that the low number of patients analyzed is a limitation of this part of the study and precludes that VLDLR plays a role in NAFLD although it might correlate with liver fat accumulation.

5. CONCLUSIONS

The findings of this study suggest that *Pparβ/δ*-deficiency results in an increase in VLDLR levels, whereas FGF21 prevents the increase in hepatic VLDLR levels. In patients with hepatic steatosis, a reduction in the levels and/or activity of PPARβ/δ was accompanied by an increase in VLDLR abundance, suggesting that this crosstalk might be involved in fatty liver development. Overall, these data suggest that modulation of PPARβ/δ and/or FGF21 activity might be a key therapeutic target for the treatment of hepatic steatosis by regulating VLDLR abundance.

AUTHOR'S CONTRIBUTION

MZ, EB, XP, JD, TQL, JCEG, LC, PR, AMV, and MVC performed the experiments; EP and SV synthesized the HRI activators; MR, MM, and RD recruited and obtained human samples; WW, YL, and FV analyzed the data and revised the results; MZ, YL, and MVC designed the experiments and revised the results; MVC was primarily responsible for writing the manuscript. All authors contributed to manuscript editing and approval.

FINANCIAL SUPPORT

This study was partly supported by funds from the Spanish Ministry of the Economy and Competitiveness (SAF2015-64146-R to MVC, SAF2014-55725 to FV, and SAF2015-65267-R to AMV) and European Union ERDF funds. CIBER de Diabetes y Enfermedades Metabólicas Asociadas (CIBERDEM) and CIBER Fisiopatologia de la Obesidad y Nutrición (CIBERobn) are Carlos III Health Institute projects. WW is supported by Start-Up Grants from the Lee Kong Chian School of Medicine, Nanyang Technological University, Singapore, and by the Région Midi-Pyrénées, France, and TQL is supported by a CONACyT (National Council for Science and Technology in Mexico) Ph.D. scholarship.

CONFLICT OF INTEREST

The authors declare no competing interests.

APPENDIX A. SUPPLEMENTARY DATA

Supplementary data related to this article can be found at https://doi.org/10.1016/j.molmet.2017.12.008.

REFERENCES

[1] Satapathy, S.K., Sanyal, A.J., 2015. Epidemiology and natural history of nonalcoholic fatty liver disease. Seminars in Liver Disease 35:221—235.

[2] Cohen, J.C., Horton, J.D., Hobbs, H.H., 2011. Human fatty liver disease: old questions and new insights. Science 332:1519—1523.

[3] Musso, G., Gambino, R., Cassader, 2009. Recent insights into hepatic lipid metabolism in non-alcoholic fatty liver disease (NAFLD). Progress in Lipid Research 48:1—26.

[4] Postic, C., Girard, J., 2008. Contribution of de novo fatty acid synthesis to hepatic steatosis and insulin resistance: lessons from genetically engineered mice. Journal of Clinical Investigation 118:829—838.

[5] Duncan, R.E., Ahmadian, M., Jaworski, K., Sarkadi-Nagy, E., Sul, H.S., 2007. Regulation of lipolysis in adipocytes. Annual Review of Nutrition 27:79—101.

[6] Jo, H., Choe, S.S., Shin, K.C., Jang, H., Lee, J.H., Seong, J.K., et al., 2013. Endoplasmic reticulum stress induces hepatic steatosis via increased expression of the hepatic very low-density lipoprotein receptor. Hepatology 57:1366—1377.

[7] Webb, J.C., Patel, D.D., Jones, M.D., Knight, B.L., Soutar, A.K., 1994. Characterization and tissue-specific expression of the human 'very low density lipoprotein (VLDL) receptor' mRNA. Human Molecular Genetics 3:531—537.

[8] Oka, K., Ishimura-Oka, K., Chu, M.J., Sullivan, M., Krushkal, J., Li, W.H., et al., 1994. Mouse very-low-density-lipoprotein receptor (VLDLR) cDNA cloning, tissue-specific expression and evolutionary relationship with the low-density-lipoprotein receptor. European Journal of Biochemistry 224:975—982.

[9] Tacken, P.J., Beer, F.D., Vark, L.C., Havekes, L.M., Hofker, M.H., Willems Van Dijk, K., 2000. Very-low-density lipoprotein binding to the apolipoprotein E receptor 2 is enhanced by lipoprotein lipase, and does not require apolipoprotein E. Biochemical Journal 347:357—361.

[10] Takahashi, S., Suzuki, J., Kohno, M., Oida, K., Tamai, T., Miyabo, S., et al., 1995. Enhancement of the binding of triglyceride-rich lipoproteins to the very low density lipoprotein receptor by apolipoprotein E and lipoprotein lipase. Journal of Biological Chemistry 270:15747—15754.

[11] Takahashi, S., Sakai, J., Fujino, T., Hattori, H., Zenimaru, Y., Suzuki, J., et al., 2004. The very low-density lipoprotein (VLDL) receptor: characterization and functions as a peripheral lipoprotein receptor. Journal of Atherosclerosis and Thrombosis 11:200—208.

[12] Tao, H., Aakula, S., Abumrad, N.N., Hajri, T., 2010. Peroxisome proliferator-activated receptor-gamma regulates the expression and function of very-low-density lipoprotein receptor. American Journal of Physiology — Endocrinology and Metabolism 298:E68—E79.

[13] Yagyu, H., Lutz, E.P., Kako, Y., Marks, S., Hu, Y., Choi, S.Y., et al., 2002. Very low density lipoprotein (VLDL) receptor-deficient mice have reduced lipoprotein

lipase activity. Possible causes of hypertriglyceridemia and reduced body mass with VLDL receptor deficiency. Journal of Biological Chemistry 277:10037—10043.

[14] Frykman, P.K., Brown, M.S., Yamamoto, T., Goldstein, J.L., Herz, J., 1995. Normal plasma lipoproteins and fertility in gene-targeted mice homozygous for a disruption in the gene encoding very low density lipoprotein receptor. Proceedings of the National Academy of Sciences of the United States of America 92:8453—8457.

[15] Goudriaan, J.R., Tacken, P.J., Dahlmans, V.E., Gijbels, M.J., van Dijk, K.W., Havekes, L.M., et al., 2001. Protection from obesity in mice lacking the VLDL receptor. Arteriosclerosis, Thrombosis, and Vascular Biology 21:1488—1493.

[16] Goudriaan, J.R., Espirito Santo, S.M., Voshol, P.J., Teusink, B., van Dijk, K.W., van Vlijmen, B.J., et al., 2004. The VLDL receptor plays a major role in chylomicron metabolism by enhancing LPL-mediated triglyceride hydrolysis. The Journal of Lipid Research 45:1475—1481.

[17] Perman, J.C., Boström, P., Lindbom, M., Lidberg, U., StÅhlman, M., Hägg, D., et al., 2011. The VLDL receptor promotes lipotoxicity and increases mortality in mice following an acute myocardial infarction. Journal of Clinical Investigation 121:2625—2640.

[18] Wang, Z., Dou, X., Li, S., Zhang, X., Sun, X., Zhou, Z., et al., 2014. Nuclear factor (erythroid-derived 2)-like 2 activation-induced hepatic very-low-density lipoprotein receptor overexpression in response to oxidative stress contributes to alcoholic liver disease in mice. Hepatology 59:1381—1392.

[19] Gao, Y., Shen, W., Lu, B., Zhang, Q., Hu, Y., Chen, Y., 2014. Upregulation of hepatic VLDLR via PPARα is required for the triglyceride-lowering effect of fenofibrate. The Journal of Lipid Research 55:1622—1633.

[20] Vázquez-Carrera, M., 2016. Unraveling the effects of PPARβ/δ on insulin resistance and cardiovascular disease. Trends in Endocrinology and Metabolism 27:319—334.

[21] Salvadó, L., Serrano-Marco, L., Barroso, E., Palomer, X., Vázquez-Carrera, M., 2012. Targeting PPARβ/δ for the treatment of type 2 diabetes mellitus. Expert Opinion on Therapeutic Targets 16:209—223.

[22] Tan, N.S., Vázquez-Carrera, M., Montagner, A., Sng, M.K., Guillou, H., Wahli, W., 2016. Transcriptional control of physiological and pathological processes by the nuclear receptor PPARβ/δ. Progress in Lipid Research 64: 98—122.

[23] Nadra, K., Anghel, S.I., Joye, E., Tan, N.S., Basu-Modak, S., Trono, D., et al., 2006. Differentiation of trophoblast giant cells and their metabolic functions are dependent on peroxisome proliferator-activated receptor beta/delta. Molecular and Cellular Biology 26:3266—3281.

[24] Omar, B.A., Andersen, B., Hald, J., Raun, K., Nishimura, E., Ahrén, B., 2014. Fibroblast growth factor 21 (FGF21) and glucagon-like peptide 1 contribute to diabetes resistance in glucagon receptor-deficient mice. Diabetes 63:101—110.

[25] Barroso, E., Rodríguez-Rodríguez, R., Chacón, M.R., Maymó-Masip, E., Ferrer, L., Salvadó, L., et al., 2015. PPARβ/δ ameliorates fructose-induced insulin resistance in adipocytes by preventing Nrf2 activation. Biochimica et Biophysica Acta 1852:1049—1058.

[26] Benveniste, R., Danoff, T.M., Ilekis, J., Craig, H.R., 1988. Epidermal growth factor receptor numbers in male and female mouse primary hepatocyte cultures. Cell Biochemistry and Function 6:231—235.

[27] Brunt, E.M., 2002. Alcoholic and nonalcoholic steatohepatitis. Clinics in Liver Disease 6:399—420.

[28] Zarei, M., Barroso, E., Leiva, R., Barniol-Xicota, M., Pujol, E., Escolano, C., et al., 2016. Heme-regulated eIF2α kinase modulates hepatic FGF21 and is activated by PPARβ/δ deficiency. Diabetes 65:3185—3199.

[29] Ron, D., Walter, P., 2007. Signal integration in the endoplasmic reticulum unfolded protein response. Nature Reviews Molecular Cell Biology 8:519—529.

[30] Chen, T., Ozel, D., Qiao, Y., Harbinski, F., Chen, L., Denoyelle, S., et al., 2011. Chemical genetics identify eIF2α kinase heme-regulated inhibitor as an anticancer target. Nature Chemical Biology 7:610—616.

[31] Lázaro, I., Ferré, R., Masana, L., Cabré, A., 2013. Akt and ERK/Nrf2 activation by PUFA oxidation-derived aldehydes upregulates FABP4 expression in human macrophages. Atherosclerosis 230:216—222.

[32] De Sousa-Coelho, A.L., Marrero, P.F., Haro, D., 2012. Activating transcription factor 4-dependent induction of FGF21 during amino acid deprivation. Biochemical Journal 443:165—171.

[33] Salvadó, L., Palomer, X., Barroso, E., Vázquez-Carrera, M., 2015. Targeting endoplasmic reticulum stress in insulin resistance. Trends in Endocrinology and Metabolism 26:438—448.

[34] Jiang, S., Yan, C., Fang, Q.C., Shao, M.L., Zhang, Y.L., Liu, Y., et al., 2014. Fibroblast growth factor 21 is regulated by the IRE1α-XBP1 branch of the unfolded protein response and counteracts endoplasmic reticulum stress-induced hepatic steatosis. Journal of Biological Chemistry 289:29751—29765.

[35] Liu, X., Zhang, P., Martin, R.C., Cui, G., Wang, G., Tan, Y., et al., 2016. Lack of fibroblast growth factor 21 accelerates metabolic liver injury characterized by steatohepatities in mice. American Journal of Cancer Research 6:1011—1025.

[36] Rodríguez-Calvo, R., Barroso, E., Serrano, L., Coll, T., Sánchez, R.M., Merlos, M., et al., 2009. Atorvastatin prevents carbohydrate response element binding protein activation in the fructose-fed rat by activating protein kinase A. Hepatology 49:106—115.

[37] Fisher, F.M., Kim, M., Doridot, L., Cunniff, J.C., Parker, T.S., Levine, D.M., et al., 2016. A critical role for ChREBP-mediated FGF21 secretion in hepatic fructose metabolism. Molecular Genetics and Metabolism 6:14—21.

[38] Chawla, A., Lee, C.H., Barak, Y., He, W., Rosenfeld, J., Liao, D., et al., 2003. PPARdelta is a very low-density lipoprotein sensor in macrophages. Proceedings of the National Academy of Sciences of the United States of America 100:1268—1273.

[39] Lee, C.H., Olson, P., Hevener, A., Mehl, I., Chong, L.W., Olefsky, J.M., et al., 2006. PPARdelta regulates glucose metabolism and insulin sensitivity. Proceedings of the National Academy of Sciences of the United States of America 103:3444—3449.

[40] Garbacz, W.G., Huang, J.T., Higgins, L.G., Wahli, W., Palmer, C.N., 2015. PPARα is required for PPARδ action in regulation of body weight and hepatic steatosis in mice. PPAR Research 2015:927057.

[41] Domouzoglou, E.M., Naka, K.K., Vlahos, A.P., Papafaklis, M.I., Michalis, L.K., Tsatsoulis, A., et al., 2015. Fibroblast growth factors in cardiovascular disease: the emerging role of FGF21. American Journal of Physiology — Heart and Circulatory Physiology 309:H1029—H1038.

[42] Tanaka, N., Aoyama, T., Kimura, S., Gonzalez, F.J., 2017. Targeting nuclear receptors for the treatment of fatty liver disease. Pharmacology & Therapeutics 179:142—157.

[43] Gross, B., Pawlak, M., Lefebvre, P., Staels, B., 2017. PPARs in obesity-induced T2DM, dyslipidaemia and NAFLD. Nature Reviews Endocrinology 13:36—49.

[44] Fernández-Miranda, C., Pérez-Carreras, M., Colina, F., López-Alonso, G., Vargas, C., Solís-Herruzo, J.A., 2008. A pilot trial of fenofibrate for the treatment of non-alcoholic fatty liver disease. Digestive and Liver Disease 40: 200—205.

[45] Bojic, L.A., Telford, D.E., Fullerton, M.D., Ford, R.J., Sutherland, B.G., Edwards, J.Y., et al., 2014. PPARδ activation attenuates hepatic steatosis in Ldlr-/- mice by enhanced fat oxidation, reduced lipogenesis, and improved insulin sensitivity. The Journal of Lipid Research 55:1254—1266.

[46] Wu, H.T., Chen, C.T., Cheng, K.C., Li, Y.X., Yeh, C.H., Cheng, J.T., 2011. Pharmacological activation of peroxisome proliferator-activated receptor δ improves insulin resistance and hepatic steatosis in high fat diet-induced diabetic mice. Hormone and Metabolic Research 43:631—635.

[47] Bays, H.E., Schwartz, S., Littlejohn 3rd, T., Kerzner, B., Krauss, R.M., Karpf, D.B., et al., 2011. MBX-8025, a novel peroxisome proliferator receptor-delta agonist: lipid and other metabolic effects in dyslipidemic overweight patients treated with and without atorvastatin. Journal of Clinical Endocrinology & Metabolism 96:2889—2897.

[48] Risérus, U., Sprecher, D., Johnson, T., Olson, E., Hirschberg, S., Liu, A., et al., 2008. Activation of peroxisome proliferator-activated receptor (PPAR)delta promotes reversal of multiple metabolic abnormalities, reduces oxidative stress, and increases fatty acid oxidation in moderately obese men. Diabetes 57:332—339.

[49] Barroso, E., Rodríguez-Calvo, R., Serrano-Marco, L., Astudillo, A.M., Balsinde, J., Palomer, X., et al., 2011. The PPARβ/δ activator GW501516 prevents the down-regulation of AMPK caused by a high-fat diet in liver and amplifies the PGC-1α-Lipin 1-PPARα pathway leading to increased fatty acid oxidation. Endocrinology 152:1848—1859.

[50] Staels, B., Rubenstrunk, A., Noel, B., Rigou, G., Delataille, P., Millatt, L.J., et al., 2013. Hepatoprotective effects of the dual peroxisome proliferator-activated receptor alpha/delta agonist, GFT505, in rodent models of nonalcoholic fatty liver disease/nonalcoholic steatohepatitis. Hepatology 58: 1941—1952.

[51] Cariou, B., Hanf, R., Lambert-Porcheron, S., Zaïr, Y., Sauvinet, V., Noël, B., et al., 2013. Dual peroxisome proliferator-activated receptor α/δ agonist GFT505 improves hepatic and peripheral insulin sensitivity in abdominally obese subjects. Diabetes Care 36:2923—2930.

[52] Dushay, J., Chui, P.C., Gopalakrishnan, G.S., Varela-Rey, M., Crawley, M., Fisher, F.M., et al., 2010. Increased fibroblast growth factor 21 in obesity and nonalcoholic fatty liver disease. Gastroenterology 139:456—463.

[53] Fisher, F.M., Chui, P.C., Antonellis, P.J., Bina, H.A., Kharitonenkov, A., Flier, J.S., et al., 2010. Obesity is a fibroblast growth factor 21 (FGF21)-resistant state. Diabetes 59:2781—2789.

Table S1. Study subjects.

Steatosis Grade	0: CT (n=5)	2: 33-66% (n=4)	3: >66% (n=6)
Sex (Male/Female)	1/4	1/3	6/0
BMI (kg/m^2)	22.7 ± 3.9	34 .9 ± 8.8	27.6 ± 2.0
ALT	35.8±23.6	56.5± 5.6	166.0±38.0
AST	26.5±5.0	34±18.4	92.3±43.9
Cholestasis	1	0	0
Portal and/or lobular Inflammation	2 Mild	2 Mild, 2 Moderate	2 Mild, 3 Moderate
Bridging fibrosis	0	0	0

Table S2. Primer sequences used for real-time RT-PCR

Gene	Primers	
hANGPLT4	for	5’-GCGAATTCAGCATCTGCAAA-3’
	rev	5’-CTTGGCCACCTCATGGTCTAG-3’
mAngplt4	for	5’-GCATGGCTGCCTGTGGTAAC-3’
	rev	5’-ATCTTGCTGTTTTGAGCCTTGA-3’
mAprt	for	5’-CAGCGGCAAGATCGACTACA-3’
	rev	5’-AGCTAGGGAAGGGCCAAACA-3’
mAtf4	for	5’-AGCAAAACAAGACAGCAGCC-3’
	rev	5’-ACTCTCTTCTTCCCCCTTGC-3’
hβ-KLOTHO	for	5’-GGCCATCTACATGATGAAGAATTTC-3’
	rev	5’-GGCAGTATAACCAAACACTCGTATTTC-3’
hCHOP	for	5`-GGAAATGAAGAGGAAGAATCAAAAAT-3`
	rev	5`-GTTCTGGCTCCTCCTCAGTCA-3`
mChop	for	5`-CGAAGAGGAAGAATCAAAAACCTT-3`
	rev	5`-GCCCTGGCTCCTCTGTCA-3`
hFGF21	for	5`-ACCAGAGCCCCGAAAGTCT-3`
	rev	5`-CTTGACTCCCAAGATTTGAATAACTC-3`
mFgf21	for	5`-CAGGGAGGATGGAACAGTGGTA-3`
	rev	5`-TGACACCCAGGATTTGAATGAC-3`
hFGFR1c	for	5’-TGTTTGACCGGATCTACACACA-3’
	rev	5’-CTCCCACAAGAGCACTCCAA-3’
hGAPDH	for	5`-GGCCTCCAAGGAGTAAGACC-3`
	rev	5`-AGGGGTCTACATGGCAACTG-3`
mHo-1	for	5’-GAAAATGTGATTCACTCCTCTGACA-3’
	rev	5’-CCTTGGTGGCCTCCTTCAA-3’
hHRI	for	5’-CCCCGAATATGACGAATCTG-3’
	rev	5’-CAGATTCGTCATATTCGGGC-3’
hL-CPT1α	for	5’-TGCTTTACAGGCGCAAACTG-3’
	rev	5’-TGGAATCGTGGATCCCAAA-3’
hNQO1	for	5’-TGCAGCGGCTTTGAAGAAGAAAGG-3’
	rev	5’-TCGGCAGGATACTGAAAGTTCGCA-3’

mNqo1	for	5’-TATCCTTCCGAGTCATCTCTAGCA-3’
	rev	5’-TCTGCAGCTTCCAGCTTCTTG-3’
mNrf2	for	5’-CGAGATATACGCAGGAGAGGTAAGA-3’
	rev	5’-GCTCGACAATGTTCTCCAGCTT-3’
hPDK4	for	5’-CCAACCAATTCACATCGTGTATG-3’
	rev	5’-GCCCGCATTGCATTCTTAAA-3’
mPdk4	for	5’-CACCACATGCTCTTCGAACTCT-3’
	rev	5’-AAGGAAGGACGGTTTTCTTGATG-3’
hPPARβ/δ	for	5’-AGCATCCTCACCGGCAAA-3’
	rev	5’-GTCTCGATGTCGTGGATCACA-3’
mPparβ/δ	for	5`-GCCACAACGCACCCTTTG-3`
	rev	5`-CCACACCAGGCCCTTCTCT-3`
hTRB3	for	5’-TCGCTGACCGTGAGAGGAA-3’
	rev	5’-GCTTGTCCCACAGGGAATCA-3’
mTrb3	for	5’-CGTGGCACACTGCCACAA-3’
	rev	5’-CCTCTCACAGTTGCTGAAGACAA-3’
hVLDLR	for	5’-CAAGAGGAAGTTCCTGTTTAACTCTGA-3’
	rev	5’-TGACCAGTAAACAAAGCCAGACA-3’
mVldlr	for	5’-TCCAATGGCCTAATGGAATTACA-3’
	rev	5’-AGCATGTGCAACTTGGAATCC-3’

Supplementary Figures

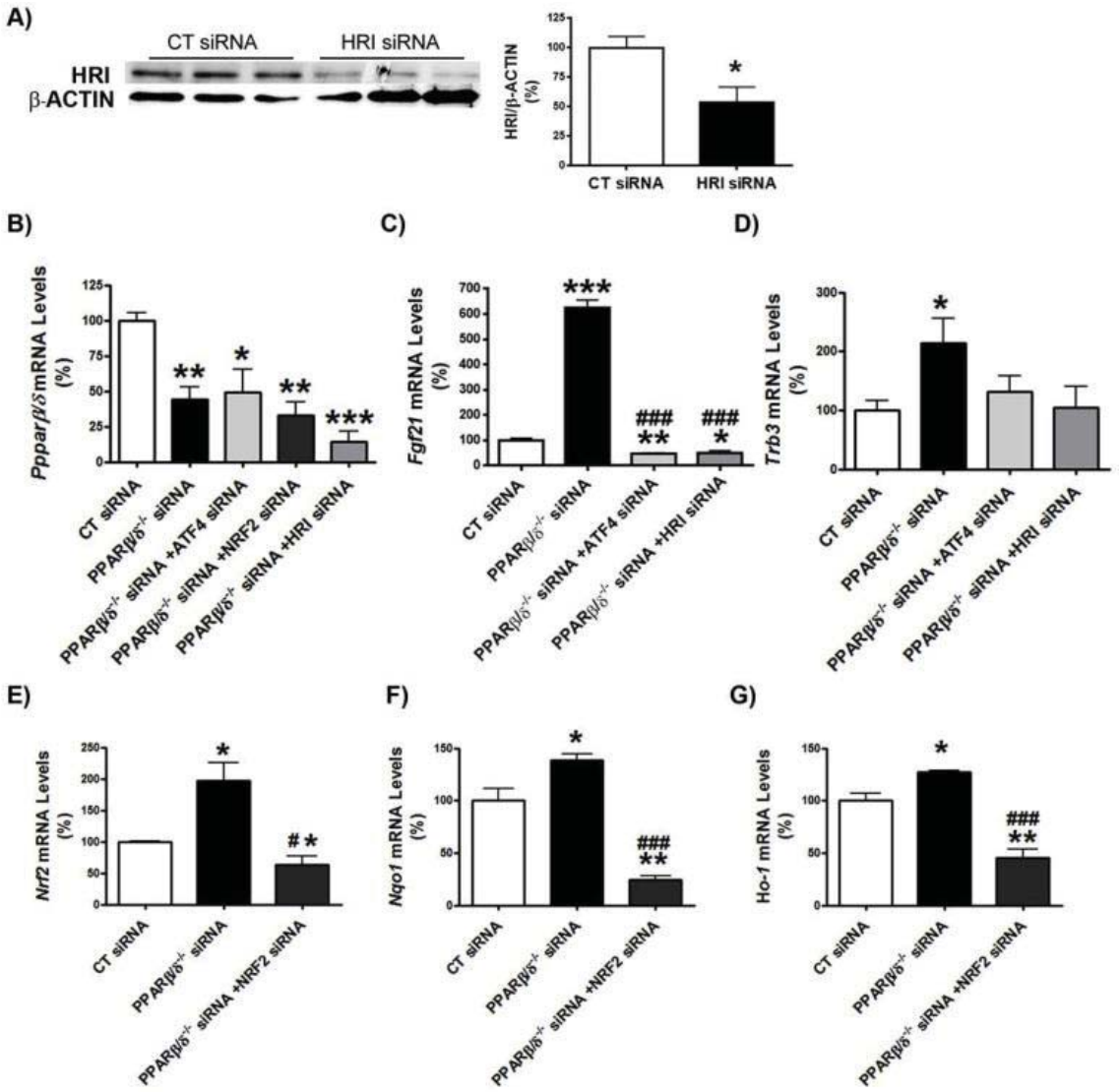

Fig. S1. A, primary hepatocytes were transfected with control or *Hri* siRNA for 24 h and the protein levels of HRI were assessed. *p<0.05 vs. control siRNA. Primary hepatocytes were transfected with control, *Pparδ, Atf4, Nrf2, Hri* and *Nrf2* siRNA for 24 h and the mRNA levels of *Pparβ/δ, Fgf21, Trb3*, *Nrf2, Nqo1* and *Ho-1* were analyzed. ***p<0.001, **p<0.01 and *p<0.05 *vs.* control siRNA. $^{\#}$p<0.05 *vs. Pparδ* siRNA. $^{\#\#\#}$p<0.001 and $^{\#}$p<0.05 *vs. Pparδ* siRNA.

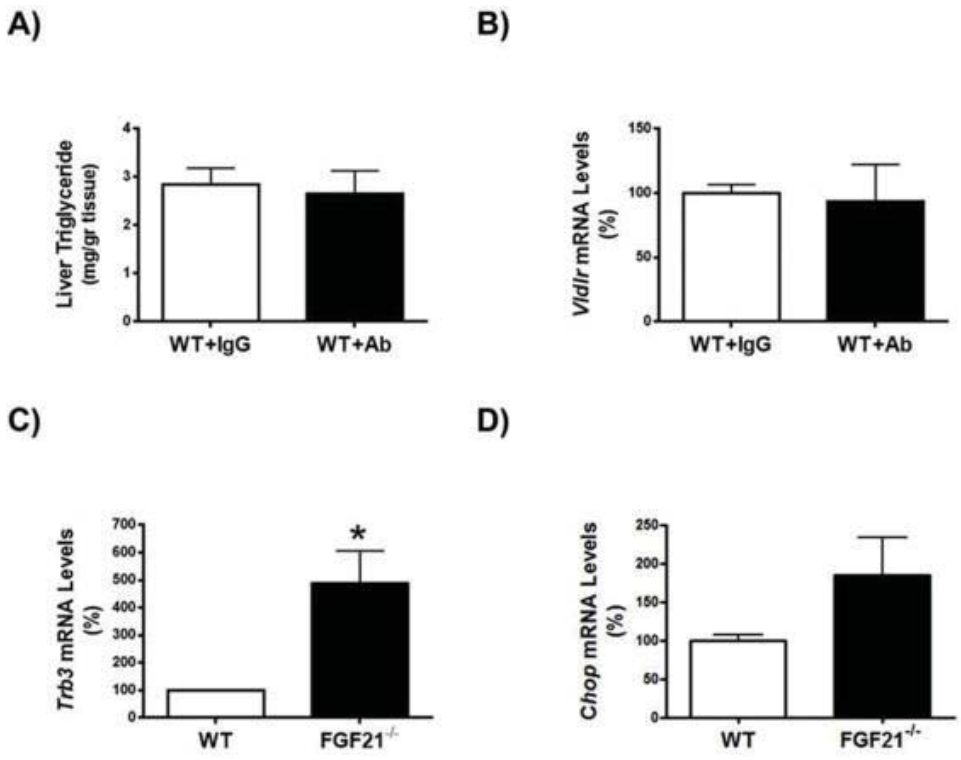

Fig. S2. Liver triglyceride levels (A) and *Vldlr* mRNA abundance (B) of livers from male wild-type (WT) mice injected intraperitoneally with IgG (9 μg/mouse) or a neutralizing antibody (Ab) (9 μg/mouse) against FGF21. *Trb3* (C) and *Chop* (D) mRNA abundance of livers from WT and *Fgf21*-null mice. Data are presented as the mean ± S.D. (n=5 per group). *p<0.05 *vs.* wild-type mice.

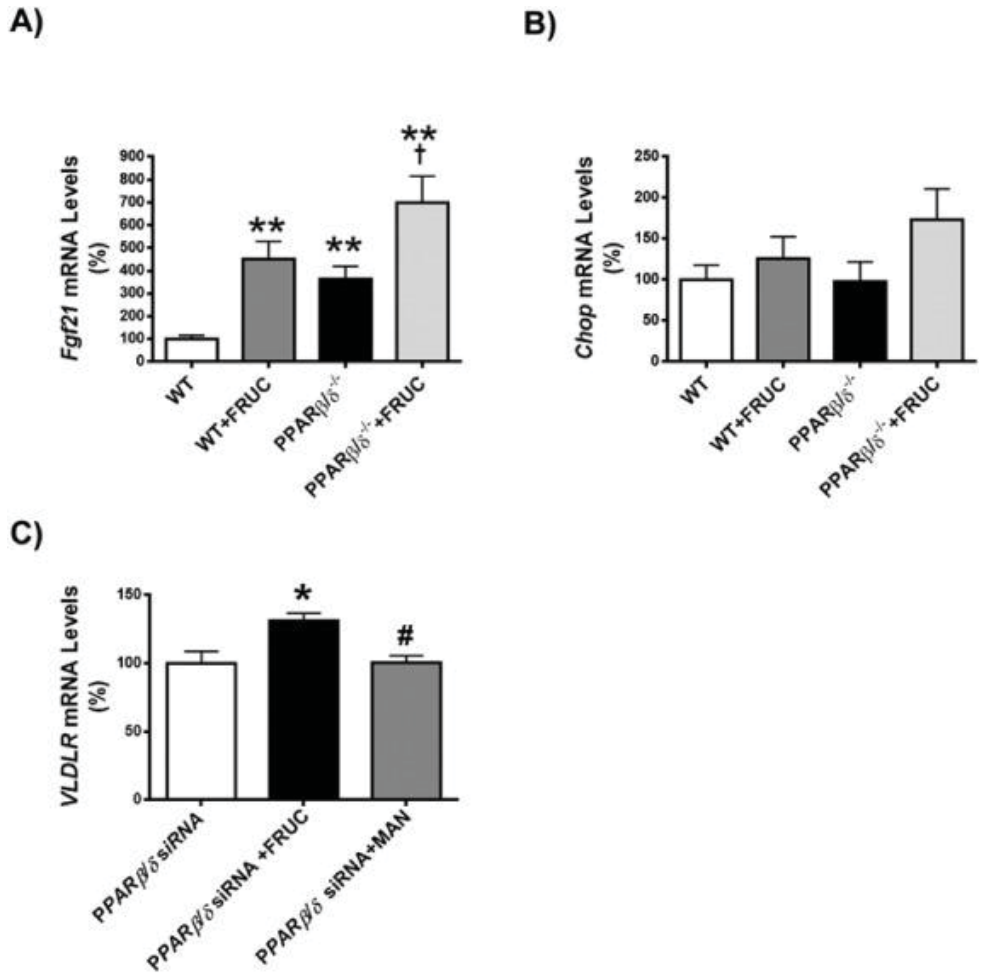

Fig. S3. Wild-type (WT) and *Pparβ/δ*-deficient mice were fed with either water or water containing 30% fructose, and the hepatic expression of (A) *Fgf21* and (B) *Chop* was assessed. Data are presented as the mean ± S.D. (n=6 per group). **p<0.01 *vs.* water-fed WT mice. †p<0.05 *vs.* vs. water-fed *Pparβ/δ*$^{-/-}$ mice. C, *VLDLR* mRNA abundance in human Huh-7 hepatocytes transfected with control and *PPARδ* siRNA for 24 hours in the presence or absence of 25 mM fructose or 25 mM mannitol. *p<0.05 *vs.* control siRNA. #p<0.05 *vs. Pparδ* siRNA transfected cells exposed to fructose.

Reciprocal effects of antiretroviral drugs used to treat HIV infection on the fibroblast growth factor-21/β-Klotho system

Journal: Antimicrobial Agents and Chemotherapy. 2018 Apr 16. pii: AAC.00029-18.

IF: 4.302 ENDOCRINOLOGY & METABOLISM 36 DE 257 (1st Quartile)

Abstract:

Following antiretroviral therapy, HIV-infected patients show increased circulating levels of the antidiabetic hormone fibroblast growth factor-21 (FGF21). In contrast, expression of the FGF21-obligatory co-receptor β-Klotho (KLB) is reduced in target tissues. This situation is comparable to the FGF21 resistance status observed in obesity and type-2 diabetes. Here, we performed the first systematic study of the effects of distinct members of different antiretroviral drug classes on the FGF21/KLB system in human hepatic, adipose, and skeletal muscle cells. Most protease inhibitors and the non nucleoside reverse transcriptase inhibitor efavirenz induced FGF21 gene expression. Neither nucleoside reverse transcriptase inhibitors nor the viral entry inhibitor maraviroc had any effect. Among integrase inhibitors, elvitegravir significantly induced FGF21 expression, whereas raltegravir had minor effects only in adipose cells. In human hepatocytes and adipocytes, known target cells of FGF21 action, efavirenz, elvitegravir, and the lopinavir/ritonavir combination exerted inhibitory effects on KLB gene expression. Drug treatments that elicited FGF21 induction/KLB repression were those found to induce endoplasmic reticulum (ER) stress and oxidative stress. Notably, pharmacological agents thapsigargin and tunicamycin, which induce these stress pathways, mimicked the effects of drug treatments. Moreover, pharmacological inhibitors of either ER or oxidative stress significantly impaired lopinavir/ritonavir-induced regulation of FGF21, but not KLB. In conclusion, current in vitro screen study identifies the antiretroviral drugs that affect FGF21/KLB expression in human cells. Present results could have important implications for the management of co-morbidities resulting from side effects of specific antiretroviral drugs for the treatment of HIV-infected patients.

zac-aac/zac00618/zac7224d18z | xppws | S=3 | 4/14/18 | 9:26 | ArtID: 00029-18 | DOI:10.1128/AAC.00029-18 | open-access | CE: CNV-kcd

Editor: Martinez | Section: Antiviral Agents | Designation: T

AMERICAN SOCIETY FOR MICROBIOLOGY | Antimicrobial Agents and Chemotherapy®

ANTIVIRAL AGENTS

Reciprocal Effects of Antiretroviral Drugs Used To Treat HIV Infection on the Fibroblast Growth Factor 21/β-Klotho System

AQ: au

Ricardo Moure,[a,b] Pere Domingo,[c,d,e,f,g] Joan Villarroya,[a,c] Laura Gasa,[a] José M. Gallego-Escuredo,[d] Tania Quesada-López,[a,b] Samantha Morón-Ros,[a,b] Alberto F. Maroto,[a] Gracia M. Mateo,[c] Joan C. Domingo,[a] Francesc Villarroya,[a,b] Marta Giralt[a,b]

[a]Department of Biochemistry and Molecular Biomedicine, Institut de Biomedicina (IBUB), University of Barcelona, Barcelona, Catalonia, Spain

[b]CIBER Fisiopatología de la Obesidad y Nutrición, Madrid, Spain

[c]Infectious Diseases Unit, Hospital de la Santa Creu i Sant Pau, Autonomous University of Barcelona, Barcelona, Catalonia, Spain

[d]Institut de Recerca Biomèdica (IRB) de Lleida, Lleida, Catalonia, Spain

[e]Department of Infectious Diseases, Hospital Universitari Arnau de Vilanova, Lleida, Catalonia, Spain

[f]Department of Infectious Diseases, Hospital Universitari de Santa María, Lleida, Catalonia, Spain

[g]Universitat de Lleida, Lleida, Catalonia, Spain

ABSTRACT Following antiretroviral therapy, HIV-infected patients show increased circulating levels of the antidiabetic hormone fibroblast growth factor 21 (FGF21). In contrast, the expression of the FGF21-obligatory coreceptor β-Klotho (KLB) is reduced in target tissues. This situation is comparable to the FGF21 resistance status observed in obesity and type 2 diabetes. Here, we performed the first systematic study of the effects of distinct members of different antiretroviral drug classes on the FGF21/KLB system in human hepatic, adipose, and skeletal muscle cells. Most protease inhibitors and the nonnucleoside reverse transcriptase inhibitor efavirenz induced FGF21 gene expression. Neither nucleoside reverse transcriptase inhibitors nor the viral entry inhibitor maraviroc had any effect. Among the integrase inhibitors, elvitegravir significantly induced FGF21 expression, whereas raltegravir had minor effects only in adipose cells. In human hepatocytes and adipocytes, known target cells of FGF21 action, efavirenz, elvitegravir, and the lopinavir-ritonavir combination exerted inhibitory effects on KLB gene expression. Drug treatments that elicited FGF21 induction/KLB repression were those found to induce endoplasmic reticulum (ER) stress and oxidative stress. Notably, the pharmacological agents thapsigargin and tunicamycin, which induce these stress pathways, mimicked the effects of drug treatments. Moreover, pharmacological inhibitors of either ER or oxidative stress significantly impaired lopinavir–ritonavir-induced regulation of FGF21, but not KLB. In conclusion, the present *in vitro* screen study identifies the antiretroviral drugs that affect FGF21/KLB expression in human cells. The present results could have important implications for the management of comorbidities resulting from side effects of specific antiretroviral drugs for the treatment of HIV-infected patients.

KEYWORDS antiretroviral drug, FGF21, β-Klotho, ER stress, hepatocyte, adipocyte

AQ: A

Successful treatment of HIV-infected patients with antiretroviral therapies (ART) has largely transformed HIV infection to a chronic medical condition (1). ART regimens can achieve strong virological control, but long-term exposure to ART, as often occurs in the growing population of older HIV patients, results in increased metabolic complications (2). Insulin resistance, metabolic syndrome, enhanced cardiovascular risk, and even overt lipodystrophy are common alterations in ART-treated HIV-infected patients (3). Several classes of antiretroviral drugs appear especially likely to elicit these alterations. For example, nucleoside analogs such as zidovudine and stavudine, which inhibit

Received 8 January 2018 **Returned for modification** 7 February 2018 **Accepted** 5 April 2018

Accepted manuscript posted online ●●●

Citation Moure R, Domingo P, Villarroya J, Gasa L, Gallego-Escuredo JM, Quesada-López T, Morón-Ros S, Maroto AF, Mateo GM, Domingo JC, Villarroya F, Giralt M. 2018. Reciprocal effects of antiretroviral drugs used to treat HIV infection on the fibroblast growth factor 21/β-Klotho system. Antimicrob Agents Chemother 62:e00029-18. https://doi.org/10.1128/AAC.00029-18.

Address correspondence to Marta Giralt, mgiralt@ub.edu.

zac-aac/zac00618/zac7224d18z	xppws	S=3	4/14/18	9:26	ArtID: 00029-18	DOI:10.1128/AAC.00029-18	**open-access**	CE: CNV-kcd

reverse transcriptase, appear to particularly exacerbate lipodystrophy, whereas protease inhibitors (PIs) have been implicated in altered glucose homeostasis (4). The molecular mechanisms that account for these toxicities are incompletely understood. More recently developed drugs (i.e., integrase inhibitors, viral entry inhibitors, and novel reverse transcriptase inhibitors and PIs) appear less prone to cause overt lipodystrophy. However, their impact on metabolic homeostasis in patients is still unclear (5).

Several studies on distinct cohorts of HIV patients have reported alterations in the fibroblast growth factor 21 (FGF21) endocrine system that manifest as abnormally high levels of FGF21 (6–8). FGF21, a hormone that was recently found to play a key role in glucose and lipid homeostasis, acts as an antidiabetic and possibly antiobesity factor (9). Several recent pilot studies have reported improvement in lipidemia and body weight after short-term treatment of obese/diabetic volunteers with FGF21 analogs (10, 11). Long-acting FGF21 analogs and agonists that mimic FGF21 action are under investigation in clinical trials in patients with obesity and diabetes (ClinicalTrials registration no. NCT02413372, NCT02538874, NCT2593331, NCT02708576, and NCT03060538). FGF21 is mainly produced in the liver and targets adipose tissue (and possibly that of the liver as well), promoting glucose uptake and oxidation (12). The effects of FGF21 are mediated by FGF receptors (FGFRs) that must interact with the cell surface protein β-Klotho (KLB) to form an FGF21-responsive receptor complex. Thus, the KLB coreceptor is essential for FGF21 action on target tissues (13). The paradoxically high FGF21 levels in HIV patients are associated with a downregulation of the molecular mediator of cellular FGF21 action, KLB. This scenario, which is reminiscent of "FGF21 resistance," is analogous to the situation found in obesity and type 2 diabetes (14, 15). It has been suggested that alterations in the FGF21 endocrine system involving liver and adipose tissues could be a major mechanism responsible for eliciting metabolic alterations in HIV patients (8, 13, 16). In this context, it has recently been reported that high FGF21 levels in HIV patients are significantly associated with altered bone homeostasis (17), consistent with previous indications of potential deleterious effects of high FGF21 levels on bone in experimental rodent models (18). Moreover, skeletal muscle, a tissue that does not express significant amounts of FGF21 in healthy individuals, shows increased expression of FGF21 under conditions in which muscle experiences mitochondrial oxidative stress (16, 19, 20), and a recent study reported enhanced expression of FGF21 in muscle from HIV patients in association with metabolic alterations (7).

Previous studies on distinct HIV patient cohorts have failed to show significant associations between abnormally high FGF21 levels and specific drugs included in ART cocktails, possibly owing to the limited number of patients and diversity of ART regimens prior to and during the study. However, several intracellular processes, including endoplasmic reticulum (ER) stress and oxidative stress, are known to induce hepatic expression of FGF21 (21–23), and there are reports that several antiretroviral drugs or drug classes (e.g., efavirenz and PIs) promote such processes (24–26). To date, less is known about molecular agents causing disturbances in the response to FGF21 in the target tissues. It has been reported that proinflammatory signaling in adipose tissue negatively regulates KLB expression (27). Then, inflammation in adipose tissue, a common condition in obesity, diabetes, and HIV lipodystrophy, may contribute to impaired FGF21 responsiveness in adipocytes.

Studies on the effects of antiretroviral drugs on human cells in culture have proven to be useful for the initial *in vitro* assessment of the potential of drugs to disturb metabolism (28–36). These studies have reported effects of several antiretroviral drugs on adipogenesis, senescence, mitochondrial toxicity, and ER stress, but none investigated their actions on the FGF21 system. In the present study, we hypothesized that antiretroviral drugs could alter the FGF21/KLB system by affecting their expression in human hepatic, adipose, and skeletal muscle cells. If so, this *in vitro* approach could be used to screen currently used antiretroviral drugs for their potential risk to cause FGF21/KLB toxicity. Here, we report a systematic analysis of the capacity of antiretroviral drugs, both "classical" and recently developed, to cause alterations in the FGF21/KLB system. That is, we analyzed their potential to promote FGF21 expression and KLB downregulation—the two key events associated with a disturbed FGF21 system in

zac-aac/zac00618/zac7224d18z	xppws	S=3	4/14/18	9:26	ArtID: 00029-18	DOI:10.1128/AAC.00029-18	**open-access**	CE: CNV-kcd

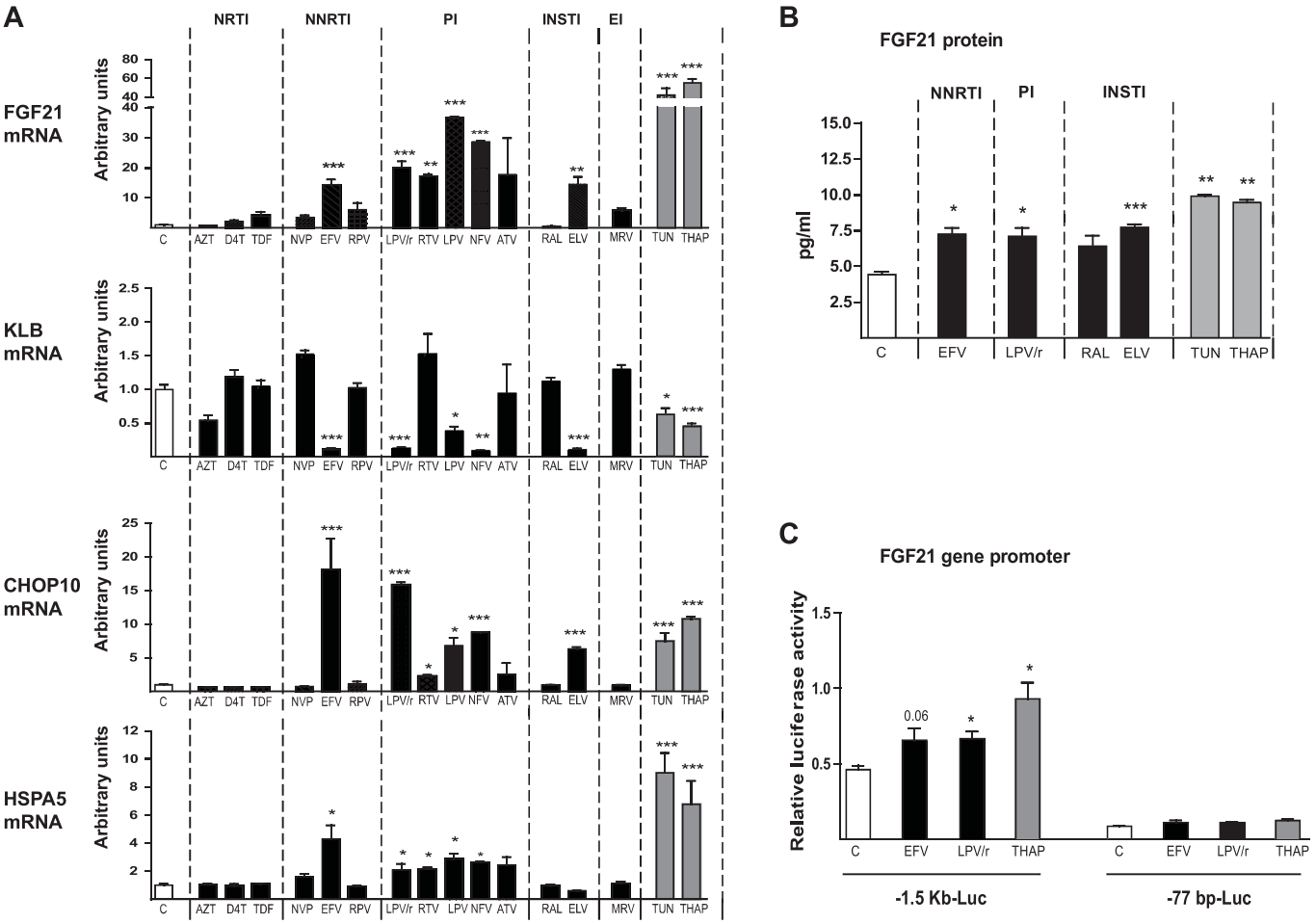

FIG 1 Effects of antiretroviral drugs on the expression of *FGF21*, KLB, *CHOP10*, and *HSPA5* mRNAs and on *FGF21* promoter activity in human hepatic HepG2 cells. Cells were exposed, when indicated, to the following drugs: zidovudine (AZT), 100 μM; stavudine (D4T), 100 μM; tenofovir disoproxil fumarate (TDF), 5 μM; nevirapine (NVP), 20 μM; efavirenz (EFV), 50 μM; rilpivirine (RPV), 10 μM; lopinavir-ritonavir 4:1 (LPV/r), 20 μM; ritonavir (RTV), 20 μM; lopinavir (LPV), 20 μM; nelfinavir (NFV), 20 μM; atazanavir (ATV), 50 μM; raltegravir (RAL), 50 μM; elvitegravir (ELV), 50 μM; maraviroc (MRV), 4 μM; tunicamycin (TUN), 2 μM; thapsigargin (THAP), 2 μM. (A) mRNA levels are presented as means ± SEM from 4 to 5 independent experiments and are expressed relative to values for control cells (defined as 1). (B) FGF21 protein levels in cell culture medium. (C) Luciferase activity in HepG2 cells transiently transfected with plasmid constructs in which luciferase is driven by the −1,497/+5 (−1.5 kb-Luc) or −77/+5 (−77 bp-Luc) 5′ regions of the *FGF21* gene. Cells were treated for 24 h with the indicated concentrations of drugs: EFV, 50 μM; LPV/r, 20 μM; THAP, 2 μM. Data are normalized to *Renilla* luciferase activity driven by the cotransfected pRL-CMV plasmid. Data are means ± SEM from 4 to 5 independent experiments. *, $P < 0.05$; **, $P < 0.01$, and ***, $P < 0.001$ for each drug treatment versus control.

patients—in human hepatic, adipose, and muscle cells. The effects of drug-induced ER stress and oxidative stress on these alterations were also explored.

AQ: B

RESULTS

Effects of antiretroviral drugs on FGF21 and KLB expression in human hepatic cells. To determine the possible effects of antiretroviral drugs on the FGF21 system, we first analyzed human hepatocytes, the main cellular source of FGF21 as well as a potential cellular target of FGF21 action. Among the antiretroviral drugs tested in HepG2 hepatic cells, all PIs, including the lopinavir-ritonavir 4:1 combination, elicited a

F1

robust induction of FGF21 expression (Fig. 1A). Neither the classical nucleoside reverse transcriptase inhibitors (NRTIs) zidovudine and stavudine nor the nucleotide analog tenofovir altered *FGF21* mRNA expression. Among nonnucleoside reverse transcriptase inhibitors (NNRTIs), efavirenz markedly induced *FGF21* expression, whereas neither nevirapine nor rilpivirine showed significant effects. Among integrase inhibitors (INSTIs), elvitegravir significantly induced *FGF21* expression, whereas raltegravir had no effect. The viral entry inhibitor maraviroc also had no effect. A parallel assessment of the effects of these drugs on *KLB* expression revealed a reciprocal pattern of alterations:

zac-aac/zac00618/zac7224d18z	xppws	S=3	4/14/18	9:26	ArtID: 00029-18	DOI:10.1128/AAC.00029-18	**open-access**	CE: CNV-kcd

most antiretrovirals that induced *FGF21* (i.e., most PIs, efavirenz, and elvitegravir) repressed *KLB* expression. *KLB* expression was unaffected by drugs that did not alter *FGF21* expression (Fig. 1A).

The induction of *FGF21* and repression of *KLB* observed in response to PIs and efavirenz, which are known to induce ER stress and oxidative stress in several cell types, including hepatocytes (24, 26), prompted us to examine whether these drugs also altered the expression of the genes encoding C/EBP-homologous protein 10 (*CHOP10*) and heat shock protein 5 (*HSPA5*), markers of ER stress and/or oxidative stress (37, 38). These analyses showed that the effects of drugs on *CHOP10* and *HSPA5* expression markedly paralleled their effects on *FGF21* expression, as evidenced by the significant upregulation of both *CHOP10* and *HSPA5* mRNAs in response to PIs, efavirenz, and elvitegravir (Fig. 1A). In addition, we treated HepG2 cells with tunicamycin and thapsigargin, two known inducers of ER stress. Both agents strongly induced *CHOP10* and *HSPA5* expression and elicited robust reciprocal effects on *FGF21* expression (induction) and *KLB* expression (repression)—the same effects produced by the aforementioned antiretroviral drugs (Fig. 1A).

The main changes found for *FGF21* mRNA expression were reflected in FGF21 protein levels released by cells to culture. Thus, efavirenz, the lopinavir-ritonavir combination, and elvitegravir caused a significant increase in FGF21 levels in HepG2 culture AQ: C medium, whereas raltegravir had no effect (Fig. 1B). The ER stress/oxidative stress inducers tunicamycin and thapsigargin caused the highest induction in FGF21 protein release by HepG2 cells (Fig. 1B).

After this initial screening, we evaluated the concentration dependence of the effects of the drugs that had been found to alter the FGF21 system at a single relatively high dose in the study above (see Fig. S1 in the supplemental material); raltegravir was used as an ineffective drug control. Efavirenz, elvitegravir, and the lopinavir-ritonavir combination caused reciprocal concentration-response effects, inducing *FGF21* and suppressing *KLB*. With one exception, we also found that these drugs induced a concentration-dependent induction of *CHOP10* and *HSPA5* expression, similar to that found for *FGF21* induction and *KLB* repression. The exception was efavirenz, which induced expression of ER stress/oxidative stress markers only at the highest concentration tested (50 μM), despite the fact that lower concentrations (20 μM) were sufficient to alter *FGF21* and *KLB* expression. Raltegravir did not alter *FGF21* or *KLB* mRNA expression, or *CHOP10* or *HSPA5* mRNA expression at any concentration tested.

To further assess FGF21 induction, we monitored the transcriptional activity of the *FGF21* promoter after transfecting HepG2 cells with an *FGF21* promoter-luciferase reporter construct in which luciferase activity is driven by the 5′ region (1.5 kb) of the *FGF21* gene (Fig. 1C). These analyses showed that thapsigargin, the positive control for ER stress induction, and the drugs efavirenz and lopinavir-ritonavir significantly induced *FGF21* promoter activity; this effect was lost when transfections were performed using AQ: D a construct comprising the −77 bp site in which most of the 5′ noncoding region of the *FGF21* gene was deleted. These results demonstrate that ER stress-inducing drugs and antiretroviral drugs that elicit increased *FGF21* mRNA expression act through the induction of *FGF21* gene transcription.

Effects of antiretroviral drugs on FGF21 and KLB expression in human adipocytes. Next, we analyzed the effects of antiretroviral drugs on adipocytes, the main cellular target of FGF21. Human Simpson-Golabi-Behmel Syndrome (SGBS) adipocytes undergoing adipogenic differentiation were exposed to the panel of antiretroviral drugs belonging to distinct classes. As was the case for hepatic cells, for this initial screen, the drugs were used at concentrations known to be nontoxic in this cell type, and *FGF21* and *KLB* mRNA expression levels were determined. Under control conditions, SGBS adipocytes expressed very low levels of *FGF21* mRNA, in agreement with the almost undetectable expression of FGF21 in human adipose tissue (13, 39, 40). However, we found that the NNRTI efavirenz and the INSTIs elvitegravir and raltegravir F2 significantly induced *FGF21* mRNA expression (Fig. 2A); treatment with lopinavir-ritonavir also produced a trend towards increased *FGF21* expression, although the

zac-aac/zac00618/zac7224d18z	xppws	S=3	4/14/18	9:26	ArtID: 00029-18	DOI:10.1128/AAC.00029-18	**open-access**	CE: CNV-kcd

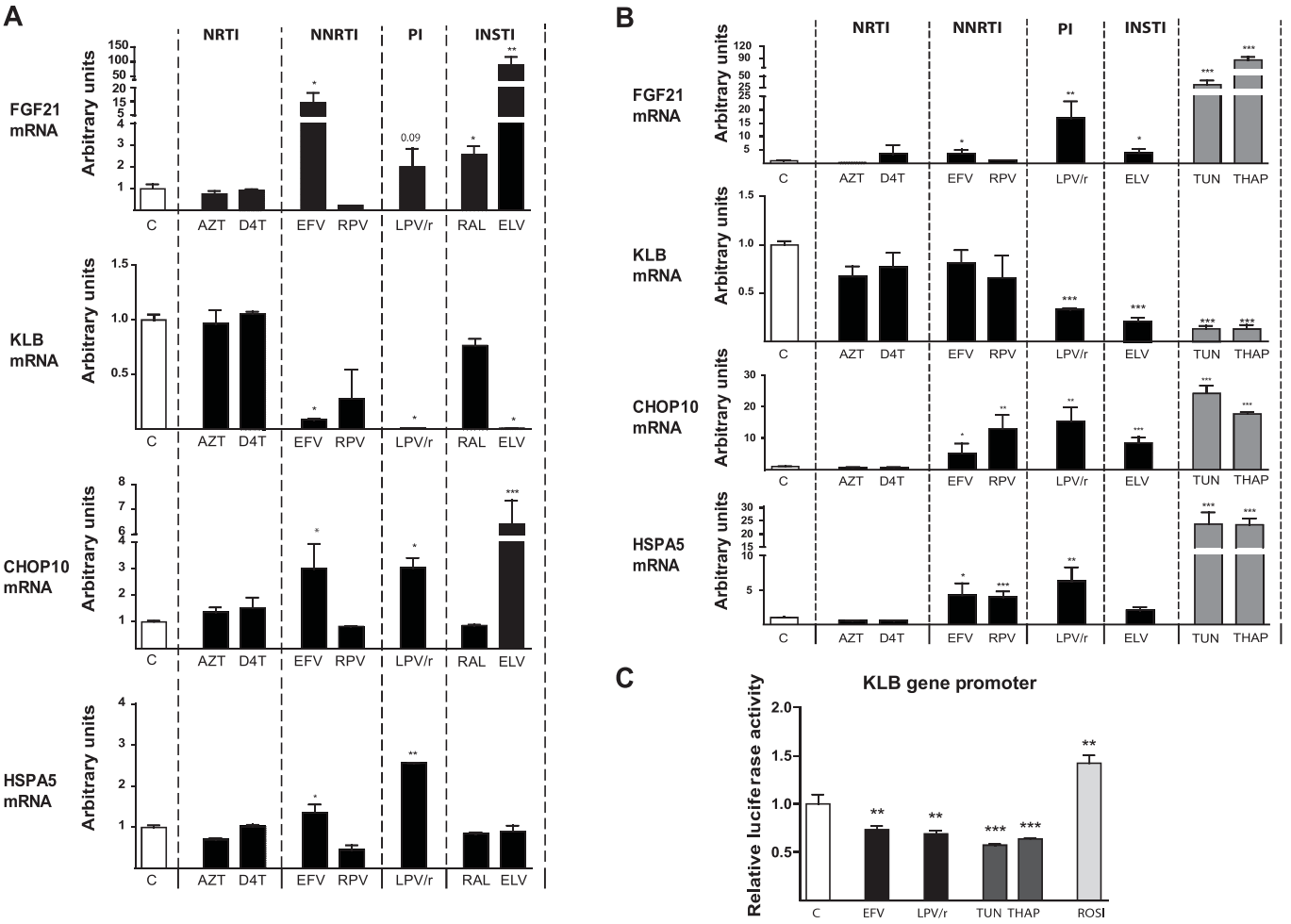

FIG 2 Effects of antiretroviral drugs on the expression of *FGF21*, *KLB*, *CHOP10*, and *HSPA5* mRNAs in human SGBS adipocytes and on *KLB* promoter activity in adipogenic cells. (A) SGBS human preadipocytes were differentiated in culture into adipocytes in the presence of the following drugs: zidovudine (AZT), 50 μM; stavudine (D4T), 50 μM; efavirenz (EFV), 5 μM; rilpivirine (RPV), 10 μM; lopinavir-ritonavir 4:1 (LPV/r), 20 μM; raltegravir (RAL), 5 μM; elvitegravir (ELV), 5 μM. (B) SGBS human adipocytes were differentiated in culture into adipocytes and treated for 24 h with the following drugs: AZT, 100 μM; D4T, 100 μM; EFV, 20 μM; RPV, 15 μM; LPV/r, 20 μM; ELV, 20 μM; tunicamycin (TUN), 2 μM; thapsigargin (THAP), 2 μM. Data are presented as means ± SEM from 4 to 5 independent experiments and are expressed relative to values for control cells (defined as 1). (C) Luciferase activity in adipogenic HIB-1B cells transiently transfected with a plasmid construct in which luciferase is driven by the −1,055/+45 region of the *KLB* gene. Cells were treated with the following drugs: EFV, 50 μM; LPV/r, 20 μM; TUN, 2 μM; THAP, 2 μM; rosiglitazone (ROSI), 2 μM. Data are normalized to *Renilla* luciferase activity driven by the cotransfected pRL-CMV plasmid. *, $P < 0.05$; **, $P < 0.01$, and ***, $P < 0.001$ for each drug treatment versus control.

differences did not reach statistical significance ($P = 0.09$). Again, these drugs exerted reciprocal repressive effects on *KLB* mRNA expression. As was the case for hepatic cells, they also induced effects on the expression of the ER stress/oxidative stress markers *CHOP10* and *HSPA5* that largely paralleled their effects on *FGF21* expression; the one exception was elvitegravir, which had no effect on *HSPA5* expression (Fig. 2A). A concentration-response analysis of the drugs that showed significant effects at single concentrations indicated that efavirenz caused overt reciprocal *FGF21* induction/*KLB* repression effects at 5 μM, lopinavir-ritonavir at 20 μM, and elvitegravir in the 1 to 2 μM range (see Fig. S2). The concentration-response effects of the three types of drug treatments remarkably paralleled those for the induction of *CHOP10*. However, only lopinavir-ritonavir induced the ER stress marker *HSPA5*.

Considering that the effects of treating adipocytes with drugs throughout their adipogenic differentiation may cause secondary effects related to alterations in the overall differentiation process, we used a second experimental paradigm in which fully differentiated human adipocytes were exposed to the drugs for 24 h. The results of these experiments were very similar to those found previously in adipogenic cells

zac-aac/zac00618/zac7224d18z	xppws	S=3	4/14/18	9:26	ArtID: 00029-18	DOI:10.1128/AAC.00029-18	**open-access**	CE: CNV-kcd

chronically treated with drugs: very low basal expression of *FGF21* and significant *FGF21* induction and *KLB* repression in response to lopinavir-ritonavir and elvitegravir (Fig. 2B). We also found that the same drugs that induced *FGF21* expression and *KLB* repression induced the ER stress/oxidative stress markers *CHOP10* and *HSPA5*; the one exception was the absence of an effect of elvitegravir on *HSPA5*. The ER stress inducers thapsigargin and tunicamycin mimicked the *FGF21* induction and *KLB* repression elicited by these drugs. Notably, in this experimental setting, rilpivirine caused a significant induction of *CHOP10* and *HSPA5* expression, but this did not translate into changes in *FGF21* or *KLB* gene expression (Fig. 2B). As was the case in the first experimental setting, a concentration-response analysis showed that efavirenz, lopinavir-ritonavir, and elvitegravir caused minor effects on *FGF21* expression that paralleled changes in *CHOP10* and *HSPA5* expression, but only at high concentrations (10 to 20 μM) (see Fig. S3).

The low range of *FGF21* mRNA expression in human adipocytes was reflected in the very low levels of FGF21 in the cell culture medium, which precluded reliable measurements of FGF21 concentration changes in response to drugs, in contrast with that in hepatic and muscle cells.

Considering that *KLB* gene expression is particularly sensitive to the differentiation status of adipocytes, we investigated whether the repression of *KLB* mRNA expression induced by drugs was attributable to impaired *KLB* gene transcription. To this end, we transfected preadipocytes with a luciferase reporter plasmid driven by the *KLB* gene promoter and exposed the cells to drugs. This analysis showed that whereas rosiglitazone (used as a positive control for *KLB* gene regulation) (27, 41) induced *KLB* gene transcription, lopinavir-ritonavir and efavirenz significantly downregulated *KLB* promoter activity, as was also the case for the ER stress positive controls, tunicamycin and thapsigargin (Fig. 2C).

Effects of antiretroviral drugs on FGF21 expression in human skeletal muscle cells. Although skeletal muscle is not considered to be a source or target of FGF21, a recent report indicated that FGF21 expression is enhanced in muscle from HIV patients (7), a phenomenon also reported in other conditions of skeletal muscle stress such as mitochondrial diseases (19, 20). *KLB* expression was virtually undetectable in differentiated human LHCN-M2 skeletal muscle cells, as expected. *FGF21* expression was also very low under control conditions, but PIs (with the exception of atazanavir) and efavirenz caused a dramatic induction of *FGF21* expression, whereas NRTIs, NNRTIs (other than efavirenz), and maraviroc had no effect (Fig. 3A). Efavirenz and the same PIs that caused *FGF21* upregulation induced the expression of *CHOP10* and *HSPA5*. Thapsigargin and tunicamycin also induced *FGF21* expression in muscle cells.

Efavirenz, the lopinavir-ritonavir combination, and the ER stress/oxidative stress inducers thapsigargin and tunicamycin caused a significant induction of the release of FGF21 protein by LHCN-M2 myotubes into culture medium, paralleling the results found for *FGF21* mRNA expression (Fig. 3B).

Effects of inhibitors of ER stress and oxidative stress on the action of antiretroviral drugs on FGF21 and KLB expression in human adipocytes. Our data demonstrating that several antiretroviral drugs, mainly PIs (e.g., lopinavir-ritonavir) and efavirenz, acted in the same manner as ER stress/oxidative stress to cause the induction of FGF21 expression and repression of KLB expression strongly suggest that ER stress and oxidative stress drive the reciprocal alterations in the FGF21 system. To test this, we used 4-phenylbutyrate (PBA), an inhibitor of ER stress, and 6-hydroxy-2,5,7,8-tetramethylchroman-2-carboxylic acid (Trolox), a vitamin E analog with antioxidant properties (Fig. 4). PBA significantly impaired the induction of ER stress. Trolox reduced thapsigargin- and tunicamycin-induced expression of *CHOP10*, but not the thapsigargin- and tunicamycin-induced expression of *HSPA5*, thus excluding HSPA5 as an oxidative stress marker; this contrasts with the dual responsiveness of CHOP10 to both ER and oxidative stress. PBA suppressed the induction of *FGF21* and repression of *KLB* expression by thapsigargin and tunicamycin, thus confirming that ER stress is capable of causing FGF21 upregulation and KLB downregulation. Both PBA and Trolox impaired the induction of *CHOP10* and *HSPA5* by lopinavir-ritonavir, suggesting that PIs are capable of causing

zac-aac/zac00618/zac7224d18z	xppws	S=3	4/14/18	9:26	ArtID: 00029-18	DOI:10.1128/AAC.00029-18	**open-access**	CE: CNV-kcd

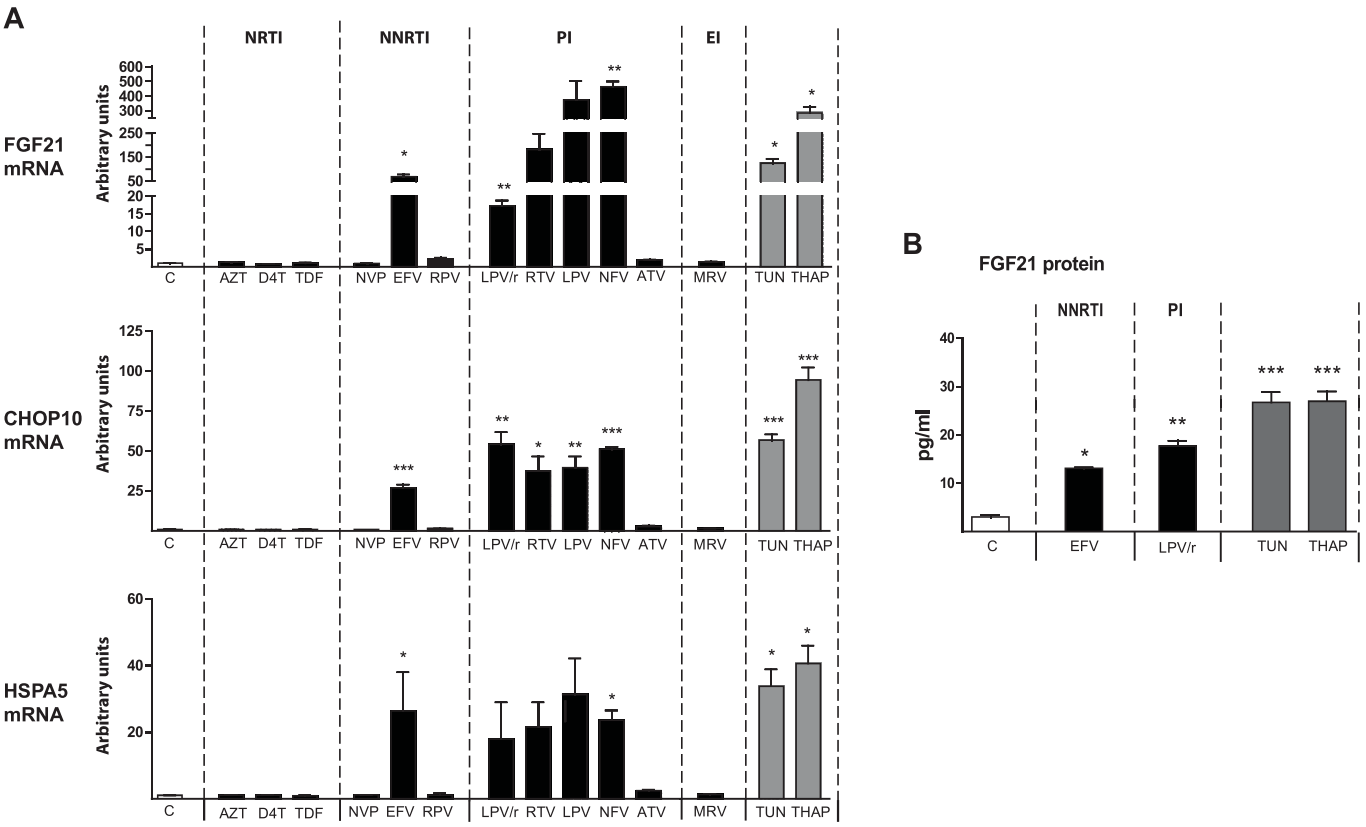

FIG 3 Effects of antiretroviral drugs, tunicamycin, and thapsigargin on the expression of *FGF21*, *CHOP10*, and *HSPA5* mRNAs and FGF21 release into the cell culture medium in human LHCN-M2 skeletal muscle cells differentiated in culture. LHCN-M2 myotubes differentiated in culture were treated for 24 h, as indicated, with the following drugs: zidovudine (AZT), 100 μM; stavudine (D4T), 100 μM; tenofovir disoproxil fumarate (TDF), 5 μM; nevirapine (NVP), 20 μM; efavirenz (EFV), 50 μM; rilpivirine (RPV), 10 μM; lopinavir-ritonavir 4:1 (LPV/r), 20 μM; ritonavir (RTV), 20 μM; lopinavir (LPV), 20 μM; nelfinavir (NFV), 20 μM; atazanavir (ATV), 50 μM; maraviroc (MRV), 4 μM; tunicamycin (TUN), 2 μM; thapsigargin (THAP), 2 μM. (A) mRNA levels are presented as means ± SEM from 4 to 5 independent experiments and are expressed relative to values for control cells (defined as 1). (B) FGF21 protein levels in cell culture medium. Data are presented as means ± SEM from 4 to 5 independent experiments. *, $P < 0.05$; **, $P < 0.01$, and ***, $P < 0.001$ for each drug treatment versus control.

both ER and oxidative stress. Similarly, PBA and Trolox blunted the induction of *FGF21* by lopinavir-ritonavir and elvitegravir. However, neither PBA nor Trolox affected the repression of *KLB* expression by these drugs, indicating that pathways other than ER stress/oxidative stress may be specifically involved in downregulating KLB in response to PIs. The downregulation of *KLB* elicited by elvitegravir was suppressed by PBA but was unaffected by Trolox. Efavirenz treatment had relatively modest effects in adipocytes under these conditions. Although it did significantly induce *CHOP10* and *HSPA5* expression, it caused only a minor induction of *FGF21*. These effects were relatively insensitive to PBA and Trolox, which at best exerted modest inhibitory actions.

Collectively, these data indicate that PIs, as well as elvitegravir and efavirenz, induce FGF21 expression through mechanisms involving ER and oxidative stress. However, although ER stress may induce KLB repression, other pathways are likely also involved in the repressive effect of PIs on KLB expression.

DISCUSSION

The results of the current study indicate that some antiretroviral drugs belonging to distinct classes alter the expression of FGF21 and the FGF21 coreceptor KLB in human cells. We found that modifications in the expression of FGF21 and KLB caused by drugs parallel those observed in HIV patients undergoing antiretroviral treatment: an induction of FGF21 levels and a repression of KLB expression (6, 7, 13). Moreover, the observed alterations are systematically reciprocal: those drugs (and drug concentrations) that induce FGF21 expression and release are largely the same as those that

zac-aac/zac00618/zac7224d18z	xppws	S=3	4/14/18	9:26	ArtID: 00029-18	DOI:10.1128/AAC.00029-18	**open-access**	CE: CNV-kcd

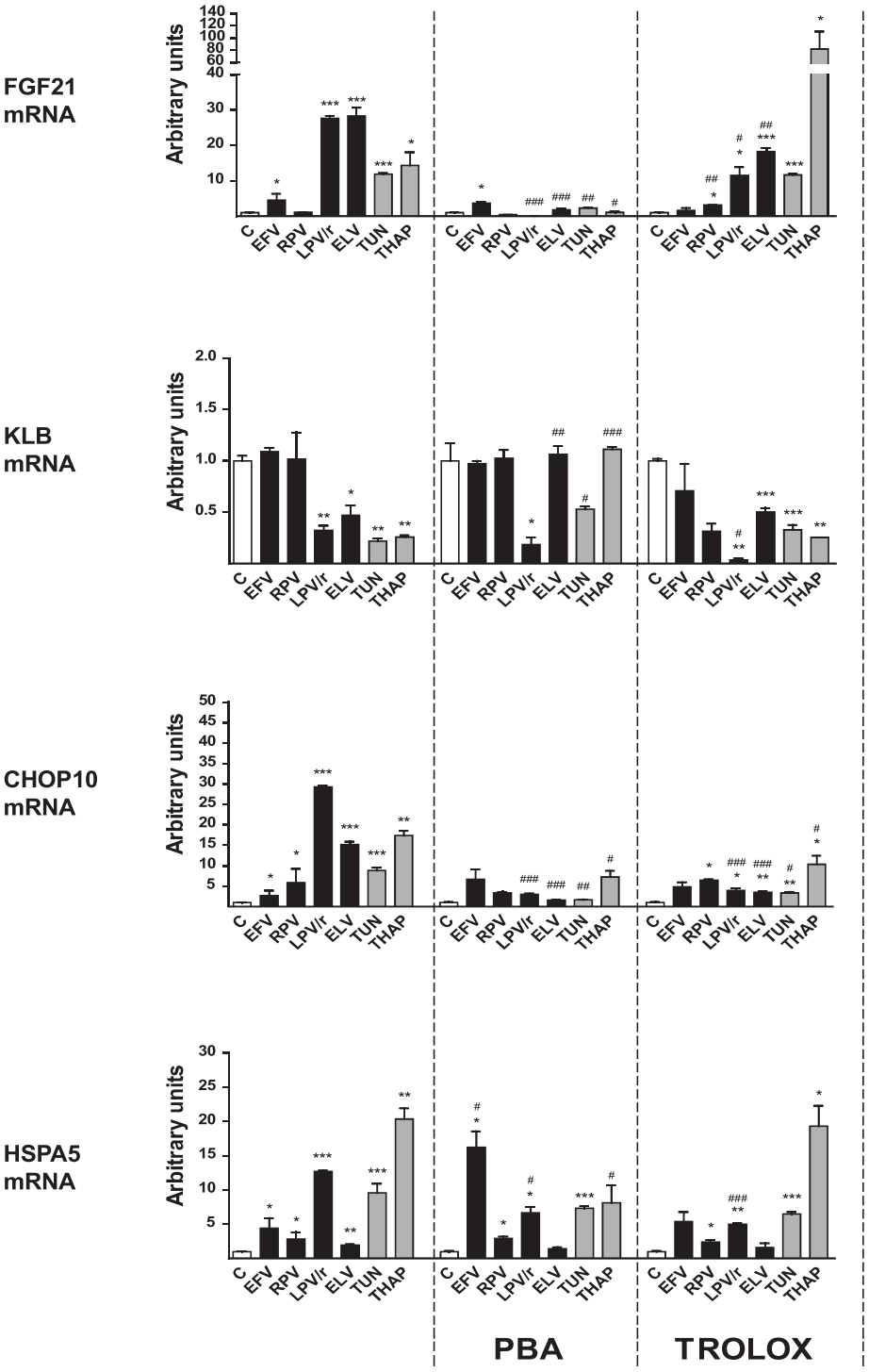

FIG 4 Effects of the ER stress-response inhibitor PBA and the antioxidant Trolox on the actions of antiretroviral drugs on the expression of *FGF21*, *KLB*, *CHOP10*, and *HSPA5* mRNAs in human SGBS adipocytes differentiated in culture. SGBS human preadipocytes were differentiated in culture into adipocytes and treated for 24 h with the following drugs: efavirenz (EFV), 20 μM; rilpivirine (RPV), 10 μM; lopinavir-ritonavir 4:1 (LPV/r), 20 μM; elvitegravir (ELV) 10 μM; tunicamycin (TUN), 2 μM; thapsigargin (THAP), 2 μM. Where indicated, cells were cultured in the presence of 2 mM PBA or 1 mM Trolox. Data are presented as means ± SEM from 4 to 5 independent experiments and are expressed relative to values for control cells (defined as 1). *, $P < 0.05$; **, $P < 0.01$, and ***, $P < 0.001$ for each drug treatment versus control; #, $P < 0.05$; ##, $P < 0.01$; ###, $P < 0.001$ for the effects of PBA or Trolox.

zac-aac/zac00618/zac7224d18z	xppws	S=3	4/14/18	9:26	ArtID: 00029-18	DOI:10.1128/AAC.00029-18	**open-access**	CE: CNV-kcd

repress KLB expression. NRTIs and the viral entry inhibitor maraviroc were universally neutral toward the FGF21/KLB system. PIs, the NNRTI efavirenz, and the INSTI elvitegravir were the drugs most capable of eliciting FGF21 induction/KLB repression effects, which otherwise followed a pattern dictated largely by the specific drug and the cell type assayed. The induction of FGF21 and repression of KLB expression in hepatic and adipose cells reflected the effects on gene transcription. Therefore, and on the basis of the remarkable concordance between the effects found here *in vitro* for several antiretroviral drugs and the alterations in the FGF21/KLB system found in HIV patients, attention should be paid to the potential of particular drugs in the ART cocktails to disturb the FGF21 system.

Subsequently, we explored the intracellular-mediated mechanisms explaining the negative effects of antiretroviral drugs on the FGF21/KLB system. In general, the drug treatments that elicited FGF21 induction/KLB repression in human hepatic, adipose, and muscle cells were also those that induced ER stress/oxidative stress. Specific pharmacological induction of ER stress/oxidative stress mimicked the effects of the drugs on the FGF21/KLB system. Moreover, the induction of ER stress/oxidative stress marker genes closely paralleled FGF21 induction and KLB repression in concentration-response analyses of lopinavir-ritonavir and elvitegravir. However, elvitegravir induced FGF21 and repressed KLB at concentrations lower than those capable of eliciting overt ER stress in hepatic cells, suggesting that pathways other than ER stress may be additionally involved in elvitegravir effects. The results obtained using inhibitors of ER stress and oxidative stress support the involvement, but not the exclusivity, of these stress pathways in the cellular actions of antiretroviral drugs on the FGF21/KLB system.

Abnormally high FGF21 levels are considered a marker of disturbed metabolism in non-HIV-infected patients with obesity, diabetes, or congenital lipodystrophy (15, 16, 42), whereas KLB repression is associated with an impairment of glucose uptake and other health effects mediated by FGF21 (27). Studies in distinct HIV patient cohorts have consistently reported that elevated FGF21 levels are associated with indicators of insulin resistance, such as homeostatic model assessment of insulin resistance (HOMA-IR), insulinemia, and glycemia (6–8, 16). Lifestyle interventions in HIV patients that achieve metabolic improvement are also associated with a decline in FGF21 levels that correlates with indications of improved energy metabolism (8). Further studies will be needed to assess if treatment only with antiretroviral drugs identified as "neutral" in our cell-based study protects HIV patients against abnormalities in the FGF21/KLB system and concomitant metabolic disturbances.

The present *in vitro* study is obviously limited with respect to the translation of results to considerations of the impact of patient treatments on the FGF21 system. The average plasma concentration of drugs in patients under standard treatment regimens is approximately 10 μM for efavirenz and lopinavir and 5 μM for elvitegravir (43–45), indicating that the effects on human adipocytes and muscle cells *in vitro* reported here occur in a concentration range that may have *in vivo* relevance. However, in our study, efavirenz and elvitegravir were added to adipocyte and myotube cell cultures in serum-free or low-serum-containing medium—culture conditions that are required for the *in vitro* differentiation of human adipocytes and muscle cells but may result in higher availability of the drugs owing to a lack of binding to proteins. Consistent with this interpretation, the concentrations of efavirenz and elvitegravir required to cause FGF21 induction/KLB repression in hepatic cells, which require 10% fetal bovine serum (FBS), were higher, implying that the presence of high levels of drug-binding proteins in the medium reduces the actual amount of drug available to the cell. On the other hand, one study that measured the accumulation of certain antiretroviral drugs in adipose tissues showed concentrations close to 100 nmol/g tissue for efavirenz and 1 nmol/g for the PI ritonavir (46); thus, intracellular concentrations, at least for efavirenz, may be higher than the plasma concentrations.

In summary, several antiretroviral drugs used in HIV therapy and belonging to distinct drug classes have been identified for the first time as triggering disturbances in the FGF21/KLB system in human hepatic, adipose, and muscle cells in culture. These

zac-aac/zac00618/zac7224d18z	xppws	S=3	4/14/18	9:26	ArtID: 00029-18	DOI:10.1128/AAC.00029-18	**open-access**	CE: CNV-kcd

drugs cause reciprocal FGF21 induction/KLB repression alterations that commonly occur in HIV patients undergoing antiretroviral treatment. ER stress/oxidative stress mechanisms appear to be involved in these effects. Considering the potential role of disruptions in the FGF21 system in metabolic, cardiovascular, and bone-related alterations, the data presented here could inspire further research designed to improve antiretroviral treatments so as to minimize the adverse effects of antiretroviral agents in HIV-1-infected patients.

MATERIALS AND METHODS

Reagents. The following chemicals/drugs were used: zidovudine (GlaxoSmithKline), stavudine (Bristol-Myers Squibb), tenofovir disoproxil fumarate (Gilead Sciences), nevirapine (Boehringer Ingelheim), efavirenz (Bristol-Myers Squibb), rilpivirine (Janssen Pharmaceuticals, Inc.), ritonavir (Abbott Laboratories), lopinavir (Abbott Laboratories), nelfinavir (Agouron), atazanavir (Bristol-Myers Squibb), raltegravir (sc-364600; Santa Cruz), elvitegravir (Gilead Sciences), maraviroc (Pfizer), tunicamycin (T7765; Sigma-Aldrich Biotechnology), thapsigargin (T9033; Sigma-Aldrich), 4-phenylbutyric acid ([PBA] P21005; Sigma-Aldrich), 6-hydroxy-2,5,7,8-tetramethylchroman-2-carboxylic acid ([Trolox] 648471; Calbiochem), and rosiglitazone (ALX-350-125; Alexis Biochemicals). The reagents for cell culture were from Sigma-Aldrich, whereas media and FBS were from Life Technologies. For initial assessments of the effects of antiretroviral drugs prior to concentration-response analyses, the drugs were used at the highest concentrations that did not cause cytotoxicity in specific cell systems. The drugs were dissolved using dimethyl sulfoxide (DMSO) as the vehicle. Controls included amounts of DMSO (≤0.1% DMSO of total cell medium volume) equal to those used in drug-treated cells.

Cell culture. The HepG2 cell line (ATCC HB-8065), used for studies on human hepatic cells, was cultured in Dulbecco's modified Eagle medium (DMEM) containing 10% FBS. The human SGBS preadipocyte cell line (47) was used for studies on adipocytes. Human SGBS preadipocytes were cultured and differentiated to adipocytes as previously reported (36). Briefly, SGBS preadipocytes were maintained in DMEM/F12 containing 10% FBS. After the cells had become confluent, adipogenic differentiation was initiated by first incubating the cells for 6 days in serum-free medium containing 20 nM insulin, 0.2 nM triiodothyronine (T3), and 100 nM cortisol, supplemented with 25 nM dexamethasone and 500 μM 3-isobutyl-methylxantine. The cells were subsequently switched to adipogenic differentiation medium containing insulin, T3, and cortisol only and maintained for up to 10 days, at which point, more than 90% of the cells had acquired a differentiated adipocyte morphology, as evidenced by lipid droplet accumulation. Depending on the experimental design, the cells were treated with drugs throughout the 10-day differentiation process or acutely for 24 h once cells had differentiated. For studies on human skeletal muscle cells, LHCN-M2 myoblastic cells were differentiated to myotubes as previously reported (23). Briefly, myoblastic LHCN-M2 cells were cultured in DMEM/medium 199 containing 15% FBS and supplemented with 60 μg/ml $ZnSO_4$, 14 μg/ml vitamin B_{12}, 55 μg/ml dexamethasone, 30 μg/ml human hepatocyte growth factor, and 10 μg/ml basic fibroblast growth factor (FGF2). When cells reached ~80% confluence, the culture medium was replaced with fresh DMEM/medium 199 supplemented with 0.5% FBS, 1 mg/ml insulin, 10 mg/ml apo-transferrin, and 55 μg/ml dexamethasone. After culturing for 2 days, the medium was replaced with DMEM/medium 199 supplemented with 55 μg/ml dexamethasone, and the cells were further cultured for 10 days, at which point, more than 90% had acquired a differentiated phenotype on the basis of their multinucleated fused myotube morphology. LHCN-M2 myotubes were exposed to drugs for 24 h. For the analysis of FGF21 protein levels, the cell culture medium was harvested 24 h after the replacement of the cell culture medium in the presence of the drugs tested.

RNA isolation, conventional reverse transcription-PCR, and quantitative reverse transcription-PCR. Total RNA was extracted from cells using an affinity column-based method (Macherey-Nagel) as previously described (36). Reverse transcription was performed in a total volume of 20 μl using random hexamer primers (Applied Biosystems) and 0.5 μg total RNA. PCR was performed on an ABI/Prism 7700 sequence detector system using 25 μl of a reaction mixture containing 1 μl of cDNA, 12.5 μl of TaqMan Universal PCR master mix, 250 nM probes, and 900 nM primers from an Assays-on-Demand gene expression assay mix (TaqMan; Applied Biosystems). The following Assay-on-Demand probes from Life Technologies were used: *FGF21*, Hs00173927; *KLB*, Hs00545621; *CHOP10*, Hs99999172; *HSPA5*, Hs99999174; *HPRT*, Hs99999909; *RPLP0*, Hs99999902; and 18S rRNA, Hs99999901. Controls with no RNA, primers, or reverse transcriptase were included in each set of experiments. The relative amount of individual mRNAs was calculated using the comparative ($2^{-\Delta\Delta CT}$) method and normalized to that of the reference control gene (*HPRT* mRNA) according to the manufacturer's instructions. Each sample was run in duplicates, and the mean value of duplicates was used in calculations. Parallel calculations performed using other reference control genes (*RPLP0* mRNA and 18S rRNA) yielded essentially the same results.

Plasmid constructions and dual luciferase reporter assays. For studies on the transcriptional activity of *FGF21* and *KLB* genes, HepG2 hepatic cells and HIB1B adipogenic cells (48), respectively, were grown in 24-well plates and transiently transfected at ~50% confluence with the corresponding promoter-luciferase reporter plasmids using Lipofectamine (Invitrogen). The reporter plasmid −1497-FGF21-Luc, containing a DNA fragment corresponding to positions −1,497 to +5 of the 5′ region of the mouse *Fgf21* gene linked to the firefly luciferase gene, and a −77-FGF21-Luc mutant construct containing only the −77/+5 region of the *FGF21* gene, were reported previously (48). The reporter plasmid driven by the *KLB* gene promoter, containing a DNA fragment corresponding to positions −1,055 to +45,

was obtained from SwitchGear Genomics. Cells were also cotransfected with a pRL-CMV expression vector for *Renilla* luciferase (Promega). Each transfection condition was assayed in triplicates. The cells were incubated for 48 h after transfection and then incubated with or without drugs, as indicated in the text, for an additional 24 h before harvesting. Luciferase activity was measured on a Glomax 96 microplate luminometer using a dual luciferase reporter assay system kit (Promega). Promoter construct-driven luciferase activity was normalized to that of *Renilla* luciferase, used as a control for variations in transfection efficiency.

FGF21 protein analysis. FGF21 protein levels in cell culture media were determine using an enzyme-linked immunosorbent assay (ELISA) specific for human FGF21 (RD191108200R; Biovendor) as described previously (48). For cultures of HepG2 cells, the medium had to be concentrated (1,000 μl to 50 μl) using centrifugal filters (UFC 50195; Amicon) to achieve measurable amounts of FGF21 in the ELISAs.

Statistical analysis. In studies comparing high concentrations of different drugs, statistical analyses were performed using Student's *t* tests to compare the effects of each drug with that of the control. In the case of concentration-response studies, statistical analyses were performed using a one-way analysis of variance (ANOVA) followed by a Dunnett's test. Differences with *P* values of <0.05 were considered statistically significant.

SUPPLEMENTAL MATERIAL

Supplemental material for this article may be found at https://doi.org/10.1128/AAC.00029-18.

SUPPLEMENTAL FILE 1, PDF file, 0.3 MB.

ACKNOWLEDGMENTS

This research was supported by grants from Fondo de Investigaciones Sanitarias, Instituto de Salud Carlos III ([ISCIII] PI14/00063, PI14/00700, PI17/00420, and PI17/00498) and the Ministerio de Economía y Competitividad ([MINECO] SAF2014-23636 and SAF2017-85722), cofinanced by the European Regional Development Fund (ERDF) and Red de Investigación en SIDA (RD16/0025/0006), ISCIII, Spain. R.M. was supported by a PFIS PhD scholarship from AES, ISCIII, MINECO, Spain. T.Q.-L. was supported by a CONACyT (National Council for Science and Technology in Mexico) PhD scholarship.

J.V. and J.M.G.-E. are "Juan de la Cierva" (MINECO, Spain) and "Sara Borrell" (ISCIII, Spain) postdoctoral researchers, respectively.

We thank the pharmaceutical companies for providing us with the antiretroviral drugs. Neither the funders nor the pharmaceutical companies had any role in the study design, data collection, and interpretation of data or preparation of the manuscript.

REFERENCES

1. Deeks SG, Lewin SR, Havlir DV. 2013. The end of AIDS: HIV infection as a chronic disease. Lancet 382:1525–1533. https://doi.org/10.1016/S0140-6736(13)61809-7.
2. Lagathu C, Cossarizza A, Béréziat V, Nasi M, Capeau J, Pinti M. 2017. Basic science and pathogenesis of ageing with HIV: potential mechanisms and biomarkers. AIDS 31(Suppl 2):S105–S119. https://doi.org/10.1097/QAD.0000000000001441.
3. Caron-Debarle M, Lagathu C, Boccara F, Vigouroux C, Capeau J. 2010. HIV-associated lipodystrophy: from fat injury to premature aging. Trends Mol Med 16:218–229. https://doi.org/10.1016/j.molmed.2010.03.002.
4. Giralt M, Domingo P, Villarroya F. 2011. Adipose tissue biology and HIV-infection. Best Pract Res Clin Endocrinol Metab 25:487–499. https://doi.org/10.1016/j.beem.2010.12.001.
5. Srinivasa S, Grinspoon SK. 2014. Metabolic and body composition effects of newer antiretrovirals in HIV-infected patients. Eur J Endocrinol 170:R185–R202. https://doi.org/10.1530/EJE-13-0967.
6. Domingo P, Gallego-Escuredo JM, Domingo JC, Gutiérrez M del, Mateo MMG, Fernández I, Vidal F, Giralt M, Villarroya F. 2010. Serum FGF21 levels are elevated in association with lipodystrophy, insulin resistance and biomarkers of liver injury in HIV-1-infected patients. AIDS 24:2629–2637. https://doi.org/10.1097/QAD.0b013e3283400088.
7. Lindegaard B, Hvid T, Grøndahl T, Frosig C, Gerstoft J, Hojman P, Pedersen BK. 2013. Expression of fibroblast growth factor-21 in muscle is associated with lipodystrophy, insulin resistance and lipid disturbances in patients with HIV. PLoS One 8:e55632. https://doi.org/10.1371/journal.pone.0055632.
8. Srinivasa S, Wong K, Fitch KV, Wei J, Petrow E, Cypess AM, Torriani M, Grinspoon SK. 2015. Effects of lifestyle modification and metformin on irisin and FGF21 among HIV-infected subjects with the metabolic syndrome. Clin Endocrinol (Oxf) 82:678–685. https://doi.org/10.1111/cen.12582.
9. Giralt M, Gavaldà-Navarro A, Villarroya F. 2015. Fibroblast growth factor-21, energy balance and obesity. Mol Cell Endocrinol 418:66–73. https://doi.org/10.1016/j.mce.2015.09.018.
10. Talukdar S, Zhou Y, Li D, Rossulek M, Dong J, Somayaji V, Weng Y, Clark R, Lanba A, Owen BM, Brenner MB, Trimmer JK, Gropp KE, Chabot JR, Erion DM, Rolph TP, Goodwin B, Calle RA. 2016. A long-acting FGF21 molecule, PF-05231023, decreases body weight and improves lipid profile in non-human primates and type 2 diabetic subjects. Cell Metab 23:427–440. https://doi.org/10.1016/j.cmet.2016.02.001.
11. Gaich G, Chien JY, Fu H, Glass LC, Deeg MA, Holland WL, Kharitonenkov A, Bumol T, Schilske HK, Moller DE. 2013. The effects of LY2405319, an FGF21 Analog, in obese human subjects with type 2 diabetes. Cell Metab 18:333–340. https://doi.org/10.1016/j.cmet.2013.08.005.
12. Markan KR, Naber MC, Ameka MK, Anderegg MD, Mangelsdorf DJ, Kliewer SA, Mohammadi M, Potthoff MJ. 2014. Circulating FGF21 is liver derived and enhances glucose uptake during refeeding and overfeeding. Diabetes 63:4057–4063. https://doi.org/10.2337/db14-0595.

13. Gallego-Escuredo JM, Domingo P, Gutiérrez MDM, Mateo MG, Cabeza MC, Fontanet A, Vidal F, Domingo JC, Giralt M, Villarroya F. 2012. Reduced levels of serum FGF19 and impaired expression of receptors for endocrine FGFs in adipose tissue from HIV-infected patients. J Acquir Immune Defic Syndr 61:527–534. https://doi.org/10.1097/QAI.0b013e318271c2c7.
14. Fisher FM, Chui PC, Antonellis PJ, Bina HA, Kharitonenkov A, Flier JS, Maratos-Flier E. 2010. Obesity is a fibroblast growth factor 21 (FGF21)-resistant state. Diabetes 59:2781–2789. https://doi.org/10.2337/db10-0193.
15. Gallego-Escuredo JM, Gómez-Ambrosi J, Catalan V, Domingo P, Giralt M, Frühbeck G, Villarroya F. 2015. Opposite alterations in FGF21 and FGF19 levels and disturbed expression of the receptor machinery for endocrine FGFs in obese patients. Int J Obes (Lond) 39:121–129. https://doi.org/10.1038/ijo.2014.76.
16. Miehle K, Ebert T, Kralisch S, Hoffmann A, Kratzsch J, Schlögl H, Stumvoll M, Fasshauer M. 2016. Serum concentrations of fibroblast growth factor 21 are elevated in patients with congenital or acquired lipodystrophy. Cytokine 83:239–244. https://doi.org/10.1016/j.cyto.2016.04.015.
17. Gallego-Escuredo JM, Lamarca MK, Villarroya J, Domingo JC, Mateo MG, Gutierrez MDM, Vidal F, Villarroya F, Domingo P, Giralt M. 2017. High FGF21 levels are associated with altered bone homeostasis in HIV-1-infected patients. Metabolism 71:163–170. https://doi.org/10.1016/j.metabol.2017.03.014.
18. Wei W, Dutchak PA, Wang X, Ding X, Wang X, Bookout AL, Goetz LR, Mohammadi M, Gerard RD, Dechow PC, Mangelsdorf DJ, Kliewer SA, Wan Y. 2012. Fibroblast growth factor 21 promotes bone loss by potentiating the effects of peroxisome proliferator-activated receptor gamma. Proc Natl Acad Sci U S A 109:3143–3148. https://doi.org/10.1073/pnas.1200797109.
19. Ji K, Zheng J, Lv J, Xu J, Ji X, Luo YB, Li W, Zhao Y, Yan C. 2015. Skeletal muscle increases FGF21 expression in mitochondrial disorders to compensate for energy metabolic insufficiency by activating the mTOR-YY1-PGC1α pathway. Free Radic Biol Med 84:161–170. https://doi.org/10.1016/j.freeradbiomed.2015.03.020.
20. Suomalainen A. 2013. Fibroblast growth factor 21: a novel biomarker for human muscle-manifesting mitochondrial disorders. Expert Opin Med Diagn 7:313–317. https://doi.org/10.1517/17530059.2013.812070.
21. Schaap FG, Kremer AE, Lamers WH, Jansen PLM, Gaemers IC. 2013. Fibroblast growth factor 21 is induced by endoplasmic reticulum stress. Biochimie 95:692–699. https://doi.org/10.1016/j.biochi.2012.10.019.
22. Wan XS, Lu XH, Xiao YC, Lin Y, Zhu H, Ding T, Yang Y, Huang Y, Zhang Y, Liu YL, Xu ZM, Xiao J, Li XK. 2014. ATF4- and CHOP-dependent induction of FGF21 through endoplasmic reticulum stress. Biomed Res Int 2014:807874. https://doi.org/10.1155/2014/807874.
23. Ribas F, Villarroya J, Hondares E, Giralt M, Villarroya F. 2014. FGF21 expression and release in muscle cells: involvement of MyoD and regulation by mitochondria-driven signalling. Biochem J 463:191–199. https://doi.org/10.1042/BJ20140403.
24. Zha BS, Wan X, Zhang X, Zha W, Zhou J, Wabitsch M, Wang G, Lyall V, Hylemon PB, Zhou H. 2013. HIV protease inhibitors disrupt lipid metabolism by activating endoplasmic reticulum stress and inhibiting autophagy activity in adipocytes. PLoS One 8:e59514. https://doi.org/10.1371/journal.pone.0059514.
25. Apostolova N, Gomez-Sucerquia LJ, Alegre F, Funes HA, Victor VM, Barrachina MD, Blas-Garcia A, Esplugues JV. 2013. ER stress in human hepatic cells treated with efavirenz: mitochondria again. J Hepatol 59:780–789. https://doi.org/10.1016/j.jhep.2013.06.005.
26. Borsa M, Ferreira PLC, Petry A, Ferreira LGE, Camargo MM, Bou-Habib DC, Pinto AR. 2015. HIV infection and antiretroviral therapy lead to unfolded protein response activation. Virol J 12:77. https://doi.org/10.1186/s12985-015-0298-0.
27. Díaz-Delfín J, Hondares E, Iglesias R, Giralt M, Caelles C, Villarroya F. 2012. TNF-α represses β-Klotho expression and impairs FGF21 action in adipose cells: involvement of JNK1 in the FGF21 pathway. Endocrinology 153:4238–4245. https://doi.org/10.1210/en.2012-1193.
28. Lagathu C, Eustace B, Prot M, Frantz D, Gu Y, Bastard JP, Maachi M, Azoulay S, Briggs M, Caron M, Capeau J. 2007. Some HIV antiretrovirals increase oxidative stress and alter chemokine, cytokine or adiponectin production in human adipocytes and macrophages. Antivir Ther 12:489–500.
29. Caron M, Auclair M, Vissian A, Vigouroux C, Capeau J. 2008. Contribution of mitochondrial dysfunction and oxidative stress to cellular premature senescence induced by antiretroviral thymidine analogues. Antivir Ther 13:27–38.
30. Gallego-Escuredo JM, Del Mar Gutierrez M, Diaz-Delfin J, Domingo JC, Mateo MG, Domingo P, Giralt M, Villarroya F. 2010. Differential effects of efavirenz and lopinavir/ritonavir on human adipocyte differentiation, gene expression and release of adipokines and pro-inflammatory cytokines. Curr HIV Res 8:545–553. https://doi.org/10.2174/157016210793499222.
31. Díaz-Delfín J, del Mar Gutiérrez M, Gallego-Escuredo JM, Domingo JC, Gracia Mateo M, Villarroya F, Domingo P, Giralt M. 2011. Effects of nevirapine and efavirenz on human adipocyte differentiation, gene expression, and release of adipokines and cytokines. Antiviral Res 91:112–119. https://doi.org/10.1016/j.antiviral.2011.04.018.
32. Capel E, Auclair M, Caron-Debarle M, Capeau J. 2012. Effects of ritonavir-boosted darunavir, atazanavir and lopinavir on adipose functions and insulin sensitivity in murine and human adipocytes. Antivir Ther 17:549–556. https://doi.org/10.3851/IMP1988.
33. Díaz-Delfín J, Domingo P, Mateo MG, Gutierrez MDM, Domingo JC, Giralt M, Villarroya F. 2012. Effects of rilpivirine on human adipocyte differentiation, gene expression, and release of adipokines and cytokines. Antimicrob Agents Chemother 56:3369–3375. https://doi.org/10.1128/AAC.00104-12.
34. Díaz-Delfín J, Domingo P, Giralt M, Villarroya F. 2013. Maraviroc reduces cytokine expression and secretion in human adipose cells without altering adipogenic differentiation. Cytokine 61:808–815. https://doi.org/10.1016/j.cyto.2012.12.013.
35. Auclair M, Afonso P, Capel E, Caron-Debarle M, Capeau J. 2014. Impact of darunavir, atazanavir and lopinavir boosted with ritonavir on cultured human endothelial cells: beneficial effect of pravastatin. Antivir Ther 19:773–782. https://doi.org/10.3851/IMP2752.
36. Moure R, Domingo P, Gallego-Escuredo JM, Villarroya J, Gutierrez MDM, Mateo MG, Domingo JC, Giralt M, Villarroya F. 2016. Impact of elvitegravir on human adipocytes: alterations in differentiation, gene expression and release of adipokines and cytokines. Antiviral Res 132:59–65. https://doi.org/10.1016/j.antiviral.2016.05.013.
37. Song B, Scheuner D, Ron D, Pennathur S, Kaufman RJ. 2008. Chop deletion reduces oxidative stress, improves beta cell function, and promotes cell survival in multiple mouse models of diabetes. J Clin Invest 118:3378–3389. https://doi.org/10.1172/JCI34587.
38. Wang S, Kaufman RJ. 2012. The impact of the unfolded protein response on human disease. J Cell Biol 197:857–867. https://doi.org/10.1083/jcb.201110131.
39. Hondares E, Gallego-Escuredo JM, Flachs P, Frontini A, Cereijo R, Goday A, Perugini J, Kopecky P, Giralt M, Cinti S, Kopecky J, Villarroya F. 2014. Fibroblast growth factor-21 is expressed in neonatal and pheochromocytoma-induced adult human brown adipose tissue. Metabolism 63:312–317. https://doi.org/10.1016/j.metabol.2013.11.014.
40. Dushay J, Chui PC, Gopalakrishnan GS, Varela-Rey M, Crawley M, Fisher FM, Badman MK, Martinez-Chantar ML, Maratos-Flier E. 2010. Increased fibroblast growth factor 21 in obesity and nonalcoholic fatty liver disease. Gastroenterology 139:456–463. https://doi.org/10.1053/j.gastro.2010.04.054.
41. Wang H, Qiang L, Farmer SR. 2008. Identification of a domain within peroxisome proliferator-activated receptor gamma regulating expression of a group of genes containing fibroblast growth factor 21 that are selectively repressed by SIRT1 in adipocytes. Mol Cell Biol 28:188–200. https://doi.org/10.1128/MCB.00992-07.
42. Zhang X, Yeung DCY, Karpisek M, Stejskal D, Zhou Z-G, Liu F, Wong RLC, Chow W-S, Tso AWK, Lam KSL, Xu A. 2008. Serum FGF21 levels are increased in obesity and are independently associated with the metabolic syndrome in humans. Diabetes 57:1246–1253. https://doi.org/10.2337/db07-1476.
43. Pérez-Molina JA, Domingo P, Martínez E, Moreno S. 2008. The role of efavirenz compared with protease inhibitors in the body fat changes associated with highly active antiretroviral therapy. J Antimicrob Chemother 62:234–245. https://doi.org/10.1093/jac/dkn191.
44. Ramanathan S, Mathias AA, German P, Kearney BP. 2011. Clinical pharmacokinetic and pharmacodynamic profile of the HIV integrase inhibitor elvitegravir. Clin Pharmacokinet 50:229–244. https://doi.org/10.2165/11584570-000000000-00000.
45. Jackson A, Hill A, Puls R, Else L, Amin J, Back D, Lin E, Khoo S, Emery S, Morley R, Gazzard B, Boffito M. 2011. Pharmacokinetics of plasma lopinavir/ritonavir following the administration of 400/100 mg, 200/150

zac-aac/zac00618/zac7224d18z	xppws	S=3	4/14/18	9:26	ArtID: 00029-18	DOI:10.1128/AAC.00029-18	**open-access**	CE: CNV-kcd

mg and 200/50 mg twice daily in HIV-negative volunteers. J Antimicrob Chemother 66:635–640. https://doi.org/10.1093/jac/dkq468.
46. Dupin N, Buffet M, Marcelin A-G, Lamotte C, Gorin I, Ait-Arkoub Z, Tréluyer J-M, Bui P, Calvez V, Peytavin G. 2002. HIV and antiretroviral drug distribution in plasma and fat tissue of HIV-infected patients with lipodystrophy. AIDS 16:2419–2424. https://doi.org/10.1097/00002030-200212060-00006.
47. Wabitsch M, Brenner RE, Melzner I, Braun M, Möller P, Heinze E, Debatin K-M, Hauner H. 2001. Characterization of a human preadipocyte cell strain with high capacity for adipose differentiation. Int J Obes Relat Metab Disord. 25:8–15. https://doi.org/10.1038/sj.ijo.0801520.
48. Hondares E, Iglesias R, Giralt A, Gonzalez FJ, Giralt M, Mampel T, Villarroya F. 2011. Thermogenic activation induces FGF21 expression and release in brown adipose tissue. J Biol Chem 286:12983–12990. https://doi.org/10.1074/jbc.M110.215889.

Supplementary Figure 1. Concentration-response effects of efavirenz, lopinavir/ritonavir, elvitegravir and raltegravir on the expression of FGF21, KLB, CHOP10 and HSPA5 mRNAs in human hepatic cells. HepG2 cells were treated with the indicated concentrations of drugs for 24 hours. Data are presented as means ± SEM from 4–5 independent experiments, and are expressed relative to values for control cells (defined as 1). *P < 0.05, **P < 0.01, and ***P < 0.001 for each drug treatment vs. control.

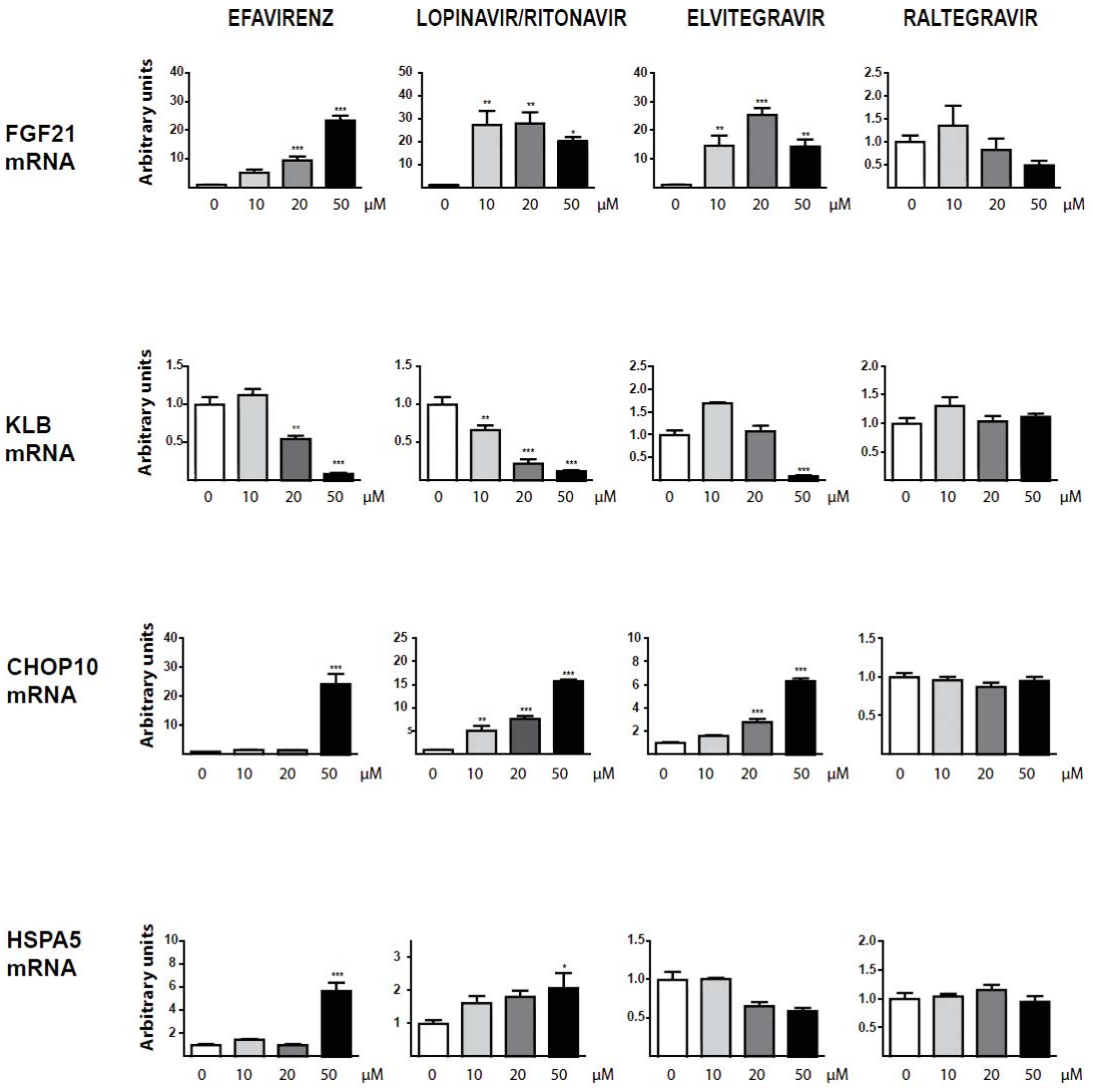

Supplementary Figure 2. Concentration-response effects of efavirenz, lopinavir/ritonavir, elvitegravir and raltegravir on the expression of FGF21, KLB, CHOP10 and HSPA5 mRNAs in human adipocytes during differentiation. SGBS human preadipocytes were differentiated in culture into adipocytes in the presence of the indicated concentrations of drugs. Data are presented as means ± SEM from 4–5 independent experiments, and are expressed relative to values for control cells (defined as 1). *P < 0.05, **P < 0.01, and ***P < 0.001 for each drug treatment vs. control.

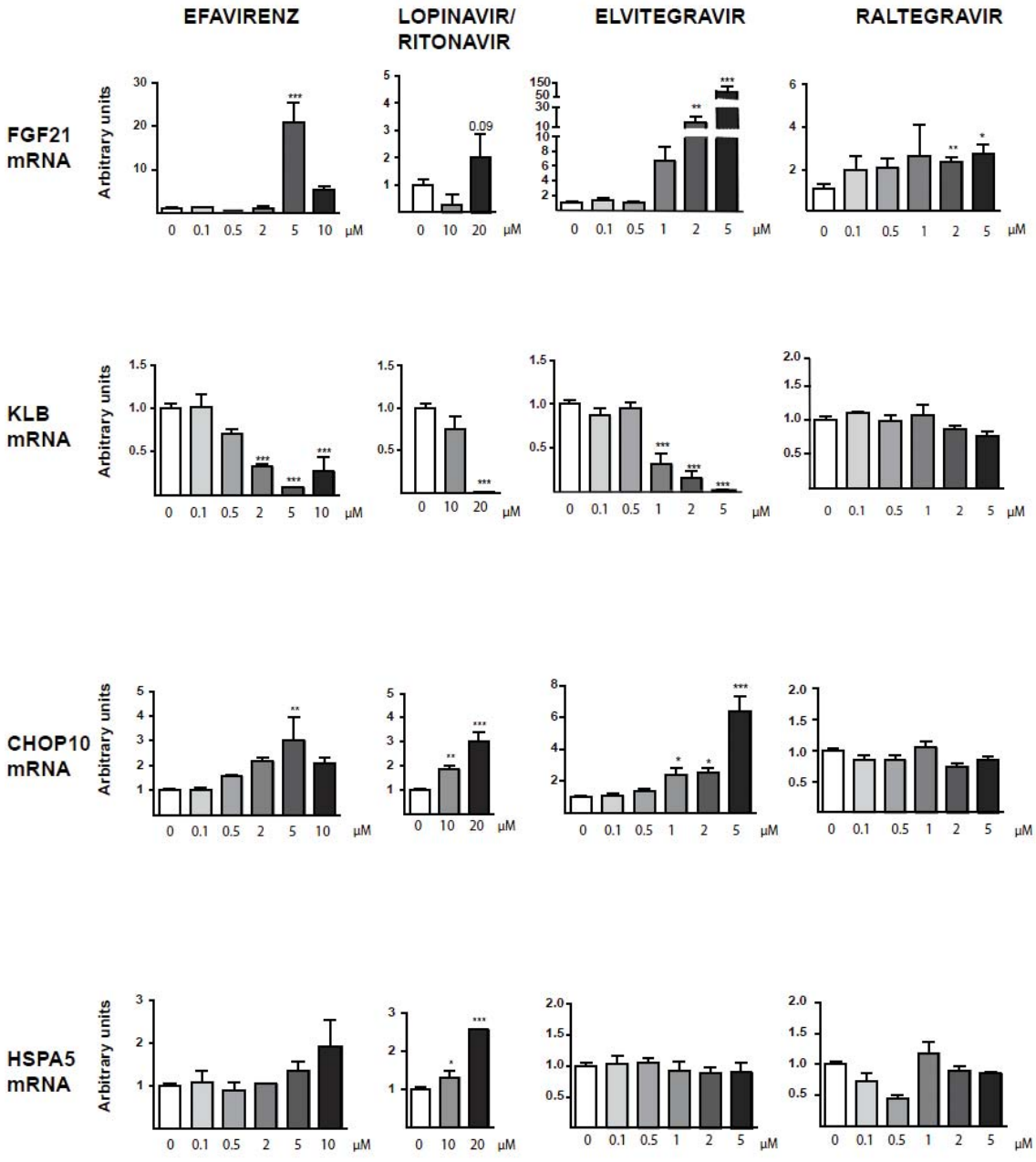

Supplementary Figure 3. Concentration-response effects of efavirenz, lopinavir/ritonavir and elvitegravir on the expression of FGF21, KLB, CHOP10 and HSPA5 mRNAs in SGBS human adipocytes differentiated in culture. SGBS human preadipocytes were differentiated in culture into adipocytes and treated with the indicated concentrations of drugs for 24 hours. Data are presented as means ± SEM from 4–5 independent experiments, and are expressed relative to values for control cells (defined as 1). *P < 0.05, **P < 0.01, and ***P < 0.001 for each drug treatment vs. control.

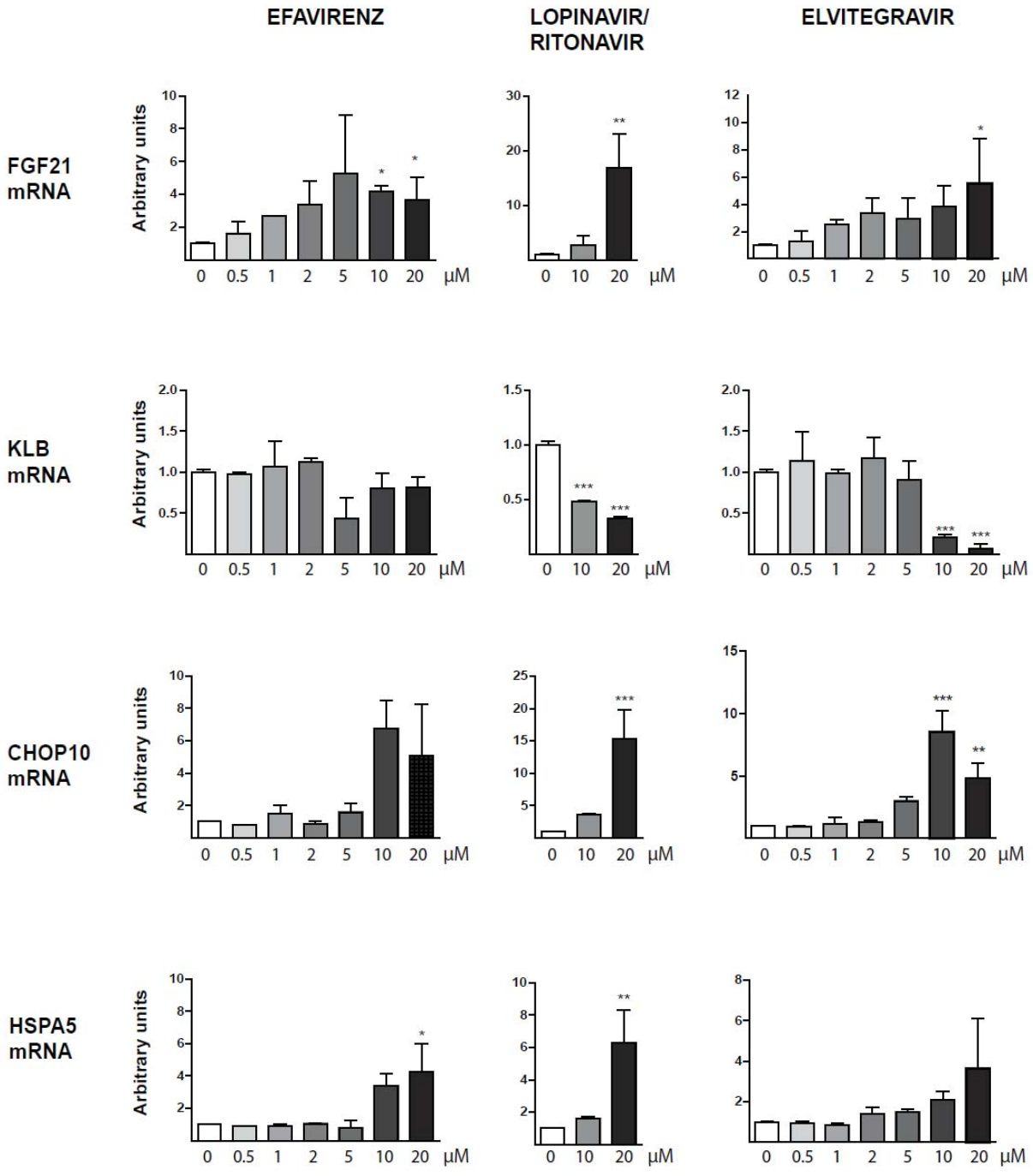

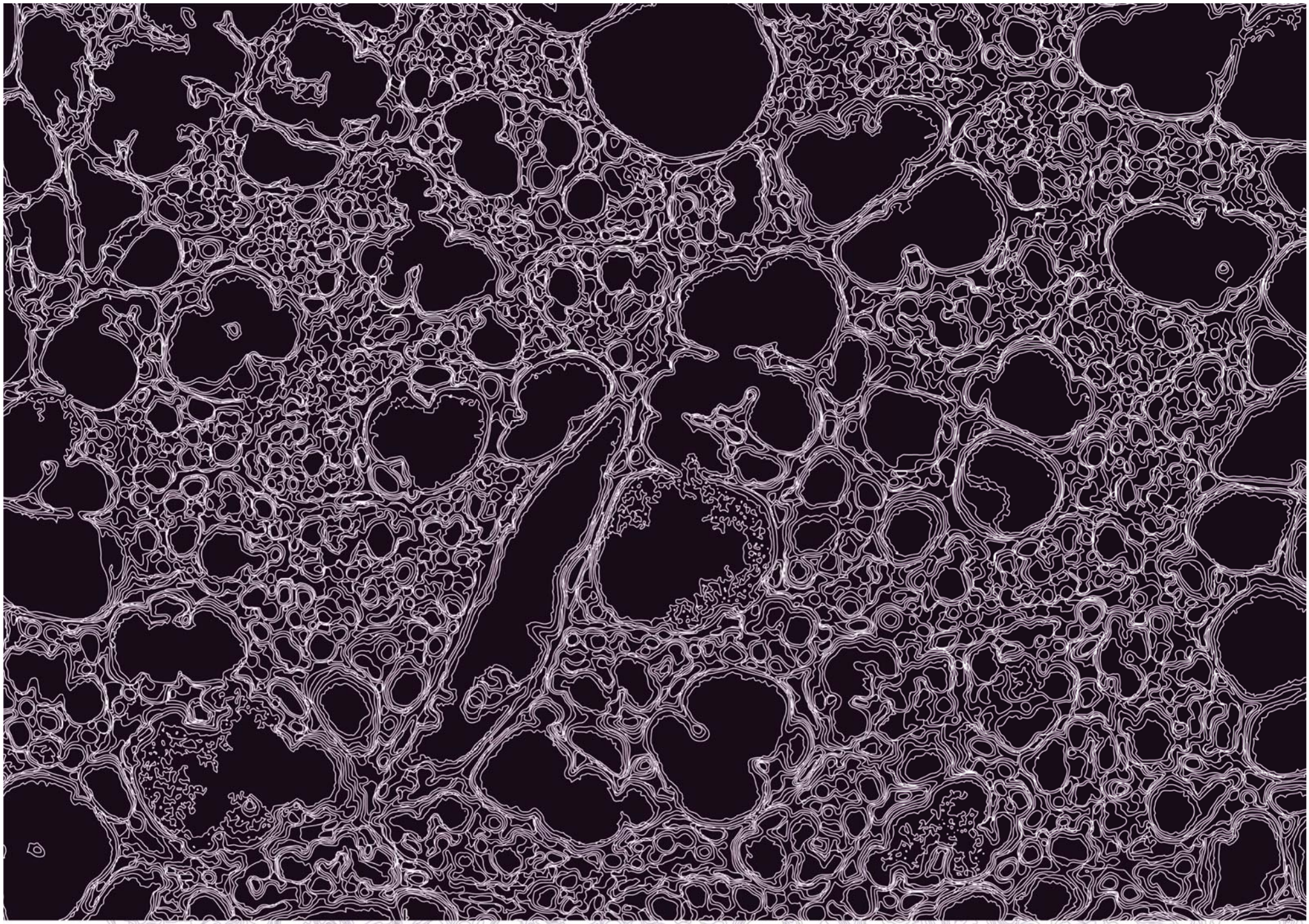

Doctoral Thesis
2018

The role of the G-protein coupled receptor 120 (GPR120) on the FGF21 system in white and brown adipose tissues

Tania Paloma
Quesada López